FUNDAMENTALS OF SHAPED CHARGES

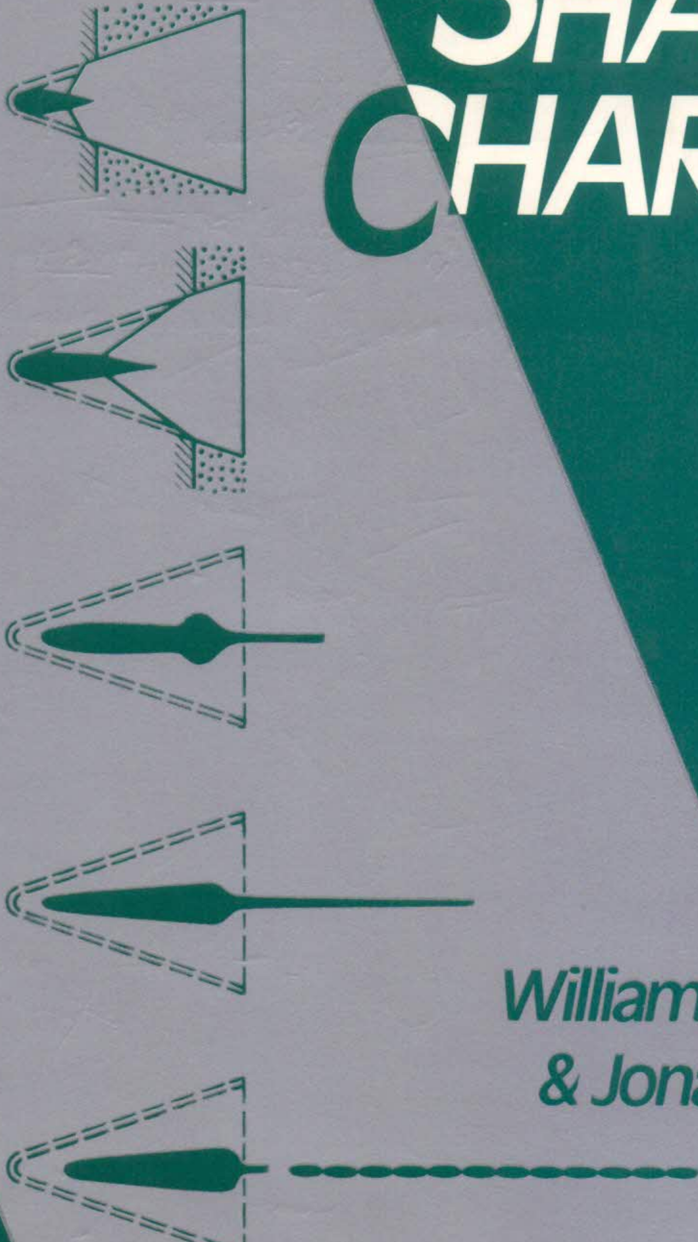

William P. Walters
& Jonas A. Zukas

FUNDAMENTALS OF SHAPED CHARGES

FUNDAMENTALS OF SHAPED CHARGES

W. P. WALTERS
U.S. Army Ballistic Research Laboratory
Aberdeen Proving Ground, Maryland

J. A. ZUKAS
Computational Mechanics Associates
Towson, Maryland

WILEY

A Wiley-Interscience Publication

JOHN WILEY & SONS

New York · Chichester · Brisbane · Toronto · Singapore

Copyright © 1989 by John Wiley & Sons, Inc.

All rights reserved. Published simultaneously in Canada.

Reproduction or translation of any part of this work beyond that permitted by Section 107 or 108 of the 1976 United States Copyright Act without the permission of the copyright owner is unlawful. Requests for permission or further information should be addressed to the Permissions Department, John Wiley & Sons, Inc.

Library of Congress Cataloging in Publication Data:

Walters, W. P. (William P.), 1943–
Fundamentals of shaped charges.

"A Wiley-Interscience publication."
Bibliography: p.
Includes index.
1. Shaped charges. I. Zukas, Jonas A. II. Title.

UF870.W35 1989 623.4′54 88-33944
ISBN 0-471-62172-2

Printed in the United States of America

10 9 8 7 6 5 4 3 2 1

PREFACE

This book originated from a series of short courses, sponsored by Computational Mechanics Associates, taught on this subject over the last four years. The voluminous notes developed for these courses became the core of this book.

It is our intent that this book provide an introduction to the basic aspects of shaped charges. We did not aim to provide exhaustive coverage of the subject. This would be an impossible task since much of the literature in this field is either classified or proprietary, insofar as specific items of hardware are concerned. What was obvious to us, from the first course onward, was the existence of a need for a basic text in this area. Thus, this book is not intended to be a "design handbook." We consistently stress the fundamental principles that must be understood before leaping into hardware design. This book will not tell the reader how to design or improve a specific hardware device. It does stress the principles and ideas that must be mastered to achieve such objectives.

The authors assume a basic background in the sciences, such as would be obtained in a first degree science or engineering curriculum in the United States. We assume also the ability to fluently convert between English and metric units as we mix both throughout the book, primarily for the sake of convenience.

Also, we deviated from the norm by relegating many figures and illustrations to the final chapter, our picture book of shaped charges. Those interested only in a brief introduction to the shaped charge field, without mathematical concepts and the like, should read Chapters 1–3 and 14. Other chapters may then be selected at will, depending on individual interest.

The authors are grateful to their many colleagues over the years, at the Ballistic Research Laboratory and elsewhere, who gave unselfishly of their time while allowing us to profit from their knowledge and experience. We also thank those who were instrumental in expediting this material for publication. Special thanks are due to B. Dale Trott, who provided an excellent review and critique of portions of the text; Steven Segletes, who generated Figures 12–19 of Chapter 5; and Manfred Held, Ben Pernick, and Chris Weickert, who generously provided considerable data and illustrations. Special thanks is also due to Dr. Pei Chi Chou, who co-authored (with WPW) in the open literature some of the material discussed in Chapters 8 and 9.

Mary G. Underwood is specially acknowledged for the meticulous preparation of a difficult manuscript. We are also grateful for the support and editorial assistance provided by John Wiley & Sons.

Finally, we remain forever indebted for the patience, understanding, and moral support provided by our wives and children

W. P. WALTERS
J. A. ZUKAS

CONTENTS

FUNDAMENTALS OF SHAPED CHARGES

CHAPTER 1

INTRODUCTION TO THE SHAPED CHARGE CONCEPT

The explosive loading of metals, especially as related to shaped charge liners and metals driven by explosives, is a vast field. Thousands of documents have been written covering many aspects of the explosive loading of materials. However, due to the intense interest in this field by the defense establishments of many nations, a great deal of the literature is either in limited distribution, classified, not available in English, or hidden in obscure government or industry documents. Also, certain industries (e.g., drilling, mining, metal forming, etc.) engaged in explosive loading of metals (or explosive loading for short) do not readily distribute information due to their highly competitive nature. This increases the number of proprietary and minimal distribution documents. In short, a great deal of information is simply not available to, or cannot be found by, even the most diligent researcher. In addition, these restrictions preclude discussion related to the design, behavior, and performance of many materials driven by an explosive.

We are certainly not aware of all the explosive loading information available. Furthermore, we will not even attempt to present all the information at our disposal. Instead, we shall present basic introductory material and cover only the major aspects of the explosive loading of metals technology and limit our discussion to shaped charges and the motion of metals driven by explosives. The material and literature covered will be that of important historical value and that material found to be most useful to us.

Our sources stem primarily from our association with the Ballistic Research Laboratory (BRL). As a direct consequence of this association, we are probably remiss in reporting the results of other government and industrial agencies, especially those that do not deal directly with the BRL. Also, reference to foreign literature is minimal. Several sources have been omitted as being

beyond the scope of this text or merely redundant or supplemental to material already included. Nevertheless, sizable bibliographies are given at the ends of chapters. Again, we do not claim that these bibliographies are complete.

1.1. THE SHAPED CHARGE CONCEPT

A cylinder of explosive with a hollow cavity in one end and a detonator at the opposite end is known as a hollow charge. The hollow cavity, which may assume almost any geometric shape such as a hemisphere, a cone, or the like, causes the gaseous products formed from the initiation of the explosive at the end of the cylinder opposite the hollow cavity to focus the energy of the detonation products. The focusing of the detonation products creates an intense localized force. When directed against a metal plate, this concentrated force is capable of creating a deeper cavity than a cylinder of explosive without a hollow cavity, even though more explosive is available in the latter case. This phenomenon is known in the United States and the United Kingdom as the Munroe effect and in Europe as the von Foerster or Neumann effect.

If the hollow cavity is lined with a thin layer of metal, glass, ceramic, or any solid, the liner may form a jet when the explosive charge is detonated if certain criteria related to the charge geometry, explosive, and liner properties are satisfied. Upon initiation, a spherical wave propagates outward from the point of initiation. This high-pressure shock wave moves at a very high velocity, typically around 8 km/s. As the detonation wave engulfs the lined cavity, the material is accelerated under the high detonation pressure, collapsing the cone. During this process, depicted in Figure 1 for a typical conical liner, the liner material is driven to very violent distortions over very short time intervals, at strain rates of 10^4–10^7/s. Maximum strains greater than 10 can be readily achieved since superimposed on the deformation are very large hydrodynamic pressures (peak pressures approximately 200 GPa, decaying to an average of approximately 20 GPa). The collapse of the conical liner material on the centerline forces a portion of the liner to flow in the form of a jet where the jet tip velocity can travel in excess of 10 km/s. Because of the presence of a velocity gradient, the jet will stretch until it fractures into a column of "jagged" particles.

When this extremely energetic jet strikes a metal plate, a deep cavity is formed, exceeding that caused by a hollow charge without a liner. Peak pressures in the metal plate of 100–200 GPa are generated, decaying to an average of 10–20 GPa. Average temperatures of 20–50% of the melt temperature and average strains of 0.1–0.5 are common. Localized temperatures and strains at the jet tip can be even higher. The penetration process occurs at strain rates of 10^6–10^7/s. The cavity produced in the metal plate due to this jet–target interaction is due not to a thermal effect but to the lateral displace-

(a)

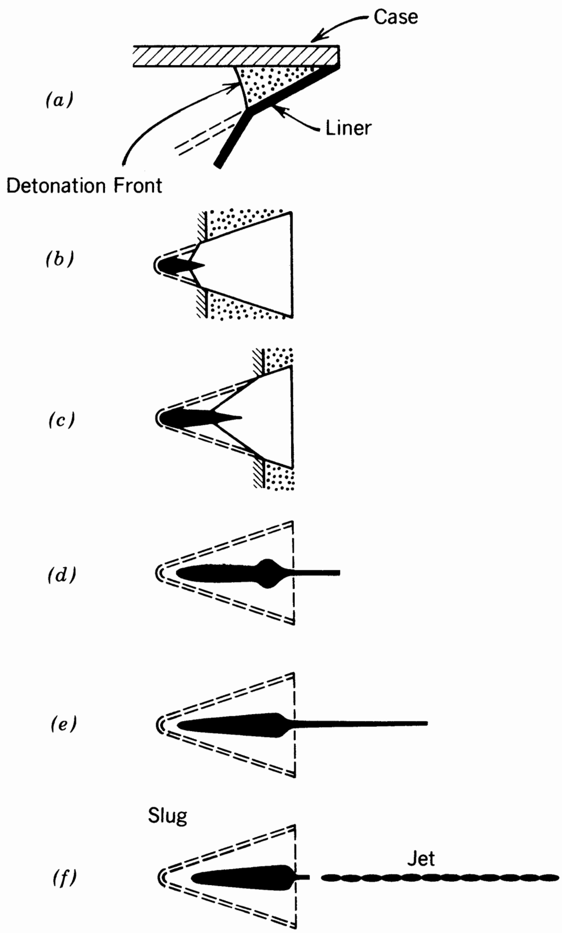

(b)

(c)

(d)

(e)

(f)

Figure 1. The collapse of a shaped charge with a conical liner.

ment of armor by the tremendous pressures created (Figure 2). The target material is actually pushed aside and the penetration is accompanied by no charge in target mass, neglecting any impact ejecta or spall from the rear surface of the target.

The cavity formed becomes deeper yet when the explosive charge containing the liner is removed some distance away from the plate. This distance, for which an optimum exists (Figure 3), is called the *standoff distance*. Devices of this nature are called *lined cavity charges* or *shaped charges*.

The shaped charge was extensively used in World War II for penetration of hardened targets, that is, tank armor, bunkers, and fuel storage containers. Today, it is employed for both military and peaceful purposes in the oil and

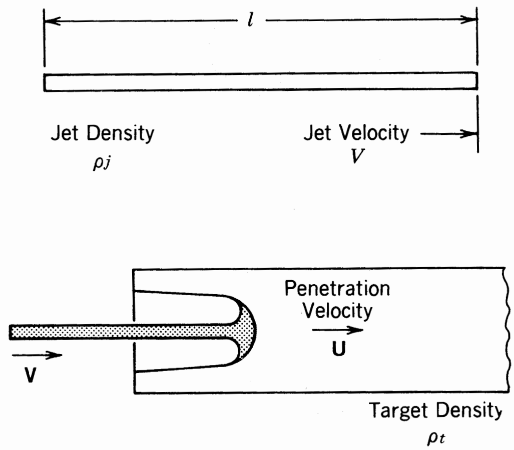

Figure 2. Jet penetration.

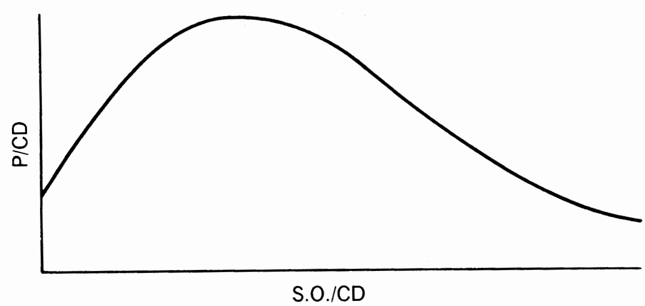

Figure 3. Penetration–standoff curve for a conical shaped charge liner.

steel industries; in geophysical prospecting, mining, and quarrying; in salvage operations; demolition work; as linear cutting charges for destruct devices in missiles; and for hypervelocity impact studies.

1.2. INTRODUCTION TO SHAPED CHARGES

The directional penetration effect observed when a hollow charge is detonated in contact with a steel plate is graphically depicted in Figure 4*a*. The crater depth is about one-half of the diameter of the hollow of the conical cavity. The cavity is produced by high-pressure, high-velocity gas erosion (the Munroe effect). When the hollow cavity is lined with a thin hollow metallic or glass cone, the lined charge results in a much deeper crater as shown in Figure 4*b*. Furthermore, when the lined cavity charge is displaced from the target block

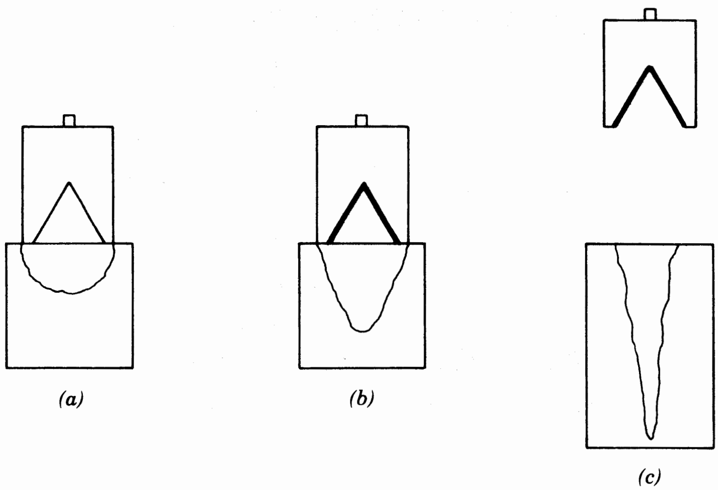

Figure 4. The lined cavity effect.

some distance (known as the standoff) the penetration increases even more as depicted in Figure 4*c*.

The increase in penetration resulting from the lined shaped charge is due to the jetting process that occurs when the liner undergoes explosive-induced high-pressure, high-velocity collapse. The mechanism of jet formation for metallic conical liners with a semi-angle (one-half of the conical apex angle) less than 60° is described later. Wide-angle conical liners and nonconical liners will be addressed in a later chapter.

Figure 5 shows a typical shaped charge configuration like that already described. Note that the explosive charge is not cylindrical but tapered. This removal of some of the explosive weight is termed *Boattailing* and does not affect the jet collapse mechanism. It is only necessary that the detonation wave front be symmetric about the longitudinal axis of the charge. A detonation wave that is plane and perpendicular to the charge axis of symmetry is assumed for simplicity.

When the detonator is fired, the detonation wave propagates through the explosive with the detonation velocity of the particular explosive used. When the detonation front reaches the conical liner, the liner is subjected to the intense pressure of the front and begins to collapse. The collapse is depicted in Figure 6 for the conical lined shaped charge of the type shown in Figure 5. For the position of the detonation wave front shown in Figure 6, the upper (apex)

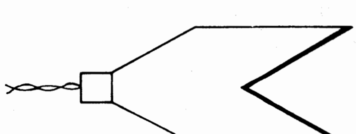

Figure 5. Typical shaped charge configuration.

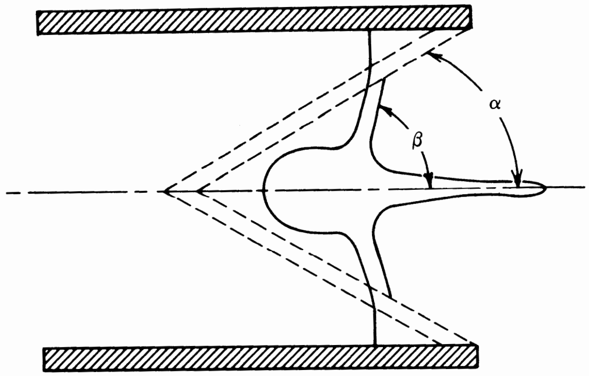

Figure 6. Schematic collapse of a typical shaped charge with a conical liner.

region of the cone has collapsed and collided on the axis of symmetry. This collision results in liner material under tremendous pressure being extruded along the axis of symmetry, as described by Kennedy (1985), Evans (1950), and Backman (1976). This extruded material is called the *jet*. When the pressures generated far exceed the yield strength of the liner material, the liner behaves approximately as an inviscid, incompressible fluid. The cone collapses progressively from apex to base under point initiation of the high explosive. A portion of the liner flows into a compact slug, the large massive portion at the rear of the jet.

This preliminary jet formation theory was advocated by Birkhoff (1943, 1947), and the steady-state, hydrodynamic theory of jet formation was formulated by Birkhoff et al. (1948). This hydrodynamic, steady-state jet formation theory was first conceived by Taylor (Tuck 1943; Taylor 1943), independently by Birkhoff (1943) and by Schumann and Schardin in Germany (Simon 1945; Schumann ca. 1945). The shaped charge jet collapse mechanism described was verified by the early flash radiograph studies of Clark et al. (Seely and Clark 1943; Clark and Rodas 1945), Tuck (1943), and Schumann and Schardin (Simon 1945; Schumann ca. 1945). These radiographs proved earlier theories of jet formation to be invalid. The earlier theories claimed that the penetrating jet was due to either a focusing of the detonation gases, the formation of multiple, interacting shock waves, the spallation of the liner material, or some combination of these effects, including the theory that jets of gas (from the detonation products) break through the metallic liner and carry fragments resulting from the rupture and erosion of the liner. An interaction of these jets then causes a strong forward wave that imparts a high velocity to the liner particles. Birkhoff (1947) and George (1945) discuss these early theories that have since been discredited by the early flash radiography data.

In fact, the shaped charge concept is not well understood by people outside the science of ordnance devices. For example, a shaped charge jet is not a "cutting plasma" and does not "burn its way through the armor" as reported

by Lawton (1986), Aronson (1986), and Schemmer (1987). Also, Kennedy (1985) addressed this issue and stated that probably 9 of 10 descriptions of shaped charge HEAT projectile functioning are in error. [See Kennedy's (1985) references 6, 21, 27, 30, 31, and 33 for example.] The acronym HEAT stands for high explosive anti-tank and does not relate to thermal effects.

A rough analogy to the jet formation can be drawn from the effect produced when a sphere is dropped into water. During impact and downward motion in the water, the cavity formed moves outward around the sphere and then reverses to collide along the axis of symmetry. On collision, vertical jets are formed that squirt upward and downward (Evans 1950; Birkhoff 1947; and Worthington 1908).

Crude rules of thumb were established by Evans (1950). Namely, about 20% of the inner surface of the metal of the cone goes into the jet. The jet diameter is about one-twentieth of the diameter of the cone. The jet tip velocity is of the order of the detonation velocity of the explosive. The distribution of the jet velocity along its length is a nearly linear function from a maximum at the tip down to about one-quarter of the detonation velocity at the tail (rear) of the jet. The velocity of the slug is of the order of one-tenth of the jet tip velocity. These values are only crude order-of-magnitude estimates and are only for moderate apex angle, copper, conical liners. Techniques will be discussed that provide more accurate estimates of the jet and slug parameters. Also, the jet formation is strongly dependent on the linear geometry, liner material, high explosive geometry, confinement geometry and material (if confinement is present), the type of high explosive used, and the mode of initiation. Great axial precision and assembly are required for reproducible and optimal performance. In any case, the goal is to direct and concentrate energy in the axial direction to enhance the damage resulting from the hollow charge.

For any liner design, a proper match between the charge-to-mass ratio (explosive charge mass to liner mass ratio) is critical. If the liner is too thick, the energy losses resulting from internal friction and heating of the liner walls during the collapse and the energy losses due to spallation of the thick liner will reduce the collision velocity below the value necessary for jet extrusion. Also, if the liner wall thickness is too thin, directed flow is not achieved due to the loss of structural integrity of the liner. If the wall is extremely thin, the liner material may undergo vaporization upon collision.

Shaped charges with wide-angle cones or hemispherical liners show a radically different collapse pattern. Hemispherical liners invert (or turn inside out) from the pole and as the detonation wave progresses toward the base of the liner, the hemispherical liner approximates a conical liner and the inverted collapse pattern reverts to that of a cone. In general, the hemispherical and large-angle conical liners usually result in larger diameter, but lower velocity jets which also have lower velocity gradients. No massive slug, per se, is formed.

Of course, jet effects are not limited to conical or hemispherical liners. Extensive use has been made of other liner designs as well as linear and

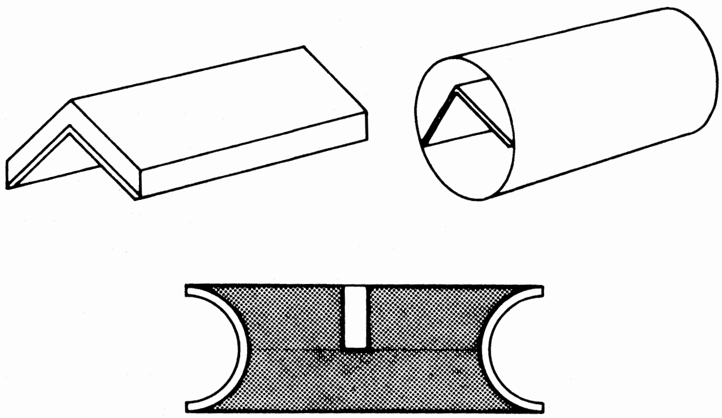

Figure 7. Linear and circular lined shaped charge configurations (Mohaupt 1966).

circular charges. The liner cross sections for linear and circular charges are wedges and semicircular configurations, respectively. The jet produced by a linear charge is in the form of a thin ribbon and in the case of a circular (torus) charge a tubular spray (Mohaupt 1966). A linear charge and a circular or torus charge are illustrated in Figure 7.

1.3. THE NOMENCLATURE

The shaped charge ordnance community has its own unique nomenclature, as shown in Figure 8. An explosive train, consisting of a detonator, booster, and the secondary high explosive (HE) fill is shown. In the figure, a conical liner is illustrated. The liner diameter (LD) is the outer diameter of the liner. The liner is encased in the cylindrical explosive billet that has a charge diameter

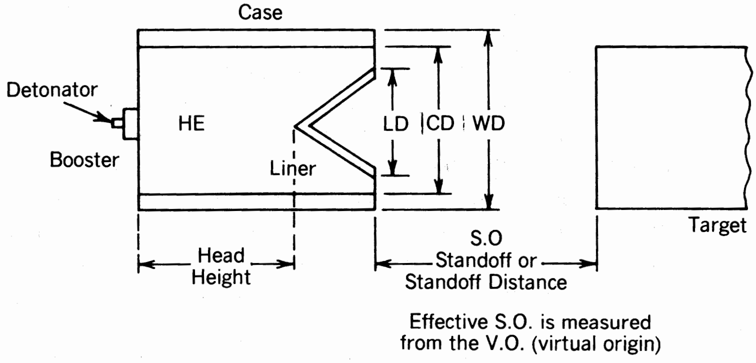

Figure 8. The nomenclature for a shaped charge configuration.

designated as CD (and not to be confused with the cone diameter, as sometimes happens). In this illustration, the LD is less than the CD or the liner is said to be subcalibered. If the charge is confined in some type of case (either to assist in casting the high explosive, to provide fragmentation effects, or to enhance the shaped charge performance), the outer diameter of the case is termed the warhead diameter (WD). Confinement effects are addressed in a later chapter. The overall length of the device is the charge length (L), and the length of the explosive fill between the apex of the liner and the booster is the head height. Finally, the distance from the base of the charge to the target is the standoff distance, or simply the standoff. The effective standoff, or virtual standoff, is the distance from the virtual origin of the warhead to the target. The virtual origin is the point from which the shaped charge jet can be assumed to originate and is discussed in a later chapter.

REFERENCES

Aronson, R. B. (1986), "Weight Is the Enemy in New Tank Designs," *Machine Design*, April 24.

Backman, M. E. (1976), "Terminal Ballistics," Naval Weapons Center Technical Publication 5780, China Lake, CA, February.

Birkhoff, G. (1943), "Mathematical Jet Theory of Lined Hollow Charges," Ballistics Research Laboratory Report No. 370, June 18.

Birkhoff, G. (1947), "Hollow Charge Anti-Tank (HEAT) Projectiles," Ballistic Research Laboratory Report No. 623, February 10.

Birkhoff, G., and MacDougall, D., Pugh, E., and Taylor, G. (1948), "Explosive with Lined Cavities," *J. Appl. Phys. 19* (6).

Clark, J. C., and Rodas, W. M. (1945), "High Speed Radiographic Studies of Controlled Fragmentation," Ballistic Research Laboratory Report No. 585, November 13.

Evans, W. M. (1950), "The Hollow Charge Effect," *Bulletin of the Institution of Mining and Metallurgy*, No. 520, March.

George, H. P. (1945), "Mechanism of Collapse of Conical Hollow Charge Liners," Frankfort Arsenal Report R-667, October.

Kennedy, D. R. (1985), "The Infantryman VS the MBT," *National Defense*, ADPA, March, pp. 27–34.

Lawton, A. T. (1986), "Lead Armour, the Soft Option to Defeat the Hollow-Charge Warhead," *Internat. Def. Rev. 19* (3).

Mohaupt, H. (1966), *Aerospace Ordnance Handbook*, F. Pollard and J. Arnold (eds.), Englewood Cliffs, NJ: Prentice-Hall, Chapter 11.

Schemmer, B. F. (1987), "An Exclusive AFJ Interview with Phillip A. Karber," *Armed Forces. J. Internat.* Part 1, May.

Schumann, E. (ca. 1945), "The Scientific Basis of the Hollow Charge Effect" Publication BIOS/Gp. 2/HEC 5919, Halstead Exploiting Center, England.

Seely, L. B., and Clark, J. C. (1943), "High Speed Radiographic Studies of Controlled Fragmentation," Ballistic Research Laboratory Report No. 368, June 16.

Simon, L. E. (1945), "Report of Special Mission on Captured German Scientific Establishments" Office of the Chief of Ordnance, Braunschweig, Germany, June 1.

Taylor, G. I. (1943), "A Formulation of Mr. Tuck's Conception of Munroe Jets," U.K. Report, A.C. 3734, SC 15-WA-638-32, March 27.

Tuck, J. L. (1943), "Note on the Theory of the Munroe Effect," U.K. Report, A.C. 3596 (Phys. Ex. 393-WA-638-24), February 27.

Worthington, A. M. (1908), *Study of Splashes*, Longmans Green, London.

CHAPTER 2

HISTORY OF SHAPED CHARGES

The term *shaped charge* has been applied to explosive charges with lined or unlined cavities although in current usage the term applies primarily to charges with lined cavities. The cavity is formed in the end of the explosive charge opposite the point of detonation. The term, however, has a more general meaning, for example, Cook (1958). The shaped charge is sometimes referred to as the hollow charge (in the United Kingdom and the United States), the cumulative charge (in the USSR), or the Hohlladung (in Germany).

2.1. THE EARLY HISTORY

The history of shaped charge conception and development is wrought with controversy. In 1792, the mining engineer, Franz von Baader (1792) allegedly noted that one can focus the energy of an explosive blast on a small area by forming a hollow in the charge. Lenz (1965) stated that Baader, in 1799 (not 1792!), observed that if depressions or shapes were cut in an explosive and placed face down on a steel plate, the detonation would cause these shapes to appear on the plate. This is known as explosive engraving. Kennedy (1983) presents additional information on the life of von Baader and his version of the history of the shaped charge effect.

The original von Baader (1792) paper, however, primarily discussed bore hole drilling and loading, confinement effects on propellants, the positioning of a small air cavity between the explosive powder and the tamping (at best, a standoff distance effect), and rock fragmentation. His original paper did not discuss explosive engraving or hollow cavity charges. However, this is a moot point since von Baader used black powder, which is not capable of detonation

or shock formation, in his experiments. Actual shaped charge devices were made possible by the discovery of blasting caps (detonators) by Alfred Nobel (Mohaupt 1966; E. I. du Pont 1980) in 1867. The explosive reaction initiated by these blasting caps could propagate through a column of explosive without the use of confinement. This was termed detonation or brisant explosion. Thus, the first demonstration of the hollow cavity effect for high explosives was achieved by von Foerster (sometimes spelled Forster, the correct spelling being Forster, with umlaut over the *o*, which may be written as *œ*) in 1883 (von Foerster 1883, 1884). A translation of some of Lieutenant von Foerster's work is given by Wisser (1886). Quoting from von Foerster (Wisser 1886):

> If a coin be placed between a gun cotton cartridge and a wrought-iron plate, the figures and letters in relief on the coin will appear in the iron as depressions after the explosion; if, instead of a coin, a green leaf be inserted, the entire skeleton of the leaf will appear on the iron plate after the explosion. The more prominent, as well as the finer veins, protect the underlying iron, the more delicate parts of the leaf, lying between the veins, cannot afford the same protection; hence the depression under the latter is the greater.

Again, this is a form of explosive engraving. Kennedy (1983) and Freiwald (1941) provide further detail on the discoveries of von Foerster and conclude that he was the true discoverer of the modern hollow charge.

Also, G. Bloem (1886) of Dusseldorf patented a shell for detonating caps that resembles a shaped charge with a hemispherical liner.

2.2. THE MUNROE EFFECT

The hollow cavity (i.e., unlined shaped charge) was rediscovered by Charles E. Munroe of the Naval Torpedo Station, Newport, Rhode Island. Munroe's discoveries date from 1888 and are well documented (1888a, 1888b, 1888c, 1894, 1900).

Munroe (1888c) detonated blocks of explosive in contact with steel plates. The explosive charge had the initials U.S.N. (United States Navy) inscribed on the charge opposite the point of initiation. The initials were reproduced on the steel plate. Munroe further observed that when a cavity was formed in a block of explosive, opposite the point of initiation, the penetration, or depth of the crater produced in the target, increased. In other words, a deeper cavity could be formed in a steel block using a smaller mass of explosive! In Munroe's own words:

> We have offered as an hypothesis to explain this phenomenon that, where spaces exist between the guncotton and the iron, portions of the undetonated guncotton, or of the products of the explosion, the indentations are produced by the impact of these moving particles. We have devised many experiments to test this theory,

> and all have tended to confirm it. Among others we have bored deeper and deeper holes in the guncotton, until we have completely perforated it, and the indentations made in the iron plates have increased with the depth of the hole in the guncotton disk until, when the hole was bored completely through the guncotton, we succeeded in completely perforating the iron plate.
>
> (Munroe 1888c; Clark (1948)

The increase in penetration results from the focusing of the explosive gases (detonation products) by the hollow cavity.

One of the first lined shaped charges (or perhaps the first shaped charge if we discount Bloem (1886) was devised by Munroe (Munroe 1894; Clark 1948). This device consisted of a tin can with sticks of dynamite tied around and on top of it, with the open end of the tin can pointing downward. It was used to punch a hole through the top of a steel safe.

Early German reference to the hollow cavity effect, after von Foerster and Bloem, occurred in 1911–1912 patents in the United Kingdom and Germany by WASAG (Westfalische Anhaltische Sprengstoff Actien Gesellschaft) (WASAG 1911a, 1911b). The WASAG patents clearly demonstrated the hollow cavity effect and the lined shaped charge effect. Also, M. Neumann (1911) and E. Neumann (1914) (who are often confused in the literature) demonstrated the hollow-cavity effect. M. Neumann (1911) shows a greater penetration into a steel plate from a cylinder of explosive with a hollow, conical cavity (247 g of Trinitrotoluol) than from a solid cylinder (310 g of Trinitrotoluol).

This clearly illustrates what is known in the United States and United Kingdom as the Munroe effect and in Germany as the Neumann effect. The depth of the crater in the target can be further increased by displacing the hollow charge some optimal distance from the target, that is, increasing the standoff distance, especially for a lined cavity charge. This situation was depicted graphically in Figure 4 of Chapter 1.

2.3. EARLY SHAPED CHARGE DEVELOPMENT

This effect was also illustrated in 1941 in Germany where a hollow cavity charge, a lined cavity charge, and a lined cavity charge detonated at a certain standoff distance above an armor plate were compared (OTIB 1941). The target plate was ship armor steel and the explosive mixture was 50% TNT and 50% cyclonite. The hollow cavity was a hemisphere with a cylindrical extension at its base equal to one-half of the diameter of the cavity (D). The liner was made of iron. The explosive contour was of the same geometry as the cavity, and the explosive thickness was 0.15 times the cavity diameter. For the (unlined) hollow charge the penetration $P = 0.4D$ at zero standoff. For the lined cavity $P = 0.7D$ at zero standoff and $P = 1.2D$ for standoffs between $0.5D$ and $1.5D$. For the iron-lined charge, D represents the inside diameter of the liner.

These formulas (OTIB 1941) are *not* accurate but are valid only for this particular experiment. They are not universal laws but do illustrate the relative increase in performance in going from unlined to lined to lined charges with a nonzero standoff distance.

Kennedy (1983) described similar studies dated from 1913 to the early 1930s, concerned with the hollow cavity effect in mining and detonation devices.

Others, notable Baum et al. (1949) and Rollings et al. (1971) attribute the hollow cavity effect to Sukharevskii (also transliterated as Sukhreski and Sucharewski) [see Murphy (1983), for example]. Indeed, Sukharevskii (1925) was the first known Soviet to investigate the shaped charge effect (in 1925–1926). He observed an increase in the explosive effect by a factor of 3–5.

The first Italian paper on the shaped charge effect was by Lodati (1932). Apparently Schardin (1954) reviewed this work and reported that Lodati did not contribute anything new to the field.

Early British development of the hollow-cavity charge was reported by Kline (1945). Eather and Griffiths (1983) provided a history of the United Kingdom contributions to the field of shaped charges that includes the achievements of Evans, Ubbelohde, Taylor, Tuck, Mott, Hill, Pack, and others. Marshall (1920) provides an early history of the unlined cavity charge and attributes its discovery to Munroe.

In the United States, the contributions of Watson (1925) on percussion fuzes and Wood (1936) on self-forging fragments (also called explosively formed penetrators, Misznay-Schardin devices, ballistic discs or *P*-charge projectiles) were significant.

The Watson percussion fuzes, patented in 1925, used a parabola-shaped booster charge with a metal lined hemispherical cavity "or arched shield" to intensify the effect of the booster charge. Watson (1925) stated that the lined cavity effect required only one-fifth to one-sixth as much explosive as an unlined booster, and the lined cavity charge would function over a "considerable air gap." This fuze is, in effect, a detonator using the shaped charge principle.

R. W. Wood (1936) of Johns Hopkins University described what is known today as an explosively formed penetrator. His paper also discussed the plastic flow of metals, deflagration, and detonation. Eichelberger (1954) credited Wood for recognizing the enhancement obtained by metal-lined hollow charges.

Also, Payman and Woodhead (1937) of the United Kingdom reported observations of jets from the cavity in the ends of detonators. They attributed this jetting process to the Munroe effect.

2.4. THE WORLD WAR II ERA

The lined cavity shaped charge research accelerated tremendously between 1935 and 1950 due primarily to World War II and the application of shaped charges to the bazooka, panzerfaust, and other devices. The history of shaped

charge development during this time frame is somewhat ambiguous in that the British, Germans, and Americans all have made significant claims to the early development of modern lined cavity charges.

The discoverers of the modern lined cavity effect were Franz Rudolf Thomanek for Germany and the Swiss, Henry Hans Mohaupt for the United Kingdom and the United States. Thomanek and Mohaupt independently perfected the hollow charge concept and developed the first effective lined cavity shaped charge penetrators.

Thomanek's early work dates from late 1935 to 1939 (Freiwald 1941; Schardin 1954; Brandmayer and Thomanek 1943; Thomanek 1978, 1959, 1942, 1960; Thomanek and von Huttern ca. 1935). The Thomanek and von Huttern patent applications (ca. 1935) pertain to hollow charges, armor-piercing shells, the shell nose design, high explosive mixtures and additives, techniques for casting high explosives, impact fuze systems, explosive initiation systems, shoulder-fired weapons, and small-caliber hand-held weapons. Unfortunately, these documents (Thomanek and von Huttern ca. 1935) are not dated by year, but the translator's note states "(Partly before 1935?)."

Thomanek (1960) claims discovery of the hollow charge lining effect on February 4, 1938. Thomanek and von Huttern (ca. 1935) describe the tests and work conducted by Thomanek and his co-worker Brandmayer.

Thomanek (1942) presents a detailed account of the hollow charge work performed by Thomanek from 1935 to 1941 in support of compensation he eventually received from the Reich. Table 1, taken from Thomanek (1942), is self-explanatory with the notes provided. The disagreement of May 1939 between Schardin and Thomanek is highlighted and taken verbatim from Thomanek (1942):

> From 1 Aug 1937 on Thomanek was employed at the Air Force Research Institute Herman Goering at Braunschweig. Before entering this employ, he submitted a collection of all his former inventions. In these von Huttern is also sometimes named as the inventor along with Thomanek. Among other things the suggestion was made to evacuate the cavity in the explosive charge doing this either by directly pumping out a finished projectile or by inserting a vacuum body into the cavities. Furthermore the general idea was presented of firing an anti tank projectile from the shoulder.
>
> Until May 1938 in Braunschweig Thomanek carried out further work on the question of hollow charges which had been done by the Air Force, especially tests with the evacuated cavity.
>
> From 1 June 1938 Thomanek worked for the Ballistic Institute of the Air Force Academy, Gatow. In accordance with informatin given by Prof. Schardin he was not permitted, according to agreement, to evaluate test results outside of the Institute or to have access to Patent records without written permission from the Director of the institute.
>
> At the instigation of Prof. Schardin and against his own previously formed opinion concerning the effect of the vacuum, Thomanek worked also on tests with inserts without a vacuum. This had been carried out in Gatow Institute

TABLE 1. Development of Hollow Charges

	Historical Survey
1883	Work by Foerster (hollow charge effect; use in projectiles).
1910	WASAG hollow charge for blasting charges of all types patented. Sheet metal liner used without knowledge of effect.
1914	Neumann, "Investigations into Hollow Charges Without Liner." (Also acute angle cone hollow charges.)
1926	Hollow charge investigations at inspection of arms and equipment.
1935–36	Development of an armor-piercing projectile by Wa A[a] with hollow charge (patent Captain Wimmer).
Late 1935	Demonstration of antitank rifle by Thomanek in presence of Hilter and Wa A.[a] No results.
1937	Resumption of test of Ordnance Research 5 (Wa Pruf 5).[a]
June 1937	Determination of favorable effect of standoff detonation with hemispherical liner (Wa F).[a]
Nov.–Dec. 1938	Proposed introduction of shells with hollow charge and aluminum liner (no increase in effect) by Wa Pruf 1.
June 1938–May 1939	Work by Thomanek (employed by Luftwaffe-Gatow); evacuated hollow charge (no improvement); recognition of liner effect by Professor Schardin; disagreement between Thomanek and Schardin.
Feb. 15, 1939	Final report by Wa Pruf 5[a] on hollow charge tests; realization of increased effect (independent of Gatow) through solid liner.
June 1939	Introduction of 7.5-cm projectile with hollow charge and aluminum liner.
Dec. 1939–Jan. 1940	Test results presented by Thomanek to Research Institute Gatow (Wa Pruf 1).[a]
May 1940	Use of hollow charge detonations (without reinforced liner) on Liege fortifications, after development by Wa Pruf 5.[a]
May 1940	Explosive Experiment Company given green light by Wa Pruf 1[a] for development.

(*continued*)

[a] Wa A is an abbreviation for Waffenamt (Army Weapons Office), which had a department designated Wa Pruf for the proof testing of weapons. Wa Pruf is an abbreviation for Waffenamt Prufwesen (Offices of Weapons Proof and Development). Wa F means Waffen Forschung (weapons research). This office researched shaped charges under the direction of Dr. Schumann. The Technische Akademie der Luftwaffe or TAL, (Technical Academy of the Air Force) was headquartered at Berlin–Gatow and headed by Dr. Schardin. It was roughly a World War II counterpart of BRL. For additional organization detail, see Simon (1947).

> since 1937 independently of Braunschweig. It was determined here that the liner without vacuum, in respect to penetration, gave the same increase of effect as the corresponding evacuated liner. Thomanek left the institute 31 May 1939.
>
> Not until Prof. Schardin brought it to light was the reason for this increase of effect found through the work carried out by Thomanek.

Simon (1947) provides further detail on the German shaped charge studies during World War II and on the organization of the German military/industrial complex.

Mohaupt independently developed and introduced the shaped charge concept to the United States. Mohaupt's early work is given by Mohaupt (1966, 1941, 1947) and Mohaupt et al. (1941). Mohaupt's (1941) patent claimed a date of November 9, 1939.

TABLE 1. Continued.

	Most Significant Results
	Casting device for hollow charges (patent applied for August 10, 1940). Acute angle cone and liner with wall thickness for armor-piercing projectiles (patent applied for September 9, 1940). Diaphragm-like liner for hollow charge (November 6, 1940). Hollow charge for rifle antitank land mine (May 29, 1941).
Sept. 7, 1940	Detonation tests by Wa F (without Thomanek) with satisfactory results with acute angle cone hollow charge (solid sheet metal liner) and standoff detonation (cast charge).
Sept. 20–30, 1940	First demonstration of antitank rifle grenade (WASAG). Hollow charge with thin liner.
Late 1940	Completion of construction of hollow charge 15 (hollow charge with heavy liner) in Gatow.
March 1941	Testing of hollow charge 15 on Maginot Line fortifications.
May 9, 1941	Delivery of 450 rifle grenades by WASAG, for use on Crete.

Steel liners (0.5–1.0 mm thick) were found to be superior to gray-iron casting (June 1940). Hollow charges with conical liners (up to 1.5 mm and with angles between 20° and 45°) and proper standoff (25–30 mm) would effect perforation of 15-mm armor plate. The charges used were cast. An increase of the diameter of the blast hole was made possible by the use of a bell-shaped hollow charge that would also permit fewer irregularities than with the acute cone. The diameter was 1 cm (of the charge).

The idea of firing a hollow charge shell from the shoulder was first conceived in 1937 (i.e., a rifle grenade).

Mohaupt, using lined cavity charges, designed practical military devices ranging from rifle grenades, to mortars, to 100-mm diameter artillery projectiles. These devices were test fired at the Swiss Army Proving Ground at Thun, at Mohaupt's laboratory, and at the French Naval Artillery Proving Ground at Gavre. These results were also demonstrated to the United Kingdom which then began development programs of its own. Following the early results of World War II, the French government authorized the release of Mohaupt's information to the United States, and in late 1940 tests were conducted at APG, Maryland, using several aspects of lined cavity shaped charges (Mohaupt 1966). The United States accepted the program, classified it, and thus excluded Mohaupt from the effort but produced the 2.36-in. HEAT machine gun grenade and the 75-mm and 105-mm HEAT artillery projectiles in 1941. Later the machine gun grenade was modified to include a rocket motor and a shoulder launcher and became the bazooka. The bazooka was first used by the United Kingdom in North Africa in 1941. Other HEAT rounds were fired from tank-mounted howitzers (Mohaupt 1966; Kennedy 1983).

Incidentally, Leslie Skinner, formerly of APG, has been called the "Father of the Bazooka" (Weston 1985). The bazooka derived its name from a homemade trombone popularized by radio comedian Bob Burns (Weston 1985).

Kennedy (1983) provides additional detail on bazookas as well as on the work of Thomanek and Mohaupt.

The German development of shaped charge warheads during World War II is discussed by Kennedy (1985, 1983), Simon (1947), Cave et al. (1945),

Birkhoff (1947), Schumann (ca. 1945), OTIB (1941), Schardin (1954), Kline (1945), Thomanek (1978, 1942, 1960), and Thomanek and von Huttern (ca. 1935). Simon (1947) and Cave et al. (1945) entered Germany near the end of World War II to study and recover German technology. Simon (1947) reported on flash X-ray photographs in Germany, including collapse studies of conical and hemispherical liners. Various other liner geometries were studied, including helmet-shaped liners, bottle-shaped liners, and ellipsoidal liners. The effect of varying the cone angle, the wall thickness, and the standoff distance was studied for various shaped charges. Also, the effect of tapering the liner with respect to thickness was studied. The Germans concluded that 60/40 cyclotol (a RDX–TNT mixture) was the optimum explosive fill for shaped charges, and aluminized explosives provided no additional advantage. According to Simon (1947), the liner materials studied were steel, sintered iron, copper, aluminum, and zinc. It was realized that copper was the best liner material, but due to the shortage of copper in Germany, zinc liners were used instead.

Schumann (1941) reports on studies relating to standoff distance effects, explosive lenses, waveshaping, and hemispherical liners. Schumann concluded that the hemisphere was an effective shaped charge liner geometry (actually a hemisphere with a cylindrical extension on its equator).

Wagner (1944) discussed the SHL (*S*chwere *H*ohl*l*adung or heavy shaped charge). The SHL 500 was a 65-cm diameter shaped charge used against light ships. The SHL 1000 was apparently an improvement to the SHL 500. The largest SHL of this series was called the Beethoven and had a diameter of 180 cm with 5000 kg of high explosive. The Beethoven was designed for use against ships and ground fortifications. During the Normandy invasion, the Beethoven destroyed two battleships and four large transport ships. The Beethoven was the forerunner of the MISTEL I and MISTEL II, discussed under shaped charge applications.

Wagner (1944) also discussed the development and production of other armor-piercing, shaped charge projectiles.

The Germans were also instrumental in transferring hollow charge research to the Japanese. There is no evidence of hollow charge research in Japan before May, 1942. At that time, two German officers of the Army Weapons Office, Colonel Paul Niemueller and Major Walter Merkel, provided Japan with data and samples of the German 30- and 40-mm hollow charge rifle grenade. The Japanese officials involved were Lt. Col. Yoshitaka, the Japanese liaison officer for the Germans and Col. A. Kobayashi, an explosives expert at the Second Army Arsenal in Tokyo (OTIR ca. 1946). Other notable Japanese researchers were Futagami, Naruse, Nasu, Nagaoka, Nakiyama, and Lt. Gen. Kan. The hollow charges were presented as a highly secret and valuable project, and the Germans and Japanese continued to exchange shaped charge data until the cessation of hostilities in 1945.

The Japanese instigated a research and development program of their own, and additional shaped charge designs were received from Germany. These

designs included the panzerfaust and a large German hollow charge called the "MISTERIE?" (This is undoubtedly the MISTEL, which evolved from the Beethoven charge, discussed earlier). From the MISTEL, the Japanese developed the large SAKURA Bombs I and II for kamikaze plane attacks against warships, discussed in Chapter 3.

In addition to the captured U.S. and U.K. ammunition, and the information received from Germany, the Japanese did considerable independent research on shaped charges (OTIR ca. 1946). This research included gas flow and gas velocity from an unlined hollow charge; the jet velocity from a lined hollow charge; penetration versus standoff distance studies; hollow charge liner geometries varying from conical to hemispherical caps; various liner materials including mild steel, copper, aluminum, zinc, asbestos, molded bakelite, tin, and paper; recovery of jet particles in sand; and dynamic (missile) effects. The Japanese preferred laminated liners (three to seven sheets) over a single, homogeneous liner of the same thickness. The Japanese also concluded that a hole in the apex of a conical or hemispherical liner was desirable. Also, the size of this hole was critical, an optimal value for the apex hole diameter being $\frac{1}{10}$ of the warhead charge diameter. (The wall thickness was taken as $\frac{1}{25}$ of the charge diameter and the liner diameter was taken to be $\frac{4}{5}$ of the charge diameter for both conical and hemispherical liners.) The optimal cone apex angle was determined to be between 35° and 50°. Other tests used 99-mm diameter, soft steel hemispherical liners with a 2.5-mm wall thickness. The optimal open apex diameter was concluded to be $\frac{3}{16}$ of the charge diameter for this warhead.

Tapered liners were designed based on the 30–40-mm German rifle grenade. They used 19° conical steel liners tapered from 0.5 mm at the apex to 1.0 mm at the base (OTIR ca. 1946). Other projectiles used constant wall thickness, laminated liners. The Japanese also developed torpedos, 18 and 21 in. in diameter using a tapered wall, 45° conical steel shaped charge liner with an open apex (OTIR ca. 1946).

Other studies related to detonation physics and methods of focusing the gas flow, calculation of the target hole volume and penetration, penetration of concrete targets, and the recovery of jet particles by reducing the explosive power (mixing dynamite with starch to reduce the "strength" of the dynamite), and capturing the jet in sand (OTIR ca. 1946).

The explosive charges used in research were spherical and formed from the arcs of two circles. Thus, the cross section of the charge looked like a new moon, quarter moon, and so on, depending on the two radii used. Cylindrical, tapered, and boattailed explosive geometries were also studied as well as the effect of the high explosive head height and the length-to-diameter ratio of the charge. In fact, the height of the charge was varied from one-half of a charge diameter to six charge diameters. A charge height of 1.5–2 charge diameters was concluded to be optimal for a 80-mm diameter charge with a 64-mm diameter soft iron, hemispherical liner and with a 2.5-mm thick wall (OTIR ca. 1946).

Futagami (OTIR ca. 1946) tested two-dimensional charges, that is, a flat, disk-shaped charge confined between two lead plates. Tests of this nature were used to evaluate various liner geometries, cone apex angles, liner wall thickness effects, and the effect of the diameter of the open apex region. All of these effects, including standoff distance studies, were also investigated with "three-dimensional" shaped charges. Futagami also studied bimetallic liners of soft iron and copper (the iron was in contact with the high explosive). As mentioned earlier, various liner materials were studied, including paper [of course, as stated in (OTIR ca. 1946), "the paper shell is tore in pieces and flys away"]. The Japanese also noted that any cavity existing between the liner and the explosive reduces the penetrating capability of the warhead.

The Japanese antitank shells, although not as effective as those developed by the Germans or the Allies, were used effectively on the Burma front. Other Japanese innovations (Kennedy 1983) included the suicidal "Lunge" mine, which was in fact a shaped charge with a wooden handle used as an antitank weapon.

Some of the research conducted in the United Kingdom in the early 1940s is reported by Monro (1943). Monro describes the research of Evans, Ubbelohde, Lennard-Jones, Devonshire, and Andrew. The British studied cadmium liners (which probably produce molten jets) and steel liners (where the jet is probably not liquid). Other topics, as pursued by the Germans, Japanese, and Americans were also investigated. Monro reports on U.S. weapons tests and on the evaluation of captured German shaped charges with aluminum, hemispherical liners and on Italian shaped charges using mild steel, parabolic liners. Tuck's (1943) work was also significant in the early 1940s.

The research and development in the United States in the 1940s is documented by Kennedy (1983), Birkhoff (1947), Cook (1958), and DM-1 (1947). DM-1 (1947) is an interesting history of weapons and demolition devices developed during World War II. Several topics are covered ranging from pocket knives to flamethrowers to Bangalore torpedos to shaped charges. A Bangalore torpedo is a long light-steel tube loaded with explosives. It is, essentially, a pipe bomb. This device was invented during World War II by Major R. L. McClintock of the Queen Victoria's own Madras Sappers and Miners near Bangalore in Mysore, India (DM-1 1947). The Bangalore torpedo was used to remove barbed wire entanglements, clear mine fields, and inserted into holes in fortifications made by shaped charge devices.

2.5. THE POST WORLD WAR II ERA

Shaped charge development, based on the early work of Mohaupt, was continued in the United States by the Du Pont Company, the Hunter Manufacturing Company, Croydon, Pennsylvania (for an M2 shaped charge), the Doblins Manufacturing Company, the Hercules Powder Company, the Atlas Powder Company, and the Corning Glass Company (for glass conical

liners). This work was directed by the Board on Engineer Equipment or Engineer Board (EB). Research was conducted by Du Pont and the Eastern Laboratory at Gibbstown, New Jersey. Demolition charges such as the M1, M2A3, M3, M3A, and others, were tested at APG in 1942 and developed by the corporations already cited. A chronology of demolition shaped charge development from 1942 to 1946 is given in DM-1 (1947). Also, specifications for the M2A3 and the M3 shaped charge are given in DM-1 (1947). The M3 weighs 40 lb, 30 of which are high explosive, and contains a welded steel cone that penetrates 60 in. of concrete. The M3 charge is 12.5 in. high and 9 in. in diameter. The M2A3 contains a glass, conical shaped charge liner; it weighs 15 lb with 11.5 lb of explosive and can penetrate 30 in. of concrete. The M2A3 has approximately the same penetrating power as the M1 (DM-1 1947); further details are given in Chapter 3 where demolition charges are discussed.

In addition to the fundamental studies performed in 1941 at the Eastern Laboratory, E. I. du Pont de Nemours and Company (Du Pont), parallel studies were undertaken by the Eastern Laboratory and Division 8, National Defense Research Committee, Bruceton, Pennsylvania. The sponsor was the Office of Scientific Research and Development. The chief scientists at the National Defense Research Committee were G. B. Kistiakowsky, D. P. MacDougall, S. J. Jacobs, and G. H. Messerly (Cook 1958).

At the same time, E. M. Pugh organized a group at the Carnegie Institute of Technology (C.I.T.). Following the war, the Carnegie Institute took over the National Defense Research Committee facilities at Bruceton. The Carnegie group employed some outstanding researchers who contributed much of the current shaped charge knowledge. The leaders at Carnegie were Heine-Geldern, N. Rostoker, Emerson Pugh, and his student Robert Eichelberger. Eichelberger is the former director of BRL.

In addition to the work at C.I.T., important postwar contributions to shaped charge research were made by L. Zernow and associates at BRL. Other laboratories making important contributions during this time period were the Naval Ordnance Laboratory, Maryland (Solem and August), the Naval Ordnance Test Station, California (Throner, Weinland, Kennedy, Pearson, and Rinehart), Picatinny Arsenal, New Jersey (Dunkle), the Stanford Research Institute, California (Poulter), and others. Additional developments in shaped charge technology, especially on the West Coast, are presented by Kennedy (1983).

Excellent bibliographical and historical information is provided by Birkhoff (1947), Parker (1950), and NRDC (1945). The following list of abbreviations from Parker (1950) serves as a library guide for the types of reports, the participating agencies, and the general terminology used during this time period. Ayton et al. (1955) is somewhat more recent. This bibliography contains references, with informative abstracts, to all pertinent literature found in books, periodicals, and reports on the subject of shaped charges, particularly their military applications. The time frame covered is basically 1930–1954, although some earlier background material has been covered.

KEY TO AGENCIES AND LIST OF ABBREVIATIONS, 1950

Issuing Agencies

- Aberdeen Proving Ground Reports
- British Reports
  - Advisory Council
  - Armament Research
  - Department of Tank Design
  - Halstead Exploiting Center
  - Intelligence Objective Sub Committee
  - Roads Research Laboratory
  - Ordnance Board Proceedings
  - Miscellaneous Agencies
- Carnegie Institute of Technology Reports
- du Pont de Nemours and Company Reports
- Frankford Arsenal Reports
- Military Attaché Reports
- National Defense Research Committee Reports
- Navy Department Reports
- Office Scientific Research & Development Reports
- Ordnance Technical Intelligence Bulletins
- Picatinny Arsenal Reports
- Miscellaneous Agencies Reports (American)
- Miscellaneous Agencies Reports (Foreign)

KEY TO ABBREVIATIONS

AAEE	Aircraft Armament Experimental Establishment
AAF	Army Air Force
AC	Advisory Council
AEC	Aerojet Engineering Corporation
APG	Aberdeen Proving Ground
ARD	Armament Research Department
ARE	Armament Research Establishment
BIOS	British Intelligence Objective Sub Committee
BM	Bureau of Mines
BMR	British Miscellaneous Report
BOB	British Ordnance Board Proceedings
BRL	Ballistic Research Laboratory
BRLM	Ballistic Research Laboratory Memorandum

BUORD	Bureau of Ordnance
CARTI	Carnegie Institute of Technology or (C.I.T.)
DMWD	Director of Miscellaneous Weapons Department
DTD	Department of Tank Design
EB	Engineer Board
EMPL	Explosives Manufacturing Practices Laboratory
ET	European Theater
FA	Frankford Arsenal
FVDD	Fighting Vehicle Design Department
GHq	General Headquarters
HEC	Halstead Exploiting Center
IR	Intelligence Report
JCSC	Joint Committee on Shaped Charges
MA	Military Attaché
MAL	Military Attaché London
MOS	Ministry of Supply
NA	Naval Attaché
NAVORD	Navy—Bureau of Ordnance
NBS	National Bureau of Standards
NDRC	National Defense Research Committee
NMSM	New Mexico School of Mines
NOL	Naval Ordnance Laboratory
NOTS	Naval Ordnance Test Station
NPF	Naval Powder Factory
NRC	National Research Council
NRCC	National Research Council of Canada
NTME	Naval Technical Mission in Europe
OCO	Office Chief of Ordnance
OP	Ordnance Program
OSRD	Office Scientific Research & Development
OTIB	Ordnance Technical Intelligence Bulletin
PA	Picatinny Arsenal
PL	Photographic Laboratory
RRL	Roads Research Laboratory
SIMR	Safety in Mines Research
WAL	Watertown Arsenal
WO	War Office

The shaped charge principle was clarified and understood as a result of the pioneering flash X-ray photographs taken in the United States by Seely and Clark (1943), Clark and Rodas (1945) and in Britain by Tuck (1943). Schumann and Schardin obtained similar flash radiographs in Germany in 1941 (Birkhoff 1947; Schumann ca. 1945; Schardin and Thomer 1941). Birkhoff (1947) and Schumann (ca. 1945) discuss the "angry priority controversy" over the first flash radiograph. X-ray photographs (or flash radiographs) are neces-

sary since ordinary photographs are uninformative due to the smoke and flame associated with the detonation.

Schardin and Thomer (1941) published excellent flash radiographs of collapsing shaped charges with hemispherical liners. These X-ray photographs clearly depict the collapse of the hemispherical liner (as it "turns inside out from the pole") and illustrates the "pinch-off effect" as the equatorial region of the liner collapses on the jet. The liner was truncated from the equator to remove this pinch-off. These phenomenon were rediscovered some 30 years later.

The Roentgenblitz or flash X-ray is made possible by the very brief discharge of a high-voltage X-ray tube. The basic apparatus was developed by Slack of Westinghouse Electric Company (Simon 1947).

Also, Linschitz and Paul (1943) experimentally studied conical lined shaped charges in different stages of collapse. Hand-tamped nitroguanidine of various densities was used as the explosive fill to achieve a partial collapse of the liner. The conical liner was recovered in water after a partial deformation, the

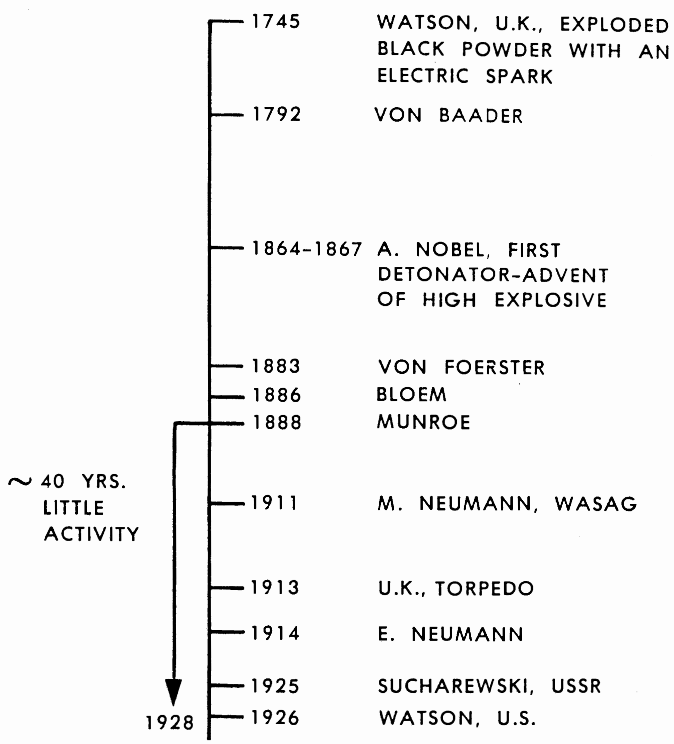

Figure 1. The time line 1745–1928.

degree of liner deformation (or collapse) corresponding to the density of the explosive fill. The results showed excellent agreement with the flash X-ray photographs.

Based on the analysis of the flash X-ray data and the partial collapse studies (Linschitz and Paul 1943), analytical models of the collapse of a lined conical shaped charge were developed and verified by Birkhoff (1943, 1947), Birkhoff et al. (1948), Evans (1950), Tuck (1943), and Pugh et al. (1952).

A bibliography and account of the weaponization of the shaped charge and similar principles are given by Backofen (1978, 1980a, 1980b, 1980c) and Backofen and Williams (1981a, 1981b, 1981c). Backofen's bibliography is extensive, especially regarding foreign sources. Earlier, World War II time frame results and bibliographical information are given by DM-1 (1947), Parker (1950), NRDC (1945), Ayton et al. (1955), Hill et al. (1944), and NDRD (1946). The time line charts in Figures 1–3 highlight the major events in shaped charge advancement.

Shaped charge theory continued to develop during the 1950s, boosted by the Korean War (Cook 1958; Kennedy 1983; Thomanek 1959, 1960; Kolsky et al. 1949; Kolsky 1949; Evans and Ubbelohde 1950a, 1950b; Pugh et al.

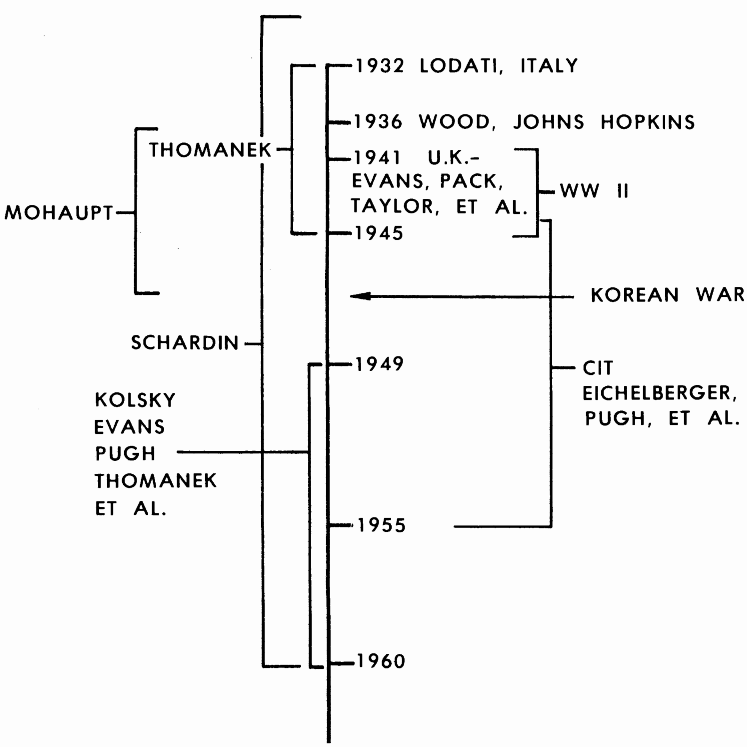

Figure 2. The time line 1932–1960.

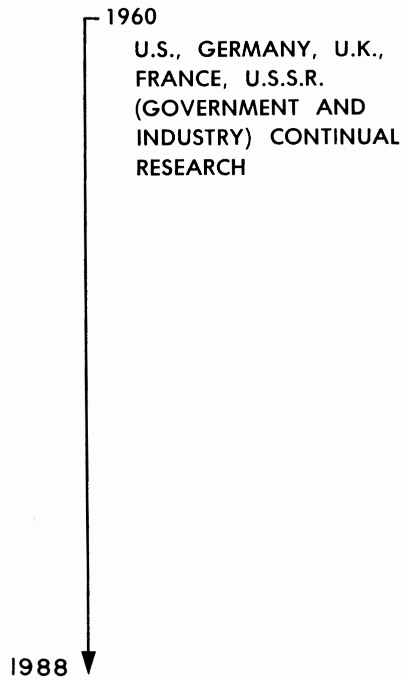

Figure 3. The time line 1960–to date.

1951; and Koski et al. 1952). During this time period, tremendous progress was made toward the understanding of the phenomena associated with shaped charge jets. Improved flash X-ray techniques were employed to observe the jet process and analytical models were improved. Efforts were made to improve existing shaped charge liners, to use detonation waveshapers, to provide spin compensation via fluted liners, to provide shaped charge follow-through mechanisms, and to enhance the overall system performance. Birkhoff (1947) discussed many of the problems still being studied today, and these concepts will be addressed in later chapters.

Starting in the 1950s–1960s, significant shaped charge developments were made possible by the perfection of experimental techniques such as high-speed photography and flash radiography. Other improvements resulted from the transition from TNT to more energetic explosives, that is, from TNT to Comp B to Octol and then to pressed explosives, notably LX-14. Also, alternate modes of initiation (other than point initiation) and waveshaping techniques have provided warhead design improvements. Other advances stemmed from the development of large computer codes to simulate the collapse, formation, and growth of the jet from a shaped charge liner. Numerical techniques and the advantages and limitations of various computer codes for wave propagation and penetration studies are discussed in detail in later chapters. These codes provide, for the most part, excellent descriptions of the formation of the jet.

Currently, shaped charge research continues in order to devise a successful countermeasure to the advanced armors currently fielded and/or contemplated; see for example, Kennedy (1985). Studies that originated in the 1950s still continue; notably, torpedo applications of shaped charge rounds, anti-aircraft rounds, fragmentation rounds, multistaged or tandem warheads, long standoff rounds, nonconical liners, and noncopper liners. Also, metallurgical and chemical aspects of the liner material as well as methods of liner fabrication remain important.

REFERENCES

Ayton, M. W., Gibson, J. R., Gurtowski, C. G., and Bledsoe, B. (1955), "Shaped Charges, an Annotated Bibliography," The Library of Congress, Technical Information Division, Washington, D.C., May.

Backofen, J. E. (1978), "The Weaponization of Shaped Charge Technology," *Proc. 4th Inter. Symposium on Ballistics*, October 17–19.

Backofen, J. E. (1980a), "Shaped Charges versus Armor," *Armor* (July–August).

Backofen, J. E. (1980b), "Shaped Charges versus Armor—Part II," *Armor* (September–October).

Backofen, J. E. (1980c), "Shaped Charges versus Armor—Part III," *Armor (November–December)*.

Backofen, J. E., and Williams, L. W. (1981a), "Antitank Mines," *Armor* (July–August).

Backofen, J. E., and Williams, L. W. (1981b), "Antitank Mines—Part II," *Armor* (September–October).

Backofen, J. E., and Williams, L. W. (1981c), "Antitank Mines—Part III," *Armor* (November–December).

Baum, F. A., Stanykovich, R. P., and Skekter, B. I. (1949), *Physics of an Explosion*, New York, Research Information Service (AD 400151), 546.

Birkhoff, G. (1943), "Mathematical Jet Theory of Lined Hollow Charges," Ballistics Research Laboratory Report No. 370, June 18.

Birkhoff, G. (1947), "Hollow Charge Anti-Tank (HEAT) Projectiles," Ballistic Research Laboratory Report No. 623, February 10.

Birkhoff, G., MacDougall, D., Pugh, E., and Taylor, G. (1948), "Explosive with Lined Cavities," *J. Appl. Phys.*, *19*(6).

Bloem, G. (1886), "Shell for Detonating Caps," Dusseldorf, Prussia, Germany, U.S. Patent 342,423, dated May 25.

Brandmayer, C., and Thomanek, F. R. (1943), "High Explosive Charge," Hungarian Patent 134,378 assigned December 9, Berlin.

Cave, J. W., Bergman, J. L., and Haley, A. (1945), "Report of Investigation of the Proving Ground at Hillersleben, Germany," 6 June, APG Misc. 063.

Clark, G. B. (1948), "Secrets of the Shaped Charge," *Ordnance*, *33*(169): 49–51.

Clark, J. C., and Rodas, W. M. (1945), "High Speed Radiographic Studies of Controlled Fragmentation," Ballistic Research Laboratory Report No. 585, November 13.

Cook, M. A. (1958), *The Science of High Explosives*, American Chemical Society Monograph Series, New York: Reinhold Publishing.

DM-1 (1947), "History of the Development of Demolitions and Obstacles, I. Demolition Explosives and Equipment," DM-1, War Department Corps of Engineers, September 9 (AD-B959585).

E. I. du Pont de Nemours and Co. (1980), *The Blaster's Handbook*, 16th ed., Wilmington, DE.

Eather, R., and Griffiths, N. (1983), "A U.K. Note on the History of Shaped Charges," Royal Armament Research and Development Establishment Report, August 1983, presented at MBB Schrobenhausen, West Germany, September.

Eichelberger, R. J. (1954), "Re-Examination of the Theories of Jet Formation and Target Penetration by Lined Cavity Charges," Ph.D. Dissertation, Carnegie Institute of Technology, Pittsburgh.

Evans, W. M. (1950), "The Hollow Charge Effect," *Bull. Inst. Min. Metall.*, No. 520, March.

Evans, W. M., and Ubbelohde, A. R. (1950a), "Formation of Munroe Jets and Their Action on Massive Targets," *Res. Sup.* (London), 3–7.

Evans, W. M., and Ubbelohde, A. R. (1950b), "Some Kinematic Properties of Munroe Jets," *Res. Supp.* (London), 3–8, May.

Freiwald, H. (1941), "The History of Hollow Charge Effect of High Explosive Charges," forward by Hubert Schardin, for German Academy of Aviation Research, Berlin, September 15.

Hill, R., Mott, N., and Pack, D. (1944), *A.R.D. Theoretical Research Report*, No. 2/44 (January 1944) and 13/44 (March 1944).

Kennedy, D. R. (1983), "The History of the Shaped Charge Effect, The First 100 Years," presented at MBB Schrobenhausen, West Germany, September.

Kennedy, D. R. (1985), "The Infantryman VS the MBT," *National Defense*, ADPA, pp. 27–34, March.

Kline, H. W. (1945), "The Cavity Charge, Its Theory and Applications to the Opening of Explosive Filled Ordnance, etc.," U.S.N.R., Ordnance Investigation Laboratory, Naval Powder Factory, Indian Head, Maryland, August 15.

Koski, W. S., Lucy, F. A., Shreffler, R. G., and Willig, F. J. (1952), "Fast Jets from Collapsing Cylinders," *J. Appl. Phys.*, *23*(12): 1300–1305.

Kolsky, H. (1949), "A Study of the Mechanism of Munroe Charges, Part II—Charges with Hemispherical Liners," *Res. Supp.* (London), 2-2: 96–98.

Kolsky, H., Snow, C. I., and Shearman, A. C. (1949), "A Study of the Mechanisms of Munroe Charges, Part I—Charges with Conical Liners," *Res. Supp.* (London), 2-2: 89–95.

Lenz, R. R. (1965), *Explosives and Bomb Disposal Guide*, Springfield, Il: Charles C. Thomas.

Linschitz, H., and Paul, M. A. (1943), "Experimental Studies of Cone Collapse and Jet Formation. Part I: Recovery of Cones from Low-powered Charges," Division 8, National Defense Research Committee of the Office of Scientific Research and Development, Report OSRD No. 2070, November 29.

Lodati, C. (1932), "An Explanation of the Explosive Behavior of Hollow Blocks of Compressed TNT," *Giornale de Chim. Ind. Ed. Appl.*, *14*:130.

Marshall, A. (1920), "The Detonation of Hollow Charges," *J. Soc. Chem. Ind.*, *39*(3): 35T.

Mohaupt, H. H. (1941), "Projectile," U.S. Patent No. 2,419,414 assigned April 22, 1947, originally filed October 3, 1941.

Mohaupt, H. H. (1947), "Projectile," U.S. Patent No. 2,974,595 assigned to Henry H. Mohaupt, 1961, filed September 11, 1947.

Mohaupt, H. (1966), *Aerospace Ordnance Handbook*, F. Pollard and J. Arnold (eds.), "Shaped Charges and Warheads," Engelwood Cliffs, NJ: Prentice-Hall.

Mohaupt, B., Mohaupt H., and Kauders, E. (1941), "An Improved Explosive Projectile," Patent, Commonwealth of Australia, assigned to Berthold Mohaupt, Henry Mohaupt, and Erick Kauders of France, August (date claimed for patent November 9, 1939).

Monro, E. A. (1943), "Shaped Charges: A Review Covering the Period August 26th, 1942 to February 28th, 1943," Advisory Council on Scientific Research and Technical Development, Shaped Charges Sub-Committee, A.C. 3827, SC 19, April 14.

Munroe, C. E. (1888a), "On Certain Phenomena Produced by the Detonation of Gun Cotton," *Newport Natural History Society*, Proceedings 1883–1888, Report No. 6.

Munroe, C. E. (1888b), "Wave-Like Effects Produced by the Detonation of Gun Cotton," *Am. J. Sci.*, *36*:48–50.

Munroe, C. E. (1888c), "Modern Explosives," *Scribner's Magazine*, Vol. III (January–June), pp. 563–576.

Munroe, C. E. (1894), Executive Document No. 20, 53rd Congress, 1st Session, Washington, D.C.

Munroe, C. E. (1900), "The Applications of Explosives," *Popular Science Monthly*, in 2 parts pp. 300–455, Vol. 56.

Murphy, M. J. (1983), "Shaped Charge Penetration in Concrete: A Unified Approach," Ph.D. Dissertation, University of California—Davis, January 1983, also Lawrence Livermore National Laboratory Report UCRL-53393.

NRDC (1945), "Annotated Bibliography of NDRC Technical Reports and Memorandums of Division 2, including pertinent division 8 Reports," May 1, NRDC (National Defense Research Council) Memorandum No. A-106M, OSRD Report No. 4830B.

NDRC (1946), "Protection against Shaped Charges," Carnegie Institute of Technology, NDRC Report No. A-384 and OSRD Report No. 6384, February.

Neumann, E. (1914), "New Hollow Bodies of High Explosive Substances," *Zeitschrift fur das Gesamte Schiess -und Sprengstoffwesen*, Darmstadt, Germany, pp. 183–187, May 15.

Neumann, M. (1911), "Einiges uber brisante Sprengstoffe, *Zeitschrift fur Angewandte Chemie*, Wittenburg, Germany, pp. 2233–2240, November 24.

OTIB (1941), "Results of Blasting Tests for Hollow Charges with and without Liners," performed in the Ballistic Institute of the Academy for Aerial Warfare, Germany, Ordnance Technical Intelligence Bulletin, 1476.

OTIR (ca. 1946), "Ordnance Technical Intelligence Report Number 11," Office of the Chief Ordnance Officer GHQ, AFPAC, Tokyo, Japan (AD 94384).

Parker, D. K. (1950), "Hollow Charges: A Bibliography," Technical Information Section, Development and Proof Services, APG, MD, APG Misc. 120, June.

Payman, W., and Woodhead, D. W. (1937), "Explosion Waves and Shock Waves, V—The Shock Wave and Explosion Products from Detonating High Explosives," *Proc. Royal Soc. 163A:*

Pugh, E., Eichelberger R., and Rostoker, N. (1952), "Theory of Jet Formation by Charges with Lined Conical Cavities," *J. Appl. Phys.*, *23*(5).

Pugh, E. M., Heine-Geldern, R. V., Foner, S., and Mutschler, E. C. (1951), "Kerr Cell Photography of High Speed Phenomena," *J. Appl. Phys.*, *22*(4): 487–493.

Rollings, R. R., Clark, G. B., and Kalia, H. N. (1971), "Penetration in Granite by Shaped Charge Liners of Various Metals," University of Missouri, Rolla, Report RMERC-TR-70-13, April.

Seely, L. B., and Clark, J. C. (1943), "High Speed Radiographic Studies of Controlled Fragmentation," Ballistic Research Report No. 368, June 16.

Schardin, H. (1954), "Development of the Shaped Charge," *Wehrtechnische Hefte*, Heft 4.

Schardin, H., and Thomer, G. (1941), "Untersuchung des Hohlkorperproblems mit Hilfe der Roentgenblitz-Methode" ("Investigation of the Hollow Charge Problems with Help of the Flash x-ray Method"), Ballistisches Institut der Luftkriegsakademie Gatow, Pruf No. 9, 20 November (Ordnance Technical Intelligence Bulletin 1628).

Schumann, E. (1941), "Wirkungssteigerung Beim Hohlsprengkorper" ("Improvement of the Effect of Hollow Charges"), Ordnance Technical Intelligence Bulletin, OTIB 1249-17, February 26.

Schumann, E. (ca. 1945), "The Scientific Basis of the Hollow Charge Effect," Publication BIOS/Gp. 2/HEC 5919, Halstead Exploiting Center, England.

Simon, L. E. (1947), *German Research in World War II*, New York: Wiley.

Sukharevskii (1925), *Technica i Snabschenie Krasnoi Armii*, No. 170: 13–18, 1925; also *Woina i Technica*, 253: 18–24, 1926.

Thomanek, F. R. (1942), OTIB 1468, "Substantiating Material in Support of Evaluation of Compensation in Favor of Explosive-Experimental Company and Diploma-Engineer, F. R. Thomanek," Ordnance Technical Intelligence Bulletin No. 411.

Thomanek, F. R. (1959), "Die Erste Hohlladungswaffe—The First Hollow Charge Weapon," *Explosivstoffe*, No. 1: 9–11.

Thomanek, F. R. (1960), "The Development of the Lined Hollow Charge," Feltman Research Laboratories, Picatinny Arsenal, Dover, NJ, Technical Notes No. FRL-TN-27, March 1961, a translation from *Explosivstoffe*, *8*(8).

Thomanek, F. R. (1978), "Meine Hohlladungs—Aktivitaten," for Periods 1932–1935, 1938–1945, 1957–1969, and from 1975 to date, March 10.

Thomanek, F. R. and von Huttern, H. (ca. 1935), OTIB (not dated but contains statement "Partly before 1935?"), "Patent Applications by Franz Rudolf Thomanek and Hellmuth von Huttern," Ordnance Technical Intelligence Bulletin 1249-19.

Tuck, J. L. (1943), "Note on the Theory of the Munroe Effect," U.K. Report, A.C. 3596 (Phys. Ex. 393-WA-638-24), February 27.

von Baader, F. (1792), *Bergmannische Journal von Kohler and Hoffman*.

von Foerster, M. (1883), *Versuche mit Komprimirter Schiessbaumwolle*, Berlin: Mittler and Son.

von Foerster, M. (1884), "Experiments with Compressed Gun Cotton," *Van Nostrand's Engineering Magazine*, Vol. 31, (July–December), pp. 113–119.

WASAG (1911a), "Verfahren zur Herstellung von Sprengkorpern," Westfalisch-Anhaltische Sprengstoffe A. G. (WASAG), German patent DRP—Anmelding W 36269, December 14, 1910 in *Zeitschrift fur das Gesamte Schiess und Sprengstoffwesen*, *6*: 358.

WASAG (1911b), "Improvement in Explosive Charges or Bodies," Patent No. 28,030 (UK) to Westfalisch-Anhaltische Sprengstoffe Actien Gesellschaft (WASAG), Berlin, December 13.

Wagner (1944), Memorandum for H. D. L. Saur by Wagner and other papers, Ordnance Technical Intelligence Bulletin, OTIB 1249, Misc-2, "Documents Connected with the Development of Hollow Charge Ammunition," November.

Watson, C. P. (1925) for "Percussion Fuzes," 1925 U.S. Patents 1,524,011 and 1,534,012, filed September 22, 1921 and August 27, 1923, both issued on April 14, 1925.

Weston, L. (1985), "APG's Contribution to World War II Was Highly Significant," *APG News*, 5B, May 22.

Wisser, J. P. (1886), *Compressed Gun Cotton for Military Use*, translated from the German of Max von Foerster with an Introduction on Modern Gun Cotton Its Manufacture, Properties and Analysis, New York: Van Nostrand.

Wood, R. W. (1936), "Optical and Physical Effects of High Explosives," *Proc. Royal Soc. (London)*, *157A:* 249–261.

CHAPTER 3

APPLICATIONS

3.1. MILITARY APPLICATIONS

Shaped charges are extremely useful when an intense, localized force is required for the purpose of piercing a barrier. The main application is in the military arena, including torpedos, missiles, high explosive antitank (HEAT) rounds including hand-held (bazooka-type) rounds, gun-launched rounds (e.g., rifle grenades), cannon-launched rounds, and various bombs. The targets are armors, bunkers, concrete or geological fortifications, and vehicles. Attacks against aircraft and spacecraft are possible. Underwater applications (torpedos) are possible with the design such that water does not enter the hollow charge area. In fact, most warheads of the type described contain an ogive to cover the liner. This ogive acts as an aerodynamic (or hydrodynamic) shield while the projectile is in flight; it can provide a housing for impact fuzes or guidance, stability, and control electronics; and it provides a built-in standoff designed to aid performance. Recall that the standoff is the distance from the base of the charge (or liner) to the target in question. Figures 1 and 2 show an old HEAT artillery projectile.

3.2. SPECIALIZED APPLICATIONS

The largest known shaped charge was a modification of the Beethoven or SHL (Schwere Hohlladung or heavy shaped charge) called the MISTEL. The SHL charges and the Beethoven were discussed in Chapter 2. The MISTEL (mistletoe) concept used a fighter aircraft mounted piggyback on the top of a large bomber aircraft. The unmanned bomber carried the MISTEL warhead in its

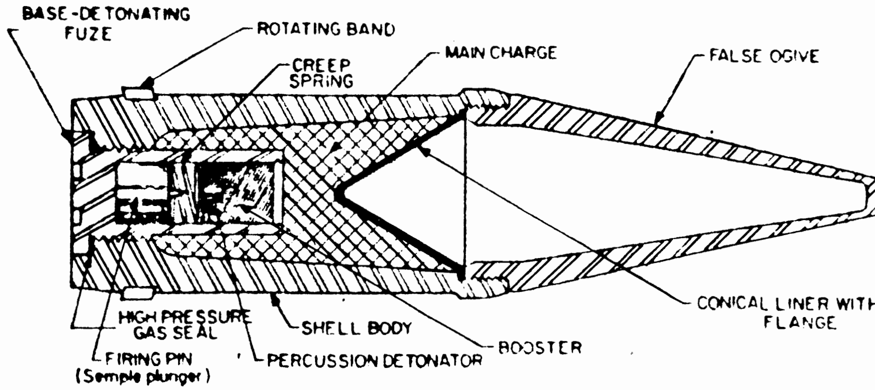

Figure 1. High explosive antitank artillery projectile, HEAT (Mohaupt 1966).

nose. The warhead consisted of a 2 m diameter, wide-angle, conical shaped charge. It is speculated that the liner had a 120° apex angle, was about 30 mm thick, and made of either mild steel or aluminum. The warhead weighed 3500 kg with an explosive weight of 1720 kg (Kennedy 1983; Coles and Rickson 1977). The fighter pilot flew the combination to the target, aimed it, released it, then returned to his base. The Germans developed this device near the end of World War II, and most were captured intact.

However, as mentioned earlier, the MISTEL technology was made available to the Japanese. The Japanese developed the SAKURA bomb, which was 1.6 m in diameter. The design and characteristics are given in Figure 3.

A shaped charge with an aluminum liner was used in an attempt to place certain identifiable man-made materials into orbit. According to Kennedy (1983), a 35° included angle aluminum shaped charge was installed on a multistage rocket assembly. The craft was fired into near space, and the warhead was detonated in an attempt to project hypervelocity fragments into Earth orbit. These tests were conducted at Holloman Air Force Base in 1955–1956. It was never established whether or not any aluminum particles were detected.

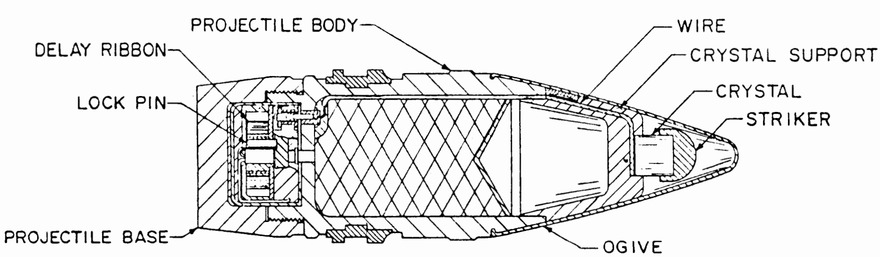

Figure 2. HEAT (High explosive antitank) projectile.

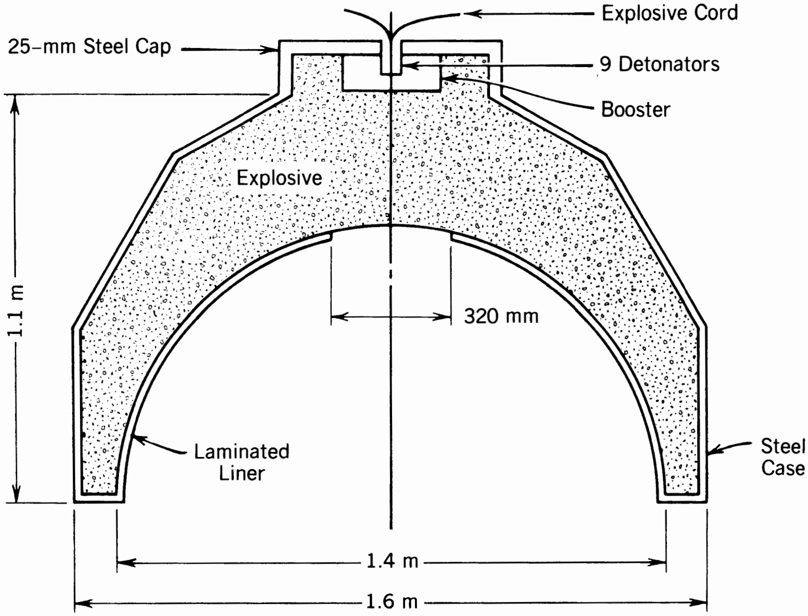

	Type I	Type II
Diameter of bomb	1.6 m	1.12 m
Length of bomb	1.1 m	1.0 m
Diameter of hemispherical liner	1.4 m	1.0 m
Size of hole at top of liner	260 mm 320 mm	200 mm
Liner, laminated steel plates	4 pc 8 mm thick (poor) 8 pc 4 mm thick (good)	4 pc 4 mm thick
Explosive (RDX)	1700 kg	500 kg
Booster (Picric Acid)	2 kg	2 kg
Case of bomb (steel)	7 mm thick	4 mm thick
Total weight	2908 kg	1300 kg

Figure 3. Design of the SAKURA Bomb, OTIR (ca. 1946) from Chapter 2.

Along the same line, S. K. Golaski, formerly of the BRL and in conjunction with the Defense Division of the Firestone Tire and Rubber Company (now owned by Physics International), developed shaped charge meteor simulators for NASA (Woodall and Clark 1966; Firestone Tire and Rubber Company 1968). The objectives of these studies were to obtain the luminous efficiency of a meteorlike body of known mass, composition, and speed during re-entry into Earth's atmosphere. The luminous efficiency is the percent of kinetic energy of the body that is converted into visible light as observed by photographic study of the visible re-entry tail. The study was designed to obtain the required mass, composition, and speed from pellets generated by a specific shaped charge design flown on a solid-state propellant vehicle. The vehicle was used to achieve the necessary velocities. Nickel and iron were the shaped charge liner

materials. The rocket engines were designed to carry the shaped charge liner above the atmosphere, turn, and allow the detonated shaped charge to accelerate at hypervelocity through Earth's atmosphere (re-entry). The intent was to simulate a body (meteor) re-entering the Earth's atmosphere. A specialized shaped charge liner design was required along with a specialized bi-explosive waveshaping device (Firestone Tire and Rubber Company 1968).

Zwicky (1947) proposed the use of a shaped charge as a method of producing artificial meteorites in 1947. He proposed launching a hypervelocity shaped charge on a V-2 rocket to exceed Earth's escape velocity and thus create an artificial meteorite. The hypervelocity jet particles could be tracked to study hypersonic aerodynamic effects. Also, the experiment could be designed to allow the jet to impact a heavenly body, such as the moon. A spectroscopic analysis of the impact flashes would reveal the elementary chemical constituents of the moon's surface. This experiment, although feasible, was never carried out.

Many other specialized shaped charge applications have been pursued by the departments of defense of several nations. These specialized designs included confinement or tamping of the explosive fill, varying the geometry or type of explosive used, altering the mode of initiation, using explosive lenses or more than one type of explosive or an explosive–nonexplosive barrier or gap, waveshaping or shaping the detonation wave (usually done to ensure a uniform wave with a short head height), or varying the standoff distance. Also, significant effects can be achieved by varying the liner material (including the use of nonmetals such as glass), varying the liner thickness, increasing the liner diameter, tapering (or causing a gradual wall thickness variation either continuously or discontinuously), or varying the liner geometry. The liner geometry variation may utilize the same basic geometry, for example, varying the conical apex angle, or may employ a radically different liner configuration. Other useful liner geometries are hemispheres, truncated (from the equator) hemispheres, disk- or dish-shaped (explosively formed penetrator) devices, tulips, trumpets, dual-angle cones, or a combination of these such as hemi-cones or tandem devices. In fact, any arcuate device may be used.

Also, spin-compensated liners may be used, especially when associated with spinning warhead applications. Gun-fired projectiles are spun in flight to provide aerodynamic stability. This angular momentum is imparted to the liner and is conserved during the liner collapse process. This leads to a large increase in the angular velocity of the jet so that centrifugal forces, if they exceed the yield strength of the material, can tear the jet apart. Without spin compensation, the jet will exhibit a radial instability (if the spin rate is high enough) and disperse radially, thus reducing the effective penetration capability. Spin compensation (i.e., causing the jet to spin enough and in the right direction to compensate for the spin of the warhead) may be achieved by metallurgical spin compensation or by the use of fluted liners. Metallurgical spin compensation is achieved by introducing anisotropies (primarily) or residual stresses into the liner during the fabrication process in order to provide rotation of the jet. Fluted liners contain raised ridges (or panels offset

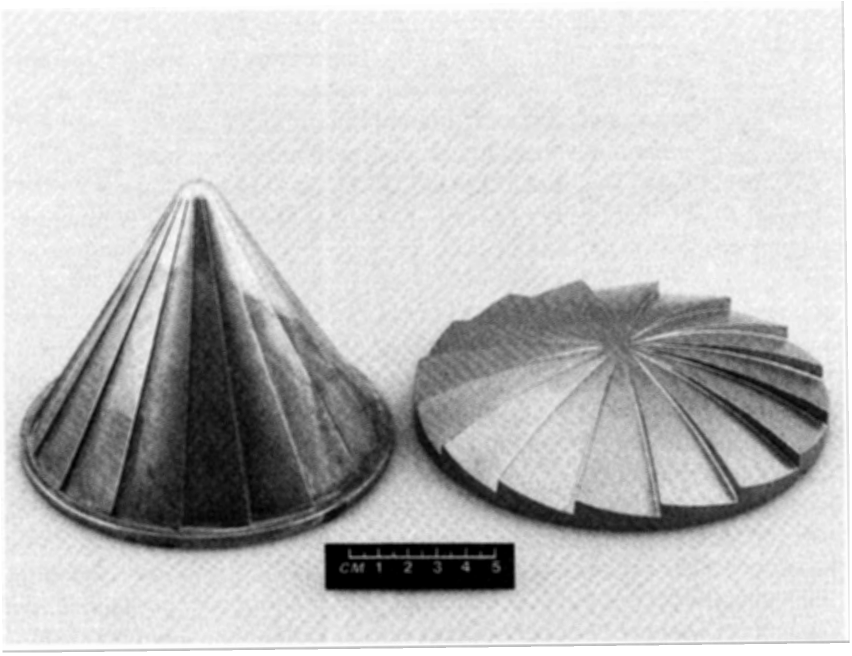

Figure 4. (*a*) Fluted liners.

with respect to the normal to a radius) either on the outside or the inside surface of the liner. A fluted liner, with ridges (flutes) on the outside surface, is shown in Figure 4. The flutes allow the jet to form with a given angular momentum to compensate for the rotation of the warhead in flight. Weickert (1986) describes fluted liners and spin-compensated liners in detail. The Firestone Tire and Rubber Company (1957) published engineering drawings for a 105-mm diameter fluted liner.

A unique shaped charge warhead design was developed by Kennedy and others in 1967 and 1970 as reported by Kennedy (1983). This particular missile design used a two-stage, tandem liner designed to produce a precursor or pre-jet to remove the guidance and control package located in the ogive of the missile. Otherwise, the main jet would have to penetrate the seeker package at a short (nonoptimum) standoff distance. Alignment difficulties in the tandem configuration made it necessary to blend the precursor liner, its standoff tube, and the main conical liner into a single piece. The result was the trumpet design configuration that is used for certain applications today. This design showed improved penetration with a relatively small standard deviation in penetration.

There exist numerous other tales of warhead development, the point being that some of the warhead concepts being pursued today are not original concepts.

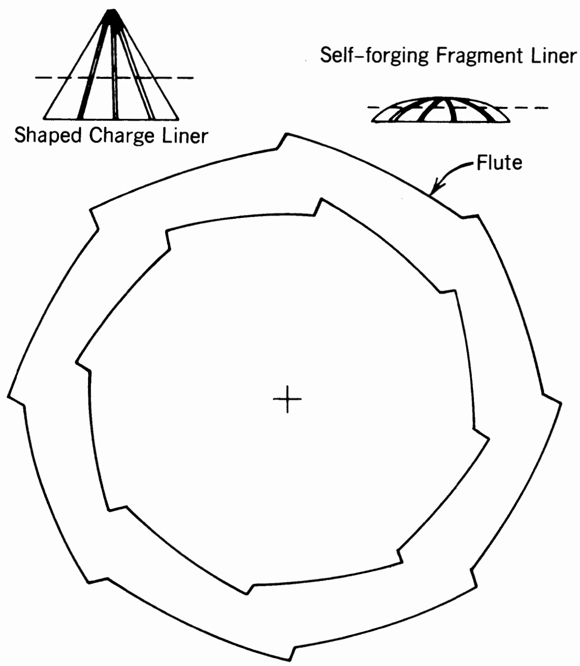

Figure 4. (*b*) Fluted liner cross-section.

3.3. CURRENT APPLICATIONS

A popular application of shaped charges is in demolition work. This area has both military and industrial application. Buildings, bridges, and other structures are the common demolition targets. Usually, demolition charges are hand placed. Demolition charges are sometimes constructed and placed in sites using a plastic explosive and a collection of liners. This technique allows for more flexibility and adjustment to the conditions at hand than a collection of fixed charges. Of course, experience on the part of the blaster is required, and this technique (the adjustment of the charge to the task) has delayed bulk charge production and research toward this particular application. The shaped charge principle is also used in construction work to break, crack, or drill holes in rock. A technique known as mudcapping is sometimes used to break rock and usually utilizes an unlined hollow charge. Shaped charges are also used in construction as earth movers, in tunneling, or to assist in well drilling. However, this usage is infrequent and highly specialized.

The shaped charge has also been employed for assorted peaceful purposes in the oil (Reinhart and Cocanower 1959) and steel industries, as a source of earth waves for geophysical prospecting and seismic exploration, mining (surface or underground) (Austin 1959, 1961; Austin and Pringle 1964), quarrying, in salvage operations, boring holes in demolition work (NAVWEPS 1962), breaking large rocks, and for hypervelocity impact studies (Merendino

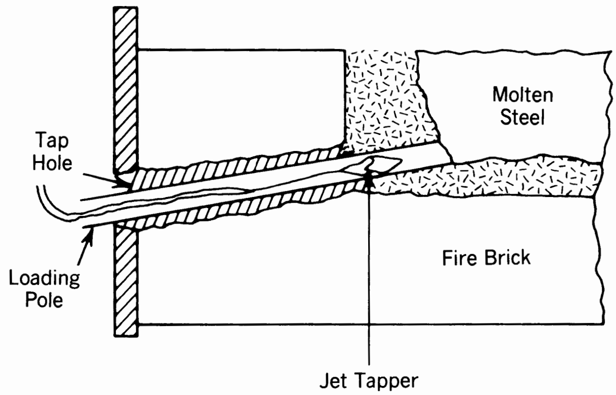

Figure 5. Steel mill furnace tapping (E. I. du Pont 1980).

et al. 1963). Other applications occur in submarine blasting, breaking log jams, breaking ice jams, and timber cutting.

Dennis (1966) describes the evaluation of standard and field-fabricated conical and linear shaped charges for felling live, sappy trees of up to 40 in. in diameter. Lined cavity linear shaped charges (described earlier) at a 4–10-in. standoff and unlined cavity conical shaped charges at zero standoff yielded effective cutting and felling of 18–43-in. diameter hickory, poplar, and oak trees with significantly less explosive than required for felling by conventional timber cutting techniques. Conventional timber cutting techniques state that the amount of explosive required P in pounds of TNT, is

$$P = D^2/40,$$

where D is the diameter, or smallest timber dimension, in inches.

Dennis (1966) reports that two unlined cavity conical shaped charges improvised from coffee cans (used as the casing) and 10 lb of C4 explosive felled trees of up to 34 in. in diameter when detonated in diametric opposition to each other. Larger-diameter trees were felled by multiples of 3–5 charges detonated symmetrically at points one-third to one-fifth the circumference of the trees.

Another application for shaped charges is in tapping steel mill furnaces. The steel mill furnace tapping problem is depicted in Figure 5 (E. I. du Pont 1980). The tapping problem requires a means of starting the flow of molten steel once the tap hole has been plugged. Steel mill furnace jet tapping is sometimes called salamander blasting since *salamander* is the term used to describe the large mass of solidified iron deposited at the base of the blast furnace after it has been in operation for some time. The tap hole is dug out as far as possible and a jet tapper is inserted into the tap hole using a loading pole. A jet tapper is a shaped charge with a conical metal or glass liner. The jet tapper is then detonated, clearing the plug, usually with a high rate of success (E. I. du Pont 1980). A commercial jet tapper is illustrated in Figure 6. The

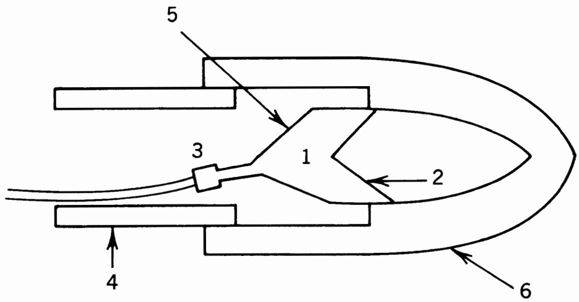

1. Explosive
2. Copper Conical Liner
3. Electric Blasting Cap
4. Loading Pole
5. Plastic Case
6. Insulating Ogive

Figure 6. The jet tapper charge (offset), (E. I. du Pont 1980).

shaped charge assembly may be aligned on axis or offset up to 10°, as shown in Figure 6, to reduce the line-of-sight thickness of the plug that must be perforated. The jet tapper assembly is insulated and special detonators are used to withstand the prolonged exposure to high temperatures.

Shaped charge liners are not always made of glass or metals. For example, Naval Proving Ground (1954) describes a shaped charge with a liner made of balsa wood. The liner consisted of flutes or wedges of balsa wood. The warhead provided a satisfactory method for producing equiaxed fragments. The liner was not satisfactory for producing a rod or a jet.

Another application of the shaped charge is in the internally coned end of certain detonators. This indented, lined cavity acts to concentrate the effect along the axis; recall Bloem (1886). Also, Cook (1948) used the original Munroe effect to engrave or stencil letters onto metal plates.

Other examples are in the oil well industry where large-diameter, but extremely short, lined shaped charges are used to penetrate various geological formations to increase the flow of oil. Oil well perforation problems present extremely difficult design problems due to the minimal amount of allowable space available in the well, the short standoff distances required, and the hostile environment within the well (Reinhart and Cocanower 1959).

The commercial use of the shaped charge in perforating oil wells was made public by McLemore (1946). Lawrence (1947) also referred to investigations in the use of shaped charges for perforating oil wells. Lawrence also discussed the use of shaped charges to fragment rocks and boulders.

The oil well perforating industry has designed several unique shaped charge devices. These devices contain a relatively small amount of explosive because of the available space and to minimize damage to the well casing and to prevent interference between neighboring charges. (Usually, several shaped charges are fired simultaneously.) The shaped charges used in the oil well industry contain conical liners, hemispherical liners, truncated conical liners, parabolic liners, and trumpet-shaped liners.

Well perforator cones usually have an apex angle of 45° to about 60°. The smaller angle increases penetration, but the hole size is small. The larger cones tend to create a tapered hole that hinders fluid flow. In addition, the interrelationship of wall thickness, wall taper, and the radius at the apex of the cone (i.e., round or pointed apex) all affect performance. If the wall is too thick, penetration will decrease, and there may be a hole-plugging slug. If the wall is too thin, the slug mass can be greatly reduced, but the jet mass will also decrease and lower the performance.

Thus, efforts have been made to design shaped charges that are slugless or noncarrot forming. (In the oil well industry the slug of a shaped charge jet is termed a *carrot*.) About 90% of the material that must be perforated consists of the cement well annulus and the rock formation. The problem is further complicated by the short standoff distances available (since the space is limited), the hostile environment (caustic and with temperatures in excess of 500°F), and the fact that the charges may have to remain in this hostile environment for several hours before they are detonated. The short standoff distance available is critical since the jet must have time and hence distance to form. Also, an optimal standoff exists to achieve maximum penetration. This optimal standoff is usually greater than three charge diameters, and these standoff distances are simply not available to the oil well perforator designer.

The first jet penetrators for oil well applications used glass liners. The glass-lined shaped charges made large holes, but the penetration depth was inadequate. Later shaped charge liner designs used steel, copper, zinc, lead, and combinations or alloys of these metals, particularly, copper and zinc.

One slugless liner design used two cones that were press fit together. The inner cone (on the air side) was copper and was approximately one-half of the composite cone wall thickness. Theoretically, this part of the liner forms the jet. The outer cone (on the explosive side) was made of a low-melting-point metal such as zinc or lead, which has little or no tendency to form a slug. However, some of the outer cone material enters the jet. Slugless charges are also made using a conical liner made entirely of a zinc alloy. Ultimately, bimetallic designs using lead or zinc alloys on the outside and copper on the inside were found to minimize the slug or carrot size without an appreciable loss in performance. The correct dimensions of each material and of the overall liner were determined experimentally. Slugless liners are also formed by preforming finely divided copper particles into molds followed by a sintering process. Another technique of slug elimination uses powdered copper but does not sinter or even bond the particles in forming the liner. Standard powder metallurgy techniques are also used.

Linear (wedge shaped, V-shaped or W-shaped) shaped charges are used as cutting charges. They generate a ribbon-shaped jet used to cut metals and other materials. Commercial cutting charges are available from several sources. For cutting charge applications, it is sometimes advantageous to use homemade cutting charges that can be optimized to the particular problem on hand. Cutting charges and hollow charges are also used as explosive separation devices, as bolt cutters, and for other applications. The shaped charge effect is

used on systems for separation, deployment, and safety destruct devices in missiles and spacecraft (Navy Bureau of Ordnance 1946; Cox 1964; Soper 1964; Sewell 1965). Garcia (1967), Brown (1969), and Sewell (1965) provide additional information on the linear cutting charge concept. Leidel (1978) discusses the design of an annular, or circular, cutting charge.

An interesting paper by Jones (1971) discusses the perforation of arctic sea-ice by large, demolition-type, shaped charges. Table 1 was compiled from the data of Jones (1971) and an army field manual FM 5-25 (1971). Table 1 describes the characteristics of three demolition charges currently in service and lists their approximate penetration capability into various targets. The M2A4 and M3A1 demolition charges were mentioned in Chapter 2. The No. 1, 6-in. Mk3 is a British-designed demolition charge.

General references on application are found in Kennedy (1983), Cook (1958), E. I. du Pont (1980), and Bawn and Rotter (1956). Certain specific applications of interest are found in Cook (1948), on engraving; Torrey (1945) on a review of shaped charge weapons of World War II; Huttl (1947) on underground blasting; Clark (1947) on concrete fragmentation; Lawrence (1947), Austin and Pringle (1964), and Austin (1961, 1959) on boulder breaking, drilling, and seismic exploration; Draper et al. (1948) on drilling; and Davidson and Westwater (1949) on cratering and boulder breaking. Overviews on application of shaped charges are available in Murphy (1983) and Baum et al. (1949).

Extensive studies are currently underway in cratering (earth removal), boulder breaking, and penetration of concrete and geological formations at several installations, notably the Waterways Experimental Station, Vicksburg, Mississippi. The demolition and cratering work performed at the Waterways Experimental Station is too extensive to cover here, but its studies cover many of the applications cited earlier. See Joachim (1983) as one example.

Extensive studies are also currently underway in the design of lined shaped charges for torpedo warheads. This work is also too extensive to cover here. See Merendino and West (1960) as one example.

Additional applications relating to explosive metal interactions, and that require an understanding of the jet formation phenomena, are explosion welding, explosion cladding, or explosion forming of metal parts. Basically, explosive welding involves using explosives to form bimetallic or trimetallic parts. A tremendous savings in material usage is thus possible because a thin layer of an often costly material can be applied to a cheaper, load-bearing substrate. The thin noble and expensive material is usually used to provide an inert or corrosion resistance barrier to the substrate material. Applications occur in chemical vessels, heat exchangers, desalination plant piping, and other areas where caustic environments exist. With explosive welding techniques, even metallurgically incompatible metals and immiscible metal combinations can be bonded, as well as compatible metal systems. *Mechanical Engineering* (1978), Rinehart and Pearson (1963), and Blazynski (1983) provide an excellent introduction to the various aspects of explosion welding. This topic will be discussed in slightly more detail in Chapter 7.

TABLE 1. Approximate Design and Performance Details of Standard Demolition Shaped Charges

	No. 1, 6-in. Mk3	M2A4	M3A1
Total weight (lb) approx.	10.0	15.0	40.0
Explosive weight (lb)	6.7	11.5	30.0
Charge diameter (in.)	6.0	6.0	9.5
Charge length (in.)	7.5	9.44	15.5
Design standoff (in.)	5.7	5.5	15.0
Casing material	Steel	Fiber	Steel
Cone diameter (in.)	6.0	4.88	9.0
Cone angle (deg.)	80.0	60.0	60.0
Cone material	Steel	Glass	Steel
Cone thickness (in.)	0.140	~ 0.350	~ 0.150
Cone weight (lb)	—	~ 1.7	~ 5.6
Penetration			
Armour depth (in.)	6.0	12.0	20.0 +
Average hole diameter (in.)	—	1.5	2.5
Mild steel depth (in.)	9.0	—	—
Thick wall, reinforced concrete			
Concrete depth (in.)	30.0	30.0	60.0
Average hole diameter (in.)	—	2.75	3.5
Minimum hole diameter (in.)	2.0	2.0	2.0
Fresh water ice depth (in.)	—	84.0	144.0
Hole diameter (in.)	—	3.5	6.0
		42 in. Standoff	
Permafrost depth (in.)	—	72.0	72.0
Hole diameter (in.)	—	1.5–6	5–8
		30 in. Standoff	50 in. Standoff
Soil depth (in.)	—	84.0	84.0
Hole diameter (in.)	—	7.0	14.5
		30 in. Standoff	48 in. Standoff

Extracted from Jones (1971) and FM5-25 (1971).

REFERENCES

Austin, C. F. (1959), "Lined Cavity Shaped Charges and Their Uses in Rock and Earth Materials," Bulletin 59, New Mexico Inst. Min. and Tech., State Bureau of Mines and Mineral Research.

Austin, C. F. (1961), "Lined Cavity Shaped Charge and Its Use as a Drilling Tool," *Trans. AIME*, *220*: 123.

Austin, C. F., and Pringle, J. K. (1964), "Detailed Response of Some Rock Targets to Jets from Lined Cavity Charges, *J. Petrol. Tech.*, January.

Bawn, C. E. H., and Rotter, G. (1956), *Science of Explosives*, C. E. H. Bawn and G. Rotter (eds.), Part I, Ministry of Supply, London (AD 127695).

Baum, F. A., Stanykovich, R. P., and Skekter, B. I. (1949), *Physics of an Explosion*, New York: Research Information Service (AD 400151), 546.

Blazynski, T. Z. (ed.) (1983), *Explosive Welding, Forming and Compaction*, New York: Applied Science Publishers.

Bloem, G. (1886), Dusseldorf, Prussia, Germany, "Shell for Detonating Caps," U.S. Patent 342,423, dated May 25.

Brown, G. E. (1969), "A New Optimization Theory for the End-Initiated Linear Shaped Charge," M.S. Thesis, Naval Postgraduate School, October.

Clark (1947), *Amer. Inst. Min. Met. Engr.*, Tech. Pubs. 2157, 2158.

Coles, R., and Rickson, P. L. (1977), "Mistletoe—The Deadly Parasite," *Air Classics Quart. Rev.*, *4*(3): 38–47, 86–99.

Cook, M. A. (1948), *Research*, *1*: 474.

Cook, M. A. (1958), *The Science of High Explosives*, American Chemical Society Monograph Series, New York: Reinhold Publishing.

Cox, C. M. (1964), "Linear and Conical Shaped Charge Performance," Firestone Tire and Rubber Company, Defense Research Division, Akron, Ohio, April.

Davidson, S. H. and Westwater, R. (1949), *Mine Quarry Eng.*, May.

Dennis, J. A. (1966), "Tree Felling with High-Explosive Shaped Charges," U.S. Army Engineer Research and Development Laboratories, Fort Belvoir, VA, Report 1876, November.

Draper, H. C., et al. (1948), *U.S. Bur. Min.*, R.I., 4371.

E. I. du Pont (1980), *The Blaster's Handbook*, 16th ed., E. I. du Pont de Nemours and Co., Wilmington, DE.

FM5-25 (1971), Headquarters, Department of the Army, "Explosives and Demolition," Department of Army Field Manual FM5-25, Washington, D.C., February.

Firestone Tire and Rubber Company (1957), "The Firestone Tire and Rubber Company on the Research and Development on Shaped Charge Liners, Akron, Ohio, 1956–1957," FTRC/2355, February.

Firestone Tire and Rubber Company (1968), "Design, Development and Testing of Bi-Explosive Shaped Charge Meteoritic Simulators," The Firestone Tire and Rubber Company, NASA CR-66615, April.

Garcia, M. A. (1967), "The End-Initiated, Linear Shaped Charge: An Analytical Model," Naval Missile Center, TM-67-64, December.

Huttl, J. B. (1947), *Eng. Min. J.*, *147*: 58.

Joachim, C. E. (1983), "Application of Shaped Charges to Rapid Atomic Demolition Munition (ADM) Emplacement," U.S. Army Engineer Waterways Experimental Station Miscellaneous Paper SL-83-20, December.

Jones, J. M. (1971), "The Design of a Large Shaped Charge Suitable for the Perforation of Arctic Sea-Ice," Defense Research Establishment, Valcartier Report, DREV TN-1907/71, PROJ D97-01-19, May.

Kennedy, D. R. (1983), "The History of the Shaped Charge Effect, The First 100 Years," presented at MBB Schrobenhausen, West Germany, September.

Lawrence, R. W. (1947), "A Scientific Approach to the Industrial Application of Shaped Charges," *Explos. Eng.*, *25* (November–December): 171.

Leidel, D. J. (1978), "A Design Study of an Annular—Jet Charge for Explosive Cutting," Ph.D. Dissertation, Drexel University, Philadelphia, June.

McLemore, R. L. (1946), *World Oil*, July 8.

Mech. Eng. (1978), "Explosive Welding" *Mech. Eng.*, May.

Merendino, A. and West, C. (1960), "A Shaped Charge Warhead for Antisubmarine Application," Ballistic Research Laboratory Technical Note No. 1357, October.

Merendino, A., Regan, J. M., and Kronman, S. (1963), "A Method of Obtaining a Massive Hypervelocity Pellet from a Shaped Charge Jet," Ballistic Research Laboratory, BRL Memorandum Report No. 1508, APG, Maryland, August.

Mohaupt, H. (1966), *Aerospace Ordnance Handbook*, F. Pollard and J. Arnold (eds.), Engelwood Cliffs, NJ: Prentice-Hall, Chapter 11.

Murphy, M. J. (1983), "Shaped Charge Penetration in Concrete: A Unified Approach," Ph.D. Dissertation, University of California—Davis, January; also Lawrence Livermore National Laboratory Report UCRL-53393.

Naval Proving Ground (1954), "Effectiveness of Balsa-Wood Shaped Charge Liners in the Controlled Fragmentation of Warheads," U.S. Naval Proving Ground, Dahlgren, VA., Report No. 1228, Testing of Warheads for Guided Missiles, January.

NAVWEPS (1962), *Demolition Materials*, Bureau of Naval Weapons Ordnance Pamphlet, NAVWEPS OP 2212, February.

Navy Bureau of Ordnance (1946), *Applications of Lined Cavity Charges*, Navy Bureau of Ordnance, OP 1647, June.

Reinhart, J. S. and Cocanower, R. D. (1959), "Concerning the Design of an Effective Shaped Charge for Oil Well Perforating," *J. Appl. Phys.*, *30*: 680–682.

Reinhart, J. S. and Pearson, J. (1963), *Explosive Working of Metals*, New York: Macmillan.

Sewell, R. G. S. (1965), "Effects of Velocity and Material Properties on Design Limits for Linear Shaped Charges," NOTS Technical Publication 3894 and NAVWEPS Report 8793, August.

Soper, W. G. (1964), *Performance of Linear Shaped Charge*, USNWL, Dahlgren, Naval Weapons Laboratory, NWL Report No. 1946, NAVWEPS Report No. 8346, September.

Torrey, V. (1945), *Explos. Engr.*, *23*: 160.

Weickert, C. A. (1986), "Spinning Self-Forging Fragments and Shaped Charges," Ph.D. Dissertation, Drexel University, Philadelphia, June.

Woodall, R. L., and Clark, E. L. (1966), "Development and Testing of Advanced Shaped Charge Meteoritic Simulators Part II—Calibration of Flight Guns," Firestone Tire and Rubber Company, NASA CR-66216, November.

Zwicky, F. (1947), "Artificial Meteors," *Ordnance*, *32*(163): 18–20.

CHAPTER 4

THE GURNEY VELOCITY APPROXIMATION

The Gurney model yields explicit algebraic relationships for estimating the velocity imparted to a metal in contact with a detonating explosive. Thus, the Gurney method can be directly and simply applied to a multitude of explosive–metal interaction problems. Design and parametric studies can be readily performed. Applications of the Gurney model include warhead and fragmentation design, the study of the efficiency of conversion of the high explosive chemical energy to the kinetic energy of the plate, explosive initiation by the impact of an explosively driven plate, the launching of a dielectric plate by electrical detonation of a metal foil, and the calculation of the speeds of layers of metal fragments in conjunction with shock wave physics (Jones et al. 1980).

The motion of metal driven by an explosive was first studied in the 1940s to early 1950s in a series of papers by Gurney (1943, 1947), Sterne (1947, 1951), and Thomas (1944) as applied to the motion of fragments resulting from the detonation of an adjacent high explosive. This simple, approximate analysis assumes that the potential (or chemical) energy of the explosive charge before detonation is converted directly to the kinetic energy of the metal after detonation and to the expansion of the explosive products. Thus, a specific energy (energy per unit mass) characteristic of a given explosive is assumed to be converted from chemical energy in the initial state to kinetic energy in the final state (Kennedy 1970). This energy is called the Gurney energy, E, and is a fraction of the total chemical energy released during detonation. The final kinetic energy is partitioned between the driven metal and the detonation product gases by an assumed linear velocity profile in the gases. The gas detonation products are assumed to expand uniformly and with constant density.

The so-called Gurney approximation is based on the conservation of momentum and energy. The results represent excellent engineering approxima-

tions, within 10%, of the experimental results or detailed numerical results. The Gurney method may be applied to any one-dimensional explosive–metal interaction system. The amazing accuracy of the relatively simple Gurney formulas, over a wide range of metal mass (M) to explosive mass (C) ratios ($0.1 \leq M/C \leq 10.0$), is apparently due to offsetting errors. These errors are caused by ignoring rarefaction waves passing through the detonation product gases, which causes the calculated velocity to be too high, and assuming an initial constant-density distribution of the detonation product gases rather than a distribution with a peak at the surface of the charge caused by the detonation wave, which causes the calculated velocity to be too low (Henry 1967).

The Gurney method, and extensions of this method, are useful analytical tools. The final flyer plate velocity depends only on the M/C ratio and the Gurney constant or Gurney characteristic velocity, $\sqrt{2E}$. Henry (1967), Jones et al. (1980), and Kennedy (1970) provide the complete derivations of all the Gurney formulas given in this chapter. As an illustration of the method, the open-faced sandwich expressions are derived in the following paragraphs.

4.1. THE GURNEY EXPRESSIONS

Figure 1 illustrates the open-faced sandwich. It consists of a slab of explosive confined by a metal on one side only. This configuration is often used in experiments to obtain constitutive properties of materials or when it is necessary to impact a large target surface. The metal plate is termed the

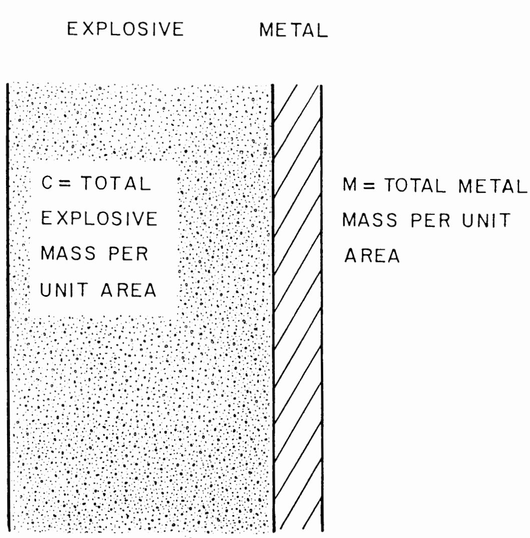

Figure 1. Open-faced sandwich.

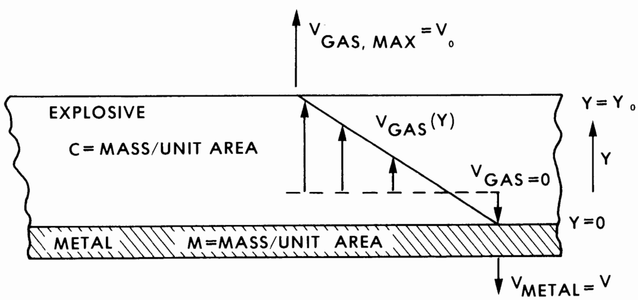

Figure 2. Linear velocity distribution for the open-faced sandwich configuration (Kennedy 1970).

slapper or driver. The motion of the metal is obtained from momentum and energy conservation. For the open-faced sandwich, Figure 2 illustrates the linear velocity distribution, which is assumed to persist for all times. From this linear velocity distribution,

$$V_{\text{gas}}(Y) = (V_0 + V)\frac{Y}{Y_0} - V. \tag{1}$$

The Y coordinate is interpreted to be Lagrangian or identified with a material particle. The magnitudes of the velocity terms used in the Gurney derivation are interpreted to be the final velocities achieved after the Gurney energy has been extracted from the detonation products. This will obviously occur only after the detonation product gases have expanded to several times their original volume. Assuming a constant density throughout the detonation product gases, the product of the instantaneous gas thickness, Y_0, times the gas density is a constant C, equal to the original mass of explosive per unit area. The value Y_0 eventually drops out of the analysis and therefore can be taken to be any value. For convenience, the value of Y_0 is taken to be the original explosive thickness, and the gas density is taken to be, ρ_e, the initial explosive density.

The energy and momentum balance equations are as follows:

$$CE = \tfrac{1}{2}MV^2 + \tfrac{1}{2}\rho_e\int_0^{Y_0}\left[(V_0 + V)\frac{Y}{Y_0} - V\right]^2 dY, \tag{2}$$

and

$$0 = -MV + \rho_e\int_0^{Y_0}\left[(V_0 + V)\frac{Y}{Y_0} - V\right] dY, \tag{3}$$

where $C = Y_0 \rho_e$
E = specific explosive kinetic energy or Gurney energy
$M = \rho_m t$, and ρ_m is the density of the metal and t is the metal thickness.
Straightforward integration of Eq. (3) results in

$$MV = \rho_e \left[(V_0 + V)\frac{Y^2}{2Y_0} - VY \right]_0^{Y_0},$$

or

$$MV = \rho_e Y_0 \left[\frac{V_0 + V}{2} - V \right].$$

Algebraic manipulation yields

$$V_0 = V\left[1 + \frac{2M}{C}\right], \tag{4}$$

and V_0 is the free surface or gas velocity V at $Y = Y_0$. Straightforward integration of Eq. (2) and algebraic manipulation yield

$$2E = \frac{MV^2}{C} + \tfrac{1}{3}\left(V_0^2 - VV_0 + V^2\right).$$

Using Eq. (4) to eliminate V_0 and with further manipulation, we have

$$V = \sqrt{2E}\left\{\frac{1}{3}\left[\left(\frac{2M}{C}\right)^2 + \frac{5M}{C} + 1\right]\right\}^{-1/2}. \tag{5}$$

If the square root term containing the M/C ratio is multiplied by 1, that is, $(1 + M/C)/(1 + M/C)$, we have

$$V = \sqrt{2E}\left[\frac{4M^3/C^3 + 9M^2/C^2 + 6M/C + 1}{3(1 + M/C)}\right]^{-1/2},$$

which can be manipulated into the form

$$V = \sqrt{2E}\left[\frac{(1 + 2M/C)^3 + 1}{6(1 + M/C)} + \frac{M}{C}\right]^{-1/2} \tag{6}$$

which is the expression given by Gurney. Note that the simpler forms

$$V = \sqrt{2E}\left[\frac{1}{3}\left[\left(\frac{2M}{C}\right)^2 + \frac{5M}{C} + 1\right]\right]^{-1/2}$$

$$= \sqrt{2E}\left[\frac{1}{3}\left(\frac{4M}{C} + 1\right)\left(\frac{M}{C} + 1\right)\right]^{-1/2}, \tag{7}$$

are equivalent to the Gurney open-faced sandwich expression [Eq. (6)].

The derivation given parallels that of Kennedy (1970). Henry (1967) and Jones et al. (1980) provide alternate but equivalent derivations (using a different choice of coordinate systems). However, all derivations result in the expression given by Eq. (5), and further manipulation is required (as shown) to obtain the Gurney form given by Eq. (6).

The equations for some common symmetric and asymmetric configurations are presented in Figures 3, 4, and 5. Henry (1967) presents a complete review of the Gurney formulas given in these figures.

Figure 3 depicts two symmetric configurations, namely, a flat sandwich and a cylinder. For the flat sandwich, M and C are the metal and explosive masses per unit area, respectively. For the cylinder, M and C are the metal and explosive masses per unit length. The term V is the resultant metal velocity.

Figure 4 presents the spherically symmetric case. For the sphere, C and M represent the entire charge and metal masses, respectively. Figure 5 shows two asymmetric configurations: an open-faced sandwich and an asymmetric sandwich that has two metal plates, one being a tamper. For these flat plate configurations, C, M, and N represent masses of unit area of the explosive, metal, and tamper plate, respectively. The derivation of these equations is

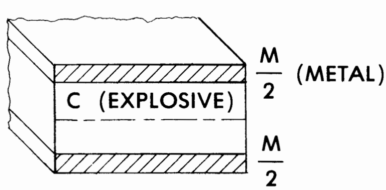

FLAT SANDWICH

$$V = \sqrt{2E}\left[\frac{M}{C} + \frac{1}{3}\right]^{-\frac{1}{2}}$$

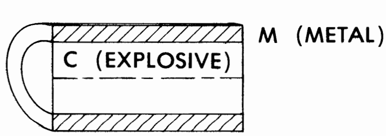

CYLINDER

$$V = \sqrt{2E}\left[\frac{M}{C} + \frac{1}{2}\right]^{-\frac{1}{2}}$$

Figure 3. The flat sandwich and cylindrical configurations.

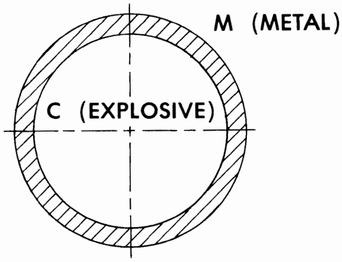

SPHERE

$$V=\sqrt{2E}\left[\frac{M}{C}+\frac{3}{5}\right]^{-\frac{1}{2}}$$

Figure 4. The spherical configuration.

relatively straightforward using the stated assumptions along with elementary calculus and algebra, for example, Henry (1967), Jones et al. (1980), and Kennedy (1970). The ratio of $V/\sqrt{2E}$ or the ratio of the metal velocity to the Gurney characteristic velocity is an explicit function of M/C, or the metal–charge mass ratio. For the asymmetric sandwich where the second metal plate may be considered to be a tamper, $V/\sqrt{2E}$ is also a function of N/C, where N/C is the mass to charge ratio of the tamper plate. The velocity expression given is that of the metal plate M.

The quantity $\sqrt{2E}$ occurs in all Gurney equations. It has the units of velocity and is termed the Gurney characteristic velocity for a given explosive. Gurney characteristic velocities have been tabulated for certain explosives by Kennedy (1970), Henry (1967), Jones et al. (1980), and many others, notably Dobratz (1982). Several explosives are tabulated from Dobratz (1982) with their density, detonation velocity, and Gurney characteristic velocity or

OPEN FACED SANDWICH

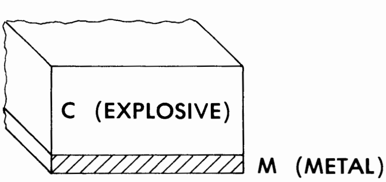

$$V=\sqrt{2E}\left[\frac{\left(1+2\frac{M}{C}\right)^{3}+1}{6\left(1+\frac{M}{C}\right)}+\frac{M}{C}\right]^{-\frac{1}{2}}$$

ASYMMETRIC SANDWICH

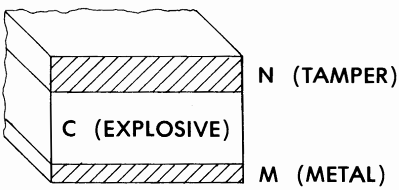

$$V_M=\sqrt{2E}\left[\frac{1+A^{3}}{3(1+A)}+\frac{N}{C}A^{2}+\frac{M}{C}\right]^{-\frac{1}{2}}$$

$$V_N=AV_M$$

$$A=\frac{1+2\frac{M}{C}}{1+2\frac{N}{C}}$$

Figure 5. Asymmetric configurations.

TABLE 1. Density, Detonation Velocity, and Gurney Constant for Several Explosives

Explosive	Density (g/cm^3)	D (km/s)	$\sqrt{2E}$ (km/s) Prompt 5–7 mm	Terminal 19–26 mm
Comp A-3	1.61	8.47	2.402	
	1.59			2.63
Comp B	1.71			2.70
	1.717	7.89	2.35	2.756–2.821
	1.717			2.71
Cast	1.68		2.402	
	1.62		2.32	
Pressed	1.59		2.335	
Comp C-4	1.52	8.37	2.176	
Comp C-3	1.60	7.63		2.68
Cyclotol 75/25	1.754	8.2–8.3		
Cast	1.69		2.286	
Pressed	1.64		2.362	
DATB	1.68	7.52	1.975	
Explosive D	1.50	6.85	1.942	
HBX-1	1.70	7.31	2.213	
HBX-3	1.81	6.9–7.1	1.984	
HMX	1.89	9.11		2.97
LX-14	1.835	8.83		2.80
NM	1.14	6.35		2.41
NQ	1.44	7.65	1.896	
Octol 75/25	1.81	8.48		2.80
	1.821			2.83
DETASHEET C				
(Du Pont)	1.48	6.8		2.1–2.3
(BRL)		7.0		2.8
PBX-9011	1.77	8.5	2.82	
PBX-9404	1.84	8.8		2.90
PBX-9502	1.885	7.71		2.377
Pentolite 50/50				
Cast	1.64	7.52	2.301	
Pressed	1.57		2.317	
PETN	1.76	8.26		2.93
RDX	1.59	8.25	2.451	
	1.77	8.70		2.93
TACOT	1.61	7.25		2.12
Tetryl	1.63	7.5	2.274	
	1.62			2.50
TNT	1.63		2.039	2.419–2.505
	1.63			2.37
Cast	1.61	6.73	2.097	
Pressed	1.54	6.93	2.103	

From Dobratz (1982).

Gurney constant (see Table 1). Note that two Gurney constants are given, one for warheads in which confining cases rupture at small expansions (prompt) and the other for warheads in which more ductile case materials are used that expand further before rupturing (terminal).

The tabulated densities are the actual density of the explosive used to determine the Gurney energy. The detonation velocities sometimes correspond to a different explosive density than that given in the table. It is recommended that the explosive of interest be accurately identified and the appropriate parameters be taken directly from Dobratz and the references therein, or any other suitable source such as Meyer (1977) or UCRL (1965).

When the Gurney constant is not available, Kennedy (1970) recommends that $E \sim 0.7H_D$ be used where H_D is the heat of detonation for the explosive. This recommendation follows from the fact that $0.61 < E/H_D < 0.76$ for most explosives. Also, La Rocca (1980) presents a simple method for accurately predicting the Gurney constant and the relative power of any explosive.

The velocity ratio $V/\sqrt{2E}$ is plotted as a function of M/C in Figure 6 for all the nontampered cases presented. Since values of $\sqrt{2E}$ have been tabulated for certain explosives, estimates of the metal velocity can be obtained for a given M/C for the geometries considered here.

Figure 7 plots the metal velocity as a function of M/C for an open-faced sandwich and a few values of the Gurney constant, $\sqrt{2E}$, corresponding to

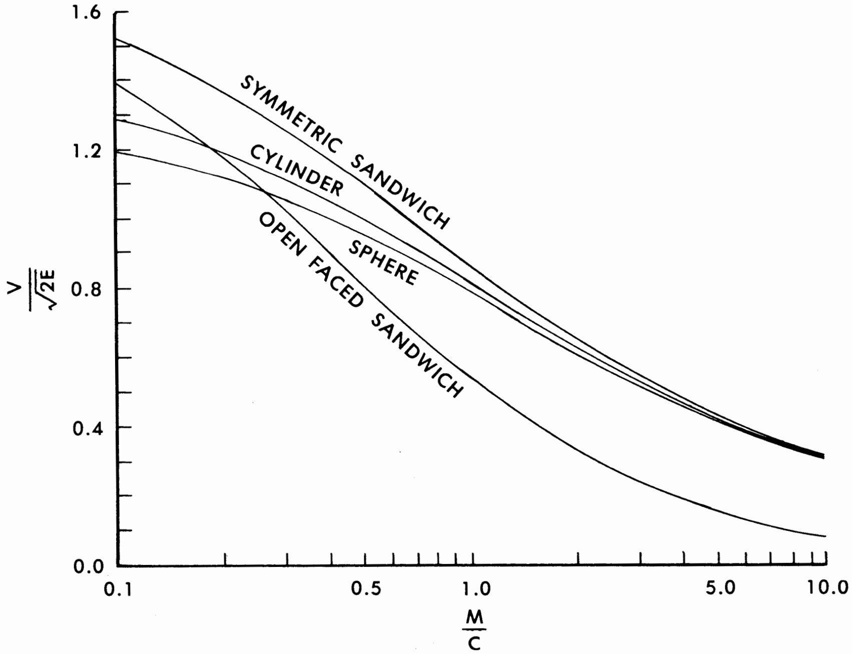

Figure 6. $V/\sqrt{2E}$ versus M/C (Kennedy 1970).

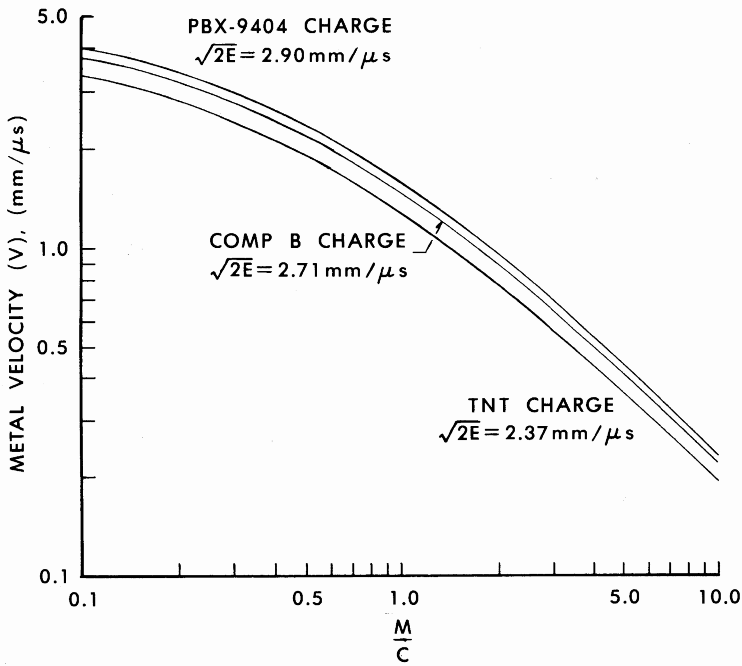

Figure 7. V versus M/C for an open-faced sandwich (Kennedy 1970).

PBX-9404, TNT, and Comp B. This plot allows easy interpolation or extrapolation to other values of the Gurney constant. The applicable range of M/C values is $0.2 < M/C < 10$ as discussed earlier. Note that as M/C decreases, for example, when adding explosive to a given metal slab or decreasing the mass of metal, the velocity approaches a constant that depends on the explosive–metal geometry, as shown in Table 2. As M/C increases, for example, as the explosive mass approaches zero or as the metal mass becomes extremely large, the velocity approaches zero.

TABLE 2. The Gurney Final Metal Velocity as $M/C \to 0$.

Geometry	Final Metal Velocity
Flat sandwich	$\sqrt{6E}$
Cylinder	$\sqrt{4E}$
Sphere	$\sqrt{\frac{10E}{3}}$
Open-face sandwich	$\sqrt{6E}$
Asymmetric sandwich ($N/C \to 0$ also)	$\sqrt{6E}$

The range of applicability of the Gurney formulas is restricted due to the simplifying assumptions in the derivation. These restrictions, according to Kennedy (1970), Jones et al. (1980), and Henry (1967), are listed and discussed in Table 3. The Gurney assumption of a linear velocity profile of constant-density detonation product gases greatly deviates from conventional gas dynamic theory. This assumption introduces the largest error in configurations involving a free explosive surface such as the open-faced sandwich, for which the Gurney method may overestimate the metal velocity and impulse. Henry (1967) used a parabolic pressure profile in the detonation products to remove the assumption that the gas density was constant at any given time. A simple gas equation of state was also used. Henry concluded that the additional mathematical complexity, inconsistent with the basic simplicity of the Gurney method, was not worthwhile based on the small improvement obtained in accuracy. Other extensions of the Gurney method are given by Hoskin et al. (1965).

The specific impulse of an explosive can also be obtained for geometries considered by the Gurney model and is directly related to the Gurney energy of the explosive.

The specific impulse delivered by the explosive can be calculated as the total momentum imparted to the metal body divided by the total explosive charge mass or

$$I_{sp} = \frac{MV}{C}. \tag{8}$$

The specific impulse, I_{sp}, will now be derived for an unconfined surface charge (Jones et al. 1980). Explosive may be detonated directly on the surface of a massive metal body in order to deliver a desired impulse for testing purposes. If the loaded body is considered to be rigid, all detonation product gases will flow away from the surface and a maximum specific impulse will be delivered to the body. For a very large metal body mass to explosive mass ratio, $M/C \gg 1$, the open-faced sandwich velocity, Eqs. (6) or (7), reduces to

$$V \sim \sqrt{2E}\sqrt{3/4}\,\frac{C}{M}, \tag{9}$$

since from Eqs. (7) for $M/C \gg 1$,

$$\left(\frac{2M}{C}\right)^2 \gg \frac{5M}{C} + 1.$$

Then, $I_{sp} \sim \sqrt{3E/2}$ from Eq. (8).

Also, from Eq. (4) for $M/C \gg 1$, $V_0 = 2VM/C$, and with V given from Eq. (9), $V_0 = \sqrt{6E}$ for the maximum free gas velocity. The final metal velocity also approaches $\sqrt{6E}$ as M/C approaches zero, as shown in Table 2.

TABLE 3. Restrictions on the Gurney Model

Restriction	Remarks and Recommendations
Range of M/C ratio	Henry (1967) claims accuracy for $0.1 < M/C < 5$, and Kennedy (1970) states a range of $0.2 < M/C < 10$ for velocity calculations. Impulse calculations are usually acceptable for $M/C > 0.2$.
Acceleration phase	The Gurney method in its basic form is not capable of analyzing motion during acceleration. However, Henry (1967) and Jones et al. (1980) used the assumption of a linear velocity profile in the uniformly dense gases in conjunction with an equation of state of the gases to yield acceleration solutions for flying metal plates. The detonation product gases must be allowed to expand sufficiently to complete the acceleration. The flying metal will reach its calculated velocity only if no external forces (or interactions) are applied during the initial acceleration phase.
Direction of detonation propagation	The detonation of the HE drives the metal at a given velocity (approximately) for a given M/C regardless of the angle between the detonation front and the metal. The direction in which the metal is driven will vary slightly with the angle (see Taylor angle discussion).
Gas velocity profile assumption	The assumed linear velocity profile and constant-density gas expansion are major assumptions. Ignoring effects of both rarefaction waves and of pressure peaks near the metal surface would seem to be canceling errors. However, these assumptions are inherent to the simplicity of the Gurney method.
One-dimensional motion	The Gurney approach is not valid for the estimate of variations in local velocity of a plate driven by a charge with a tapered thickness (or a tapered metal thickness). In this case, an average value of M/C could be used to estimate the final velocity of the entire plate.
Metal strength effects	Forces exerted by the metal to oppose deformation are not considered, other than inertia. Hoop stresses in cylinders and spheres can reduce the metal velocity in explosions and the strength effect is greater in implosions.
Metal spallations	Metal spallation may occur when $M/C < 2$ for high-density explosives and metals. Spallation can, in some cases, be avoided by introducing an air gap of a few millimeters between the explosive and the metal. This results in a small decrease in metal velocity.
Early case fracture	The leakage of the detonation product gases through fractures in the metal case can decrease the final metal velocity perhaps significantly depending on the nature and extent of the leakage.

The impulse delivered to a body by the explosive can be increased by tamping or confining the explosive with an outer layer of metal. Tamping acts to hold back the detonation gases, keeps the pressure high, and forces the detonation gases to do useful work against the body. A tamping and a confinement are analogous. The Gurney method can be used to estimate the change in impulse as a function of the tamper areal density. If the heavy metal body sandwich is considered to be rigid, it resembles the plane of symmmetry in the symmetrical flat sandwich configuration shown in Figure 3. The velocity of the tamper plate is then given by the flat sandwich of Figure 3 with the tamper to explosive mass ratio N/C used instead of M/C or

$$V = \sqrt{2E}\left[\frac{N}{C} + \frac{1}{3}\right]^{-1/2}. \qquad (10)$$

The effective specific impulse of the explosive for a tamping ratio of N/C follows from the equation for the asymmetric sandwich of Figure 5, namely,

$$V_M = \sqrt{2E}\left[\frac{1 + A^3}{3(1 + A)} + \frac{N}{C}A^2 + \frac{M}{C}\right]^{-1/2},$$

where

$$A = \frac{1 + 2M/C}{1 + 2N/C}. \qquad (11)$$

Assuming $M/C \gg 1$ and $M/C \gg N/C$, which implies $A \gg 1$, the specific impulse from Eq. (11) becomes

$$V_M \sim \sqrt{2E}\left[\frac{A^2}{3} + \frac{NA^2}{C}\right]^{-1/2}$$

with

$$A \sim \frac{M/C}{1/2 + N/C},$$

or

$$V_M \sim \sqrt{2E}\left[\frac{(M/C)^2}{(1/2 + N/C)^2}\left(\frac{1}{3} + \frac{N}{C}\right)\right]^{-1/2},$$

and finally

$$V_M \sim \frac{\sqrt{2E}\,(N/C + 1/2)}{(M/C)(N/C + 1/3)^{1/2}}.$$

Thus,

$$I_{sp,\,tamped} = \frac{V_M M}{C} \sim \frac{\sqrt{2E}\,(N/C + 1/2)}{(N/C + 1/3)^{1/2}}. \tag{12}$$

Note that when $N/C = 0$, that is, no tamper, Eq. (12) yields $I_{sp} \sim \sqrt{\frac{3}{2}E}$ as derived earlier for the open-faced sandwich.

For the case where both $M/C \gg 1$ and $N/C \gg 1$, A approaches $(M/C)/(N/C)$, and from Eq. (11),

$$\frac{V}{\sqrt{2E}} \sim \left[\frac{1 + [(M/C)/(N/C)]^3}{3[1 + (M/C)/(N/C)]} + \frac{(M/C)^2}{N/C} + \frac{M}{C}\right]^{-1/2},$$

$$\sim \left[\frac{(N/C)^3 + (M/C)^3 + [1 + (M/C)/(N/C)] \times \left[3(N/C)^2(M/C)^2 + (3M/C)(N/C)^3\right]}{3(N/C)^3[1 + (M/C)/(N/C)]}\right]^{-1/2},$$

and neglecting terms of the third power as compared to terms to the fourth power,

$$\frac{V}{\sqrt{2E}} \sim \left[\frac{M/C(M/C + N/C)}{N/C}\right]^{-1/2}.$$

If $M = N$, then

$$\frac{V}{\sqrt{2E}} \sim \left(\frac{2M}{C}\right)^{-1/2}$$

or

$$I_{sp,\,tamped}\,(M = N) \sim \sqrt{E}\sqrt{M/C}\,.$$

4.2. EXTENSIONS OF THE GURNEY METHOD

Hirsch (1986) improved the basic Gurney formulas for exploding cylinders and spheres to extend their applicability toward lower M/C values. This improvement is based on the observation that the acceleration time of light plates is so short that only that part of the explosive that is close to the plate participates in its acceleration. The contribution of the inner part of the explosive is negligible. Accordingly, the explosive volume is divided into a

hard core and an outer part in which the gas velocity distribution is assumed to be linear. This division is chosen in such a way that the plate velocity is a maximum under the model restrictions. It provides a crude fit to the actual gas velocity distribution, which is better than assuming linearity in the whole explosive volume. The model predicts the same Gurney escape velocity of the explosive products (or maximum free gas velocity) for all the geometries in which Mach waves are not formed. The Gurney escape velocity is $\sqrt{6E}$ for small M/C ratios for sandwich, cylindrical, and spherical configurations. Thus, the explosive products escape velocity does not depend on the initial geometry of the explosive when no Mach waves are formed. The agreement with experimental data is very good for $0.6 \leq M/C < 1.5$.

The equations of Hirsch (1986) are analogous to those of Gurney except they involve additional terms of various powers of r_H/R, where r_H is the radius of the hard core and R is the liner inner (or explosive outer) radius. In order to maximize the velocity of the metal, r_H/R becomes a function of M/C only, and thus the velocity of the metal remains a function of M/C and the Gurney constant alone.

The acceleration of explosively driven metal plates can also be determined by using the Gurney assumption of a linear velocity profile in uniformly dense gases in conjunction with an equation of state for the gases. Acceleration calculations showing the displacement as a function of time or speed are important when estimating the effects of venting in a perforated casing. Henry (1967) and Jones et al. (1980) calculate the acceleration of the casing for various sandwich configurations. Kornhauser (1981) published an extension of Henry's model for improved explosive casing expansion.

Note that the Gurney method does not consider the propagation of shock waves through metals, but only the terminal effect of the shock propagation. Duvall (1963) provides an excellent description of shock wave propagation, transmission, and reflection. He describes a plane wave lens, a plane wave generator, and methods of forming oblique shock waves. He also states the pressure levels attained by the various methods of shock wave generation. Duvall's (1963) article explains shock wave phenomena without recourse to advanced mathematical concepts. Thus, Duvall (1963) is an excellent introductory article for the layman. Courant and Friedrichs (1948) provide an excellent mathematical treatment of shock wave physics. Shock wave propagation through solid media is an important aspect of explosive–metal interaction but is beyond the scope of this introductory book.

An extension of the Gurney method was given recently by Chanteret (1983). Chanteret developed an analytical model for symmetrical geometries with energy partitioning during expansion. This model allows a calculation of the Gurney energy as a function of the expansion ratio. The expansion ratio is $(R/R_0)^n$ where R is the current value of the radius of the explosive–metal interface and R_0 is the undetonated radius of the explosive–metal interface. The constant n depends on the geometric configuration ($n = 1$ for symmetrical plane sandwiches, and $n = 2$ for cylinders with a constant wall thickness). Chanteret's results can be used in conjunction with the classical Gurney

formulas to obtain the entire velocity–time curve for all symmetrical steady-state configurations. Also, Chanteret extended the Gurney model to include imploding cylinders by introducing a fictitious rigid boundary in the explosive cylinder. The results are claimed to agree well with available experimental data and two-dimensional hydrocode results.

Hennequin (1986) used the HEMP code to guide the development of an analytical model that accurately predicted the distribution of velocities of the fragments from a cylindrical warhead initiated at one end. The influence of the end closures was taken into account.

Yadav et al. (1986) solved the equation of motion for an incompressible metal plate, accelerated by a plane detonation wave with a general value of the adiabatic exponent γ in the detonation products equation of state. The effect of γ on the terminal velocity of the plate was investigated. The adiabatic exponent was determined to be 2.8 from measured flyer plate velocities at various C/M ratios. The flyer plate velocity decreases as γ decreases and γ decreases as the explosive density decreases. This may explain the difference between theoretical and experimental flyer plate velocities when the plate is accelerated by a low-density explosive as observed by Deribas et al. (1967).

Butz et al. (1982) measured fragment terminal velocities from symmetric sandwich configurations with low values of the metal–explosive mass ratio. The M/C ratio was varied from 0.05 to 0.175, and the Gurney equation as well as the Taylor angle formula were found to adequately predict the low M/C experimental results.

Fucke et al. (1987) and Bol and Honcia (1977) measured flying plate velocities for high values of the metal–explosive mass ratio. Fucke et al. (1987) added correction terms to the Gurney formula for an asymmetric sandwich with $M/C > 10$. These correction terms were designed to account for plate thicknesses, lateral plate dimensions, and the structure of the explosive layer. The structure of the explosive layer is specified by the type of explosive used and the fraction of the volume between the plates that is filled with explosive.

The Gurney method is one dimensional, ignores rarefaction effects, and ignores the shock characteristics of metals. Thus, one can expect errors to occur when these effects are important. An example is a short, open-ended cylinder that deviates from the Gurney prediction near its ends. This deviation results from the fact that short cylinders introduce two-dimensional effects.

Also, the difference in shock impedance between different metals will alter the energy coupling, and as a result, the same M/C ratios with different metals but with the same explosive will yield different velocity histories. However, the final plate velocity is achieved after multiple shock reflections in the plate, which damps out shock impedance differences. Thus, the Gurney method predicts accurate final plate velocities but does not address early time plate motion.

Several other Gurney-like formulas relating to flat plates and imploding devices have been developed. A representative few of these expressions are given in the following paragraphs.

For shaped charge studies, which will be addressed in detail in the next chapter, a popular formula for a single flat plate backed by a slab of explosive is given by Chou and Flis (1986) as

$$V_0 = \sqrt{2E}\left[\frac{3}{4\mu^2 + 5\mu + 1}\right]^{1/2}, \tag{13}$$

where $\mu = M/C$ and V_0 is the liner collapse velocity. Equation (13) applies to the same geometry as Eq. (7), the Gurney equation for an open-faced sandwich. For this same configuration, with the detonation wave (of velocity D) propagating in a direction tangent to the liner, Duvall et al. (1958, 1969), used the hydrodynamic theory to obtain the collapse velocity formula

$$V_0 = D\left[1 + \frac{27\mu}{16}\left(1 - \sqrt{1 + 32/(27\mu)}\right)\right]. \tag{14}$$

Kleinhanss (1971) also presented Eq. (14) as well as another formula, credited to Trinks, based on semi-empirical data related to the explosive launching of plates

$$V_0 = 0.36D \arctan\left(\frac{2}{3\mu}\right). \tag{15}$$

These formulas were developed for flat plates, and although they are quite accurate, they do not account for the effect of curvature such as in implosive geometries, for example, a conical shaped charge. Kleinhanss, in experiments with imploding cylindrical charges, showed a strong dependence of the liner collapse velocity (V_0) on its radius. He obtained the semi-empirical formula

$$V_0 = D\left[\frac{r_i - \sqrt{\varepsilon(2r_i - \varepsilon)}}{r_i - \varepsilon} \cdot \frac{1}{(C_0 + \varepsilon f(b))}\right], \tag{16}$$

where ε is the metal thickness, $b = r_0 - r_i$, r_0 and r_i being the outer and inner explosive radii, respectively, and thus b is the explosive thickness. Empirical constants C_0 and $f(b)$ depend on the type of explosive and metal being used. Other studies on implosive geometries were given by Chanteret (1983) as discussed earlier, Chou et al. (1981), and Hennequin (1983). All of these studies provide improved results over the basic Gurney model for implosive geometries.

Other formulas are available for plate acceleration and are often used in shaped charge liner collapse and explosive welding models. For example, Singh (1956) considers the velocity of the casing of a thin-walled cylinder filled with explosive and detonated at one end. The velocity of the casing at the time of fracture is given by

$$V_0 = \frac{D}{4}(1 + \sin\alpha), \tag{17}$$

where each element of the casing subtends an angle α with the axis of propagation of detonation.

Deribas (1972) gives

$$V_0 = 1.2D\left[\frac{\sqrt{1 + 32/(27\mu)} - 1}{\sqrt{1 + 32/(27\mu)} + 1}\right], \tag{18}$$

where μ again is the mass to charge ratio and V_0 is the plate velocity. Equation (18), except for the factor of 1.2, is identical to Eq. (14) as can be shown by simple algebraic manipulation. Deribas (1972) conducted several experiments using low detonation velocity granular explosives and flyer plates of several different materials. The factor of 1.2 was added to the equation to improve the agreement with the experimental data.

Shushko et al. (1975) give

$$V_0 = 0.61D\left[\frac{18\mu^2 + 12\mu + 1 - 6\mu\sqrt{9\mu^2 + 12\mu + 2}}{1 + 6\mu}\right]. \tag{19}$$

Mikhailov and Dremin (1974) provide several frequently used expressions for the metal plate speed. They include

$$\frac{V_0}{D} = \frac{\sqrt{1 + 32/(27\mu)} - 1}{\sqrt{1 + 32/(27\mu)} + 1},$$

which is identical to Eq. (14), derived from hydrodynamic theory assuming that the ratio of specific heats or adiabatic exponent of the explosive products (γ) is equal to 3 (Duvall et al. 1958, 1969; Deribas 1972; Mikhailov and Dremin 1974), and

$$V_0 = \frac{0.602D}{1 + 2\mu}.$$

Also, Aziz et al. (1961) made theoretical predictions of a flying plate velocity by considering a rigid piston under detonation loading. The terminal piston (metal) velocity was given as Eq. (14) with μ interpreted to be the piston mass to explosive mass ratio. Again, hydrodynamic theory was used for $\gamma = 3$. Note that the choice of $\gamma = 3$ allows a particularly easy solution of the hydrodynamic equations using the method of characteristics. Complete details as well as more realistic values of γ are given by Hirschfelder et al. (1954).

Smith et al. (1971) used formulas analogous to Eq. (7) and (18) to determine the terminal velocity of flyer plates used in plate acceleration experiments. Smith et al. (1971) also calculated the flyer plate terminal bend angle, which will be discussed shortly. Both the bend angles and flyer plate terminal velocities are in agreement with the experimental values obtained from three different low-velocity, granular explosives.

Explosive–metal interaction models are also useful in fragmentation calculations. Fragmentation, of course, does not always result from an explosive–metal interaction. For example, fragments are generated when gas-pressurized pipes or vessels fail. A knowledge of the velocity of the fragments following a gas-pressurized system failure is necessary in order to determine the damage to neighboring equipment or structures. Fragment velocities resulting from a

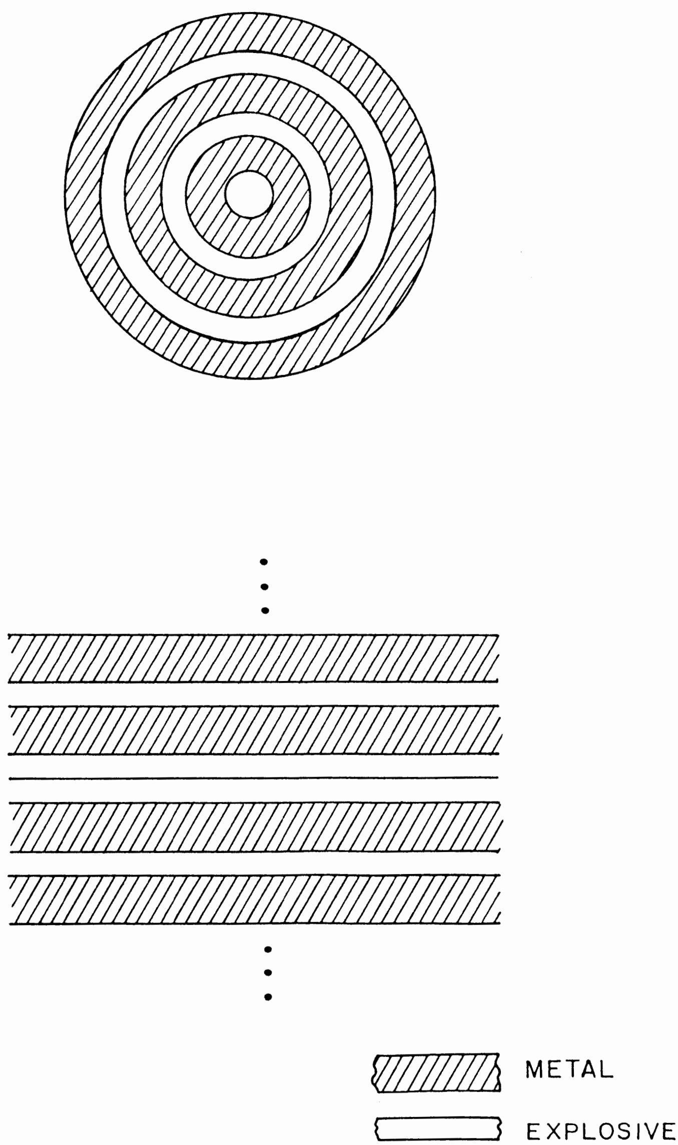

Figure 8. The jelly roll (top) and the dagwood (bottom) configurations.

pressurized pipe or vessel failure are usually predicted by the Moore equation (Moore 1967). The Moore equation is semi-empirical based on experimental data from the velocity of explosively generated fragments (i.e., Gurney data).

Another method for estimating the fragmentation velocity from ruptured pipes or vessels follows from the theoretical model of Baum (1984). Also, Baker et al. (1977, 1980) published voluminous manuals dealing with fragmentation resulting from the bursting of pressure vessels and other structures.

Of course, other Gurney-like models are also available. The literature on explosive welding and on jet formation provides references to other metal acceleration models. Walters (1979) and Walters and Harrison (1980) provide several references (mostly Soviet) related to the acceleration of metals by high explosives. Dehn (1984) published an overview of Gurney-type velocity approximation models as well as the Taylor angle (grazing incidence) models. Dehn provides additional historical information and correctly analyzes geometric configurations such as the jelly roll, the dagwood, and similar explosive–metal multilayer arrangements. The jelly roll and dagwood configurations (Dehn 1984) are shown in Figure 8. Henry (1967) also discusses the jelly roll and other geometries.

Basically, none of the Gurney-like models provide significant improvement over the basic Gurney expressions, but they serve to extend the Gurney method to geometries not covered by the Gurney assumptions, for example, implosive geometries, or extension of the M/C range of validity.

Finally, care must be taken in comparing the various explosive–metal interaction formulas with respect to geometries considered and the applicable M/C range. Also, many authors use M/C as a key parameter. Other authors prefer C/M as the parameter. In fact, in this book, the authors converted all expressions with C/M as a parameter to M/C.

In Chapter 5, where shaped charge liner collapse is discussed, additional plate push or Gurney-like models will be discussed, especially for the case where grazing detonation waves occur.

4.3. THE TAYLOR ANGLE APPROXIMATION

The Gurney equations assume that the metal moves in a direction normal to its surface. This is true when the detonation wave encounters the metal at normal incidence. It is not true when the detonation wave encounters the metal plate at a grazing incidence. The grazing incidence is treated by another model known as the Taylor angle approximation.

The Taylor approximation (Taylor 1941) is shown in Figure 9, which depicts a grazing (parallel) incidence of the detonation wave to the metal surface. The plate is deflected at an angle θ from its initial position. Acceleration of the metal to its final velocity is assumed to be instantaneous. For this steady-state condition, the metal plate is assumed to undergo pure rotation,

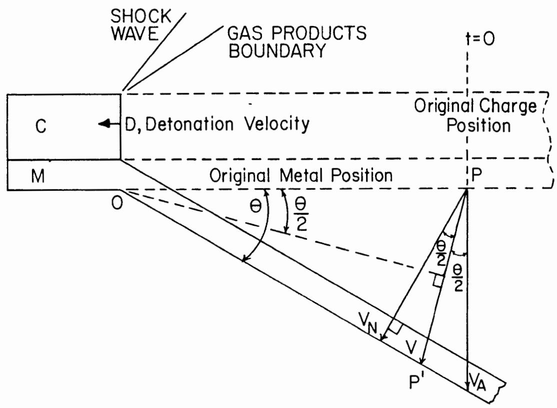

Figure 9. Direction of metal projection by a grazing detonation wave.

that is, no net shear flow or no change in length or thickness. Thus, the plate element that was at P initially will be at P' after launch and the lengths $\overline{OP} = \overline{OP'}$.

As shown in Figure 9, a line was constructed from O, perpendicular to $\overline{PP'}$. This line bisects the angle θ since OPP' is an isosceles triangle. If the time t is measured from the time when the detonation wave passes point P, then

$$\overline{OP} = Dt,$$

$$\overline{PP'} = Vt$$

and

$$\sin\frac{\theta}{2} = \frac{\overline{PP'}/2}{\overline{OP}} = \frac{Vt}{2Dt} = \frac{V}{2D}, \tag{20}$$

as shown in Figure 10. An estimate of the direction in which the metal plate is projected is the angle $\theta/2$, which can be determined from Eq. (20) with V known from the Gurney method and D determined from the specified explosive. As the plate moves, it will be tilted at an angle θ from its initial position and, by assumption, will not be rotating.

When using a streak camera located perpendicular to the initial charge axis, a component of the velocity, namely V_A, the apparent velocity, was measured by Kury et al. (1965). This velocity can be related to V by the geometry shown in Figure 11 or

$$V_A = D\tan\theta, \tag{21}$$

then

$$\frac{V}{V_A} = \frac{2D\sin\theta/2}{D\tan\theta} = \frac{2\sin\theta/2}{\sin\theta/\cos\theta} = \frac{\cos\theta(2\sin\theta/2)}{2\sin(\theta/2)\cos(\theta/2)},$$

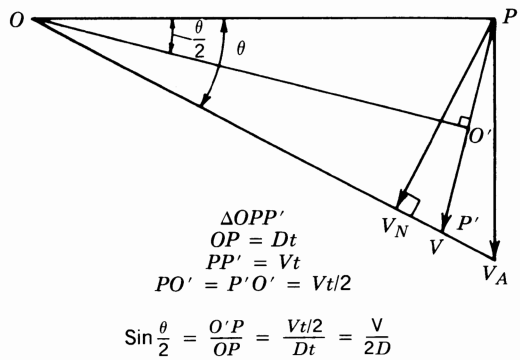

Figure 10. Taylor angle computational details.

or

$$\frac{V}{V_A} = \frac{\cos\theta}{\cos\theta/2}. \tag{22}$$

Hoskin et al. (1965) expressed their results in terms of the velocity component V_N, the velocity component normal to the flight plane of the plate, since this velocity is of interest when the flying plate is used in impact studies. Since the angle between V_A and V_N is θ, then

$$V_N = D\sin\theta, \tag{23}$$

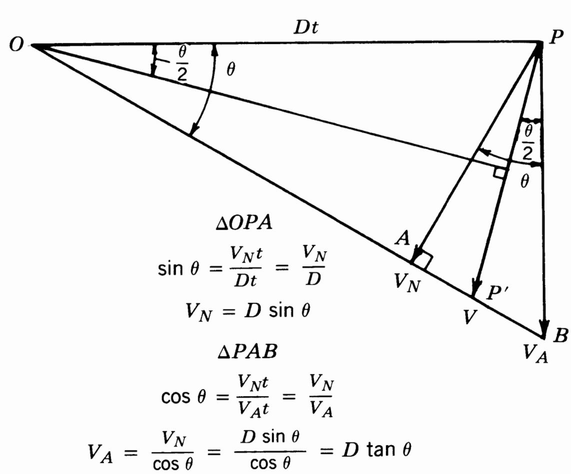

Figure 11. Expressions for the apparent velocity, V_A, and the velocity component normal to the flight plane, V_N.

and

$$\frac{V}{V_N} = \frac{2D\sin\theta/2}{D\sin\theta} = \frac{1}{\cos\theta/2} = \sec\frac{\theta}{2}, \tag{24}$$

from Figure 11. The difference between V, V_N, and V_A is usually only a few percent. Also, the term $V/2D$ is approximately the same for many explosives. Thus, θ is approximately constant. If the mass of the plate (its thickness) being driven is fixed, then increasing the detonation velocity of the explosive implies an increase in the plate velocity such that $V/2D$ is approximately constant. These concepts are used to analyze jet formation.

4.4. APPLICABILITY OF THE GURNEY AND TAYLOR METHODS

Karpp and Predebon (1974, 1975) showed that fragment velocity predictions based on the Gurney and Taylor formulas are adequate for cases when the flow is one dimensional (radial) and for practical ranges of charge to metal

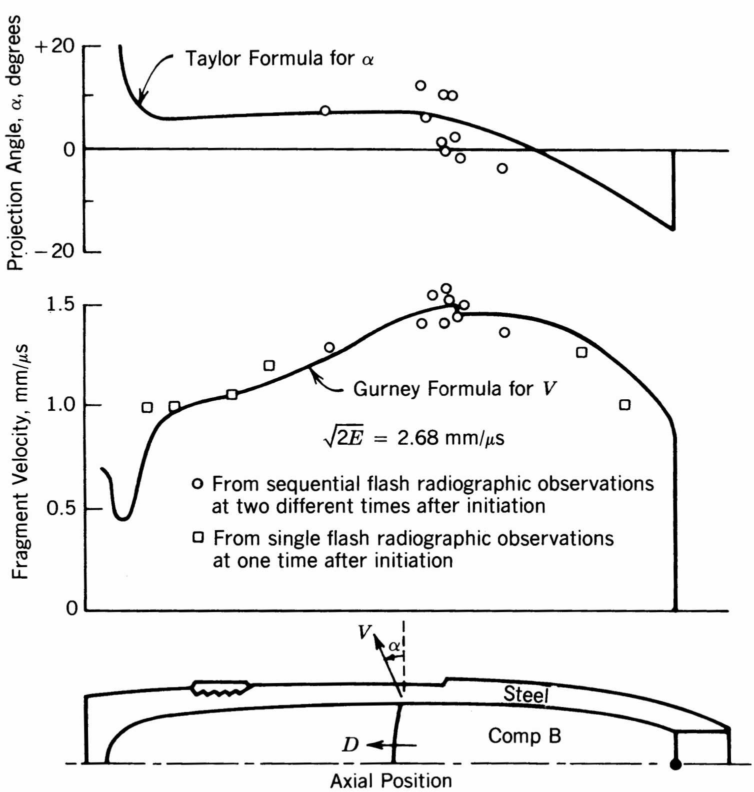

Figure 12. Comparison of Gurney and Taylor formula predictions with experimental data (Karpp and Predebon 1975).

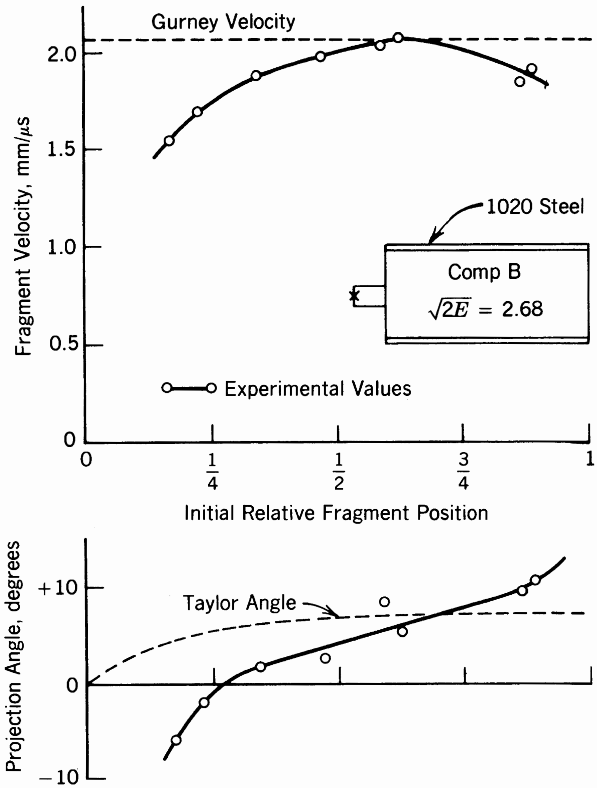

Figure 13. Comparison of Gurney and Taylor formula predictions with experimental data (Karpp and Predebon 1975).

ratios ($0.1 < C/M < 2$). An example is shown in Figure 12. Note that for an axisymmetric explosive–metal system with a variable diameter, the C/M ratio is computed locally as a function of axial position. Thus, the speed computed from the Gurney formula varies with axial position. Also, in the Taylor angle formula for the projection angle, both the fragment speed and the rate at which the detonaton wave traverses the casing varies with axial position. The agreement between the Gurney and Taylor angle predictions and the experimental data for the typical HE projectile shown in Figure 12 is quite good.

However, for a two-dimensional case the agreement between theory and data is not good. Figure 13 shows the Taylor angle and Gurney velocity compared to experimental data for a steel cylinder with length to diameter ratio of 2 filled with Comp B explosive and initiated on axis at one end. Figure 13 illustrates the degree to which end effects may influence the fragment speed and projection angle.

The standard cylinder test developed by the Lawrence Livermore National Laboratory provides a great deal of data on the expansion of explosive-filled cylinders (Lee et al. 1968). These standard cylinder tests used three different

explosive fills, namely, TNT, Comp B, and Octol, and three different cylinder materials, namely, copper, stainless steel, and mild steel. Karpp and Predebon (1975) observed that for most of the data, nearly all of the metal acceleration has occurred when the expansion ratio $R/R_0 = 2$. Even at $R/R_0 = 1.75$ at least 92% of the final velocity has been achieved. Here, R is the current radius of the casing and R_0 is the initial radius of the casing. Nevertheless, it was deemed desirable to include the effects of gas leakage in time-dependent, two-dimensional hydrocode calculations to obtain accurate predictions of fragment velocities especially in the regions influenced by end rarefaction waves.

Karpp and Predebon (1974, 1975) used the HEMP two-dimensional, transient, finite-difference hydrocode to model naturally fragmenting munitions. The JWL (Jones, Wilkins, Lee) equation of state (Lee et al. 1968), discussed in Chapter 11, was used for the explosive, the cylinder was modeled as an elastic-plastic material, and a gas leakage model was developed and used in conjunction with the HEMP code. The gas leakage model was designed to simulate explosive gas leakage around fragments after casing breakup. Comparisons were given between the code calculations and experimental data. The experimental data was obtained from cylinders of various steels with $L/D = 2$. The explosive fills were TNT, Comp B, and Octol. The C/M, for each explosive fill, was 0.4 and 0.8. The experimental details are given by Karpp et al. (1973). The agreement between the data and the code calculations, with the gas leakage model, was excellent. Again, the Gurney and Taylor angle formulas exhibit poor agreement for these two-dimensional cases.

It is the authors' recommendation that two-dimensional explosive–metal interaction problems be addressed with a two-dimensional computer code with a gas leakage model such as used by Karpp and Predebon (1974, 1975) or with an analytical/semi-empirical model derived for the exact problem under consideration.

REFERENCES

Aziz, A. K., Hurwitz, H., and Sternberg, H. M. (1961), "Energy Transfer to a Rigid Piston under Detonation Loading," *Phys. Fluids*, *4*(3): 380–384.

Baker, W. E., Kulesz, J. J., Ricker, R. E., Bessey, R. L., Westine, P. S., Parr, V. B., and Oldham, G. A. (1977), "Workbook for Predicting Pressure Wave and Fragment Effects of Exploding Propellant Tanks and Gas Storage Vessels," NASA Contractor Report, NASA CR-134906, NASA Lewis, September.

Baker, W. E., Westine, P. S., Kulesz, J. J., Wilbeck, J. S., and Cox, P. A. (1980), "A Manual for the Prediction of Blast and Fragment Loadings on Structures," DOE/TIC-11268, November (AD A111849).

Baum, M. R. (1984), "The Velocity of Missiles Generated by the Disintegration of Gas-Pressurized Vessels and Pipes," *J. Pressure Vessel Tech., Trans. ASME*, *106*(Nov.): 362–368.

Bol, J. and Honcia, G. (1977), "Velocity of H.E. Accelerated Plates for Low Values of α," *Proc. 3rd Int. Symp. on Ballistics*, Karlsruhe, Germany, March.

Butz, D. J., Backofen, J. E., and Petrousky, J. A. (1982), "Fragment Terminal Velocities from Low Metal to Explosive Mass Ratio Symmetric Sandwich Configurations," *J. Ballistics*, *6*(1): 1304–1323.

Chanteret, P. Y. (1983), "An Analytical Model for Metal Acceleration by Grazing Detonation," *Proc. 7th Int. Symp. on Ballistics*, The Hague, Netherlands, April.

Chou, P. C., and Flis, W. J. (1986), "Recent Developments in Shaped Charge Technology," *Propell. Explos. Pyrotech. 11*: 99–144.

Chou, P. C., Carleone, J., Hirsch, E., Flis, W. J., and Ciccarelli, R. D. (1981), "Improved Formulas for Velocity, Acceleration and Projection Angle of Explosively Driven Liners," *Proc. 6th Int. Symp. on Ballistics*, Orlando, FL, October 27–29.

Courant, R., and Friedrichs, K. O. (1948), *Supersonic Flow and Shock Waves*, New York: Wiley-Interscience.

Dehn, J. T. (1984), 'Models of Explosively Driven Metal," BRL Technical Report, BRL-TR-2626, December.

Deribas, A. A. (1972), *Physics of Explosive Work-Hardening and Welding*, Novosibirsk: Nauka.

Deribas, A. A., Kudinow, V. M., Matveenkov, F. I., and Simonov, V. A. (1967), *Combus., Explos. Shock Waves*, *3*: 182–186.

Dobratz, B. M. (1982), "LLNL Explosives Handbook. Properties of Chemical Explosives and Explosive Stimulants," LLNL Report UCRL-52997, March 1981, with Errata dated January 1982.

Duvall, G. E. (1963), "Shock Waves in Solids," *Internat. Sci. Tech.*, April, New York: Conover-Mast.

Duvall, G. E., and Erkman, J. O. (1958), Technical Report No. 1, Stanford Research Institute, No. GU-2426.

Duvall, G. E., Erkman, J. O., and Ablow, C. M. (1969), "Explosive Acceleration of Projectiles," *Israel J. Tech.*, *7*(6): 469–475, January (AD 709810).

Fucke, W., Bol, J., and Schumann, St. (1987), "Velocity of Sandwich Plates Driven by Thin H.E. Layers," *Proc. 10th Int. Symp. on Ballistics*, Vol. 2, San Diego, October.

Gurney, R. W. (1943), "The Initial Velocities of Fragments from Bombs, Shells and Grenades," BRL Report 405, September.

Gurney, R. W. (1947), "Fragmentation of Bombs, Shells and Grenades," BRL Report 635, March.

Hennequin, E. M. (1983), "Analytical Model of the Shaped Charge Liner Collapse," *Proc. 7th Int. Symp. on Ballistics*, The Hague, Netherlands, April 19–21.

Hennequin, E. M. (1986), "Influence of the Edge Effects on the Initial Velocity of Fragments From a Warhead," *Proc. 9th Int. Symp. on Ballistics*, Shrivenham, U.K., April–May.

Henry, I. G. (1967), "The Gurney Formula and Related Approximations for the High-Explosive Deployment of Fragments," Hughes Aircraft Company, Culver City, CA, Report No. PUB-189, April (AD 813398).

Hirsch, E. (1986), "Improved Gurney Formulas for Exploding Cylinders and Spheres Using Hard Core Approximation," *Propell., Explos., Pyrotech.*, *11*: 81–84.

Hirschfelder, J. O., Curtiss, C. F., and Bird, R. B. (1954), *Molecular Theory of Gases and Liquids*, New York: Wiley.

Hoskin, N. E., Allan, J. W. S., Bailey, W. A., Lethaby, J. W., and Skidmore, I. C. (1965), "The Motion of Plates and Cylinders Driven by Waves at Tangential Incidence," *The Fourth Symposium on Detonation Preprints*, Vol. I, NOL, MD, October.

Jones, G. E., Kennedy, J. E., and Bertholf, L. D. (1980), "Ballistics Calculations of R. W. Gurney," *Am. J. Phys.*, *48*(4): 264–269.

Karpp, R. R., and Predebon, W. W. (1974), "Calculation of Fragment Velocities from Fragmenting Munitions," *First Int. Symp. on Ballistics*, Orlando, FL, November.

Karpp, R. R., and Predebon, W. W. (1975), "Calculations of Fragment Velocities from Naturally Fragmenting Munitions," BRL Memorandum Report No. 2509, July.

Karpp, R. R., Kronman, S., Dietrich, A. M., and Vitali, R. (1973), "Influence of Explosive Parameters on Fragmentation," BRL Memorandum Report 2330, October.

Kennedy, J. E. (1970), "Gurney Energy of Explosives: Estimation of the Velocity and Impulse Imparted to Driven Metal," Sandia National Laboratories, SC-RR-70-790, December.

Kleinhanss, H. R. (1971), "Experimentelle Untersuchungen Zum Kollapsprozess bei Hohlladungen," *Proc. Third Int. Symp. on Military Applications*, FRG, September, 1971, and FSTC-HT-23-794-73, March, 1973.

Kornhauser, M. (1981) "An Improved Approximate Model of Explosive Casing Expansion," *Proceedings of the Seventh Symposium (International) on Detonation*, Naval Surface Weapons Center, June.

Kury, J. W., Hornig, H. C., Lee, E. L., McDonnel, J. L., Ornellas, D. L., Finger, M., Strange, F. M., and Wilkins, M. L. (1965), "Metal Acceleration by Chemical Explosives," *The Fourth Symposium on Detonation Preprints*, Vol. I, NOL, MD. October.

La Rocca, E. W. (1980), "Advances in Predicting the Relative Power of High Explosives and the Correlation with Fragment Velocity," General Dynamics, TM-6-348-1.13-4, October 28.

Lee, E. L., Hornig, H. C., and Kury, J. W. (1968), "Adiabatic Expansion of High Explosive Detonation Products," UCRL-50422, May 2.

Meyer, R. (1977), *Explosives*, Weinheim and New York: Verlag Chemie.

Mikhailov, A. N., and Dremin, A. N. (1974), "Flight Speed of a Plate Propelled by Products From a Sliding Detonation," *Fizika Goreniya i Vzryva*, *10*(6): 877–884.

Moore, C. V. (1967), *Nuclear Engineering and Design*, Vol. 5, pp. 81–97.

Shushko, L. A., Shekhter, B. I., and Krys'kov, S. L. (1975), "Bending of a Metal Strip by a Sliding Detonation Wave," *Fizika Goreniya i Vzryva*, *11*(2): 264–274.

Singh, S. (1956), "Spatial Distribution of Fragments of Explosively Loaded Thin-Walled Steel Cylinders," *Proc. Phys. Soc., London*, *69*: 1089–1094.

Smith, Jr., E. G., Laber, D., and Linse, V. D. (1971), "Explosive Plate Acceleration Studies Using a Dual-Channel Flash X-Ray Technique," *The Third International Conference of the Center for High Energy Forming*, Vail, Colorado, July.

Sterne, T. E. (1947), "A Note on the Initial Velocities of Fragments from Warheads," BRL Report 648, September.

Sterne, T. E. (1951), "The Fragment Velocity of Spherical Shell Containing an Inert Core," BRl Report 753, March.

Taylor, G. I. (1941), "Analysis of the Explosion of a Long Cylindrical Bomb Detonated at One End," in *The Scientific Papers of Sir Geoffrey Ingram Taylor*, Vol. III, G. K. Batchelor (ed.), Cambridge: University Press, 1963.

Thomas, L. H. (1944), "Theory of the Explosion of Cased Charges of Simple Shape," BRL Report 475, July.

UCRL (1965), "Properties of Chemical Explosives," University of California, Lawrence Radiation Laboratory, UCRL-14592, December.

Walters, W. P. (1979), "Influence of Material Viscosity on the Theory of Shaped Charge Jet Formation," BRL Memorandum Report, ARBRL-MR-02941, August.

Walters, W. P., and Harrison, J. T. (1980), "Modeling of the Shaped Charge Jet Formation," *Proceedings of the Army Symposium on Solid Mechanics, 1980—Designing for Extremes: Environment, Loading and Structural Behavior*, AMMRC MS 80-4, September.

Yadav, H. S., Kamat, P. V., and Sundaram, S. G. (1986), "Study of an Explosive-Driven Metal Plate," *Propell., Explos., Pyrotech., 11*: 16–22.

CHAPTER 5

SHAPED CHARGE JET FORMATION

Birkhoff et al. (1948) formulated the first theory of conical shaped charge jet formation assuming that the detonation wave produces such large pressures during the collapse process that the material strength of the liner may be neglected. The calculation given in Appendix A justifies this assumption. In fact, the liner is treated as an inviscid, incompressible fluid. The conical liner is modeled as a wedge, and a steady-state collapse model is assumed. Thus, the liner elements are instantaneously accelerated to their final collapse velocity. The steady-state model predicted a jet with a constant length equal to the slant height of the cone. It has been observed, however, that the shaped charge jets possess a velocity gradient with the tip traveling much faster than the tail, causing the jet to stretch and eventually break up. This steady-state theory was later modified by Pugh et al. (1952) to include the jet velocity gradient. The modified "nonsteady" theory is based on the same principles as the original theory except that the velocity at which the various liner elements collapse is not constant but depends on the original position of the element in the liner. An examination of the Birkhoff et al. (1948) steady-state model follows.

5.1. THE BIRKHOFF ET AL. THEORY

As the detonation wave impacts the conical liner, the pressure on all sides of the liner is assumed to be equal and the liner walls are assumed to collapse inward at a constant velocity, say V_0. The angle 2β between the moving walls is greater than the original apex angle 2α because of the finite time required for the detonation wave to sweep the liner surface from apex to base. Figure 1 describes the geometry of the collapse process. The conical liner is symmetric

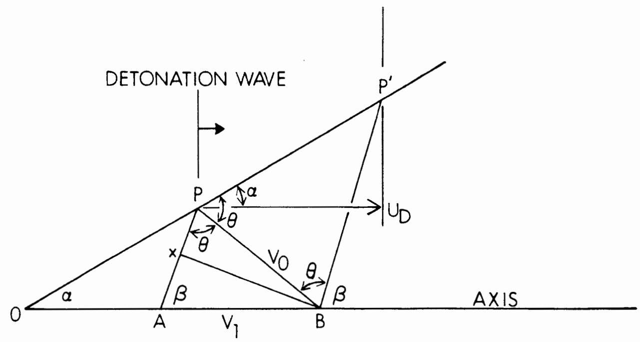

Figure 1. Geometry of the collapse process (Birkhoff et al. 1948).

so α represents one-half of the liner apex angle and β represents the collapse angle. The liner assumes a velocity V_0, which bisects the angle APP' of Figure 1. To show this, consider a coordinate system having a constant velocity such that the origin moves from point P to P' in a unit time. In this coordinate system, steady-state conditions exist at the origin and the liner moves inward along $\overline{P'P}$ and flows outward along the path $\overline{PA}$. The velocity of the liner passing through this region changes its direction but not its magnitude because the pressure forces are everywhere perpendicular to the motion. $\overline{P'P}$ and $\overline{P'B}$ represent the entering and emerging velocities, respectively, of the liner in the moving coordinate system. $\overline{P'B}$ is constructed parallel to $\overline{PA}$ and $\overline{P'P}$ and $\overline{P'B}$ are equal in magnitude. Since the velocity in the moving coordinate system is $\overline{PP'}$, the velocity of the collapsing liner in the stationary system is the vector sum

$$\overline{PP'} + \overline{P'B} = \overline{PB} = V_0.$$

Since $\overline{P'P} = \overline{P'B}$, the triangle BPP' is isosceles and since $\overline{P'B}$ is parallel to $\overline{PA}$, $\measuredangle BPP' = \measuredangle PBP' = \measuredangle BPA$. Call these angles θ. Thus, V_0 bisects angle APP' as claimed earlier.

The walls of the collapsing liner are two planes moving inward. The junction of these planes moves from A to B with a velocity V_1:

$$V_1 = \frac{V_0 \cos[(\beta - \alpha)/2]}{\sin \beta}. \tag{1}$$

This follows from Figure 1, where $\measuredangle OPA = \phi$ and $\alpha + \phi + 180 - \beta = 180$ or $\phi = \beta - \alpha$, that is, the sum of the angles of a triangle equals 180°. The line segment $\overline{XB}$ is constructed perpendicular to $\overline{PA}$. The angle γ is defined to be $\measuredangle XBP$. Next, consider the triangle PXB where $180 = 90 + \theta + \gamma$ or $\gamma = 90 - \theta$. In triangle XAB, $180 = 90 + \beta + \measuredangle ABX$ or $\measuredangle ABX = 90 - \beta$. Then

along the line $\overline{OPP'}$,

$$2\theta + \phi = 180, \quad \text{or} \quad \theta = 90 - \frac{\phi}{2} = 90 - \left(\frac{\beta - \alpha}{2}\right),$$

from above. Then since $\gamma + \theta = 90$,

$$\gamma + 90 - \left(\frac{\beta - \alpha}{2}\right) = 90 \quad \text{or} \quad \gamma = \left(\frac{\beta - \alpha}{2}\right).$$

Angle $PP'B = \phi$ since in triangle $PP'B$ we have $2\theta + \measuredangle PP'B = 180$ or $180 - \phi + \measuredangle PP'B = 180$ or $\measuredangle PP'B = \phi$. This establishes the geometry of Figure 1. Now for some trigonometry.

In triangle APB by the law of sines, $V_1/\sin\theta = V_0/\sin\beta$ or $V_1 = V_0 \sin\theta/\sin\beta$. The

$$\sin\theta = \sin\left[90 - \left(\frac{\beta - \alpha}{2}\right)\right] = \cos\left(\frac{\beta - \alpha}{2}\right)$$

and

$$V_1 = \frac{V_0 \cos[(\beta - \alpha)/2]}{\sin\beta} = \frac{V_0 \cos(\phi/2)}{\sin\beta}. \tag{2}$$

A moving observer positioned at A would observe any point P in the upper plane approaching him with a velocity $V_1 \cos\beta + V_0 \cos\theta$. This velocity, V_2, becomes

$$V_2 = V_1 \cos\beta + V_0 \cos\left[90 - \left(\frac{\beta - \alpha}{2}\right)\right] = V_1 \cos\beta + V_0 \sin\left(\frac{\beta - \alpha}{2}\right),$$

and from Eq. (2),

$$V_2 = V_0 \left\{\frac{\cos[(\beta - \alpha)/2]}{\tan\beta} + \sin\left(\frac{\beta - \alpha}{2}\right)\right\}. \tag{3}$$

Also $U_D = U\cos\alpha$ where U is along $\overline{PP'}$ and using the law of sines for triangle PBP',

$$\frac{V_0}{\sin(\beta - \alpha)} = \frac{U}{\sin\theta},$$

or

$$U = \frac{V_0}{\sin(\beta - \alpha)} \sin\left[90 - \left(\frac{\beta - \alpha}{2}\right)\right] = \frac{V_0 \cos[(\beta - \alpha)/2]}{\sin(\beta - \alpha)},$$

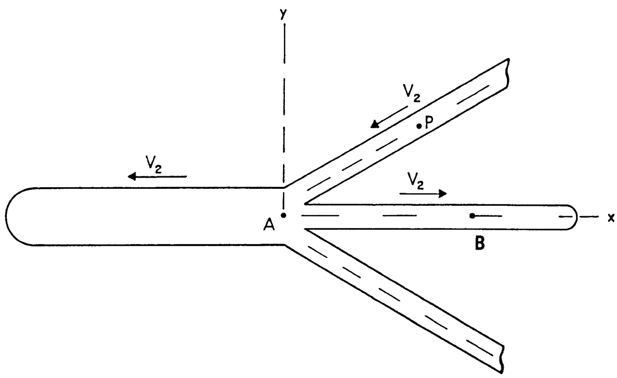

Figure 2. The formation of a jet and slug by a wedge from the point of view of an observer stationed at the moving junction at A (Birkhoff et al. 1948).

then

$$\frac{U_D}{\cos\alpha} = \frac{V_0\cos[(\beta - \alpha)/2]}{\sin(\beta - \alpha)}. \tag{4}$$

Returning to V_2 from Eq. (3), the observer sees a "jet" moving to his right and a "slug" moving to his left, as in Figure 2. Also, as viewed by this observer, the whole process appears to be unchanged by the lapse of time, or steady-state motion exists. This, with the earlier assumptions of inviscid, incompressible, and one-dimensional flow allows the use of the Bernoulli equation or

$$P + \tfrac{1}{2}\rho_0 U^2 = \text{const.}, \tag{5}$$

which relates the pressure and the corresponding velocity U. The pressure at any point in the liner determines the velocity at that point. Assume the liner moves away from the detonation so fast that the pressure of the surface decreases rapidly, and the pressure on all surfaces of the collapsing liner is constant. This allows free streamlines, that is the boundary streamlines are at constant pressure and density (and hence velocity). As viewed by the observer, the jet and slug will appear to recede with exactly the same speed, V_2, as the walls approach in Figure 2.

Returning to the stationary system of coordinates, it is seen that the jet, traveling to the right in Figure 2, has a velocity

$$V = V_1 + V_2,$$

while the slug, traveling to the left in the moving system of Figure 2, has a velocity to the right given by

$$V_s = V_1 - V_2.$$

To further visualize this process consider that the point P (fixed in the upper plane) travels to point B (fixed in space) in unit time. The material from the inner surface of the upper plane included between $\overline{PA}$ and $\overline{AB}$ moves into the jet, and the front of the jet moves to the right a distance $\overline{PA} + \overline{AB}$ in the same time, forming a high-velocity jet. This jet velocity is $V = V_1 + V_2$ and from Eqs. (2) and (3):

$$V = V_0\left\{\frac{\cos[(\beta - \alpha)/2]}{\sin\beta} + \frac{\cos[(\beta - \alpha)/2]}{\tan\beta} + \sin\left(\frac{\beta - \alpha}{2}\right)\right\}. \tag{6}$$

Also, the outer surface of each plane forms a slug moving with the lower velocity $V_s = V_1 - V_2$ or

$$V_S = V_0\left\{\frac{\cos[(\beta - \alpha)/2]}{\sin\beta} - \frac{\cos[(\beta - \alpha)/2]}{\tan\beta} - \sin\left(\frac{\beta - \alpha}{2}\right)\right\}. \tag{7}$$

Conservation of momentum dictates the division of material between the jet and the slug. Let m be the total liner mass per unit length of the two collapsing planes (sides of the wedge) approaching the junction. Let m_j represent that part of the liner mass entering the jet and m_s represent that part entering the slug, so

$$m = m_j + m_s. \tag{8}$$

Equating the horizontal momentum components entering and leaving junction A of Figure 2 in the moving coordinate system yields

$$mV_2\cos\beta = m_sV_2 - m_jV_2. \tag{9}$$

Solving Eqs. (8) and (9) simultaneously gives

$$m_j = \tfrac{1}{2}m(1 - \cos\beta), \tag{10}$$

and

$$m_s = \tfrac{1}{2}m(1 + \cos\beta). \tag{11}$$

According to this model, the velocities of the jet and slug and their cross-sectional areas are constant.

The analysis assumed a wedge configuration. A conical liner may be treated in the same way. In the conical case, the walls converge on the axis from all sides. The moving observer must travel at the same rate as in the case of the wedge. In order for the process to appear stationary to him, the total mass per unit distance along the axis must be constant. This is approximately true for a constant wall thickness liner. More accurately, the liner wall thickness would have to be tapered to be inversely proportional to the distance from the apex.

For the detonation wave traveling parallel to the axis with speed U_D, as in Figure 1, Eqs. (6) and (7) become, from Eq. (4),

$$V = \frac{U_D}{\cos\alpha}\sin(\beta-\alpha)\left[\csc\beta + \operatorname{ctn}\beta + \tan\left(\frac{\beta-\alpha}{2}\right)\right], \tag{12}$$

and

$$V_S = \frac{U_D}{\cos\alpha}\sin(\beta-\alpha)\left[\csc\beta - \operatorname{ctn}\beta - \tan\left(\frac{\beta-\alpha}{2}\right)\right]. \tag{13}$$

The jet velocity V increases as α decreases since β also decreases. The jet velocity approaches a maximum as $\alpha \to 0$, or $V = U_D\{1 + \cos\beta + \tan\beta/2\}$ or $\beta \to 0$ as $\alpha \to 0$ so $V = 2U_D$, which means that the jet velocity cannot exceed twice the detonation velocity. Also, as $\alpha \to \beta \to 0$, $V_S \to 0$. Note that as $\alpha \to 0$ the conical liner approaches a cylinder. Cylindrical liners are capable of generating high-velocity (and low mass) jets.

For the hypothetical case of a conical wave front moving perpendicular to the surface of a conical liner such that the wave strikes all surfaces at the same time, $\beta = \alpha$ and the velocities of the jet and slug from Eqs. (6) and (7) this time become

$$V = \frac{V_0}{\sin\alpha}(1 + \cos\alpha) \quad \text{and} \quad V_S = \frac{V_0}{\sin\alpha}(1 - \cos\alpha).$$

With this type of wave front the jet velocity could be increased indefinitely by decreasing α. However, as $\alpha \to 0$, $V_0 \to 0$, $m_j \to 0$, and jet momentum

$$m_j V = \frac{mV_0}{2}\sin\alpha \to 0.$$

Finally, the theory of Birkhoff et al. (1948) predicts steady-state jet and slug velocities as in Eqs. (6) and (7) or Eqs.(12) and (13), and masses as in Eqs. (10) and (11) for conical or wedge-shaped liners.

5.2. COMMENTS ON THE BIRKHOFF ET AL. SOLUTION

The steady-state model provides quantitative agreement with flash radiograph experiments. The model tends to overpredict the jet velocities. Also, the jet possesses a velocity gradient from tip to tail and continues to stretch after the walls have collapsed giving a jet length greater than the slant height of the cone. The steady-state analysis does not predict jet elongation. The velocity gradient along the jet causes the jet to stretch however. If the jet were formed from a brittle material, a stream of particles would form which would separate

in time. A jet formed from a ductile material can, however, elongate to a considerable extent as a continuous stream before the jet finally separates into a stream of particles.

Important modifications have been made to the steady-state theory of Birkhoff et al. notably by Pugh, Eichelberger, and Rostoker (1952) and Godunov et al. (1975). Pugh et al developed a nonsteady theory, hereafter referred to as the PER theory, based on the same concepts as Birkhoff et al. (1948) except that the collapse velocities of the various liner elements are not the same for all elements but vary depending on the original position of the liner element. Thus, the collapse velocity decreases continuously from the cone apex to its base, producing significant jet elongation.

In the Soviet Union, Godunov et al. (1975), hereafter referred to as the visco-plastic theory, modified the steady-state theory to include visco-plastic behavior, that is, strain rate dependence.

Both of these models will be discussed in turn.

5.3. THE PER THEORY

The PER theory assumes a variable instead of a constant collapse velocity for the walls of the conical (or wedge) liner. This condition greatly improves the steady-state theory results. The collapse velocity decreases from the apex to the base of the cone, and Figure 3 illustrates the effect of these velocity variations. Note that as the collapse angle β increases, the jet velocity decreases, but the portion of the liner entering the jet increases. Figure 3 also shows how the decreasing collapse velocity increases β. As the detonation wave travels from P to Q along the conical surface APQ, the liner element originally at P collapses to J. The liner element originally at P' starts later and collapses slower than P and arrives at M at the same time P arrives at J. The element P' would have reached N when P reached J if their collapse velocities were identical. Thus, with a constant collapse velocity, the surface

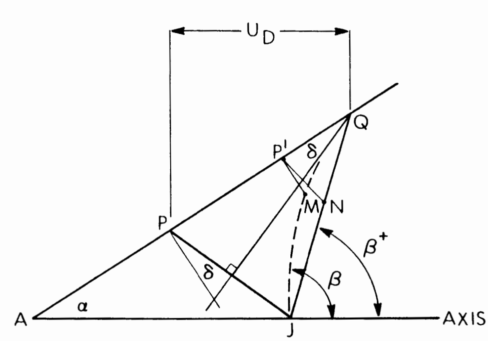

Figure 3. The collapse process for a variable collapse velocity liner (Pugh et al. 1952).

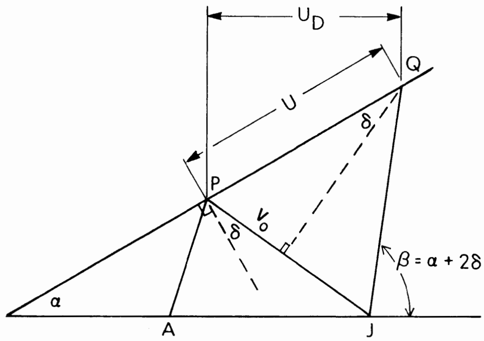

Figure 4. Velocity vectors of a collapsing conical liner element (Pugh et al. 1952).

remains conical, or $\overline{QNJ}$ is a straight line. However, since P' has a slower collapse velocity than P, the collapsing liner has the nonconical contour $\overline{QMJ}$ of Figure 3. The angle β is greater than β^+, the "steady-state" β. This assumes that each liner element is thin and not affected by its neighbors, consistent with the hydrodynamic assumption.

Next, Figure 4, which is similar to the steady-state model of Birkhoff et al. (1948), illustrates the flow situation. $\overline{QJ}$ is parallel to $\overline{PA}$ and equal in length to $\overline{PQ}$. If the magnitudes of $\overline{QP}$ and $\overline{QJ}$ are equal to U, they represent the velocities in the moving coordinate system of the liner elements entering and leaving the region P. The vector $\overline{PJ} = \mathbf{V}_0$ is the velocity of the collapsing liner element in a stationary system of coordinates. Thus, the arguments of Birkhoff et al. (1948) are valid. The liner element does not move perpendicular to its original surface but along a line that makes a small angle δ with the normal. This angle, from Figure 4, is

$$\sin\delta = \frac{V_0}{2U}. \tag{14}$$

If V_0 is constant, $\beta = \beta^+$ and $\delta = (\beta - \alpha)/2$, and all the PER results relax to the steady-state model.

By the proper choice of coordinate systems, the geometric relationships at the moving junction (J) are shown in Figure 5. The axis of the cone is along $\overline{JR}$ and $\overline{OJ}$ is the element of the liner moving toward the axis. This element has a velocity $\overline{OJ} = \mathbf{V}$ in moving coordinates. The velocity of the moving coordinate is $\overline{JR} = \mathbf{V}_1$. Using the law of sines from Figure 5 yields

$$V = \frac{V_0 \cos(\alpha + \delta)}{\sin\beta}, \tag{15}$$

and

$$V_1 = \frac{V_0 \cos(\beta - \alpha - \delta)}{\sin\beta}. \tag{16}$$

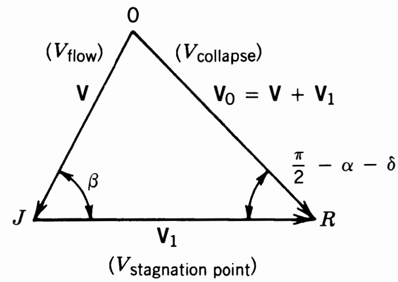

Figure 5. Relationship between $\mathbf{V}_0$, the liner collapse velocity, $\mathbf{V}$ the collapse velocity relative to the collision point, and $\mathbf{V}_1$ the collision point velocity.

In fixed coordinates, the velocities of the jet and slug are $V_j = V_1 + V$ and $V_s = V_1 - V$, respectively. Using Eqs. (15) and (16), along with some trigonometric manipulations, the jet and slug velocities become

$$V_j = V_0 \csc\frac{\beta}{2}\cos\left(\alpha + \delta - \frac{\beta}{2}\right), \tag{17}$$

and

$$V_s = V_0 \sec\frac{\beta}{2}\sin\left(\alpha + \delta - \frac{\beta}{2}\right), \tag{18}$$

respectively. Note that for $\beta = \beta^+ = \alpha + 2\delta$, these equations relax to the Birkhoff et al. (1948) jet and slug velocities, after some trigonometric manipulation.

Elimination of δ from Eqs. (17) and (18) using Eq. (14) yields

$$V_j = V_0 \csc\frac{\beta}{2}\cos\left(\alpha - \frac{\beta}{2} + \sin^{-1}\frac{V_0}{2U}\right), \tag{19}$$

and

$$V_s = V_0 \sec\frac{\beta}{2}\sin\left(\alpha - \frac{\beta}{2} + \sin^{-1}\frac{V_0}{2U}\right). \tag{20}$$

These equations are valid in either the steady-state case when V_0 is constant or in the nonsteady case where V_0 varies. In the steady-state case, however, β could be expressed in terms of α, U, and V_0 and need not appear in the equation.

Of the four unknowns, V_j, V_s, m_j, and m_s, expressions for m_j and m_s are still required. These equations follow from the conservation of mass and momentum, or, where m is the liner mass and m_j and m_s are the jet and slug masses, respectively,

$$dm = dm_j + dm_s,$$

$$\frac{dm_j}{dm} = \sin^2\frac{\beta}{2}, \tag{21}$$

$$\frac{dm_s}{dm} = \cos^2\frac{\beta}{2}. \tag{22}$$

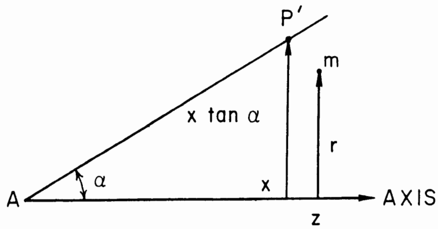

Figure 6. The coordinate directions.

Equations (21) and (22) are identical to the steady-state theory [Eqs. (10) and (11)].

Equations (19)–(22) describe the mass separation and the velocities of each element of a conical liner. They depend on the cone angle 2α and the detonation velocity $U_D = U\cos\alpha$, and on the collapse angle β and velocity V_0, both of which are variables.

From Figure 3, observe that the calculation of the angle β^+ would be more straightforward than the calculation of β since V_0 is different for each element of the liner, and thus the contour of the collapsing liner is not straight but curved as line $\overline{QMJ}$ of Figure 3. Toward this end, let the cylindrical coordinates of M be (r, Z) and the coordinates of P' be $(X\tan\alpha, X)$ in Figure 3. The coordinate directions are indicated in Figure 6. Then,

$$Z = X + V_0(t - T)\sin A, \tag{23}$$

and

$$r = X\tan\alpha - V_0(t - T)\cos A, \tag{24}$$

where t is the elapsed time since the detonation wave passed the apex of the cone, $T = X/U_D = X/(U\cos\alpha)$, and the angle $A = \alpha + \delta$. The slope of the contour of the collapsing liner at any time t can be obtained from the $\partial r/\partial Z$ using Eqs. (23) and (24) and some calculus. The time when a given element reaches the axis is found from Eq. (24) with $r = 0$ or

$$t - T = \frac{X\tan\alpha}{V_0\cos A}, \tag{25}$$

and $\partial r/\partial Z$ evaluated at $r = 0$ is the $\tan\beta$. Using the Taylor relationship, Eq. (14), to simplify results in

$$\tan\beta = \frac{\sin\alpha + 2\sin\delta\cos A - X\sin\alpha(1 - \tan A\tan\delta)V_0'/V_0}{\cos\alpha - 2\sin\delta\sin A + X\sin\alpha(\tan A + \tan\delta)V_0'/V_0}. \tag{26}$$

Since $2\delta = \beta^+ - \alpha$ and $2A = \beta^+ + \alpha$, Eq. (26) may be further simplified to yield

$$\tan\beta = \frac{\sin\beta^+ - X\sin\alpha(1 - \tan A\tan\delta)V_0'/V_0}{\cos\beta^+ + X\sin\alpha(\tan A + \tan\delta)V_0'/V_0}. \tag{27}$$

The term V_0' represents the partial derivative of V_0 with respect to X.

The angle $\beta > \beta^+$ since $V_0' < 0$, that is, the collapse velocity decreases from apex to base, and for cone angles (2α) that are not extremely large. Additional mathematical details and a more complete discussion can be found in Pugh et al. (1952) and Eichelberger's doctoral dissertation (Eichelberberger 1954).

Careful attention should be paid to the quadrant in which the angles calculated in Eqs. (26) and (27) may fall. For angles in the second quadrant, minor modifications of the equation may be necessary, and numerical algorithms that calculate trigonometric functions should be checked for the proper quadrant.

The PER theory provides expressions for m_j, m_s, V_j, V_s, δ, and β, and the number of unknowns exceed the number of independent equations. Experimental evidence that verifies the model and the assumptions of the PER theory was given by Eichelberger and Pugh (1952). Also, Eichelberger (1955) noted a systematic discrepancy between the theoretical and experimental results. It was noted that the liner acceleration to the axis was assumed instantaneous in the PER model, but the effect of a finite acceleration time would influence the value of β. Allison and Vitali (1962), in another classic paper, used a radioactive tracer technique and obtained excellent agreement between the PER theory and experiment. The radioactive tracer technique is described by Bryan et al. (1957) and Gainer (1960).

Bryan et al. (1957) related the jet velocity to its position in the parent liner. The experimental technique involved the use of a rotating mirror camera to determine emerging jet velocity as a function of target plate thickness. Next, M9A1 conical steel shaped charge liners were plated on the inside (air side) with narrow bands of radioactive material at given axial locations. The plated cones were then fired into steel targets identical to those used in the emerging velocity experiments. An analysis of each target provided the depth at which the tagged element was located. The resulting correlation between the depth of each element and its position in the cone was combined with the correlation between depth of each element and its velocity to yield the required velocity–position curve.

The radioactive plating material was Fe^{59}. This isotope was selected based on its half-life and strong gamma emission, which is required for adequate detection of the tracer deposited within the target.

Similar measurements can be made by an indirect method that involves the collection and weighing of a portion of the jet and the slug for which the velocity has been measured. The two methods of determining jet velocity versus axial position exhibit overall qualitative agreement. However, a definite discrepancy exists near the base of the cone. Bryan et al. (1957) provide further detail especially regarding the sources of error in both measurements.

Gainer (1960) used radioactive tracers to study the contribution of different segments of a 105-mm copper conical liner to the penetration of steel targets by the jet. Both confined (in a $\frac{3}{8}$-in. thick steel body) and unconfined rounds were studied. Gainer (1960) improved the experimental procedure developed

by Bryan et al. (1957) by using Ag^{110} as the tracer. This increased the resolution by increasing the activity per band and by narrowing the band. Penetration velocities were also measured and other improvements were reported.

No radioactivity was detected in the slug, which implies that the entire inside surface of the liner contributed to the jet. Also, large differences were observed in the velocity gradients between the confined and unconfined charges. Gainer found that in a confined charge, the base region of the liner contributed significantly to the penetration. However, for the unconfined charge, the base region contributed little to the penetration. Penetration–time measurements showed that the jet velocities at the maximum depth of penetration were nearly the same for both confined and unconfined warheads.

Thus, the PER theory has been verified experimentally and constitutes the basis of all analytical shaped charge jet formation models. Many extensions have been made to the PER model and auxiliary equations have been added to facilitate and extend the solution.

The plate bending angle or the Taylor angle (δ) can be determined by the formula proposed by Richter (1948) and Defourneaux (1970):

$$\frac{1}{2\delta} = \frac{1}{\phi_0} + \frac{\rho \varepsilon K}{e}, \tag{28}$$

where ρ and ε are the density and thickness of the liner wall, respectively, and e is the explosive thickness driving the liner. K and ϕ_0 are constants that are determined from the type of explosive used and the angle of incidence, i, which the detonation wave makes with the liner. Equation (28) is coupled with the PER theory in the analytical jet formation codes BASC (Harrison 1981a, 1981b) and DESC (Carleone et al. 1975; and probably others). Defourneaux (1970) also presents a good discussion of the liner collapse and formation that is an excellent supplement to the PER study. Kerdraon (1975, 1977) modified Eq. (28) by including terms to account for the effect of liner radius in imploding cylindrical liner charges.

The PER theory assumes the liner element is instantaneously accelerated to the axis as depicted in Figure 7*a*. The first-order correction is the assumption that the liner acceleration is constant over a finite period of time, as first proposed by Eichelberger (1955) and used by Carleone et al. (1975). The velocity then increases linearly over a short period, as shown in Figure 7*b*, until it reaches its final velocity or collapses on the axis. In Carleone et al. (1975) the acceleration is given by

$$a = c\frac{P_{CJ}}{\rho\varepsilon},$$

where P_{CJ} is the Chapman–Jouguet pressure of the explosive, ρ and ε are the liner density and thickness, respectively, and c is an empirical constant.

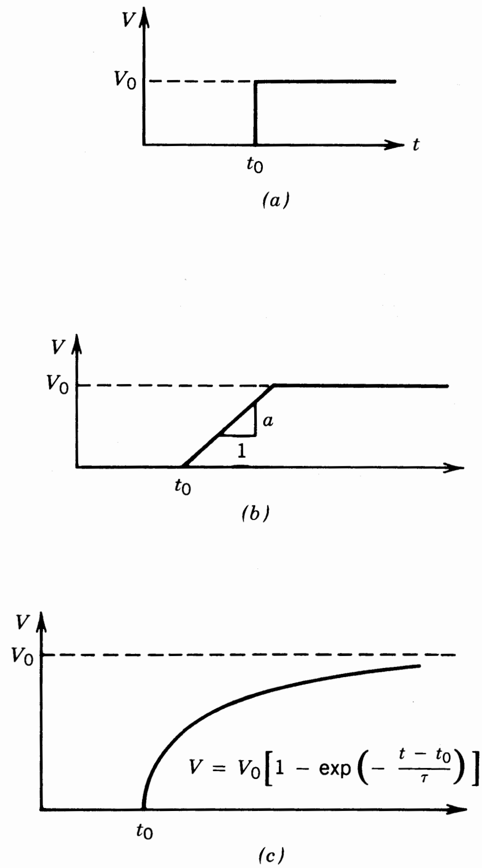

Figure 7. Liner acceleration histories: (a) instantaneous acceleration; (b) constant acceleration; (c) exponential acceleration (Chou and Flis 1986).

Possibly, a more realistic form of the liner velocity history is given as an exponential form by Randers-Pehrson (1976):

$$V(t) = V_0\left[1 - \exp\left(-\frac{t - t_0}{\tau}\right)\right],$$

as shown in Figure 7c. This formula requires knowledge of the time constant, τ, for which Chou et al. (1981a) recommend

$$\tau = c_1\frac{MV_0}{P_{\mathrm{CJ}}} + c_2,$$

where M is the initial mass per unit area of the liner and c_1 and c_2 are empirical constants.

Considering the effects already mentioned, Chou et al. (1981a, 1981b) provide a more exact expression for the projection (Taylor) angle,

$$\delta = \frac{V_0}{2U} - \frac{1}{2}\tau V_0' + \frac{1}{4}\tau' V_0,$$

where the prime denotes differentiation along the liner. Randers-Pehrson (1976) proposed a similar formula. Randers-Pehrson (1976) and Chou et al. (1981a, 1981b) all show better agreement with the hydrocode results than the Taylor angle (steady-state) formula for δ.

Hirsch et al. (1986) formulated the general equations of motion of a thin, smooth explosively driven liner. Liner curvature was considered and the equations of motion were solved in closed form for certain cases. In general, approximate solutions were obtained for the projection (Taylor) angle δ and the liner elongation ratio, dL/dL_0, where L_0 is the initial liner length and L is the liner length at some later time t. The analysis was applied to conical, cylinder, and hemispherical liners and good agreement was obtained between the model and two-dimensional computer simulations.

Models of this type, for acceleration to the liner axis during the collapse process, have been incorporated into the PER theory. These one-dimensional computer programs use the analyses presented in this section to calculate the Taylor angle δ, the flow velocity V, the collapse velocity V_0, the stagnation point velocity V_1, the collapse velocity gradients V_0', the jet velocity V_j, the slug velocity V_s, the collapse angle β, the jet mass m_j, and the slug mass m_s. The input values consist of the complete geometry and material density of the conical liner and the explosive charge. The mode of initiation of the charge and the type of HE (high explosive) must be known to determine the HE density and detonation velocity. The mode of initiation determines the shape of the detonation wave (i.e., plane or spherical) and the angle of incidence between the detonation wave and the liner wall. Also, the relative distribution of the kinetic energy entering the jet and slug are given as

$$\frac{dE_j}{dE} = \cos^2\left(\alpha + \delta - \tfrac{1}{2}\beta\right), \tag{29}$$

and

$$\frac{dE_s}{dE} = \sin^2\left(\delta + \delta - \tfrac{1}{2}\beta\right), \tag{30}$$

respectively.

The stretching jet radius is also calculated assuming the jet to be circular in cross section. In addition, the material near the liner apex does not have sufficient time to reach its theoretical collapse velocity, and hence the earliest formed portions of the jet have lower velocities than the jet material formed behind them. This "piling up" of jet particles causes the formation of the

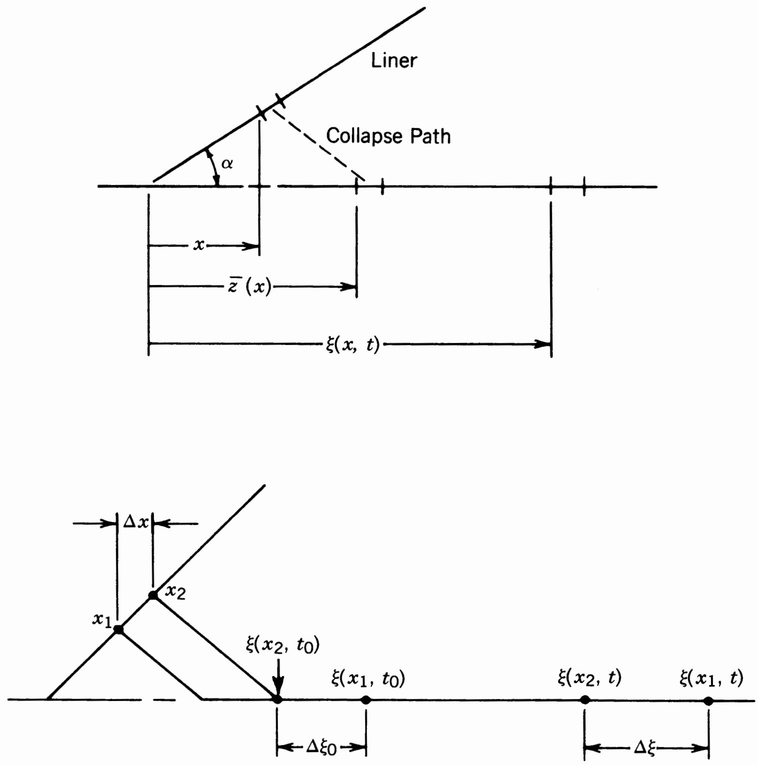

Figure 8. Relations between the liner coordinate x, and the jet coordinate ξ (Chou and Flis 1986).

inverse velocity gradient, and this coalescence of particles is treated separately to calculate the jet tip velocity. All these effects are included in most jet formation codes such as BASC (Harrison 1981a, 1981b) along with certain other parameters such as momentum, jet strain, and strain rate.

To calculate the strain, jet length, and jet radius, it is necessary to relate the position of a jet element back to its original position in the liner. This was done by Carleone and Chou (1974) by using a simple Lagrangian coordinate definition. The coordinate x is used for the axial liner position and coordinate ξ for the position of the jet, as shown in Figure 8. The jet position is given as

$$\xi(x, t) = Z(x) + (t - t_0)V_j(x), \tag{31}$$

where t_0 is the time when the liner element first arrives at the axis, $Z(x)$ is the location of the formation, and $V_j(x)$ is the jet velocity. Note that V_j is a function of a liner position, but ξ is a function of both liner position and time. Outside the inverse velocity gradient region, a liner element with a smaller x always proceeds (is ahead of, or has a larger ξ than) an element with a larger

x. The strain rate, η, is given as

$$\eta = \lim_{x_2 \to x_1} \frac{\Delta\xi - \Delta\xi_0}{\Delta\xi} = \frac{(\partial\xi/\partial x)_t}{(\partial\xi/\partial x)_{t_0}} - 1. \tag{32}$$

Equations (31) and (32), with the statements made earlier, allow the jet length and radius to be calculated.

Special techniques are necessary to calculate the jet tip velocity, as discussed earlier. The PER theory indicates that the jet velocity decreases monotonically from tip to tail. Thus, the gradient of the jet velocity is negative with respect to the original liner position or positive with respect to the jet position. As mentioned earlier, liner elements near the apex collide on the axis before reaching their final collapse velocity, V_0. This reduced collapse velocity results in a reduced jet speed, so that the jet velocity gradient with respect to the liner position is positive. This is termed the inverse-velocity gradient (Kiwan and Wisniewski 1972). In the apex region, each jet element has a higher velocity than the one ahead of it, causing a "piling-up" of jet mass. This piled-up mass forms the jet tip as verified experimentally (Chou et al. 1977). For conventional conical charges, the first 30–40% of the liner from the theoretical apex forms the tip of the jet. The tip has a much larger radius than the rest of the jet.

Figure 9 shows the inverse-velocity gradient with respect to X, the liner element position. The velocity of the jet tip is given as

$$V_{j0} = V_{\text{tip}} = \frac{\int_0^{X_{\text{tip}}} V_j(dm_j/dX)\,dX}{\int_0^{X_{\text{tip}}}(dm_j/dX)\,dX}, \tag{33}$$

based on the conservation of momentum.

Hirsch (1977) extended the PER model to include nonsteady effects at the collision point (or formation point) by assuming that relative to this point, the

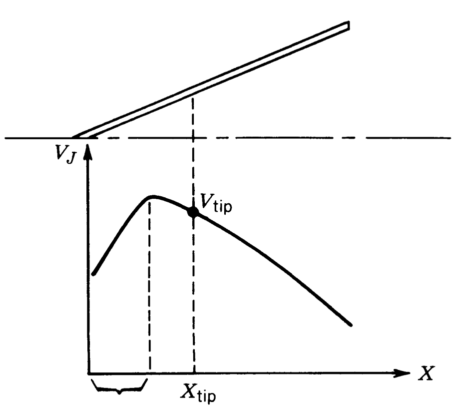

Figure 9. A typical jet velocity distribution curve showing that the inverse-velocity gradient region near the apex of the liner forms the jet tip particle (Chou and Flis 1986).

jet and slug velocities, V_j and V_s, are not equal to the incoming liner velocity V as the PER theory assumed from the Bernoulli equation.

Recently, Lampson (1987) devised a method to account for the velocity gradient through the liner thickness for conical liners. The existence of a velocity gradient through the liner walls was first noted by Sterne (1950) for collapsing cylindrical shells.

Other studies involve modifications or extensions of the PER theory, such as Perez et al. (1977), who modified PER to account for two-dimensional effects of the flow near the collapse axis, and Hirsch (1979). Leidel (1978) provides an overview of the PER model and analyzes annular cutting charges, or cookie cutter warheads as first conceived by Glass et al. (1969). Harrison (1978) and Harrison and Karpp (1977) compare the simple one-dimensional models to hydrocodes and experimental data.

Other shaped charge publications of interest include Hornemann and Senf (1974) on wide-angle cones, Van Thiel and Levatin (1978), Trinks (1975) for his shaped charge discussion and historical inferences, Rostoker (1953), Simon and DiPersio (1972), and the USSR studies by Novikov (1962), and Titov (1979). These papers relate to jet formation and collapse and relevant topics pursuing the concepts reviewed so far. An excellent Soviet paper was published by Ivanova and Rozantseva (1953), which is very long and very informative. It provides a detailed discussion and derivation of the PER theory and simple penetration models including experimental data and numerous flash radiographs or X-ray photographs of shaped charge jets. The USSR models are discussed in more detail later in the next chapter.

Excellent flash radiography data and analysis thereof is given by Breidenbach (1952) and by Heine-Geldern and Pugh (1953). Classical papers on jets and jet formation are given by Harlow and Pracht (1966) and on collapsing cylinders by Koski et al. (1952).

Zernow and Simon (1955) investigated the behavior of jets from several different shaped charge materials. Aseltine (1980) studied the effect of several different warhead asymmetries on the behavior and performance of shaped charge jets. Also, Panzarella and Longobardi (1952) investigated conical shaped charge liners that were intentionally deformed, and investigated deficiencies in charge explosive casting. Merendino et al. (1963) altered a shaped charge liner, that is, inhibited the collapse of the liner, to obtain a massive hypervelocity pellet in lieu of a jet. Other studies regarding shaped charge analyses are given in the papers by Robinson (1984, 1985) and Lee (1985).

Kolsky et al. (1949) studied the formation and penetration of conical shaped charge liners. Kolsky (1949) continued his studies to include the formation and penetration of hemispherical shaped charge liners. The formation and collapse of hemispherical liners were also studied via hydrocodes by Kiwan and Arbuckle (1977), Arbuckle et al. (1980), Chou et al. (1981), Aseltine et al. (1978), Chou et al. (1983), and Lacetera and Walters (1979).

Studies on the formation of hemispherical shaped charge liners were presented by Lee (1985), Singh (1955), Shepherd (1956), and Grace et al. (1984). A closed-form analytical expression (analogous to the PER theory for

conical liners) for the collapse and formation of hemispherical shaped charge liners does not currently exist.

Vigil and Robinson (1987) provided a theoretical model to analyze the three-dimensional collapse, jetting, and penetration of a linear shaped charge. The results were in agreement with the available experimental data.

5.4. GENERALIZATION OF SHAPED CHARGE JET FORMATION MODEL

The PER jet formation model was modified by Behrmann (1973) [and later by Carleone (1987)] to account for deviations from conical liner geometry and variations in the explosive initiation point. These modifications allow the study of a generally shaped liner, for example, a trumpet configuration or any geometry that jets analogously to a cone. Thus, a hemispherical liner is excluded. Also, a spherical or toroidal detonation wave (as well as a plane detonation wave) is allowed.

The first equation is

$$V_j = \frac{V_0}{\sin \beta/2} \cos\left(\alpha + \delta - \frac{\beta}{2} \right), \tag{34}$$

as given by the PER model. Also, for generalization, U, the detonation velocity of the explosive along the liner surface is replaced by $U_D/\cos \varepsilon(x)$, where U_D is the detonation velocity of the explosive (as given in tables such as Dobratz for various explosives) and $\varepsilon(x)$ is the angle between the detonation front normal and the liner surface evaluated at the liner surface. The Taylor angle relationship is generalized as

$$\sin \delta = \frac{V_0 \cos \varepsilon}{2U_D}. \tag{35}$$

The PER theory assumed a constant liner apex angle, a constant liner wall thickness, and a plane wave initiation. To remove these assumptions, Figure 10 from Behrmann (1973) defines δ and V_0 (the liner collapse velocity) as in the PER model. Also, α becomes the angle between the tangent to the liner at a point x and the axis of the liner. The angle between the collapsing liner wall and its axis is β. The angle between the explosive detonation velocity vector and the tangent to the liner is ε.

From Figure 10, the following expressions are derived:

$$\tan(\alpha - \varepsilon) = \frac{r_1 - D}{x - d}, \tag{36}$$

$$T(x) = \frac{1}{U_D}\left[(x - d)^2 + (r_1 - D)^2 \right], \tag{37}$$

$$r(x) = r_1(x) - V_0(x)[t(x) - T(x)]\cos[\alpha(x) + \delta(x)], \tag{38}$$

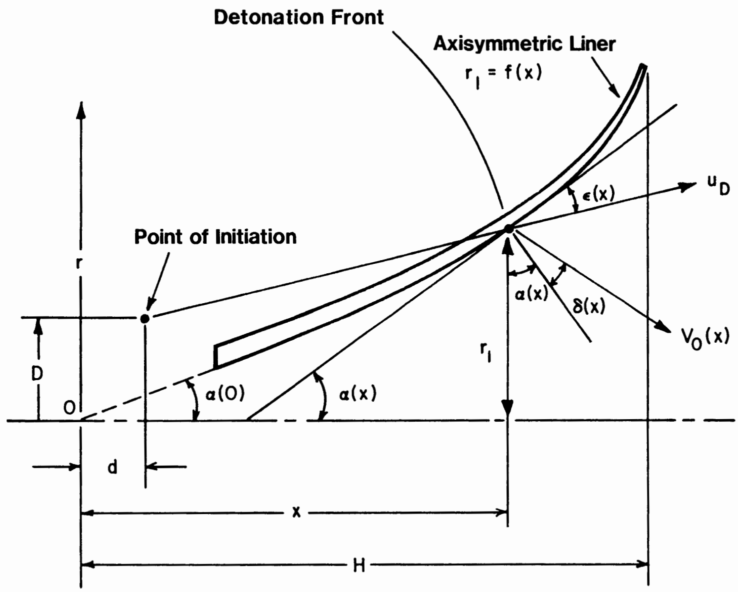

Figure 10. Generalized axisymmetric shaped charge configuration (Behrmann 1973).

and

$$Z(x) = x + V_0(x)[t(x) - T(x)]\sin[\alpha(x) + \delta(x)], \tag{39}$$

where r_1 is the radius of the liner at a point x; T is the time the detonation front takes to reach a point x on the liner; t is the time it takes for a point x on the liner to reach a radius r, and Z is the corresponding x coordinate. The tangent of the collapse angle β at any given time t is by definition the partial derivative of r with respect to Z at a constant t.

Following the same mathematical attack as in the PER theory, the collapse angle of interest occurs at $r = 0$ when an element at the point x on the liner reaches the axis. Therefore, from Eq. (38), the corresponding time at $r = 0$ is

$$t - T = \frac{r_1}{V_0 \cos A}, \tag{40}$$

where $A = \alpha + \delta$.

From the preceding equations, the collapse angle can be shown to be

$$\tan\beta|_{r=0} = \frac{\tan\alpha + r_1[(\alpha' + \delta')\tan A - V_0'/V_0] + V_0 T' \cos A}{1 + r_1[(\alpha' + \delta') + (V_0'/V_0)\tan A] - V_0 T' \sin A}, \tag{41}$$

where

$$\delta' = \tan\delta\left(\frac{V_0'}{V_0} - \varepsilon'\tan\varepsilon\right), \tag{42}$$

$$\varepsilon' = \alpha' + \frac{\cos^2(\alpha - \varepsilon)}{x - d}\left[\tan(\alpha - \varepsilon) - \tan\alpha\right], \tag{43}$$

$$T' = \frac{(x - d)}{U_D^2 T}\left[1 + \tan(\alpha - \varepsilon) - \tan\alpha\right], \tag{44}$$

and the prime denotes differentiation with respect to x.

Equations (34), (35), and (41)–(44), and the PER theory differential mass equations (21) and (22) form a sufficient set of equations to calculate the jet

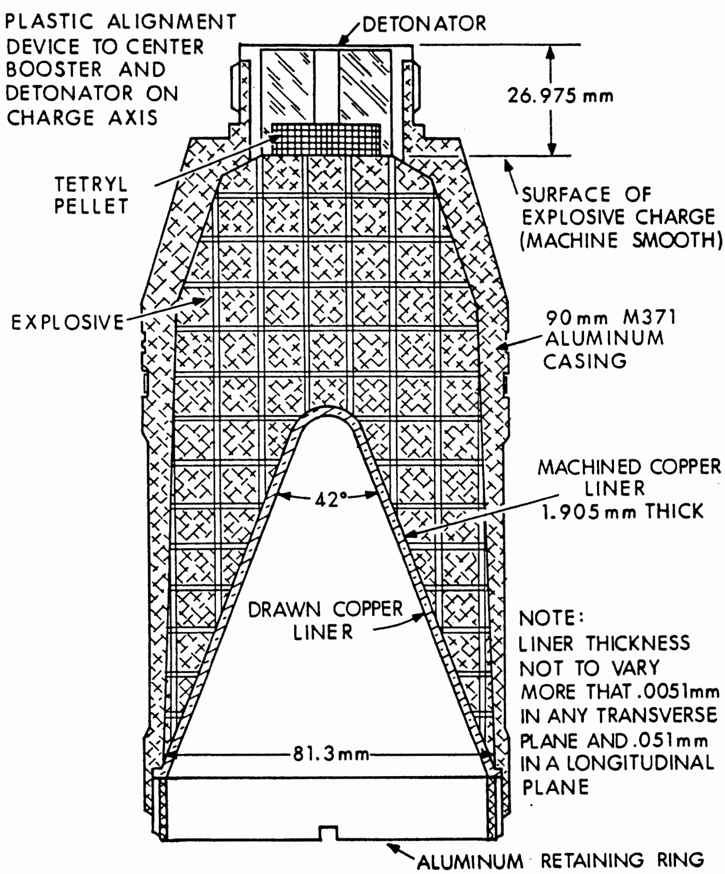

Figure 11. Standard shaped charge (Aseltine 1980).

parameters from a generalized axisymmetric shaped charge liner once the liner geometry, mode of initiation, and collapse velocities are known.

In summary, four basic independent equations exist (ignoring the slug calculations). Examination of these equations reveal five unknowns, namely, dm_j/dm, β, V_j, V_c, and δ. The additional unknown is removed when an explosive–metal interaction equation, for example, a Gurney-like model, is introduced.

5.5. A SAMPLE CALCULATION

The PER theory, as implemented in computer codes such as BASC, yields excellent agreement with the experimentally observed jet parameters. In the following figures, a sample calculation was performed to illustrate typical output from models such as the PER theory. The calculation was performed for a standard, precision shaped charge. The shaped charge is shown in Figure 11 from Aseltine (1980). The computational results are given in Figures 12–19, which present the deflection angle (ϕ), collapse angle (β), the flow velocity, stagnation point velocity, and jet velocity all as a function of liner position. Note that the jet tip formation technique is used to determine the jet tip velocity (Figure 16). Also, the jet cumulative momentum, kinetic energy, and mass are shown plotted versus jet velocity.

To simplify the calculations, the charge was assumed to have a pointed, instead of rounded, apex although this assumption is not necessary. The

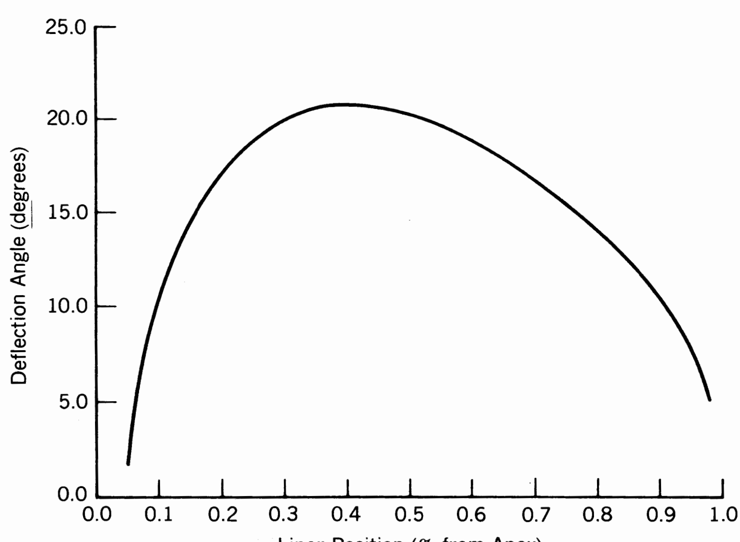

Figure 12. Deflection angle versus liner position.

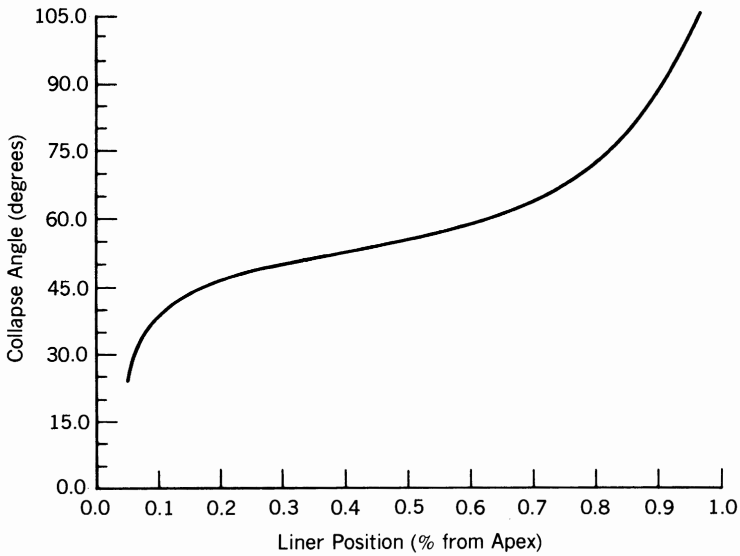

Figure 13. Collapse angle versus liner position.

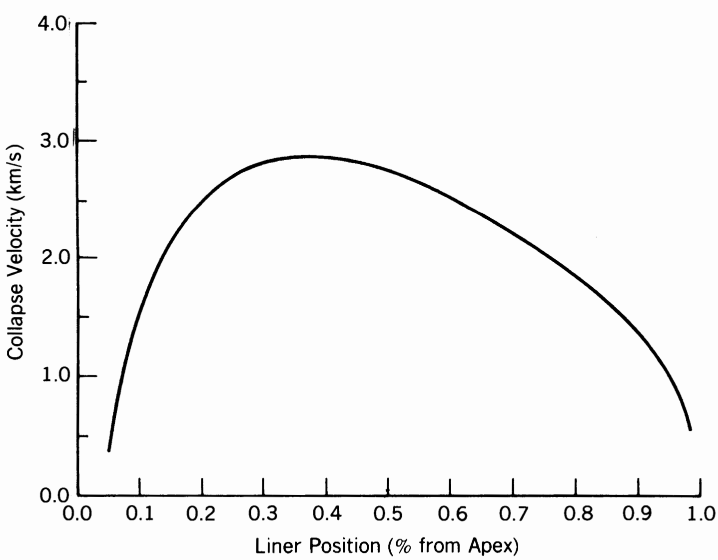

Figure 14. Collapse velocity versus liner position.

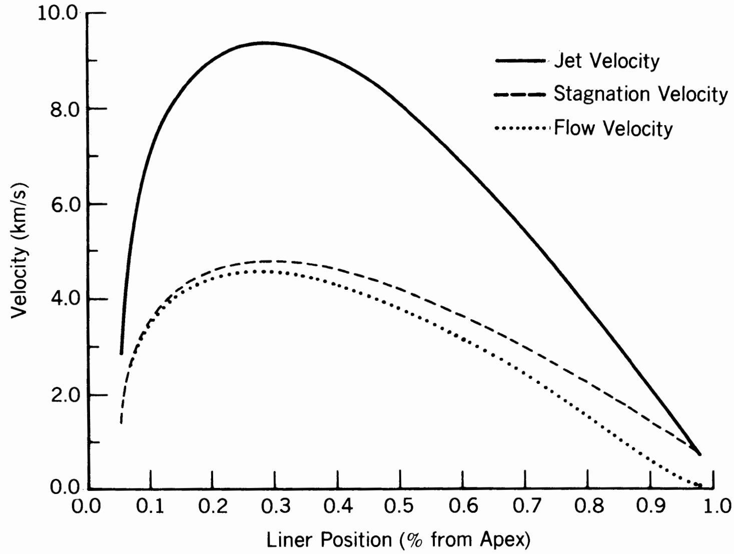

Figure 15. Jet formation velocities versus liner position.

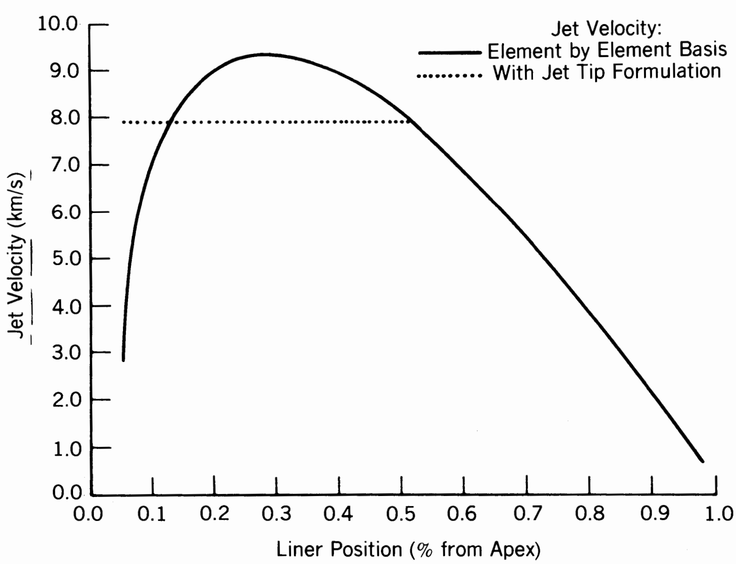

Figure 16. Jet velocity and jet tip velocity versus liner position.

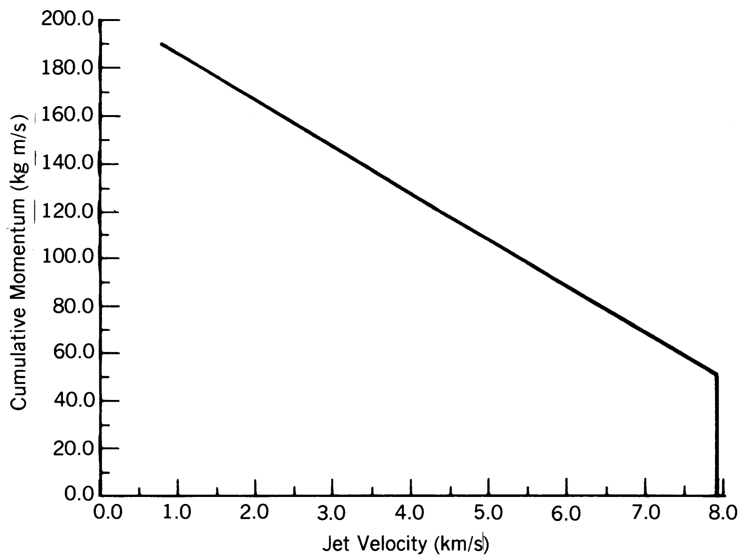

Figure 17. Cumulative momentum versus jet velocity.

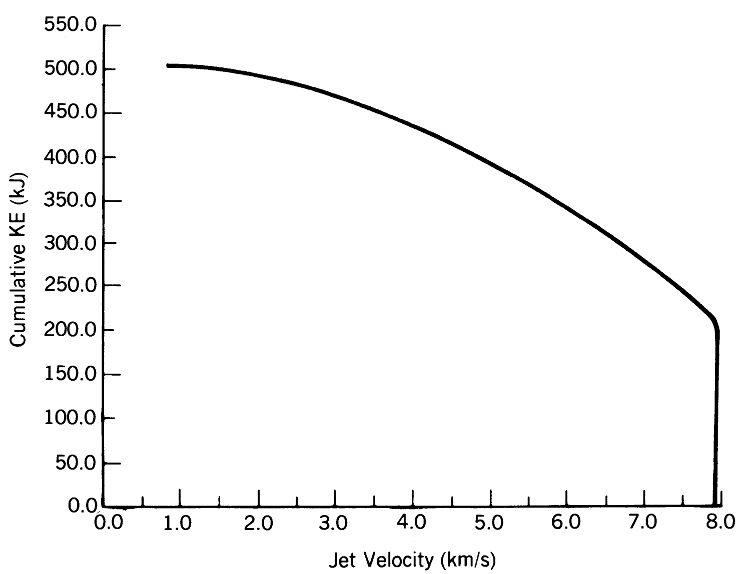

Figure 18. Cumulative kinetic energy versus jet velocity.

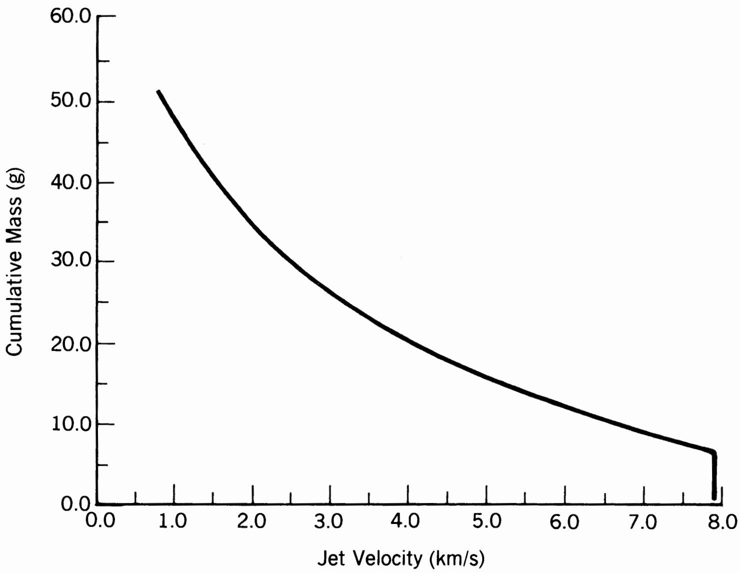

Figure 19. Cumulative jet mass versus jet velocity.

calculated PER results are very typical of measured values from shaped charges with conical liners.

APPENDIX A THE HYDRODYNAMIC ASSUMPTION JUSTIFICATION

The familiar Bernouilli equation expresses the total pressure, P_T as

$$P_T = \tfrac{1}{2}\rho_j V^2$$

when the static pressure is neglected. For a jet of copper with density $\rho_j = 8.9\ \text{g/cm}^3$ and a typical flow velocity of 4 km/s,

$$P_T \sim 71.2 \times 10^9\ \text{Pa} \sim 10.3 \times 10^6\ \text{psi} \sim 0.7 \times 10^6\ \text{atm},$$

or the resulting pressure is of the order of 10^6 (one million!) atm, which far exceeds the dynamic yield strength of copper (1.5 kbars or about 1.5×10^3 atm) or even steel (10 kbars or about 10^4 atm).

REFERENCES

Allison, R. E., and Vitali, R. (1962), "An Application of the Jet Formation Theory to a 105 mm Shaped Charge," BRL Report No. 1165, March.

Arbuckle, A. L., Walters, W. P., and Aseltine, C. L. (1980), "Analysis of Uniform Wall and Tapered Hemispherical Liners with Several Explosive Confinement Geometries," ARBRL-TR-02222, March.

Aseltine, C. L. (1980), "Analytical Predictions of the Effect of Warhead Asymmetrics on Shaped Charge Jets," Technical Report ARBRL-TR-02214, February.

Aseltine, C. L., Walters, W. P., Arbuckle, A. L., and Lacetera, J. E. (1978), "Hemispherical Shaped Charges Utilizing Tapered Liners," *Proc. 4th Int. Symp. Ballistics*, Monterey, CA, October 17–19.

Behrmann, L. A. (1973), "Calculation of Shaped Charge Jets Using Engineering Approximations and Finite Difference Computer Codes," AFATL-TR-72-160, September.

Birkhoff, G., MacDougall, D., Pugh, E., and Taylor, G. (1948), "Explosives with Lined Cavities," *J. Appl. Phys.*, *19* (6).

Breidenbach, H. I. (1952), "The Evolution of Jets From Cavity Charges as Shown by Flash Radiographs," BRL Report No. 808, April.

Bryan, G. M., Eichelberger, R. J., MacDonald, D., and Zigman, P. E. (1957), "Application of Radioactive Tracers to the Study of Shaped Charge Phenomena," *J. Appl. Phys.*, *28* (10): 1152–1155.

Carleone, J. (1987), Section 3, "Mechanics of Shaped Charges," Course Notes, *Basic Principles of Hypervelocity Impact and Related Topics*, April, Computational Mechanics Associates, Baltimore, MD.

Carleone, J., and Chou, P. C. (1974), "A One-Dimensional Theory to Predict the Strain and Radius of Shaped Charge Jets," *Proc. 1st Int. Symp. on Ballistics,* Orlando, FL, November 13–15.

Carleone, J., Chou, P. C., and Tanzio, C. A. (1975), "User's Manual for DESC-1, A One-Dimensional Computer Code to Model Shaped Charge Liner Collapse, Jet Formation, and Jet Properties," Dyna East Corporation. Technical Report No. DE-TR-75-4, December.

Chou, P. C., and Flis, W. J. (1986), "Recent Developments in Shaped Charge Technology," *Propell., Explos., Pyrotech.*, *11*: 99-114.

Chou, P. C., Carleone, J., and Jameson, R. (1977), "The Tip Origin of a Shaped Charge Jet," *Propell. Explos.*, *2*: 126–130.

Chou, P. C., Ciccarelli, R. D., Arbuckle, A. L., and Walters, W. P. (1981), "Jet Formation of an Implosively Loaded Hemispherical Liner," Contract Report ARBRL-CR-00470, September.

Chou, P. C., Carleone, J., Hirsch, E., Flis, W. J., and Ciccarelli, R. D. (1981a), "Improved Formulas for Velocity, Acceleration, and Projection Angle of Explosively Driven Liners," *Proc. 6th Int. Symp. on Ballistics,* Orlando, FL, October 27–29.

Chou, P. C., Hirsch, E., and Ciccarelli, R. D. (1981b), "An Unsteady Taylor Angle Formula for Liner Collapse," BRL Contractor Report, ARBRL-CR-00461.

Chou, P. C., Ciccarelli, R. D., and Walters, W. P. (1983), "The Formation of Jets from Hemispherical Liner Warheads," *Proc. 7th Int . Symp. on Ballistics,* The Hague, Netherlands, April 19–21.

Defourneaux, M. (1970), "Theorie Hydrodynamique des Charges Creuses," *Mem. l'artillerie Francaise, 44*(2): 293–334.

Eichelberger, R. J. (1954), "Re-Examination of the Theories of Jet Formation and Target Penetration by Lined Cavity Charges," CEL Report No. 1., June (also Ph.D. Dissertation).

Eichelberger, R. J. (1955), "Re-Examination of the Non-Steady Theory of Formation by Lined Cavity Charges," *J. Appl. Phys., 26*(4).

Eichelberger, R. J., and Pugh, E. M. (1952), "Experimental Verification of the Theory of Jet Formation by Charges with Lined Conical Cavities," *J. Appl. Phys., 23*(5).

Gainer, M. K. (1960), "The Application of Radioactive Tracers to Shaped Charge Liners," BRL Memorandum Report No. 1242, January.

Glass, C. M., Kronman, S., and Golaski, S. K. (1969), "The Cookie Cutter Warhead," BRL Report No. 1455, October.

Godunov, S. K., Deribas, A. A., and Mali, V. I. (1975), "Influence of Material Viscosity on the Jet Formation Process during Collisions of Metal Plates," translated from *Fizika Goreniya i Vzryya*, Vol. 11, No. 1, pp. 3–18, January–February.

Grace, F. I., Golaski, S. K., and Scott, B. R. (1984), "The Nature of Jets from Hemispherical Lined Explosive Charges," *Proc. of 8th Int. Symp. on Ballistics*, Orlando, FL, October.

Harlow, F. H., and Pracht, W. E. (1966), "Formation and Penetration of High-Speed Collapse Jets," *Phys. Fluids, 9*(10).

Harrison, J. T. (1978), "A Comparison between the Eulerian, Hydrodynamic Computer Code (BRLSC) and Experimental Collapse of a Shaped Charge Liner," BRL Memorandum Report ARBRL-MR-02841, June.

Harrison, J. T. (1981a), "Improved Analytical Shaped Charge Code: BASC," BRL Technical Report No. ARBRL-TR-02300, March.

Harrison, J. T. (1981b), "BASC, An Analytical Code for Calculating Shaped Charge Properties," *Proc. 6th Int. Symp. on Ballistics,* Orlando, FL, October 27–29.

Harrison, J. T., and Karpp, R. R. (1977), "Terminal Ballistic Application of Hydrodynamic Computer Code Calculations," BRL Report 1984, April.

Heine-Geldern, R. V., and Pugh, E. M. (1953), "The Photography of High-Speed Metallic Jets," *Meteoritics, 1*(1): 5–10.

Hirsch, E. (1977), "An Analytical Model for the Nonsteady Shaped Charge Jet Formation Junction," *Proc. 7th Int. Symp. on Ballistics,* Karlsruhe, West Germany, March.

Hirsch, E. (1979), "A Simple Representation of the Pugh, Eichelberger, and Rostoker Solution to the Shaped Charge Jet Formation Problem," *J. Appl. Phys., 50*(7).

Hirsch, E., Chou, P. C., and Ciccarelli, R. D. (1986), "General Kinematical Solution to the Motion of an Explosively Driven Liner," *Propell. Explos., Pyrotech., 11*: 53–64.

Hornemann, U., and Senf, H. (1974), "Parameter Studies of 120° Flat-Cone Shaped Charges," *Proc. 3rd Int. Symp. on Ballistics*, Weil am Rhein, June 1971, FSTC-HT-23-797-73, September.

Ivanova, V., and Rozantseva, V. (1953), "Theoretical and Experimental Investigation of the Shaped-Charge Effect," *Meckhanika, Sbrorniki Penevodov i Obzonov Inostrannoy Periodicheskoy Literatury*, *4*(2): 51–105, FSTC-HT-426-82.

Kerdraon, A. (1975), "Etude de la Projection Cylindrique Convergente," ISL Symposium, St. Louis, France, October.

Kerdraon, A. (1977), "Study of Converging Cylindrical Projection," *Proc. 3rd Int. Symp. on Ballistics*, Karlsruhe, W. Germany, March 23–25.

Kiwan, A. R., and Arbuckle, A. L. (1977), "Study of Liner Collapse, Jet Formation and Characteristics from Implosive Shaped Charge Systems," BRL Report 2028, November.

Kiwan, A. R., and Wisniewski, H. (1972), "Theory and Computations of Collapse and Jet Velocities of Metallic Shaped Charge Liners," BRL Report No. 1620, November.

Kolsky, H. (1949), "A Study of the Mechanism of Munroe Charges, Part II—Charges with Hemispherical Lines," *Res. Supp.*, London, 2-2, 96–98.

Kolsky, H., Snow, C. I., and Shearman, C. A. (1949), "A Study of the Mechanism of Munroe Charges, Part I—Charges with Conical Liners," *Res. Supp.*, London, 2-2, 89–95.

Koski, W. S., Lucy, F. A., Schreffler, R. G., and Willig, F. J. (1952), "Fast Jets from Collapsing Cylinders," *J. Appl. Phys.*, **23**(12): 1300–1305.

Lacetera, J. E., and Walters, W. P. (1979), "Theoretical and Experimental Studies of Hemispherical Shaped-Charged Liners," *Transactions of the Twenty Fifth Conference of Army Mathematicians*, ARO Report 80-1, held at Johns Hopkins University, Baltimore, June.

Lampson, M. (1987), "Jet Formation from Collapsing Conical Shells," *Proc. 10th Int. Symp. on Ballistics*, Vol. 2, San Diego, October.

Lee, W. H. (1985), "High Explosive Modeling in 2D Euler Code for Shaped Charge Problems," Los Alamos National Laboratory Report, LA-UR-85-2954.

Leidel, D. J. (1978), "A Design Study of an Annular-Jet Charge for Explosive Cutting," Ph.D. Dissertation, Drexel University, Philadelphia, June.

Merendino, A., Regan, J. M., and Kronman, S. (1963), "A Method of Obtaining a Massive Hypervelocity Pellet from a Shaped Charge Jet," BRL Memorandum Report No. 1508, August.

Novikov, N. P. (1962), "High-Speed Shaped Jets," *PMTF*, No. 6, 22–28, FSTC-HT-1384-82.

Panzarella, J., and Longobardi, J. (1952), "Performance of Shaped Charges with Intentionally Deformed Liners," Ballistic Research Laboratory Report No. 811, March.

Perez, E., Fauquignon, C., and Chanteret, P. (1977), "Fundamental Studies of Shaped Charge Mechanisms,"*Proc. 3rd Int. Symp. on Ballistics*, Karlsruhe, West Germany, March.

Pugh, E., Eichelberger, R., and Rostoker, N. (1952), "Theory of Jet Formation by Charges with Lined Conical Cavities," *J. Appl. Phys.*, *23*(5).

Randers-Pehrson, G. (1976),"An Improved Equation for Calculating Fragment Projection Angle," *Proc. 2nd Int. Symp. on Ballistics*, Daytona Beach, FL, March 9–11.

Richter, H. (1948), "On the Theory of Shaped Charges: Motion of Thin Layers of Plastic Material on the Surface of a Plane Explosive," Note Technique ILS No. 6a/48.

Robinson, A. C. (1984), "Asymptotic Formulas for the Motion of Shaped Charge Liners," Sandia Report SAND 84-1712, Unlimited Release UC-35, September.

Robinson, A. C. (1985), "SCAP—A Shaped Charge Analysis Program—User's Manual for SCAP 1.0," Sandia Report SAND 85-0708, Unlimited Release UC-35, April.

Rostoker, N. (1953), "The Formation of Craters by High-Speed Particles," *Meteoritics*, *1*(1): 11–27.

Shepherd, W. C. F. (1956), "Strength of High Explosives and Effects due to Shape," in *Science of Explosives*, C. E. H. Bawn and G. Rotter (eds.), Ministry of Supply, London.

Simon, J., and DiPersio, R. (1972), "Jet Formation and Utilization," *Proc. of Behavior and Utilization of Explosives in Engineering Design*, L. Davison and J. E. Kennedy (eds.), N. Mexico Section of the ASME, March.

Singh, S. (1955), "On the Jet Formation by Explosives with Lined Hemispherical Cavities," Research Notes, *Proc. Phys. Soc.*, Vol. 68B, London, pp. 785–789, October 1.

Sterne, T. E. (1950), "A Note on Collapsing Cylindrical Shells," *J. Appl. Phys.*, *21*(2): 73–74.

Titov, V. M. (1979), "Possible Regimes for Hydrodynamic Cumulation during the Collapse of a Casing," *Doklady Academic Nauk SSSR*, *247*(5): 1082–1084.

Trinks (1975), "German WW II Calculation Methods for Shaped Charges," MBB Report No. SOB-583, MWD-DEA G 1060 Meeting at ISL/Weil, FSTC 1198-76, October.

Van Thiel, M., and Levatin, J. (1978), "Jet Formation Experiments and Computations with Lagrange Code," LLNL, UCRL-82834, September.

Vigil, M. G., and Robinson, A. C. (1987), "Analytical-Experimental Comparison of 150 and 220 Grain per Foot Linear Shaped Charge Performance Parameters," *Proc. 10th Int. Symp. on Ballistics*, Vol. 2, San Diego, CA, October.

Zernow, L. and Simon, J. (1955), "High Strain Rate Plasticity of Liner Materials and Jet Behavior," BRL Report No. 954, August.

CHAPTER 6

THE VISCO-PLASTIC JET FORMATION THEORY

Other studies involving the collapse and formation of shaped charge liners were advanced by Soviet researchers. Returning to the collapse of conical liners or wedges, the USSR used the results of Birkhoff et al. (1948), or perhaps Lavrent'ev, as the basis for their studies, Lavrent'ev (1957) having claimed prior discovery. In any case, the results of Birkhoff or Lavrent'ev were extended to include visco-plastic effects by Godunov et al. (1975).

6.1. THE VISCO-PLASTIC CONCEPT

The visco-plastic model follows from Lavrent'ev (1957), Godunov et al. (1975, 1972, 1970), Deribas et al. (1967), Novikov (1963), and Simonov (1971). A detailed derivation and discussion of this model is given by Walters and Harrison (1980). The basic, visco-plastic model does not include transient effects. Typically, in the axisymmetric hydrocode models used in the West, compressible flow is assumed, and the material constitutive relationships are based on elastic–perfectly plastic, work hardening models or more sophisticated models, for example, Steinberg and Sharp (1980) and Steinberg et al. (1980). The USSR analytical models typically assume an incompressible flow but use a rate-dependent, visco-plastic material constitutive equation, for example, Godunov and Deribas (1972), and Godunov et al. (1975), and Walters (1979). This equation is usually of the form $\sigma = \sigma_y + \mu\dot{\varepsilon}$, where the stress σ is related to the strain rate $\dot{\varepsilon}$, by the yield stress σ_y and the constant dynamic viscosity coefficient μ.

Thus, the visco-plastic models require a knowledge of the dynamic viscosity coefficient, and many Soviet investigators have deduced viscosity coefficients

from experimental measurements under shock loading conditions. Walters (1979) summarizes many of the experimental viscosity values. Additional data related to viscosity measurements and the collapse of metallic bodies by high explosives are given by Al'tshuler et al. (1977), Deribas and Zakharenko (1974), Gordopolov et al. (1976, 1977, 1978), Shusnko et al. (1975), Lobanov (1975), Efromov (1975a, 1975b), Bezhanov (1977), Pogorelov et al. (1977), Sanasaryan (1971), Kozin et al. (1977), Shursnalov (1975), Rubtsov (1977a, 1977b), Mikhailov et al. (1974), Godunov et al. (1969), Ivanov (1966), Ivanov et al. (1977), Bichenkov and Lobanov (1974), Shekhter et al. (1977), and Laptev et al. (1974). The pioneering work of Walsh et al. (1953), as discussed later, served as the basis for many of the USSR studies.

Material viscosity values have also been experimentally determined in the United States, under shock loading conditions [see, e.g., Walters (1979) and Chhabildas and Asay (1979)]. The viscosity values deduced from various experimental measurements depend on many parameters, primarily strain rate, pressure, and temperature. Thus, the viscosity coefficient is not constant. In fact, for solid materials, the dynamic viscosity may range from typically 10 to 10^5 Pa-s (10^2–10^6 poise) depending on the strain rate, pressure, and temperature and the experimental method used to measure μ. Usually, the U.S. measured viscosity values under shock loading conditions may be as much as two orders-of-magnitude lower than the USSR measured viscosity values [e.g., Walters (1979), Al'tshuler et al. (1977), Deribas and Zakharenko (1974), Gordopolov et al. (1976, 1977, 1978), Shusnko et al. (1975), Lobanov (1975), Efromov (1975a, 1975b), Bezhanov (1977), Pogorelov et al. (1977), Sanasaryan (1971), Kozin et al. (1977), Shursnalov (1973), Rubtsov (1977a, 1977b), Mikhailov (1974), Godunov et al. (1969), Ivanov (1966), Ivanov et al. (1977), Bichenkov and Lobanov (1974), Shekhter et al. (1977), Laptev et al. (1974), and Chhabildas and Asay (1979)]. The uncertainty in the U.S. measured μ values is $\pm$ a factor of 10. The USSR methods may even have a greater amount of uncertainty. Experimental determination of μ in the United States, as performed by Chhabildas and Asay (1979), involves measurement of the shock rise time via velocity interferometry. The maximum stress is taken to be proportional to the strain rate, $\sigma = \mu\dot{\varepsilon}$, and the maximum stress is determined from the Rayleigh line and the shock Hugoniot pressures. The strain rate is calculated as the strain induced by the shock divided by the shock rise time, which is resolution limited. The time resolution is limited to 1–3 ns (Chhabildas and Asay 1979).

6.2. THE VISCO-PLASTIC MODEL

The Godunov shaped charge liner collapse model includes the influence of viscosity on the jet formation process. A jet formation criterion is derived that is based not on taking into account the compressibility effects or shock wave effects as in Walsh et al. (1953) or Chou et al. (1976), or on consideration of a

critical Mach number as in Harrison et al. (1979), but on taking into account the viscous (visco-plastic) properties of metals. A jet formation criterion attempts to guarantee that the jet is coherent, which means that it does not disperse or spread out in a radial direction, that is, has a radial component of velocity. Incoherent jets are also sometimes called bifurcated, overdriven, or diverging jets.

Following Godunov et al. (1975), an appropriate method is used to estimate the effect of viscosity in the plane (two-dimensional) problem of jet collisions. The fluid is incompressible, the motion irrotational and steady state, and the coefficient of viscosity is constant. Then the solutions of the Euler equations automatically satisfy the Navier–Stokes equations of motion, and the difference between the problems of ideal and viscous jet collisions is the condition on the free surface of the jet. The flow fields are taken to be Newtonian. For the flow fields to agree in the ideal and viscous flow problems, some forces must be applied to the free surface in the viscous flow case (Godunov et al. 1975). Consideration of the influence of these forces on the flow resulting from the collision between jets of an ideal fluid will provide a measure of the influence of viscosity in the jet formation problem (Godunov et al. 1975).

The formation of a reverse jet (slug) is possible only if the horizontal component of the viscous force, acting on the free surfaces of the reverse jet, is less than the force resulting from the symmetric collision of two plane fluid jets (Godunov et al. 1975). This inequality allows one to define a Reynolds number and a critical Reynolds number for jet formation.

The visco-plastic shaped charge jet collapse model derived by Godunov et al. (1975) relaxes to the classical U.S. models reviewed earlier when the dynamic viscosity is zero. Basically, the visco-plastic model yields a lower jet velocity and a lower flow velocity than the U.S. models. However, the visco-plastic model predicts a higher slug velocity than the U.S. models. The USSR (visco-plastic) criterion to form a coherent jet is that the Reynolds number,

$$\mathrm{Re} = \frac{tU \sin^2 \beta}{\nu(1 - \sin \beta)} \tag{1}$$

be greater than 2. The wall thickness is denoted by t, ν is the kinematic viscosity equal to μ/ρ, 2β is the collision angle, and U is the inviscid flow velocity as given by Defourneaux or the PER model, for example. The Reynolds number greater than 2 criterion is based on experimental observations [see Godunov et al. (1975) and Walters (1979)]. Detailed formulas for the jet strain rate, jet velocity, viscid flow velocity, and slug velocity are given in Godunov et al. (1975) and Walters (1979). Also, by setting Re = 2 in Eq. (1), an expression for the critical flow velocity as a function of β, t, and ν can be obtained. If the critical flow velocity is greater than the flow velocity, a coherent jet will not form. Simonov (1971) and others [e.g., Walters (1979),

Al'tshuler et al. (1977), Deribas and Zakharenko (1974), Gordopolov et al. (1977, 1978), Efromov (1975a), Pogorelov et al. (1977), Kozin et al. (1977), Mikhailov et al. (1974), Godunov et al. (1969), Rubtsov (1977b), and Bichenkov and Lobanov (1974)] define collapse angles for the transition from the jet regime to the jetless regime for explosive bonding applications. These investigators defined collapse angles below which only incoherent jets will form and collapse angles below which no jet at all will form. Again, Walsh et al. (1953) had an obvious influence on these studies.

6.3. THE EQUATIONS FOR THE VISCO-PLASTIC JET FORMATION MODEL

For the transient flow (PER) case, the stagnation point velocity (V_c) is given as

$$V_c = D_a \frac{\sin(\beta - \alpha) - \sin(\beta - \alpha - \phi)}{\sin \beta}, \tag{2}$$

where D_a is the speed of the detonation wave, 2α is the conical liner apex angle, and $\phi = 2\delta$ is the plate bending angle. Equation (2) is used in both the PER and visco-plastic models. The flow velocity is given by

$$U = D_a \frac{\sin(\alpha + \phi) - \sin \alpha}{\sin \beta} \tag{3}$$

in the PER model. The visco-plastic flow velocity U_2 can be expressed in the form

$$U_2 = U\left(1 - \frac{2}{\mathrm{Re}}\right)^{1/2}, \tag{4}$$

Godunov et al. (1975) and Walters (1979) for Re > 2. Also, $U_2 = U$ when the dynamic viscosity, μ, is zero.

In the PER model, the jet velocity and slug velocity are, respectively,

$$V_j = V_c + U, \tag{5}$$

and

$$V_s = V_c - U. \tag{6}$$

In the visco-plastic model, the jet and slug velocities are

$$V_j = V_c + U_2, \tag{7}$$

and

$$V_s = V_c - U_2. \tag{8}$$

In both models,

$$V_j + V_s = 2Vc.$$

For steady-state collapse, analogous formulas are available from Godunov et al. (1975) and Birkhoff et al. (1948).

For both the steady-state and transient version of the visco-plastic theory, the PER theory can be obtained by setting the dynamic viscosity, μ, or the kinematic viscosity, $\nu = \mu/\rho$ equal to zero. Walters and Harrison (1980) discuss the PER and the visco-plastic models, and comparison is made to the experimental data obtained by Allison and Vitali (1962). Figure 1 shows this comparison and the excellent agreement between the two analytical models and the experimental data.

The strain rates calculated by the visco-plastic model (Godunov et al. 1975) are of the order of 10^6/s and show little variation with liner element position. Chou and Carleone (1975) calculated strain rates for an 81-mm diameter precision charge with a copper conical liner with a 42° apex angle and a 1.9-mm wall thickness and found a larger variation of strain rate with liner element position including liner elements in both compression and tension.

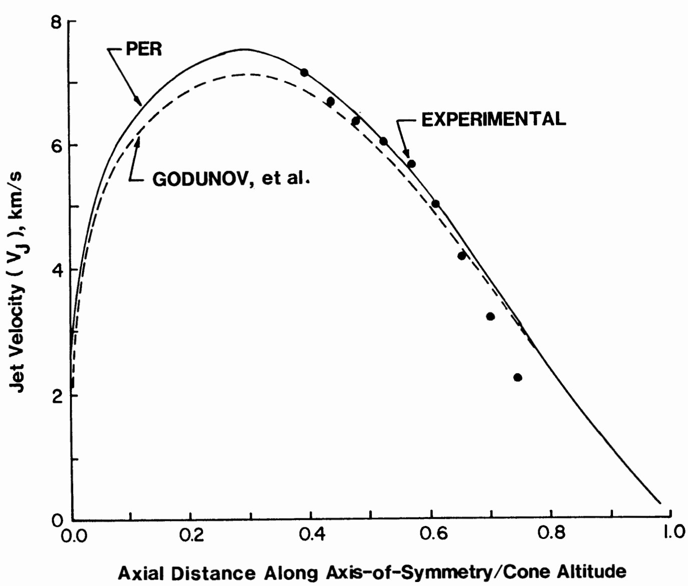

Figure 1. Jet velocity distribution for a 105-mm diameter conical copper liner with a 42° apex angle, a plane wave detonation velocity of 8 km/s, a wall thickness of 2.69 mm, and transient flow (Walters and Harrison 1980).

The peak strain rate was $10^5/s$. Experimental measurements of the strain rate of collapsing liners are not available, but Bauer and Bless (1979) measured the strain rate of exploding copper tubes to be about $10^4/s$, and Walters deduced the strain rates of stretching jets to be also of the order of $10^4/s$.

Additional data on various shaped charge jets are given by DiPersio et al. (1967) and Defourneaux (1970).

6.4. JET COHERENCY

The visco-plastic coherent jet or noncoherent jet criterion is based on a critical Reynolds number being greater than 2 (Godunov et al. 1975) or some other number, such as 5 or 10 (Mali et al. 1974). The Walsh et al. (1953), Chou et al. (1976), or the Harrison et al. (1974) criterion is based on inviscid flow, but compressibility effects are taken into consideration in the determination of the cohesiveness of the jet.

Walsh et al. (1953) studied the compressibility effect in the jet formation process as related to the oblique impact of explosively driven plates. The symmetric plate collision, as viewed from a moving coordinate system, reduces to a flow field analogous to two impinging streams. Walsh et al. (1953) concluded that jetting always occurs if the fluid is incompressible or if the collision velocity in the moving coordinate system is subsonic. For supersonic flow, jetting always occurs if $\beta > \beta_c$, where β_c is the critical turning angle for an attached oblique shock wave at the collision velocity. Walsh et al. (1953) did not address jet cohesiveness per se since their primary interest was explosive bonding. Cowan and Holtzmann (1963) present additional flow criteria for explosive bonding.

In the studies of Chou et al. (1976, 1974), jetting criteria for plane axisymmetric cases are presented along with a measure of the jet quality. Chou et al. state the following:

1. For subsonic collisions (or the collision velocity $V < C$, the material bulk speed of sound), a solid coherent jet always forms.
2. For supersonic collisions ($V > C$) jetting occurs if $\beta > \beta_c$, but the jet is not coherent. The angle β_c is the maximum angle that an attached shock wave can form at a prescribed supersonic velocity, V.
3. For supersonic collisions ($V > C$) but $\beta < \beta_c$, a jet will not be formed.

For shaped charge applications, the major criterion for jetting is that the formation process be subsonic. Otherwise, the jet will be incoherent and spread out radially.

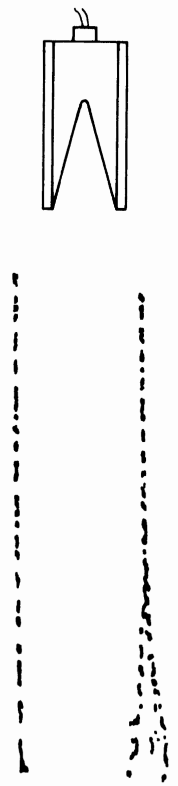

(a) (b)

Figure 2. Radiographs of jets from two typical conical charges. (a) 40° copper-lined charge, subsonic collision, coherent jet, and (b) 20° copper-lined charge, supersonic collision, noncoherent jet.

The speed of sound referred to is usually taken to be the bulk speed of sound of the material as opposed to a longitudinal or transverse shear speed of sound. The appropriate speed of sound, as well as its exact value under the extreme pressures and temperatures encountered in the formation region, is not well known. Also, the actual flow field is compressible and two dimensional (at least), and hence the subsonic collision condition is useful only as a general principle. In practice, it has been observed that the value of the critical Mach number based on the static bulk speed of sound is about 1.2 for conical copper liners (Harrison et al. 1974; Harrison 1981; Walters and Harrison 1980). In other words, the liner velocity divided by the bulk speed of sound, that is, the Mach number, could be as high as 1.2 and still achieve a cohesive jet for a conical, copper liner. A flow velocity of 4.8 km/s (1.23 times the bulk speed of sound of copper) is the calculated flow velocity above which 20° copper liners have been observed to have incoherent jet tips (Harrison et al. 1974). Figure 2 shows a flash radiography photograph of a copper, coherent and incoherent jet.

REFERENCES

Allison, F. E., and Vitali, R. (1962), "An Application of the Jet-Formation Theory to a 105 mm Shaped Charge," BRL Report No. 1165, March.

Al'tshuler, L. V., Kanel', G. I., and Chekin, G. S. (1977), "New Measurements of the Viscosity of Water behind a Shock Wave Front," *Sov. Phys. JETP*, *45*(2).

Bauer, D. P., and Bless, S. J. (1979), "Strain Rate Effects on Ultimate Strain of Copper," AFML-TR-79-4021, May.

Bezhanov, K. A. (1977), "Irregular Interaction of a Moving Shock Wave with a Tangential Discontinuity," *PMM, 41*(6).

Bichenkov, E. I., and Lobanov, V. A. (1974), "Acceleration of Metallic Plates by Explosion," *Fizika Goreniya i Vzryva*, *10*(2).

Birkhoff, G., MacDougall, D., Pugh, E., and Taylor, G. (1948), "Explosives with Lined Cavities," *J. Appl. Phys.*, *19*(6).

Chhabildas, L. C., and Asay, J. R. (1979), "Rise-Time Measurements of Shock Transitions in Aluminum, Copper, and Steel," *J. Appl. Phys.*, *50*(4).

Chou, P. C., and Carleone, J. (1975), "Calculation of Shaped Charge Jet Strain, Radius and Breakup Time," BRL CR 246, July.

Chou, P. C., Carleone, J., and Karpp, R. R. (1976), "Criteria for Jet Formation from Impinging Shells and Plates," *J. Appl. Phys.*, *47*(7).

Chou, P. C., Carleone, J., and Karpp, R. R. (1974), "The Effect of Compressibility on the Formation of Shaped Charge Jets," *Proc. 1st Int. Symp. on Ballistics*, Orlando, FL, November 13–15.

Cowan, G. R., and Holtzman, H. (1963), "Flow Configurations in Colliding Plates: Explosive Bonding, Part 1" *J. Appl. Phys.*, *34*(4): 928–939.

Defourneaux, M. (1970), "Hydrodynamic Theory of Shaped Charge and of Jet Penetration," Memorial De L'art Ille'rie Francasise-T, 44.

Deribas, A. A., and Zakharenko, I. D. (1974), "Surface Effects with Oblique Collisions between Metallic Plates," *Fizika Goreniya i Vzryva*, *10*(3).

Deribas, A. A., Kudinov, V. M., Matveenkov, F. I., and Simonov, V. A. (1967), "Determination of the Impact Parameters of Flat Plates in Explosive Welding," *Fizika Gorniya i Vzryva*, *3*(2).

DiPersio, R., Jones, W., Merendino, A., and Simon, J. (1967), "Characteristics of Jets from Small Caliber Shaped Charges with Copper and Aluminum Liners," BRL MR 1866, September.

Efromov, V. V. (1975a), "Oblique Impacts of Metallic Plates in an Elastic Formulation," *Zh. Prikladnoi Mekhaniki i Technicheskoi Fiziki*, (5).

Efromov, V. V. (1975b), "Investigation of Oblique Collisions of Metal Plates in an Elastic Formulation," *Zh. Prikladnoi Mekhaniki i Technicheskoi Fiziki*, (1).

Godunov, S. K., and Deribas, A. A. (1972), "Jet Formation upon Collision of Metals," *Doklady Akademii Nauk. SSSR*, *202*(5).

Godunov, S. K., Deribas, A. A., and Mali, V. I. (1975), "Influence of Material Viscosity on the Jet Formation Process during Collisions of Metal Plates," *Fizika*

Goreniya i Vzryva, *11*(1).

Godunov, S. K., Deribas, A. A., Zabrodin, A. V., and Kozin, N. S. (1970), "Hydrodynamic Effects in Colliding Solids," *J. Comp. Phys.*, *5*.

Godunov, S. K., Kazhdan, Ya. M., and Simonov, V. A. (1969), "Shock Wave Incidence on a V-Shaped Cavity," *Zh. Prikladnoi Mekhaniki i Technicheskoi Fiziki*, *10*(6).

Gordopolov, Yu. A., Dremin, A. N., and Mikhailov, A. N. (1976), "Experimental Determination of the Dependence of the Wavelength on the Angle of Collision in the Process of the Explosive Welding of Metals," *Fizika Goreniya i Vzryva*, *12*(4).

Gordopolov, Yu. A., Dremin, A. N., and Mikhailov, A. N. (1977), "Wave Formation with the High-Speed Collision of Metallic Bodies," *Fizika Goreniya i Vzryva*, *13*(2).

Gordopolov, Yu. A., Dremin, A. N., and Mikhailov, A. N. (1978), "Theory of Waves on the Interface of Metals Welded by Explosion," *Fizika Goreniya i Vzryva*, *14*(4).

Harrison, J. T. (1981), "Improved Analytical Shaped Charge Code: BASC," Ballistic Research Laboratory, Technical Report ARBRL-TR-02300, March.

Harrison, J., DiPersio, R., Karpp, R., and Jameson, R. (1974), "A Simplified Shaped Charge Computer Code: BASC," DEA-AF-F/G-7304 Technical Meeting: *Physics of Explosives*, Vol. II, April–May, Paper 13 Presented at the Naval Ordnance Laboratory, Silver Spring, Maryland.

Ivanov, V. A. (1966), "Disintegration of a Liquid Jet," *Zh. Prikladnoi Mekhaniki i Technicheskoi Fiziki*, *7*(4).

Ivanov, A. G., Novikov, S. A., and Kochkin, L. I. (1977), "Detonation Wave Collision on Surface of an Inert Material," *Fizika Goreniya i Vzryva*, *13*(4).

Kozin, N. A., Mali, V. I., and Rubtsov, M. V. (1977), "Tangential Explosion with Collapse of a Bimetallic Casing," *Combus., Explos. Shock Waves*, *13*(4).

Laptev, V. I., and Trishin, Yu. A. (1974), "Increase of Initial Velocity and Pressure upon Impact on an Inhomogeneous Target," *Zh. Prikladnoi Mekhaniki i Technicheskoi Fiziki*, (6).

Lavrent'ev, M. A. (1957), "A Cumulative Charge and the Principle of Its Work," *Usp. Mat. Nauk.*, *12*(4).

Lobanov, V. F. (1975), "Numerical Simulation of Flow during Compression of Cylindrical Samples by a Glancing Detonation Wave," *Zh. Prikladnoi Mekhaniki i Technicheskoi Fiziki*, (5).

Mali, V. I., Pai, V. V., and Skovpin, A. I. (1974), "Investigation of the Breakdown of Flat Jets," *Fizika Goreniya i Vzryva*, *10*(5).

Mikhailov, A. N., and Dremin, A. N. (1974), "Flight Speed of a Plate Propelled by Products from a Sliding Detonation," *Fizika Goreniya i Vzryva*, *10*(6).

Novikov, N. P. (1963), "Certain Properties of High-Speed Cumulative Jets," *Zh. Prikladnoi Mekhaniki i Technicheskoi Fiziki*, (1).

Pogorelov, A. P., Glushok, B. L., Novikov, S. A., Sinitsyn, V. A., and Chernov, A. V. (1977), "Dependence of Recoil Impulse from a Rigid Barrier under Sliding Conditions of Detonation of an Explosive Layer," *Fizika Goreniya i Vzryva*, *13*(5).

Rubtsov, M. V. (1977a), "Deformation of Liquid Line with the Collision of Jets," *Zh. Prikladnoi Mekhaniki i Technicheskoi Fiziki*, (6).

Rubtsov, M. V. (1977b), "Measurement of Velocity of a Cumulative Jet," *Fizika Goreniya i Vzryva*, *13*(6).

Sanasaryan, N. S. (1971), "Explosive Viscoplastic Deformation of a Tube and Its Relationship with the Properties of the Surrounding Medium," *Fizika Goreniya i Vzryva*, (4).

Shekhter, B. I., Shusko, L. A., and Krys'kov, S. L. (1977), "Investigation of the Squeezing Process of the Lining of an Elongated Hollow-Charge Pedicle," *Fizika Goreniya i Vzryva*, *13*(2).

Shursnalov, L. V. (1975), "Calculation of Cumulative Jets," *Izvestiya Akademii Nauk. SSSR*, *Mekhanika Znidkosti i Gaza*, (4).

Shusnko, L. A., Shekhter, B. I., and Krys'kov, S. L. (1975), "Bending of a Metal Strip by a Sliding Detonation Wave," *Fizika Goreniya i Vzryva*, *11*(2).

Simonov, V. A. (1971), "Flows due to an Incident Impact Wave on a Wedge Shaped Cavity," *Fizika Goreniya i Vzryva*, *7*(2).

Steinberg, D. J., and Sharp, R. W. (1980), "An Elastic-Viscoplastic Constitutive Model for Metals," LLNL UCRL-85086, October.

Steinberg, D. J., Cochran, S. G., and Guinan, N. W. (1980), "A Constitutive Model for Metals Applicable at High Strain Rate," *J. Appl. Phys.*, *51*(3): 1498–1504.

Walsh, J. M., Shreffler, R. G., and Willig, F. J. (1953), "Limiting Conditions for Jet Formation in High Velocity Collisions," *J. Appl. Phys.*, *24*(1).

Walters, W. P. (1979), "Influence of Material Viscosity on the Theory of Shaped Charge Jet Formation," BRL Memorandum Report, ARBRL-MR-02941, August.

Walters, W. P., and Harrison, J. T. (1980), "Modeling of the Shaped Charge Jet Formation," *Proceedings of the Army Symposium on Solid Mechanics, 1980—Designing for Extremes: Environment, Loading, and Structural Behavior,* AMMRC MS 80-4, September.

CHAPTER 7

COMMENTS ON EXPLOSIVE WELDING, BONDING, AND FORMING

This chapter will briefly address the concepts of explosive welding, explosive bonding, and explosive forming. These concepts, especially explosive welding and bonding, are related to jet collapse and formation.

The explosive working of metals and concepts related to explosive effects, standoff systems, contact systems, shock physics, and material effects are presented in an excellent introductory book by Rinehart and Pearson (1963).

7.1. EXPLOSIVE FORMING

An explosive forming procedure is shown in Figure 1. A die assembly holding the workpiece is positioned in a tank of water. A vacuum is drawn below the workpiece, and an explosive charge is detonated in the water. The workpiece then assumes the shape of the die (if all goes well). This technique represents one of many ways to fabricate a shaped charged liner.

A method for bulging cylindrical tubing is shown in Figure 2. The explosive charge is sealed in plastic and positioned in the cylindrical workpiece filled with water. The ends are sealed to add confinement and reduce water splash. The charge is detonated within the cylinder held by a split die assembly. Figure 2 shows the bulging cylinder produced. This technique is another example of explosive forming.

7.2. EXPLOSIVE WELDING AND BONDING

In explosive welding or bonding applications, two or more plates are driven together at high velocities, and surface jetting occurs. This results in a bond between the two driven metals and can result in a wavy interface of high

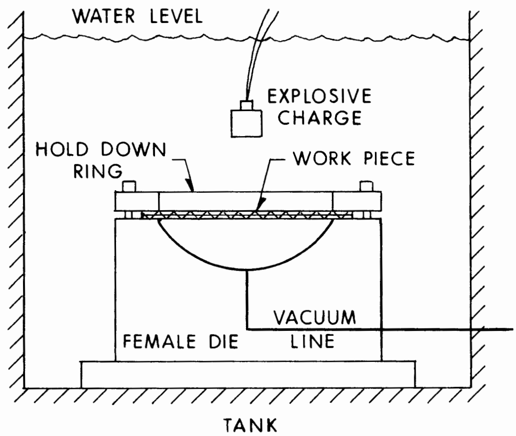

Figure 1. Explosive forming (Rinehart and Pearson 1963).

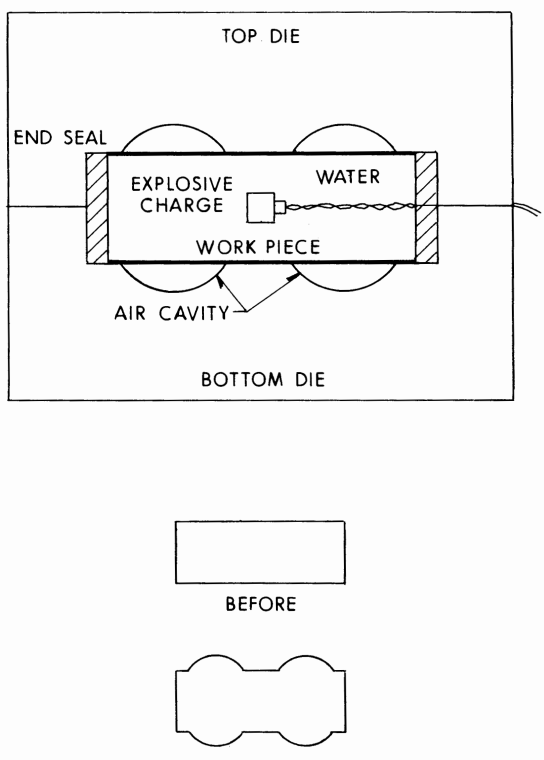

Figure 2. Bulging cylinder tube (Rinehart and Pearson 1963).

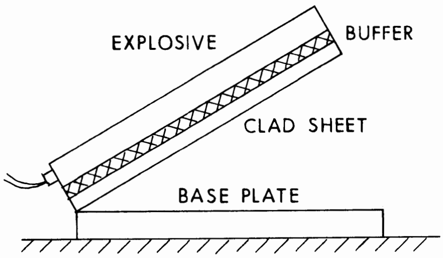

Figure 3. Surface cladding (Rinehart and Pearson 1963).

strength between the welded materials. If the plate impact velocities are too high (relative to the material properties), the interface material will jet as a shaped charge, and the bonding will not occur at the interface. The velocity must be such that plastic deformation occurs at the interface and only local surface jetting occurs. The requirements for welding to occur are (Blazynski 1983):

1. The existence of a jet at the interface.
2. An increase in pressure, associated with the rapid dissipation of kinetic energy, to a sufficient level for a sufficient time to achieve stable interatomic bonds. The pressure is determined by the impact velocity, and the time available for bonding is determined by the velocity of the collision point.

The final geometry of the explosive–metal system will vary depending on the geometry and materials of the parts to be welded. The nature of the interface between the welded parts will vary depending on the materials welded and the nature of the explosive–metal interaction system.

Figure 3 shows a surface cladding test arrangement. The top plate, or flyer plate, only is driven by the explosive force in order to weld a thin sheet of material onto a heavy sheet. This technique is useful in plating a good structural material with a thin cladding to protect it from a corrosive or hazardous environment.

Explosive welding is similar to explosive cladding, but two flyer plates are used to form an explosively welded final product. Figure 4 depicts an explosively welded sandwich or a three-layer weld.

Other examples of the explosive working of metals, as well as the details associated with these processes, can be found in Rinehart and Pearson (1963).

Blazynski (1983) provides a recent collection of papers dealing with many aspects of the explosive working of metals. Pearson [in Chapter 1 of Blazynski (1983)] describes the explosive hardening of austenitic manganese steels subjected to severe impact and abrasion. These steels are used in railroad frogs, rock crusher jaws, grinding mills, and similar devices. To explosively harden a steel, a thin layer of explosive is detonated in contact with the surface to be hardened, usually at grazing incidence. The propagation of the shock through

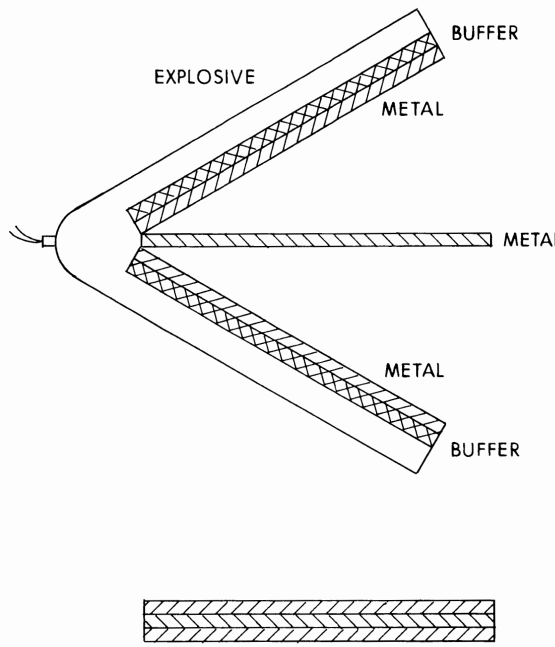

Figure 4. Explosive welding, a three-layer weld (sandwich) (Rinehart and Pearson 1963).

the material increases the metal hardness (BHN) throughout the material. This also increases the yield and tensile strength of the metal, making it more resistant to impact wear and with less tendency to deform. Duvall (1963) discusses shock wave propagation in metals.

Pearson [in Blazynski (1983)], discusses explosive compaction where explosive loads are applied either directly or through a loading system to compact powders. Two methods involve the use of gun powder cartridges and the use of explosives to drive pistons into the powder compaction chamber. Explosive compaction can produce parts from powders that cannot be produced by conventional pressing. Improved material properties with a high percent of the theoretical density can be produced. Explosive compaction is extremely valuable in the powder metallurgy field.

Pearson and El-Sobky [Chapters 1 and 6 of Blazynski (1983)] discuss explosive welding. This area has been mentioned previously, and the following discussion will highlight some of the major points of Blazynski's book.

Explosive welding is a solid-phase welding process in which high explosives are used to join the weld surfaces in a high-velocity collision. This collision produces severe, localized plastic flow at the interface between the two surfaces. Explosive welding is used to weld metal combinations, many of which cannot be welded by conventional means.

The weld is usually formed by oblique impact of the plate surfaces with the weld, progressing from the apex along the collision interface by a process similar to the collapse of a shaped charge liner. The parameters involved in explosive welding include the physical and mechanical properties of the metals to be welded, the type and amount of explosive used, the mode of initiation, the initial geometry of the weld operation, and the type and geometry of buffer sheets (if used) between the metal and the explosive. These parameters influence the collision angle, the impact velocity, and the collision point velocity.

It is generally agreed that jet formation at the collision point is essential for welding [e.g., El-Sobky, Chapter 6 of Blazynski (1983)]. This is because, at least in part, jetting produces chemically clean surfaces that allow interatomic bonding under the high-pressure conditions.

The jet–no jet criterion, or the limiting condition for jet formation, discussed in Chapter 6, is based on the studies of Cowan and Holtzman (1963), Walsh et al. (1953), Chou et al. (1976), and Harlow and Pracht (1966). These studies relate to shock formation and critical collapse angles and are also applied to shaped charge jets. [Note that the explosive weld geometry is a two-dimensional (wedge) shaped charge.] The mathematical description for the explosive welding of oblique plates involves relationships similar to those used in jet formation theory and in the Gurney-type equations. In addition to Gurney, impact velocity equations are given by Deribas et al. (1967) and others as reviewed by El-Sobky [Chapter 6 of Blazynski (1983)]. El-Sobky reviews the jet formation criterion as well as minimum impact pressures and standoff distance requirements that must be met. El-Sobky notes that the collision velocity and plate impact velocity should be less than the bulk speed of sound of either welding component. However, Wylie et al. (1971) suggest that the bulk speed of sound may be exceeded by as much as 25% with satisfactory welds. It is interesting that this coincides with the jet–no jet criterion observed by Harrison (1981a, 1981b) and Harrison et al. (1974) for copper jets, that is, Mach number of 1.23. Also, the visco-plastic critical Reynolds number criterion, discussed in Chapter 6, was derived from explosive welding experiments [see Walters (1979) and Walters and Harrison (1980)].

A major area of study in explosive welding is the interfacial periodic deformation or the interfacial waves. Often a regular wavy interface pattern appears, but the nature of the interfacial waves varies depending on the materials and system geometry used.

When regular waves are produced, they are very similar to the surface deformations found on solid surfaces subjected to erosive action of high-speed liquid films, jet drags, for example, in pump and steam turbine blades, and at the air–sea interface, for example, ocean waves. A review of the mechanisms for wave formation is given by El-Sobky [Chapter 6, Blazynski (1983)].

A good general discussion of explosive welding is given in *Mechanical Engineering* (1978). Jetting phenomena, the weld interface, and the explosive

load and standoff distance required for various weld combinations are discussed. Other excellent sources of information include the Soviet sources, given in the discussion on the visco-plastic jet formation model and viscosity measurements, for example, Walters (1979) and Walters and Harrison (1980). Schroeder (1984) recently edited a text on explosive welding and related areas. Deribas (1972) authored a classic text on explosive welding and work hardening. Duvall (1963) presents an excellent supplementary discussion on shock propagation and transmission through solids. Sewell (1965) also discusses explosive welding regarding jet–no jet criterion.

This concludes the discussion of explosive working of metals. The information provided in this section is not complete, nor was it intended to be. The intent was merely to provide an overview of explosive welding and related fields. The goal was to provide a brief introduction and a few fundamental references into this field and to note the similarity to shaped charge jetting phenomenon.

REFERENCES

Blazynski, T. Z. (ed.) (1983), *Explosive Welding, Forming and Compaction*, New York, Applied Science Publishers.

Chou, P. C., Carleone, J., and Karpp, R. R. (1976), "Criteria for Jet Formation from Impinging Shells and Plates," *J. Appl. Phys.*, *47*(7): 2975–2981.

Cowan, G. R., and Holtzman, A. H. (1963), "Flow Configurations in Colliding Plates: Explosive Bonding," *J. Appl. Phys.*, *34*(4): 928–939.

Deribas, A. A., Kudinov, V. M., Matveenkov, F. I., and Simonov, V. A. (1967), "Determination of the Impact of Flat Plates in Explosive Welding," *Fizika Goreniya i Vzryva*, *3*(2): 291–298.

Deribas, A. A. (1972), *Physics of Explosive Work-Hardening and Welding*, Novosibirsk: Nauka.

Duvall, G. E. (1963), "Shock Waves in Solids," *Internat. Sci. Tech.* April. A Conover-Mast Publication, N.Y.

Harlow, F. H., and Pracht, W. E. (1966), *Phys. Fluids*, *9*:1951–1959.

Harrison, J. T. (1981a), "Improved Analytical Shaped Charge Code: BASC," Ballistic Research Laboratory Technical Report ARBRL-TR-02300, March.

Harrison, J. T. (1981b), "BASC, An Analytical Code for Calculating Shaped Charge Properties," *Proc. 6th Int. Symp. on Ballistics*, Orlando, Florida, October 27–29.

Harrison, J. T., DiPersio, R., Karpp, R. R., and Jameson, R. (1974),"A Simplified Shaped Charge Computer Code: BASC," DEA-AF-F/G-7304 Technical Meeting, *Phys. Explos.*, Vol. II, April–May. Paper 13 presented at the Naval Ordnance Laboratory, Silver Spring, Maryland.

Mechanical Engineering (1978), "Explosive Welding," May.

Rinehart, J. S., and Pearson, J. (1963), *Explosive Working of Metals*, New York: Macmillan.

Schroeder, J. W. (ed.) (1984), *High Energy Rate Fabrication*, Foster Wheeler Development Corp., Livingston, N.J. (ASME Special Publications, Book No. H00381).

Sewell, R. G. S. (1965), "Effects of Velocity and Material Properties on Design Limits for Linear Shaped Charges," NAVWEPS Report 8793, NOTS TP 3894, October.

Walsh, J. M., Shreffler, R. G., and Willig, F. J. (1953), "Limiting Conditions for Jet Formation in High Velocity Collisions," *J. Appl. Phys.*, *24*(3): 349–359.

Walters, W. P. (1979), "Influence of Material Viscosity on the Theory of Shaped Charge Jet Formation," Ballistic Research Laboratory Memorandum Report AR-BRL-MR-02941, August.

Walters, W. P., and Harrison, J. T. (1980), "Modeling of the Shaped Charge Jet Formation," *Proceedings of the Army Symposium on Solid Mechanics, 1980—Designing for Extremes: Environment, Loading and Structural Behavior,* AMMRC MS 80-4, September.

Wylie, H. K., Williams, P. E. G., and Crossland, B. (1971), "Further Experimental Investigation of Explosive Welding Parameters," *Proc. 3rd Int. Conf. of the Center for High Energy Rate Forming*, University of Denver, Colorado.

CHAPTER 8

THE BREAKUP OF SHAPED CHARGE JETS

A typical shaped charge jet has a relatively high tip velocity and a low tail velocity. This velocity gradient causes the jet to stretch to great lengths at sufficiently large standoff distances. This length, which is directly proportional to the penetration capability of the jet, is limited by the eventual axial breakup of the jet into segments or particles. Once the jet particulates, the penetration decreases steadily and significantly. Consequently, an understanding of the jet breakup phenomena and methods of delaying its onset are of major importance to the shaped charge designer. In recent years, many investigators have studied this problem, notably Chou, Carleone, Walsh, Hirsch, Pfeffer, Haugstad, and Miller. In general, three approaches have been used: hydrocode studies, one-dimensional analytical models, and semi-empirical formulas. The following discussion parallels and extends the excellent overview article of Chou and Flis (1986).

8.1. HYDROCODE SIMULATION

One of the earliest hydrocode simulations of jet breakup was performed by Karpp and Simon (1976). Using the Lagrangian code HEMP, they demonstrated that jets with a uniform initial radius under continuous stretching eventually develop "necks." The rate of necking depends on the wavelength of the initial surface perturbation. Karpp and Simon (1976) also employed the conservation of angular momentum of a spinning jet to estimate the strength of copper under dynamic conditions. They estimated a strength value of 0.1 GPa. As shown in the following discussion, the dynamic strength value is necessary to accurately predict jet breakup times.

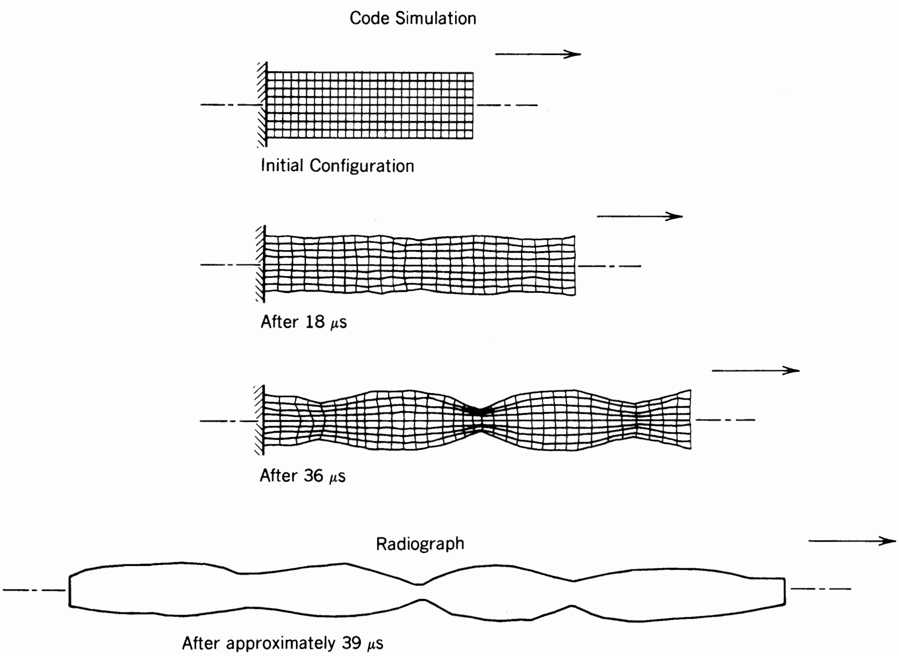

Figure 1. Comparison between hydrocode simulation of jet necking due to stability and flash radiograph of a jet at approximately the same time (Chou and Flis 1986).

Chou and Carleone (1976, 1977) and Chou et al. (1977) used HEMP for parametric calculations, varying the values of yield strength, jet density, and the initial disturbance wavelength and amplitude. They showed that perturbations in jet strength (flow stress) or velocity cause a plastic instability to occur. In fact, the critical wavelength seems independent of the perturbed physical quantity that triggers the instability. Figure 1 shows a comparison of their hydrocode simulations with the flash radiograph of a typical jet.

Miller (1981) calculated the elongation of a copper shaped charge jet using a two-dimensional hydrocode (PISCES). The hydrocode was modified to allow usage of the Steinberg–Cochran–Guinan constitutive equation. This constitutive model is applicable at high strain rates and includes the effects of pressure, temperature, and equivalent plastic strain on yield stress and shear modulus. Thus, it accounts for strain hardening and thermal softening. Other inputs to the code included initial jet geometry and end conditions (for the BRL 105-mm diameter, unconfined 42° conical copper shaped charge), jet axial and radial velocity fields, initial jet stress state, and initial jet temperature (assumed to be 450°C throughout the jet). Also, a steady-state tip or lead particle was included.

The calculation revealed the formation of a single neck at early time between the steady-state tip particle and the stretching jet. At later times, this

neck becomes more pronounced, and additional necks begin to form behind the original neck once the material yield strength reaches saturation (i.e., the onset of thermal softening). A similar behavior was observed at the rear of the jet. However, the time required for the necks to progress from the ends to the center of the jet was longer than that observed experimentally. Miller (1982) later concluded that these results were probably due to the "perfect" numerical jet. In a real jet, random necks would be present throughout the jet, caused by the imperfect formation of the jet. These random necks would cause the jet to neck down prematurely compared to a "perfect" numerical jet.

Osborn (1981) used the two-dimensional code TOODY to study the jet breakup problem. Pfeffer (1980) also simulated jet breakup using the STRESS-2 code.

8.2. ANALYTICAL JET BREAKUP MODELS

In the one-dimensional modeling of the jet breakup phenomenon, the approach is similar to that used in the study of stability of liquid jets. One-dimensional governing differential equations are first written in Lagrangian coordinates. The initial and boundary conditions are specified. Some small disturbance is then introduced. If the disturbance grows in amplitude, the jet is unstable and necking will occur. A familiar liquid jet instability is water flowing from a faucet; at first it has a constant diameter, then becomes wavy with necks, and finally turns into droplets. But, whereas the controlling force in the water jet is the surface tension, the governing factors for shaped charge jets are the material strength and inertia force.

In a series of papers and reports, Chou and Carleone studied jet breakup using a one-dimensional model. In Chou and Carleone (1976, 1977), they modeled the jet with linearized equations and showed that the ratio Y/ρ of jet flow stress to jet density controlled the growth of the instability. A low value of this ratio causes the jet to neck down more slowly than a material with a large value, all other conditions being equal. This early version of the theory, however, could not predict the critical wavelength. Carleone et al. (1977) extended the theory to include the stress concentration at the jet necks. The resulting equations clearly showed the existence of a critical wavelength as discussed earlier. The linearized solution of the theory showed the critical wavelength to be independent of the jet stretching rate, with a value 2.22 times the jet diameter d_0 at the time of onset of the instability. However, detailed two-dimensional hydrocode simulations, also presented by Carleone et al. (1977), clearly showed the critical wavelength to be a function of jet stretching rate. Carleone et al. (1979, 1981) solved the nonlinear equations by a finite-difference method, with results showing the observed dependence of critical wavelengths on jet stretching rate. The correct number of jet segments was also obtained from the solution. The use of a finite-difference solution removes the necessity of linearizing the equations in order to obtain a solution. Thus,

more advanced, for example, visco-plastic, constitutive equations may be used in the model since the equations are solved numerically.

Miller (1982) also obtained a one-dimensional solution to the jet necking problem. The solution is based on a perturbation technique that allows linearization of the governing equations. The solution is obtained by separation of variables and a Fourier integral representation of the solution. The jet was assumed to be long and nearly cylindrical (a small neck at the center of the jet was assumed), an initial linear velocity gradient was assumed, and a perfectly plastic constitutive equation was used.

The one-dimensional solution predicted the generation of a progression of new necks from an existing neck. Also, the formation of necks near the tip of the stretching jet was accurately simulated. These results were verified by two-dimensional finite-difference calculations using the same initial conditions and constitutive equations. A more sophisticated constitutive model, the Steinberg–Cochran–Guinan equation, predicted the same behavior.

Walsh (1984) carried out a dimensional analysis based on the one-dimensional equations and performed a detailed parametric calculation on the effects of surface roughness, the effects of nonuniform initial velocity gradients, and the effects of nonuniform material yield strength (all of which are kinds of initial disturbances). He also proposed a scaling relation. His conclusions are in general agreement with those of Carleone et al. (1979, 1981). Walsh, however, provides considerable insight into the mechanisms related to plastically stretching metal jets. His results show that the breakup time is only mildly dependent on the amplitude of the initial disturbance. Walsh also concluded that breakup could be delayed by reducing the shaped charge fabrication tolerances and/or increasing the homogeneity of the shaped charge components. Also, breakup time delays can be achieved by reducing the jet material yield strength. Since the material yield strength is substantially modified during jet collapse and formation, by shock heating and severe plastic work, measurement of the yield strength for a stretching jet is required. Such measurements could lead to the eventual control of the jet strength.

8.3. SEMI-EMPIRICAL FORMULAS

Quite a few empirical formulas have been proposed. Hirsch (1979, 1981a) presented a phenomenological formula for the jet breakup time. In this formula, the breakup time is related to the smallest characteristic dimension (original liner thickness) and an empirical constant V_{pl}, the velocity that characterizes the metal and that may be related to the velocity difference between segmented jet particles or to $\sqrt{Y/\rho}$. This formula is

$$t_b = \frac{2r_0}{V_{pl}} \tag{1}$$

where r_0 is the initial jet radius or radius when the jet elongation begins. Equation (1) can be expressed as

$$t_b = \frac{1}{V_{pl}} \sqrt{8RT_L} \sin\frac{\beta}{2},$$

where t_b is the breakup time measured from the arrival of the detonation wave at the liner element from which the jet originates, R is the radius of the element, T_L is its thickness, and β is the collapse angle.

Equation (1) gives reasonable breakup times for certain charges, but because it is independent of the stretching rate, its application is limited.

Hirsch (1981b) also comments on the natural jet spread and tumbling of the particles after breakup.

Pfeffer (1980) also presented a formula for jet breakup time. He performed two-dimensional hydrocode calculations of jet stability and fit a simple formula as follows

$$t_b = \frac{1.4}{\eta_0} + 48.5\frac{r_0}{C_0}, \tag{2}$$

where η_0 is the initial strain rate, r_0 is the initial jet radius, and C_0 is the shock velocity in the jet. Since this formula is independent of jet strength, its application is also limited. Pfeffer showed correctly that the critical wavelength is approximately independent of jet diameter. Detailed comparisons of Hirsch's and Pfeffer's results with experimental data may be found in Carleone et al. (1979, 1981) and Carleone and Chou (1981).

Haugstad and Dullum (1983) and Haugstad (1983) postulate two formulas based on the constitutive equation

$$\sigma = \sigma_0 + \mu\eta, \tag{3}$$

which is an elastic-visco-plastic material model where μ has the form of a viscosity, σ is the stress, η is the strain rate, and σ_0 is the quasistatic yield stress.

For the case where $\mu \to 0$, Haugstad and Dullum (1983) take

$$t_b = \frac{\alpha d_0}{(\sigma_0/\rho)^{1/2}} - \frac{1}{\eta_0}, \tag{4}$$

where α is a constant, ρ is the liner material density, d_0 is the initial stretching jet diameter, and η_0 is the initial strain rate. If the Hirsch velocity V_{pl} is taken to be $(\sigma_0/\rho)^{1/2}/\alpha$, then Eq. (4) results in a formula similar to that given by Hirsch with a correction term for the strain rate.

For the case where the visco-plastic (μ) effects dominate, Haugstad and Dullum (1983) propose

$$t_b = \beta \frac{\mu}{\sigma_0} - \frac{1}{\eta_0}, \tag{5}$$

where β is a constant.

Haugstad notes that an exact description of the jet breakup cannot be formulated within the framework of continuum mechanics, which does not account for material microstructure. Only "first-order" effects resulting from mechanical properties (such as density, yield strength, etc.) can be obtained from the application of continuum mechanics to shaped charge jet breakup. Also, due to the high strain rates involved (10^4–10^6/s), dynamic effects are evident.

Haugstad and Dullum (1983) also addressed necking of a jet in uniaxial tension and obtained a similar behavior to that reported by Chou, Carleone, and others. Haugstad concluded that an increase in the breakup time of a shaped charge jet should correlate with a decrease in σ_0 and an increase in μ. In turn, an increase in μ would result from a reduction in grain size of the liner material or a trend toward superplasticity. Haugstad also noted that a dependence on material viscosity would tend to preclude the scaling of breakup time with charge size.

The model comparison between Chou–Carleone, Pfeffer, and Hirsch, given by Carleone et al. (1979, 1981) and Carleone and Chou (1981), shows that the breakup model developed by Chou and Carleone (1976, 1977), Chou et al. (1977), Carleone et al. (1977, 1979, 1981), and Carleone and Chou (1981) provides the best available correlation over a wide spectrum of experimental data. These data include several different liner geometries and liner materials. Walters provided most of the experimental data used to derive and evaluate the model. The analytical results of Walsh (1984), Haugstad and Dullum (1983), and Haugstad (1983) provide additional insight into the jet breakup phenomena.

8.4. THE CHOU - CARLEONE MODEL

The current understanding of the jet breakup phenomenon will now be summarized and a practical design formula will be presented. The summary and formulas are from Chou and Flis (1986). First, the jet necking instability will be examined.

Figure 2 shows schematically a stretching jet that has a wavy surface due to some initial disturbance. The amplitude of the wave initially is very small (the figure shows an exaggerated surface). Consider a small element bounded by surfaces 1 and 2. Section 2 is near the neck, so the average axial stress there is higher than that at section 1 because of stress concentration. It is known that

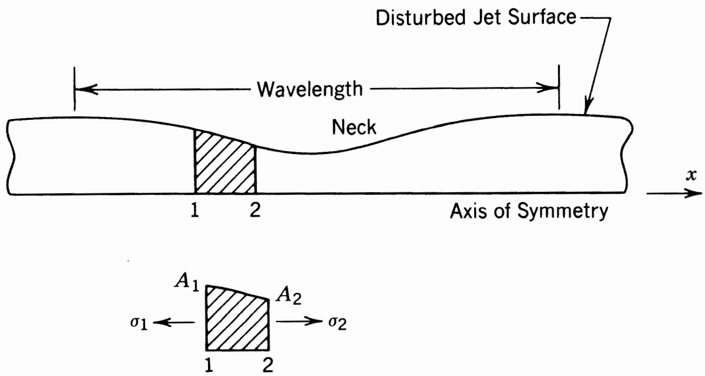

Figure 2. Schematic diagram showing the necking instability of shaped charge jets. Section 2 has a smaller area than section 1, but due to stress concentration, has larger flow stress. If $A_1\sigma_1 > A_2\sigma_2$, the jet is unstable and the neck gets smaller (Chou and Flis 1986).

the stress near the neck is inversely proportional to the radius of curvature. Therefore, the smaller the wavelength of the disturbance, the higher the difference between the stresses at sections 2 and 1. The area at section 1 is larger. The net surface force acting at this element is

$$F = \sigma_2 A_2 - \sigma_1 A_1. \tag{6}$$

If this force is positive, it pulls the element toward the neck, causing it to heal and thus stabilizing the jet. If negative, the element moves away from the neck, and the amplitude of the disturbance becomes larger, so the jet is unstable. In the actual case, there is a critical wavelength that is most unstable. For disturbances of random wavelength, the critical one grows the fastest and forms deep necks that determine the fragment length in the broken jet.

The jet breakup process can be divided into two phases. The first is the increase in amplitude of the wavy surface and the forming of necks due to plastic instability, as already discussed. The second phase is the actual breakup, or separation, at the necks. While the disturbance with the critical wavelength starts to grow and form necks, the jet is still stretching and the neck radius gets smaller. The amount of stretching, or necking, at which the jet breaks is another property of the material. The term f is used to represent the degree of necking, where

$$f = \frac{A_{\text{avg}} - A_{\text{min}}}{A_{\text{avg}}}, \tag{7}$$

and A_{avg} is the current average cross-sectional area and A_{min} is the current minimum area (at the neck). The term f_s, the dynamic ductility, is defined to be the value of f at which the jet breaks. In general, f_s is a property of the jet material.

From dimensional analysis and one-dimensional calculations, the breakup time in dimensionless form becomes

$$\bar{t}_b = 3.75 - 0.125\bar{\eta}_0 + \frac{1}{\bar{\eta}_0}, \tag{8}$$

where $\bar{t}_b$ = dimensionless breakup time = $C_p t_b / r_0$
$C_p = \sqrt{Y/\rho_o}$
η = dimensionless strain rate = $\eta_0 r_0 / C_p$
η_0 = initial strain rate $\Delta V / \Delta X$,

and t_b is the breakup time, Y the yield strength, ΔV the change in velocity over the length ΔX. The subscript 0 designates initial values when the liner element first arrives at the axis of symmetry. This equation is obtained with a value of dynamic ductility f_s of 0.3, which seems to fit most experimental data, as shown in Figure 3. The three experimental points with a large t_b do not agree with the model for $f_s = 0.3$. These data points are from a 127-mm diameter, ETP copper cone with a 60° apex angle, and a 1.5% (1.905-mm) wall thickness, that is, a fairly standard round. The reason for the discrepancy between theory and experiment is unknown.

Equation (8) shows that in dimensionless form, the breakup time is a function of the initial stretching rate only. This conclusion is in agreement with Walsh's (1984) results, for if his formula for jet length at breakup is transformed into breakup time, it will also be a function of $\bar{\eta}_0$ only. The strain rate can be found from the one-dimensional jet formation and collapse theory (e.g., Carleone and Chou 1974).

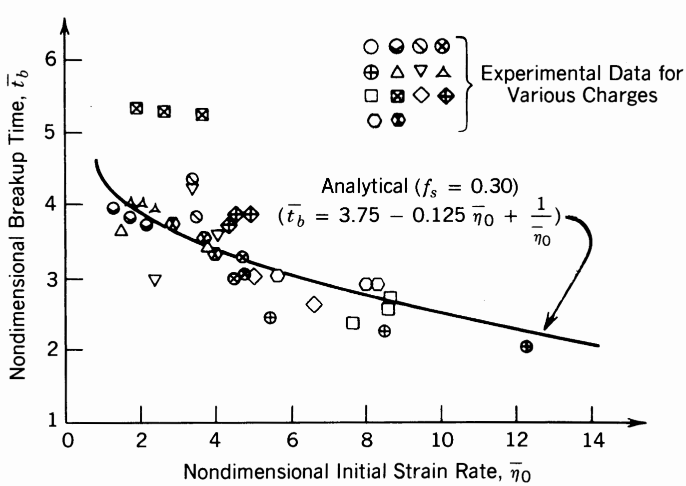

Figure 3. Comparison between the analytical breakup time formula and some experimental data (Chou and Flis 1986).

If a value of dynamic ductility larger than 0.3 is chosen, the constants in Eq. (8) will change and the $\bar{t}_b$ curve in Figure 3 will move up. Equation (8) contains three terms on the right-hand side. The first two represent a straight line with intercept 3.75 and slope -0.125. The third term contributes significantly only at small values of $\bar{\eta}_0$. In dimensional form, Eq. (8) is

$$t_b = \frac{r_0}{C_p}\left(3.75 - 0.125\frac{\eta_0 r_0}{C_p} + \frac{C_p}{\eta_0 r_0}\right). \tag{9}$$

It can be seen that scaling applies, if all dimensions of a charge are doubled, while all other properties remain the same, then the breakup time will also double. This is because the stretching rate η_0 is inversely proportional to ΔX; therefore, if the velocity for each mass point remains the same, $\eta_0 r_0$ does not change with charge dimensions. This apparent scaling may result from the linearized solution of the governing equations. However, from the results of this analysis and from available experimental data, it is evident that the breakup time scales at least within $\pm 20\%$. The experimental data considered were for charge sizes between 60 and 178 mm. For charge diameters outside this range, it is difficult to study scaling due to variability of liner metallurgy, the difficulties associated with the explosive casting of large charges, and the precision of fabrication required for small charges. At any rate, with due consideration given to the round-to-round variability, the breakup time appears to approximately scale. Scaling will be discussed in detail in a later chapter.

From Eq. (9), one can observe that the breakup time increases as η_0 decreases. The dependence of t_b on C_p is not obvious because the first two terms of Eq. (9) have opposite signs. It can be shown easily that for $\bar{\eta}_0$ less than 15, which covers most practical shaped charges, the derivative $\partial t_b / \partial C_p$ is negative, and thus the breakup time is inversely proportional to C_p. The breakup time will increase with decreasing yield strength Y and with increasing jet density ρ_0.

In Eqs. (8) and (9), the jet yield strength Y is not necessarily the static handbook value. In Carleone et al. (1979, 1981), values of Y for certain metals and the method by which it was determined are given. Some of these values are listed here:

Liner Material	Y, Jet Yield Strength (Pa)
Copper	
ETP	2×10^8
OFHC	2.7×10^8
Aluminum	1×10^8

Carleone (1987) provides the mathematical details and pertinent hydrocode results for the Chou–Carleone breakup time prediction model. This model is also capable of calculating the number of jet segments resulting after jet breakup. Several trends are shown by Carleone (1987), namely, the number of jet segments decreases as the cone apex angle increases or as the conical liner wall thickness increases. The Chou–Carleone model shows that the jet does not instantaneously breakup but breaks from tip to tail showing a distribution of breakup times. In fact, the jet always breaks from tip to tail by the Chou–Carleone model, which is usually, but not always, the case. Finally, the model shows that the breakup times can be increased as follows:

1. Increasing the jet radius
2. Decreasing the jet stretching rate
3. Decreasing the jet strength
4. Increasing the jet density
5. Increasing the jet dynamic ductility

In general, if all other parameters remain the same, increasing the jet breakup time increases the penetration, especially at the optimum standoff. These effects are discussed in Chapter 9.

8.5. MAXIMUM JET VELOCITY

The maximum velocity attainable by a shaped charge jet was estimated by Carleone and Chou (1981). Standard jet formation theory and the subsonic collision conditions for jet coherence (Chou et al. 1974, 1976) were used to obtain the following formula:

$$V_j \leq 2.41C. \tag{10}$$

Equation (10) states that the maximum jet velocity is 2.41 times the bulk speed of sound of the liner material.

REFERENCES

Carleone, J. (1987), "Mechanics of Shaped Charges," Section 3, Course Notes, *Basic Principles of Hypervelocity Impact and Related Topics*, April, Computational Mechanics Associates, Baltimore, MD.

Carleone, J., and Chou, P. C. (1974), "A One-Dimensional Theory to Predict the Strain and Radius of Shaped Charge Jets," *Proc. 1st Int. Symp. on Ballistics*, Orlando, FL, November 13–15.

Carleone, J., and Chou, P. C. (1981). "Maximum Jet Velocity and Comparison of Jet Breakup Models," BRL Contractor Report ARBRL-CR-00458, July.

Carleone, J., Chou, P. C., and Ciccarelli, R. D. (1977), "Shaped Charge Jet Stability and Penetration Calculations," U.S. Army Ballistic Research Laboratory (BRL) Contractor Report No. 351, April.

Carleone, J., Chou, P. C., and Walters, W. P. (1981), "An Improved Shaped Charge Jet Breakup Calculation and Measurement of Jet Properties," U.S. Army Ballistic Research Laboratories (BRL) Contractor Report No. ARBRL-CR-00445, January.

Carleone, J., Chou, P. C., Walters, W. P., Jameson, R., and Ciccarelli, R. D. (1979), "Prediction of Shaped Charge Jet Breakup Time and Calculation of Penetration," U.S. Army Ballistic Research Laboratory (BRL) Contractor Report No. ARBRL-CR-00396, April.

Chou, P. C., and Carleone, J. (1976), "Breakup of Shaped Charge Jets," *Proc. 2nd Int. Symp. on Ballistics*, Daytona Beach, FL, March 9–11.

Chou, P. C., and Carleone, J. (1977), "The Stability of Shaped Charge Jets," *J. Appl. Phys.*, *48*(10): 4187–4195.

Chou, P. C., and Flis, W. J. (1986), "Recent Developments in Shaped Charge Technology," *Propell., Explos., Pyrotech.*, *11*: 99–114.

Chou, P. C., Carleone, J., and Karpp, R. R. (1974), "Study of Shaped Charge Jet Formation and Breakup," BRL Contractor Report BRL-CR-138, February.

Chou, P. C., Carleone, J., and Karpp, R. R. (1976), "Criteria for Jet Formation from Impinging Shells and Plates," *J. Appl. Phys.*, *47*(7): 2975–2981.

Chou, P. C., Carleone, J., Tanzio, G. A., and Ciccarelli, R. D. (1977), "Shaped Charge Jet Breakup Studies Using Radiograph Measurement and Surface Instability Calculations," U.S. Army Ballistic Research Laboratory (BRL) Contractor Report No. 337, April.

Haugstad, B. (1983), "On the Breakup of Shaped Charge Jets," *Propell., Explos., Pyrotech.*, *8*: 119–120.

Haugstad, B. S., and Dullum, O. (1983), "The Jet Fragmentation Problem and Its Relation to Shaped Charge Engineering," Shaped Charge Symposium, MBB, Schrobenhausen, FRG, September.

Hirsch, E. (1979), "A Formula for the Shaped Charge Jet Breakup Time," *Propell. Explos.*, *4*: 89–94.

Hirsch, E. (1981a), "A Model Explaining the Rule for Calculating the Breakup Time of Homogeneous Ductile Metals," *Propell. Explos.*, *6*: 11–14.

Hirsch, E. (1981b), "The Natural Spread and Tumbling of the Shaped Charge Jet Segments," *Propell. Explos.*, *6*: 104–111.

Karpp, R. R., and Simon, J. (1976), "An Estimate of the Strength of a Copper Shaped Charge Jet and the Effect of Strength on the Breakup of a Stretching Jet," U.S. Army Ballistic Research Laboratory, BRL Report No. R1893, June, AD #B012 141.

Miller, C. W. (1981), "A New Approach to the Numerical Analysis of Shaped Charge Jets," *Proc. 6th Int. Symp. on Ballistics*, Orlando, FL, October.

Miller, C. W. (1982), "Generation of Necks in an Elongating Shaped Charge Jet," *Proceedings of the BRL Symposium on Ballistics*, ADPA, November.

Osborn, J. J. (1981), "Effects of Material Properties on the Deformation and Necking of Rods Stretching under Large Velocity Gradients," 7th Annual Technical Meeting, DEA-AF/71-F/G-7304, Lawrence Livermore Laboratory, October 21–23.

Pfeffer, G. (1980), "Determination par Simulations Numeriques de L'etat et des Lois de Fragmentation des Jets de Charges Creusses," *Proc. 5th Int. Symp. on Ballistics*, Toulouse, France, April 16–18.

Walsh, J. M. (1984), "Plastic Instability and Particulation in Stretching Metal Jets," *J. Appl. Phys.*, *56*(7): 1997–2006.

CHAPTER 9

SHAPED CHARGE JET PENETRATION MODELS

NOTATION

B_{max}	Brinell hardness of target
CD	charge diameter
D	rod diameter
E_1	energy in last part of projectile
g	gap distance between particles
g_0	empirical constant
H_D	dynamic hardness of target
H_0	height of interaction region
k_j	jet body shape factor
k_T	target body shape factor
l	jet length
L	rod length
M	jet mass
P	penetration depth
P_0	penetration depth at zero standoff
r_j	jet radius
S or SO	standoff
t	time
t_0	time for jet to reach the target
t_b	jet breakup time
T	time at end of penetration
U	penetration velocity
U_{min}	minimum penetration velocity

V	jet velocity
V_I	velocity at top of the interaction region
V_{min}	minimum jet velocity
V_0	jet tip velocity
Y	target strength
α, β	empirical constants
γ	$(\rho_t/\rho_j)^{1/2}$
$d\xi$	incremental length of jet
λ	empirical constant
μ	dynamic viscosity
ρ_j or ρ_0	jet density
ρ_T or ρ_{T_0}	target density
σ_j	dynamic strength of jet
σ_p	dynamic strength of penetrator
σ_{SD}	stress state of deforming penetrator
σ_t	dynamic strength of target

Other specialized symbols are defined as used.

9.1. INTRODUCTION

Analytical models capable of predicting the penetration of the jets from shaped charges into a variety of target materials are extremely valuable to the terminal ballistician. Many disciplines are involved since shaped charge jets are used to penetrate or perforate armor, as well as rocks, soil, wood, ice, and other nonmetallic materials. These analytical models provide fast analytical predictions where the time and resources available prohibit large hydrocode computer solutions. Also, the target may be monolithic or it may consist of several layers of different materials including air or liquids. Thus, analytical penetration expressions usually assume one-dimensional flow and employ other simplifying assumptions.

Early analytical penetration models (1940 vintage) were based on the Bernoulli principle. Later, empirical factors were introduced to account for particulation of the jet. Eventually, non-uniform-velocity (i.e., stretching) jets were incorporated into the models. Other authors included terms to account for jet and target strength effects, compressibility effects, and the effects of jet drift, particle dispersion, and particle tumbling. These models were based primarily on the Bernoulli principle or on a rod-type penetration model. Other models included transient effects based on a one-dimensional conservation of mass and momentum without recourse to the rod models or the Bernoulli concept.

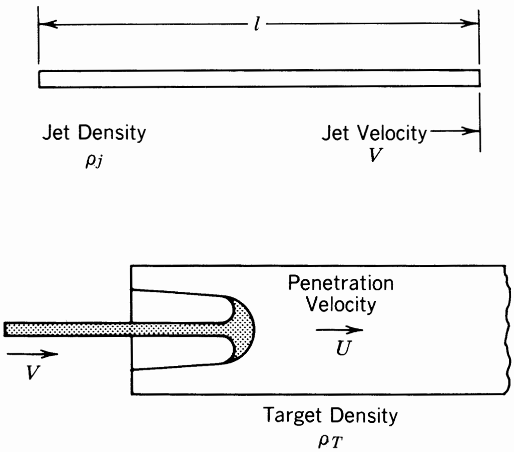

Figure 1. Jet penetration.

9.2. SHAPED CHARGE JET PENETRATION

Birkhoff et al. (1948) and Hill et al. (1944) developed a simple penetration theory from the hydrodynamic theory of impinging jets. This theory is further documented in NDRC (1946).

Because of the hypervelocity associated with shaped charge jets, the pressures produced during jet–target impact far exceed the yield strength of most materials. Thus, to a first approximation, the strengths and viscosities of the jet and target materials can be neglected, allowing usage of the familiar hydrodynamic assumption of incompressible, inviscid fluid flow.

Consider a shaped charge jet of length l, density ρ_j, and velocity V penetrating a semi-infinite, monolithic target of density ρ_T. The penetration velocity is U, as shown in Figure 1. The penetration is simpler when viewed from a system of coordinates moving with the penetration velocity U, as shown in Figure 2. In this system the hole profile is fixed, and the jet moves to the right at a velocity $V - U$, and the target moves left at a velocity U. The

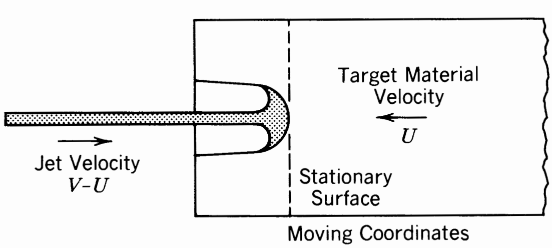

Figure 2. Jet penetration with a coordinate system moving at the penetration velocity, U.

pressure on the two sides of the interface between the jet and the target must be the same. Now, since the phenomenon is steady state in this system of coordinates, Bernoulli's equation may be applied along the axial streamline so that

$$\tfrac{1}{2}\rho_j(V - U)^2 = \tfrac{1}{2}\rho_T U^2. \tag{1}$$

Figure 2 shows the jet being eroded while penetrating the target. Assuming that steady state is reached instantaneously and that the penetration ceases when the rear of the jet strikes the target, then the total penetration P is the penetration velocity times the penetration time or

$$P = U\frac{l}{V - U} \quad \text{or} \quad P = l\left(\frac{\rho_j}{\rho_T}\right)^{1/2} \tag{2}$$

using Eq. (1). This simple equation indicates that the penetration is independent of the jet velocity. However, the rate at which the jet erodes and the final stretched length of jet depends on the jet velocity through the term l. Note that for real jets, l is a function of time.

There are several limitations to this simple theory. First, after the last jet particle strikes the target, that is, after the jet is consumed, the residual inertia of the penetrator may cause the hole to continue to grow in depth (and width). This additional depth has been called the secondary penetration (NDRC 1946), or afterflow. The depth of the crater when the jet vanishes is called the primary penetration.

Second, even the primary penetration is not predicted exactly, as effects other than density come into play. For example, a greater penetration into mild steel is observed than in armor steel, even though both have the same density. Also, greater penetration into soft materials, such as lead, occurs than would be directed by the density law. These results undoubtedly occur because material strength, strain, strain rate dependence, and other material properties are not included in the simple penetration model. These effects are especially important at low jet velocities and less important at hypervelocities. In short, a density (and even a yield strength) is usually not sufficient to characterize a target material for purposes of calculating the jet penetration.

Third, for real jets, the average penetration into a given target increases, reaches a peak value, and then decreases as the distance between the base of the charge and the target (the standoff) increases. Figure 3 illustrates a typical penetration–standoff curve for a shaped charge with a conical liner versus armor steel. This variation with standoff is not predicted by the simple penetration model, as discussed later.

If the jet is particulated (broken up) and separated such that the particles do not interfere with each other, the particles retain their velocity $(V - U)$ and cross sectional area (A) until they impact the target, assuming the

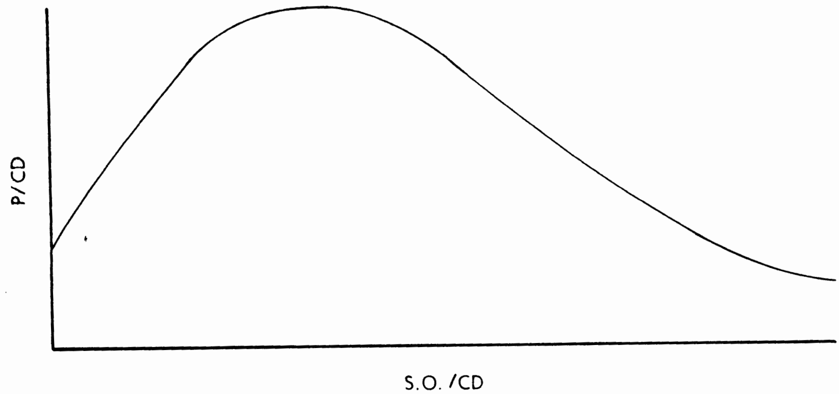

Figure 3. Penetration–standoff curve for a conical liner.

particles remain perfectly aligned and do not tumble, spread, or diverge from the penetration axis.

Upon impact, the dynamic pressure produced by a jet particle can be approximated by dividing the total force by the total cross-sectional area the jet strikes. Following Evans (1950), the total force given by the rate of change of momentum is $\rho_j A(V - U)^2$ and the average pressure on the impact surface is $\rho_j(V - U)^2$. Equating this pressure to the pressure in the target material at the point of impact, from Bernoulli's equation, yields,

$$\rho_j(V - U)^2 = \tfrac{1}{2}\rho_T U^2. \tag{3}$$

Comparison with Eq. (1) leads to

$$\lambda\rho_j(V - U)^2 = \rho_T U^2, \tag{4}$$

where λ is a constant that was claimed to equal 1 for a continuous jet and 2 for a particulated jet. ρ_j is then the average jet density including the gaps between particles. For jets particulated partially or particulated during the penetration process, $1 < \lambda < 2$. Then from Eq. (2) the ideal primary penetration becomes

$$P = l\left(\frac{\lambda\rho_j}{\rho_T}\right)^{1/2}. \tag{5}$$

This quantitative hydrodynamic theory of penetration by hypervelocity jets was developed by Hill, Mott, and Pack [see Hill et al. (1944), Evans (1950), and Pack and Evans (1951)] and independently by Pugh (1944). Additional details regarding the development of the hydrodynamic, hypervelocity penetration theory are given by Birkhoff et al. (1948), Eichelberger (1956),

Birkhoff (1947), and NDRC (1946). Birkhoff (1947) relates the parameter λ to the drag coefficient and calculates the penetration for a rotating jet.

This simple theory does not take into account jet velocity gradients, jet–target interactions, jet alignment, shock physics, compressibility effects, aerodynamic drag, variable-area jets, transient effects, and jet–target material properties. Pack and Evans (1951) and Eichelberger (1956) provide additional information regarding penetration theory and secondary penetration (or after-flow effects).

Other equations useful in penetration theory are, by definition,

$$P = \int U\,dt \quad \text{or} \quad U = \dot{P}, \tag{6}$$

where $\dot{P}$ denotes the derivative of P with respect of time, and

$$dl = (V - U)\,dt. \tag{7}$$

Equations (6) and (7) yield

$$P = \int \frac{U}{V - U}\,dl. \tag{8}$$

Early models attempted to improve the accuracy of the simple theory to better account for jet particulation (and spread) and standoff effects; these models were semi-empirical in nature. Let S denote the standoff and α be some constant depending on the jet velocity gradient; also, let β be a constant that determines the rate of jet spreading (dispersion). Then, for continuous (or very recently particulated) jets

$$P = \frac{P_0(1 + \alpha S)}{1 + \beta S} \tag{9}$$

where P_0 is the penetration at zero standoff distance (Birkhoff et al. 1948). For fully particulated jets where $\lambda = 2$, the penetration may be given as

$$P = P_0' \frac{\sqrt{2}\,(1 + \alpha S)^{1/2}}{1 + \beta S}, \tag{10}$$

where P_0' is the value of P from Eq. (9) at $S = S_1$ where the jet breaks up (Birkhoff et al. 1948). This model assumes that the ratio of the effective jet length at some standoff S to that at $S = 0$ is $1 + \alpha S$. Also, the ratio of the effective cross-sectional area of the jet at standoff S to that at $S = 0$ is assumed to be $(1 + \beta S)^2$ from Birkhoff et al. (1948). Other models, due to Pugh (NDRC 1946; Pugh 1944), assume that the ratio of the cross-sectional area of the jet at standoff S to that at $S = 0$ is $1 + \beta S^2$ instead of $(1 + \beta S)^2$. In either model, the constants α and β must be determined experimentally.

Pack and Evans (1951) also noted the importance of target material strength on jet penetration. To account for strength, they propose correcting Eq. (2) by a semi-empirical factor,

$$P = \left(\frac{\rho_j}{\rho_t}\right)^{1/2} l \left(1 - \frac{\alpha Y}{\rho_j V^2}\right). \tag{11}$$

They showed that for steel, the correction term $\alpha Y/\rho_j V^2$ is as great as 0.3; that is, the effect of strength is to reduce penetration by as much as 30%.

For the penetration of ductile targets, such as lead, by a shaped charge jet, Pack and Evans (1951) modify Eq. (11) by adding a secondary penetration term equal to the radius of the hole made by the jet.

Significant progress was made when Eichelberger (1956) conducted penetration-versus-time measurements. He verified that the hydrodynamic formula, Eq. (1), is very accurate for early times and short standoffs where the jet has a high velocity and is not yet broken. He found that when the jet is broken, λ in Eq. (4) should actually be less than one if ρ_j is taken as the original density of the liner. Furthermore, at low jet speeds, the strengths of the jet and target are important. Eichelberger proposed the formula

$$\lambda \rho_j (V - U)^2 = \rho_t U^2 + 2\sigma \tag{12}$$

where $\sigma = \sigma_t - \sigma_j$, in which σ_t and σ_j are the "resistance to plastic deformation" for the target and jet, respectively. These strength terms are taken as one to three times the static uniaxial yield stress, with the factor attributed to strain rate effects and to the state of nonuniaxial stress at the yield site in the target.

The importance of target strength can be observed by comparing the penetration of a copper shaped charge jet into RHA and mild steel. RHA has a larger yield strength and Brinell hardness than mild steel. Pugh (1944) states that the depth of penetration in armor plate is 20% less than in mild steel. Klamer (1964) states that the penetration in armor plate is 10–15% less than in mild steel. The higher percentage reduction in penetration seems to be more realistic.

Beyond this point, the quasisteady hydrodynamic theory has evolved along two lines, the shaped charge jet with variable velocity and the kinetic energy rod with uniform initial velocity. For stretching jets, work has been directed toward analytical solutions and quantifying the degradation in penetration beyond the point of jet breakup. For rods of uniform velocity, models treating the deceleration and deformation (shortening) of the penetrator have been developed; these models are applicable to broken jets or short length to diameter ratio rods.

9.3. VARIABLE-VELOCITY JETS

For a jet of nonuniform velocity distribution, such as produced by a shaped charge, the jet length is not constant but increases with time. In this case, Eq. (2) is not directly applicable.

As a first step, Abrahamson and Goodier (1963) derived explicit formulas for the penetration of continuous, straight jets of nonuniform velocity. They concluded that, if strength is neglected, addition of a constant velocity over the entire jet actually decreases penetration since the jet has less time to stretch before penetrating. If, however, the rear of the jet is too slow to overcome the strength of the target, addition of a uniform velocity may increase penetration. They derived a formula for the penetration of an idealized jet, which serves as a theoretical maximum. In their analysis, they took the jet length as known at a given distance from the target but did not consider the relationship between jet length and distance from the charge; this makes their results less useful for practical purposes.

Allison and Vitali (1963) further extended the theory to account for jet segmentation, with the following assumptions and conclusions:

1. Existence of a Virtual Origin It is known that the velocity of each jet particle remains nearly constant. In addition, if the spatial distribution of velocity is linear, as for most jets from constant-thickness conical liners, then a "virtual origin," or point source, of the entire jet can be located, as first proposed by Allison and Bryan (1957). This is a point on the distance–time plane from which all jet particles appear to originate.

2. Negligible Strength The strengths of the jet and target materials were neglected by Allison and Vitali (1963). Then, to characterize the termination of the penetration by the slow-moving rear of the jet, a minimum jet velocity for penetration, $V_{\min}$, is defined. This $V_{\min}$, and the penetration process at low velocity, must depend on the strengths of the jet and target. This is an artificial method to terminate the penetration.

3. Negligible Compressibility They also studied the effect of compressibility on penetration from equation-of-state data and the compressible-flow Bernoulli's equation. They concluded that, first, there is no effect for identical jet and target materials, and second, for dissimilar materials, the effect is small, provided the compressibilities do not differ greatly (e.g., only 1% difference in penetration velocity between the compressible and incompressible flow equations for a copper jet against a titanium target at shaped charge velocities). Harlow and Pracht (1966) confirmed this in two-dimensional code simulations of iron and aluminum jets impacting similar targets. (It will be shown later that compressibility is indeed negligible for a metal jet on a metal target; for a metal jet on a low-sound-speed target, such as Plexiglas, compressibility is not insignificant.)

Before jet breakup, penetration P as a function of time t was derived by Allison and Vitali as

$$P(t) = V_0 t\left(\frac{t_0}{t}\right)^{\gamma/(1+\gamma)} - t_0 V_0 \tag{13}$$

where $\gamma = (\rho_t/\rho_j)^{1/2}$ and t_0 is the time of arrival at the target of the jet tip, which has velocity V_0.

4. Simultaneous Breakup In Allison and Vitali (1963), the entire jet is assumed to break simultaneously. This assumption has also been used by other investigators (Simon et al. 1965; DiPersio and Simon 1964, 1966, 1968a; DiPersio et al. 1965a). In general, for conventional shaped charges, where the jet particulates or breaks up over a time interval from tip to tail, the simultaneous jet breakup assumption is, at best, a first-order approximation. Usually, as verified by the studies of Simon et al. (1965), DiPersio and Simon (1964, 1966, 1968a), and DiPersio et al. (1965a), this assumption is satisfactory for conventional warheads.

In reality, there exists a distribution of jet particulation from tip to tail where several microseconds are required before particulation is complete. For unconventional warheads, where the breakup does not proceed from tip to tail, this assumption (of a simultaneous, constant breakup time) is invalid.

5. Each Broken-Jet Segment Penetrates as a Continuous Jet The basic principles involved in Eichelberger's hydrodynamic penetration theory are Bernoulli's equation and the continuity equation,

$$\frac{dP}{U} = -\frac{d\xi}{V - U}, \tag{14}$$

where $d\xi$ is the incremental length of the jet. Allison and Vitali (1963), in calculating the penetration of a segmented jet, assumed that Eqs. (1) and (14) are applicable for short separated jet segments as well. This assumption is questionable because the penetration of finite segments is affected more by unsteady effects and is often less than that calculated from steady formulas. Under this assumption, once the jet breaks, penetration remains constant with further increase in standoff. In actuality, penetration decreases with standoff after the jet is broken. Experiments by Chou et al. (1975) and Chou and Toland (1977) indicate that the penetration of two segments with an intervening gap is less than that of two segments with no gap. Two-dimensional computer code calculations by Harlow and Pracht (1966) also demonstrate that during the initial transient period, penetration is less than in the steady-state case. Segmented penetrators are discussed later in this chapter.

The principles proposed by Allison and Vitali (1963) are still used today as the basis for penetration calculations. DiPersio and Simon (1964) presented

explicit formulas based on Allison and Vitali's theory, for three cases: (a) penetration before jet breakup ($T < t_b$), (b) jet breaks during penetration ($t_0 < t_b \leq T$), and (c) jet breaks before reaching the target ($t_b < t_0 \leq T$), where T is the time at the end of penetration, t_b the time of jet breakup, and t_0 the time when the tip reaches the target. For case (a), the total penetration depth P is

$$P = S\left[\left(\frac{V_0}{V_{\min}}\right)^{1/\gamma} - 1\right], \tag{15}$$

where S is the distance from the virtual origin to the target, or the effective standoff distance. In this case S is bounded by

$$0 \leq S < V_{\min} t_b \left(\frac{V_{\min}}{V_0}\right)^{1/\gamma}$$

and

$$U_{\min} = \frac{V_{\min}}{1 + \gamma}.$$

For case (b), the penetration is

$$P = \frac{(1 + \gamma)(V_0 + t_b)^{1/(1+\gamma)} S^{\gamma/(1+\gamma)} - V_{\min} t_b}{\gamma} - S, \tag{16}$$

where S is bounded by

$$V_{\min} t_b \left(\frac{V_{\min}}{V_0}\right)^{1/\gamma} < S < V_0 t_b.$$

Finally, for case (c), the penetration is

$$P = \frac{(V_0 - V_{\min}) t_b}{\gamma}, \tag{17}$$

for standoffs in the range given by

$$V_0 t_b < S < \infty.$$

Recall that $\gamma = \sqrt{\rho_T/\rho_j}$.

These formulas are the results of the so-called DSM (DiPersio, Simon, and Merendino) theory (DiPersio and Simon 1964). Other works related to studies of this type are given by Simon et al. (1965, 1967), DiPersio and Simon (1964,

1966, 1968a, 1968b, 1968c), DiPersio et al. (1965a, 1965b), Merendino and Vitali (1968), and Simon and DiPersio (1969a, 1969b).

These results can be manipulated to yield the velocity V_p of that point in the jet that is currently penetrating at a depth P in the target. For example, Eq. (15) becomes

$$V_p = V_0 \left[\frac{S}{P + S} \right]^{\gamma}.$$

This is also, of course, the emergent velocity of a continuous jet after penetrating a target of finite thickness P.

Based on Eqs. (15)–(17), DiPersio and Simon (1964) also compared their calculated penetration depth with experimental data. In general, good agreement was obtained at short standoffs, up to about three charge diameters. At larger standoffs, the formulas give higher than measured values. They attributed the declining performance of actual jets mainly to asymmetric wavering of the jet.

In 1965, DiPersio et al. (1965a) conducted an extensive experimental program to determine the causes for decreased penetration at long standoff. They reached the following conclusions:

1. Jets from precision charges travel in very straight lines; jet particles show no appreciable tumbling, deceleration, or mass ablation due to air friction. For conical liners, the jet velocity distribution is nearly linear, and the assumption of a virtual origin is valid.
2. The minimum jet velocity for penetration is not constant for a given jet or target, but increases with standoff.

Since $V_{\min}$ is not a constant, they proposed a new criterion for terminating penetration based on a minimum penetration velocity $U_{\min}$. From test data they noticed that the penetration velocity U at the time penetration stops was constant for different standoffs. The penetration velocity of a broken jet was obtained, in essence, by drawing a smooth curve through the penetration history. The slope of this curve at the cessation of penetration was taken to be a constant, $U_{\min}$, regardless of standoff. For the standard charge they used, $U_{\min}$ was about 1.0 km/s.

Next, DiPersio and Simon modified the penetration formulas in all three regimes by replacing the $V_{\min}$ criterion with a $U_{\min}$ criterion. The new formulas yield penetrations that decrease with standoff, in better agreement with experimental data (DiPersio et al. 1965a).

Equations (15)–(17) were taken to be valid except for the $V_{\min}$ terms. The equations for the total penetration, using $U_{\min}$ as a jet cutoff criterion instead

of $V_{\min}$, follow. For case (a),

$$P = S\left[\left(\frac{V_0}{(1+\gamma)U_{\min}}\right)^{1/\gamma} - 1\right], \tag{18}$$

where S is bounded by

$$0 \leq S < (1+\gamma)U_{\min}t_b\left[\frac{(1+\gamma)U_{\min}}{V_0}\right]^{1/\gamma}$$

For case (b), the penetration is now

$$P = \frac{(1+\gamma)(V_0t_b)^{1/(1+\gamma)}S^{\gamma/(1+\gamma)} - \sqrt{(1+\gamma)U_{\min}t_b(V_0t_b)^{1/(1+\gamma)}S^{\gamma/(1+\gamma)}}}{\gamma}$$

$$-S, \tag{19}$$

where S ranges from

$$(1+\gamma)U_{\min}t_b\left[\frac{(1+\gamma)U_{\min}}{V_0}\right]^{1/\gamma} < S < V_0t_b.$$

For case (c), when the jet particulates before penetration begins,

$$P = \frac{V_0t_b - \sqrt{U_{\min}t_b(V_0t_b + \gamma S)}}{\gamma}, \tag{20}$$

where S lies in the interval

$$V_0t_b < S \leq \frac{V_0t_b}{\gamma}\left(\frac{V_0 - U_{\min}}{U_{\min}}\right)$$

and $P = 0$ when S equals its upper bound.

For the $U_{\min}$ criteria, Eqs. (18)–(20) are used in lieu of Eqs. (15)–(17), respectively. The total length of jet that contributes to the penetration process may be obtained by multiplying the appropriate value of P [from Eqs. (18), (19), or (20)] by γ.

DiPersio and Simon subsequently conducted many informative experiments. In DiPersio and Simon (1966), they reported a study on "residual penetration," penetration by a jet into a main target after perforating a series

of skirting plates. In DiPersio and Simon (1968a), they studied the effect of jet breakup on penetration (the earlier the breakup, the less the penetration) and also discussed the effect of jet rotation. In DiPersio and Simon (1968b, 1968c) and Simon and DiPersio (1969b), they verified experimentally that penetration decreases as target strength, or hardness, increases. Merendino and Vitali (1968) made the same observation.

Simon and DiPersio (1969a), using flash radiography and other techniques, revealed that the rear portion of the jet that does not contribute to penetration actually piles up at the bottom of the hole. They also mentioned a "valve action," whereby the rear of the jet is trapped by the small hole created by the front of the jet. DiPersio et al. (1965a, 1965b), DiPersio and Simon (1968b, 1968c), Simon and DiPersio (1969a, 1969b), and Simon et al. (1967) present several comparisons of the DSM theory with experimental data.

Note that in all these studies the basic hydrodynamic equation (1) was used to describe the penetration process, while efforts were made to determine the termination of penetration, V_{min} or U_{min}, by empirical means.

Eichelberger's formula [Eq. (12), which contains the material strength term] was not used at all. Thus, the material is described only by an empirical constant and its density.

The penetration criteria based on the minimum velocities V_{min} and U_{min} provide useful practical formulas but do not directly address the physical causes of the decrease in jet penetration with standoff. These phenomena, which include jet segmentation, wavering, and tumbling of jet particles, have been the focus of several recent studies. Note that since U is the penetration velocity and by definition $U = \dot{P}$, so U_{min} (the minimum penetration velocity) is zero when the penetration ceases, or the penetration–time curve asymptotes.

It is generally recognized that three-dimensional effects (or two-dimensional effects if the target is impacted at normal obliquity) are the true mechanisms involved in jet cutoff or penetration termination. A U_{min} or V_{min} cutoff criterion is simply a device to allow the one-dimensional models to be effective. This is not meant as a critique of the DSM theory alone since all analytical models suffer this limitation. Basically, the DSM limitation is the a priori determination of U_{min}, which is often not a constant, but varies strongly with standoff and charge diameter for a given jet–target configuration. This is documented in the CUMIN report where Majerus and Scott (1978) provided several plots of the U_{min} variation. Unfortunately, this variation of U_{min} with standoff and charge diameter is highly erratic and cannot be readily modeled or curve fit. Nonetheless, Majerus and Scott (1978) is a useful aid in the application of the DSM theory. Held (1987) presents a useful application of the U_{min} concept.

Jet waving, jet tumbling, jet drift, and crossing (or transverse) velocity effects (where the target moves as the jet penetrates) have been analyzed by several authors. Notably, these analyses are found in Majerus et al. (1977) and Segletes (1984) on the effects of transverse velocity, Segletes (1983, 1987) on the effects of jet drift velocity, and Held (1983) and Golesworthy (1983) on the effects of transverse velocity.

9.4. PARTICULATED JETS

Carleone et al. (1982), in an augmented version of the one-dimensional jet formation code DESC, developed a theory for predicting the breakup of shaped charge jets and introduced an approximate method for determining the decrease in penetration with standoff. First, the breakup time of each portion of the jet is calculated or measured. If a given segment of jet reaches the target before its computed breakup time, its penetration is calculated from Eichelberger's equation (4) for a continuous jet. If the segment of jet has broken, however, its actual penetration dP' is reduced from the continuous-jet penetration dP by the formula

$$dP' = dP\left(1 - \frac{g}{g_0}\right) \tag{21}$$

where g is the gap distance between jet particles, nondimensionalized with respect to the increment of jet length, and g_0 is an empirical constant. According to this formula, penetration is degraded as the particles move farther apart, so that after breakup, penetration decreases (as expected) with standoff. Comparisons with experimental data show good agreement when $g_0 = 6.5$ for precision shaped charges and 4–6 for nonprecision or small charges. An advantage of this simple theory is that only one empirical constant need be specified.

A more sophisticated approach was taken by Smith (1981), who applied the Monte Carlo technique to the effects of tumbling, dispersion (or wavering), and breakup, which are considered as stochastic processes. The values of the parameters governing these processes are assumed to follow prescribed probability distributions. Then, random values consistent with these distributions are chosen for the parameters of each jet particle. Finally, jet penetration is determined by applying Tate's method for rod penetrators [Tate (1967) discussed later] to each particle. With proper selection of the statistical parameters (mean, standard deviation), describing the distribution of tumbling rate, dispersion angle, and breakup time, excellent agreement with measured penetrations can be achieved. The chief shortcoming of this approach is the difficulty in determining, a priori, proper values of all of these parameters. Nevertheless, this method is useful for interpolating and extrapolating penetration data; once the parameters have been calibrated by experimental data, penetrations at other standoffs or against other targets can be estimated with some confidence. Improvements to this model (Smith 1981) are possible by coupling the Monte Carlo technique with a model more suitable to shaped charge penetration than Tate's rod model (Tate, 1967).

Zaid (1960) formulated a penetration/perforation model based on the conservation of mass and momentum. Zaid considered shear stress terms and modeled a nondeforming cylindrical penetrator.

Walters and Majerus (1977, 1978, 1979), Majerus et al. (1978), Walters et al. (1979), and Majerus and Walters (1978, 1981) developed a penetration model based on the conservation of mass and momentum using an integral approach and a control volume concept. They divided the penetration process into two regions, the undeformed portion of the penetrator and the interaction region of deforming target and penetrator materials at the bottom of the crater. Global equations of motion are derived for each region in terms of normal stresses and shear stresses, the latter using a Newtonian fluid approximation. The resulting system of ordinary differential equations is solved by numerical integration. With proper selection of values for target strength and viscosity, good agreement with measured penetration can be achieved. The dynamic viscosity values are obtained from the American or Soviet experimental data. See the papers by Walters and Majerus already cited, for example. The strength term represents a dynamic value analogous to that used in Eqs. (11) and (12).

Walters and Majerus used an approximation of broken jets involving two steps. First, the broken jet is replaced by a continuous jet of equal length, of density the same as the average of the broken jet, as suggested by Allison and Vitali (1963). Then the continuous jet is shortened to the sum of the lengths of the particles in the original jet.

The model defines the termination of penetration to occur when U, the penetration velocity, reaches zero. This can happen after the jet length (which is also calculated) is consumed, thereby providing a measure of the secondary penetration or afterflow. The model is also capable of analyzing layered, multimaterial targets including air gaps (Walters and Majerus 1979).

The conservation of momentum yields

$$\frac{d}{dt}(MU) = \pi r_j^2(\sigma_j - \sigma_T) + \pi r_j^2 \rho_0 (V_I - U)^2 - \pi r_j^2 \rho_{T_0} U^2 - 2\pi H_0 \mu U \quad (22)$$

for a continuous jet. In this equation M is the mass of the jet, U is the penetration velocity, r_j is the jet radius, σ_j and σ_T are the dynamic strength values of the jet and target, respectively, ρ_0 and ρ_{T_0} are the jet and target densities, respectively, H_0 is the height of the interaction region between the penetrator and the target, and V_I is the velocity at the top of the interaction region. Walters and Majerus (1977, 1978, 1979), Majerus and Walters (1978, 1981), Majerus et al. (1978), Walters et al. (1979) and especially Walters and Majerus (1979) present the derivation of Eq. (22) and provide analogous equations for particulated jets. Expressions for V_I, H_0, r_j, and the jet length are also given for continuous and particulated jets. The jet length, jet radius, and jet density determine the jet mass, M. Walters and Majerus (1977, 1978, 1979), Majerus and Walters (1978, 1981), Majerus et al. (1978), and Walters et al. (1979) present several penetration depth and penetration time predictions and comparison with experimental data. Walters and Majerus (1977,

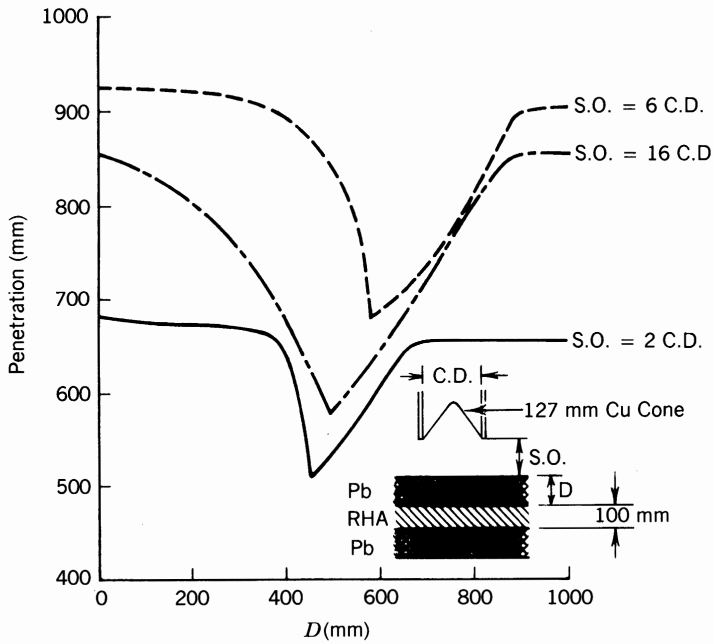

Figure 4. Predicted penetration versus a layered target (Walters et al. 1979).

1978), Majerus et al. (1978), and Majerus and Walters (1978) extend the model to include penetration by long or short rods.

One interesting application of this model was the accurate prediction of the data presented in NDRC (1946). In NDRC (1946), a series of 1-in. plates of lead were stacked, and a single 1-in. RHA (rolled homogeneous armor) plate was inserted in the stack at various depths, for example, first as the top plate, then as the second plate, and so on. The test objective was to predict penetration into the stack as a function of the position of the hard (RHA) plate from the top of the stack. For penetration by a shaped charge jet, there exists an optimum position of the hard plate from the top to minimize the penetration. The experiment was also conducted using mild steel plates instead of lead. The Walters–Majerus model (Walters et al. 1979) successfully predicted the optimum location of the RHA plate for either case given in NDRC (1946) and for a new experimental test using an RHA plate in an aluminum stack. In addition, this effect was found to be standoff dependent. See Figure 4, for example, where an RHA plate in a lead stack was analyzed. This study was significant in that many models experience difficulty in providing accurate penetration depth and penetration–time predictions into multimaterial layered targets since any material parameters or semi-empirical constants in use must change during the penetration process.

Most other models in use are based on an extension or duplication of those described in this section. For example, a simple analytical model based on the concepts given earlier was developed by Szendrei (1983). Other models that

contain original concepts are due to Evans and Ubbelohde (1950a, 1950b), Luttwak et al. (1982), Andersson et al. (1983), Sagomonyan (1974), and Murphy (1983). Also, Shear et al. (1981) used optimization techniques to relate shaped charge liner parameters to the penetration performance. Chou and Foster (1987) addressed the penetration of layered targets by jets with a nonlinear velocity gradient.

A multitude of models or correlations exist to determine both penetration and perforation of metallic and nonmetallic substances. Models have been developed for cratering or sphere impact, micrometeorite impact, and general penetration studies that relate to special problems or special jet–target interaction effects. Wilkinson (1969) and Seizew et al. (1978) considered the impact of micrometeorites on various structures. Hill (1980) considered the shape of the nose on a uniform rod penetration. High-speed impact was studied by Zlatin (1962), Stepanov (1969a), Merzhievskii and Titov (1975), Mar'yamov (1975), Gordopolov et al. (1977), and Stepanov (1969b). Stepanov (1970) also considered the effect of target temperature on the depth of penetration. Other interesting penetration studies follow from Senf (1974), Banks and Chandrasekhara (1962), Alekseevskii et al. (1973), Belyakov and Zlatin (1968), Defourneaux (1973), Greenspon (1978), Johnson (1977), and as related to explosive welding Zakharenko and Mali (1972) and Godunov et al. (1970).

A frequently used model for shaped charge jet penetration follows from Alekseevskii (1966), Sanasaryan (1975), and Sagomonyan (1975, 1977, 1978). The simple penetration model is based on a modified Bernoulli equation,

$$H_D + k_T \rho_T U^2 = \sigma_{SD} + k_j \rho_j (V - U)^2, \tag{23}$$

using the notation introduced earlier, and where H_D is the dynamic hardness of the target, taken as the Vickers hardness. The terms k_T and k_j are the body shape factors of the target and jet, respectively, which depend on the flow geometry and the effect of internal forces; they are difficult to determine and Alekseevskii (1966) takes $k_T = k_j = \frac{1}{2}$. Finally, σ_{SD} is the part of the stress state of the deforming penetrator determined by the internal forces and is called the dynamic yield point (Alekseevskii 1966). The cutoff velocity, or velocity below which the jet will cease to penetrate, akin to the V_{min} of the DSM theory discussed earlier, is

$$V_{min} = \sqrt{\frac{H_D - \sigma_{SD}}{k_j \rho_j}} \, . \tag{24}$$

Equation (24) follows from Eq. (23) for $U = 0$. Since $U = \dot{P}$, determination of U implies P by numerical integration.

Recent Soviet penetration models were presented by Kozlov (1986) and Agafonov (1986). These models are similar to the Walters–Majerus model discussed earlier, but they address both the jet and target viscosity instead of

the viscosity of the interaction region between the jet and target. The strain rate during penetration is related to the penetration velocity in an analogous manner. The major difference between the models is that Kozlov (1986) and Agafonov (1986) derive their respective equations using a static force balance whereas Walters and Majerus employ a conservation of momentum or dynamic force balance.

9.5. COMPRESSIBLE MODELS

As discussed earlier, Allison and Vitali (1963) and Harlow and Pracht (1966) indicated that the effect of compressibility on penetration of metal jets into metal targets is slight. However, Haugstad (1981) and Haugstad and Dullum (1981) showed that for nonmetallic targets compressibility effects may be significant. Furthermore, if the jet velocity is sufficiently high for shocks to occur, the penetration can be much less than that predicted by the incompressible theory (20% reduction for a copper jet against Plexiglas at 10 km/s).

The form of the Bernoulli equation presented earlier neglects compressibility, consideration of which requires an additional term (the flow work) that depends on the compressibilities of the jet and target materials. If the compressibilities are similar (as for a copper jet impacting a steel target), this term is negligible. If the target is appreciably more compressible than the jet (as for a copper jet against a Plexiglas target), the effect of this term is to significantly reduce penetration as compared to incompressible flow theory, as shown in Figure 5.

Flis and Chou (1983) extended the compressible theory to include more general equations of state (including Mie–Grüneisen and Tillotson) and reconfirmed the conclusions of previous researchers. Also, they applied the compressible model to a stretching jet using the virtual origin assumption, and showed that the penetration of such a jet can theoretically be as much as 50% less than predicted by the incompressible theory. This greater degradation in penetration for a stretching jet is explained by observing that, when the front of the jet penetrates less, the rear portion has less distance to stretch, and therefore also penetrates less.

Experimental evidence of the importance of compressibility has not been convincing. Experiments by White and Wahll (1981) and White et al. (1982) of nonprecision shaped charges against Plexiglas, aluminum, steel, and several liquids as target materials showed no correlation of target penetration resistance with compressibility.

Chick et al. (1984) applied the compressible theory to a jet with nonlinear velocity distribution, for which a virtual origin was not assumed. For such a jet projected by a small copper-lined conical charge into a Plexiglas target, a difference in penetration rate of only about 4% is predicted by the compressible and incompressible theories, but they claimed that their experimental results were in better agreement with the compressible theory. Coincidentally,

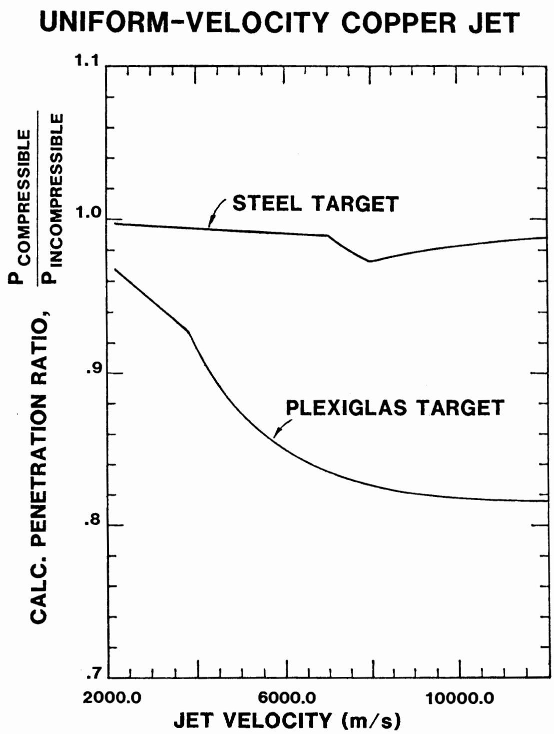

Figure 5. Effect of compressibility on penetration by a uniform-velocity copper jet (Flis and Chou 1983).

they point out that, for their jet, the error involved in neglecting compressibility is comparable to assuming a single virtual origin for the entire jet.

Woidneck (1986) fired copper rod projectiles into water, glycerol, and methanol at velocities of 2500 and 5000 m/s. Even at the higher velocity, the effect of compressibility makes a difference of only 3.3% (for water) in the early-time penetration rate, which he did not discern in his experiments.

9.6. THE VIRTUAL ORIGIN CONCEPT

The virtual origin concept is used in penetration calculations to determine the effective standoff distance and to allow an accurate prediction of short standoff penetration. Most of the penetration models assume that the jet velocity is linearly distributed in space and rely on the virtual origin approach first used by Allison and Vitali (1963) to integrate the penetration over the length of the jet. Recently, Chou et al. (1981) examined the accuracy of the virtual origin approximation, concluding that for charges with simple conical or hemispherical liners, the maximum error involved is less than 0.2 charge

diameters and is constant with standoff. However, Foster (1981), using a mass summation technique to analyze jet radiographs before breakup, has shown a significant nonlinearity in the velocity distribution of a biconic shaped charge.

9.7. ROD PENETRATION MODELS

Penetration models for long rod projectiles are sometimes used in shaped charge penetration or EFP penetration studies. A large number of these exist [see Backman and Goldsmith (1978) and Zukas et al. (1982) for surveys of existing models]. However, many assume the projectile to be nondeforming. This eliminates much unpleasantness in modeling as well as a good deal of reality. Thus, only a few of the rod models can be applied to jet or EFP penetration studies.

Smith (1981), Alekseevskii (1966), and Sanasaryan (1975), among others, have noted that an analogy exists between rod and jet penetration, hence the justification for the use of the rod models. Since rod models were developed mainly to explain results observed at ordnance velocity impacts (0.5–2 km/s), greater emphasis is placed in them on target and projectile strength effects and on projectile failure or erosion. Penetration by a shaped charge jet typically occurs at velocities exceeding 2 km/s so that jet penetration models represent a closer approximation to pure hydrodynamic flow. For a shaped charge jet, the jet velocity can be established since the velocity gradient of the jet from tip to tail is approximately linear. However, for rodlike projectiles that deform and erode and do not penetrate at constant velocity, the rod velocity during penetration (as well as the penetration velocity) is unknown. Both must be inferred from a combination of experiments and analytical models, as demonstrated by Wright (1983). On the other hand, for shaped charge jet penetration studies, one must consider the eventual breakup of the jet and analyze penetration of segmented jet particles.

During the 1960s based on a large number of experimental observations, a phenomenological model of hypervelocity penetration was formulated that still influences model development (Herrmann and Wilbeck 1987). Penetration of a semi-infinite target was taken to consist of four stages:

1. Transient Shock Regime Shock waves are formed in target and striker on initial contact. Density and compressibility are the key parameters governing material response. For hypervelocity impacts, the shock pressures are great enough to cause extensive plastic flow, melting, or vaporization. The duration of this phase depends on the geometry of the colliding solids, that is, the time required for release waves to relieve the initial shock pressures.

2. Steady-State Regime After several reverberations of release waves, conditions for steady-state flow are established. The projectile erodes while at the same time causing crater formation. Pressures at the projectile–target

interface are approximated from Bernoulli's equation. The duration of this phase depends on the geometry of the projectile.

3. Cavitation Regime The crater continues to expand after complete consumption of the projectile as a result of its own inertia and the residual energy trapped in the target material. This growth will continue until multiple wave reverberations reduce target pressures to the order of the material strength.

4. Recovery Regime Elastic rebound will slightly diminish the maximum dimensions of the crater. The rebound may produce tensile stresses that can cause spallation.

Although many of the hypervelocity impact experiments of the 1960s were performed with compact [length-to-diameter (L/D) ratios of 3 or less] projectiles, this phenomenological model explains many observations with long rod projectiles and has been verified computationally many times [e.g., Kimsey and Zukas (1986) wherein finite-element simulations of long rod impact at velocities of 1.1–3.75 km/s showed complete agreement with the above model and the experimental data of Hohler and Stilp (1977)].

Allen and Rogers (1961) conducted a series of experiments with rods of various materials impacting aluminum targets. Comparing their data with Eichelberger's formula [Eq. (12)], they concluded that the net strength $\sigma = \sigma_t - \sigma_p$ is nearly independent of penetrator material, or that σ_p is negligible compared to σ_t. Further, they postulated that the target strength is strain rate dependent and expressed σ_t as a function of the penetration velocity U. In addition, they observed "secondary penetration" in high-velocity impacts of dense (gold) rods against light (aluminum) targets. In this case, at the end of the usual penetration process, penetrator material that has been deflected by the crater bottom still has a net velocity into the target and can thus cause additional penetration.

Christman and Gehring (1966) developed a model by considering the effects of the primary and secondary phases of penetration. For a velocity range of 2.0–6.7 km/s, they report good agreement with experimental data. The dimensionless penetration into semi-infinite metal targets is expressed as

$$\frac{P}{L} = \left(1 - \frac{D}{L}\right)\left(\frac{\rho_p}{\rho_t}\right)^{1/2} + 2.42\frac{D}{L}\left(\frac{\rho_p}{\rho_t}\right)^{2/3}\left(\frac{\rho_t V^2}{B_{\max}}\right)^{1/3} \tag{25}$$

The first term represents the primary (or hydrodynamic) phase of penetration. The effective length of the penetrator for this phase is reduced by one rod diameter. This remaining diameter of length is assumed to contribute to the secondary phase of penetration, as represented by the remaining empirical term. The terms are self-explanatory, except perhaps $B_{\max}$, the Brinell hardness of the target. This model allows the final penetration to be greater than that predicted by the one-dimensional, hydrodynamic theory.

Doyle and Buchholz (1973) used a modified form of the Christman–Gehring equation (25) to predict the penetration of mass focused slugs (or EFPs) at long standoff distances. Their equation was

$$\frac{P}{L} = \left(1 - \frac{D}{L}\right)\left(\frac{\rho_p}{\rho_t}\right)^{1/2} + \frac{0.13}{L}\left(\frac{\rho_p}{\rho_t}\right)^{1/3}\left(\frac{E_1}{B_{\max}}\right)^{1/3}. \tag{26}$$

where P = target penetration depth (in.)
L = length of projectile (in.)
D = diameter of projectile (in.)
ρ_p = density of projectile
ρ_t = density of target
E_1 = energy in last caliber (last part) of the projectile (joules)
$B_{\max}$ = target hardness beneath the penetrating projectile (kg/mm^2).

Doyle and Buchholz (1973) state that Eq. (26) essentially assumes that the first part of the slug (all except the last caliber) performs like a shaped charge jet. The last part (last caliber) performs like a ballistic projectile. Thus, total penetration in metallic targets can be represented by this two-part equation that separates the contributions from primary and secondary penetration phases. Primary penetration is a function of projectile length and density and target density. Secondary penetration is a function of projectile density and kinetic energy and target density and strength.

A major contribution to the one-dimensional theory of rod penetration was made by Tate (1967, 1969, 1977, 1979, 1986a, 1986b) who accounted for the deceleration and shortening of the rod during penetration. (A similar model was developed independently by Alekseevskii (1966).) Equation (12), the Bernoulli equation with strength, is used with the equation of motion of the undeformed part of the rod,

$$\rho_p L\, dV/dt = \sigma_p \tag{27}$$

and the kinematic relation $dL/dt = V - U$ where L is the current length of the rod. Tate presented several explicit solutions to this system of equations for special cases of density and material strength; the general case may be solved by numerical integration. Tate recommended the value of σ_p as the Hugoniot elastic limit of the projectile material and σ_t at 3.5 times the Hugoniot elastic limit of the target material.

Tate considered two classes of impacts, $\sigma_p > \sigma_t$ and $\sigma_p < \sigma_t$. In the former case (hard penetrator, soft target), the penetration process passes through two stages: at a sufficiently high impact velocity, the penetrator and target first both flow hydrodynamically; later, after the penetrator has decelerated, it ceases to flow and penetrates as a rigid body. When a soft penetrator impacts a hard target (the case of most interest), both materials initially behave hydrodynamically; then, after the penetrator decelerates below a critical

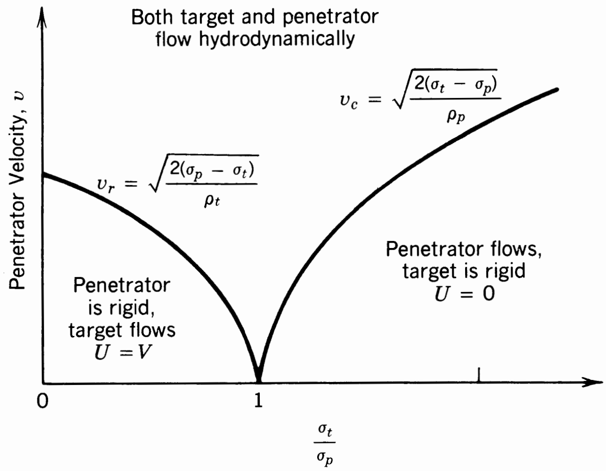

Figure 6. Phase diagram of rod penetration according to one-dimensional theory (Chou and Flis 1986).

velocity, the target ceases to flow so that penetration stops, while the penetrator continues to deform. For both cases, if the impact velocity does not exceed a critical velocity calculated from Eq. (12), the initial stage of purely hydrodynamic behavior is absent. These phenomena are summarized in the phase diagram (Figure 6).

Chou and Flis suggested a different set of values for σ_p and σ_t. They reasoned that, since the deforming part of the penetrator is in a state of uniaxial stress, σ_p should be chosen as the uniaxial yield stress rather than the Hugoniot elastic limit (the strength under a condition of uniaxial strain). Then by comparing with experiments and hydrocode calculation, they showed that taking the target resistance σ_t as 2.5 times the Hugoniot elastic limit gave the best agreement. In addition, in a computer code for integrating Tate's equations (Flis 1979), they included an approximate method for computing the secondary penetration observed by Allen and Rogers (1961) and also by Tate.

In the absence of firm guidelines for their determination, the parameters $R_t(\sigma_t)$ and $Y_p(\sigma_p)$ in Tate's theory have frequency been used as adjustable parameters. Thus, comparison of Tate's theory with experimental results tended to vary from poor to excellent, depending on the skill with which these parameters were selected. In two recent works, Tate (1986a, 1986b) has extended his theory and provided means for estimating R_t and Y_p for some materials based on their dynamic yield strengths. Correlation with experimental data for projectiles with L/D from 3–12 is quite good.

Wright (1981) established a rigorous theoretical basis for the models of Tate (1967, 1969) and Alekseevskii (1966) and indicated the actual assumptions involved in the derivation. Wright also compared these models with instrumented impact experiments.

Perez (1978, 1982) modified Tate's approach by substituting a condition of conservation of kinetic and distortional energy in place of Bernoulli's equation. A more sophisticated estimate of strength effects can then be made by deriving the amount of energy absorbed in plastic deformation of the target and penetrator materials. Good agreement is shown between calculations using this model with the experimental data of his own and of Hohler and Stilp (1977) for several combinations of projectile and target materials. However, Perez does not present any comparison with Tate's original model.

An integral theory of impact has been developed by Donaldson et al. (1976) and Contiliano et al. (1978). This theory was extended to include a rod penetrator model applicable to a wide range of impact velocities and materials. Good correlations with experimental data have been reported. The penetrator is modeled as a head, from which material can erode, and a rigid shaft that is decelerated by interface stresses at the head. The target material is characterized by two properties: E_{*p}, energy absorbed during plastic deformation, and E_{*e}, energy absorbed by elastic deformation. Simple formulas have been derived to determine these constants from laboratory tests. The determination of these constants for a variety of materials has identified certain hard, brittle, nonmetallic materials as effective armor materials.

In Figure 7, three calculations are compared based on Tate's deceleration model [using the RODPEN code, Flis (1979), Donaldson's integral theory of impact, and Christman and Gehring's semi-empirical formula] with impact experiments performed by Hohler and Stilp (1977). These results show good agreement among RODPEN, Donaldson, and the experiments, while Christman and Gehring's formula seems useful here only at the high velocities, and indeed was developed from high-velocity data.

Matuska (1982) investigated steady-state jet penetration by a computational approach. From simulations with the two-dimensional Eulerian hydrocode HULL, he determined the values of the parameters in a modified form of Bernoulli's equation,

$$\frac{\gamma}{2}\rho_j(V-U)^2 + \beta\sigma_j = \frac{\rho_t U^2}{2} + \alpha\sigma_t. \tag{28}$$

The values determined for the parameters are

$$\alpha = 1$$
$$\beta = 0.3$$
$$\gamma = 0.47 + 0.028\rho_j + 0.00086\rho_j^2 + 0.072\ln V,$$

where the density is in g/cm^3 and the velocity is in km/s. The deviation of γ from its theoretical value of unity was attributed to the target's resistance to radial flow. This deduction was based on results of simulations of two impinging jets of equal radius, for which γ had a value very close to 1.

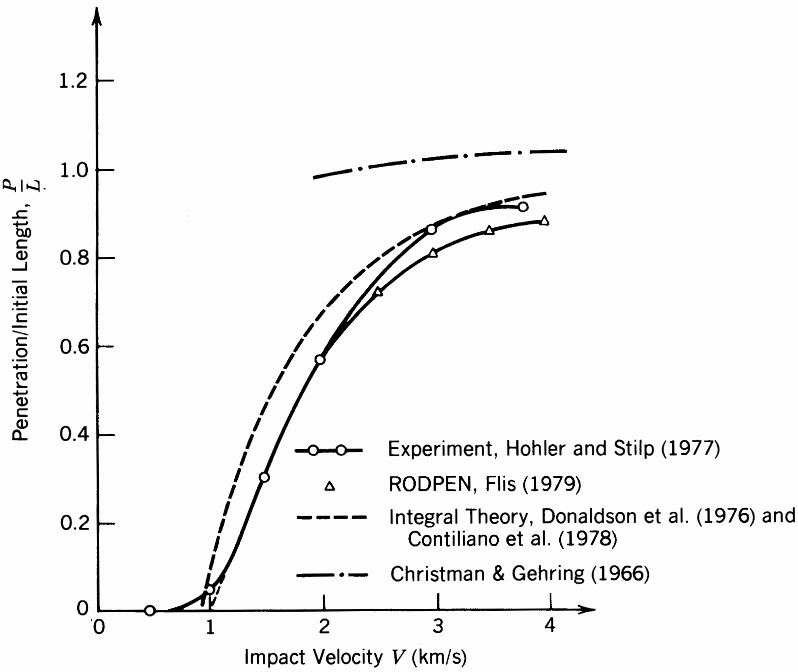

Figure 7. Comparison of three one-dimensional theoretical calculations with experimental penetrations of steel rods impacting armor steel.

This model was extended to rod penetrators by substituting the above equation for the Bernoulli equation in Tate's model. The steady-state portion of penetration is calculated by numerically integrating the resulting equations. Steady-state penetration is considered to cease when the rod has eroded to a length equal to its diameter [as suggested by Christman and Gehring (1966)] or when the penetration velocity has dropped to a prescribed value.

Byrnside et al. (1972) extended the model of Goodier (1965) for hard and soft spheres impacting various targets at velocities that were either very high or very low. The Byrnside et al. model is also applicable at intermediate velocities, and the effects of projectile strength were determined for aluminum alloy spheres impacting aluminum targets. The test results were in good agreement with theory.

Woodward (1982) developed a numerical model for the penetration of metal targets where the jet–target interaction was viewed as two colliding cylinders. His numerical method was an extension of that developed by Hashmi and Thompson (1977). Other studies were given by Dong and Chen (1981) and Dullum and Haugstad (1981). Perforation of thin plates by projectiles was studied by Awerbuch and Bodner (1973a, 1973b) and Ravid and Bodner (1982). Also, Franzen (1987) studied the penetration of slender, hollow cylinders.

Ravid et al. (1987a, 1987b) also extended the hydrodynamic approach to penetration calculations. They derived a two-dimensional model that accounts for the strong shock compression prevailing in target and projectile for short times after impact and that influences the initiation of the penetration process. The model accounts for strain-rate-dependent plastic flow and also for inertial forces due to local and convective accelerations, thus permitting determination of the target cavity diameter. The model is valid in the transient shock wave regime and permits determination of forces, penetration velocity, deformed geometry, strain rates, and flow stresses in projectile and target. It has been applied to both monolithic and layered targets.

Other rod models and data are discussed by Walters and Majerus (1978), Belyayev et al. (1976), Weihrauch (1971) (an excellent experimental study), Clark (1983), and Dehn (1979), who discusses the history of rod penetration, presents a survey of rod penetration models, and develops new rod penetration concepts based on estimated or semi-empirically determined parameters. Allen et al. (1957) introduce a drag coefficient concept and present a model for a noneroding bullet penetrating sand.

There is considerable interest in segmented penetrators today. Their potential benefit is based on the quantitative advantage of multiple impacts of well-aligned and well-separated penetrator segments when compared to that of a single "equivalent" penetrator. The concept is not new. Eichelberger (1956) suggested that a perfect, particulated jet should penetrate about 40% more than a continuous jet. Numerical studies by Kucher (1982), deRosset (1981), and deRosset and Kimsey (1986) also indicate, for perfectly aligned penetrators, that increases in penetration depth of 40–160% are possible at velocities approaching the sound speed (approximately 5 km/s). The degree of improvement depends on the striking velocity, the number of segments, and the spacing of the segments. Segmented penetrators were studied experimentally by Chou et al. (1975) and Chou and Toland (1977) and both analytically and experimentally by Sedgwick and Wilkinson (1987).

At this stage, it is not possible to quantify the difference in performance between segmented penetrators and "equivalent" monolithic penetrators. A large number of parameters (velocity, rod geometry and spacing, material strength, and failure characteristics) must be examined and compared. Thus far, all modeling has involved two- and three-dimensional wave propagation codes since the problem is not analytically tractable. Because of the expense involved, studies have been performed only for specific cases. The required range of parameters remains to be explored, although Sedgwick and Wilkinson (1987) have taken an important step in this direction.

Dehn (1986) published a generalized equation of motion for penetration. In various specialized forms, this equation is used to calculate penetration by rods, jets, or fragments. The generalized equation of motion describes the target force resisting penetration as a second-order polynomial in the penetration speed. The force and coefficients of the penetrator speed must be determined for each case. This equation was also presented by Johnson (1970)

and Allen et al. (1957) and is a generalized form of the Robins–Euler equation. Dehn (1986) also provides a comprehensive overview and survey of jet and rod penetration models. However, his comments on jet penetration models (especially regarding jet length calculations and visco-plastic, high strain rate behavior) are misleading.

Some of the material presented in this chapter is also discussed by Chou and Flis (1986) and Walters et al. (1987, 1988).

Excellent surveys of penetration by rods are given by Wright (1983), Backman and Goldsmith (1978), Dehn (1979), and in the books by Goldsmith (1960) and Johnson (1970). Studies involving rod penetration, experimental data, and hydrocode simulation are given by Jonas and Zukas (1977, 1978) and Zukas (1980). Zukas summarizes many of the penetration and hydrocode simulation methods (Zukas et al. 1982). In addition, many interesting articles on experimental, analytical and numerical aspects of hypervelocity impact are to be found in the *Proceedings of the 1986 Hypervelocity Impact Symposium,* which appears as Volume 5 of the 1987 *International Journal of Impact Engineering*.

Finally, brief comments regarding radial hole growth are given in Appendix A, which follows.

APPENDIX A RADIAL HOLE GROWTH

From the previous discussions it is evident that considerable effort has been devoted to modeling the penetration rate and penetration depth (*axial* hole growth) for high-velocity impacts into thick targets. A somewhat smaller number of studies consider the radial (or direction perpendicular to the penetration axis) flow of material during penetration. It is not the intent here to discuss this subject exhaustively. This would require several chapters, perhaps even a new book. Instead, we provide an introduction to this important area as well as citations to the relevant literature to permit further study.

In the following, we distinguish between *radial hole growth* models, which usually involve perforation of thin plates, and *crater volume* models, which involve penetration into thick (semi-infinite) plates and require determination of both axial and radial dimensions of the crater. Most hole growth–crater volume models are one-dimensional in nature or at best axisymmetric. Three-dimensional hole growth can only be treated numerically. Projectiles are generally assumed to be metallic materials. Much of the experimental foundation for this work, and a number of models, are to be found in the various hypervelocity impact symposia. An overview of hypervelocity impact and a thorough description of optical methods of capturing data are provided by Swift (1982a, 1982b). The current state of the art is summarized in Volume 5 of the *International Journal of Impact Engineering*, which is devoted to the 1986 hypervelocity impact symposium. In this regard, see also the books by Kornhauser (1964), Vollrath (1967), Kinslow (1970), Caldirola and Knoepfel

(1971), and Kawata and Shioiri (1979). Impacts involving fluid jets and projectiles leading to material erosion are treated by Springer (1976), Preece (1979), and Adler (1979). Analytical models are reviewed by Backman and Goldsmith (1978) and Zukas et al. (1982). Impacts involving lunar and planetary materials are considered in Roddy et al. (1977) and Öpik (1936). Silsby (1984) presents extensive data for long rods striking semi-infinite targets. Other pertinent references include Tate et al. (1978), Hohler et al. (1978), Woodward (1981), Stilp (1987), Hohler and Stilp (1987), Piekutowski (1981), Baker (1969), and Lambert (1978).

Formulation of Crater Growth Models

Bethe (1941) formulated a theory of armor penetration for both thin and thick plates. A normal impact was considered and cylindrical coordinates were used with the penetration direction parallel to the Z axis. Axial symmetry was assumed. Bethe's configuration is depicted in Figure A.1. In region C, the material was assumed to be elastic, while in regions A and B the stresses were assumed sufficient to produce plastic deformation. The distinction between regions A and B is in the behavior of the hoop stress, σ_θ, which is also a principal stress in this configuration. In region A, the hoop stress was assumed to be negligible whereas in region B it was assumed to be finite and tensile. Bethe determined the stresses in regions A, B, and C using the Tresca–Mohr yield condition, assuming perfect plasticity and ignoring inertial effects. Stress continuity was assumed at r_1 and r_2. Extensions to this model, such as inclusion of inertial terms, work-hardening effects, and so on were suggested

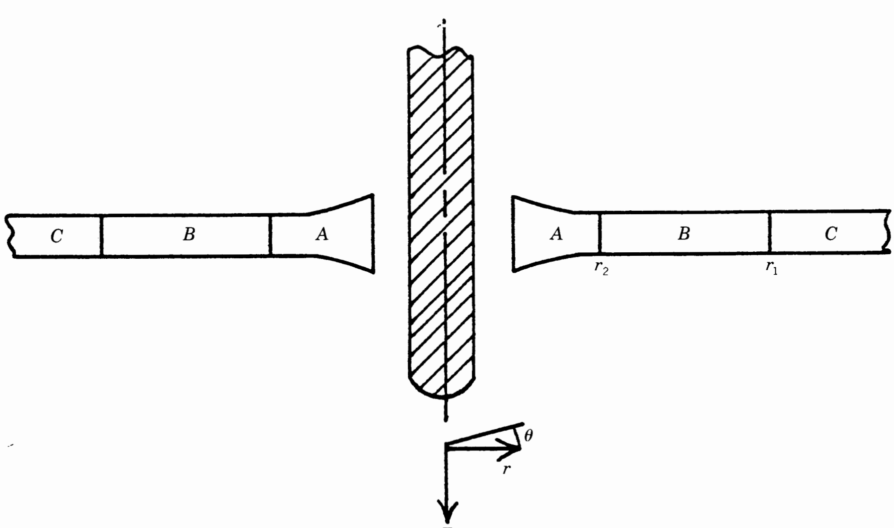

Figure A.1. Bethe's (1941) thin plate configuration.

but were not pursued. Bethe argued that within region A, at least for the static condition, the radial stress was a finite constant, while the hoop and axial stresses were zero. In later investigations by Taylor (1941, 1948), Bethe's constant region A stress state assumption was relaxed to allow the ratios of principal stress (σ_i) differences to be proportional to the incremental strain (e_i) differences (the von Mises approximation) or

$$\frac{\sigma_r - \sigma_\theta}{e_r - e_\theta} = \frac{\sigma_\theta - \sigma_z}{e_\theta - e_z} = \frac{\sigma_z - \sigma_r}{e_z - e_r}. \tag{A1}$$

Using the von Mises approximation, Taylor obtained a static stress solution within regions A, B, and C. The greatest difference between Taylor's and Bethe's results occurs in the large strain, plastic region A where instead of a constant radial stress, the stress is significantly larger near the hole surface. The hoop stress in this region is no longer zero but finite and tensile near the hole surface and eventually becomes compressive midway through region A. At r_2, the interface between large and small plastic strains, the hoop stress is discontinuous. It is difficult to ascertain experimentally the validity of either Bethe's or Taylor's approximations since both approaches neglected the inertial terms, that is, an equilibrium solution was obtained for a dynamic problem. Taylor (1941) investigated the case of a constant radial velocity and concluded that for radial velocities greater than $\sqrt{0.39\sigma_\theta/\rho}$ the hypothesis that $\sigma_\theta = 0$ requires a discontinuity of σ_θ at the r_2 interface. Experimental observations, Kineke and Vitali (1963), Eichelberger and Kineke (1967), Turpin and Carson (1970), and Holloway (1963), show that for actual conditions the radial velocity usually exceeded this limit but is far from being constant.

A more general approach to the dynamic problem was published by Freiberger (1952). Bethe's stress hypothesis was utilized and inertial terms were included in the radial equation of motion. Freiberger (1952) assumed the Tresca–Mohr yield condition and plastic incompressibility. They then expressed the dynamic equations in characteristic form. Simple wave solutions were obtained under the condition of uniform velocity and uniform velocity followed by expansion under a constant, positive acceleration. The initial conditions for the existence of the simple wave solutions involve a singularity along the axis of symmetry. The determination of realistic values of these conditions for practial applications was not addressed and consequently comparison with experimental data was not made. The experimental data already cited show that the majority of the hole expansion process involves a deceleration process that limits Freiberger's approach to extremely small times (much less than 1 μs) during the initial stages of hole formation.

The hole enlargement and growth to the final hole size for thin plates was discussed by Walters and Scott (1985). Thick plates were addressed by Scott (1984). In fact, Scott (1984, 1986) presents an excellent, and fairly recent, overview of the hole growth and crater volume studies. Also, Scott (1984) developed a hole growth rate model that, coupled with an axial penetration

model, provided the crater volume. The studies of Scott (1984) and Walters and Scott (1985) are based on the pioneering work of Bethe (1941), Taylor (1941, 1948), and Freiberger (1952).

Additional data are provided by Frasier et al. (1965), Rolsten et al. (1964), Hill (1980), Seizew et al. (1978), Hopkins (1960), Merzhievskii and Titov (1975), Stepanov (1969), Allison (1965), Wilkins and Guinan (1973), Whiffin (1948), Goldsmith (1960), Johnson (1972), Housen et al. (1983), Glass and Bruchey (1984), Christman et al. (1965), Eichelberger and Gehring (1962), Perez (1978), Atkins (1960), Christman and Gehring (1966), Kineke (1960), Payne (1965), Halperson (1965), and Feldman (1959, 1960).

The Walters–Majerus model derives expressions to calculate the radial hole size and growth rate. The DiPersio–Simon studies (discussed here and in Chapter 10) present a method to calculate the final crater volume, but not the crater growth rate, based on the hypothesis that the crater volume is proportional to the kinetic energy of the jet. This concept was first utilized by Rinehart and Pearson (1954), Feldman (1959), and Kornhauser (1964).

However, Murphy (1987), noted that the jet (or penetrator) kinetic energy divided by the hole volume is not a material constant. This was also noted by Majerus and Scott (1978). Murphy states that the value of the penetrator kinetic energy divided by the hole volume is

Primarily a function of velocity and appears to be parabolic with a minimum in the 3- to 4-km/s range;

At a given velocity, primarily a function of the target material;

At a given velocity, for a given target, is influenced only slightly by the impactor material.

The hypervelocity impact symposia, cited earlier, provide an excellent overview of the hole/crater growth rate field. The terminal phase of perforation/hole growth, that is, petalling, plugging, mushrooming, and spallation is discussed by Scott (1986) and in detail by Zukas et al. (1982).

Finally, we mention again that this brief appendix only highlights the radial hole growth field. The literature cited is not comprehensive. It represents only introductory material for further study.

REFERENCES

Abrahamson, G. R., and Goodier, J. N. (1963), "Penetration by Shaped Charge Jets of Nonuniform Velocity," *J. Appl. Phys.*, *34*.

Agafonov, A. V. (1986), "Consideration of Viscosity during Subsonic Penetration of a

Solid Body into Isotropic Barriers," trans. from *Zhurnal Prikladnoi Mekhaniki i Tekhnicheskoi Fiziki*, (3): 120–125.

Alekseevskii, V. P. (1966), "Penetration of a Rod into a Target at High Velocity," *Fizika Goreniya i Vzryva, 2*(2): 99–106.

Alekseevskii, V. P., Biletskii, A. K., Fot, N. A., and Yarosh, V. V. (1973), "Inertial Motion of a Ring of Plastic Material Subjected to a Pulse Load," *Prikladnaya Mekhanika, 9*(4): 81–86.

Allen, W. A., Mayfield, E. B., and Morrison, H. L. (1957), "Dynamics of a Projectile Penetrating Sand," *J. Appl. Phys., 28*(3): 370–376.

Allen, W. A., and Rogers, J. W. (1961), "Penetration of a Rod into a Semi-Infinite Target, *J. Franklin Institute, 272*.

Allison, F. E., and Bryan, G. M. (1957), "Cratering by a Train of Hypervelocity Fragments," *Proc. 2nd Hypervelocity Impact Effects Symp.,* Vol. 1, p. 81, December.

Allison, F. E., and Vitali, R. (1963), "A New Method of Computing Penetration Variables for Shaped Charge Jets," Ballistic Research Laboratory Report No. 1184.

Andersson, G., Holmberg, L., and Mellgard, I. (1983), "Experimental Study of the Penetration Mechanisms of Hollow Charge Jets in Nonmetallic Target Materials," *Proc. 7th Int. Symp. on Ballistics,* The Hague, Netherlands, April.

Awerbuch, J., and Bodner, S. R. (1973a), "Experimental Investigation of Normal Perforation of Projectiles in Metallic Plates," MED Report No. 41, Material Mechanics Laboratory, Israel Institute of Technology, June.

Awerbuch, J., and Bodner, S. R. (1973b), "Analysis of the Mechanics of Perforation of Projectiles in Metallic Plates," MED Report No. 40, Material Mechanics Laboratory, Israel Institute of Technology, May.

Backman, M. E., and Goldsmith, W. (1978), "The Mechanics of Penetration of Projectiles into Targets," *Int. J. Engr. Sci, 16:* 1–99.

Banks, R. B., and Chandrasekhara, D. V. (1962), "Experimental Investigation of the Penetration of High Velocity Gas Jet through a Liquid Surface," *J. Fluid Mech., 15.*

Belyakov, L. V., and Zlatin, N. A. (1968), "Rate of Penetration of a Metal Cylinder into a Massive Target," *Soviet Physics-Technical Physics, 12*(10).

Belyayev, V. I., Kovalevskiy, V. I., Smirnov, G. V., and Chokan, V. A. (1976), "High Speed Deformation of Metals," (Vysokoskorostnaya Deformatsiya Metalov) Minsk, *Nauka i Tekhnika*, FSL24517.

Birkhoff, G. (1947), "Hollow Charge Anti-Tank (HEAT) Projectiles," Ballistic Research Laboratory Report No. 623, February 10.

Birkhoff, G., MacDougall, D., Pugh, E., and Taylor, G. (1948), "Explosives with Lined Cavities," *J. Appl. Phys., 19*(6).

Byrnside, N. C., Torvik, P. J., and Swift, H. F. (1972), "Impact Crater Formation at Intermediate Velocities," *J. Basic Engr.—Trans. ASME*, June.

Carleone, J., Chou, P. C., Flis, W. J., and Tanzio, C. (1982), "User's Manual for DESC-2," Dyna East Corporation Technical Report, DE-TR-75-4, Revision 3, July.

Chick, M. C., Frey, R. B., Trimble, J. J., and Bines, A. (1984), "Jet Penetration in Plexiglas," *Proc. 8th Int. Symp. on Ballistics,* Orlando, FL, October 23–25.

Chou, P. C., and Flis, W. J. (1986), "Recent Developments in Shaped Charge Technology," *Propell., Explos., Pyrotech., 11:* 99–114.

Chou, P. C., and Foster, J. C. (1987), "Theory of Penetration by Jets of Non-Linear

Velocity and in Layered Targets," *Proc. 10th Int. Symp. on Ballistics,* Vol. 2, San Diego, October.

Chou, P. C., and Toland, R. H. (1977), "Experimental Study of Multiple Interior Impacts," *Exper. Mech., 17*(6): 201–206.

Chou, P. C., Hirsch, E., and Walters, W. P. (1981), "The Virtual Origin Approximation of Shaped Charge Jets," *Proc. 6th Int. Symp. on Ballistics,* Orlando, FL, October 27–29.

Chou, P. C., Minnich, M., and Gause, L. (1975), "Experimental Study of Multiple Interior Impacts," Ballistic Research Laboratory Contract Report No. 199.

Christman, D. R., and Gehring, J. W. (1966), "Analysis of High-Velocity Projectile Penetration Mechanics," *J. Appl. Phys., 37*(4).

Clark, G. D. (1983), "Study of Kinetic Energy Penetration of Multi-Layered Targets," M.S. Thesis, Air Force Institute of Technology, AFIT/GAE/AA/83S-1, September.

Contiliano, R. M., McDonough, T. B., and Swanson, C. V. (1978), "Application of the Integral Theory of Impact to the Qualification of Materials and the Development of a Simplified Rod Penetrator Model," ARAP Report No. 368, November.

Defourneaux, M. (1973), "Examination of the Theories Dealing with the Penetration of a Projectile into a Plastic Material," Franco-German Research Center of Saint-Louis, France, pp. 645–671 (Incl. #1) R423300 and FSTC-HT-23-0110-74, September.

Dehn, J. T. (1979), "The Particle Dynamics of Target Penetration," Ballistic Research Laboratory Technical Report, ARBRL-TR-02188, September.

Dehn, J. T. (1986), "A Unified Theory of Penetration," Ballistic Research Laboratory Technical Report, ARBRL-TR-2770, December.

deRosset, W. S. (1981), "Multiple Impacts on Monolithic Steel," *Proc. 6th Int. Symp. on Ballistics,* Orlando, FL, October 27–29.

deRosset, W. S., and Kimsey, K. D. (1986), "Calculation of Multiple Copper Rod Impacts on Steel Targets," *Proc. 9th Int. Symp. on Ballistics,* Schrivenham, U.K., April 29–May 1.

DiPersio, R., and Simon, J. (1964), "The Penetration–Standoff Relation for Idealized Shaped Charge Jets," Ballistic Research Laboratory Memorandum Report 1542.

DiPersio, R., and Simon, J. (1966), "Theory of Residual Penetration by Ideal Shaped Charge Jets," Ballistic Research Laboratory Report No. 1313.

DiPersio, R., and Simon, J. (1968a), "The Effect of Jet Breakup Time on the Penetration Performance of Shaped Charges," Ballistic Research Laboratory Memorandum Report No. 1897.

DiPersio, R., and Simon, J. (1968b), "Resistance of Solid Homogeneous Targets to Shaped Charge Jet Penetration," Ballistic Research Laboratory Report No. 1417, October.

DiPersio, R., and Simon, J. (1968c), "The Effect of Hardness on the Penetration Capability of Shaped Charge Jets," Ballistic Research Laboratories Report No. 1408, July.

DiPersio, R., Simon, J., and Merendino, A. B. (1965a), "Penetration of Shaped Charge Jets into Metallic Targets," Ballistic Research Laboratory Report No. 1296, September.

DiPersio, R., Simon, J., and Merendino, A. B. (1965b), "Shaped Charge Warhead Performance, Part I—Experimental Observations, J. Simon and Part II—Mathe-

matical Relationships. R. DiPersio," *Proc. 4th Warhead Research Symp.,* TP No. 3984 Naval Weapons, held at the Naval Ordnance Test Station, China Lake, CA, September 28–30.

Dong, Y., and Chen, T. (1981), "An Experimental Research of the Vertical Penetrating Process of High-Velocity Long-Rod Armor-Piercing Projectiles," *Binggong Xuebao (Acta Armamentarii),* No. 2, May.

Dullum, O., and Haugstad, B. (1981), "On the Effect of Finite Strength in Long Rod Penetration," FFI/RAPORT-81/4001, January (NDRE Report).

Donaldson, C. D., Contiliano, R., and Swanson, C. (1976), "The Qualification of Target Materials Using the Integral Theory of Impact," Aeronautical Research Associates of Princeton Report No. 295.

Doyle, J. R., and Buchholz, R. L. (1973), "Design, Development, Fabrication and Testing Program to Demonstrate Feasibility of the Mass Focus/Fragmentation Warhead," Honeywell Technical Report AFATL-TR-72-187, September.

Eichelberger, R. J. (1956), "Experimental Test of the Theory of Penetration by Metallic Jets," *J. Appl. Phys., 27*(1): 63–68.

Evans, W. M. (1950), "The Hollow Charge Effect," *Bulletin of the Institution of Mining and Metallurgy,* March 9.

Evans, W. M., and Ubbelohde, A. R. (1950a), "Some Kinematic Properties of Munroe Jets," *Res. Supp.*, London, 3-8.

Evans, W. M., and Ubbelohde, A. R. (1950b), "Formation of Munroe Jets and Their Action on Massive Targets," *Res. Supp.*, London, 3-7.

Flis, W. J. (1979), "RODPEN, A One-Dimensional Computer Code for Penetration Calculations," Dyna East Corporation Technical Report No. DE-TR-79-2.

Flis, W. J., and Chou, P. C. (1983), "Penetration of Compressible Materials by Shaped Charge Jets," *Proc. 7th Int. Symp. on Ballistics,* The Hague, Netherlands, April 19–21.

Foster, J. (1981), "Integrated Flash Radiograph Analysis—an Approach to Studying Time-Dependent Phenomena in the Explosive Formation and Projection of Metals," *Proc. 7th Annual Technical Mtg. on Physics of Explosives,* Livermore, CA, October 21–23.

Franzen, R. R. (1987), "Notes on Tubular Hyper-Velocity Penetrators," *Proc. 10th Int. Symp. on Ballistics,* Vol. 2, San Diego, October.

Godunov, S. K., Deribas, A. A., Zabrodin, A. V., and Kozin, N. S. (1970), "Hydrodynamic Effects in Colliding Solids," *J. Comp. Phys., 5:* 517–539.

Goldsmith, W. (1960), *Impact—Theory and Physical Behavior of Colliding Solids*, London: Edward Arnold Publishers.

Golesworthy, R. C. (1983), "The Effect of Transverse Velocity on Shaped Charge Performance," *Proc. 7th Int. Symp. on Ballistics,* The Hague, Netherlands, April.

Goodier, J. N. (1965), "On the Mechanics of Indentation and Cratering in Solid Targets of Strain-Hardening Metal by Impact of Hard and Soft Spheres," *Proc. 7th Hypervelocity Impact Symp.,* Vol. III, Tampa, FL: Martin Company.

Gordopolov, Yu. A., Dremin, A. N., and Mikhailov, A. N. (1977), "Wave Formation with the High Speed Collision of Metallic Bodies," *Fizika Goreniya i Vzryva, 13*(2): 288–291.

Greenspon, J. E. (1978), "A Study of the Mechanics of Perforation," AMSAA-TR-212, August.

Harlow, F. H., and Pracht, W. E. (1966), "Formation and Penetration of High-Speed Collapse Jets," *Phys. Fluids, 9*(10).

Hashmi, M. S. J., and Thompson, P. J. (1977), "A Numerical Method of Analysis for the Mushrooming of Flat-Ended Projectiles Impinging on a Flat Rigid Anvil," *Int. J. Mech. Sci., 19:* 273–283.

Haugstad, B. S. (1981), "Compressibility Effects in Shaped Charge Jet Penetration," *J. Appl. Phys., 42*(3): 1243–1246.

Haugstad, B. S., and Dullum, O. S. (1981), "Finite Compressibility in Shaped Charge Jet and Long Rod Penetration—The Effect of Shocks," *J. Appl. Phys., 52*(8): 5066–5071.

Held, M. (1983), "Characterizing Shaped Charge Performance by Stand-Off Behavior," *Proc. 7th Int. Symp. on Ballistics,* The Hague, Netherlands, April 19–21.

Held, M. (1987), "Refined Shaped Charge Jet Penetration Measurement in Various Materials Versus Hydrodynamic Prediction," *Proc. 10th Int. Symp. on Ballistics,* Vol. 2, San Diego, October.

Herrmann, W., and Wilbeck, J. (1987), "Review of Hypervelocity Penetration Theories," *Int. J. Impact Engng., 5*(1–4): 307–322.

Hill, R. (1980), "Caviation and the Influence of Headshape in Attack of Thick Targets by Non-Deforming Projectiles," *J. Mech. Phys. Solids, 28:* 249–263.

Hill, R., Mott, N., and Pack, D. (1944), A.R.D. Theoretical Research Report No. 2/44 (January) and 12/44 (March).

Hohler, V., and Stilp, A. J. (1977), "Penetration of Steel and High Density Rods in Semi-Infinite Steel Targets," *Proc. 3rd Int. Symp. on Ballistics,* Karlsruhe, Germany.

Johnson, G. R. (1977), "Liquid-Solid Impact Calculations with Triangular Elements," *J. Fluids Engr., Trans. ASME*, September.

Johnson, W. (1970), *Impact Strength of Materials*, New York: Arnold.

Jonas, G. H., and Zukas, J. A. (1977), "Armor Penetration: Theory and Experiment," *Proc. 14th Annual Mtg. of the Society of Engineering Sci.,* Lehigh University, PA, November.

Jonas, G. H., and Zukas, J. A. (1978), "Mechanics of Penetration: Analysis and Experiment," *Int. J. Engr. Sci., 16:* 879–903.

Kimsey, K. D., and Zukas, J. A. (1986), "Contact Surface Erosion for Hypervelocity Problems," Ballistic Research Laboratory, BRL-MR-3495, February.

Klamer, O. A. (1964), "Shaped Charge Scaling," Ammunition Engineering Directorate, Picatinny Arsenal, Technical Memorandum 1383, Dover, NJ, March.

Kozlov, V. S. (1986), "Penetration Model That Accounts for the Ductile Properties of the Materials of Colliding Bodies," trans. from *Problemy Prochnosti*, No. 3, 47–52.

Kucher, V. (1982), "Multiple Impacts on Monolithic Steel," Ballistic Research Laboratory Technical Report, ARBLR-TR-02406, April.

Luttwak, G., Kivity, Y., and Abetser, A. (1982), "Effects of a Hypervelocity Jet on a Layered Target," *Int. J. Engr. Sci., 20:* 946–961.

Majerus, J. N., and Scott, B. R. (1978), "CUMIN: A Computer Code for Determining Certain Jet/Target Parameters from Experimental Data," Ballistic Research Laboratory Technical Report ARBRL-TR-02129, December.

Majerus, J. N., and Walters, W. P. (1978), "Axial Penetration and Radial Growth for Kinetic Energy and Shaped Charge Jet Penetrators," *Proc. of DEA-G-1060 Ballistic Research and Development Mtg.,* Naval Surface Weapons Center, Dahlgren, VA; also published in the TTCP-TPW-1 Kinetic Energy Ammunition Conference, Ballistic Research Laboratory, May.

Majerus, J. N., and Walters, W. P. (1981), "A Predictive Penetration Model Utilizing an Effective-Flow Viscosity of the Interaction Region," *Proc. 6th Int. Symp. on Ballistics,* Orlando, FL, October 27–29, 1981.

Majerus, J. N., Kucher, V., and Simon, J. (1977), "Influence of Transverse Velocity upon the Penetration Performance of Shaped Charge Warheads," Ballistic Research Laboratory Memorandum Report, ARBRL-MR-2742, April.

Majerus, J. N., Walters, W. P., and Neitzel, G. P. (1978), "Impact Models for Penetration and Hole Growth," *Proc. 4th Int. Symp. on Ballistics,* Monterey, CA, October 17–19, 1978.

Mar'yamov, A. N. (1975), "Calculation of the High Velocity Impact of Solids on the Basis of a Viscoplastic Model," *Vestnik Moskovskogo un-ta-matematika, mekhanika, 1*(6): 99–102.

Matuska, D. A. (1982), "A Model for High Velocity Penetration," *Proc. of ARO Workshop on Computational Aspects of Penetration Mechanics,* Aberdeen Proving Ground, MD, April.

Merendino, A. B., and Vitali, R. (1968), "The Penetration of Shaped Charge Jets into Steel and Aluminum Targets of Various Strengths," Ballistic Research Laboratory Memorandum Report No. 1932.

Merzhievskii, L. A., and Titov, V. M. (1975), "Perforation of Plates through High-Velocity Impact," *(ZPMFA Novosibirsk), J. Appl. Mech. Tech. Phys.,* (5): 102–111.

Murphy, M. J. (1983), "Shaped Charge Penetration in Concrete: A Unified Approach," Ph.D. Dissertation, University of California, Davis, also UCRL-53393 and DE 83009181, January.

NDRC (1946), "Protection Against Shaped Charges," Carnegie Institute of Technology, NDRC Report No. A-384 and OSRD Report No. 6384, February.

Pack, D. C., and Evans, W. M. (1951), "Penetration by High-Velocity ('Munroe') Jets: 1," *Proc. Phys. Soc. (London), B64:* 298.

Perez, E. (1978), "A Theory for Armor Penetration by Hypervelocity Long Rods," *Proc. 4th Int. Symp. on Ballistics,* Monterey, CA, October 17–19, 1978.

Perez, E. (1982), "Experimental and Theoretical Study on the Penetration of Semi-Infinite Metal Targets by Great-Length Metal Projectiles with a Velocity Higher Than 2000 m/s," *Sciences et Techniques de l'Armement*, Vol. 56, No. 1, Paris.

Pugh, E. M. (1944), "A Theory of Target Penetration of Jets," National Defense Research Committee Armor and Ordnance, Report No. A-274 (OSRD No. 3752) Division 2, June.

Ravid, M., and Bodner, S. R. (1982), "Dynamic Perforation of Viscoplastic Plates by Rigid Projectiles," Material Mechanics Laboratory, Israel Institute of Technology, July.

Ravid, M., Bodner, S. R., and Holcman, I. (1987a), "Analysis of Very High Speed Impact," *Int. J. Engr. Sci., 25*(4): 473–482.

Ravid, M., Bodner, S., and Holcman, I. (1987b), "A Two-Dimensional Engineering Model for Perforation of Layered Targets," *Proc. 10th Int. Symp. on Ballistics,* Vol. 2, San Diego, October.

Sagomonyan, A. Ya. (1974), *Penetration of Solids Into Compressible Continuous Media*, Moscow University, trans. by DARPA, January 1980.

Sagomonyan, A. Ya. (1975), "Plate Piercing by a Slender Solid Projectile," *Vestnik Moskovskogo Universiteta, Seriya 1, Matematika, Mekhenika,* No. 6, 104–111, FSTC-HT-1065-81.

Sagomonyan, A. Ya. (1977), "The Penetration of an Obstacle by a Cylindrical Object," *Vistnik Moskovskogo un-ta, Seriya Matematika, Mekhanika,* (5): 111–118, Izd-vo Mosk. un-ta.

Sagomonyan, A. Ya. (1978), *Penetration of Solids into Compressed Continuous Media*, "Penetration of Solids after High Speed Impact," Chapter 3, UDC 534.26 and 539.374, May.

Sanasaryan, N. S. (1975), "Penetration of a Cumulative Jet into a Barrier," *Izvestiya Akademii Nauk SSSR, Mekhanika Zhidkosti i Gaza,* No. 6, 151–154.

Sedgwick, R. T., and Wilkinson, M. G. (1987), "High Velocity Long Rod Impact: Theory and Experiment," *Proc. 10th Int. Symp. on Ballistics,* Vol. 2, San Diego, October.

Segletes, S. B. (1983), "Drift Velocity Computations for Shaped Charge Jets," Ballistic Research Laboratory Memorandum Report, ARBRL-MR-03306, September.

Segletes, S. B. (1984), "A Model of Effects of Transverse Velocity on the Penetration of a Shaped Charge Jet," Ballistic Research Laboratory Memorandum Report, ARBRL-MR-3409, November.

Segletes, S. B. (1987), "Improved Drift Velocity Computations for Shaped Charge Jets," Ballistic Research Laboratory Technical Report, BRL-TR-2823, June.

Seizew, M. R., Kuhl, A. L., and Blankenship, V. D. (1978), "The Role of Viscosity of Solids in Microparticle Cratering," *Acta Astronautica, 5:* 1129–1144.

Senf, H. (1974), "Effects of Fragmentation Against Hard Targets," Fraunhofer Gesellschaft zur Forderung der Angewandten Forschung, E. V.: Arbeitsgruppe fur Ballistische Forschung, Weil am Rhein, September.

Shear, R. E., Brundick, F. S., and Harrison, J. T. (1981), "A Link between Shaped Charge Performance and Design," Ballistic Research Laboratory Technical Report, ARBRL-TR-02361, September.

Simon, J., and DiPersio, R. (1969a), "Experimental Verification of Standoff Effects on Shaped Charge Jet Cutoff in Solid Targets," Ballistic Research Laboratory Memorandum Report No. 1976.

Simon, J., and DiPersio, R. (1969b), "The Effect of Target Density and Hardness on the Penetration Capability of Precision Shaped Charge Warheads," *Proc. 3rd Symp. on Lightweight Armor Materials,* Cleveland, August 12–15, 1968, Sponsored by U.S. Army Materials and Mechanics Research Center, Watertown, MA, Report No. AMMRC-MS-69-02, April.

Simon, J., DiPersio, R., and Merendino, A. (1965), "Penetration Capability and Effectiveness of a Precision Shaped Charge Warhead," Ballistic Research Laboratory Memorandum Report No. 1636, March.

Simon, J., DiPersio, R., and Merendino, A. B. (1967), "Shaped Charge Warhead Performance (II)," *Proc. 5th Warhead Research Symp.,* Naval Weapons Center, China Lake, CA, September, NWC-TP4446, December.

Smith, J. (1981), "Shaped Charge Penetration at Long Standoff," Air Force Armament Laboratory Report No. AFATL-TR-81-25, February.

Stepanov, G. V. (1969a), "High Speed Impact of Solid Particles and Obstacles of Various Angles," *PKMKA, Soviet Applied Mechanics, 5*(8): 110–112.

Stepanov, G. V. (1969b), "Hypervelocity Projectile Impact in Semi-Infinite Targets," *Problemy Prochnosti, 5*(11): 71–75.

Stepanov, G. V. (1970), "Influence of Target Material Temperature on the Depth of Craters Produced by High-Velocity Particles," *Soviet Physics–Technical Physics, 15*(3).

Szendrei, T. (1983), "Analytical Model of Crater Formation by Jet Impact and Its Application to Calculation of Penetration Curves and Hole Profiles," *Proc. 7th Int. Symp. on Ballistics,* The Hague, Netherlands, April.

Tate, A. (1967), "A Theory for the Deceleration of Long Rods after Impact," *J. Mech. Phys. Solids, 15:* 387–399.

Tate, A. (1969), "Further Results in the Theory of Long Rod Penetration," *J. Mech. Phys. Solids, 17:* 141–150.

Tate, A. (1977), "A Possible Explanation for the Hydrodynamic Transition in High Speed Impact," *Int. J. Mech. Sci., 19:* 121–123.

Tate, A. (1979), "A Simple Estimate of the Minimum Target Obliquity Required for the Ricochet of a High Speed Long Rod Projectile," *J. Phys. D: Appl. Phys., 12:* 1825–1829.

Tate, A. (1986a), "Long Rod Penetration Models—Part I. A Flow Field Model for High Speed Long Rod Penetration," *Int. J. Mech. Sci., 28*(8): 535–548.

Tate, A. (1986b), "Long Rod Penetration Models—Part II. Extensions to the Hydrodynamic Theory of Penetration," *Int. J. Mech. Sci., 28*(9): 599–612.

Walters, W. P., and Majerus, J. N. (1977), "Hypervelocity Impact Models for Hole Growth and Geometry," *Proc. 3rd Annual Vulnerability / Survivability Symp.,* ADPA, Naval Amphibious Base, Coronada, CA.

Walters, W. P., and Majerus, J. N. (1978), "Impact Models for Penetration and Hole Growth," Ballistic Research Laboratory Technical Report, ARBRL-TR-02069, May.

Walters, W. P., and Majerus, J. N. (1979), "Shaped Charge Penetration Model, Part I: Monolithic Penetration and Comparison with Experimental Data," Ballistic Research Laboratory Technical Report, ARBRL-TR-02184, AD B041747.

Walters, W. P., Majerus, J. N., and Neitzel, G. P. (1979), "Developing Target Armor Using a Jet Penetration Model," *Proc. 4th Vulnerability-Survivability Symp.,* Tyndall AFB, FL, March.

Walters, W. P., Chou, P. C., and Flis, W. J. (1987), "Shaped Charge Jet Penetration," Ballistic Research Laboratory Technical Report, BRL-TR-2826, July.

Walters, W. P., Flis, W. J., and Chou, P. C. (1988), "A Survey of Shaped Charge Jet Penetration Models," *J. Impact Engr., 7*(3).

Weihrauch, G. (1971), "The Behavior of Copper Pins upon Impacting Various Materials at Velocities of 50–1650 m/s," Ph.D. Dissertation, Karlsruhe University.

White, J. J., and Wahll, M. J. (1981), "Shaped Charge Jet Interactions with Liquids," *Proc. 6th Int. Symp. on Ballistics,* ADPA, Orlando, FL, October.

White, J. J., Wahll, M. J., and Backofen, J. E. (1982), "Observation of Compressibility-Related Effects in Shaped Charge Jet Penetration," *J. Appl. Phys., 53*(6).

Wilkinson, J. P. D. (1969), "A Penetration Criterion for Double-Walled Structures Subject to Meteoroid Impact," *AIAA J., 7*(10).

Woidneck, C. P. (1986), "Rod Penetration in Liquids," *Proc. 9th Int. Symp. on Ballistics,* Shriveham, U.K., April 29–May 1.

Wright, T. W. (1981), "Penetration with Long Rods: A Theoretical Framework and Comparison with Instrumented Impacts," Ballistic Research Laboratory Technical Report, ARBRL-TR-02323, May.

Wright, T. W. (1983), "A Survey of Penetration Mechanics for Long Rods," Ballistic Research Laboratory Technical Report, ARBRL-TR-02496, June.

Woodward, R. L. (1982), "Penetration of Semi-Infinite Metal Targets by Deforming Projectiles," *Int. J. Mech. Sci., 24*(2): 73–87.

Zaid, M. (1960), "An Analytical Approach to Hypervelocity Impact Mechanics," *Hypervelocity Impact*, Vol. 3, Fourth Symposium, APGC-TR-60-39, September.

Zakharenko, I. D., and Mali, V. I. (1972), "Viscosity of Metals in Explosion Welding," *Goreniya i Vzryva*, Moscow: Izd-vo Nauka, pp. 575–578.

Zlatin, N. A. (1962), "On the Theory of Metal Bodies in High Speed Impact," *(ZTEPA) J. Tech. Phys., 6*(8).

Zukas, J. A. (1980), "Impact Dynamics: Theory and Experiment," Ballistic Research Laboratory Technical Report, ARBRL-TR-02271, October 1980; also "Impact Dynamics," in *Emerging Technologies in Aerospace Structures, Design, Structural Dynamics and Materials,* J. R. Vinson (ed.); New York: ASME.

Zukas, J. A., Nicholas, T., Swift, H. F., Greszczuk, L. B., and Curran, D. R. (1982), *Impact Dynamics*, New York: Wiley-Interscience.

REFERENCES APPENDIX A

_______ (1955), *Proc. 1st Hypervelocity and Impact Effects Symp.,* Santa Monica, CA, May.

_______ (1957), *Proc. 2nd Hypervelocity Impact Effects Symp.,* Washington, D.C., May.

_______ (1959), *Proc. 3rd Symp. on Hypervelocity Impact,* Chicago, IL, October.

_______ (1960), *Proc. 4th Symp. on Hypervelocity Impact,* Eglin AFB, FL, April.

_______ (1961), *Proc. 5th Symp. on Hypervelocity Impact,* Denver, CO, April.

_______ (1963), *Proc. 6th Symp. on Hypervelocity Impact,* Cleveland, OH, April/May.

_______ (1965), *Proc. 7th Symp. on Hypervelocity Impact,* Tampa, FL, November.

_______ (1969), *Proc. AIAA Hypervelocity Impact Conf.,* Cincinnati, OH, April/May.

_______ (1987), *Hypervelocity Impact: Proc. 1986 Symp., Int. J. Impact Eng., 5*(1–4).

Adler, W. (ed.) (1979), *Erosion: Prevention and Useful Applications,* ASTM-STP-664.

Allison, F. E. (1965), "Mechanics of Hypervelocity Impact," *Proc. 7th Hypervelocity Impact Symp.*, Vol. I, Tampa, FL.

Atkins, W. W. (1960), "Hypervelocity Penetration Studies," *Proc. 4th Hypervelocity Impact Symp.*, Eglin AFB, FL, September.

Backman, M., and Goldsmith, W. (1978), "The Mechanics of Penetration of Projectiles into Targets," *Int. J. Engng. Sci.*, *16:* 1–99.

Baker, J. R. (1969), "Rod Lethality Studies," Naval Research Laboratory, NRL-6920.

Bethe, H. A. (1941), "Attempt of a Theory of Armor Penetration," Frankford Arsenal Rep., Philadelphia, PA.

Caldirola, P., and Knoepfel, H. (eds.) (1971), *Physics of High Energy Density*, New York: Academic Press.

Christman, D. R., and Gehring, J. W. (1966), "Analysis of High-Velocity Projectile Penetration Mechanics," *J. Appl. Phys.*, *37*(4).

Christman, D. R., Wenzel, A. B., and Gehring, J. W. (1965), "Penetration Mechanisms of High Velocity Rods," *Proc. 7th Hypervelocity Impact Symp.*, Tampa, FL, February.

Eichelberger, R. J., and Gehring, J. W. (1962), "Effects of Meteroid Impacts on Space Vehicles," *ARS J.*, *32*(10): 1583–1591.

Eichelberger, R. J., and Kineke, J. H. (1967), "Hypervelocity Impact," in *High-Speed Physics*, K. Vollrath and G. Thomer (eds.), New York: Springer-Verlag.

Feldman, J. B. (1959), "Volume-Energy Relation from Shaped Charge Jet Penetrations," *Proc. 3rd Symp. on Hypervelocity*, Chicago, February.

Feldman, J. B. (1960), "Volume-Energy Relation from Shaped Charge Jet Penetrations," *Proc. 4th Symp. on Hypervelocity Impact*, Eglin AFB, FL, September.

Frasier, J. T., Karpov, B. G., and Holloway, L. S. (1965), "The Behavior of Wax Targets Subjected to Hypervelocity Impact," *Proc. 7th Hypervelocity Impact Symp.*, Vol. V, Tampa, FL.

Freiberger, W. (1952), "A Problem in Dynamic Plasticity: The Enlargement of a Circular Hole in a Flat Sheet," *Proc. Cambridge Phil. Soc.*, 48, London.

Glass, J., and Bruchey, W. (1984), "Internal Deformation and Energy Absorption During Penetration of Semi-Infinite Targets," *Proc. 8th Int. Symp. on Ballistics*, Orlando, FL, October 23–25.

Goldsmith, W. (1960), "Impact, The Theory and Physical Behavior of Colliding Solids," London: Edward Arnold.

Halperson, S. M. (1965), "Comparisons Between Hydrodynamic Theory and Impact Experiments," *Proc. 7th Hypervelocity Impact Symp.*, Tampa, FL, February.

Hill, R. (1980), "Cavitation and the Influence of Headshape in Attack of Thick Targets by Non-Deforming Projectiles," *J. Mech. Phys. Solids*, *28:* 249–263.

Hohler, V., and Stilp, A. (1987), "Long Rod Penetration Mechanics," *Int. J. Impact Engr.*, *5*(1–4).

Hohler, V., Schneider, E., Stilp, A., and Tham, R. (1978), "Length and Velocity Reduction of High Density Rods Perforating Mild Steel and Armor Steel Plates," *Proc. 4th Intl. Symp. on Ballistics*, Monterey, CA, October 17–19.

Holloway, L. S. (1963), "Observations of Crater Growth in Wax," Ballistic Research Laboratory Report, USABRL-M-1526.

Hopkins, H. G. (1960), "Dynamic Expansion of Spherical Cavities in Metals," in *Progress in Solid Mechanics*, I. N. Sneddon and R. Hill (eds.), Vol. I, Chapter 3, Amsterdam: North Holland.

Housen, K., Schmidt, R., and Holsapple, K. (1983), "Crater Ejecta Scaling Laws: Fundamental Forms Based on Dimensional Analysis," *J. Geophys. Res., 88*(B3): 2485–2499, March 10.

Johnson, W. (1972), *Impact Strength of Materials*, New York: Edward Arnold.

Kawata, K., and Shioiri, J. (eds.) (1979), *Proc. IUTAM Symp. on High Velocity Deformation of Solids,* Berlin: Springer-Verlag.

Kineke, J. H. (1960), "An Experimental Study of Crater Formation in Metallic Targets," *Proc. 4th Hypervelocity Impact Symp.,* Eglin AFB, FL.

Kineke, J. H., and Vitali, R. (1963), "Transient Observations of Crater Formation in Semi-Infinite Targets," *Proc. 6th Symp. on Hypervelocity Impact,* Vol. II, Part 2, Cleveland.

Kinslow, R. (ed.), (1970), *High Velocity Impact Phenomena*, NY, Academic Press.

Kornhauser, M. (1964), *Structural Effects of Impact*, Baltimore: Spartan Books.

Lambert, J. P. (1978), "The Terminal Ballistics of Certain 65 gram Long Rod Penetrators Impacting Steel Armor Plate," Ballistic Research Laboratory Report, ARBRL-TR-02072, May.

Majerus, J., and Scott, B. R. (1978), "CUMIN: A Computer Code for Determining Certain Jet/Target Parameters from Experimental Data," Ballistic Research Laboratory Technical Report, ARBRL-TR-02129, December.

Merzhievskii, L. A., and Titov, V. M. (1975), "Perforation of Plates Through High-Velocity Impact," *(ZPMFA Novosibirsk), J. Appl. Mech. Tech. Phys.,* No. 5, 102–110.

Murphy, M. J. (1987), "Survey of the Influence of Velocity and Material on the Projectile Energy/Target Hole Volume Relationship," *Proc. 10th Int. Symp. on Ballistics,* San Diego, October.

Öpik, E. (1936), "Researches of the Physical Theory of Meteor Phenomena: 1. Theory of the Formation of Meteor Craters," *Acta Comm. Univ. Tartuensis.*

Payne, J. J. (1965), "Impacts of Spherical Projectiles of Aluminum, Stainless Steel, Titanium, Magnesium, and Lead into Semi-Infinite Targets of Aluminum and Stainless Steel," AEDC-TR-65-34, ARO, Inc., February.

Perez, E. (1978), "A Theory for Armor Penetration by Hypervelocity Long Rods," *Proc. 4th Int. Symp. on Ballistics,* Monterey, CA, October 17–19.

Piekutowski, A. J. (1981), "A Compendium of Data from Laboratory-Scale High Explosive Cratering and Ejecta Studies," AFWL-TR-8-86.

Preece, C. (ed.) (1979), *Treatise on Materials Science and Technology. Vol. 16, Erosion,* New York: Academic Press.

Rinehart, J., and Pearson, J. (1954), "Behavior of Metals under Impulsive Loads," *Amer. Soc. for Metals.*, Cleveland.

Roddy, D. J., Peppin, R. O., and Merrill, R. B. (eds.) (1977), *Impact and Explosion Cratering*, New York: Pergamon Press.

Rolsten, R. F., Wellnitz, J. N., and Hunt, H. H., (1964), "An Example of Hole Diameter in Thin Plates due to Hypervelocity Impact," *J. Appl. Phys., 35.*

Scott, B. R. (1984), "Radial Expansion of Cavities Produced by the Axisymmetric Steady Penetration of Hypervelocity Rods," Ph.D. Dissertation, University of Delaware, Newark, DE.

Scott, B. R. (1986), "Analytical Penetration and Hole Growth Models," in Course Notes *Fundamentals Aspects of Hypervelocity Impact and Shaped Charge Phenomena*, Vol. 2, Computational Mechanics Associates, Baltimore, April.

Seizew, M. R., Kuhl, A. L., and Blankenship, V. D. (1978), "The Role of Viscosity of Solids in Microparticle Cratering," *Acta Astronautica, 5:* 1129–1144.

Silsby, G. (1984), "Penetration of Semi-Infinite Steel Targets by Tungsten Long Rods at 1.3 to 4.5 km/s.," *Proc. 8th Int. Symp. on Ballistics,* Orlando, FL, October 23–25.

Springer, G. S. (1976), *Erosion by Liquid Impact*, New York: Wiley.

Stepanov, G. V. (1969), "High Speed Impact of Solid Particles and Obstacles of Various Angles," *(PKMKA), Soviet Appl. Mech., 5*(8): 110–112.

Stilp, A. (1987), "Long Rod Penetration Mechanics," in Computational Mechanics Associates Course Notes, *High Velocity Impact Dynamics*, Baltimore, MD.

Swift, H. (1982a), "Hypervelocity Impact Mechanics," in *Impact Dynamics*, J. A. Zukas et al., New York: Wiley-Interscience.

Swift, H. (1982b), "Image Forming Instruments," in *Impact Dynamics*, J. A. Zukas et al., New York: Wiley-Interscience.

Tate, A., Green, K. E. B., Chamberlain, P. G., and Baker, R. G. (1978), "Model Scale Experiments on Long Rod Penetration," *Proc. 4th Int. Symp. on Ballistics,* Monterey, CA, October 17–19.

Taylor, G. I. (1941), "Notes on H. A. Bethe's Theory of Armor Penetration, II. Enlargement of a Hole in a Flat Sheet at High Speeds," Ministry of Home Security Rep., R.C. 280.

Taylor, G. I. (1948), "The Formation and Enlargement of a Circular Hole in a Thin Plastic Sheet," *Quart. J. Mech. Appl. Math., 1.*

Turpin, W. C., and Carson, J. M. (1970), "Hole Growth in Thin Plates Perforated by Hypervelocity Pellets," Air Force Materials Lab. Report 70-83, Wright-Patterson AFB, OH.

Vollrath, G. (ed.) (1967), *Kurzzeitphysik*, New York: Springer-Verlag.

Walters, W. P., and Scott, B. R. (1985), "The Crater Radial Growth Rate Under Ballistic Impact Conditions," *Comput. Struct., 20*(1–3): 641–648.

Whiffin, A. C. (1948), "The Use of Flat-Ended Projectiles for Determining Dynamic Yield Stress, II. Tests on Various Metallic Materials," *Proc. R. Soc. London Ser. A, 194.*

Wilkins, M., and Guinan, M. (1973), "Impact of Cylinders on a Rigid Boundary," *J. Appl. Phys., 44.*

Woodward, R. L. (1981), "Ballistic Experiments with Laminated Metal Targets," Ballistic Research Laboratory Report, ARBRL-TR-02303.

Zukas, J. A., Nicholas, T., Swift, H., Greszczuk, L., and Curran, D. (1982), *Impact Dynamics*, New York: Wiley.

CHAPTER 10

OTHER ASPECTS OF SHAPED CHARGES

This chapter contains a potpourri of data representing certain practical aspects of shaped charge manufacture and assembly. In addition, size effects (scaling), aerodynamic effects, and analytical/experimental methods of determining the temperature of a shaped charge jet are discussed.

10.1. FABRICATION OF SHAPED CHARGE LINERS

To date, specification of the optimum method for fabricating shaped charge liners is not a straightforward procedure. However, in the last few years a great deal has been learned about liner metallurgy, liner metallurgical requirements, and liner fabrication processes. Perhaps, in the near future, for a given liner geometry and metallurgical requirements, an optimum method of fabrication will be apparent. The method of fabrication must depend on the grain size, grain orientation, and other metallurgical factors required. This in turn, describes the amount of work (rolling, forming, deformation, etc.) that must go into the starting plate or stock. Annealing and other intermediate cycles are important. Finally, the metallurgical characteristics of the starting material must be translated into the correct metallurgical characteristics of the final liner configuration, which in turn must be translated into the correct shaped charge jet material characteristics.

Basically, from Leidel (1978), Vidosic (1984), and Degramo (1957), manufacturing processes can be classified as (1) casting processes, (2) forming processes (such as powder metallurgy techniques, hot-working techniques and cold-working techniques), (3) machining processes, and (4) other techniques such as grinding and metallizing. These processes will be discussed in turn.

Casting produces the desired part by the introduction of a molten material into a previously formed mold or cavity.

In a powder metallurgy process, the parts are produced in their final form by pressing fine metal powders, usually in metal molds and under considerable pressure, and then heating the compacted powder for a period of time at a temperature below the melting point of the major constituent. Powder metallurgy processes consist of at least four basic steps: (1) producing a fine metal powder, (2) mixing and preparing the powder, (3) pressing the powder into the final shape, and (4) heating (sintering) the shape at elevated temperature.

Hot working is the plastic deformation of metals above the recrystallization temperature. Recrystallization occurs when a metal is heated to a high enough temperature, after being cold worked, that new, equiaxed, unstrained crystals are formed. The temperature at which recrystallization takes place varies with each metal and with the amount of cold deformation. Usually, the greater the amount of cold work, the lower the recrystallization temperature. However, there is a practical lower limit below which recrystallization will not occur over a reasonable period of time.

When plastic deformation takes place within a single crystal of most metals at ordinary room temperatures, a permanent displacement takes place due to the slipping of one plane of atoms over an adjacent plane. The slippage that occurs between any two adjacent atomic planes is very small in magnitude. As slippage occurs, a phenomenon results that increases the resistance to further slip. This phenomenon is termed strain hardening, or work hardening, and means that as resistance to slip increases, the metal becomes harder, with a corresponding decrease in the ductility.

Strain hardening does not occur above the recrystallization temperature, and thus hot working does not cause an increase in the yield strength or hardness. Thus, it is possible to drastically alter the shape of some metals by hot working without causing them to rupture.

In general, stronger metals have higher recrystallization temperatures than the weaker ones. Since the strength properties of metals decrease considerably at elevated temperatures, the strong metals (usually the ones of engineering importance) may be deformed much more readily and with smaller forces. This means that less energy is required and thus less massive and expensive equipment is required.

Hot working can refine and improve the grain structure of the metal. When molten metal solidifies and cools, the size of the grains increases until a critical temperature is reached, after which the grain size remains constant. If a metal of given grain size is heated from below the critical temperature, new grains are formed in the critical range until only new, smaller grains exist. If the temperature is increased further, the newly formed grains continue to grow until the melting point is reached. If the temperature increase is halted above the critical range and the metal is permitted to cool, the grain size continues to increase until the critical temperature is again reached. If a coarse-grained metal is heated above the critical temperature and then hot worked, recrystal-

lization occurs and new, small grains may exist when the metal cools below the critical temperature if the metal is not held too long above the critical temperature.

In theory, if hot working continued down to the critical temperature, the resulting grains would be extremely fine. However, hot working usually ceases a safe distance above the critical temperature because the metal does not remain at a uniform temperature throughout and because strain hardening would occur if the working continued at too low a temperature. Hence, some grain growth does occur.

Another improvement in grain structure may result from hot working. When a metal part is plastically deformed, particles of impurities are elongated into stringers in accordance with the flow of the metal during deformation. Hence, the deformed metal may not have uniform strength in all directions due to the orientation of these weak stringers. By proper hot-working procedures, a fiber pattern can be produced that is advantageous for resisting the imposed stresses, yielding greater effective strength for a given weight of material.

Manufacturing processes of interest for liner fabrication are (a) rolling, which consists of passing hot metal between two rollers that revolve in opposite directions to squeeze and elongate the material; (b) forging, or the hot working of metal by localized compressive forces exerted by power hammers, presses, or special forging machines; (c) hot drawing, or causing heated metal to be drawn through the opening in a die; (d) extrusion, or forcing the metal through a die that controls the cross section of the resulting product; and (e) hot spinning, or the forming of metal parts from a flat, rotating disk by applying controlled pressure to one side and causing the metal to flow against a rotating male form that is held against the opposite side.

Cold-working processes, for some materials, are worthy of consideration. Cold working is the plastic deformation of metals below the recrystallization temperature. The working of metals at low temperatures (room temperature in many cases) has several advantages and disadvantages as compared with hot working. These advantages and disadvantages are listed in Table 1.

The major headings of cold-working operations are squeezing, bending, shearing, and drawing (Degramo 1957). Table 2 classifies these operations and includes many operations that are not relevant to shaped charge fabrication. Note that annealing is often required during intermediate stages of cold working to prevent rupture. Cold-working processes of importance here are cold rolling, cold forging, and coining (the cold working of metal by means of a positive displacement punch while completely confined within a set of dies).

Bending is the plastic deformation of metals about a linear axis with little or no change in the surface area. When two or more bends are made simultaneously with the use of a die, the process is called forming.

Cold drawing is the forming of parts from sheet material where plastic flow occurs, usually along a curved axis. Spinning (or shear spinning or rotary extrusion) is a cold-working process in which a rotating disk of metal is drawn

TABLE 1. Advantages and Disadvantages of Cold-Working Processes Compared with Hot-Working Processes

Advantages
Improved surface finish
Improved strength properties
Better dimensional control
No requirement for heating
Reproducibility and interchangeability of parts
Directional properties can be imparted
Disadvantages
Higher forces are required for deformation
Heavier forming equipment is required
Metal surfaces must be clean and scale free
Detrimental directional properties may result
Strain hardening occurs

From Degramo (1957).

TABLE 2. Classification of Cold-Working Operations

Squeezing	
a. Rolling	g. Staking
b. Swaging	h. Coining
c. Cold forging	i. Peening
d. Sizing	j. Burnishing
e. Extrusion	k. Die hobbing (hubbing)
f. Riveting	l. Thread rolling
Bending	
a. Angle	d. Seaming
b. Roll	e. Flanging
c. Roll forming	f. Straightening
Shearing	
a. Shearing	d. Notching
Slitting	Nibbling
b. Blanking	e. Shaving
c. Piercing	f. Trimming
Lancing	g. Cut-off
Perforating	h. Dinking
Drawing	
a. Bar and tube drawing	d. Embossing
b. Wire drawing	e. Stretch forming
c. Spinning	f. Shell drawing

From Degramo (1957).

over a male form by applying localized pressure to the outside of the disk by means of a round-ended tool or a roller. Stretch forming involves gripping a sheet of metal with two sets of jaws. The motion of these jaws stretches the metal and wraps it around the form block as the latter moves upward. Various combinations of stretching, wrapping, and upward motion of the form block may be used, depending on the desired shape of the final part. Shell drawing is a punch and die procedure usually used to form rectangular or cylindrical shapes.

Rubber, sand, hydraulic pressure, and other mechanisms are sometimes used as a substitute for a female die. The operational principle is that many materials will act as fluids when completely confined and thus transmit force in all directions.

Also, because of the forces required in cold working of metals, many types of presses are available. Hydraulic presses are in common use for drawing operations. The use of several hydraulic cylinders makes it possible to apply a load to the ram at several points, and to provide any desired force and timing to the blank holder.

Turning operations are yet another way to fabricate metal parts. Turning is the production of an external surface through the relative longitudinal action of a single-point cutting tool and a rotating workpiece. Facing is a special case of turning where the cutting tool moves across the work in a direction normal to the axis of rotation, instead of parallel to the axis. Boring operations are simply internal turning operations. Lathes provide the most effective method of turning.

Another method of forming parts is grinding. Grinding involves the cutting of metals by the use of a multipoint cutting tool, made up of a number of abrasive particles that have been bonded together into a grinding wheel of the desired shape. The abrasive grains are hard and irregularly shaped so that each one constitutes a very small cutting edge. Honing and lapping are similar processes. Lapping and honing operations use finer abrasive surfaces than grinding.

Another technique for fabricating metal parts is metallizing. Metallizing is a process wherein metal is melted and atomized in a special torch, gun, or the like and sprayed onto a base material or mandrel. This process is sometimes called metal spraying. Plasma spray techniques and chemical vapor deposition operations are related to metallizing but exhibit a finer control of the metal porosity, grain size, and grain orientation.

Electroplating is also related to metallizing. Electroplating is the electrodeposition of an adherent coating on a base metal. The part to be plated is made the cathode and immersed in a solution that contains dissolved salts of the metal to be deposited. The anode is a suspended piece of the metal to be deposited. Other materials may be added to the electrolyte to increase its conductivity. When a direct current is applied, metallic ions migrate to the cathode and, upon losing their charge, are deposited as metal upon it. Variables include the electrolyte solution, the current applied, the time of immersion, and the temperature of the electrolyte.

Some techniques for manufacturing liners from given plate or stock material will be discussed. It is presumed that the starting material has been worked to the extent that the metallurgical characteristics are favorable and that the liner (if the shaped charge liner is not formed directly) will have the same characteristics as the starting stock or plate.

Some of the available techniques, as discussed above for general fabrication processes, are (a) turning, for example, lathe operations; (b) using a progressive die and punch or deep draw operations, for example, to form conical liners; (c) hydroforming, or using a large hydraulic press and a die to form the liner, for example, hemispherical liners; and (d) explosively forming the liner to final shape. In Chapter 7, explosive forming was stated to be a viable fabrication process. Also, the liner material could be directly deposited on a mandrel using (e) electroplating techniques, (f) plasma spray techniques, or (g) chemical vapor deposition techniques. Other liner fabrication techniques consist of (h) spinning or shear spinning operations and (i) hot or cold forging processes. Many of these processes require a finish machining or grinding operation to shape the liner to its final thickness specifications. Engineering details are given by Leidel (1978), Vidosic (1964), Degramo (1957), and Baumeister and Marks (1967) for most of these processes.

Another fabrication process that is feasible for liners of certain materials (e.g., aluminum, lead, etc.) is casting. Cast liners are not common.

The most common, or most widely used, method of fabricating conical liners is a deep drawing process. This process is described by Simon and Martin (1958). The various drawing stages are shown in Figure 1. Figure 2

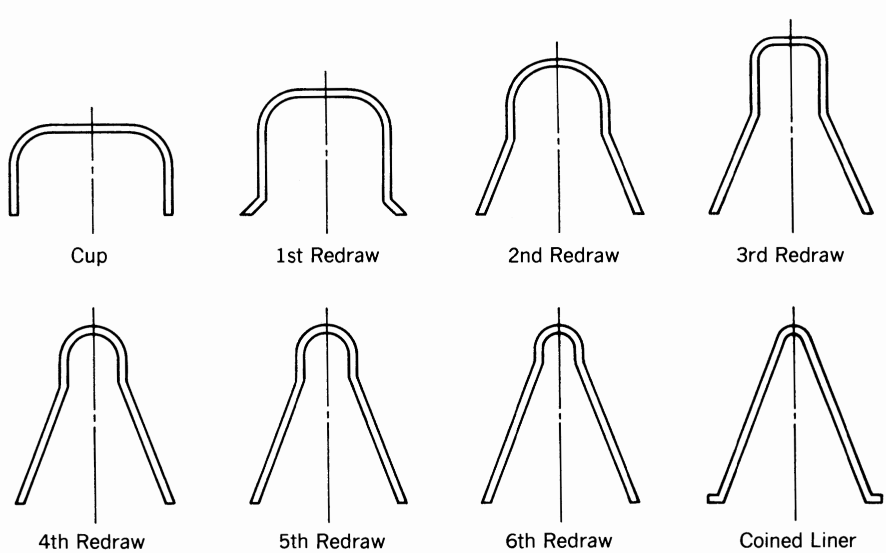

Figure 1. Progressive layout of drawing stages (Simon and Martin 1958).

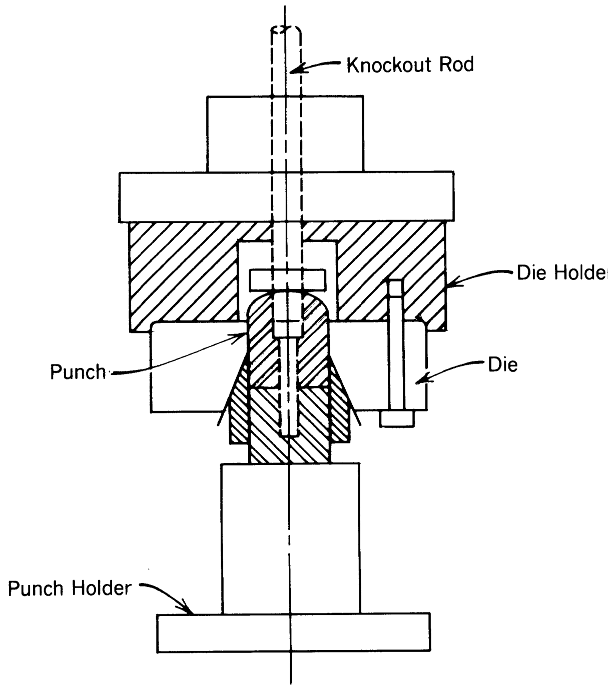

Figure 2. Typical set of draw stage tool assembly (Simon and Martin 1958).

shows a tool assembly for one stage of the deep drawing process. Other popular methods of fabricating conical liners include spin forming (also called rotary extrusion, shear forming, or shear spinning). Figure 3 illustrates this process. Liners formed by rotary extrusion or shear spinning are also used for spin compensation by relating the preferred orientation of the crystal planes with respect to the surface of the cone. Glass et al. (1959) and Gainer and Glass (1962), clearly explain this aspect of shaped charge liner fabrication. Grain size effects are discussed by Dante and Golaski (1985) and Zerilli and Armstrong (1987).

The rotary forging process is a relatively new technique in the United States. This process can be used to form dish-type or shallow devices such as EFPs, Miznay-Schardin devices, and the like. Rotary forging, or orbital forging, is a metal cold-forming process that uses two dies to deform only a small portion of the workpiece at a time in a progressive or continuous manner. In rotary forging, the axis of one die is tilted at a small angle with respect to the other die, and it rotates in such a way that only a small area of the die is in contact with the workpiece at any one time. The die rotates around the workpiece continuously deforming it until a final shape is achieved. Rotary forges can, in effect, be used as small-scale rolling presses to cold work and reduce the grain size of the workpiece. Chou and Labriola (1985) provide an excellent discussion and description of the rotary forge process.

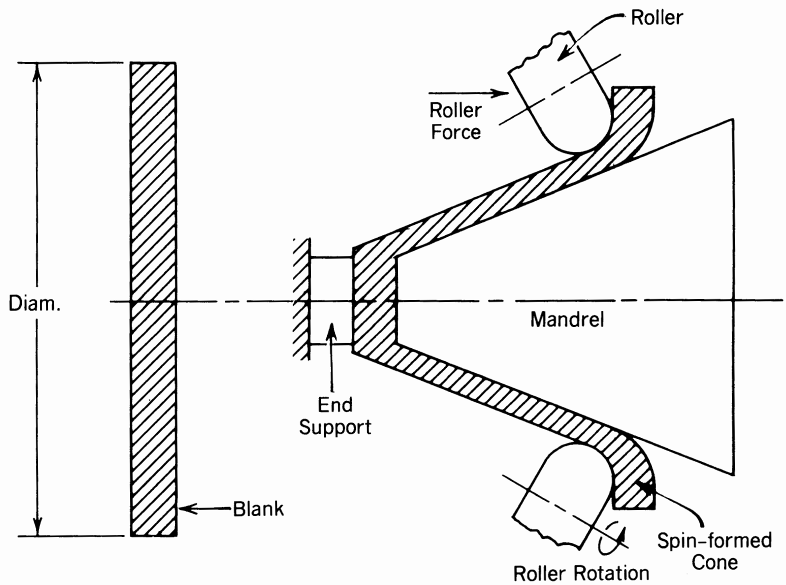

Figure 3. Essential elements of spin forming (Vidosic 1964).

Often metalworking processes are sought that will lead to jet ductility. To a shaped charge designer, jet ductility refers to jets that break in a smooth, "nonjagged" fashion or neck down gradually. To a metallurgist, ductility simply means the ability of a material to be drawn into a wire (i.e., elongated plastically without localized necking or fracture).

In conclusion, liner metallurgical effects (e.g., liner microstructure) are important for spin compensation, jet ductility, jet breakup, and finally, jet penetration. This is an old field, recently revisited, with new insight and with more advanced experimental diagnostic techniques including X-ray diffraction, particle recovery, flash radiography, and camera coverage. The shaped charge jet properties desired are related to the liner microscopic properties, which are controlled by the fabrication process.

10.2. SHAPED CHARGE PRECISION ASSEMBLY

A shaped charge requires precision in the assembly and fabrication of its components. Precision tolerances for a typical 81 mm copper cone [e.g., Aseltine (1980)] require that the wall thickness in the transverse plane be held to ± 0.0002 in., the concentricity to the casing or TIR (total indicated readout) be held to ± 0.002 in., and the maximum variation in wall thickness be held to ± 0.001 in. For a typical nonprecision charge of the same diameter, the wall thickness in the transverse plane has a tolerance of ± 0.002 in., a concentricity (TIR) of ± 0.004 in., and a maximum variation of liner wall thickness of

± 0.004 in. Note that linear tolerances are not absolute but should scale with charge diameter. Thus, for small liners, precision tolerances are difficult to achieve (DiPersio et al. 1967). These small precision tolerances are required to eliminate poor performance, especially at long standoff distances (> 5 CD). The processes of jet collapse, jet formation, and penetration are strongly dependent on the maintenance of axisymmetric flow. In other words, radial velocity components must be avoided.

Many aspects of shaped charge fabrication and assembly can cause radial jet velocity components. These aspects include variations of the liner wall thickness, variations in the case thickness or asymmetric confinement of the high explosive, inhomogeneities in the explosive fill, and misalignment of the liner axis with respect to the warhead axis of symmetry or the axis of symmetry of the detonation wave. These effects will be discussed in detail later.

Figure 4 contrasts the penetration versus standoff (performance) difference between a precision and a nonprecision shaped charge. Figure 5 depicts the standard charge used in this study, and Table 3 gives the gauging data for the precision and nonprecision charge. Returning to Figure 4, the I beams represent the spread of the data and the dots denote the average penetration (about five shots at each standoff) into RHA. The curve labeled "ideal jet performance" is a theoretical penetration from the model of DiPersio et al. (1965) based on an ideal jet with all jet particles moving above a minimum jet velocity as described in an earlier penetration model by DiPersio and Simon (1964). The curve labeled "ideal jet in air" accounts for aerodynamic deceleration of the shaped charge jet in flight. The importance of air drag was first observed by DiPersio et al. (1965) who noticed an increase in penetration and hole volume when jets were fired into a reduced atmospheric pressure, that is, penetration and hole volume increased as the chamber or ambient pressure decreased. DiPersio et al. (1965) noted that atmospheric effects may result in the following:

Loss of jet velocity due to air drag
Loss of jet particle mass due to ablation
A greater tendency for the jet to waver and for the jet particles to tumble

In order to quantify the jet velocity loss in air, various shaped charges were fired through air interspersed with metal screens to measure the position–time history of the jet and hence its velocity–distance behavior. These data are shown in Figure 6. DiPersio et al. (1965) concluded:

The decrease in jet particle velocity is proportional to the distance traveled through air and is not dependent on the initial jet velocity.

The decrease in jet particle velocity over a given distance of air travel is inversely proportional to the particle size for particles of similar shape.

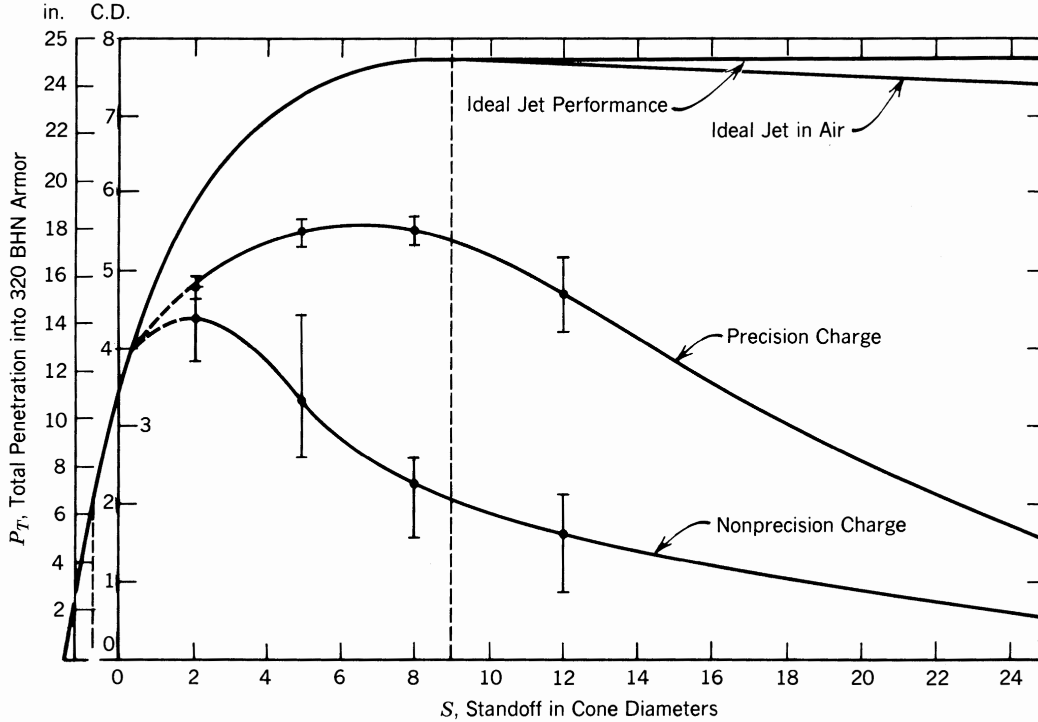

Figure 4. Penetration performance of the standard charge (DiPersio et al. 1965).

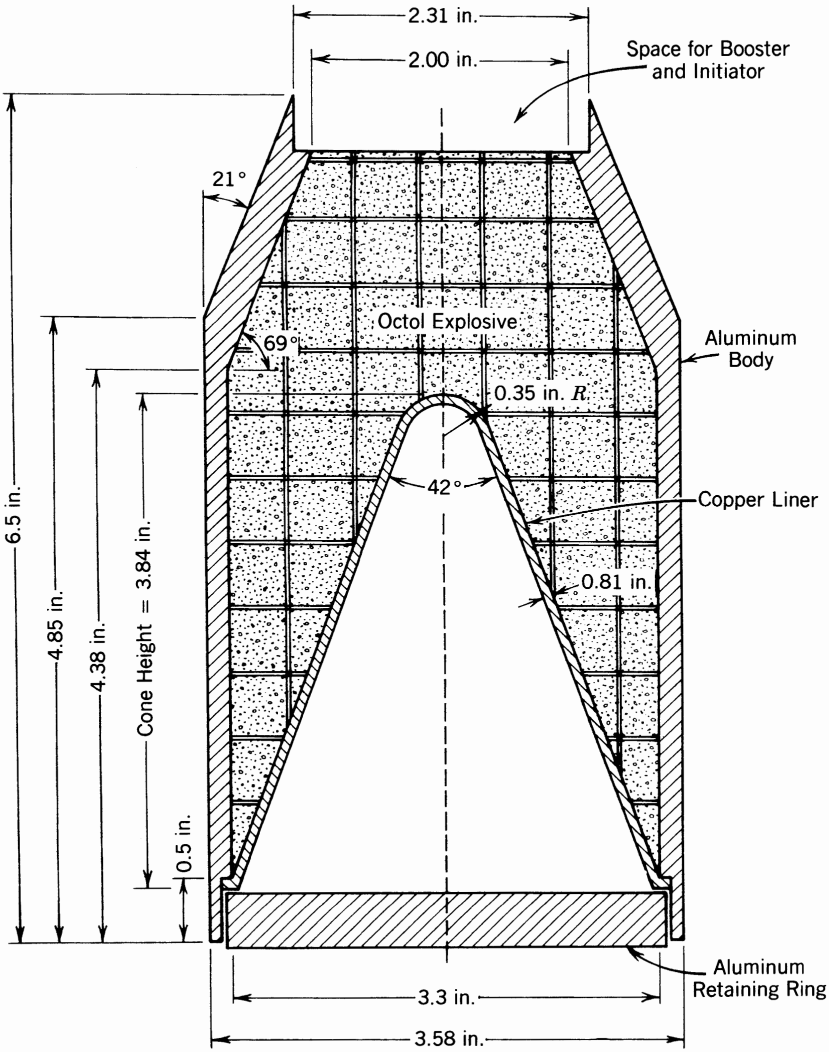

Figure 5. Diagram of standard shaped charge (DiPersio et al. 1965).

Low-density jet particles are retarded more by travel through air than high-density jet particles of the same size.

DiPersio et al. (1965) also presented camera records of the shock (flow) field near the tip of a shaped charge jet. It was noted that no evidence of ablation of the jet tip could be seen on the camera or flash X-ray pictures. Additional details and descriptions of the test charges and results can be found in DiPersio et al. (1965).

TABLE 3. The Gauging Data for the Precision and Nonprecision Charges

	Precision Charge	Nonprecision Charge
Wall thickness variation in any liner transverse plane (in.)	0.00007	0.0043
Maximum variation in wall thickness throughout the liner (in.)	0.0010	0.0040
Concentricity of liner with casing (in.)	0.0020	0.0036

Note: The loading procedure was kept the same for both groups of charges. From DiPersio et al. (1965).

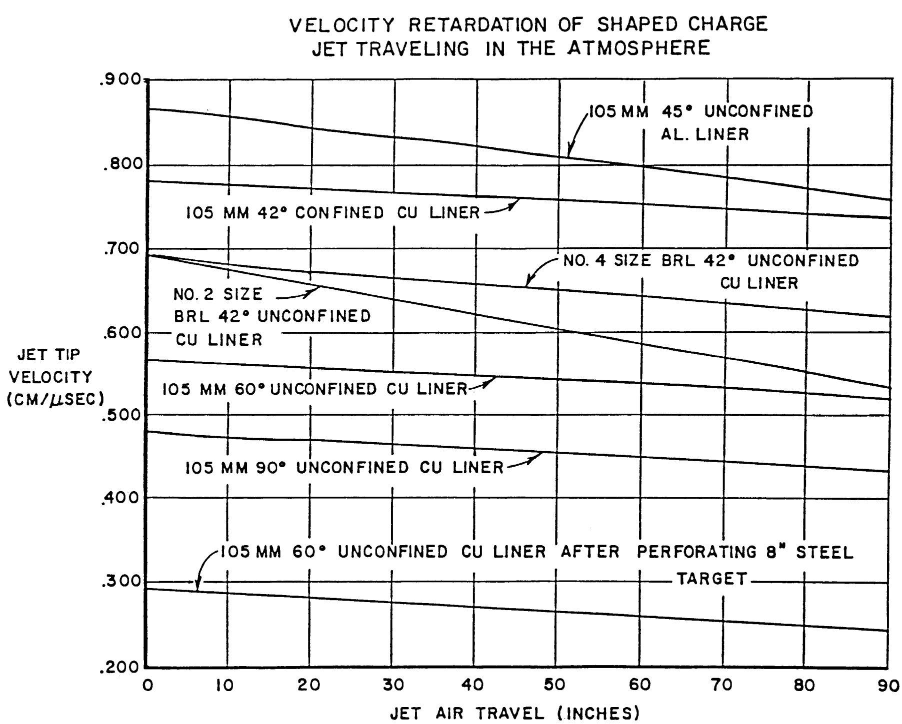

Figure 6. Jet travel in air (DiPersio et al. 1965).

Returning to the discussion of shaped charge assembly precision, Leidel (1978) presented an excellent overview on the precision requirements for shaped charges. Earlier studies that proved the advantages of precision over nonprecision charges were given by Thorn (1967) and Taglairino (1966).

Leidel (1978) discusses liner manufacturing methods, liner tolerance requirements, the fabrication of precision linear shaped charges, and presents analytical design studies regarding linear shaped charges.

The deep drawing technique for fabricating shaped charge liners as well as the manufacturing tolerances required are discussed by Taglairino (1966) and the DRD report (1962). Taglairino (1966) also describes spin forming techniques and electro-deposition as means of manufacturing shaped charge liners.

Panzarella and Longobardi (1952) intentionally deformed steel M9A1 shaped charge liners to study (in an exaggerated sense) the effect of warped liners, liner wall thickness variations, and other asymmetries. Also, Leidel (1978) studied the effect of precision in manufacture by deliberately varying the liner and charge geometry, as well as the charge assembly, and the explosive casting technique. Cox (1964) studied the effect of the liner apex angle.

The high explosive (HE) fill can degrade shaped charge performance if inhomogeneities occur in the HE fill. According to Leidel (1978), inhomogeneity may consist of one or both of the following conditions:

Chemical inhomogeneity	Distribution of the explosive constituents is nonuniform throughout the mixture.
Physical inhomogeneity	The presence of voids, gas inclusions, or pores in the cast explosive.

In fact, Frey and Melani (1976) investigated the effect of explosive porosity by implanting artificial voids in the HE fill. They showed that voids large enough to degrade penetration may be too small to be detected by X-ray nondestructive testing. Thus, a precision explosive fill is required, and Leidel (1978) defines a precision explosive cast to mean control of the porosity, the cast temperature, the cooling rate, as well as chemical inhomogeneities. A precision loading technique for Comp B as used at the old Ravenna Army Ammunition Plant in Ravenna, Ohio, follows (Leidel 1978):

1. Composition B, which complies with Military Specification Mil-C-401C 15 May 1963 was melted without vacuum at 210°F.
2. The charge casing was preheated to 190°F. All charge assemblies were properly cleaned and degreased prior to loading.
3. The charge was cast using vibration to eliminate air inclusions, and the riser kept hot. Vibration was maintained for 10 min. No vacuum was used during casting.

4. The charges were allowed to cool slowly on a hot platen from casting temperature to ambient temperature for 1 h.
5. The additional explosive and riser were removed.
6. All charges were X-ray inspected for voids or air inclusions and found to be satisfactory.

Additional data on the effects of the HE fill are given by Panzarella and Longobardi (1952) and Simon and Martin (1958). Simon et al. (1965) present data that show that variability in penetration performance may result from imperfections in the explosive components, the shaped charge liner, and the assembly of the metal components. Also, improper alignment of the liner axis with the axis of the charge or improper alignment of the initiation system is detrimental to the penetration performance. In fact, jets that are bowed or curved near the tip (which of course degrades penetration) are most likely due to a nonprecision TIR on the initiation assembly. Jets that are bowed over their entire length most likely suffer from a nonprecision TIR on the body or HE fill, that is, the cone must be concentric to the body and the explosive.

Leidel (1978) conducted a liner tolerance study for a 66 mm (2.5 in.) 42° conical copper liner with a 0.040 in. wall thickness. The liner was electrolytic tough pitch copper machined from bar stock. Leidel maintained the following tolerances in the manufacturing of the liners:

1. The straightness of the exterior surface of the liner was held within 0.001 in. in the longitudinal plane.
2. The roundness or variation of liner radius with respect to the centerline of the exterior surface was maintained within 0.001 in.
3. The concentricity of the liner to datum was maintained within 0.002 in. on the diameter.
4. The thickness at any station point on the liner was 0.040 ± 0.001 in.
5. All noncritical dimensions of the liner were toleranced as ± 0.010 in.

These specifications, with a quality explosive cast and alignment, resulted in a high-performance charge. DiPersio et al. (1967) also discuss the precision tolerances required for shaped charge liners.

Evans (1950) noted that the jet characteristics can be drastically altered by asymmetries. He described these asymmetries as variations in thickness and/or strength of the liner, which can cause unstable jets that deviate from the axial direction as they travel forward in space. This effect dissipates the jet over larger areas of the target and thus reduces the effective penetration. Such perturbations also occur when the detonation wave that impacts the liner is not symmetric, which is usually caused by a misalignment between the body, explosive, and liner, or lack of good contact between the explosive and the liner.

Aseltine (1980) also studied asymmetries associated with the liner, explosive, and confinement. Explosive loading quality was also studied. The baseline charge used by Aseltine was an 81.3 mm precision charge. The wall thickness was 1.905 mm with tolerance requirements of less than 0.0051 mm (± 0.0002 in.) in any transverse plane and less than 0.051 mm (± 0.002 in.) in any longitudinal plane. These liner tolerance requirements, liner thickness variations, the homogeneity (or composition variation) of the explosive fill, and the effects of confinement asymmetry were studied analytically. Aseltine (1980) concluded that the liner tolerances were required and adequate as specified and that the explosive fill homogeneity is the greatest single source of asymmetry for this round.

Brown et al. (1987) studied asymmetries of the confining case of a shaped charge, and Mayseless et al. (1987) studied, both theoretically and experimentally, the effects of asymmetries for peripherally initiated and point-initiated shaped charges.

10.3. SCALING OF SHAPED CHARGES

A linear relationship exists for scaling charges of the same geometry. All linear dimensions in the large scale are larger than the small scale by a given scale factor, that is, one charge is a photographic enlargement of the other by a linear factor. The charges are geometrically similar, or homologous scaling is obtained. Baker et al. (1973) give an excellent discussion of similitude and scaling including a chapter on penetration scaling.

Scaling a shaped charge involves maintaining the same geometric shape, for example, cone apex angle, but increasing the liner diameter, the charge diameter, charge length, confinement, liner wall thickness, standoff distances, and booster dimensions, all by the same linear scale factor. Of course, the liner material, confinement material, and explosive must remain the same.

The final jet parameters theoretically scale as follows:

1. The jet tip velocity remains unchanged. This is not surprising since the conical apex angle and the charge-to-mass ratio are unchanged.
2. The jet diameter and jet length increase by the linear scale factor.
3. The jet mass and total jet kinetic energy increase by the cube of the scale factor.
4. The penetration depth and the jet breakup time increase by the linear scale factor.
5. Since the hole volume is proportional to the jet kinetic energy, the hole volume should increase by the cube of the scale factor.

In other words, if a 3 in. charge diameter shaped charge is compared to a 6 in. diameter shaped charge, where the 6 in. charge is a linear scale of the 3 in.

charge, the scale factor is 2. The two charges will have the same tip velocity. The jet diameter, jet length, and breakup time will be twice as big for the 6 in. charge. The 6 in. charge will have eight times the jet mass and jet kinetic energy and eight times the hole volume of the 3 in. charge. The penetration depth divided by the charge diameter will be the same for both charges.

The theoretical considerations given have been verified experimentally. Such verification was necessary since many of the jet formation processes, jet breakup time considerations, and penetration discussions invoke nonlinear and/or rate-dependent parameters, which usually do not exhibit homologous scaling behavior. However, a few caveats enter the picture. First, scaling is apparent over a limited range of liner diameter, namely, from approximately 40 to 178 mm. Scaling is not apparent below about a 40 mm charge diameter since for small charges precision tolerances are difficult to achieve. Also, the small head height associated with small-scaled charges causes the detonation wave to nonplanar (or curved). The deviation from scaling for small charges (charge diameters of $1\frac{1}{2}$ and $\frac{3}{4}$ in.) was presented by DiPersio et al. (1967).

Scaling is also absent for shaped charges with a liner diameter greater than 178 mm. This is due, in part, to the fact that large shaped charges are usually loaded in stages, and hence the explosive fill is not uniform and the liner metallurgy and mechanical properties are harder to control for large (thick) liners.

Another caveat is that even precision shaped charges exhibit a round-to-round variability. Precision was discussed earlier. Round-to-round variability means that the jet parameters, penetration, and hole volume vary from shot to shot. In other words, the same value for any given parameter will rarely remain the same over a several shot average.

In general, the jet tip velocity measurement is usually within ± 0.1 km/s for jet tip velocities of 4–10 km/s. This is due, in part, to experimental error. Flash radiographs of the collapse process for scaled shaped charges look like photographic enlargements, that is, the collapse process appears to scale at least in a global sense. Jet parameters such as the velocity gradient, jet diameter, jet mass, and breakup time exhibit a round-to-round variability of as much as $\pm 20\%$. The particulated jet particle length and the location of the virtual origin varies sometimes more than $\pm 20\%$. Also, the virtual origin location and particle length do not appear to scale homologously. This may be due to the fact that some jets possess a nonlinear velocity distribution from tip to tail, that is, along their length (Chou and Foster 1987).

Round-to-round variability of the jet mass is due in part to the method of calculating the jet particle mass from a two-dimensional flash X-ray. The jet density is assumed to be the liner initial density. The jet particle volume is calculated by assuming the particle to be some combination of axisymmetric geometries such as cylinders, cones, conical frustums, or hemispheres. This can introduce errors since orthogonal flash X-rays reveal that jets are sometimes oblong or elliptic in cross section. Thus, the mass calculation could be in error and also could appear to vary from shot to shot if the jet rotates (slowly) in flight.

TABLE 4. Precision Shaped Charge Performance

Standoff (CD)	Average Penetration (CD)	Minimum Penetration (CD)	Maximum Penetration (CD)	Standard Deviation (CD)
2	4.81 (29 shots)	4.50	5.19	0.17
5	5.36 (5 shots)	5.00	5.69	0.26
7	5.42 (5 shots)	4.84	5.91	0.34
10	4.81 (65 shots)	3.19	5.88	0.55
15	3.09 (5 shots)	2.47	3.88	0.47
20	2.59 (24 shots)	1.34	4.31	0.67

Nevertheless, with the above round-to-round variability caveats, the jet parameters exhibit homologous scaling over the limited, but fortunately practical, range of liner diameters (40–178 mm).

Shaped charge jet penetration also exhibits a round-to-round variability. For a representative precision shaped charge, the penetration versus standoff data are given in Table 4. Several shots were fired at each standoff distance from identical rounds. Note that the penetration data varies from round-to-round, and the standard deviation (in general) increases with standoff. Also, as mentioned previously, note the peak in the penetration–standoff curve. It is also instructive to note the range of penetration values. For example, at a 10 CD standoff, the penetration ranged from 3.9 to 5.88 CD, for supposedly the same shaped charge and the same target, namely, stacked plates of RHA (rolled homogeneous armor).

With the caveats already noted, scaling has been demonstrated over the liner diameter range indicated by DiPersio et al. (1960). In this classic study, DiPersio et al. tested three homologously scaled 42° electrolytic tough pitch (ETP) copper cones loaded with Comp B high explosive. The three scaled liner diameters were 1.89, 2.835, and 3.780 in. (48, 72, and 96 mm, respectively). Figure 7 presents the pertinent liner dimensions for all three scaled charges. Figure 8 shows the case and booster dimensions for the three charges. DiPersio et al. (1960) presented data that revealed the following:

1. The jet velocity gradient can be approximated by a constant at any given time except for the first few particles near the jet tip. Its value varies inversely with the charge diameter at the same time, and inversely with time for a given charge diameter.
2. Approximately 20% of the liner (cone) mass enters the jet.

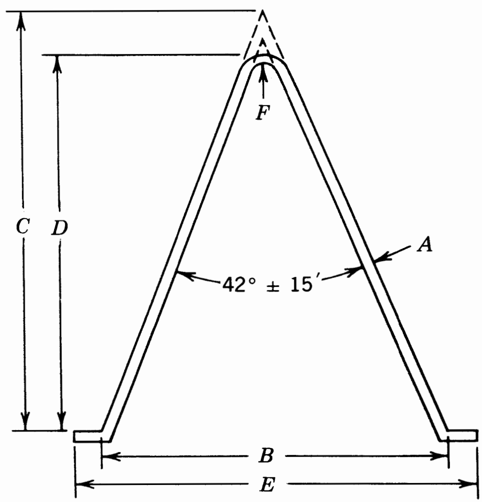

Dimensions	Scale Size No. 2	3	4
A Nominal wall thickness ⊥ wall (in.)	0.070	0.105	0.140
B Cone diameter (in.)	1.890	2.835	3.780
C Theoretical altitude (in.)	2.4618	3.6927	4.9236
D Geometrical height (in.)	2.238	3.357	4.476
E Flange diameter (in.)	2.050	3.075	4.100
F Inside radius (in.)	0.0625	0.093	0.125
Measured cone mass (g)	82.53	278.8	662.9

Figure 7. Dimensions of the BRL scaled copper liners (DiPersio et al. 1960).

3. Jets from scaled conical liners in scaled warheads produce approximately the same number of particles after breakup. The average particle length scales directly with the charge diameter. Thus, the average particle volume and mass varies as the cube of the charge size.
4. Scaled shaped charges produce scaled penetration depths at scaled standoffs. The penetration velocities, jet velocities, and relative penetration depths are the same at scaled times during the penetration process.

The scaled penetration in cone diameters versus the penetration time divided by the cone diameter is shown in Figure 9. The penetration time is the time that the jet pierced each element of the target stack as recorded on an oscilloscope by means of electrical contacts sandwiched between the plates. The target was 1 in. thick mild steel plates and the standoff was 3 CD. The closely spaced experimental points shown in Figure 9 allow a smooth curve to represent all the charges studied, regardless of size.

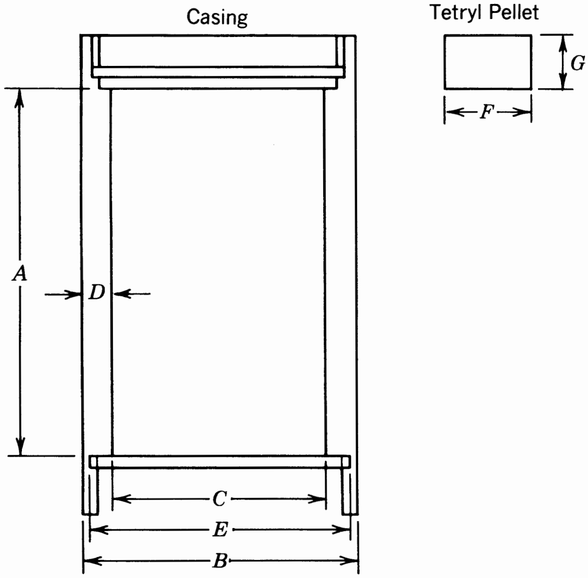

Casings	Scale Size No. 2	3	4
A—length (in.)	3.271	4.894	6.525
B—O.D. (in.)	2.366	3.545	4.726
C—I.D. (in.)	1.892	2.837	3.782
D—wall thickness (in.)	0.237	0.354	0.472
E—flange register	2.051	3.076	4.101
tetryl pellets			
F—diameter (in.)	0.683	1.042	1.378
G—length (in.)	0.455	0.683	0.912

Figure 8. Scaled dimensions for casings and tetryl pellets (DiPersio et al. 1960).

Additional data on the scaling of shaped charges is given by Klamer (1964). For conventional shaped charge designs, the penetration versus standoff curve, normalized by the charge diameter, scales approximately within the limitations given.

The hole volume produced by a shaped charge warhead is discussed by DiPersio et al. (1965), where it was postulated that the hole volume was directly proportional to the jet kinetic energy. Thus, as discussed earlier, the hole volume varies as the cube of the scale factor. In general, the hole volume remains approximately constant for various shaped charges of the same diameter and at a given standoff. For example, for shaped charges of various liner materials and various wall thicknesses, the penetration depth varies, but the hole diameter also varies such that the hole volume is practically un-

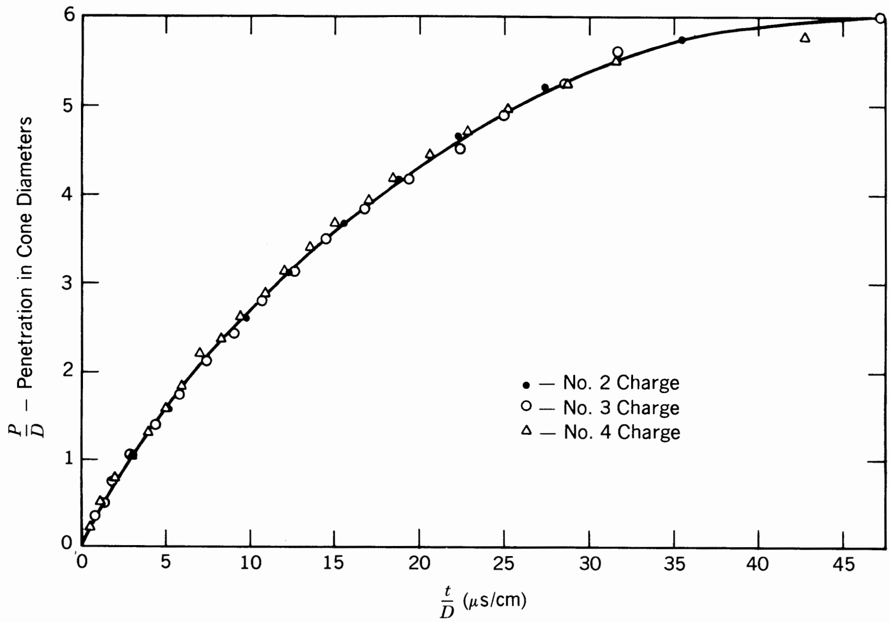

Figure 9. Scaled target penetration versus time (DiPersio et al. 1960).

Types of Charges

Types	Distance in ϕ	Crater		$\sum_{1}^{n}$ Volume in ϕ^3
		Depth in ϕ	Width in ϕ	
Blast Charge 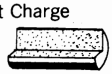	0	0.2–0.4	0.8–1.0	$\frac{0.9^2 \times \pi}{4} \times 0.3 \sim 0.19$
Hollow Charge 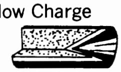	1.5–6	5–9	0.1–0.3	$\frac{0.2^2 \times \pi}{4} \times 6 \sim 0.19$
Flat Cone Charge 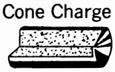	3–8	2–3	0.25–0.40	$\frac{0.3^2 \times \pi}{4} \times 2.7 \sim 0.19$
Projectile Charge 	$1–10^3$	0.55–0.60	0.6–0.7	$\frac{0.65^2 \times \pi}{4} \times 0.57 \sim 0.19$
Fragment Charge 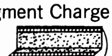	$1–10^3$	0.05–0.10	0.05–0.15	$\frac{0.10^2 \times \pi}{4} \times 0.08 \times 300 \sim 0.19$

Figure 10. Comparison of the conventional high explosive charges with respect to standoffs, penetration depths, and diameters expressed in terms of caliber, and the volumes of the holes computed from depth and diameter values (Held 1976).

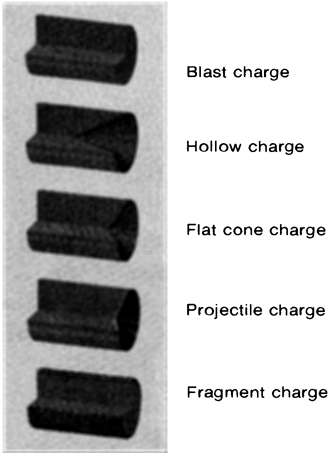

Figure 11. Basic types of conventional high explosive charges (Held 1976).

changed (Klamer 1964). This is because the hole volume varies directly with specific explosive energy. Thus, for a fixed explosive energy, the hole volume is fixed, and the hole depth times the hole area remains approximately constant.

Further, Held (1976) observed that the hole volume remains approximately constant for a variety of explosive devices. In Figure 10, several conventional high explosive charges are compared with respect to standoffs, penetration depths, and crater diameters, all expressed in calibers. The volumes of the holes in the target are computed from the hole depth and diameter. Figure 10 shows that all types of charges generate about the same hole volume in calibers, including the fragmenting charge where the separate hole volumes have to be summed. The scaled hole volume of $0.19D^3$ (D = charge diameter) is unique to this experiment and is not a "universal" constant. However, indications are that for a given explosive energy only a certain amount of target deformation can occur. The basic warheads listed in Figure 10 are shown in Figure 11 (Held 1976).

10.4. SHAPED CHARGE JET TEMPERATURE STUDIES

In a series of publications, von Holle and Trimble (1976a, 1976b, 1977) developed a temperature measurement technique for shocked metals based on two-color infrared radiometry. Their results include the application of their method to the residual temperature measurement of thin copper plates shocked in the 30–50 GPa range. Data on the temperature measurements of shaped charge jets in flight are also presented.

In von Holle and Trimble (1976a), the temperature of the jet from a 81.3 mm diameter, 42° apex angle, copper conical liner was measured. The explosive fill was Comp B and a four-shot average of the jet temperature was 432°C with a standard deviation of 76°C. The jet was fired into a vacuum.

Von Holle and Trimble (1976b) measured the jet temperature from basically the same round for both Comp B- and Octol-loaded charges. The jet temperature was obtained after the jet tip had traveled eight charge diameters from the base of the cone. The basic copper liner was altered such that both pointed and rounded apex liners were tested. The pointed apex liner was used since it contained less debris at the tip than the rounded apex liner.

For the Comp B-loaded charges, considering an 11-shot average, which included both pointed and rounded apex liners, the average temperature was 428°C with a standard deviation of 67°C. The pointed apex cone revealed a higher temperature than the rounded apex cone.

For the Octol-loaded charges, all with rounded apex cones, a three-shot average gave a jet temperature of 537°C with a standard deviation of 20°C.

In von Holle and Trimble (1977), additional shots were fired using both rounded and pointed apex cones and both Comp B and Octol explosive fills. Averaging all data from von Holle and Trimble (1976a, 1976b, 1977) gave a 12-shot average temperature for the Comp B-loaded charges of 441°C with a standard deviation of 80°C. For the Octol-loaded charges a 6-shot average temperature was 521°C with a standard deviation of 40°C.

For the pointed apex conical copper jets, the temperature versus distance from the jet tip was measured. The trend of the data indicated that the jet temperature rises behind the tip and then levels off. Also, the jet tip was viewed end-on for an Octol-loaded charge in order to measure the jet temperature during formation. The temperature appeared to decrease at later times after formation.

Also, von Holle and Trimble (1977) measured the jet temperature of a 60° apex angle, 81.3 mm diameter, tin–lead eutectic liner. The liner wall thickness was 2.54 mm and the explosive fill was Comp B. The conical apex was slightly rounded to a 1 mm radius. A four-shot average revealed a jet temperature of 569°C with a standard deviation of 34°C. The tin–lead liner had a jet tip velocity of 6.3 km/s compared to the copper liner jet velocity of nearly 8 km/s.

Von Holle and Trimble concluded that the copper jet was solid and the lead–tin jet was liquid in spite of any scatter in their data. The von Holle–Trimble experiments were the first of a kind and represent an excellent approach to a difficult problem, although some uncertainty exists in the recorded data. The explanation of the experimental technique and the interpretation of the data is given in von Holle and Trimble (1976a, 1976b, 1977).

Walters et al. (1985) performed hydrocode calculations to calculate the temperature gradients in collapsing lead hemispherical liners. The wall thickness of the liner was varied, and free-flight flash radiograph coverage of the jet revealed that the jet quality improves as the wall thickness increases. That is, the jet becomes less fluid, or more solid, in appearance as the wall thickness increases.

The HULL, HELP, and EPIC codes were all used to study the hemispherical liner collapse and formation. Temperature calculations throughout the jet

were obtained, and the general temperature trends were in qualitative agreement with the appearance of the jets from the lead hemispherical liners (i.e., transitions from liquid to solid were revealed). Also, the temperatures measured by von Holle and Trimble for Octol-loaded copper liners were calculated and were within the scatter of the experiment data.

The code-calculated temperatures were obtained from the initial temperature, the density, the internal energy, and the specific heat of the liner material. The specific heat was assumed to be a constant, which is probably not realistic. Other computational errors would result from lack of data on materials under high-pressure, high-temperature, and high-strain rate conditions, for example, exact constitutive equations and exact equations of state.

Nevertheless, the experimental and theoretical information provided by the preliminary studies cited represent an important first step toward the estimation of the temperature and temperature gradients of a shaped charge jet.

REFERENCES

Aseltine, C. L. (1980), "Analytical Predictions of the Effect of Warhead Asymmetries on Shaped Charge Jets," Ballistic Research Laboratory Technical Report, BRL-TR-02214, February.

Baker, W. E., Westine, P. S., and Dodge, F. T. (1973), *Similarity Methods in Engineering Dynamics*, Rochelle Park, NJ: Spartan Books, Hayden Book Company.

Baumeister, T., and Marks, L. (eds.) (1967), *Standard Handbook for Mechanical Engineers*, 7th ed., New York: McGraw-Hill.

Brown, J., Cullis, I. G., and Griffiths, N. (1987), "The Effects of Confining Studies on Shaped Charges," *Proc. 10th Int. Symp. on Ballistics*, Vol. 2, San Diego, October.

Chou, A., and Labriola, M. (1985), "Rotary Forging—A Precision Process," *Mech. Eng.*, March: 73–77.

Chou, P. C., and Foster, J. C. (1987), "Theory of Penetration by Jets of Non-Linear Velocity and in Layered Targets," *Proc. 10th Int. Symp. on Ballistics*, Vol. 2, San Diego, October.

Cox, C. M. (1964), "Memorandum Report on Linear and Conical Shaped Charge Performance," The Firestone Tire and Rubber Company, Defense Research Division, Report No. DRD-4, May.

Dante, J. G., and Golaski, S. K. (1985), "Micrograin and Amorphous Shaped Charge Liners," *Proc. of ADPA Bomb and Warhead Section*, White Oak, Maryland, May.

Degramo, E. P. (1957), *Materials and Processes in Manufacturing*, New York: McMillan.

DiPersio, R., and Simon, J. (1964), "The Penetration-Standoff Relation for Idealized Shaped Charge Jets," Ballistic Research Laboratory Memorandum Report, BRL-MR-1542, February.

DiPersio, R., Simon, J., and Martin, T. H. (1960), "A Study of Jets from Scaled Conical Shaped Charge Liners," Ballistic Research Laboratory Memorandum Report No. 1298, August.

DiPersio, R., Simon, J., and Merendino, A. B. (1965), "Penetration of Shaped Charge Jets Into Metallic Targets," Ballistic Research Laboratory Report No. 1296, September.

DiPersio, R., Jones, W. H., Merendino, A. B., and Simon, J. (1967), "Characteristics of Jets from Small Caliber Shaped Charges with Copper and Aluminum Liners," Ballistic Research Laboratory Memorandum Report, BRL-MR-1866, September.

DRD Report (1962), "Manufacturing Summary of Spin Compensated Shaped Charge Liners," Defense Research Division, Firestone Tire and Rubber Company, Report No. DRD-1, October.

Evans, W. M. (1950), "The Hollow Charge Effect," *Bull. Instit. Mining Metall.*, No. 520, March.

Frey, R., and Melani, G. (1976), "The Effect of Voids on Metal Acceleration by Explosives and its Implication for Octol Loaded Shaped Charges," Ballistic Research Laboratory Memorandum Report, BRL-MR-2582, February.

Gainer, M. K., and Glass, C. M. (1962), "A Study of Metallurgical Effects in High Velocity Deformation of Copper Using Rotary Extruded Liners," U.S. Army Ballistic Research Laboratory Report No. 1167, May.

Glass, C. M., Gainer, M. K., and Moss, G. L. (1959), "Effects of Anisotropies in Rotary Extruded Liners," U.S. Army Ballistic Research Laboratory Report No. 1084, November.

Held, M. (1976), "The Performance of the Different Types of Conventional High Explosive Charges,"*Proc. 2nd Int. Symp. on Ballistics*, Daytona, FL, March.

Klamer, O. A. (1964), "Shaped Charge Scaling," Ammunition Engineering Directorate, Picatinny Arsenal, Dover, N.J., Technical Memorandum 1383, March.

Leidel, D. J. (1978), "A Design Study of an Annular-Jet Charge for Explosive Cutting," Ph.D. Dissertation, Drexel University, Philadelphia.

Mayseless, M., Miller, S., Niv, E., and Peretz, D. (1987), "Experimental and Computational Analysis of the Effect of Asymmetries on Peripherally Initiated Shaped Charges," *Proc. 10th Int. Symp. on Ballistics*, Vol. 2, San Diego, October.

Panzarella, J., and Longobardi, J. (1952), "Performance of Shaped Charges with Intentionally Deformed Liners," U.S. Army Ballistic Research Laboratory, Report No. 811, March.

Simon, J., and Martin, T. H. (1958), "Spin Compensation of Shaped Charge Liners Manufactured by the Rotary Extrusion Process," U.S. Army Ballistic Research Laboratory Memorandum Report No. 1181, December.

Simon, J., DiPersio, R., and Merendino, A. B. (1965), "The Penetration Capability and Effectiveness of a Precision Shaped Charge Warhead," Ballistic Research Laboratory Memorandum Report, BRL-MR-1636, March.

Taglairino, J. J. (1966), "A Discussion of Some Effects of Variables on Shaped Charge Warhead Performance," Picatinny Arsenal Technical Report No. 3446, October.

Thorn, G. S. (1967), "Research Related to Basic Warhead Mechanism for End Item Application," Report No. DRD-13, The Firestone Tire and Rubber Company, Defense Research Division, December.

Vidosic, J. P. (1964), *Medal Machining and Forming Technology*, Atlanta: Georgia Institute of Technology.

von Holle, W. G., and Trimble, J. J. (1976a), "Temperature Measurement of Shocked Copper Plates and Shaped Charge Jets by Two-Color IR Radiometry," *J. Appl. Phys.* *47*(6): 2391–2394.

von Holle, W. G., and Trimble, J. J. (1976b), "Shaped-Charge Temperature Measurement," The Sixth Symposium on Detonation, San Diego, August 24–27.

von Holle, W. G., and Trimble, J. J. (1977), "Temperature Measurement of Copper and Eutectic Metal Shaped Charge Jets," Ballistic Research Laboratory Report, BRL-R-2004, August.

Walters, W. P., Jonas, G. H., and Zukas, J. A. (1985), "Explosive Loading of Lead Hemispherical Liners," *Comput. Struct.*, *20*(1–3): 615–621.

Zerilli, F. J., and Armstrong, R. W. (1987), "Dislocation Mechanics—Based Constitutive Relations for Material Dynamics Calculations," *J. Appl. Phys.*, *61*(5): 1816–1825.

CHAPTER 11

COMPUTATIONAL ASPECTS OF EXPLOSIVE–METAL INTERACTIONS

The analytical models described thus far for shaped charge formation and jet penetration prove to be very valuable in day-to-day applications. When conditions exist that are close to the assumptions inherent in the models, comparison of model predictions with experiments tends to be quite good. The models also serve in developing an appreciation for the dominant physical phenomena occurring in a given loading situation as well as for sorting and clarifying experimental data. Recall, however, that most are one-dimensional representations of two- and three-dimensional phenomena. If a complete solution to an explosive–metal interaction or penetration situation is required, recourse must be made to numerical simulation. This is especially true for oblique impact situations where a three-dimensional stress state is dominant, for there are virtually no models that can deal with such complexity. Two- and three-dimensional computer codes obviate the need for various simplifying assumptions and are capable of treating very complex geometries and loading states. They do have several limitations, however. Their accuracy and utility is limited by the material description embodied in the constitutive equations. Equally important to achievement of physically plausible results is the use of constants (or data) for these constitutive descriptions obtained from wave propagation-type experiments at strain rates appropriate to those in the simulation. Excellent results have been obtained for situations where material behavior is well understood and characterized. However, use of these codes as "black boxes," with inappropriate models and data obtained as quasistatic conditions can lead to nonsensical results. The old adage, "garbage in, garbage out" applies. Numbers are not sanctified simply by passing through a computer.

Simulation of explosive loading phenomena and high-velocity penetration is based on a continuum mechanics formulation using the equations of mass,

momentum, and energy conservation, together with appropriate descriptions of material behavior. The formulation is completed by specifying initial and boundary conditions appropriate to the problem of interest. The resulting system of partial differential equations is nonlinear, hence the need for numerical evaluation in situations where simplifications are not appropriate. The problems addressed by such computations involve intense dynamic loads generated by impact or explosive detonation and acting over extremely short time periods (nanoseconds to microseconds). Inertial effects dominate initial stages and the interaction of stress waves with material boundaries, geometric boundaries, and each other must be adequately simulated.

In many situations, the primary interest is in the response of the materials subjected to impact or explosive loading. The explosive is modeled with a simple programmed burn—initiation takes place at a given time or pressure, and the energy of the explosive is transferred to materials in contact with it in accordance with the detonation velocity and geometry of the explosive. No account is taken of the reaction kinetics of the explosive. If such information is required, then the various approaches described in the monograph by Mader (1979) must be employed.

A number of two- and three-dimensional wave propagation codes exist. Those that are applicable to problems in warhead dynamics are discussed in Chapter 12. Before discussing the numerical techniques embodied in these codes and the characteristics of the codes themselves, it is worthwhile to classify the main features of the three problem areas to which they have been applied, the latter two being of greatest interest for our purposes:

1. Kinetic Energy Penetration The behavior of both inert (solid) projectiles and barriers (often in the form of plates) at impact velocities of 0.5–2 km/s is dominated by inertia with material failure as an added complication. Since the problem is momentum driven, the key ingredients are the equations of motion and the descriptions of material failure. Large plastic flow is highly localized and is typically accounted for with an incremental elastic-plastic relationship. Experience has shown that this is adequate for many practical problems (e.g., Wilkins 1984a, b). For good correlation with experiments, it is *crucial* that material parameters be determined from dynamic (wave propagation) experiments.

2. Hypervelocity Impact Hydrodynamic pressure dominates the behavior of solids for impact velocities above the speed of sound of the material. Hence, the equations of motion and a high-pressure equation of state are the key descriptors of material behavior. Material strength is only significant for the very late stages of the energy-driven problem. It can often be represented by a simple elastic–perfectly plastic relationship with an appropriate value of yield strength obtained from dynamic experiments. Spallation is a frequently encountered failure mechanism. Because of the short time scale of the material response, simple time-independent failure criteria for space (e.g., Rinehart 1951, 1952, Drucker 1978) often give satisfactory results.

3. Warhead Formation The collapse of an explosively formed metal to form a short [length-to-diameter (L/D) ratio between 2–3] slug or long jet moving at velocities of 2–8 km/s results in a striker under extremely high pressures (0.2–1 Mbars), with metal temperatures ranging from one-half to near the melt temperature of the material. Computations of liner collapse phenomena have had to assume failure strains in excess of 100% in order to obtain decent correlation with experiments. This problem is dominated by extremely large plastic flows under conditions of extreme temperature and pressure. Questions have been raised regarding the adequacy of incremental plasticity theories for such applications since these are normally derived assuming isotropy, neglecting compressibility and thermal effects with large deformations assumed to be in the 10–30% range [see the discussions in Nemat-Nasser et al. (1984) for the state of the art in this area].

Excluded here are problems involving very low velocity impacts (striking velocity $V_s \ll c$, the material sound speed). Such problems fall in the category of structural dynamics where *both* the geometry of the structure and the material constitution play an important role in the response of the structure to transient loading. See Belytschko and Hughes (1983) and Donea (1978) for details.

We hope to make clear in the following chapters that computer codes are not stand-alone tools in the study of explosive–metal interactions or penetration phenomena. However, coupled iteratively with experiments and material characterization at high strain rates, they can be very effective tools in achieving cost-effective designs without excessive computations, testing, or material evaluation. Examples of this approach can be found in the NMAB (1980) report and the paper by Herrmann (1977).

Consider next the numerical simulation of impact and explosive loading phenomena. The primary emphasis is on methods capable of treating intense impact or explosive loads where both loading and response times are in the submillisecond regime. Deformations resulting from such loading will be highly localized and determined principally by the constitution and properties of the colliding materials. The global characteristics of the structure in which they are contained will be only of secondary interest, mainly insofar as the location of material boundaries and free surfaces is concerned. Representative problem areas include the design of lightweight armor systems, including fabric body armors for the protection of police officers, executives in business and government, and military personnel; the vulnerability of military vehicles, aircraft, and assorted structures subjected to impact and explosive loading; the erosion and fracture of solids subjected to multiple impacts by liquid and solid particles; protection of spacecraft from meteoroid impact; explosive forming and welding of metals, explosive formation of jets or slugs, and jet penetration.

Problems of this type are usually referred to as "impact" or "wave propagation" problems. They are distinct from problems that fall in the

"structural dynamics" category, which are characterized by loading and response times measured in milliseconds and where the geometry of the overall structure plays a significant role in determining the response of the system to external stimuli (e.g., safe demolition of prestressed concrete structures; the transportation safety of hazardous materials; crashworthiness of vehicles and protection of their occupants and cargo; safety of nuclear reactor containment vessels subjected to missile impact from external sources, such as aircraft and tornado-borne debris, or internal ones such as extreme pressures from reactor excursions, debris and fragments from failed components). Yet, both problems have a common origin since both types can be described mathematically by the wave equation, which in simplified form is

$$c^2u_{,xx} - u_{,tt} = f(u, u_{,t}, x, t) \tag{1}$$

where, u represents a displacement vector, f a generalized loading function, and subscripts denote derivatives with respect to spatial (x) or temporal (t) quantities. The general solution to the wave equation can be obtained in one of two forms: the normal mode solution or the traveling-wave approach.

The *normal mode solution* is a technique for solving structural response problems in terms of variables that are multiples of the free, undamped mode shapes (eigenvectors) of the structure. The solution is postulated to be separable into functions of the spatial and temporal variables, that is,

$$u = \phi(x)\kappa(t). \tag{2}$$

An eigenvalue problem for the structure is formed, the appropriate eigenvalues and eigenvectors determined, and the result written in the form

$$u = \sum_i A_i \sin(\omega_i t)\sin\frac{\omega_i x}{c} \tag{3}$$

where the ω_i are eigenvalues of the system. The summation is carried out to the desired degree of accuracy. The approach is useful in situations where the response of the structure is affected principally by a few dominant modes, usually the lower harmonics. Problems in this category include vibratory response of structures, the safe design of nuclear reactors subject to internal impulsive and external impact or seismic loading, transportation safety of hazardous materials, crashworthiness of vehicles, and many other industrial problems.

In the *traveling-wave* approach, the disturbances induced by the applied loads are viewed as propagating through a system of waves that interact with geometric and material boundaries as well as each other. It can be shown (e.g., Achenbach 1975; Wasley 1973) that the most general solution of the one-

dimensional wave equation is

$$\psi = f(x - ct) + g(x + ct) \tag{4}$$

where f and g are arbitrary functions of the arguments $x - ct$ and $x + ct$, respectively. The quantities f and g must be consistent with the requirements of continuity, small amplitude, and the various imposed boundary conditions. Two functions are necessary because the wave equation is of second order.

There is a simple interpretation for Eq. (4) in the one-dimensional situation. For purposes of illustration, consider only the function f. Then, at any time t, ψ is a function of x only and can be represented by a certain curve, shown in Figure 1.

The specific shape of the curve is determined by the form of f. After time is increased by an amount Δt, the argument of the function becomes $x - c(t + \Delta t)$. Since we are dealing with a one-dimensional ideal elastic medium where c is a constant, the shape of the wave does not change during propagation. The function f will remain unchanged provided that simultaneously with the increase by Δt the points along x change by an amount $x = c\,\Delta t$. This means that the curve ψ as shown for the time t in the figure can also be used for the time $t + \Delta t$ if it is appropriately displaced in the x direction. Hence, f in Eq. (4) represents a wave moving in the direction of the positive x axis with a constant velocity c. In the same manner, it can be shown that the function g represents a wave traveling in the direction of the negative x axis. Thus Eq. (4) physically represents two waves progressing along the x axis in opposite directions, each with constant velocity.

This approach to the solution of the wave equation is most appropriate (and computationally efficient) for problems involving intense, short-duration loading, especially where the energy carried by waves can result in material failure when the waves interact with material interfaces, free surfaces, or each other. Examples include the impact of meteoroids and small particles with space structures at velocities that exceed the speed of sound in the colliding materials, the penetration and perforation of solids impacted by high-speed

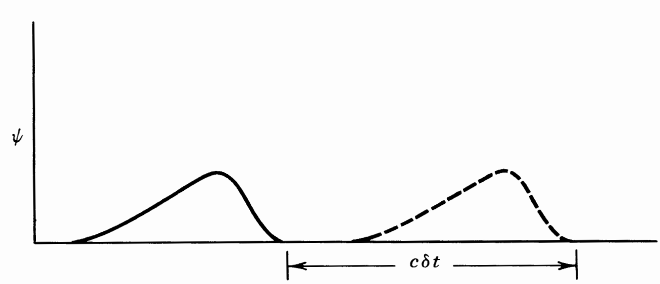

Figure 1. Propagation of an idealized one-dimensional elastic wave.

TABLE 1. Low-Velocity Impact Phenomena

Extent of deformation	Global
Modal Response	Low frequency
Loading/response time	Milliseconds–seconds
Strains	0.5–10%
Strain rates	10^{-2}–10^{1} s^{-1}
Hydrodynamic pressure magnitude	0 (σ_y)
Failure	Large plastic flow

TABLE 2. High-Velocity Impact Phenomena

Extent of deformation	Local
Modal response	High frequency
Loading/response time	Submilliseconds
Strains	> 60%
Strain rates	> 10^5 s^{-1}
Hydrodynamic pressure magnitude	10–100σ_y
Failure	Physical separation of material

missiles, the erosion and fracture of solids subjected to multiple impacts by liquid and solid particles, and the explosive loading of metals.

The physical characteristics of low- and high-velocity impact problems are summarized in Tables 1 and 2. In high-velocity impact situations, loading and response times are typically measured in nanoseconds to microseconds. Extremely high pressures are generated that exceed by several orders of magnitude the strength of the colliding materials. Typical values (peak and average) for pressure, temperature, and strain rate are shown for representative ordnance problems in Tables 3 and 4 (NMAB 1980). The remaining sections of this chapter address the problem of obtaining practical, quantitative solutions to these problems.

TABLE 3. Range of Conditions—Projectile Formation

	Pressure (GPa)	Homologous[a] Temperature	Strain	Strain Rate (s^{-1})
Shaped charge jet (3–10 km/s)	Peak ~ 200 Avg. ~ 20	Peak > 1 Avg. ~ 0.5–0.7	> 10	Peak ~ 10^6–10^7 Avg. ~ 10^4–10^5
Self-forging fragment (1.5–3 km/s)	Peak ~ 40 Avg. ~ 10	Peak ~ 0.5–0.8 Avg. ~ 0.2	Peak ~ 2 Avg. ~ 0.7	Peak ~ 10^6–10^7 Avg. ~ 10^4
Fragmentation (1.3–3 km/s)	Peak ~ 30 Avg. ~ 2	Ductile ~ 0.3–0.5 Brittle ~ 0.1	Ductile ~ 0.5–1.5 Brittle ~ 0.1–0.2	Peak ~ 10^6–10^7 Avg. ~ 10^4

[a]Temperature divided by the melting temperature.

TABLE 4. Range of Conditions—Target Response

	Pressure (GPa)	Homologous[a] Temperature	Strain	Strain Rate (s^{-1})
Gun launched (0.5–1.5 km/s)	Peak ~ 20–40 Avg. ~ 3–5	Peak ~ 0.2–0.3 Avg. ~ 0.1	Peak > 1 Avg. ~ 0.2–0.3	Peak ~ 10^6–10^7 Avg. ~ 10^4–10^5
Self-forging fragment (1.5–3 km/s)	Peak ~ 70 Avg. ~ 10	Peak ~ 0.4–0.5 Avg. ~ 0.2	peak ~ 1 Avg. ~ 0.2–0.3	Peak ~ 10^6 Avg. ~ 10^4–10^5
Shaped charge jet (3–10 km/s)	Peak ~ 100–200 Avg. ~ 10–20	Peak > 1 Avg. ~ 0.2–0.5	Peak ≫ 1 Avg. ~ 0.1–0.5	Peak ~ 10^6–10^7 Avg. ~ 10^4–10^5

[a]Temperature divided by the melting temperature.

11.1. THE GOVERNING EQUATIONS

The equations governing the behavior of solids under impact or impulsive loading conditions are well known, straightforward, and can be summarized on the back of a business-size envelope. Their solution is another matter. Hence, the existence of large finite-difference and finite-element wave propagation codes where the governing equations are contained in one or two short subroutines and the remainder of the code (10,000–150,000 FORTRAN statements) is devoted to input/output operations and various bookkeeping techniques to advance the solution in time.

The basic equations are grouped into four categories:

1. Conservation equations
   - Mass
   - Linear momentum
   - Angular momentum
   - Energy
2. Constitutive relations
   - Volumetric response
   - Deviatoric response
3. Failure criteria
   - Instantaneous
   - Time-dependent (cumulative damage)
   - Micromechanical
4. Postfailure prescriptions

Detailed consideration will be given to constitutive equations and failure models in later sections. For now, we concentrate on the conservation laws of continuum mechanics.

Conservation Equations

Consider the motion of a material body Ω in three-dimensional Euclidean space R^3. Choose a time scale so that at $t = 0$ the body occupies a reference configuration in which its geometry is known. To this end, postulate the existence of an inertial (fixed) frame of reference so that points in R^3 can be defined by their position $x = (x_1, x_2, x_3)$. Denote the material particles of the body by $X = (X^1, X^2, X^3)$. The X^i associated with particle $X \subset \Omega$ are called *material coordinates* of the particle X, and x_i associated with position $x \subset R^3$ are called *spatial coordinates* of x. A motion of Ω is described by

$$x_i = \eta_i(X, t), \tag{5}$$

where η_i is assumed to be a single-valued function differentiable with respect to the arguments.

The motion (5) can be considered as a transformation from X to x at time t. The Jacobian of this transformation is

$$J = \det\left[\frac{\partial x_i}{\partial X^j}\right]. \tag{6}$$

The particle velocity v is given by

$$v = \frac{\partial}{\partial t}\eta(X, t). \tag{7}$$

With this notation established, we can now consider the conservation equations. For additional background material consult Fung (1965) or Herrmann and Nunziato (1972).

Conservation of Mass Let $\rho_0(X, t)$ and $\rho(X, t)$ denote the densities of the body in the reference configuration and current configuration, respectively. The principle of mass conservation may be expressed as

$$\int_\Omega \rho_0 \, dV_0 = \int_\Omega \rho \, dV$$

where

$$dV_0 = dX^1 \, dX^2 \, dX^3 \quad \text{and} \quad dV = J \, dV_0.$$

Alternatively, this may be expressed as

$$\frac{d\rho}{dt} + \rho \frac{\partial v_i}{\partial x_i} = 0. \tag{8}$$

Here, d/dt denotes the material time derivative, and repeated indices imply summation.

Conservation of Linear Momentum Let σ be the Cauchy stress tensor (referred to and measured with respect to the spatial coordinates x_i), and let f be the body force per unit mass. The local form of the principle of linear momentum is given by

$$\rho \frac{dv_i}{dt} = \frac{\partial \sigma_{ij}}{\partial x_j} + \rho f_i. \tag{9}$$

Conservation of Angular Momentum In the absence of microstructural effects (nonpolar media), angular momentum conservation leads to the symmetry of the stress tensor:

$$\sigma_{ij} = \sigma_{ji}. \tag{10}$$

If the medium is *polar* (polyatomic and certain non-Newtonian fluids), a body torque vector **Q** per unit mass and a couple stress tensor **R**, in addition to the body force vector **f** and stress tensor $\boldsymbol{\sigma}$ must be introduced. This leads to

$$\rho \frac{dL_i}{dt} = \rho Q_i + \frac{\partial}{\partial x_j} R_{ji} + \varepsilon_{jki}\sigma_{jk}, \tag{11}$$

where L_i is the component of an intrinsic angular momentum due to the presence of body torque **Q** and couple stress **R**. The ε_{ijk} is the permutations symbol. Observe that if **Q** and **R** are zero, $\varepsilon_{jki}\sigma_{jk} = 0$, which implies that $\sigma_{jk} = \sigma_{kj}$.

Conservation of Energy Let q denote the rate of heat flow per unit area across the surface of Ω, S be the rate of internal heat generation per unit mass, and T be the specific internal energy. Then the local form of the energy conservation principle may be written as

$$\rho \frac{de}{dt} = \frac{\partial}{\partial x_j}(\sigma_{ji} v_i) - \frac{\partial q_i}{\partial x_i} + \rho S + \rho f_i v_i, \tag{12}$$

where

$$e = \tfrac{1}{2} v_i v_i + I.$$

The form of the conservation equations is similar for Lagrangian (grid fixed in the material and distorting with it) and Eulerian (grid fixed in space with material flowing through it) mesh descriptions. The differences occur because

of the definition of

$$\frac{d}{dt} = \frac{\partial}{\partial t} + v_i \frac{\partial}{\partial x_i}. \tag{13}$$

This derivative, variously known as the material derivative, substantial derivative, or total time derivative, is used in the Euler approach in calculating quantities that are transported between cells since they are associated with the mass flow. Thus, the conservation equations for an Eulerian system, neglecting heat sources and sinks, would be

$$\frac{\partial \rho}{\partial t} + \frac{\partial}{\partial x_i}(\rho v_i) = 0,$$

$$\frac{\partial v_i}{\partial t} + v_j \frac{\partial v_i}{\partial x_j} = f_i + \frac{1}{\rho}\frac{\partial \sigma_{ji}}{\partial x_j},$$

$$\frac{\partial e}{\partial t} + v_i \frac{\partial e}{\partial x_i} = f_i v_i + \frac{1}{\rho}\frac{\partial}{\partial x_j}(\sigma_{ij} v_i).$$

The conservation equations are summarized in Table 5. Included are the Hugoniot jump conditions-conservation equations across a shock front. For their derivations, see Zukas et al. (1982).

Constitutive Equations

The conservation laws apply to any continuous material body without regard to its physical constitution. To complete our description, we need to add relationships that govern both the high-pressure (volumetric) and deformation (deviatoric) behavior of bodies under applied loads. Since impact loading is a very rapid process, we will assume that it is adiabatic (no heat is transferred from the system).

A few additional quantities need to be introduced first. The stress tensor σ_{ij} can be expressed as the sum of a *hydrodynamic* component, $P\delta_{ij}$, and a *deviatoric* stress, s_{ij}

$$\sigma_{ij} = -P\delta_{ij} + s_{ij}, \tag{14}$$

where

$$s_{ii} = 0; \qquad \sigma_{ii} = 3P(\rho, I)$$

P is obtained from an equation of state. The strain rate tensor and spin tensor

TABLE 5. Conservation Equations

Conservation of mass

$$\dot{\rho} + \rho \dot{u}_{i,i} = 0$$

Conservation of linear momentum

$$\rho \ddot{u}_i = \sigma_{ji,j} + \rho f_i$$

Conservation of angular momentum

a. Polar media

$$\rho \dot{L}_i = \rho Q_i + R_{ji,j} + \varepsilon_{jkl} \sigma_{jk}$$

b. Nonpolar media

$$\sigma_{ij} = \sigma_{ji}$$

Conservation of energy

$$\rho \dot{e} = \left(\sigma_{ji} \dot{u}_i\right)_{,j} - q_{i,i} + \rho S + \rho \dot{u}_i f_i$$
$$e = I + \tfrac{1}{2} \dot{u}_j \dot{u}_j$$

Hugoniot jump conditions

$$\rho_0 U_s = \rho\left(U_s - u_p\right)$$
$$P - P_0 = \rho_0 U_s u_p$$
$$I - I_0 = \tfrac{1}{2}(P + P_0)\left(\frac{1}{\rho_0} - \frac{1}{\rho}\right)$$

U_s = shock velocity; u_p = particle; I = internal energy; $\dot{u} = du/dt = v$.

TABLE 6. Constitutive Equations

Fluid flow

$\dot{d}_{ij} = \dot{\varepsilon}_{ij} - \frac{1}{3} \dot{\varepsilon}_{kk} \delta_{ij}$	$\dot{s}_{ij} = c_{ijkl} \dot{d}_{kl}$ (anisotropic)
$\dot{d}_{kk} = 0$	$\dot{s}_{ij} = 2G \dot{d}_{ij}$ (homogeneous, isotropic)

are given by

$$\dot{\varepsilon}_{ij} = \frac{1}{2}\left(\frac{\partial v_i}{\partial x_j} + \frac{\partial v_j}{\partial x_i}\right),$$

$$\omega_{ij} = \frac{1}{2}\left(\frac{\partial v_i}{\partial x_j} - \frac{\partial v_j}{\partial x_i}\right).$$

The deviatoric strain rate tensor is defined by

$$\dot{d}_{ij} = \dot{\varepsilon}_{ij} - \tfrac{1}{3}\dot{\varepsilon}_{kk}\delta_{ij}; \qquad \dot{d}_{kk} = 0.$$

TABLE 7. Constitutive Equations

Elastic-plastic material

a. Stress deviators

$$\dot{s}_{ij} = 2G\left(\dot{\varepsilon}_{ij} - \tfrac{1}{3}\delta_{ij}\dot{u}_{k,k}\right)$$

b. Velocity strains

$$\dot{\varepsilon}_{ij} = \tfrac{1}{2}\left(\dot{u}_{i,j} + \dot{u}_{j,i}\right)$$
$$\dot{\omega}_{ij} = \tfrac{1}{2}\left(\dot{u}_{i,j} - \dot{u}_{j,i}\right)$$

c. Jaumann stress rate

$$\hat{\sigma}_{ij} = \sigma_{ij} + \sigma_{im}\omega_{mj} - \omega_{im}\sigma_{mj}$$

d. Total stress

$$\sigma_{ij} = s_{ij} - \delta_{ij}P$$
$$s_{ii} = 0 \qquad \sigma_{ii} = -3P(\rho, I)$$

e. Von Mises yield criterion

$$s_{ij}s_{ij} \le \tfrac{2}{3}Y^2$$

if yield stress exceeded

$$s_{ij} = s_{ij}\left[\frac{2Y^2}{3s_{ij}s_{ij}}\right]^{1/2}$$

TABLE 8. Equations of State

Mie–Grüneisen
$$P = P_H\left(1 - \frac{\Gamma\mu}{2}\right) + \Gamma\rho(I - I_0)$$
$$P_H = \begin{cases} k_1\mu + k_2\mu^2 + k_3\mu^3 & \text{if } \mu \geq 0 \\ k_1\mu & \text{if } \mu < 0 \end{cases}$$
$$\mu = \frac{\rho}{\rho_0} - 1$$
Tillotson
For $\rho > \rho_0$ and $0 \leq I \leq I_s$
$$P = P\pi + A\mu + B\mu^2$$
$$P\pi = I\rho\left[a + \frac{b}{I/(I_0\eta^2) + 1}\right]$$
for $\rho < \rho_0$ with $I > I_s$
$$P = aI\rho\left\{\frac{bI\rho}{[1 + I/(I_0\eta^2)]} + A\mu e^{-\beta(1/\eta - 1)}\right\} e^{-\alpha(1/\eta - 1)^2}$$
$$\eta = \frac{\rho}{\rho_0}$$

Constitutive equations for fluid flow are summarized in Table 6. Constitutive equations for elastic-plastic behavior are listed in Table 7. Representative high-pressure equations of state for solids, gases, and explosives are shown in Tables 8 and 9.

Note that the equations governing material behavior under high rate loading are rate equations. Although the Cauchy stress tensor is frame invariant the stress rate tensor is not. Several frame-invariant stress rate tensors can be constructed. The one most often used in computations is due to Jaumann:

$$\hat{\sigma}_{ij} = \frac{d\sigma_{ij}}{dt} + \sigma_{im}\omega_{mj} - \omega_{im}\sigma_{mj} \tag{15}$$

The tensor $\hat{\sigma}_i$ is called a *stress flux* and measures the rate of change of the stress components with respect to a rectangular Cartesian system that participates in the rotation of the material.

Nagtegaal and de Jong (1982) observed that for a simple finite shear problem, using a bilinear elasto-plastic stress–strain relationship, use of the Jaumann rate of the Cauchy stress produced a radical difference in shear stress response depending on the assumption made for the hardening behavior. The isotropic hardening assumption led to a monotonically increasing shear stress,

TABLE 9. Equations of State

Los Alamos

$$P = \begin{cases} [A\mu + \rho_0 I(B + \rho_0 IC)]/(\rho_0 I + \phi_0) & \text{if } \mu \geq 0 \\ [\mu A_1 + \rho_0 I(B_0 + \mu B_1 + \rho_0 IC)]/(\rho_0 I + \phi_0) & \text{if } \mu \leq 0 \end{cases}$$

Wilkins

$$P = a\eta^{\alpha} + b\left(1 - \frac{\omega}{R}\eta\right)e^{-R/\eta} + \omega\eta I$$

Gamma law

$$P = (\gamma - 1)(1 + \mu)I$$

Jones, Wilkins, Lee (JWL)

$$P = \mathrm{A}\left(1 - \frac{\omega\eta}{R_1}\right)e^{-R_1/\eta} + B\left(1 - \frac{\omega\eta}{R_2}\right)e^{-R_2/\eta} + \omega\eta I$$

as expected. However, the kinematic assumption led to a periodically varying shear stress. Dienes (1979, 1984a, 1986) proposed a solution to the problem. He defined a rate of material rotation on which the rate of change of stress should be dependent, resulting in a change of stress rate from that of Jaumann to one attributed to Green and Naghdi (1965) see Figure 2. Other forms of frame-invariant stress rates have been suggested by Johnson and Bammann (1984) and Halleux and Donea (1985).

Such simple problems are excellent vehicles for uncovering defects, or exposing limitations, of various formulations and algorithms. It can be logically asked, therefore, why the limitations of the Jaumann rate were not discovered previously, especially since wave propagation and impact calculations have been performed routinely for over 25 years. Recall, however, that the penetration problem is everything but simple. Failure in impacted materials occurs by a variety of mechanisms that take turns in dominating the response at different stages of penetration (Zukas 1982; Wright 1983). Material response is highly nonlinear with plastic strains exceeding 60%. High temperature and hydrodynamic pressure fields are superimposed on the stress state generated by impact and impulsive loads and, due to the interaction of waves with free surfaces and material interfaces, both the intensity and nature (tension, compression) of the loading charges dramatically over short (submicrosecond) time intervals.

Recall further that the Jaumann rate has been shown to give good results to strain levels of 40%. Near this value, failure occurs in many materials, especially high-strength steels. Since most codes do not track cells or elements labeled as failed (i.e., stress states are no longer computed), the deficiency in

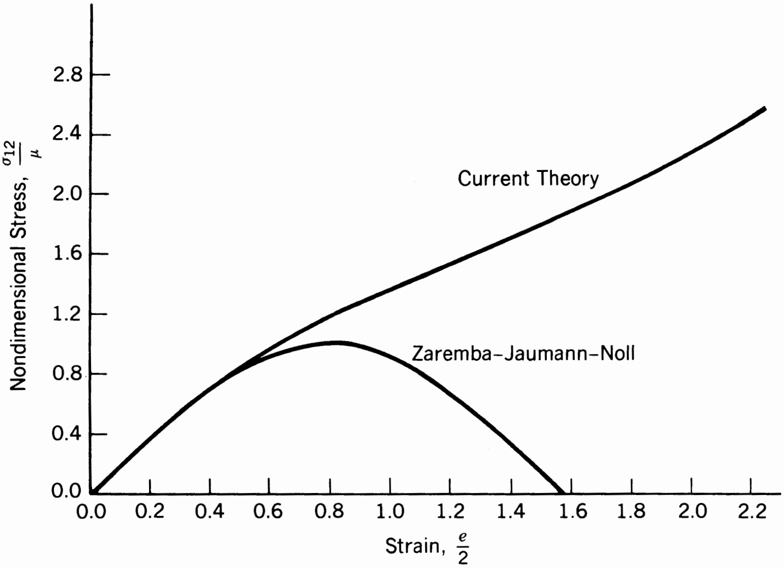

Figure 2. Effects of stress rate measures on material response. (Dienes, 1986)

the stress rate would not easily be observed. Finally, for most ballistic experiments, calculations are compared to postmortem results (deformed profiles of target and projectile, net mass loss, residual velocity), integral quantities that are not *sensitive* to the fine points of constitutive equations. Only recently with the advent of dynamic measurements of strain and pressure *during* and impact event [see Zukas (1982), Chapter 5] have experimental methods begun to approach the capabilities of computer codes to determine local (stress, strain, pressure) variables and thus provide a sensitive discriminant for constitutive equations.

The Dienes formulation was incorporated in a version of the EPIC-2 code and simulations performed for the case of an $L/D = 10$ rod of C110W steel striking a semi-infinite target of HzB20 armor steel at a velocity of 3.114 km/s. Details are given in the report by Kimsey and Zukas (1986). Comparisons of displacements, effective plastic strain contours, effective stress contours, and pressure contours using both the Jaumann and Dienes rates show that:

Displacement profiles were virtually identical for both rates.

Effective plastic strain contours showed a difference of a few percent at most near the crater in the target and were identical at locations some one or two crater diameters removed from the impact interface.

Effective stress contours (Figures 3–5) showed somewhat more pronounced differences, especially near the impact interface.

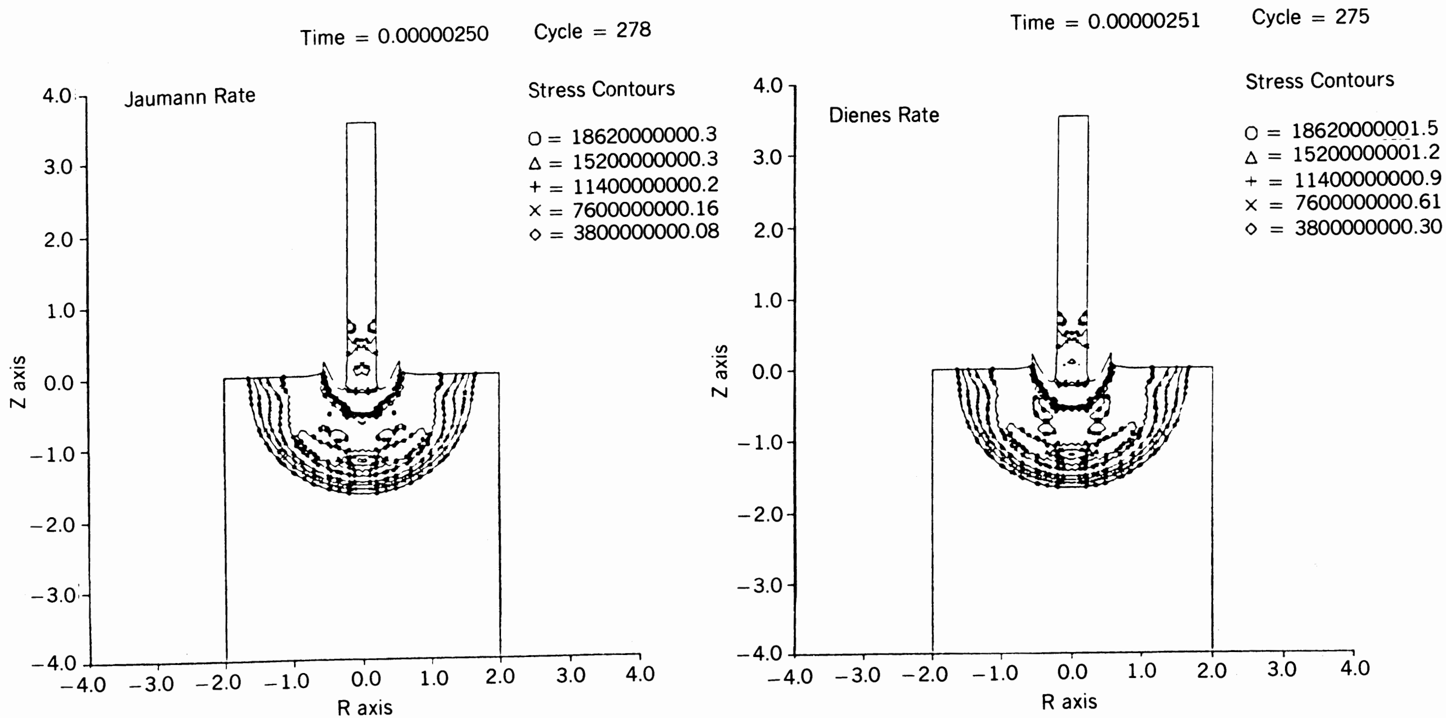

Figure 3. Effective stress contours for different stress rates, $t = 2.5\ \mu s$.

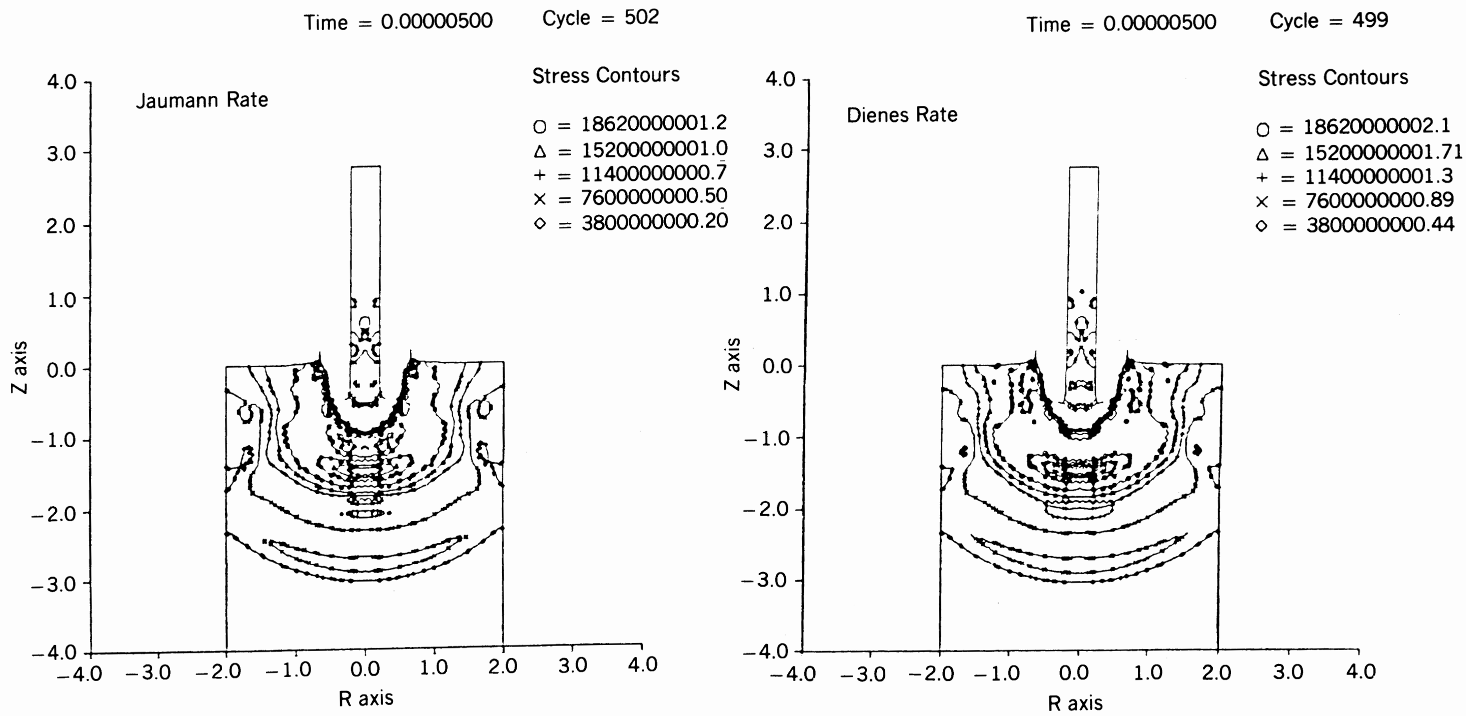

Figure 4. Effective stress contours for different stress rates, $t = 5\ \mu s$.

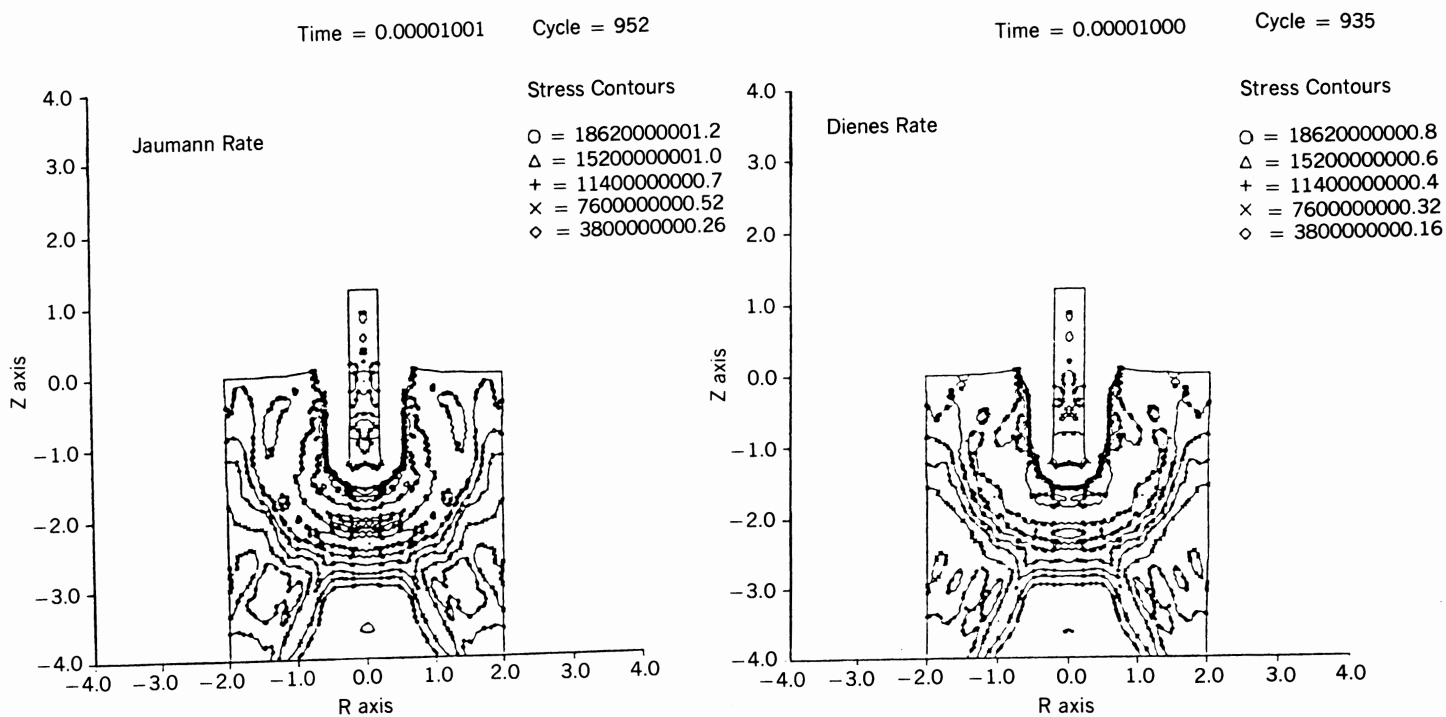

Figure 5. Effective stress contours for different stress rates, $t = 10\ \mu s$.

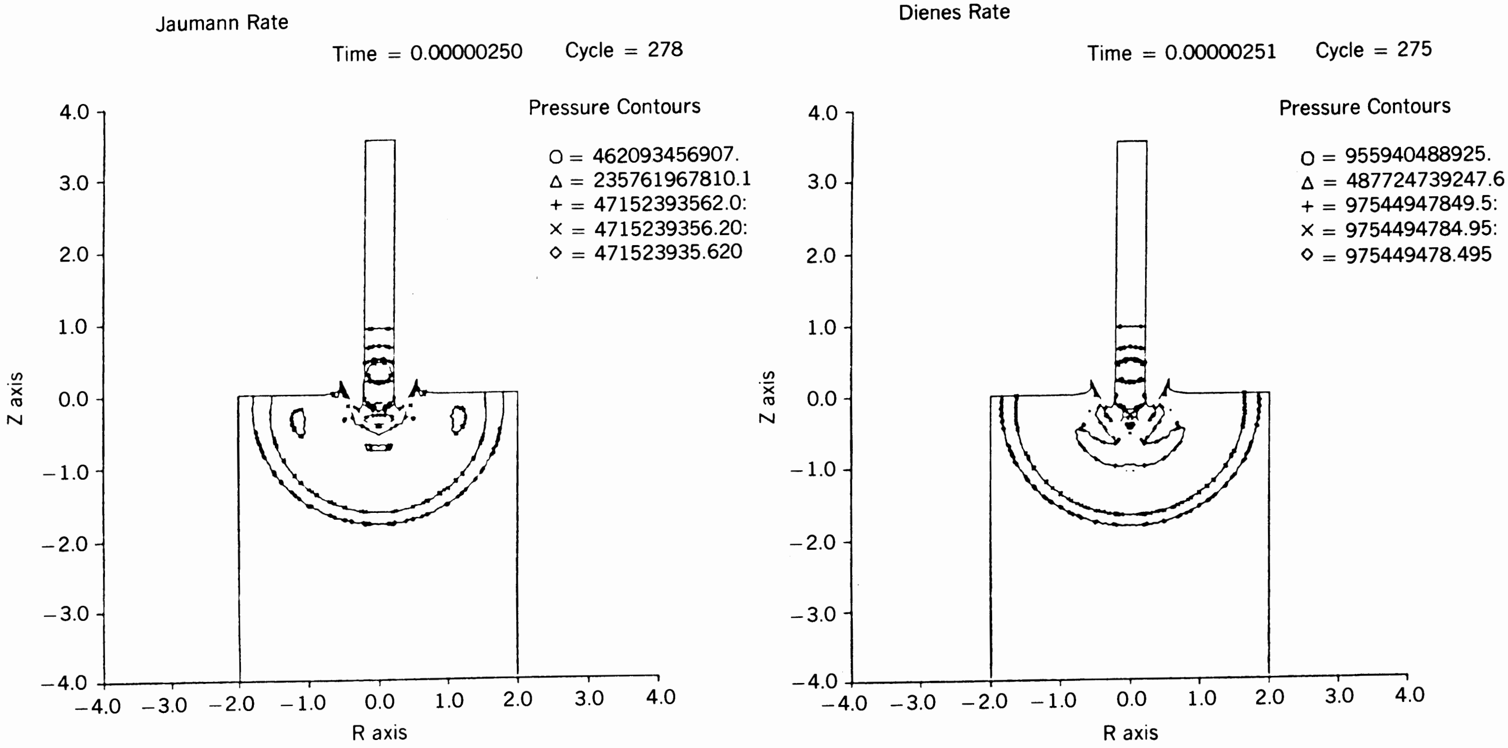

Figure 6. Pressure contours for different stress rates, $t = 2.5\ \mu s$.

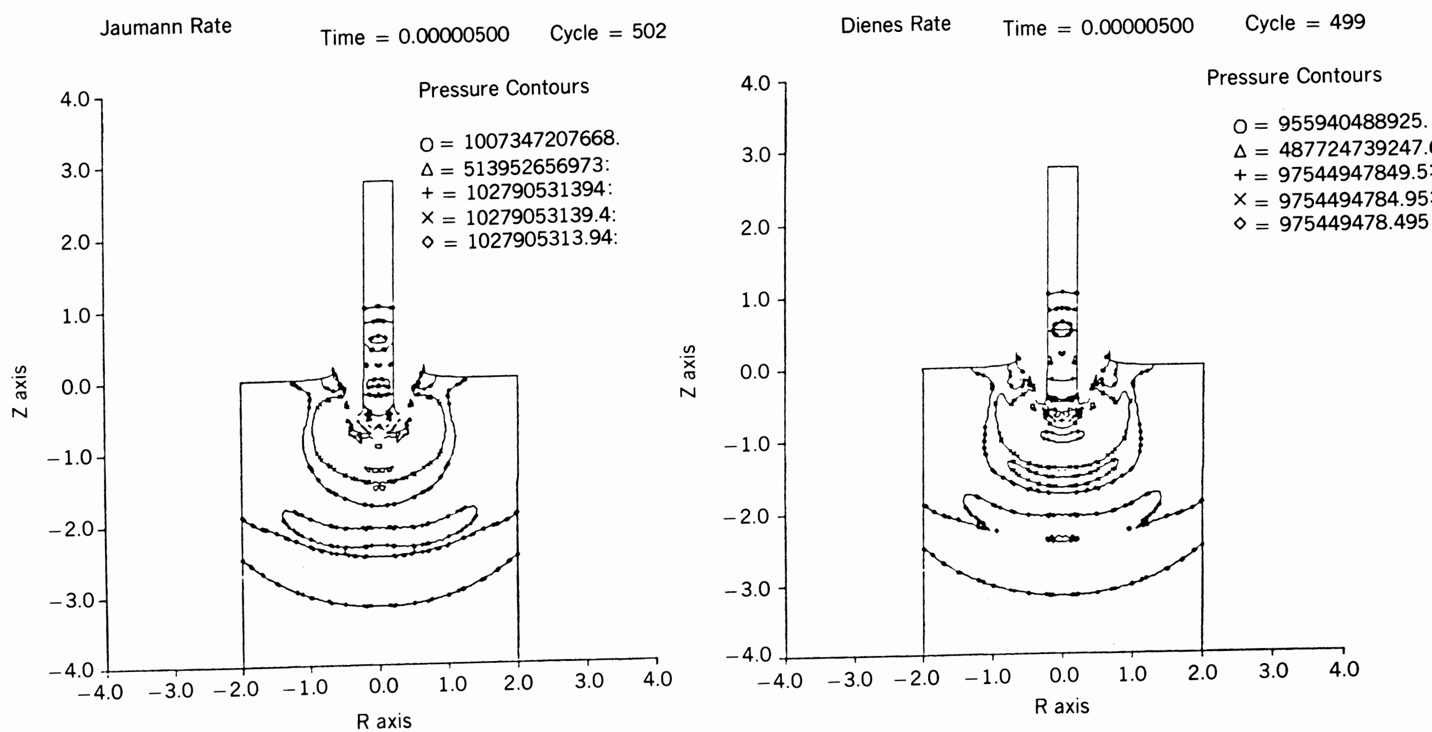

Figure 7. Pressure contours for different stress rates, $t = 5\ \mu s$.

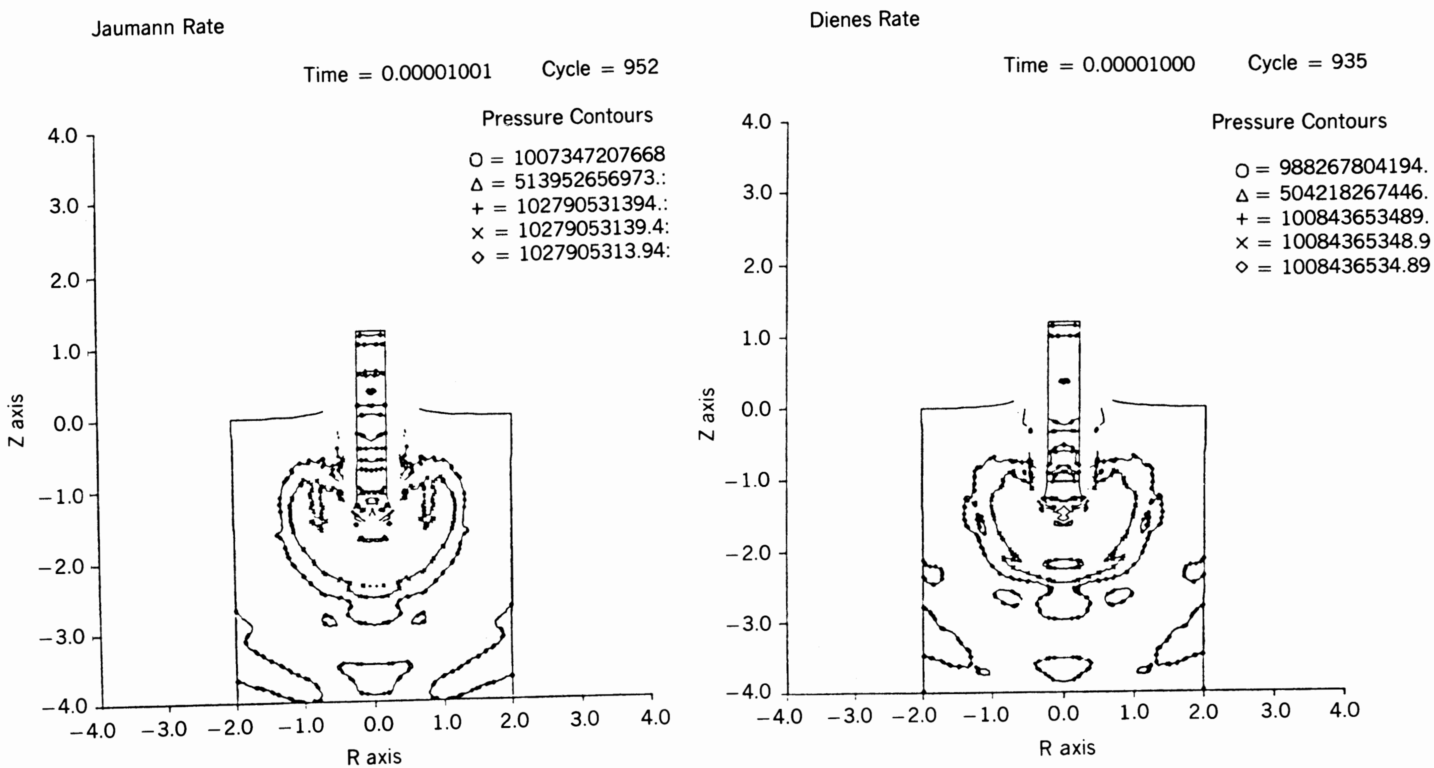

Figure 8. Pressure contours for different stress rates, $t = 10\ \mu s$.

Pressure calculations showed the greatest differences at early times and near the projectile–target interface (Figures 6–8). Differences in pressure and other variables diminished with time and, at any given time, with distance from the projectile–target interface.

The Green–Naghdi rate is gradually being incorporated in wave codes. Until all existing codes have been updated, users should be aware of potential difficulties with the Jaumann rate. Whether this will have a pronounced effect on accuracy of the results depends strongly on the material model and the results sought. If displacements or global quantities are of primary interest, results are virtually unaffected by the choice of stress rate. If local quantities are sought, the Jaumann rate will serve well for strains up to 40%. Beyond that, some differences can be expected, depending on the nature of the problems and the stress rate chosen.

11.2. SPATIAL DISCRETIZATION

The differential equations of the previous section are easy to write down but (except in highly idealized circumstances) difficult to solve. This is true of partial differential equations in general. The solutions of a few classic equations —the Laplace and Poisson equations come to mind readily—have been obtained and examined in great detail, but hardly any techniques exist that allow one to obtain a general solution to nonlinear partial differential equations.

Numerous techniques, however, exist for solving algebraic equations. It is logical, therefore, to seek to construct an analogous set of algebraic equations that, in the limit, will exhibit the same behavior as our original partial differential equations. The two methods used in all production codes for wave propagation and impact studies are the finite-difference and finite-element methods.

The following observations will not make an expert of the reader in these techniques. They are intended only to bring out two points: (a) the nature of the approximations introduced by way of each technique, and (b) the form of the resulting algebraic equations is the same, regardless of the method used.

There are very many books on finite-element and finite-difference methods that may be consulted. Two of the most readable and rewarding are the books by Fried (1979) and Bathe (1982).

The finite-difference method may be thought of as an approximate solution technique to an exact problem because in the usual approach one manipulates the governing physical relationships into differential equation form. Then, derivatives are systematically replaced with analogous difference operators. This is done for the governing differential equations, boundary conditions, and initial conditions. This procedure then results in a set of algebraic equations

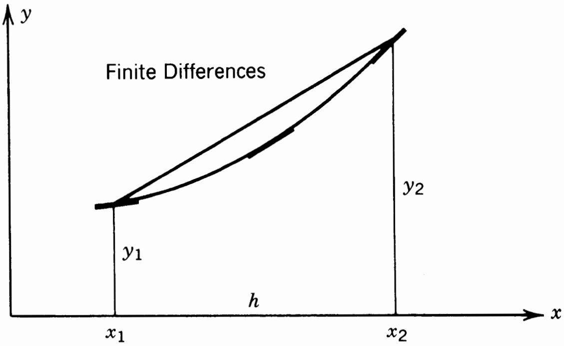

Figure 9. Finite difference approximations.

$$y'(x) = (y_2 - y_1)/h \qquad x_1 \leq x \leq x_2$$

Difference scheme is
backward if $x = x_1$ in $y'(x)$
forward if $x = x_2$ in $y'(x)$
central if $x = \dfrac{x_1 + x_2}{2}$ in $y'(x)$

(the number depending on the degree of accuracy desired) that can then be solved numerically using standard techniques.

As Fried (1979) has observed: "Replacement of differentials by differences is the paramount step in algebraization of the differential equation." Consider Figure 9, which shows some portion of a function $y(x)$ over an interval h. One way to obtain a difference approximation of the first derivative $y'(x)$ is to approximate the tangent by the chord. That is, at any point within the interval $x_1 \leq x \leq x_2$, the first derivative of $y(x)$ is approximated by

$$y'(x) = \frac{y_2 - y_1}{h} \tag{16}$$

This approximation is always exact if y is a linear function of x, but for wave propagation problems we can expect both nonlinear and highly transient behavior. This implies that our interval $h = x_2 - x_1$ will be rather small to satisfy accuracy requirements (i.e., we're giving up 20 or so partial differntial equations that we can't solve for many thousands of algebraic equations that we can solve, albeit tediously) and also that for most points in our chosen interval the replacement of the curve by straight line segments is only an approximation. However, by Rolle's theorem, there will be at least one point within the interval where the equality holds.

Our finite-difference approximation will be termed backward, forward, or central (Figure 9) depending on the point in the interval at which we elect to approximate $y'(x)$.

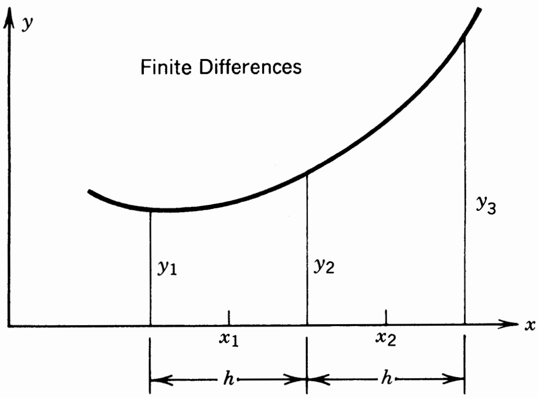

Figure 10. Formation of derivatives.
Second derivatives obtained from successive formation of $(y')'$

$$y_1' \approx y'(x_1) = h^{-1}(y_2 - y_1)$$

$$y_2' \approx y'(x_2) = h^{-1}(y_3 - y_2)$$

$$y''(x) = h^{-1}(y_2' - y_1') = h^{-2}(y_1 - 2y_2 + y_3)$$

Higher-order difference schemes may be generated by successively forming expressions for high derivatives, that is, $y''(x) = [y'(x)]'$ and so forth. See Figure 10 for an example of the procedure for obtaining $y''(x)$. There are more systematic procedures for doing this (Fried 1979), but this illustration is sufficient for our purposes.

It is natural next to inquire as to the degree of error incurred in replacing differentials by finite differences. Fried (1979) demonstrates that through the use of Taylor's theorem, it is possible to establish that the central difference method is second order accurate—$O(h^2)$. This implies that as the interval length h is halved, the error of the approximation is reduced by a factor of 4. By contrast, forward and backward schemes are only first order accurate—$O(h)$.

An alternate method for discretizing partial differential equations in the spatial domain is the finite-element method. Here, the discretization is introduced at the outset. There is no playing with differential equations and replacement of derivatives—the continuum with its infinite degrees of freedom is replaced at the outset by a substitute finite degree of freedom system whose characteristics approximate those of the original model. Once this approximation is made, the resulting equations are solved exactly. For this reason, the finite-element method is sometimes referred to as an exact solution to an approximate problem.

Consider Figure 11. Here we depict a cylindrical striker making initial contact with a flat, cylindrical plate. Both are continuous bodies, yet for

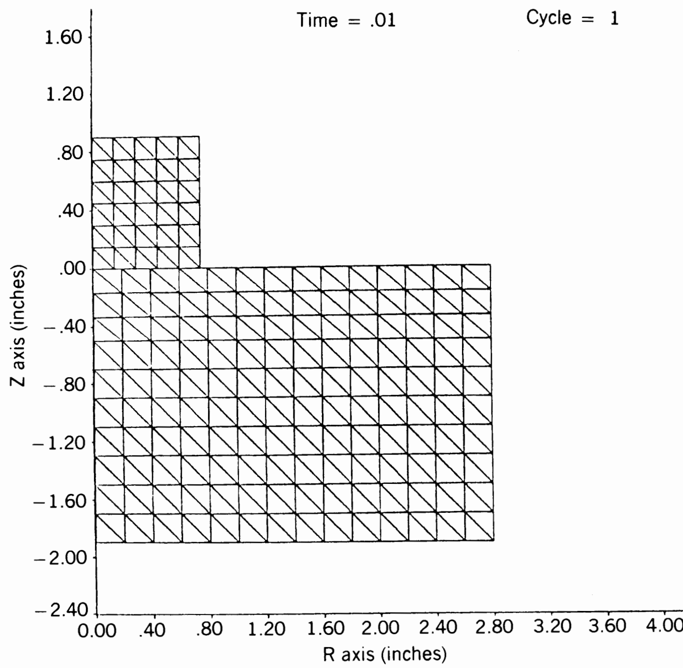

Figure 11. Finite-element approximation of a continuum.

purposes of computations we have broken them into triangular regions. We assume these regions interact only at a finite number of points, called nodes. The displacement of these nodal points are the unknowns of our problem. If it is desired to know displacements or other variables *within* an element, we will interpolate from the (known) nodal quantities. Hence, central to the finite-element process is the need to *assume* some admissible distribution of the unknowns in terms of functions defined throughout the regions of the solid.

The discretization procedure for the finite-element technique is outlined in Table 10. The nodal displacements are the unknowns of the problem. Once

TABLE 10. Finite-Element Method

Discretize at outset
Outline of procedure
- Divide continuum into finite number of regions (elements). Elements interact only at discrete number of points (nodes).
- Postulate functions to define displacements within element in terms of nodal displacements
- Define state of strain from displacement functions
- Define state of stress from constitutive relationship
- Define element nodal forces
- Assemble global arrays
- Solve for nodal displacements using standard techniques

these are obtained, all other unknowns may be found through constitutive equations or compatibility constraints.

The choice of approximating (or interpolating) functions is not completely arbitrary (it is common practice to choose a polynomial series as the approximating function). Care must be taken that the number of terms in the chosen series equals the total number of degrees of freedom of an element. Furthermore, the approximating function and certain of its derivatives must be continuous within an element. Compatibility must exist between adjacent elements. The approximating function must be able to accommodate rigid-body motions and, as the mesh is refined, a state of constant strain should be approached in the element.

Whether by finite differences or by finite elements, we arrive at a system of discrete algebraic equations of the form

$$[M]\{\ddot{u}\} + [C]\{\dot{u}\} + [K]\{u\} = F. \tag{17}$$

For wave propagation studies, where loading and response times are in the submillisecond regime, explicit use is not made of the damping matrix. We can then write our equations in the form

$$[M]\{\ddot{u}\} = F^{\text{ext}} - F^{\text{int}}. \tag{18}$$

If the mass matrix is diagonal (lumped mass formulation), it is possible to perform the integration on an element-by-element basis and bypass the explicit use of the stiffness matrix $[K]$ entirely. This greatly simplifies computations and data storage procedures (Bathe 1982) and is the approach used in all Lagrangian finite-element wave codes.

Note that a common property of both the finite-difference and finite-element methods is the local separation of the spatial dependence from the time dependence of the dependent variable (i.e., at this point in our development we have a semidiscrete system—algebraic expressions for the spatial behavior of our unknowns but still partial derivatives for the time dependence). This permits us to treat space and time grids separately.

Since for many cases the discrete forms of the equations of motion of the finite-element method are equivalent to those of the finite-difference method, there is no basic mathematical difference between the two methods. Therefore, they should have the same degree of accuracy in numerical computations. The main differences lie not in the methods themselves but in the data management structure of the computer programs that implement them.

Finite-element codes have a distinct advantage in treating irregular geometries and variations in mesh size and type because in the finite-element method, the equations of motion are formulated through nodal forces for each element and do not depend on the shape of the neighboring mesh. In the finite-difference method, equations of motion are expressed directly in terms of the pressure gradients of the neighboring meshes. This is not inherently a

problem, but the difference equations must be formulated separately for irregular regions and boundries.

Another major difference occurs in numbering of meshes. In finite-difference programs, the regularity of the mesh implicity establishes the connectivity information. In finite-element programs, mesh connectivity is explicitly stored, a feature that facilitates automatic generation of complex mesh systems. This limitation can be overcome for finite-difference methods, but versatility is generally achieved at the expense of large computer storage and central processor (CPU) time.

11.3. MESH DESCRIPTION

Another decision to be made is whether this spatial discretization is to be made in an Eulerian or Lagrangian framework. Mesh descriptions are covered in some detail in Section 10.2 of Zukas et al. (1982). Hence, only a relevant outline and current developments will be presented here.

In the Lagrangian scheme of things (Figure 12), a grid is embedded in the material and distorts with it. In other words, the Lagrangian world tracks motion of fixed elements of mass. In the Eulerian approach (Figure 13), the grid is fixed in space and mass flows through it. Both schemes have their advantages and disadvantages for various problem classes. Often, features of both are required in a calculation so the tendency today is toward development of computer codes with Eulerian and Lagrangian capabilities.

There are a number of advantages to a Lagrangian system. Since there are no convective terms for the motion of material through a grid as in the Eulerian case, Lagrangian codes are conceptually straightforward and, in principle, should require fewer computations per cycle. Since the grid deforms with the material, time histories are easily obtained and material interfaces and geometric boundaries are sharply defined.

However, in order to account for momentum transfer between colliding bodies, Lagrangian codes incorporate elaborate logic for sliding interfaces. Examples of situations requiring sliding interface logic are shown in Table 11. A number of different options are available (Figure 14):

Sliding with or without friction

Sliding with or without separation

Tied sliding (a technique to maintain displacement continuity across regions of substantial changes in grid size)

In most Lagrangian calculations, the bulk of the computation time is spent in the sliding interface logic. The more elaborate and general that logic, the more useful the code. However, the computational penalty incurred in very general sliding interface routines more than offsets the advantages of not having to

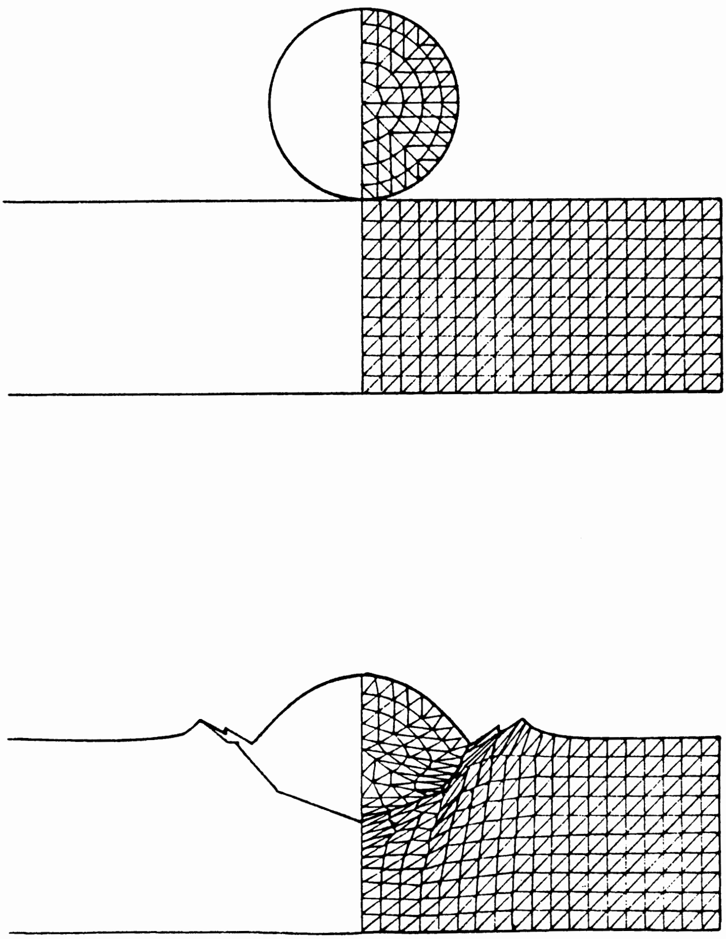

Figure 12. Deformation in Lagrangian systems.

deal with convection insofar as computation time is concerned. In addition to the references in Zukas et al. (1982), the papers by Oden (1983), Wilkins (1982), Oden and Pires (1983), Pires and Oden (1983), Kalker (1977), Bathe (1984), Bathe and Chaudhary (1984), Hyman (1984), and Hallquist et al. (1985) represent a good bibliography on sliding interface techniques for both wave propagation and structural dynamics codes.

Sliding interface logic is ridiculously simple to describe (Table 12). Indeed, the equations governing sliding can be written on a 3 × 5 file card. Implementation in a computer code, however, is a formidable problem. Indeed, about 80% of the computation time in a Lagrange calculation is spent on the interface logic. Lagrange codes succeed or fail in large part based on the implementation of the sliding interface logic.

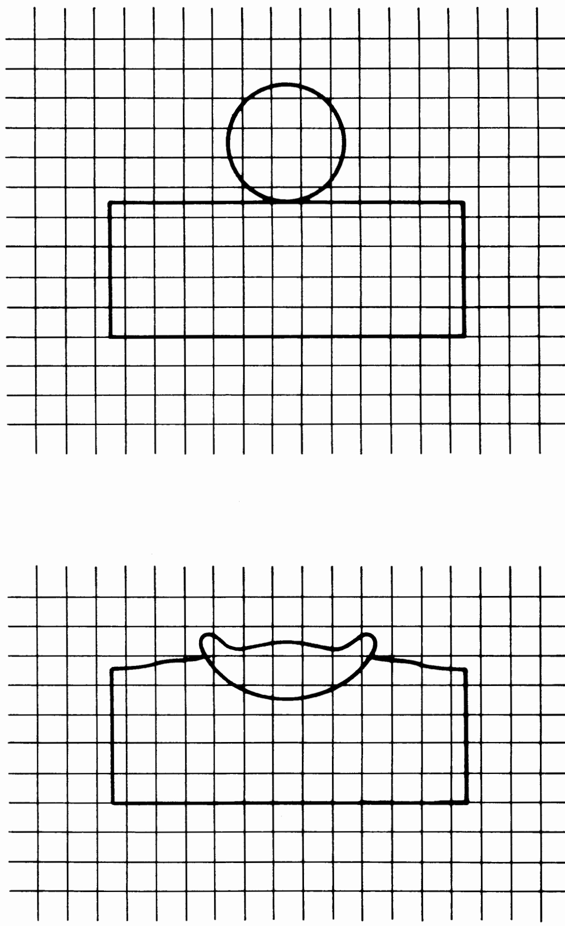

Figure 13. Deformation in an Eulerian system.

The computational procedure is shown in Table 13. The user designates nodes that make up both master and slave surfaces. The interface logic then checks for intrusions during the computational cycle, corrects them, and ensures that momentum is conserved. *Energy*, however, is *not conserved* in most sliding interface prescriptions. The total energy of each calculation must therefore be carefully monitored. Losses of 5–10% on the sliding interfaces are reasonable for most high-velocity impact problems. Anything greater than 10% should prompt a close scrutiny of the calculations for other problems.

Some care had to be taken in older codes in specifying master and slave surfaces. Most recent codes (post-1980) or revisions of older codes now incorporate a symmetric treatment of the interface–master and slave designations are interchanged and both sides of an interface are checked for intru-

TABLE 11. Lagrangian System

Sliding interfaces: Required when sliding or separation of materials can be expected
Examples
- Interactions of gases and fluids with solid walls
- Penetration of targets
- Contact between colliding bodies
- Regions with large shear distortions
- Internal fracture (material separation)

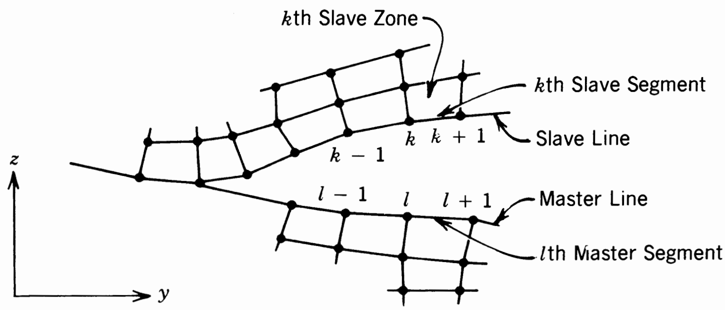

sions prior to application of momentum balance and frictional restraints. Here, the designation of master and slave surfaces is arbitrary.

Experience of analysts with a given program is the key to success. There is no theoretical basis to assume convergence of calculations based on the sliding interface scheme employed. Acceptance of a particular "prescription" is based on close correlation between experiments and computations for a large number of cases. Interface schemes deemed successful are carried on from one code to another.

Because a Lagrangian mesh distorts with the material, very large distortions soon occur in impact problems that have very deleterious effects. Figure 15 shows a portion of a calculation where initially uniform triangular elements with 1 : 1 aspect ratio have been stretched at the interface to unreasonable proportions. Such large distortions give rise to several problems:

1. Because the time step in the wave propagation codes is based on the smallest element dimension, large distortions render computations economically unfeasible. As the element volume approaches zero, the time step approaches zero. The computation is barely advanced in time at great CPU cost while truncation errors grow.

2. Four-node quadrilateral elements can turn inside out, resulting in calculation of negative volumes, and therefore negative masses. This invalidates the calculation, requiring a fresh start or remedial action. Triangular elements cannot be driven to a negative volume condition without first going through a

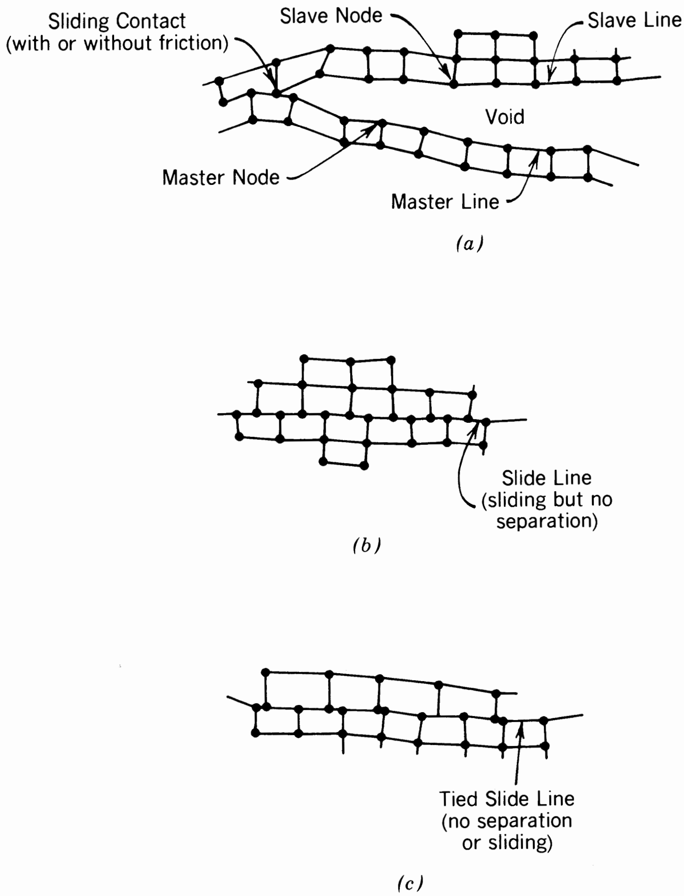

Figure 14. Examples of contact algorithm options: (*a*) sliding with voids; (*b*) sliding only; (*c*) tied sliding.

TABLE 12. Lagrangian System

Sliding interfaces
Approach:
Designate master and slave material
Decompose $\ddot{u}$, $\dot{u}$ into normal and tangential components
In *normal* direction
Motion continuous during contact
Independent when separated
In *tangential* direction
Independent when materials separated or interface frictionless
Modified when there is contact or frictional force acts
Tied sliding—maintain displacement compatibility at abrupt grid changes

TABLE 13. Lagrangian System

Sliding interfaces

Computational procedure

a. Identify a series of nodes that make up the master surface
b. Identify a series of nodes that make up the slave surface
c. For each Δt, apply equations of motion to both master and slave nodes.
d. Check for interference between slave nodes and master surface
   Define search region
   Check each slave node not on master surface
   If penetration occurs, move slave node to master surface. Examples:
      Insert linear spring into stiffness matrix
      Move slave node to master surface in direction $\perp$ master surface
   Reduce Δt to inhibit penetration
e. Once slave nodes moved onto master surface
   Invoke momentum balance
   Apply frictional forces
   Open voids (if tensile forces present)
f. Repeat c–e for each Δt

state of infinite pressure. However, pressure oscillations in neighboring triangular elements can occur when they are subjected to the extreme distortions shown in Figure 15. One triangle will have a very large negative pressure, its neighbor a large positive pressure. If averaged, the pressure for the quadrilateral forming the two triangles will be nearly correct, but individual element pressures will be well off the mark. This oscillation not only imparts excessive stiffness to the grid but can produce erroneous qualitative as well as quantitative information if failure criteria based on stress or pressure wave profile are used in the calculation. Some of these problems may be alleviated by special arrangements of triangles in computational grid (Nagtegaal et al. 1974).

3. Errors in evaluation of the constitutive equation also occur for highly distorted elements, especially if one-point integration is used. One cell or element covering a large region undergoing large, rapid deformation will average, or diffuse, material history.

The general solution to the large distortion problem is rezoning. A new mesh is overlaid on the distorted one; mass, momentum, energy, and the constitutive equation are conserved and the calculation continued. There is an excellent discussion of rezoning (indeed of Lagrangian computations in general) in the article by Herrmann and Bertholf (1983). Although rezoning solves the large distortion problems and allows a calculation to continue, there are penalties to be paid. Frequent rezones average the material histories of several distorted elements into a single large element, thus making the mesh semi-Eulerian. Indeed, if rezoning were performed each cycle, the mesh would be Eulerian. Although many codes now have automatic rezoners, some user

Lagrangian System

Mesh Distortion

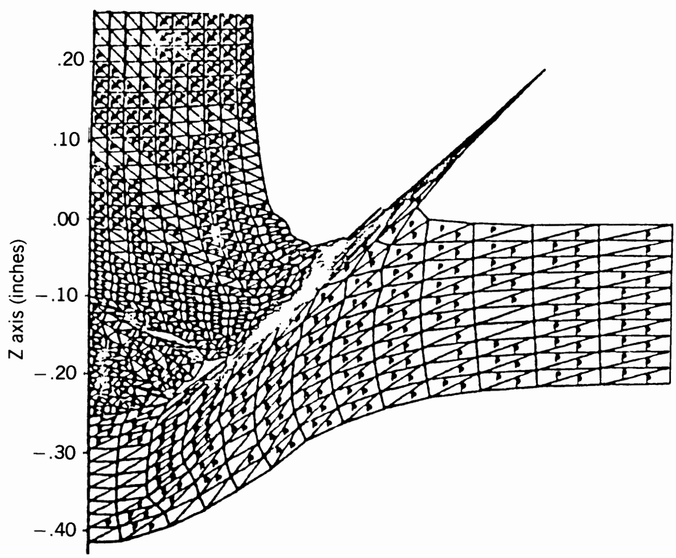

Large mesh distortions → Large truncation errors.

Rezoning: Overlay new grid on old.
Map mesh quantities of old grid to new.
Satisfy:
Mass, momentum energy conservation.
Constitutive equations.

Figure 15. Mesh distortion.

intervention is still required to assure that the rezoner is functioning properly. As with slidelines, success is directly dependent on the experience of the code user.

Most codes employ criteria based on energy or time step reaching a critical value to activate the rezoning logic. Once the criterion is met, a restart file is written to a mass storage device, either user assisted or automatic rezoning is performed, and the calculation then continues until the rezoning criterion is again met. An example of a rezone operation, taken from Weickert (1983), is shown in Figure 16.

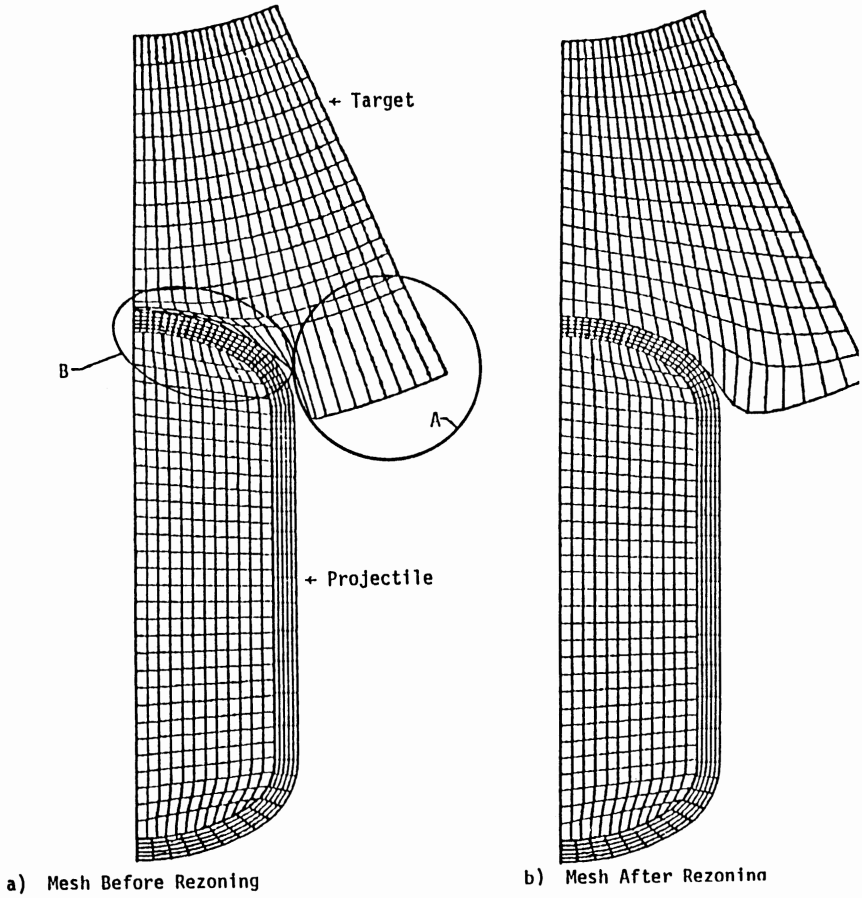

Figure 16. Rezoning (Weickert 1973).

Another technique for dealing with large distortions in situations for which the large deformations are highly localized (i.e., high-velocity penetration problems) is referred to in the literature as "eroding slidelines." The term *erosion* in this context does not refer to a physical failure mechanism. Rather, it describes bookkeeping procedures that allow *redefinition* of master and slave surfaces in the course of a computation where very large, localized, distortions occur. The overall result makes it appear that the penetrator and target are "eroding."

The Lagrangian codes developed in the 1970s required that the contact surface or sliding interface specified at the beginning of the problem remain unchanged throughout. This requirement was imposed not from physical considerations but to simplify the interface logic. Its effect was to prohibit total failure of material dictated by the physical problem, resulting in either unrealistic distortions of the computational mesh leading to large truncation

errors or to temporal integration increments that render further computation uneconomical.

The eroding contact surface concept has been under active investigation at a number of centers since 1978 and is now finding its way into production codes. The most comprehensive treatment is to be found in the DYSMAS/L code developed by Massmann, Poth, and their associates at Industrieanlagen-Betriebsgesellschaft mbH (Ottobrun, West Germany). The contact processor in DYSMAS/L is based on a generalized master–slave concept. Structural surfaces that are to be controlled by the contact processor are defined as master planes and slave points. Both master surface erosion and internal cracking can be treated. In the case of element separation (crack opening) the separated nodal masses of the affected elements are designated as slave points to permit calculation of momentum exchange in case of further contact. Redefinition of the contact surface in case of erosion or cracking is treated automatically, requiring no user intervention.

Methods for dynamic redefinition of sliding interfaces in the presence of total element failure have also been developed by G. R. Johnson. The earlier approach, implemented in the EPIC-3 code, had several limitations and restrictions (i.e., only obliquities of 45° or less could be treated, and users had to specify a priori the extent of target damage) and has not been used extensively. Many of these have been removed from the techniques now used in current versions of EPIC-2 and EPIC-3. Snow implemented logic to dynamically redefine the master surface as element failure occurs in the EPIC-2 code. The approach retained the requirement in the original version of

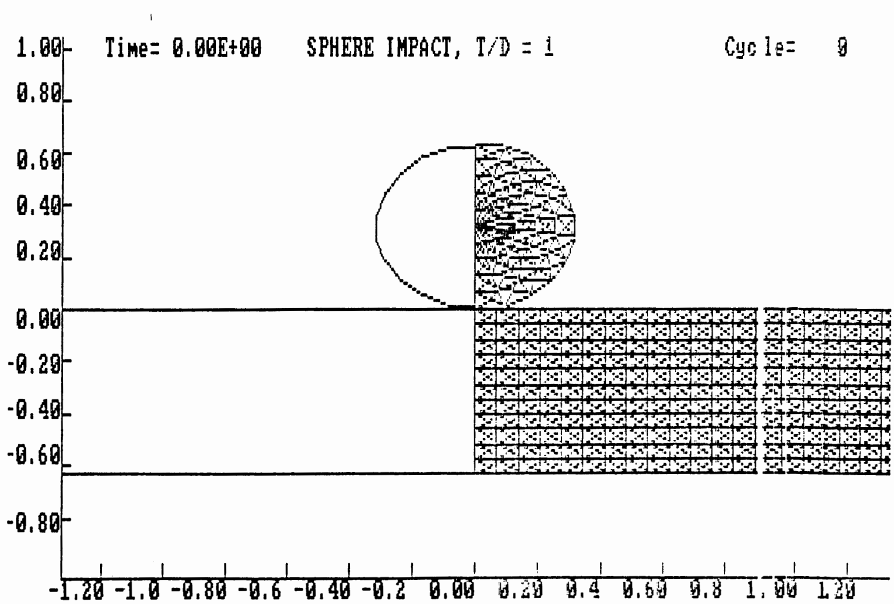

Figure 17. Initial configuration.

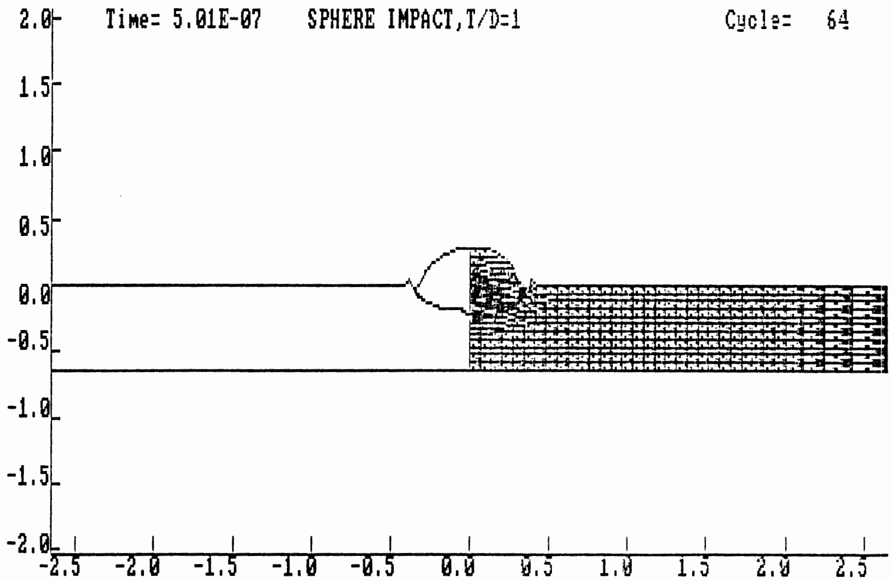

Figure 18. Deformation at 0.5 μs after impact.

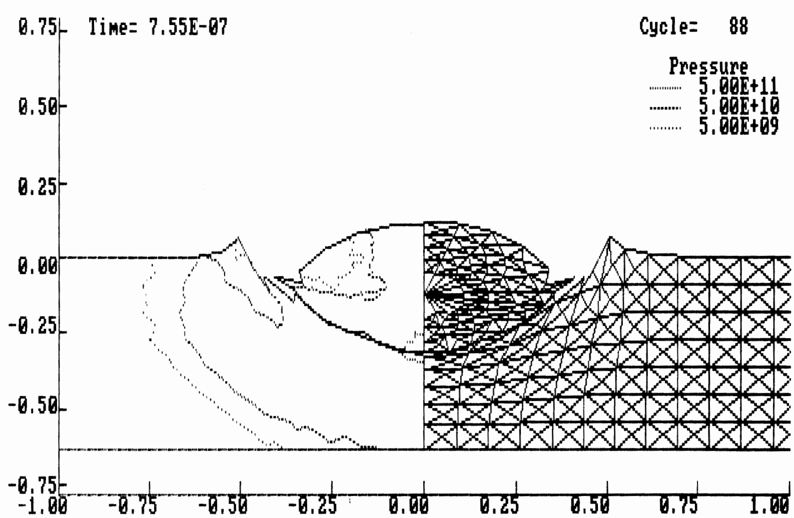

Figure 19. Pressure contours and deformation 0.75 μs after impact.

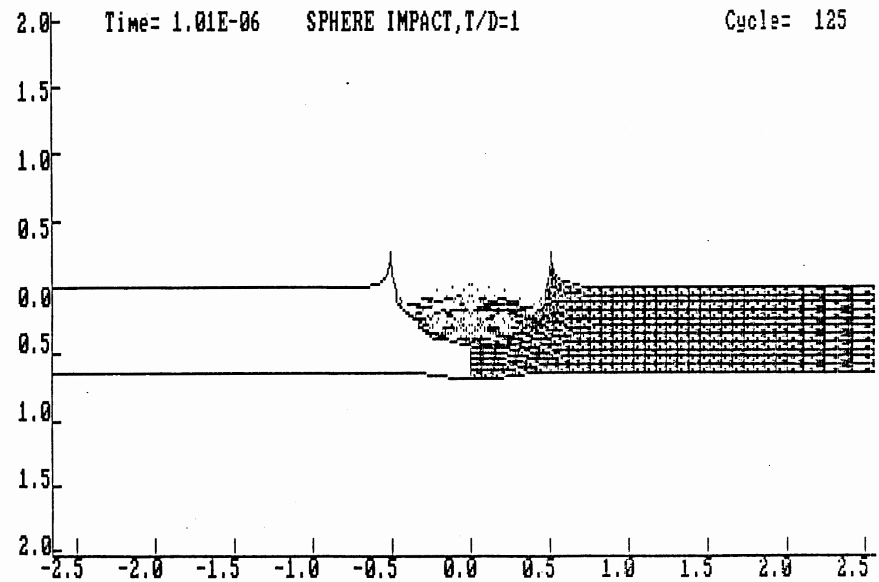

Figure 20. Deformation and projectile breakup at 1 μs after impact.

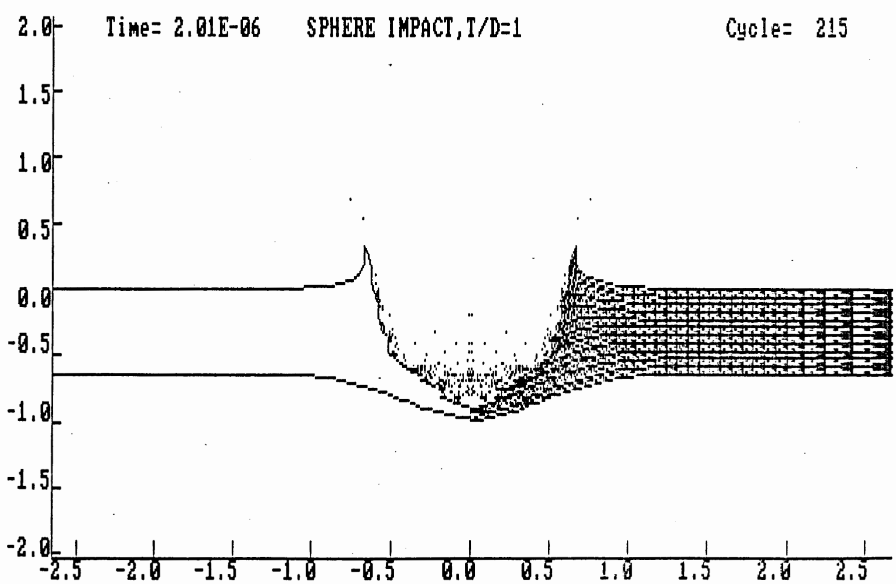

Figure 21. Hole growth at 2 μs after impact.

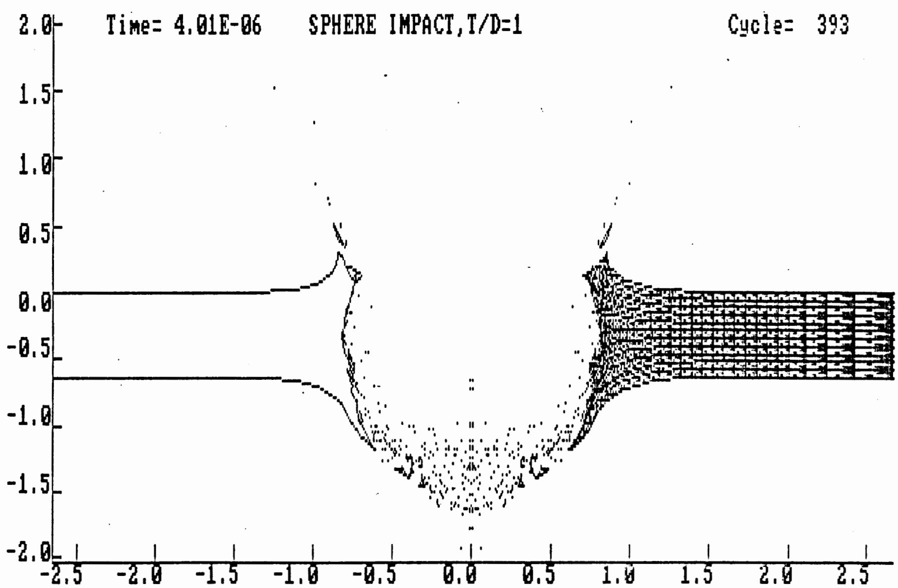

Figure 22. Hole growth and perforation at 4 μs after impact.

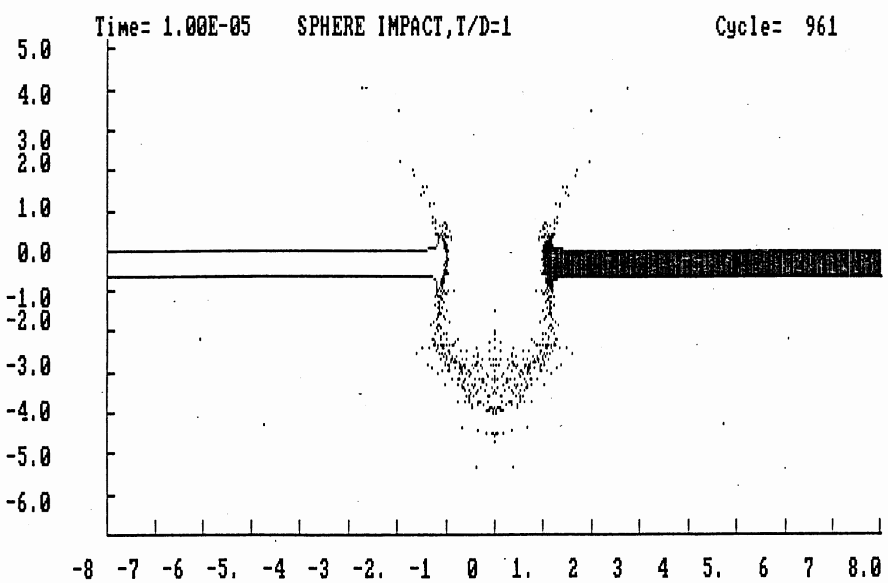

Figure 23. Crater and projectile debris, 10 μs after impact.

the code that the master surface remain continuous and employed an asymmetric interface treatment. Most recently Belytschko has introduced eroding contact surface concepts into the EPIC-3 code, making use of an eight-node hexahedral elements and hourglass viscosity to stabilize spurious deformation modes caused by one-point integrations. References to the above, as well as an alternative treatment of contact surface erosion are given by Kimsey and

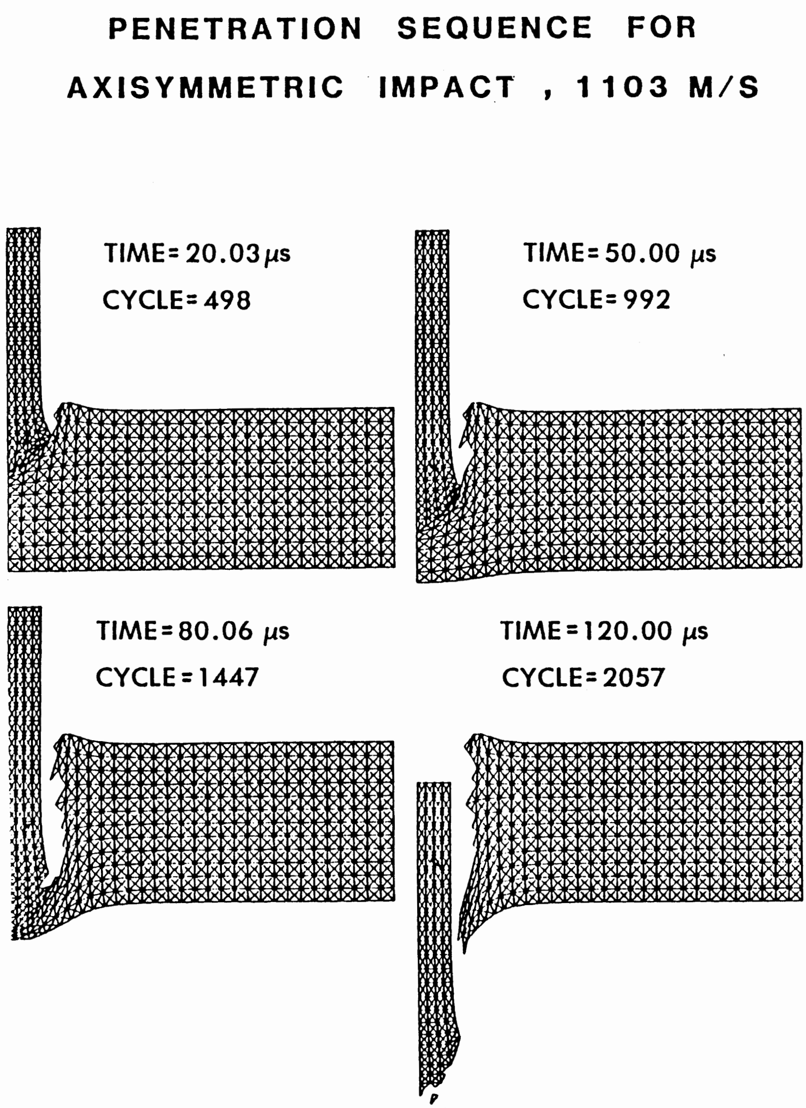

Figure 24. Finite thickness plate perforation at normal incidence.

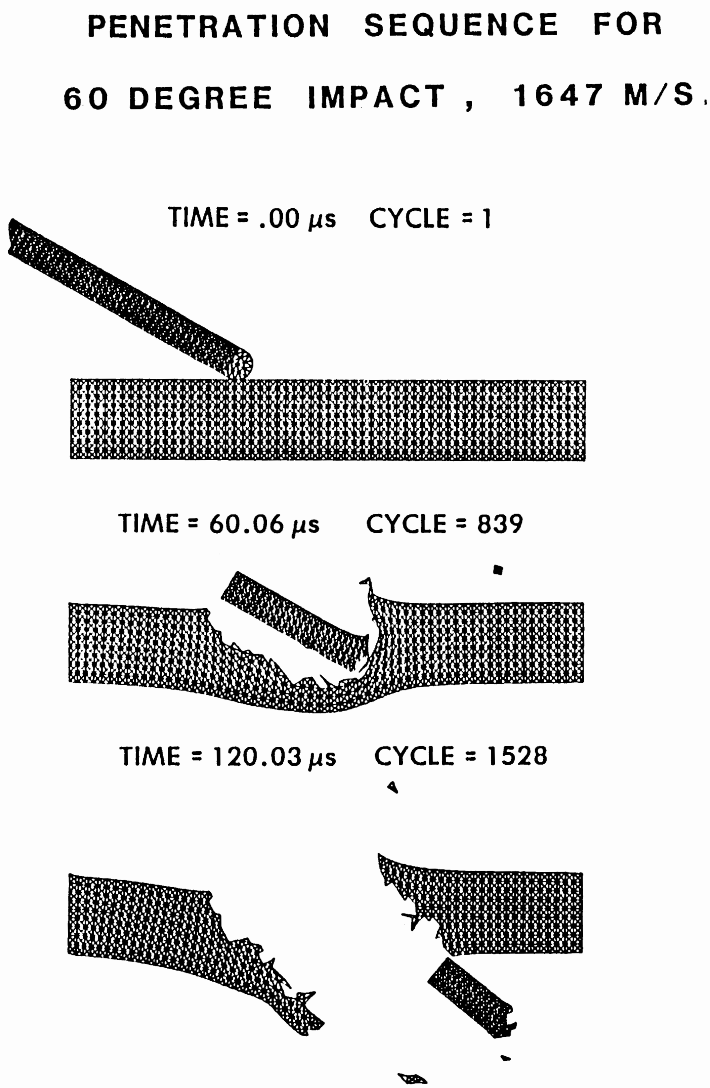

Figure 25. Finite thickness plate perforation at oblique incidence.

Zukas (1984, 1986). Ringers (1983) developed a variant of the sliding interface logic in the DYSMAS code (see Chapter 12) to treat plugging problems.

Figures 17–23 show results of a calculation performed with the ZEUS code for the case of an aluminum sphere striking an aluminum target at 7 km/s. Figures 24 and 25 show normal and (plane strain) oblique calculations performed with EPIC-2. Table 14 compares experimental and computational results for the EPIC-2 calculations. In general, excellent agreement is obtained for the normal impact cases. The quantitative agreement is poor for the plane

TABLE 14. Calculated and Measured Residual Parameters[a]

		Residual Velocity (m/s)		Residual Mass (g)	
θ	V_s (m/s)	Calculated	Measured[a]	Calculated	Measured[b]
0°	1219	925	910	34.5	39.1[c]
0°	1103	709	690	32.1	32.7
60°	1647	1202	1145	22.9	16.8

[a]Parameters used: $L/D = 10$; 65 g; $D = 1.0$ cm.
[b]Reference ARBRL-TR-02072, May 1978.
[c]Estimated from radiograph.

strain case, as one would expect, although qualitatively the results are reasonable.

Recall that with any sliding interface algorithm, acceptance is based on a large number of successes, there being no theoretical basis to guarantee convergence of interface algorithms to correct (unique) physical results. Calculations performed thus far with erosion algorithms show good agreement with experiment for the limited class of problems for which they were designed. Many more comparisons need to be made to establish confidence in the method.

For problems in which large distortions predominate or where mixing of materials initially separated occurs, an Eulerian description of material behavior is necessary. In the Eulerian approach, the computational grid is fixed in space while material passes through it (Figure 13). Material can be represented as either discrete points or a continuum. A number of approaches are available in existing Eulerian codes. In one, the material transport terms are included in the difference algorithm for the partial derivatives for the outset, for example, Roache (1972). In another, at each time step a Lagrangian calculation is performed, followed by a separate calculation of the convective transport terms, which in effect resembles a rezone of a distorted Lagrangian grid back to the undistorted Eulerian grid, for example, Hageman et al. (1975) and Matuska and Durrett (1978).

Unless special provisions are made for locating material surfaces and interfaces, these will diffuse rapidly throughout the computational grid. A number of techniques have been invented. In one technique, the actual positions of surfaces and interfaces are calculated by introducing massless Lagrangian tracer particles. Such particles can also be used to provide material history data, but this introduces considerable computational complexity and expense. Diffusion may also be limited by resorting to preferential transport of materials. In some techniques, care is taken to identify the materials being transported from the donor mesh to the acceptor mesh and to transport only one material until it is exhausted in the donor mesh. Material surfaces and interfaces are thereby defined only to within one mesh width, but they do not progressively diffuse.

11.4. NUMERICAL INTEGRATION

To complete the full discretization of our original partial differential equations, it is necessary to prescribe methods to discretize in time. Explicit time integration schemes are employed in wave propagation codes while implicit schemes are generally used for problems in structural dynamics.

Time integration methods are discussed in Section 10.4 of Zukas et al. (1982) as well as in excellent articles by Key, Belytschko, and Owen in Donea (1980). The articles by Belytschko, Hughes and Geradin, Hogge and Idelson in Belytschko and Hughes (1983) are also well worth reading.

Methods for integrating the discretized equations of continuum mechanics are called *explicit* if displacements at some time $t + \Delta t$ in the computational cycle are independent of the accelerations at the time. Table 15 gives a flow chart for explicit integration. Note that both velocities and displacements are computed in terms of quantities known at the previous time step. This is in effect a central difference algorithm in time and is very simple to program.

The computed response may become unstable (grow without bound) in explicit integrations unless care is taken to restrict the size of the time step. This problem has been studied rigorously for linear problems by Courant, Friedrichs, and Lewy (1928), who found that in explicity integration the computation will be stable if the time step Δt satisfies the relation

$$\Delta t \leq \frac{2}{\omega}, \tag{19}$$

where ω is the highest natural frequency of the mesh. No rigorous stability

TABLE 15. Numerical Integration Flow Chart for Explicit Integration Scheme

1. Set initial conditions ($t = t_0$)
   Velocities [$\dot{u}(t)$]
   Displacements [$u(t)$]
2. Find $\dot{u}(t + \Delta t/2)$, $u(t + \Delta t)$ from

$$\begin{aligned} u(t + \Delta t) &= u(t) + \Delta t[\dot{u}(t + \Delta t/2)] \\ \dot{u}(t + \Delta t/2) &= \dot{u}(t - \Delta t/2) + \Delta t[\ddot{u}(t)] \end{aligned}$$

3. Find internal nodal forces by looping through all elements in mesh
   Compute strain rates and strains
   Compute stresses from constitutive law
   Find nodal forces from element stresses
4. Compute external load nodal forces
5. Find $\ddot{u}(t + \Delta t)$ from equations of motion
6. Increment forward in time ($t = t + \Delta t$)
7. Go to 2.

criterion has been determined for nonlinear problems, but it is customary to determine the time step from

$$\Delta t = \frac{kl}{c}, \tag{20}$$

where l is the minimum mesh dimension in the computational grid, c the sonic velocity, and k a factor chosen to be less than unity, generally between 0.6 and 0.9.

In an implicit scheme, the displacements at any time $t + \Delta t$ cannot be obtained without a knowledge of the accelerations at the same time. The relationships among velocity, displacement, and accelerations must be combined with the equations of motion and the resulting set of simultaneous equations solved for the displacements. The resulting nonlinear equations are generally solved by some kind of linearization method. Among the most popular methods are predictor–corrector schemes, trapezoidal techniques such as Houbolt's method, the Wilson method, and the Newmark method (see the references cited previously).

Many implicit methods have been shown to be unconditionally stable. However, the price of stability is the need to solve a set of equations at each time step. The local truncation error of most implicit and explicit schemes is of order Δt^3. While this is insignificant for explicit schemes, it is a matter of concern for implicit methods where the time step is so much larger.

Problems involving high-velocity impact (0.5–2 km/s) result in a strong initial shock wave (alternatively, a large stress or velocity gradient) that can lead to material failure and must be accurately resolved. This demands fine spatial as well as temporal resolution and results in very small time steps and a large number of computational cycles.

Typically, for design problems, computations must be run to tens or hundreds of wave transit times across the characteristic length dimension of the problem. As a general rule, it has been found that, for wave propagation problems, the time step for implicit methods must be about the same as that for explicit methods to satisfy accuracy requirements. Since implicit methods require considerably more computations per cycle than explicit integrations, their use had generally been limited to problems where the details of wave propagation are not as significant as the overall response of the material.

11.5. ARTIFICIAL VISCOSITY

A characteristic of high-amplitude wave propagation in solids is the presence of shock waves. Even if shocks are not introduced by intial or boundary conditions, they may arise spontaneously in the body by the steepening of compressive waves due to the nonlinear response of the material.

Shock waves are mathematical discontinuities. The formulation of Section 1 is predicated on the assumption that we are dealing with a continuum. This contradiction was resolved by von Neumann and Richtmyer (1950) who introduced the concept of an "artificial viscosity," added to the pressure term from an equation of state, that has the effect of smearing a shock wave over several mesh widths, thus converting it to a step stress gradient that continuum formulations can accommodate. There is some distortion of the solution, but it is localized in the neighborhood of the shock wave and permits the convenience of retaining a continuum description of the process.

Other methods—natural viscosity, internal floating boundaries—could be used to track shock waves. Internal boundary, or shock-matching logic, has been tried in one-dimensional calculations but proves to be intractable in two- and especially three-dimensional calculations. Natural viscosity is a very small quantity for most materials. It would not spread shock fronts significantly and still require extremely small mesh sizes (and a large number of cells/elements) to adequately resolve each shock front. Thus, the von Neumann and Richtmayer approach has been incorporated in existing production codes. In order to diffuse the shock wave and damp spurious oscillations, a two-term viscosity expression

$$q = c_1 \rho c \, \Delta x \left| \frac{d\dot{x}}{dx} \right| - c_2^2 \rho (\Delta x)^2 \left| \frac{d\dot{x}}{dx} \right| \frac{d\dot{x}}{dx} \tag{21}$$

is added to the equation of state. The coefficients c_1 and c_2 are specified by the user. The linear coefficient c_1 is typically in the range of 0.05–0.5 while the quadratic coefficient c_2 is typically set at 2. The effect of the q term is to diffuse a shock front over approximately four cells/elements and to suppress spurious oscillations behind the shock front. The solution is thus compromised locally (we solve for a finite but steep pressure gradient that a continuum formulation can handle instead of a pressure discontinuity that cannot be accommodated) for the purpose of retaining the advantages of a continuum formulation but is unaffected some distance away from the front.

Figures 26–29 show the effects of varying the linear coefficient for an elastic impact of a steel rod onto a rigid surface at 10 ft/sec. It is clear that use of excessive viscosity can overdamp a solution and suppress meaningful information. The effect is very much mesh size dependent. Artificial viscosity should be used with great care. Calculations with very fine resolution may not need it, nor calculations where extreme gradients do not exist. Use of excessive viscosity in coarsely gridded calculations, especially those involving energetic materials, will cause disturbances to propagate at high, nonphysical rates and can lead to instabilities. Experience is the key to success.

The artificial viscosity method is discussed very lucidly in the report by Noh (1976) and paper by Wilkins (1980) who derives extensions of Eq. (21) to two- and three-dimensional cases. Both should be in your library.

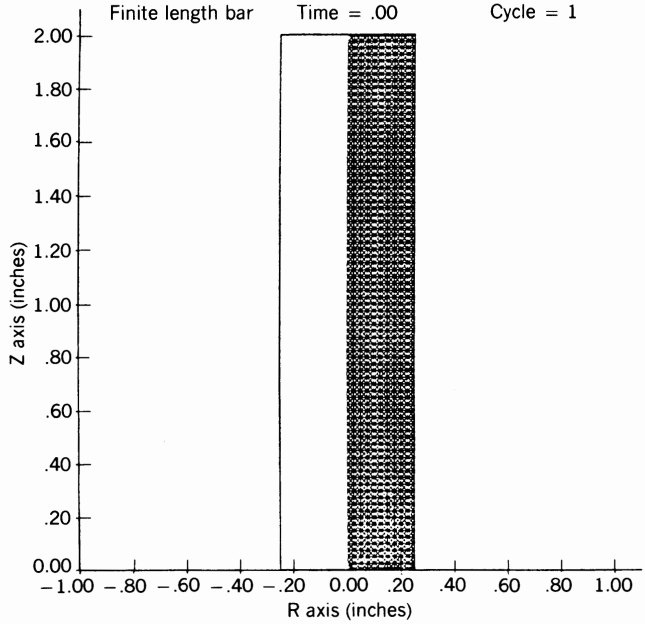

Figure 26. Initial geometry.

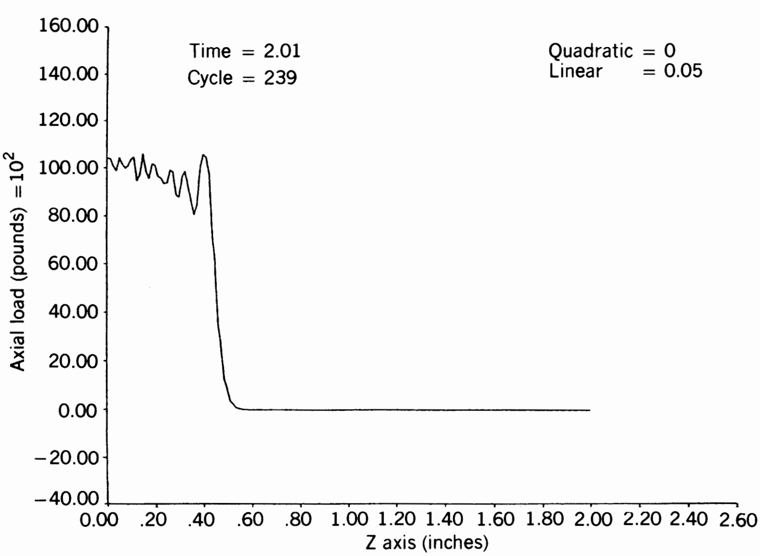

Figure 27. Axial force versus distance.

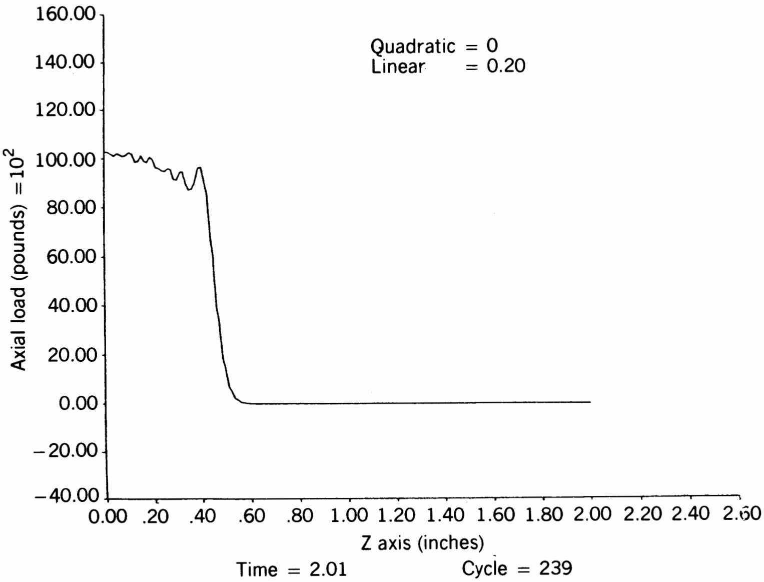

Figure 28. Axial force versus distance.

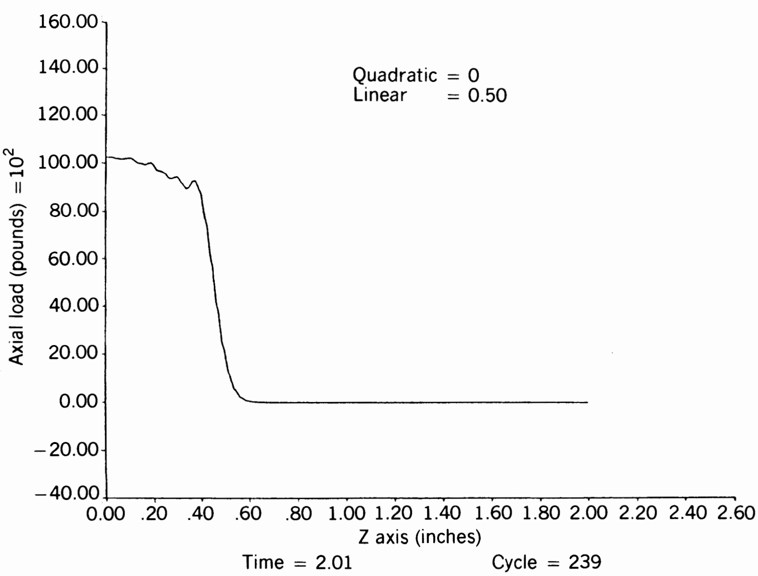

Figure 29. Axial force versus distance.

In addition to the von Neumann–Richtmyer viscosity, another type of viscosity, referred to as hourglass or tensor viscosity, is used in computer programs with underintegrated elements. As an example, a four-node quadrilateral element should be integrated using a 2×2 Gauss quadrature rule (i.e., the constitutive equation is evaluated at four points in the element). This, however, is computationally expensive and in some situations leads to stiff results. To save time and money, it is possible to evaluate the stresses and strains at one point in the element—the center. This makes for economical calculations but results in certain types of motions in two and three dimensions that are not resisted by internal forces. An example is the velocity field shown in Figure 30, which leads to an hourglass-type instability not resisted by either internal element forces or the von Neumann-type viscosity. To retain the advantages and economics of one-point integration but counter destabilizing motions, viscosity expressions are introduced for the purpose of mesh stabilization. No one method has achieved universal acceptance as yet. Various schemes have been proposed by Wilkins (1980), Park (1984), Belytschko et al. (1984), Belytschko and Lin (1985), Jacquotte and Oden (1984), Flanagan and Belytschko (1981), Kosloff and Frazier (1978), Belytschko and Liu (1983, 1986), Schulz (1985), Schulz and Heimdahl (1986), and Verhegghe and Powell (1986).

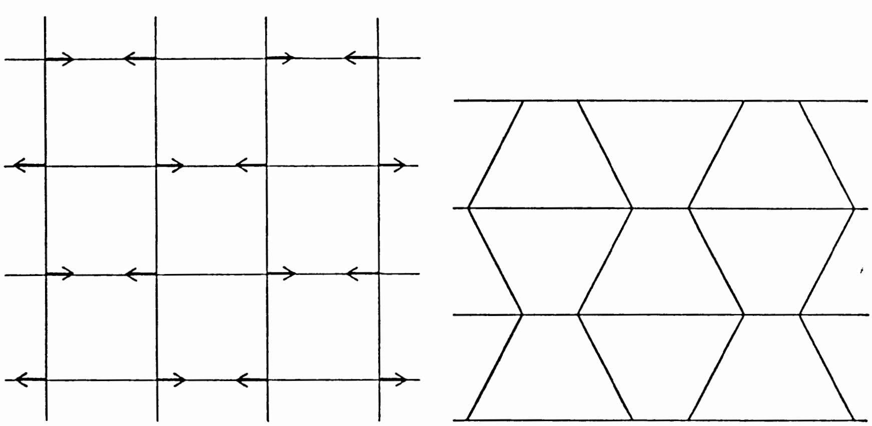

Figure 30. Hourglass distortions.

11.6. MATERIAL MODELS

A. Metals

It is the practice in current production codes for wave propagation and impact problems to divide the response of the material into volumetric and deviatoric parts and to treat these independently.

The volumetric behavior is described in terms of an equation of state relating pressure, volume, and some thermal parameter, usually the internal energy or temperature. The Mie–Grüneisen equation of state is favored for impacts below the speed of sound, while the Tillotson equation (see Section 1) tends to be used for hypervelocity impact studies.

For solid–solid impacts in the 0.5–2 km/s velocity regime, only moderate pressures (300–500 kbars) are generated, and these decay rapidly to values comparable to the strength of the material. Hence, in this regime, the equation of state is of secondary importance. A good description of material behavior at high strain rates and a good failure model (if failure dominates the response) are crucial for successful calculations. Data to drive these models must come from a wave propagation experiment. Entirely erroneous results will be obtained if quasistatic data are used. See Kimsey and Zukas (1986) for an illustration. For impacts above the speed of sound, high pressures dominate throughout the event. Material strength is of importance only in the late stages of the response and can well be approximated by an elastic–perfectly plastic model with the yield strength obtained from a dynamic (wave propagation) experiment. There are a number of collections of equation of state data, namely, Kohn (1969), van Thiel (1977), and Marsh (1980). If material data are not available in existing compilations, techniques for rapid and accurate characterization exist.

An incremental elastic-plastic formulation is used to describe the shear response of metals in present finite-difference and finite-element codes. The plasticity descriptions are based on an assumed decomposition of the velocity strain tensor, $\dot{\boldsymbol{\varepsilon}}$, into elastic and plastic parts

$$\dot{\boldsymbol{\varepsilon}} = \dot{\boldsymbol{\varepsilon}}^e + \dot{\boldsymbol{\varepsilon}}^P \tag{22}$$

together with incompressibility of the plastic part. The von Mises yield criterion, and Prandtl–Reuss flow rules are used to represent plastic behavior. Excellent descriptions of material modeling in computer codes have been written by Wilkins (1984a, 1984b). A generic stress–strain curve for metals is shown in Figure 31. The constitutive model for metals is summarized in Table 16.

A variant on this approach is the model proposed by Steinberg et al. (1980). Their model, for use at high strain rates where saturation has occurred and rate effects no longer dominate, assumes that the shear modulus and yield

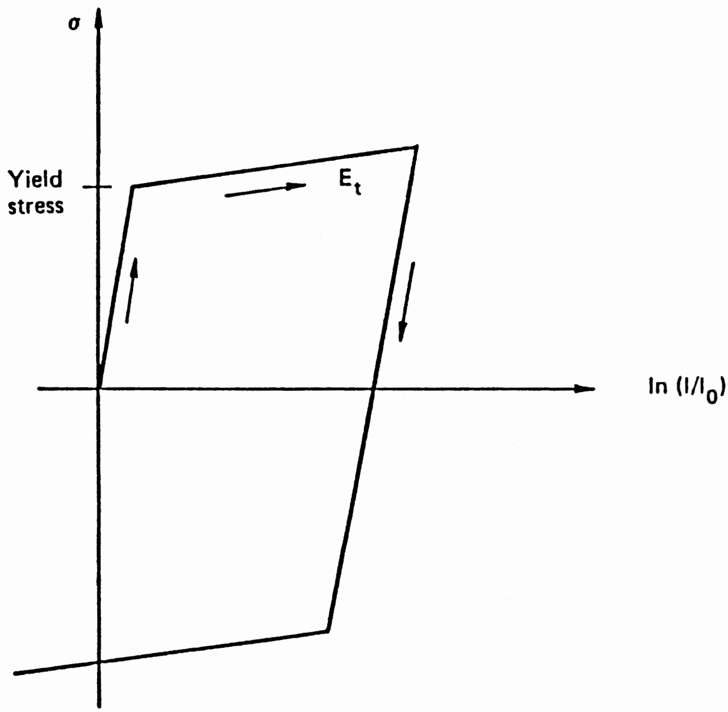

Figure 31. Generic stress–strain curve for metallic materials.

TABLE 16. Constitutive Model for Metals

Volumetric	Shear
$P = P(\rho, E)$	$\dot{s}_{ij} = 2G(\dot{\varepsilon}_{ij} - \frac{1}{3}\delta_{ij}\dot{u}_{k,k,})$
Tillotson	$\dot{\varepsilon}_{ij} = \frac{1}{2}(\dot{u}_{i,j} + \dot{u}_{j,i})$
Mie–Grüneisen	
Ad hoc for Explosives Concrete Geological materials	$\sigma_{ij} = s_{ij} - \delta_{ij}(P + q)$ $s_{ij}s_{ij} \le \frac{2}{3}Y^2$ $s_{ij} = s_{ij}\left[\dfrac{2Y^2}{3s_{ij}s_{ij}}\right]^{1/2}$
	Provision for Strain hardening Thermal softening Compressibility effects

strength are functions of equivalent plastic strain, pressure, and internal energy. The parameters needed to implement the model were determined for 14 metals. The model was successful in reproducing measured stress and free surface velocity versus time data for a number of shock wave experiments.

B. Nonmetals

A variety of models, many ad hoc, exist for sand, rock, concrete, and other nonmetallic materials. They can broadly be grouped into two categories: (a) models based on the p–α model suggested by Herrmann (1969) and (b) CAP-type models. We will briefly outline each in turn.

A generic stress–strain curve for porous/crushable media is shown in Figure 32. Such models are designed to account for permanent loss of porosity and void volume produced by tensile failure. Figure 33 shows an implementation of such a model in the TENSOR code by Maenchen and Sack (1974). The crushable foam model is designed to account for the permanent loss of porosity as well as the void volume produced by tensile failure.

Referring to Figure 33, the material initially loads along the virgin path A. If the maximum compression is less than ζ_m, unloading also occurs along path

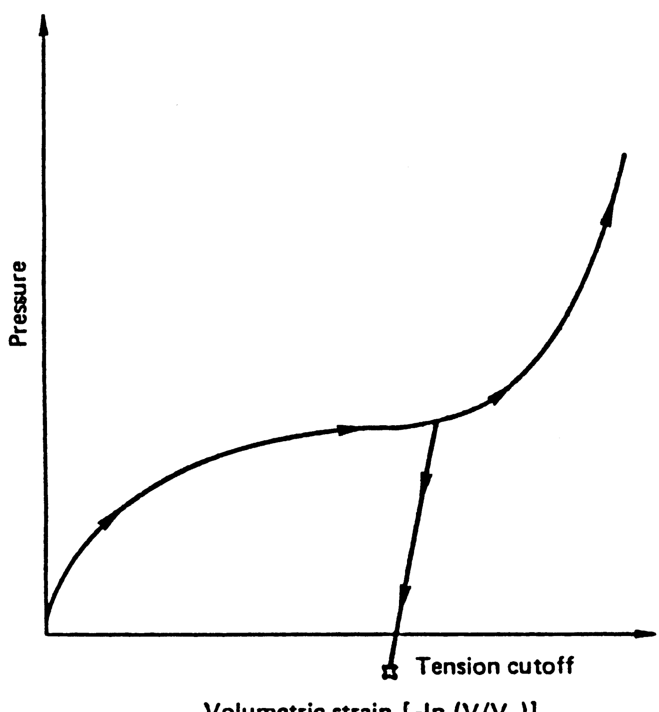

Figure 32. Generic stress–strain curve for porous crushable materials.

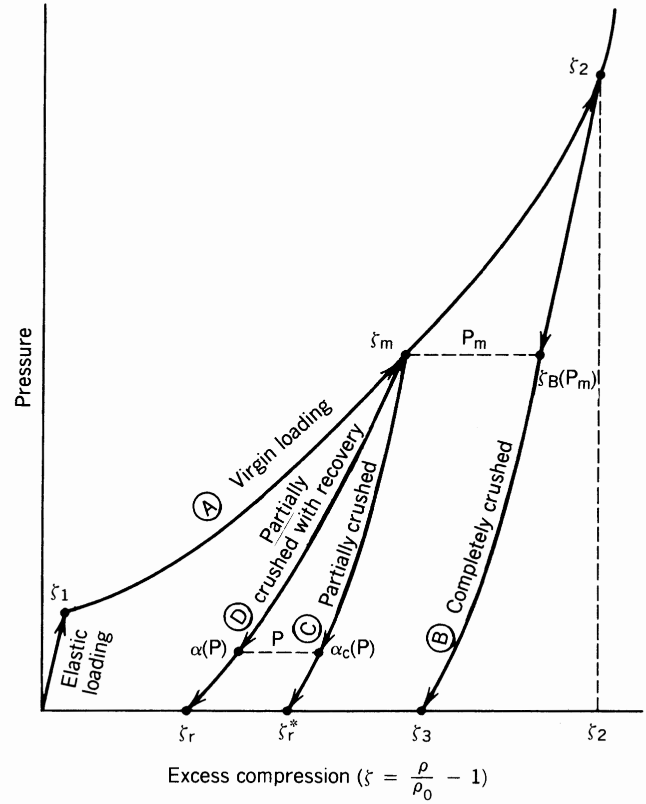

Figure 33. Crushable material model.

A. A totally crushed material would unload along path *B*. For partially crushed materials the unloading path would be *C* unless there is elastic recovery, in which case the unloading path becomes *D*. In order to create such a pressure–compression map, the points ζ_1, ζ_2, ζ_3 and the residual porosity α must be determined through laboratory tests, which can involve the iterative use of computations with an assumed constitutive model and indirect experiments. It is not a simple matter of looking up the data in a handbook. This general form has been adapted for concrete. This model is incorporated in the EPIC and HULL codes and described in the references cited for each code in the code survey chapter.

CAP-type models are also popular for describing the behavior of nonmetallic materials. A comprehensive description of the derivation of a CAP-type model for reinforced concrete as well as experiments to determine the necessary model parameters are given in the report by Gupta and Seaman (1979). Figure 34 shows a generic CAP model. Many porous materials yield under shear loading, compact irreversibly under compressive loading, and separate

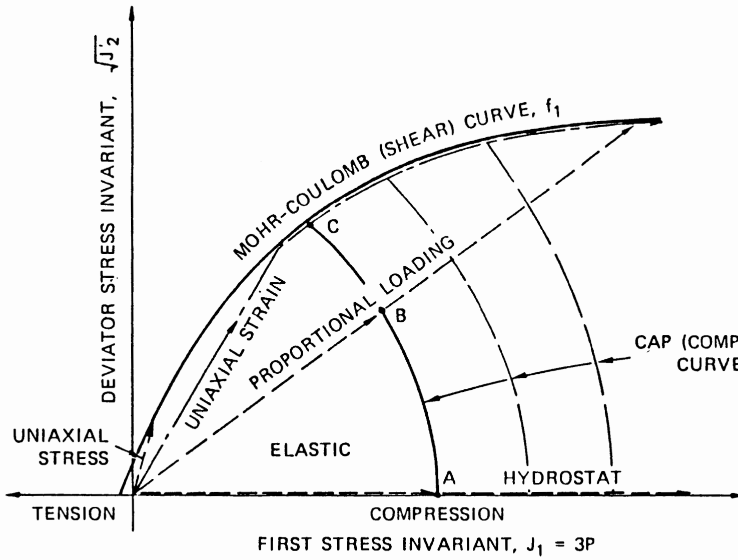

Figure 34. Generic CAP model.

in tension. In concrete and rock materials, the shear strength increases with increasing pressure. Also, increasing shear stress reduces the resistance to compaction. This shear-enhanced compaction is common to porous materials . The stiffness of the material also increases with pressure, hence the elastic moduli are a function of the stress state. This behavior is described by CAP models, which generally include the following:

Elastic stress–strain relations, including variation of the moduli from initial loading to consolidation

Mohr–Coulomb (or shear) curve, including plastic stress–strain relations on the curve

CAP curve, including plastic stress–strain relations on the CAP curve and description of the strain hardening of the CAP curve

Tensile curve, which is the continuation of the Mohr–Coulomb curve into the tension region, stress–strain relation and stress reduction on the curve, and a fracture and separation process.

The Gupta and Seaman model is outlined in Table 17.

11.7. MATERIAL FAILURE

This section concentrates on the description of material failure in two- and three-dimensional finite-difference and finite-element computer programs that

TABLE 17. Material Models

Cap Model: Continuum incremental plasticity theory for concrete and geological materials using two yield curves

1. Mohr–Coulomb curve accounts for yielding and dilation

$$F_1 = \sqrt{J_2'} - [A_1 + A_2 \exp(J_1/A_3) + A_4 \exp(J_1/A_5)]$$

where A_1–A_5 experimentally determined parameters

$$\begin{aligned} J_1 &= 3P = \Sigma\sigma_{ij} \\ J_2 &= \tfrac{1}{2}\Sigma s_{ij} s_{ij} \\ s_{ij} &= \sigma_{ij} - P\delta_{ij} \end{aligned}$$

2. Cap curve accounts for compaction

$$F_2 = J_1^2/9 + J_2'/W^2 - P_H^2(\varepsilon_v^p)$$

where

$$\begin{aligned} \varepsilon_v^p &= \Sigma\varepsilon_{ii}^p \\ P_H &= \text{pressure on hydrostat} \\ W &= \text{parameter from experiments} \end{aligned}$$

Inside the cap, material behaves elastically according to

$$\begin{aligned} dP &= K \Sigma\, d\varepsilon_{ii}^E \\ ds_{ij} &= 2G\, d\varepsilon_{ij}'^E \\ d\varepsilon_{ij}'^E &= d\varepsilon_{ij}^E - \tfrac{1}{3}\delta_{ij}(\Sigma\, d\varepsilon_{ii}^E) \end{aligned}$$

where

$$\begin{aligned} P &= \text{hydrostatic pressure} \\ K &= \text{bulk modulus} \\ s_{ij} &= \text{deviatoric stress} \\ \varepsilon_{ij}' &= \text{deviatoric strain} \\ \varepsilon_{ij}^E &= \text{elastic strain} \end{aligned}$$

Yield functions F_1, F_2 are defined so that

$$\begin{aligned} F(\sigma_{ij}) &= 0 \text{ at yielding} \\ F(\sigma_{ij}) &< 0 \text{ denotes elastic behavior} \\ F(\sigma_{ij}) &> 0 \text{ are inaccessible states} \end{aligned}$$

From Gupta and Seaman (1979).

model the response of materials to short-duration loading. For the most part, attention will be restricted to metals and metallic structures.

A solid on which a deformation is imposed at an arbitrary rate can accommodate this deformation by six basic modes (Curran et al. 1977): elastic distortion, homogeneous plastic flow, phase changes, nucleation and growth of ductile microvoids, nucleation and growth of brittle microcracks, and nucleation and growth of shear instabilities. The last four processes can lead to material failure. In many situations involving high loading rates—that is, the integrity of nuclear reactor pressure vessels, crashworthiness of vehicles, design of containment structures, protection of spacecraft from meteoroid impact—any or all of these modes may be excited although not necessarily simultaneously. A complete mathematical description of the dynamics of impacting solids must account for the geometry of the interacting bodies; elastic, plastic, and shock wave propagation; hydrodynamic flow; finite strains, typically exceeding 60%; thermal and frictional effects as well as the initiation and propagation of failure.

The effects observed in colliding solids can be characterized in many ways on the basis of a number of parameters [see, e.g., Backman and Goldsmith (1978), Johnson (1972), and Zukas et al. (1982) as well as the simplified approach given earlier].

Loading of the type described can lead to various failure mechanisms some of which are shown in Figure 35. Although one of these may dominate, it is not unusual for several modes to be active in situations involving long event times. For a comprehensive discussion of factors leading to material failure under impact loading see Woodward (1987a, 1987b) as well as Chapters 5 and 9 of Zukas et al. (1982).

Analytical modeling of hypervelocity events is relatively straightforward. In numerical simulations, the accuracy achievable and the problems addressable are limited mainly by the speed and memory of the computer. The compressible fluid analogy serves well for many practical engineering applications. In addition, a large number of semi-analytical models for penetration (e.g., Walters and Majerus (1980), radial hole growth (e.g., Scott 1984; Perez 1982), and other aspects are available. In addition, a large collection of empirical models is available [see Backman and Goldsmith (1978) and Zukas et al. (1982) for examples and citations to the literature].

The greatest uncertainties are in the modeling of the explosive loading of thin structures, that is, jet and self-forging fragment formation. The adequacy of the plasticity model used in large-scale computations is a much more critical consideration than the mechanics of material failure, although the two are intimately coupled. Not yet resolved are questions of an adequate material model in the presence of large strains ($> 100\%$), temperatures approaching the melting temperature, and pressures well in excess of material strength for much of the event time. These questions are not likely to be resolved in the near future since controlled experiments under these conditions are nearly impossible to perform. Existing methods, using primarily X-ray radiography

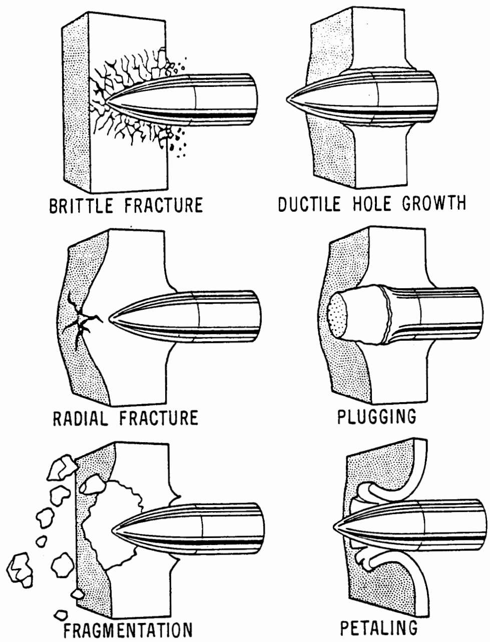

Figure 35. Failure modes in impacted plates (Backman 1976; Backman and Goldsmith 1978).

or X-ray cinematography [see Held (1988) and the references therein for a good description of the state of the art], yield only marginal data, mainly the exterior configuration of the jet or fragment. In engineering design, code calculations are combined with semi-analytical models to determine jet or fragment characteristics that are then used to assess penetration effects in various configurations.

In the high-velocity regime (often referred to as the ordnance velocity regime), the problem is complicated by the presence of boundaries, either as free surfaces or material interfaces. Very high pressures are generated on impact, but due to the presence of these surfaces they rapidly decay to the order of the material strength (except at the impact interface). Strain rates vary from above 10^5/s at the striker–target interface to 10^2–10^3/s in a zone of about 2–4 striker diameters, beyond which primarily elastic loading is encountered. For long rod impacts, the situation has been succinctly depicted by Wright (1983) (Figure 36) who also reviews analytical methods for such problems. Material failure, through a variety of mechanisms occurring at different stages of the penetration process, is a dominant feature of the response and requires careful consideration.

Many of the problems to which wave codes are applied result in damage where treatment of each crack individually becomes too difficult. Physically, material failure under high rate loading conditions can be thought of as a

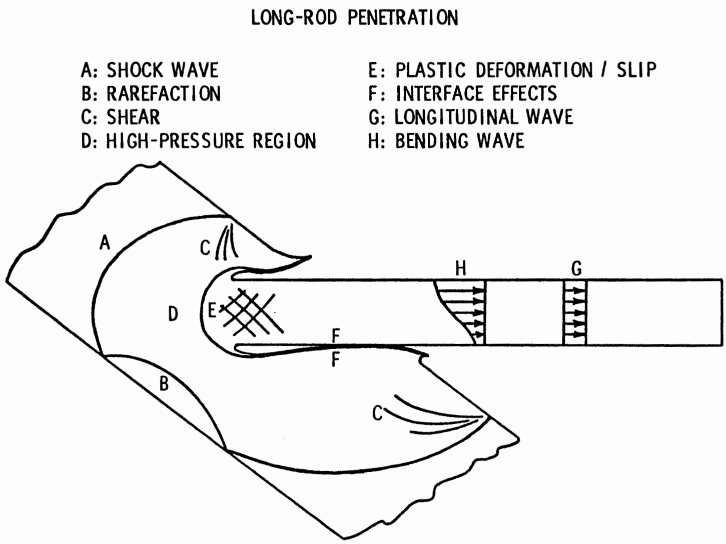

Figure 36. Long rod penetration mechanics (Wright 1983).

four-stage process (Seaman 1975):

1. Rapid nucleation of microfractures at a large number of locations in the material
2. Growth of the fracture nuclei in a rather symmetric manner
3. Coalescence of adjacent microfractures
4. Spallation or fragmentation by formation of one or more continuous fracture surfaces through the material

Ideally, failure prediction would be accomplished by treating some key measures of average microscopic void behavior as internal state variables in the constitutive relations for the material. Thus, in addition to the usual variables in continuum wave codes, microvoid concentration, and size distribution functions would be included in the description of the current state of the material. In this approach, the fracture process is built into the stress–strain relationship for the material (Curran 1982). When wave propagation codes first became available in the mid-1960s, such information was not available. Fracture was modeled, if at all, with very simple, time-independent criteria. Considerable effort has been expended in developing micromechanically based failure models for incorporation into continuum codes since then, especially in the last 10 years. However, no definitive model has yet emerged. Neither is a library of data available to drive the various models for materials of practical interest. Therefore, for want of an adequate data base for advanced failure models, most calculations are performed with the simplest failure models for

several reasons:

1. Material characterization costs are kept to a minimum.
2. Since material failure will be incorrectly modeled, it should be done so as simply and as cheaply as possible.
3. In many cases, simple models produce results in agreement with experiments.

It is now clearly established that the following material descriptors that most affect computational results are:

1. The flow stress, determined at a strain rate appropriate to the problem being considered
2. A good failure model *in those loading regimes where it is required*

Problems of accounting for dynamic material behavior and fracture are difficult but not insurmountable, even in view of our present limited knowledge. A practical approach has been suggested by the National Materials Advisory Board Committee on Materials Response to Ultra-High Loading Rates (NMAB 1980). It recommended an iterative procedure of successive refinements involving computations with existing relatively simple failure descriptions, dynamic material characterization employing relatively simple and standardized techniques, and experimentation to produce useful results for design purposes in many applications. The report suggests that

> rough computations, using simple material models with published or even estimated material properties, may be used in conjunction with exploratory test firings to scope an initial design. Comparison of test data with predictions may reveal discrepancies which suggest refinements in the computations or material models, and the need for some dynamic material property measurements. Once reasonable agreement has been achieved, another round of computations may then be performed to refine the design. Test firings of this design might use more detailed diagnostic instrumentation. This sequence is iterated, including successively more detail in computational models, material property tests and ordnance test firings, until a satisfactory design is achieved. In this procedure *unnecessarily detailed computations, material property studies or test firings are minimized*; only those details necessary to achieve a satisfactory design are included.

Failure Criteria and Post-failure Models

A number of different descriptions are available in computer codes to model failure of metals. Each involves a criterion for initiation and a prescription for the treatment of material in a computational cell or element once failure has occurred. For the most part, the initiation criterion is based on attainment of critical values of pressure, some measure of stress or strain, plastic work,

internal energy, or some combination of these. Current efforts are directed at development of cumulative criteria, dependent on the history of stress or strain. Models have also been developed that attempt to account explicitly for the nucleation and growth of voids, cracks, and shear bands. The initiation criteria used in representative production computer codes for wave propagation and impact problems are summarized in Table 18.

The simplest, and one of the earliest models, is the pressure cutoff. When the hydrostatic pressure (or mean stress) reaches a critical value in tension, failure is assumed to occur instantaneously. The pressure is not allowed to grow beyond this user-specified critical value and further expansion occurs at this value of mean stress. Any shear stresses in the computational element are set to zero. Recompression is permitted, and if this occurs the material can again carry compressive pressures.

Related to this are the volumetric strain ($V/V_0 - 1$) and maximum distension criteria, with postfailure modeled as already described. These criteria were first used in the early finite-difference codes developed to solve problems in the hypervelocity impact regime where hydrodynamic pressures dominate. They prove useful in situations where loading and response times are sufficiently brief so that micromechanical considerations may be ignored as a first-order approximation.

For situations where pressures are on the order of material strength for the bulk of the response time, initiation criteria based on some measure of stress (maximum principal stress, effective plastic stress) or strain (maximum principal strain, effective plastic strain, octahedral shear strain, or the second invariant of the strain deviator) have been more effective. Postfailure response has been modeled in a number of different ways. In the simplest approach, all stresses are set to zero instantaneously. In a variant of this, stresses may be relaxed to zero over several computational cycles. An approach gaining in popularity is the introduction of discrete free surfaces along failure planes to model such events as spall, fragmentation, or plugging. These free surfaces may either be introduced manually (e.g., Bertholf et al. 1975) or logic may be incorporated in the code to automatically permit void opening and closing (e.g., Trigg et al. 1981); Poth et al. 1981, 1983; Ringers 1983. Another approach assumes that the failure plane is normal to the maximum principal direction. The stress tensor calculated for undamaged material is then modified to account for the fact that the failure plane has been weakened (Bertholf et al. 1976). Compressive stresses may be transmitted if the opening subsequently closes in all these descriptions.

Some situations cannot be effectively addressed by models based on a single field variable. Successful use has been made of the so-called P/Y model, where P represents hydrodynamic pressure and Y the flow stress. This is based on the work of Hancock and MacKenzie (1976) who showed that the ductility of steel depends markedly on the triaxiality of the state of stress existing within the steel. The high hydrodynamic pressure present in many impact situations can have a strong effect on the strain to fracture. Combining

TABLE 18. Failure Initiation Criteria

Failure Criterion	Computer Code
	Instantaneous Criteria
Tensile pressure cutoff	All
Effective plastic strain	STEALTH, DYNA3D, EPIC-2, EPIC-3, PEPSI, DYSMAS, DEFEL, KEPIC, PISCES
Principal stress/principal strain	PEPSI, DYSMAS, HULL, TOODY IV
Volumetric strain/maximum distension	DYNA3D, EPIC-2, EPIC-3, DEFEL, KEPIC, DYSMAS, HELP, METRIC, CSQII, SOIL, DORF, PISCES 3DELK
Plastic work	TOODY IV, HELP
Internal energy	DYSMAS
Hancock–MacKenzie	HULL, PISCES 2DELK
	Cumulative Damage
Tuler–Butcher	Ad hoc in many codes; not production versions.
G. R. Johnson	EPIC-2
	Micromechanical Models
SRI NAG-FRAG-SNAG	CHEMP, TOODY IV (BFRACT), some versions of HELP
SANDIA models	Incorporated into in-house codes, mainly 1D.
LOS ALAMOS models	

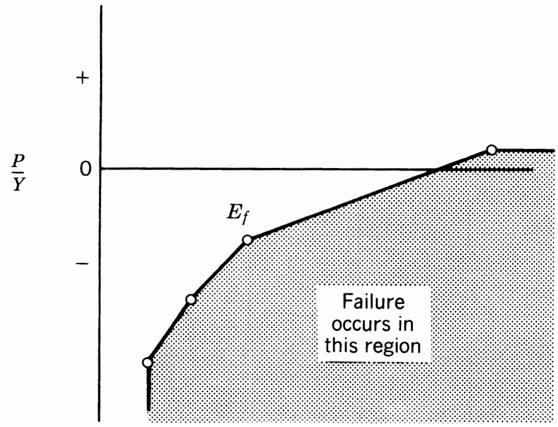

Hancock–MacKenzie (1976): $\varepsilon_f = f(\dot{\varepsilon}, T, P, \sigma)$
High-strength material:

$$\varepsilon_F = \alpha \exp\left(\frac{-3P}{2\bar{\sigma}}\right)$$

Substantial plastic flow before void nucleation:

$$\varepsilon_F = e_N + \alpha \exp\left(\frac{-3P}{2\bar{\sigma}}\right)$$

e_N = void nucleation strain

ε_F = maximum principal tensile strain

Figure 37. Hancock–MacKenzie model.

the effective stress

$$Y^2 = \tfrac{1}{2}\left[(\sigma_1 - \sigma_2)^2 + (\sigma_2 - \sigma_3)^2 + (\sigma_3 - \sigma_1)^2\right]$$

with the hydrodynamic pressure determined from an equation of state

$$P = f(\rho, I),$$

where ρ represents density and I the internal energy [or from $P = (\sigma_1 + \sigma_2 + \sigma_3)/3$ at lower loading levels] provides a single nondimensional parameter P/Y that gives a measure of the stress state triaxiality. In this model the plastic strain and the state of stress, as characterized by P/Y, become the field variables characterizing fracture (Figure 37).

The determination of P/Y versus effective plastic strain curves is straightforward (Nash and Cullis 1984; Matuska and Osborn 1981). A typical example for rolled homogeneous armor is shown in Figure 38. This criterion has

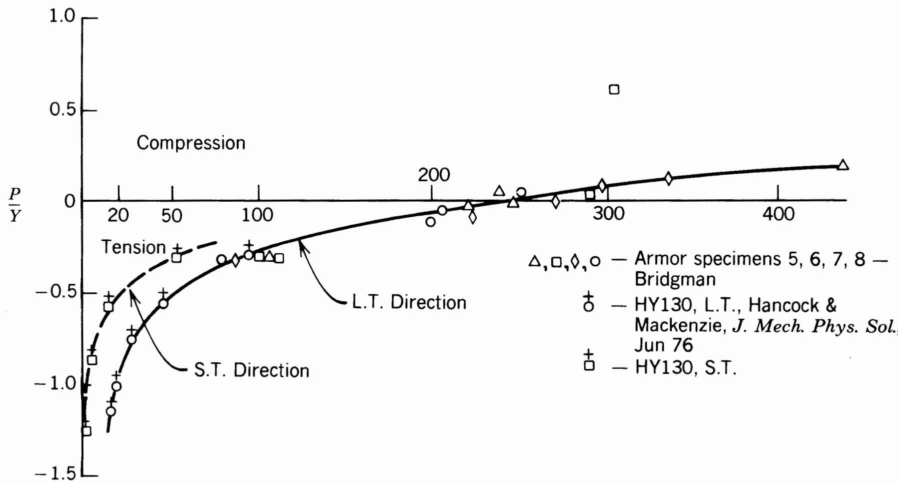

Figure 38. Room temperature failure strain for armor steels.

been incorporated in the HULL code (Matuska and Durrett 1978, Matuska et al. 1982). Material fracture is simulated by relaxing a failed material cell to its ambient density. A numerically significant quantity of void is introduced into the cell and allowed to grow or recompress depending on the loading. The stress tensor is modified to account for the changing volume of damaged material in the cell. Provided the cell size is sufficiently small, this process has the appearance of void growth on the continuum scale. (Figure 39 shows a calculation of a copper rod impacting spaced steel plates. The shaded areas indicate damaged material.) Voids grow as long as the fracture criterion is satisfied and may completely occupy a computational cell or neighboring cells if the loading situation decrees such growth. Compression of failed material is permitted and may ultimately close voids previously formed. Excellent results have been obtained by Nash and Cullis (1984) for a number of impact and explosive loading situations with this criterion.

In reality, material failure does not occur instantaneously as described by these models. This was shown clearly in a number of plate impact experiments performed to study spall failure in metals. Spallation is material failure due to the interaction of two or more rarefaction waves and occurs at locations far removed from the point of application of the load. In their review, Oscarson and Graff (1968) noted that in many experiments the velocity of the flyer plate required to cause incipient spall decreased with increasing flyer plate thickness in an approximately linear manner. Since impact velocity is directly related to stress [e.g., Johnson (1972)] and flyer thickness can be similarly related to the duration of the stress pulse, a definite time dependence for spall failure is implied.

Oscarson and Graff detail several types of models for spall damage. Cumulative models account for the effects of stress amplitude and duration in

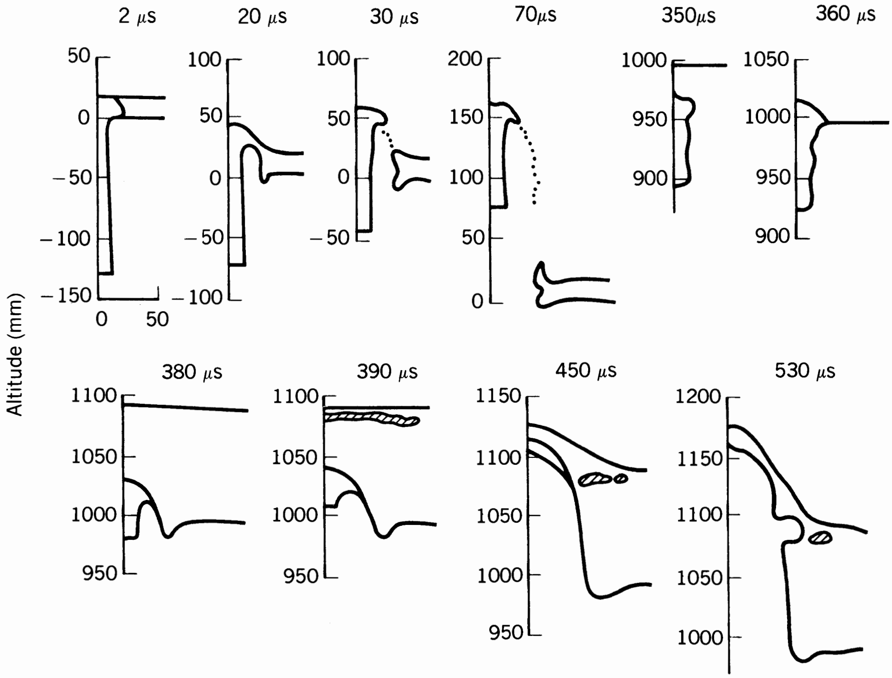

Figure 39. HULL code results of spaced plate calculation.

attempting to predict spall for an arbitrary pulse shape from previously generated data with rectangular pulses. Energy models are based on the assumption that the mechanical energy supplied to the spall plane up to the time of fracture is invariant. Stress rate models use the criterion that the tensile strength of a material is dependent on its tensile unloading characteristics (stress rate or stress gradient). All such models incorporate a number of empirical factors and require a fair degree of material characterization. The current tendency in dealing with spall failure is to view it as a sequence of nucleation, growth, and coalescence of voids or cracks. A comprehensive review is given by Meyers and Aimone (1983).

The Tuler and Butcher (1968) criterion was one of the first cumulative damage criteria proposed and has been used in a number of studies of spallation in steel. Three parameters must be determined experimentally. Mescall and Papirno (1973) found better correlation with HEMP code analyses and experiments using the Tuler–Butcher criterion than with instantaneous criteria. Recently Gordon Johnson (Johnson and Cook 1985) incorporated the cumulative damage model shown in Figure 40 in the EPIC-2 code. Parameters D_1–D_5 must be determined experimentally. Note that the first term in the brackets is equivalent to the Hancock–MacKenzie criterion. The model has been tested for a limited number of cases and found to provide

STRENGTH MODEL FOR VON MISES TENSILE FLOW STRESS

$$\sigma = \underbrace{[A + B\epsilon^{n}]}_{\text{STRAIN}}\underbrace{[1 + C\ln\dot{\epsilon}^{*}]}_{\text{STRAIN RATE}}\underbrace{[1 - T^{*m}]}_{\text{TEMPERATURE}}$$

WHERE A, B, n, C, m ARE MATERIAL CONSTANTS

FRACTURE MODEL

$$D = \sum \frac{\Delta\epsilon}{\epsilon^{f}} \qquad \text{(DAMAGE)}$$

$$\epsilon^{f} = \underbrace{[D_1 + D_2 \exp D_3\sigma^{*}]}_{\substack{\text{PRESSURE} \\ \sigma^{*} = \sigma_m/\bar{\sigma}}}\underbrace{[1 + D_4\ln\dot{\epsilon}^{*}]}_{\text{STRAIN RATE}}\underbrace{[1 + D_5T^{*}]}_{\text{TEMPERATURE}} \qquad \text{(FRACTURE STRAIN)}$$

WHERE $D_1 \ldots\ldots D_5$ ARE MATERIAL CONSTANTS

$D \geq 1.0$ GIVES FRACTURE

Figure 40. Strength and fracture models in EPIC codes (Courtesy G. R. Johnson).

qualitative agreement with experiments. Reasons stated for the discrepancy between computations and experiments include the following:

The model and/or the data do not extrapolate well to the high regions of strain rate, temperature, and pressure encountered in high-velocity impact situations.

Uncertainties in the fracture characteristics of the materials studied (OFHC copper, ARMCO iron).

Damage does not accumulate as stated in the model

Cumulative damage models have the advantage of being more realistic (failure depends on a critical level of stress acting over a *finite* time). They are advantageous from a computational standpoint since, lacking the very strong dependence on peak stress of the instantaneous failure models, good results are possible with relatively large computational cells. Moreover, data from experiments with simple pulse shapes can readily be extended to treat more general shapes (Oscarson and Graff 1968).

However, the degree of material characterization is increased. Several well-designed experiments must be performed to determine the three or more parameters of a time-dependent damage model. Existing experimental techniques can generate data at average strain rates of 10^3/s for uniaxial stress experiments and 10^5/s for uniaxial strain experiments (Nicholas 1982), but these models are often employed in ballistic impact situations where considerably higher strains, three-dimensional stress states, and exceedingly high

temperatures and pressures dominate. Furthermore, some of the quantities required by these models cannot be measured directly and must be inferred from a combination of experiments and computer simulations. Thus, there is a significant increase in facilities and manpower requirements to develop data for these models, in contrast to the single parameter required for instantaneous models that can often be inferred from existing data.

Criteria involving more than one damage measure have been devised by Davison and Stevens (1972) and Davison et al. (1977). A number of micromechanical models for metals and geological materials (e.g., Shockey et al. 1984, 1985; Dienes 1985) exist. These descriptions, though suitable for incorporation in computer codes, have not been used extensively since model parameter determination for two- and three-dimensional situations is a costly and time-consuming task.

Very comprehensive discussions of material failure under impact loading and recommendations for both ad hoc procedures and long-term research are given in the NMAB (1980) report. Zukas (1987) has reviewed numerical modeling of failure under stress wave loading in wave propagation codes. The current practice can be summarized very simply. Most calculations are performed with the simplest possible failure criteria discussed previously. This is done not out of ignorance of better approaches but for a want of data to drive advanced failure models. Basic *zeroth-order* data for cumulative damage and micromechanical models are simply not available for materials of interest in engineering design. Today's research dollars fund short-term projects resulting in shiny, tangible hardward. High-risk, long-term research, no matter how invaluable or how cost effective over an accounting period greater than one year is not readily funded.

This situation is of great concern for those working at lower (0.5–2 km/s) impact velocities whose main concern is material behavior. In the explosive loading area, other factors predominate, as already discussed, so that material failure in the case of jet formation, breakup, and penetration is a secondary consideration. The validity of the computational models, especially for the plastic behavior of metals, is a far greater concern at this point. And indeed, if it were possible to develop material failure models for shaped charge and explosively formed fragment situations, the experimental techniques to validate such models simply do not exist at this time.

The best approach is still that recommended in NMAB (1980). Many institutions have adopted their ad hoc procedures. The long-term research still remains to be done.

REFERENCES

Achenbach, J. D. (1975), *Wave Propagation in Elastic Solids*, New York: American Elsevier.

Backman, M. E. (1976), *Terminal Ballistics*, Naval Weapons Center, NWC TP 578.

Bachman, M. E., and Goldsmith, W. (1978), "The Mechanics of Penetration of Projectiles into Targets," *Int. J. Engr. Sci.*, *16*(1).

Bathe, K-J. (1982), *Finite Element Procedures in Engineering Analysis*, Englewood Cliffs, NJ: Prentice-Hall.

Bathe, K-J. (1984), "Soloution Method for Large Deformation Contact Problems," Ballistic Research Laboratory, BRL-CR-534, October.

Bathe, K-J., and Chaudhari, A. (1984), "On Finite Element Analysis of Large Deformation Frictional Contact Problems," *Proc. 7th Invitational Symp. on the Unification of Finite Elements, Finite Differences and Calculus of Variations*, University of Connecticut, Storrs, CT, May.

Belytschko, T., and Hughes, T. J. R. (eds.) (1983), *Computational Methods for Transient Analysis*, Amsterdam: North-Holland.

Belytschko, T., and Lin, J. I. (1985), "A New Interaction Algorithm with Erosion for EPIC-3," Ballistic Research Laboratory, BRL-CR-540, February.

Belytschko, T., and Liu, W. K. (1983), "On Mesh Stabilization Techniques for Underintegrated Elements," in *Computational Aspects of Penetration Mechanics*, J. Chandra and J. E. Flaherty (eds.), Heidelberg: Springer-Verlag.

Belytschko, T., and Liu, W. K. (1986), "Improved Spurious Mode Control through Mixed Variational Principles," in *Finite Element Methods for Nonlinear Problems*, P. Bergan, K-J. Bathe, and W. Wunderlich (eds.), Berlin: Springer-Verlag.

Belytschko, T., et al. (1984), "Hourglass Control in Linear and Nonlinear Problems," *Comp. Methods Appl. Mech. Engr.*, *43*(3): 251.

Bertholf, L. D., et al. (1975), "Damage in Steel Plates from Hypervelocity Impact: Part II—Numerical Results and Spall Measurements," *J. Appl. Phys.*, *46*(9): 3776–3783.

Bertholf, L. D., et al. (1976), "Kinetic Energy Projectile Impact on Multilayered Targets: Two-Dimensional Stress Wave Calculation," Sandia National Laboratories, SAND-76-0375.

Courant, R., Friedrichs, K. O., and Lewy, H. (1928), "Über die Partiellen Differenzengleichungen der Mathematischen Physik," *Mathematische Annalen*, *100*: 32–74.

Curran, D. R. (1982), "Dynamic Fracture," in *Impact Dynamics*, J. A. Zukas et al., New York: Wiley-Interscience.

Curran, D. R., Seaman, L., and Shockey, D. A. (1977), "Dynamic Failure in Solids," *Physics Today*, *30*: 46.

Davison, L., and Stevens, A. L. (1972), "Continuum Measures of Spall Damage," *J. Appl. Phys.*, *43*(3): 988–994.

Davison, L., Stevens, A. L., and Kipp, M. E. (1977), "Theory of Spall Damage Accumulation in Ductile Metals," *J. Mech. Phys. Solids*, *25*(11).

Dienes, J. K. (1979), "On the Analysis of Rotation and Stress Rate in Deforming Bodies," *Acta Mech.*, *32* 217.

Dienes, J. K. (1984a), "The Effect of Finite Rotation on a Problem in Plastic Deformation," in *Proc. Intl. Symp. on Plasticity*, A. S. Khan (ed.), Bell Anniversary Volume, Norman, OK, July 30–August 3.

Dienes, J. K. (1984b), "A Statistical Theory of Fragmentation Processes," Los Alamos National Laboratory, LA-UR-84-3173.

Dienes, J. K. (1985), "Foundations of Statistical Crack Mechanics," Los Alamos National Laboratory, LA-UR-85-3264.

Dienes, J. K. (1986), "A Discussion of Material Rotation and Stress Rate," *Acta Mechanica*, *65*: 1–11.

Donea, J. (ed.) (1980), *Advanced Structural Dynamics*, London: Applied Science Publishers.

Drucker, D. C. (1978), "Approximate Calculations of Spall and Cratering in High Speed Impact," in *High Velocity Deformation of Solids*, K. Kawata and J. Shioiri (eds.), Berlin: Springer-Verlag.

Flanagan, D. P., and Belytschko, T. (1981), "A Uniform Strain Hexahedron and Quadrilateral with Orthogonal Hourglass Control," *Int. J. Num. Methods Engr.*, *17*: 679.

Fried, I. (1979), *Numerical Solution of Differential Equations*, New York: Academic Press.

Fung, Y. C. (1965), *Foundations of Solid Mechanics*, Englewood Cliffs, NJ: Prentice-Hall.

Green, A. E., and Naghdi, P. M. (1965), "A General Theory of an Elastic-Plastic Continuum," *Arch. Rat. Mech. Anal.*, *2*: 197.

Gupta, Y. M., and Seaman, L. (1979), "Local Response of Reinforced Concrete to Missile Impact," Electric Power Research Institute, EPRI-NP-1217.

Hageman, L. J. et al. (1975), "HELP, a Multi-Material Eulerian Program for Compressible Fluid and Elastic-Plastic Flows in Two Space Dimensions and Time," Systems, Science and Software, SSS-R-75-2, July.

Halleux, J. P., and Donea, J. (1985), "A Discussion of Cauchy Stress Formulations for Large Strain Analysis," in *Finite Element Methods for Nonlinear Problems*, P. Bergan, K-J. Bathe, and W. Wunderlich (eds.), Berlin: Springer-Verlag.

Hallquist, J. O., Goudreau, G. L., and Benson, D. J. (1985), "Sliding Interfaces with Contact-Impact in Large-Scale Lagrangian Computation," *Comp. Mech. Appl. Mech. Engr.*, *51*: 107.

Hancock, J. W., and MacKenzie, A. C. (1976), "On the Mechanisms of Ductile Failure in High-Strength Steels Subjected to Multi-Axial Stress Rates," *J. Mech. Phys. Solids*, *24*: 147–169.

Held, M. (1988), *Fundamentals of Shaped Charges*, Course Notes Computational Mechanics Associates, Baltimore, MD.

Herrmann, W. (1969), "Constitutive Equation of the Dynamic Compaction of Ductile Porous Materials," *J. Appl. Phys.*, *40*(6): 2490.

Herrmann, W. (1977), "Current Problems in the Finite Difference Solution of Stress Waves," in *Nonlinear Waves in Solids*, T. C. T. Ting, R. J. Clifton and T. Belytschko (eds.), Proc. Workshop at U. of Illinois Chicago Circle, March 21–23, 1977, US Army Research Office.

Herrmann, W., and Bertholf, L. D. (1983), "Explicit Lagrangian Finite-Difference Methods," in *Computational Methods for Transient Analysis*, T. Belytschko and T. J. R. Hughes (eds.), Amsterdam: North-Holland.

Herrmann, W., and Nunziato, J. W. (1972), "Nonlinear Constitutive Equations," in *Dynamic Response of Materials to Intense Impulsive Loading*, P. C. Chou and A. K. Hopkins (eds.), Washington, D.C.: U.S. PO.

Hyman, J. M. (1984), "Numerical Methods for Treating Interfaces," *Physica*, *12D*: 396.

Jacquotte, O-P., and Oden, J. T. (1984), "Analysis of Hourglass Instabilities and Control in Underintegrated Finite Elements," in *Proc. Intl. Conf. on Innovative Methods for Nonlinear Problems*, W. K. Liu, T. Belytschko, and K. C. Park (eds.), Swansea, UK: Pineridge Press.

Johnson, W. (1972), *Impact Strength of Materials*, London: Edward Arnold.

Johnson, G. C., and Bammann, D. J. (1984), "A Discussion of Stress Rates in Finite Deformation Problems," *Int. J. Solids Structures*, *20*(8): 725.

Johnson, G. R., and Cook, W. H. (1985), "Fracture Characteristics of Three Metals Subjected to Various Strains, Strain Rates, Temperatures and Pressures," *Engr. Fracture Mech.*, *21*(1): 31–48.

Kalker, J. J. (1977), "A Survey of the Mechanics of Contact between Solid Bodies," *ZAMM*, *57*, T3.

Kimsey, K. D., and Zukas, J. A. (1984), "Contact Surface Erosion for Impact Problems," *Proc. 8th Intl. Symp. on Ballistics*, Orlando, FL, October.

Kimsey, K. D., and Zukas, J. A. (1986), "Contact Surface Erosion for Hypervelocity Problems," Ballistic Research Laboratory, BRL-MR-3495.

Kohn, B. J. (1969), "Compilation of Hugoniot Equations of State," USAF Weapons Laboratory, AFWL-TR-69-38, April.

Kosloff, D., and Frazier, G. A. (1978), "Treatment of Hourglass Patterns in Low Order Finite Element Codes," *Int. J. Num. Anal. Methods Geomech.*, *2*: 57.

Mader, C. L. (1979), *Numerical Modeling of Detonations*, Berkeley: University of California Press.

Maenchen, G., and Sack, S. (1964), "The Tensor Code," in *Methods in Computational Physics*, *Vol. 3*, *Fundamental Methods in Hydrodynamics*, B. Alder et al. (eds.), NY: Academic Press.

Marsh, S. P. (ed.) (1980), *LASL Shock Hugoniot Data*, Berkeley: University of California Press.

Matuska, D. A., and Durrett, R. E. (1978), "The HULL Code, A Finite Difference Solution to the Equations of Continuum Mechanics," Air Force Armament Laboratory, AFATL-TR-78-125.

Matuska, D. A., Durrett, R. E., and Osborn, J. J. (1982), "HULL Users Guide for Three-Dimensional Linking with EPIC-3," Ballistic Research Laboratory, ARBRL-CR-00484.

Matuska, D. A., and Osborn, J. J. (1981), "HULL/EPIC Linked Eulerian/Lagrangian Calculations in Three Dimensions," Ballistic research Laboratory, ARBRL-CR-00467.

Mescall, J., and Papirno, R. (1973), "Spallation in Cylinder-Plate Impact," *Exp. Mech.*, 257–266, July.

Meyers, M. A., and Aimone, C. T. (1983), "Dynamic Fracture (Spalling) of Metals," *Prog. Mat. Sci. 28*: 1–96.

Nagtegaal, J. C., and DeJong, J. E. (1982), "Some Aspects of Nonisotropic Work-Hardening in Finite Strain Plasticity," in *Plasticity of Metals at Finite Deformation*, E. H. Lee and R. L. Mallett (eds.), Stanford, CA: Stanford University Press.

Nagtegaal, J. C., Parks, D. M., and Rice, J. R. (1974), *Comp. Methods Appl. Mech. Engr.*, *4*: 153.

Nash, M. A., and Cullis, I. G. (1984), "Numerical Modeling of Fracture—A Model for Ductile Fracture in Triaxial States of Stress," in *Proc. 3rd Conf. on Mechanical Properties at High Rates of Strain*, J. Harding (ed.), Institute of Physics Conference Series #70, Institute of Physics, London.

Nemat-Nasser, S., Asaro, R. J., and Hegemier, G. A. (eds.) (1984), *Theoretical Foundation for Large-Scale Computations of Nonlinear Material Behavior*, Dordrecht: Martinus Nijhoff.

Nicholas, T. (1982), "Material Behavior at High Strain Rates," in *Impact Dynamics*, J. A. Zukas et al., New York: Wiley-Interscience.

NMAB (1980), *Materials Response to Ultra-High Loading Rates*, National Materials Advisory Board, NMAB-356, Washington, D.C.

Noh, W. (1976), Lawrence Livermore Lab, UCRL-52112.

Oden, J. T. (1983), "Comments on Some Problems in Computational Penetration Mechanics," in *Computational Aspects of Penetration Mechanics*, J. Chandra and J. E. Flaherty (eds.), Heidelberg: Springer-Verlag.

Oden, J. T., and Pires, E. B. (1983), "Nonlocal and Nonlinear Friction Laws and Variational Principles for Contact Problems in Elasticity," *J. Appl. Mech.*, *50*(1): 67.

Oscarson, J. H., and Graff, K. F. (1968), Battelle Memorial Institute, BAT-197A-4-3.

Park, K. C. (1984), "Locking, Spurious Mechanisms and Pressure Divergence in Penalty Finite Element Methods for Stokes Flow Problems," *Comp. Methods Appl. Mech. Engr.*, *47*: 315.

Perez, E. (1982), "Experimental and Theoretical Study on the Penetration of Semi-Infinite Metal Targets by Great-Length Metal Projectiles with a Velocity Higher Than 2000 m/s," *Sciences et Techniques de L'Armement*, Vol. 56, No. 1, Paris, National Printing Office.

Pires, E. B., and Oden, J. T. (1983),"Analysis of Contact Problems with Friction Under Oscillating Loads," *Comp. Methods Appl. Mech. Engr.*, *39*: 337.

Poth, A. et al. (1981), "Experimental and Numerical Investigation of the Ricochetting of Projectiles from Metallic Surfaces," *Proc. 6th Intl. Symp. on Ballistics*, American Defense Preparedness Association.

Poth, A. et al. (1983), "Failure Behavior of an Aluminum Plate Under Impact Loading," *Proc. Intl. Conf. on Application of Fracture Mechanics to Materials and Structures*, Freiburg, West Germany.

Roache, P. J. (1972), *Computational Fluid Dynamics*, Albuquerque: Hermosa Publishers.

Rinehart, J. S. (1951), "Some Quantitative Data Bearing on the Scabbing of Metals under Explosive Attack," *J. Appl. Phys.*, *22*(5): 555.

Rinehart, J. S. (1952), "Scabbing of Metals under Explosive Attack: Multiple Scabbing," *J. Appl. Phys.*, *23*(11): 1229.

Ringers, B. E. (1983), "New Sliding Surface Techniques Enable Lagrangian Code to Handle Deep Target Penetration/Perforation Problems," in *Computational Aspects of Penetration Mechanics*, J. Chandra and J. E. Flaherty (eds.), Heidelberg: Springer-Verlag.

Schulz, J. C. (1985), "Finite Element Hourglassing Control," *Int. J. Num. Methods Engr.*, *21*: 1039.

Schulz, J. C., and Heimdahl, O. E. R. (1986), "Hourglassing Control Through Boundary Smoothing," *Comm. Appl. Num. Methods*, *2*: 369.

Scott, B. (1984), Ph.D. Dissertation, University of Delaware.

Seaman, L. (1975), "Fracture and Fragmentation Under Shock Loading," in *Shock and Vibration Computer Programs*, W. Pilkey and B. Pilkey (eds.), Washington, D.C.: Shock and Vibration Information Center.

Shockey, D. A., Seaman, L., and Curran, D. R. (1984), "A Computational Shear Band Model for Armor Design," *Proc. 1984 Army Symposium on Solid Mechanics,* Newport, RI, October 1–3.

Shockey, D. A. et al. (1985), "Development of Improved Failure Models," SRI Project 3722, report for US Army Research Office (AD A 155 586).

Steinberg, D. J., Cochran, S. G., and Guinan, M. W. (1980), "A Constitutive Model for Metals Applicable at High Strain Rates," *J. Appl. Phys.*, *51*(3): 1498.

Trigg, M. et al. (1981), "PISCES 3DELK User's Manual," Physics International, San Leandro, CA.

Tuler, F. R., and Butcher, B. M. (1968), "A Criterion for the Time Dependence of Dynamic Fracture," *Int. J. Fract. Mech.*, *4*: 431.

van Thiel, M. (1977), Lawrence Livermore Laboratory, UCRL-50108, Vols. 1–3.

Verhegghe, B., and Powell, G. H. (1986), "Control of Zero-Energy Modes in 9-Node Plane Element," *Int. J. Num. Methods Engr.*, *23*: 863.

von Neumann, J. and Richtmyer, R. D. (1950), "A Method for the Numerical Calculation of Hydrodynamic Shocks," *J. Appl. Phys.*, *21*: 232–237.

Walters, W. P., and Majerus, J. N. (1980), "Impact Models for Penetration and Hole Growth," Ballistic Research Laboratory, ARBRL-TR-02069.

Wasley, R. J. (1973), *Stress Wave Propagation in Solids*: *An Introduction*, New York: Marcel Dekker.

Weickert, C. A. (1983), "Evaluation of Selected Computer Codes for Impact and Explosive Detonation Calculations," Defence Research Establishement Suffield, Memorandum #1059, April.

Wilkins, M. L. (1980), "Use of Artificial Viscosity in Multidimensional Fluid Dynamic Calculations," *J. Comp. Phys.*, *36*: 281.

Wilkins, M. L. (1982), "Calculation of Elastic-Plastic Flow," Lawrence Livermore National Laboratory, UCRL-7322, Rev. 2.

Wilkins, M. L. (1984a), "Modeling The Behavior of Materials," in *Structural Impact and Crashworthiness*, *Vol. 2*, *Conference Papers*, J. Morton (ed.), London: Elsevier Applied Science Publishers.

Wilkins, M. L. (1984b), "Modeling the Behavior of Materials," in *Theoretical Foundation for Large-Scale Computations of Nonlinear Material Behavior*, S. Nemat-Nasser, R. J. Asaro, and G. A. Hegemier (eds.), Dordrecht: Martinus Nijhoff Publishers.

Wright, T. W. (1983), "A Survey of Penetration Mechanics for Long Rods," in *Computational Aspects of Penetration Mechanics*, J. Chandra and J. E. Flaherty (eds.), Heidelberg: Springer-Verlag.

Woodward, R. L. (1987a) "Analytical Modelling of Target Perforation," in Course Notes for the Short Course *High Velocity Impact Dynamics*, Computational Mechanics Associates, Baltimore.

Woodward, R. L. (1987b), "Dynamic Failure Mechanisms" in Course Notes for the Short Course *High Velcoity Impact Dynamics*, Computational Mechanics Associates, Baltimore.

Zukas, J. A., Nicholas, T., Swift, H. F., Greszczuk, L. B., and Curran, D. R. (1982), *Impact Dynamics*, New York: Wiley-Interscience.

Zukas, J. A. (1987), "Stress Waves and Fracture," in *Materials at High Strain Rates*, T. Z. Blazynski (ed.), London: Elsevier Applied Science Publishers.

CHAPTER 12

WAVE PROPAGATION CODES FOR SHAPED CHARGE STUDIES

This chapter summarizes the capabilities and limitations of two- and three-dimensional production computer codes used for problems involving the explosive loading of metals and high-velocity penetration effects.

The wave propagation codes to be reviewed here were originally developed to solve problems characterized by:

1. The presence of shock waves (alternatively, steep stress or velocity gradients)
2. Localized materials response (i.e., situations where the overall geometric configuration of a structure is of secondary importance compared to the constitution and characteristics of the material in the vicinity of the applied load)
3. Loading and response times in the submillisecond regime.

Characteristics of computer codes to solve these problems are outlined in Table 1. Contrast these with the analogous situation for low-velocity loading and structural response simulations given in Table 2.

Excellent results can and have been obtained with the wave codes described here, involving many different materials in engineering designs with very complex shapes. Good accuracy has been achieved, in comparison to exact solutions or with experimental results *when the materials involved are very well known and characterized*. When this is not done, when the codes are used as black boxes with engineering materials that are not well understood or characterized, it is not uncommon to obtain *qualitatively* incorrect solutions. *The greatest limitations on accuracy in wave propagation calculations are the*

TABLE 1. Characteristics of Computer Codes for High-velocity Impact

Mesh description	Eulerian and Lagrangian
Spatial discretization	Finite-difference/finite-element, linear, and constant strain elements
Temporal integration	Explicit
Artificial viscosity	Explicit formulation
Material model	Incremental elastic-plastic
Failure criteria	Instantaneous maxima of field variable (principal stress, strain, plastic work, pressure); cumulative damage, micromechanical models
Methods of material characterization	Wave propagation methods Split Hopkinson bar Plate impact Bar-bar impact Exploding cylinder
Hydrodynamic pressure	High-pressure equation of state [$P = P(\rho, E)$]
Boundary conditions	Reflective and transmittive
Initial conditions	Velocity

TABLE 2. Characteristics of Computer Codes for Low-velocity Impact

Mesh description	Predominantly Lagrangian
Spatial discretization	Predominantly finite element; high-order elements
Temporal integration	Predominantly implicit
Artificial viscosity	None or implicit through discretization scheme
Material model	No definite model (small strain–large rotation common)
Failure criteria	Plastic flow
Methods of material characterization	Conventional hydraulic test machines
Hydrodynamic pressures	$P = \dfrac{(\sigma_{11} + \sigma_{22} + \sigma_{33})}{3}$
Boundary conditions	Wide selection of internal and boundary constraints
Initial conditions	Force, displacement, velocity

material descriptions embodied in the constitutive equations, particularly with regard to material failure.

In addition, the material data (the various coefficients of the constitutive description) must be appropriate to the characteristic time scale of the problem studied. If the material is responding at strain rates of 10^5/s, good results should not be expected if the input data comes from handbooks where the data was determined at strain rates of 10^{-4}/s!

Wave propagation codes share a number of common features.

Spatial Discretization The earliest (pre-1975) wave codes made use of finite-difference methods to approximate the solution of the governing partial differential equations [see Chapter 11 or Appendices A–C of Zukas et al. (1982)] for problems of interest. Typical of these is the differencing technique used in the TOODY code as described by Walsh (1973). The newer (post-1980) codes are based on finite-element techniques, making use of linear and constant strain triangular and quadrilateral elements in two dimensions, hexahedral or tetrahedral elements in three dimensions. Over the years, experiments have been performed with higher-order elements such as those found in typical structures codes (e.g., ADINA, MARC, MAGNA, ANSYS). These, however, have not been adopted for general use since problems modeled with such codes include shock waves (mathematically, discontinuities). There is no gain in accuracy in modeling discontinuities with high-order polynomials, but a considerable increase in computational effort. Hence, production codes rely on the simplest spatial discretization techniques.

Time Integration Solutions are advanced in time through the use of an explicit central difference algorithm (see Table 5 of Chapter 11). This procedure is straightforward and easily implemented in computer codes. However, it is only conditionally stable so that the maximum time step, Δt, is controlled by the Courant stability criterion

$$\Delta t = \min \frac{\Delta x}{\max(c + u)}$$

where c is the characteristic sound speed of the material, u the particle velocity, and the minimization is taken over the entire mesh. In short, the smallest cell or element governs the time step for the entire mesh. This has important implications insofar as the cost of a calculation is concerned.

Consider a two-dimensional calculation with a constant cell/element size of Δx in both coordinate directions. The total number of computations performed during a given time step is proportional to the number of cells/elements in the mesh. Assuming N cells in each direction, $N \times N$ calculations are performed each cycle to cover the geometric region. Assuming further that M

cycles are necessary to reach the desired simulation time ($M\Delta t$), the total computational effort for a given simulation is proportional to $M \times N \times N$.

If now, for the sake of accuracy, the grid must be refined using a cell size of 0.5 Δx (i.e., double the resolution), then the time step, which is dependent on the cell size, must also be halved. Hence, the total computational load now becomes $2M \times 2N \times 2N = 8M \times N \times N$! If even greater resolution is required, the calculation can become economically prohibitive or even impossible if the available memory space in the computer is exceeded.

Hence, there is a need to balance physical and economic factors in many computational efforts. If the wave structure and its related variables (pressure, stress, strain) are required, then the resolution must be good enough so that the shortest wavelength of interest is defined by at least 2 cells/elements. This situation will arise if material failure due to shock wave interactions with material interfaces, geometric boundaries, or each other must be carefully modeled, especially if the failure criterion requires a definition of the pulse shape or an accurate value of peak pressure. Each shock wave will be spread over 3–5 cells/elements and must be tracked from inception to peak value.

If, on the other hand, only bulk properties are required—center of mass velocity, the overall shape of the colliding objects—then grid requirements can be relaxed considerably. In some cases, these quantities may be obtained to a first approximation without explicitly accounting for material failure in the calculation.

A committee of the National Materials Advisory Board (NMAB 1980) has reviewed the state of the art in numerical simulation of high-velocity impact phenomena. Recommendations were made for both long-term research and interim procedures. Those interested in analytical and numerical work in this field would be well advised to obtain a copy (available from the National Technical Information Service).

Artificial Viscosity Shock waves, as mathematical discontinuities, cannot be directly accommodated in the continuum formulation, which is the basis of present-day wave codes. To get around this problem, an artificial viscosity is introduced that smears shock fronts over several mesh widths in a calculation. At least linear and quadratic terms are available. The former serves principally to spread the wave front over several cells in the direction of propagation and lower the peak amplitude. The latter is used principally to supress spurious oscillations behind the wave front. The generalized viscosity term, which is added to the pressure computed from an equation of state, is of the form

$$q = c_1 \rho c \, \Delta x \left| \frac{d\dot{x}}{dx} \right| - c_2^2 \rho (\Delta x)^2 \left| \frac{d\dot{x}}{dx} \right| \frac{d\dot{x}}{dx}$$

where c_1 and c_2 are user-defined constants, Δx is a characteristic grid length, c the local sound speed, $d\dot{x}/dx$ the volumetric strain rate, and ρ the density.

Expressions for strain rate and characteristic length are given by Wilkins (1980). A very good discussion of the artificial viscosity concept is given by Noh (1976).

With quadrilateral or hexahedral elements that are underintegrated, an instability can occur, called hourglassing, that is not resisted by internal forces. Artificial viscosity formulations for grid stabilization differ. See the papers by Wilkins (1980), Belytschko et al. (1987), Flanagan and Belytschko (1981), Malkus and Hughes (1978), Maenchen and Sack (1964), and Schultz (1985) for representative examples.

Material Models Metals, until recently, were the materials of primary interest. Hence, the material model in most codes decouples the effects of volumetric and shear behavior. The hydrodynamic component of stress is taken from an equation of state. For impacts where the striking velocity is below the sonic velocity, some variant of the Mie–Grüneisen equation of state is commonly used. Beyond this range (hypervelocity impact), the Tillotson equation of state is favored. The constitutive model of elastic-plastic behavior is typically in incremental form, employing a von Mises yield criterion and providing for some form of hardening, thermal softening, and strain rate effects. By and large, the essential physics in these codes can be written down on the back of a business envelope. Encoded in FORTRAN, it is usually contained in two or three subroutines. The remainder of the coding—between 10,000 and 125,000 FORTRAN statements— is devoted to assorted bookkeeping: input/output operations, sliding interface logic, material transport, and the like.

Because of interest in porous materials, various geological materials, and concrete, many of the newer codes incorporate material models for crushable materials.

Limitations The greatest uncertainty in code computations for explosive loading problems involving thin structures is the validity of the plasticity model since those in existence were not derived for situations involving large superimposed hydrodynamic pressures well in excess of the material strength, temperatures approaching the melting temperature, and strains exceeding 100%. This question is not likely to be resolved in the near future. Compounding the problem is the paucity of detailed experimental data for materials under these conditions.

For computations in the ordnance velocity regime, the principal obstacle is a poor knowledge of the mechanisms of failure under impact and explosive loading. Micromechanically based failure models applicable in the high-pressure regime for multiaxial transient loading situations are generally not available. Those that exist (Curran 1982) require an inordinate degree of material characterization. Hence, failure models for codes tend to be simple, instantaneous failure models that require minimal material characterization.

Essential features of wave propagation codes are summarized in Tables 3 and 4.

TABLE 3. Code Characteristics

Material Model	Numerical Model
Conservation equations	Finite difference
Mass	First or second order
Momentum	Finite element
Energy	Constant and linear strain elements
Constitutive Relationship	Artificial viscosity
Elastic-plastic behavior	Linear and quadratic terms
Equation of State	Explicit integration algorithms
Hydrodynamics behavior	
Fracture/failure model	
Failure criterion	
Postfailure behavior	

Some high rate loading problems exhibit characteristics that require features found in both wave propagation and structures codes. For example, the impact of a foreign object onto a rotating turbine blade can produce shock waves and failure due to wave interaction that must be carefully tracked. This is best done with the explicit schemes and material models found in wave codes. This loading, however, typically lasts from 50 to 100 *micro*seconds at which time the foreign object is totally consumed. If the target has not been totally destroyed, the deposited energy will be expended by vibrations and other mechanisms, leading to peak deflections of the blade tip some 2–3 *milli*seconds after the initial loading. Since from 100 μs onward the details of the wave motion are no longer required, implicit integration schemes with their larger time steps can economically provide the required solution at 3 ms.

TABLE 4. Constitutive Model for Metals

Volumetric	Shear
$P = P(\rho, E)$	$\dot{s}_{ij} = 2G(\dot{\varepsilon}_{ij} - \frac{1}{3}\delta_{ij}\dot{u}_{k,k})$
Tillotson	$\dot{\varepsilon}_{ij} = \frac{1}{2}(\dot{u}_{i,j} + \dot{u}_{j,i})$
Mie–Grüneisen	
Ad hoc for	$\sigma_{ij} = s_{ij} - \delta_{ij}(P + q)$
Explosives	$s_{ij}s_{ij} \leq \frac{2}{3}Y^2$
Concrete	$s_{ij} = s_{ij}\left[\dfrac{2Y^2}{3s_{ij}s_{ij}}\right]^{1/2}$
Geological materials	
	Provision for
	Strain hardening
	Thermal softening
	Compressibility effects

To attempt this with explicit schemes would require thousands of additional cycles and lead to roundoff errors that, in all probability, would mask the actual solution.

Several codes originally developed to solve problems of structures subjected to transient loading have been modified to incorporate sliding interface logic to permit direct treatment of impact problems. In their original formulation, surface loads were required to drive an impact problem. The exact nature of this pressure pulse is often not known so that typically a shape is assumed and iterations performed on it until the desired end result is obtained. This is both uneconomical and undesirable since a good deal of subjective bias enters into the calculation [for examples of this approach see Gupta et al. (1980), Nimmer and Boehman (1981), Brown and Krahula (1981), and Misey et al. (1980)]. With the sliding interface logic, only initial velocities of the colliding bodies need be specified. The loading function is computed as a by-product of the calculation.

In contrast to wave codes, structures codes tend to be predominantly finite-element codes, contain a large library of structural (beam, plate, shell) elements, and one or two continuum elements. Whereas finite-element wave codes inevitably use a lumped mass formulation for the mass matrix (allowing the solution to be developed on an element-by-element basis), structures codes use a consistent mass matrix, an explicit stiffness matrix, and a variety of implicit integration schemes. Most of these are unconditionally stable and permit the use of large time steps. Even though large time steps are permitted, the accuracy requirements of the physical problem must govern each simulation, and this may limit the allowable time step. The nature of the physical problem should determine which type of code should be used. Considerable research is going on in developing explicit–explicit as well as explicit–implicit partitions. It is therefore likely that the next generation of codes will be able to tackle both types of problems with equal efficiency.

Considerations in Computing

A number of points need to be considered before undertaking large-scale computations. The selection of a computational mesh involves tradeoffs between accuracy and economics. This was pointed out very clearly in an article by Herrmann (1977). Consider a problem involving stress wave propagation. These are usually characterized by a high-frequency content, but discrete methods cannot reproduce the entire frequency spectrum. The mesh or element size acts as a filter and is unable to reproduce frequency components with wavelengths less than two mesh widths. If we consider a simple case of uniform mesh spacing with N meshes in the characteristic length, the resolution is $N/4$. Herrmann suggests, on the basis of experience, that the minimum resolution needed for most stress wave problems is on the order of 25, implying that in our problem at least 100 meshes are needed in the characteris-

TABLE 5. Computer Resource Requirements

One-dimensional Calculations	
Total number of meshes	10^2
Total number of time cycles	2×10^2
Number of mesh point calculations	20K
CDC 7600 CPU time	22 s ($2.20)[a]
Memory requirement	1K words
Two-dimensional Calculations	
Total number of meshes	$10^2 \times 10^2$
Total number of cycles	2×10^2
Number of mesh point calculations	2M
CDC 7600 CPU time	1.1 h ($400)[a]
Memory requirements	190K words
Three-dimensional Calculations	
Total number of meshes	$10^2 \times 10^2 \times 10^2$
Total number of time cycles	2×10^2
Number of mesh point calculations	200M
CDC 7600 CPU time	200 h ($70K)[a]
Memory requirement	27M words

[a]$360 per CPU hour.

tic length. Depending on the problem and the severity of pressure or stress gradients, even higher resolution may be required.

The minimum time of interest in stress wave problems generally involves at least two wave transits across the characteristic length dimension of the problem. Thus, for the minimum resolution of 100 meshes, 200 time steps will be required as a minimum. Again, in many practical problems, the motion may need to be followed for tens or hundreds of transit times, with a corresponding increase in the number of time steps.

Table 5, adapted from Herrmann (1977), lists the computer resources and costs required for one-, two-, and three-dimensional problems. One- and two-dimensional calculations can be performed with reasonable accuracy and costs. Indeed, one-dimensional problems with high resolution can be run in minutes while production two-dimensional calculations can be done in several hours or less on current supercomputers. However, a $100 \times 100 \times 100$ grid is quite coarse for three-dimensional simulations and run times quite expensive.

This does not necessarily imply that three-dimensional calculations cannot be done. Quite a few practical problems have been addressed with three-dimensional codes [Chapter 10 in Zukas et al. (1982)]. However, compromises are required, and these in turn require a keen understanding of the physical

problem and the effects that various numerical artifacts such as uneven resolution in three coordinate directions, mixing of explicit and implicit integration schemes or explicit–explicit partitions (Belytschko and Lin 1987), choice of mesh or element type, and use of artificial and hourglass viscosity have on the solution. Anyone can perform finely resolved one- and two-dimensional calculations if cost is no object. A keen knowledge of the problem and numerical simulation methods is required, though, for successful three-dimensional simulations that, with all the compromises, will still be expensive.

12.1. SUMMARY OF WAVE PROPAGATION CODE CHARACTERISTICS

Tables 6–11 summarize the characteristics of two- and three-dimensional wave propagation codes that are or have been used to study problems involving the explosive loading of thin metallic liners to form either long jets ($L/D > 100$) or relatively short ($L/D \approx 2$–3) projectiles. Penetration effects have been studied with either Eulerian codes or Lagrangian codes with a rezoning or eroding slideline capability. Other codes are available, and have been used, to study such problems. The codes listed in the tables are considered to be *production codes*, readily (more or less) available to interested users. There exists for these codes not only ample documentation of successes and failures but a large body of experienced users as well. Proprietary and in-house codes probably outnumber those listed in the tables, but they are not readily obtainable and generally were written for the benefit of a specific, small group. Documentation, if it exists, is generally spartan and limited to in-house reports that may not be current. Acquiring such codes is generally more trouble than it is worth.

Although Tables 6–11 are intended to be self-sufficient, a few comments are in order. The tables concentrate on material descriptions and numerical techniques needed to solve the physical problem. Pre- and postprocessing details are not covered here. Although mesh generation techniques differ for Lagrangian and Eulerian codes, current codes can, with relative ease, generate almost any geometric configuration for study. Typical projectile shapes are long cylindrical rods, solid or hollow, straight or tapered, with hemispherical, conical, or ogival nose shapes (again, solid or hollow). Targets are often modeled as some combination of circular or square plates, either contiguous or spaced, composed of one or more materials. Mesh generators are available in almost all codes to quickly and easily generate such shapes with minimal user input. Provision is also made for manual generation of lines of nodes or cells/elements. These can be used with automatic mesh generation features to generate arbitrary geometrical forms.

The degree of postprocessing capability varies considerably from code to code, but all can, at minimum, generate plots of deformed and undeformed mesh geometries, contour plots of various stress and strain measures, and

TABLE 6. Lagrangian Codes

	DYNA2D	DYNA3D	EPIC-2	EPIC-3	DEFEL	HEMP	HEMP3D	TOODY	ZEUS	HULL	DYSMAS/L	AUTODYN	PISCES2DELK	PISCES3DELK
Discretization														
Finite difference						×	×	×		×		×	×	×
Finite element	×	×	×	×	×				×		×			
Dimensionality														
Two dimensional	×		×		×	×		×	×	×	×	×	×	
Three dimensional		×		×			×			×	×			×
Artificial viscosity														
von Neumann	×	×	×	×	×	×	×	×	×	×	×	×	×	×
Hourglass	×	×	×	×		×				×		×	×	
Time integration														
Explicit	×	×	×	×	×	×	×	×	×	×	×	×	×	×
Implicit														
Rezoning														
Automatic	×							×		×				
Manual			×		×					×			×	
None		×		×		×	×		×		×			×
Interactive												×		
Initial conditions														
Velocity	×	×	×	×	×	×	×	×	×	×	×	×	×	×
Acceleration	×	×												
Spin	×	×												
Boundary conditions														
Pressure	×	×			×							×	×	×
Shear	×	×											×	
Concentrated forces	×	×			×									×
Velocity–time history	×	×			×									
Other										×	×			
Eroding interfaces			×	×					×		×			

pressure as well as velocity vectors. Time histories of various field variables at specific locations can also be obtained.

Since neither Eulerian nor Lagrangian methods alone are adequate to address some problems, a number of codes incorporating both capabilities have been developed. These include HULL, DYSMAS, AUTODYN, and the PISCES family of codes. The codes have the ability to model both Eulerian and Lagrangian regions in a single calculation. Thus, regions undergoing very large distortions may be modeled as Eulerian, quiescent regions with mild to moderate distortions as Lagrangian. In addition, most coupled codes also include the capability to model materials as rigid and may include structural

TABLE 7. Eulerian Codes

	HELP	METRIC	CSQII	SOIL	HULL	DYSMAS/E	AUTODYN	PISCES2DELK	PISCES3DELK
Discretization									
Finite Difference	×	×	×	×	×	×	×	×	×
Finite element									
Dimensionality									
Two dimensional	×		×	×	×	×	×	×	
Three dimensional		×		×	×	×			×
Artificial viscosity									
von Neumann	×	×	×	×	×	×	×	×	
Implicit in numerics	×	×	×	×	×	×			×
Rezoning									
Automatic					×		×		
User assisted						×			
Manual	×		×		×			×	
Cell combination	×								
Grid translation				×	×			×	
Void opening/closing	×								
None		×		×					×
Interface Definition									
Mixed cells	×	×	×	×	×	×	×		×
Slide lines	×						×	×	
Other	×					×	×		
Diffusion control									
Lagrangian boundary	×						×	×	
Preferential transport		×	×	×	×	×	×	×	×
Boundary conditions									
Lagrange					×		×		
Transmittive	×	×	×		×	×		×	×
Reflective	×	×	×		×	×		×	×
Rigid		×							
Other						×			
Applied Loads									
Shear								×	
Pressure			×	×			×	×	
Gravity			×					×	

TABLE 8. Lagrangian Codes—Materials Models

	DYNA2D	DYNA3D	EPIC-2	EPIC-3	DEFEL	HEMP	HEMP3d	TOODY	ZEUS	HULL	DYSMAS/L	AUTODYN	PISCES2DELK	PISCES3DELK
Deviatoric														
Incremental—e-p	×	×	×	×	×	×	×	×	×	×	×	×	×	×
Work hardening	×	×	×	×	×	×	×	×	×	×	×		×	×
Thermal softening	×	×	×	×	×				×	×			×	
Compressibility			×	×	×				×	×			×	
Strain rate			×	×						×	×			
Programmed burn	×	×	×	×	×	×	×	×	×	×	×	×	×	×
Other	×	×								×		×	×	
Volumetric (EOS)														
Mie–Grüneisen	×	×	×	×	×		×	×	×	×			×	×
Tillotson											×	×	×	×
JWL	×	×	×	×			×	×		×		×	×	×
Polynomial	×	×				×	×			×				
Gamma law	×	×	×	×	×	×	×	×	×	×		×	×	×
Ad hoc						×	×						×	
Other	×	×		×						×		×	×	×
Crushable/porous	×	×	×	×	×			×		×		×	×	
Properties														
Isotropic	×	×	×	×	×	×	×	×	×	×	×	×	×	×
Orthotropic	×	×		×	×			×			×	×	×	
Materials Library			×	×						×				

elements such as shells to facilitate modeling. Communication between different regions is established through boundary conditions—Eulerian regions pass pressure to Lagrangian regions, which in turn compute detailed stress distributions and boundary deflections that are returned to the Euler region. This information is used to update pressures and densities, and the cycle continues.

The intended advantage of such processes is to limit detailed calculations to those regions that require them. Quiescent regions can be modeled as rigid or Lagrangian with efficient computational techniques and large grids, while regions undergoing large distortions are more finely zoned and modeled in an Eulerian sense. Provision can also be made, as in the HULL code, to donate highly distorted Lagrangian cells to the Eulerian mesh so that long rods and jets can be efficiently modeled without the need to explicitly account for void or air regions surrounding the jet. This minimizes both storage requirements and errors due to diffusion.

TABLE 9. Eulerian Codes—Materials Models

	HELP	METRIC	CSQII	SOIL	HULL	DYSMAS/E	AUTODYN	PISCES2DELK	PISCES3DELK
Deviatoric									
Incremental e-p	×	×	×	×	×	×	×	×	×
Work hardening					×				
Thermal softening	×	×	×		×	×		×	
Compressibility	×	×	×		×	×			
Strain rate					×	×		×	
Programmed burn	×	×	×		×	×	×	×	×
Other					×	×	×	×	
Volumetric									
Mie–Grüneisen				×	×			×	×
Tillotson	×	×		×		×	×	×	×
JWL	×		×	×	×	×	×	×	×
Polynomial					×				
Gamma law	×	×		×	×		×	×	×
Crushable/porous					×	×	×	×	
Ad hoc					×	×	×		
Other			×		×		×	×	
Properties									
Isotropic	×	×	×	×	×	×	×	×	×
Orthotropic							×		
Materials library	×				×				

Another new development is the implementation of these codes on personal computers. Both AUTODYN and ZEUS are designed to run on desktop machines. An entire family of codes to study the behavior of energetic materials has been developed in one and two dimensions based on descriptions in Mader (1979) and implemented on personal computers. For example, the TDL code (Mader 1987a, 1987b) is capable of treating both inert and energetic materials. For the latter, a variety of reaction kinetics models are available (Forest Fire, C-J Volume, Sharp Shock Burn, Arrhenius, Gamma Law, Taylor Wave) together with appropriate equation of state formulations. Metals are treated as described in Chapter 11, and a variety of initial and boundary conditions may be selected. These are fully two-dimensional finite-difference and finite-element codes, every bit the equivalent of their mainframe counterparts, not some stripped-down versions of two-dimensional codes. Naturally, execution time on a personal computer (PC) is considerably longer than on a mainframe, but a number of other factors need to be considered:

TABLE 10. Lagrangian Codes—Failure Criteria

	DYNA2D	DYNA3D	EPIC-2	EPIC-3	DEFEL	HEMP	HEMP3D	TOODY	ZEUS	HULL	DYSMAS/L	AUTODYN	PISCES2DELK	PISCES3DELK
Instantaneous														
P_{min}	×	×	×	×	×	×	×	×	×	×	×	×	×	×
Effective plastic strain		×	×	×	×				×		×	×	×	×
Principal stress/strain								×		×	×			
Volumetric strain/maximum distension		×	×	×	×				×					×
Plastic work								×						
Internal energy											×			
Hancock–McKenzie										×			×	
Other						[a]	[a]				×			
User supplied												×		
Cumulative damage														
Tuler–Butcher	Ad hoc in many codes: Not in production versions													
G. R. Johnson			×											
Micromechanical														
SRI NAG/FRAG/SNAG							×	×						
Sandia Models	Incorporated in in-house codes, mainly one dimensional													
Los Alamos models	Incorporated in in-house codes, mainly one dimensional													

[a] See documentation for advanced fracture models not in production versions of HEMP.

1. A simple comparison of execution times is illusory. Granted a supercomputer is much faster than a PC; it is also much more complex and much more utilized. To use the supercomputer, it is necessary to learn complex communications protocols and job control languages. That done, one then submits a problem and waits. If the machine is close to being overloaded, 15 min of CPU time may require a full day of real time (i.e., the time between submission and receipt of output). The PC, in the meantime, can be dedicated to a single code, is relatively user friendly, easy to learn, and relatively inexpensive —after the initial purchase price it requires only electricity, paper, and occasional maintenance. A problem that runs for 1 h on a supercomputer may run 24 h on current 286 PC machines, but the real-time turnaround may be no worse if one is dealing with a heavily utilized mainframe. At worst, assuming a 20-h run time, one is guaranteed at least five calculations per week. This might be no worse than can be achieved on some mainframes.

2. A charge must be paid each time a calculation is performed on a mainframe. With PC-based codes, there is an initial expenditure for the PC and the code. There will also be smaller charges for annual updates and

TABLE 11. Eulerian Codes—Failure Criteria

	HELP	METRIC	CSQII	SOIL	HULL	DYSMAS/E	AUTODYN	PISCES2DELK	PISCES3DELK
Instantaneous									
P_{min}	×	×	×	×	×	×	×	×	×
Effective plastic strain						×	×	×	×
Principle stress/strain					×				
Volumetric strain/maximum distension	×	×		×		×			×
Plastic work	×								
Internal energy									
Hancock–McKenzie					×			×	
User supplied							×		
Other						×			
Cumulative damage									
Micromechanical									
SRI NAG/FRAG/SNAG	×								

improvements. Thereafter, the cost of calculations is limited to electricity and paper. This makes PC-based codes ideal as training devices, where mistakes can be made cheaply and often. They can also be used for preliminary screening calculations, prior to submission of a long run to a mainframe. Finally, for those organizations that cannot afford mainframe time but need a computational capability that goes beyond back of the envelope, they may serve for production calculations. PC-based codes can now do respectable computations in 6–20 h. As the capabilities of PCs increase, run times will decrease while problem size (or resolution) increases.

12.2. CODE SELECTION CRITERIA

In too many cases the decision to acquire a large-scale wave propagation code is made lightly. The common motivations include the following:

1. A variant of "keeping up with the Joneses." Someone, usually a mid-level manager, is impressed by a show-and-tell briefing featuring three-dimensional color renditions of computational results and decides that his organization, to be competitive, should also do computations. This decision is usually influenced by information that a particular problem required n hours or minutes of supercomputer time for such beautiful results. Inevitably omitted from such briefings are reminders that such codes required from 15 to 25 man-years of development, that they are in no way easy-to-use "black boxes" and require a

minimum commitment of six months to two years just to implement the code on an in-house computer and learn to use it with a reasonable degree of competency. During this period, adherence to a "one person–one code" philosophy is necessary. Equally necessary is contact with other experienced code users or code developers during the learning period. Mandatory is the acquisition of material data for the constitutive equations employed in the code determined from wave propagation experiments at strain rates appropriate for the problems being addressed.

Assuming all this has been done—it almost never is—there still remains the problem of rendering the results of code computations in usable graphical form. While most current wave codes are readily transportable, postprocessing routines are still highly device dependent. The color slides and movies produced readily at one installation may require a major investment in graphics hardware at another—a minor detail often missed in the course of a well-prepared briefing!

None of these mistakes would be made if the discussion involved acquisition of an experimental facility. There is, however, a mindset regarding computer codes that takes into account only the initial cost and totally ignores the much larger cost of training and continuing support of a computational facility. The inevitable result is that a junior engineer, with little or no experience with wave propagation phenomena, is reassigned or recruited to perform calculations and is usually expected to reproduce the types of results seen in the literature in three months or less.

2. "My friend has one" and has been getting good results with his code. The friend may be working on one type of problem, say structural impact, at low striking velocities and hydrodynamic pressures comparable to material strength, but the code is acquired for a completely different application (say, hypervelocity impact). Not only is a lot of time and money wasted trying to do a problem that the code was never intended to solve, but the acquisition and learning process has to be started all over again when a code suitable for the problem is finally acquired, usually after some help from an experienced (and expensive) consultant.

3. "It's free." Indeed, many codes described here were developed under government contracts and are available to qualified users through government laboratories at no cost or for a nominal charge. So far, so good, but now who is going to help you learn it and run it? That part certainly isn't free. In addition, all the cost factors cited in the first motivation apply.

The acquisition of a computer code and its intelligent use implies commitment of significant manpower and equipment costs. Properly utilized, this capability can result in considerable savings in the engineering design cycle. Herrmann (1977) cites an example where savings of $1.1 million and 10 months were made possible by the use of computer simulations in the design of an item of military hardware. Such savings do not occur by default. They

TABLE 12. Code Selection Criteria: Nature of the Physical Problem

Impact Velocity	
	$v/c < 0.2$
	$0.2 < v/c < 0.75$
	$v/c > 1.0$
Response time	
Microseconds	
Milliseconds	
Seconds	
Hydrodynamic pressure	
	$P = O(\sigma)$
	$P > \sigma$
	$P \gg \sigma$
Explosive loading	
Simple burn	
Reaction kinetics	
Degree of distortion	
Materials	
Failure modes	

require consideration of a number of factors (Tables 12 and 13) prior to making a commitment.

First and foremost should be consideration of the types of problems to be solved. If the main interest is in the long-term response of a structure due to impact or impulsive loading (i.e., where the details of wave propagation are unimportant) and expected deformations are moderate, then a structures-type

TABLE 13. Code Selection Criteria: Other Considerations

Budget
- Manpower costs
- Computer costs

Experience of code user(s)
- Documentation
- Availability of training/support

Type of computer

Access to computer

Corporate/laboratory atmosphere

Availability of materials data

Access to experiments

code with an implicit time–integration scheme is called for. Many such codes are available. However, if the contact problem must be solved explicitly (i.e., one knows initial velocities and geometries of the contacting bodies but not the nature of the loading pulse), then a code with explicit sliding interface logic is required. This, among structures codes, reduces the choices to ADINA, MAGNA, and NIKE [see Zukas (1987) and references therein for a summary of code capabilities]. The sliding interface logic allows the contact force to be computed as a by-product of the calculation.

Problems in the "ordnance velocity" regime (1–3 km/s) are characterized by high-pressure pulses that initially exceed the strength of the material by an order of magnitude or more but, because of the presence of free surfaces and material interfaces, decay rapidly to the order of the material strength. These are accompanied by high strain rates, especially at the impact interface and plastic strains in excess of, for example, 60%. All these features result in large, but highly localized deformations. In addition, fracture due to the interaction of stress waves with material interfaces and free surfaces can occur by a wide variety of mechanisms (Zukas et al. 1982; Woodward 1987). Such problems can be addressed by Eulerian codes or Lagrangian codes that feature continuous rezoners or an eroding interface capability. They can also be treated by coupled codes, with the highly distorted region being modeled as Eulerian while the quiescent portions of the grid are treated in a Lagrangian manner. Hypervelocity impact situations almost inevitably call for Eulerian codes, although recent results with Lagrangian codes with eroding interface capabilities have been very promising.

If explosives are involved in the calculation, a decision must be made regarding the acceptability of the simple burn models contained in wave codes. An initiation time, location, and a detonation velocity are specified by the user. The code then sweeps the detonation front through the explosive material at the prescribed velocity, with the detonated explosive being treated by a simple gas law equation of state. This approach is adequate if the main interest is in transferring the energy of the explosive to another body. If reaction kinetics are important, then the explosives codes described by Mader (1979) must be used.

A proper constitutive model and characterization of the materials at appropriate loading rates are the keys to many successful simulations. The models in production codes were initially formulated for metals. Excellent results have been obtained over the past 25 years for metallic materials and structures vis-á-vis experimental results. Until very recently, experiments yielded only global data–deformed profiles of striker and target, net velocities, and the overall extent of damage. Since the equations solved by wave propagation codes include inertia effects, which dominate most high-velocity impact processes, and since a large body of high rate data for such materials has been developed, accurate values of displacements and velocities are easily obtained. The rate equations for elasto-plastic-hydrodynamic behavior have not been severely tested for their ability to predict local phenomena—strains, stresses,

adiabatic shearing phenomena, and so on. Experimental techniques now exist to measure strains during an impact event, dynamic pressures, wave arrival times, and related quantities. If the localized material behavior is the main object of study, then it may become necessary to implement other constitutive equations in existing codes. For determination of integral quantities and comparison with analytical methods or postmortem experiments, good results can be expected if the metals involved have been well characterized.

Materials such as composites and ceramics are not well characterized insofar as their high rate behavior is concerned, not do definitive models exist for incorporation into codes. Many ad hoc calculations are performed using some form of the elasto-plastic rate equations with limits imposed on the maximum tensile pressures and strains that the material may experience. Failure modes for these materials are either unknown or guessed at. Some calculations have shown fair agreement with experiments, but this is purely fortuitous since the correct physics is not incorporated in the codes.

Based on the answers to these questions, a preliminary decision may be made as to the code most suitable to address it. This, however, should be tempered by the considerations listed in Table 13.

A realistic estimate of costs, manpower, code acquisition, and maintenance and computing costs should be made at the outset. It may indicate that, if only a few calculations are needed yearly, it is cheaper to have these done under contract than to establish an in-house group.

The experience of code users will be another important factor in the selection of a code. An inexperienced group will require a code that is well documented. The availability of outside support, in the form of formal training and informal contacts with code developers or experienced users, is another factor. Starting off with a coupled code would not be appropriate for such a team. Instead, developing expertise with one- and two-dimensional codes and the numerical techniques associated with them would be good training before moving on to more complex codes. At least six months should be allowed such a group to become familiar with the tools of their new trade and establish contacts with other code users before imposing any requirements for results. Experienced users familiar both with computational techniques for wave propagation problems and with the physical problems to be addressed can begin with more complex codes and, after an initial break-in period (6 months to 2 years, depending on the code), can be expected to make simple modifications to the code, such as replacing constitutive models, failure criteria, or integration schemes.

The type of computer as well as access to it will govern selection of a code. The codes described here run on a variety of machines. Run times, however, vary depending on the speed of the machine and the efficiency of a particular code. If the in-house computer is a supercomputer with ample time available, two- and three-dimensional calculations can readily be performed with any of the codes mentioned. If it happens to be a VAX, complicated calculations may require the full memory capacity of the machine and run upward of 200 h.

Unless the machine is specifically dedicated to the code, this may be an unacceptable situation, especially if the computer is used in a time-sharing mode by the entire organization.

Finally, there is nothing more futile or frustrating than running computations in isolation from the rest of the world, especially during the first few years of developing familiarity with a code. The computational group should work closely with experimentalists in the problem area of concern. Equally, strong efforts should be made to keep in touch with computational groups at other laboratories as well as sources of materials data. The iteration of computations, experiments, and material characterization, as advocated in NMAB (1980) is a very cost-efficient approach to solving high-velocity impact problems. The time spent establishing such contacts and attending relevant conferences should be built into the planning cycle and budget when establishing a computational facility.

All the items listed in Tables 12 and 13 can be assigned a priority and existing codes evaluated against these criteria. This will result in one or two codes that must closely suit in-house capabilities and needs. An example of this procedure can be found in Weickert (1983).

12.3. APPLICATIONS

Three-Dimensional Computer Simulation of a Linear Self-Forging Device

Many of the geometries of interest in the study of self-forging fragments (SFF) [alternatively, explosively formed penetrators (EFP)] can be routinely modeled using two-dimensional computer codes. However, devices using nonaxisymmetric liners are also of interest in demolition and mining applications. Weickert and Kimsey (1983) used an earlier version of the EPIC-3 code (Johnson 1981) to study linear self-forging fragment devices. A linear self-forging fragment device produces an explosively formed long rod fragment that flies in a direction transverse to its longitudinal axis and has the capability to produce a long cut in the target. This "cutting" property makes these devices attractive for demolition applications.

The linear self-forging fragment device studied by Weickert and Kimsey (1983), consisting of a steel liner and castable HMX explosive, is shown in Figure 1. The corresponding computational mesh is shown in Figure 2. Taking advantage of symmetry, only half the device was modeled. The Jones–Wilkins–Lee equation of state was used to describe the pressure–volume–energy behavior of the detonation products of the high explosive. Explosive properties for the explosive were obtained from Dobratz (1981). The incremental elastic-plastic constitutive relationship described in Chapter 11 was used for the steel, taking the yield strength to be 331 MPa and the ultimate strength as 517.2 MPa. The steel liner was modeled using 3 layers of elements

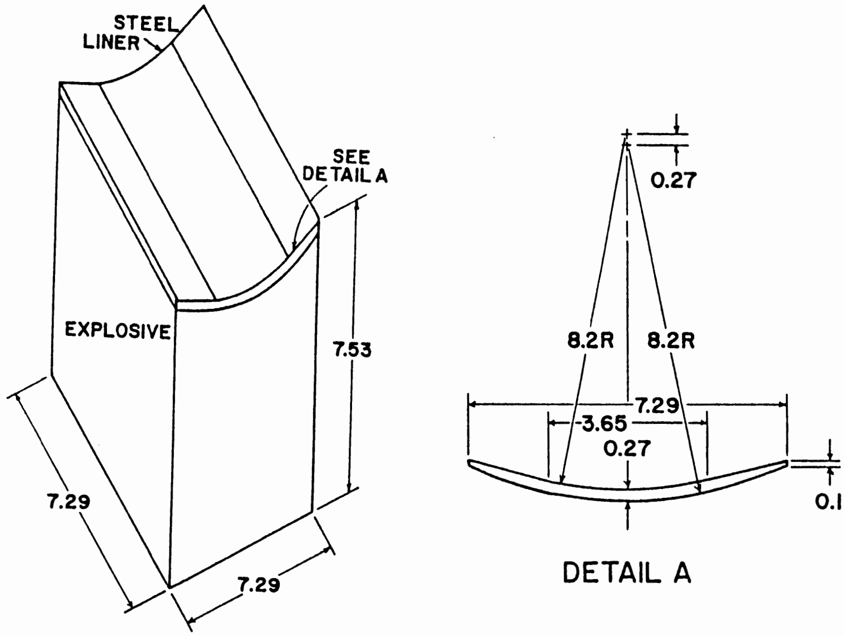

Figure 1. Schematic of linear self-forging fragment device (all dimensions in centimeters).

through its thickness while 10 layers of elements were used through the explosive. Thus, the liner model consisted of 3444 nodes and 14,400 elements. The explosive model contained 2541 nodes and 12,000 elements.

The mesh generators available in EPIC-3 at the time had the capability to automatically generate computational grids for plates, disks, spheres, and rods with various nose shapes. However, none of these applied to the geometry being studied. As a result, the computational mesh had to be generated on a node-by-node, element-by-element basis. This manual generation of the computational mesh, which consists of 5985 nodes and 26,400 elements, consumed *approximately one man-month of time*.

The relative motion of materials at material interfaces is a paramount consideration in any analysis of explosive–metal interactions. In explosively formed penetrator analysis, sliding surfaces are typically placed at the liner–explosive, liner–case, and explosive–case interfaces. The sliding surface algorithm in EPIC-3 required that all the nodes of a given sliding surface be core resident. This requirement prevented the modeling of the material interface along the explosive–case interface, and the casing has not been included in the model. Only one sliding surface, between the liner and explosive material, has been modeled.

The explosive is point initiated at the center of the back face of the explosive. By 25 μs (see Figure 3), the pressure in the detonation products is

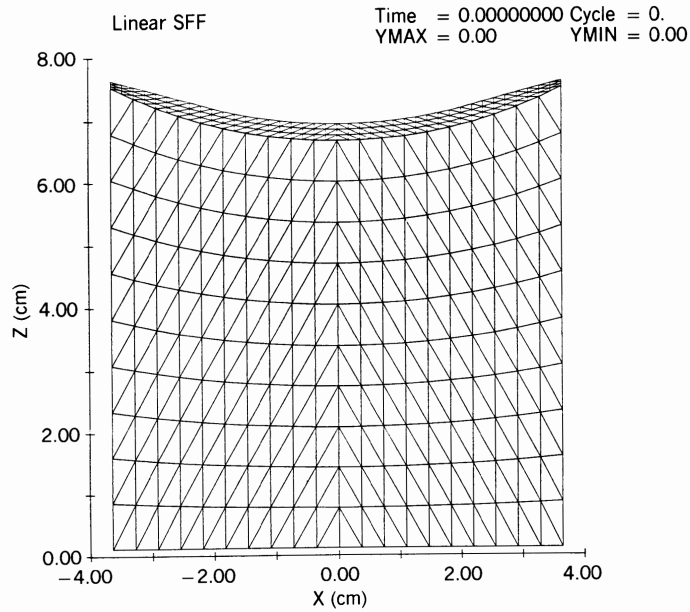

Figure 2. Computational mesh.

approximately one-half of one percent of the detonation pressure. In addition, the net velocity at the center of gravity of the liner is a constant 2.22 km/s. At this point, all of the explosive elements were removed from the computation. The formation process of the liner was terminated at 80.8 μs (Figure 4) for two reasons. First, the time increment, being controlled by the severely distorted elements on the trailing edge of the fragment, was extremely small. Due to the large computer resource requirements of this simulation, it was considered cost prohibitive to remove these severely distorted elements and continue the computation. Second, the basic shape excluding the trailing edges did not change appreciably between 60 and 80 μs. Hence, steady-state conditions had been achieved and further computations were not warranted.

The computations described here required 16 CPU hr on a CDC 7600 machine and 220,000 octal words of central memory. The availability of supercomputers would reduce the CPU time considerably, making such calculations economically feasible. The calculation does point out, however, the need for user-friendly software packages for rapid generation of input data as well as comprehensive postprocessing of the extensive information generated during the simulation. Development of such packages for the major production codes, where they do not already exist, represents a substantial, one-time investment, but is well worth the cost. Although introducing additional computer resource costs to perform the requisite graphics, large savings in analyst manhours can be achieved through the use of efficient, user-friendly pre- and postprocessing packages.

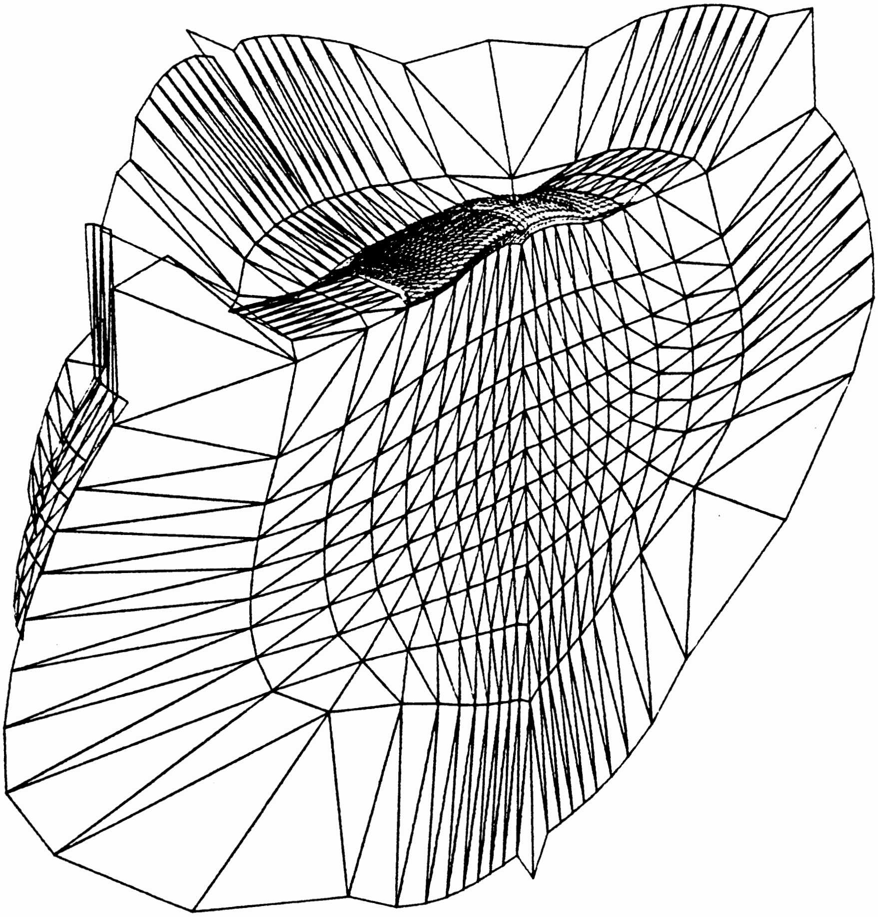

Figure 3. LSFF formation at 25 μs.

Explosive Loading of Lead Hemispherical Liners

A combined experimental-computational study of the behavior of lead hemispheres of various thicknesses subjected to explosive shock loading was performed by Walters et al. (1985), as mentioned in Chapter 10. The study shows the advantages of a combined program with computations supplementing the data obtained from experiments. It points out the need for adequate resolution in numerical simulations in order to match the salient features observed in experiments even though this may increase the cost of computations. Finally, it points out that the methods for calculating kinetic, internal, and total energies in the various codes can play a crucial role in determining valid temperature profiles in the colliding solids.

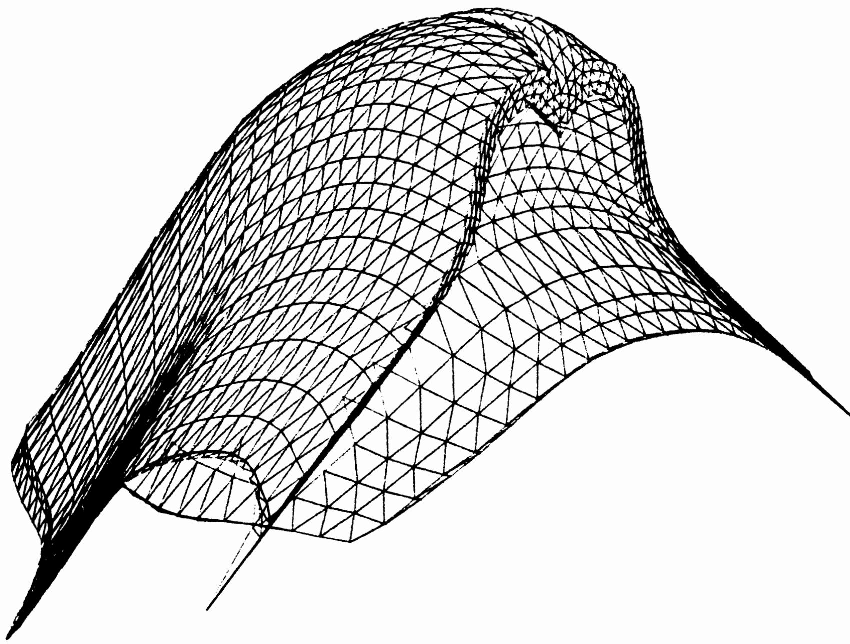

Figure 4. LSFF formation at 80.8 μs.

Traditionally, jets from lead-lined shaped charges exhibit fluid characteristics (Evans 1950) due at least in part to the low bulk sound speed and the low melting temperature of lead. This has resulted in poor performance for the penetration of monolithic and spaced target arrays in comparison with other liner materials. Table 14 shows a comparison of lead and copper properties. Copper is a proven performer in hemispherical shaped charge liners.

In this study, lead hemispheres of different wall thicknesses were examined under explosive loading conditions. Lead is an attractive material due to its ready availability, low cost, and high density, hence the motivation for recurring attempts to put it to practical use. The test configuration consisted of a uniform wall hemispherical liner that was press fit into an aluminum confined cylindrical charge with 75/25 OCTOL as the high explosive. The lead

TABLE 14. Material Properties

Property	Lead	Copper
Density (kg/m^3)	11.35×10^3	8.9×10^3
Melting temperature (°C)	327	1082
Bulk sound speed (km/s)	2.03	3.96

liner outer diameter was 127 mm while the aluminum cylinder was 190.5 mm high with a wall thickness of 3.2 mm (see Chapter 14). The charge was point initiated with a head height of 127 mm.

Three different wall thicknesses for the lead liner were studied. These are given in Table 1, Chapter 14, together with experimental results. The intent of the program was to improve the quality of the shaped charge jet resulting from the liner configuration. The target plates were stacked against each other and were 203 × 203 × 50 mm thick. The standoff distance was 17.15 CD (charge diameters), where the charge diameter was 127 mm. The choice was an arbitrary one, made for the convenience of stacking the targets and positioning of the X-ray film. Flash radiographs depicting jets from the three configurations are shown in Chapter 14. Since the liners were machined from remelted lead, the liner material undoubtedly contained some impurities. Additionally, the liners were not fabricated to the usual precision demanded of shaped charge liners since the specified tolerance on the normal wall thickness was ±0.001 in. (±0.0254 mm) as opposed to the usual shaped charge tolerances of ±0.0005 in. (0.0127 mm) since liner precision is not as critical in spherical charges as in conical charges. Table 1 of Chapter 14 also lists characteristics of a small diameter (50.8 mm) lead hemispherical liner as scaled from the 127-mm liner, except that the wall thickness was 1.9 mm. This liner was tested to provide data regarding the rear of the jet. The delay times were altered to allow the tip of the jet to leave the field of view covered by the film in order to provide coverage of the jet tail. Radiographic data for this jet is also shown in Chapter 14.

These figures clearly show that jet quality improves as the wall thickness increases (i.e., the jet becomes less fluid, more solid in appearance as wall thickness increases). Correspondingly, the jet tip velocity decreases as wall thickness increases since the liner becomes more massive. Penetration into the target array increases with increasing wall thickness but does not appear to do so linearly with increasing thickness. Keep in mind, however, that these conclusions are based on "one-shot statistics" and require further study. It can be postulated, however, that some optimum wall thickness for lead liners should exist since increasing wall thickness leads to a reduction in jet fluidity while at the same time reducing tip velocity, which affects penetrability of target arrays.

Figure 79 of Chapter 14, included to show the tail structure of the jet, illustrates that a fluid region exists near the rear of the jet and shows that the massive slug generated by conical linear designs in other materials is not present. The liner shown here (round No. 3157) has a wall of thickness similar to that of round No. 2952 and diminished target penetration at the long standoff of 31 CD. The rear view of the jet is a valuable asset in determining the quality of jet over its length as well as in determining the total length.

Two interesting points may be raised in view of these results. First, it would be fruitful to investigate even thicker liners with regard to their jet quality and performance against monolithic RHA targets. In fact, a lead hemispherical

liner with a 16% wall (20.3 mm) was studied analytically. The ultimate goal of such a study would be to obtain penetration as a function of wall thickness at a given standoff to deduce an optimum liner design for lead. This design, albeit heavy, should yield performance results more consistent with metals having high melting temperatures.

A second point of interest is the obvious transition of the fluid characteristics of the jet as the wall thickness increases. The thin wall liner yields a jet with considerable amounts of vapor present. The vapor content of jets from thicker liners is markedly reduced. Most probably they are in a solid or liquid phase. Information regarding liquefaction of the jet can be obtained by firing the jet into a target at an oblique angle to the jet axis. A liquid jet would exhibit considerable splatter against an oblique plate, whereas a much cleaner (and deeper) penetration channel would be obtained from a solid jet.

Further studies to assess jet phase, quality, and tip velocity as functions of wall thickness can be performed with large-scale computer codes. Such codes can readily assess the effects due to the variation of single liner parameter on jet behavior and penetration capability. The series of experiments described here provides an excellent challenge for codes, especially their capability to predict characteristics related to thermodynamic behavior such as internal jet energy and temperature gradients in jets. The jet shown in Figure 76 of Chapter 14 should show high temperatures and correspondingly large amounts of vapor. The temperature gradient should decrease as the liner wall thickness increases. Lead has negligible strength (as compared to other materials used in shaped charge liners) so that a pure hydrodynamic analysis should be sufficient, avoiding unknown constitutive relationships.

Calculations were performed with HULL and EPIC. Initial calculations with HULL for round No. 2952 indicated a tip velocity of 3.25 km/s, a value considerably below that found in the experiment. This caused some concern, so a calculation was performed with a similar geometry but with a copper liner and results compared with experiment and HELP code calculations (for this case, the aluminum cylinder height was 17.8 cm, its wall thickness was 3.2 mm, and the liner thickness was 3.3 mm). HULL again underpredicted the tip velocity but was within 10% of the experimental value and showed the same trends as the HELP code results (Arbuckle et al. 1980). EPIC predicted a tip velocity of 3.79 km/s when using five quadrilateral cells across the wall thickness for round No. 2952.

Assuming that the materials were sufficiently well characterized, the authors performed several additional calculations using HULL with both copper and lead liners, varying the size and number of computational cells. Results are shown in Table 15. It is evident that results are quite sensitive to cell size and that problems of this type require adequate spatial resolution if good comparison with experiment is to be expected. If these results are extrapolated to the experimentally determined tip velocity, then adequate resolution would be obtained with a cell size of 0.25 mm for lead liners. However, this would require an excessive amount of computer time.

TABLE 15. Spatial Resolution Effects

	Lead (5.08-mm wall)		Copper (3.3-mm wall)		
Cell Size (mm)	No. of Cells Through Wall Thickness	Tip Velocity (km/s)	No. of Cells Through Wall Thickness	Tip Velocity (km/s)	CPU Time (hr)
0.5	10.0	3.65	6.6	4.26	8.0
1.0	5.1	3.25	3.3	3.99	2.0
1.5	3.4	3.13	2.2	3.68	0.5

Two additional HULL calculations with the lead liners were carried out, one with a 2.97 mm wall thickness, the other with a 20.32 mm wall thickness. Both used the fine grid size (0.5 mm). The resulting tip velocities were 4.35 and 3.29 km/s, respectively. The thin liner results were again within 10% of experiment and again on the low side. EPIC calculations for the 2.97 mm wall thickness lead liner gave a tip velocity of 4.8 km/s, which was an overprediction. No experimental data were available for the extremely thick-wall liner.

Reliable estimates of jet temperature could not be obtained from the HULL calculations. Temperatures are derived from internal energies that in turn are obtained from the differences between total and kinetic energies, two large numbers resulting in unreliable internal energy values. However, the calculations did show a trend of lower temperature in the jet with increasing wall thickness, which is consistent with decreased vaporization seen experimentally as liner thickness increases.

On the other hand, EPIC is reported to predict reliable temperatures. As a check, a 42° conical copper shaped charge liner calculation was performed to compare with experimental measurements obtained by von Holle and Trimble (1976, 1977). Experimental measurements of temperature were made by radiometry methods, therefore, only measuring temperatures on the surface of the front portion of the jet. Temperatures in EPIC are determined from

$$T = T_0 + \frac{E_s}{C_s \rho_0},$$

where T_0 is the initial temperature in an element, E_s the internal energy per unit original volume, C_s the specific heat, and ρ_0 the original density. The calculated temperatures were within the scatter of the experimental data obtained by von Holle and Trimble (1976, 1977). The results of the 2.97- and 5.08-mm wall calculation, using EPIC and a value for specific heat of 1.59×10^6 erg/g °C, show that temperature increases in the radial direction of the jet as you approach the center and the higher temperatures were present along the

axis near the tip for the thinner wall liner. Temperatures range from near 300°C along the exterior of the jet to temperatures up to 1200°C along the center line. The interior of the jet is well above the melting temperature for lead. A check was also made with EPIC on the effect of zoning with respect to temperature. For the 2.97 mm wall thickness calculation, the quadrilateral cells across the liner were reduced from 5 to 2. The tip velocity was reduced from 4.8 to 4.35 km/s, but in essence the temperature contours were similar.

It should be noted that the equation of state data for lead at elevated temperatures are sparse. However, the limited available data are sufficient to identify trends in thermal properties.

REFERENCES

Arbuckle, A. L., Walters, W. P., and Aseltine, C. L. (1980), "Analysis of Uniform Wall and Tapered Hemispherical Liners with Several Explosive Confinement Geometries," Ballistic Research Laboratory, ARBRL-TR-02222, March.

Belytschko, T. B., Lin, J. I., and Jonas, G. H. (1987), "Modifications in EPIC-2 Subcycling and Quadrilaterals," Ballistic Research Laboratory, BRL-CR-569, June.

Brown, K. W., and Krahula, J. L. (1981), "Linear-Nonlinear Interface for Finite Element Impact Analysis," American Society of Mechanical Engineers, ASME Paper 81-TG-39, presented at the *Intl. Gas Turbine Conf. and Products Show*, Houston, TX, March 9–12.

Curran, D. R. (1982), "Dynamic Fracture," in *Impact Dynamics*, J. A. Zukas et al., New York: Wiley-Interscience.

Dobratz, B. M. (1981), "LLNL Explosives Handbook. Properties of Chemical Explosives and Explosive Simulants," Lawrence Livermore Laboratory, UCRL-52997, March.

Evans, W. M. (1950), "The Hollow Charge Effect," *Bull. Min. Metall.*, *250*:9–25.

Flanagan, D. P., and Belytschko, T. (1981), "A Uniform Strain Hexahedron and Quadrilateral with Orthogonal Hourglass Control," *Int. J. Num. Meth. Engng.*, *17*:679–706.

Gupta, A. D., Misey, J. J., and Wortman, J. D. (1980), "The Response of a Long Steel Penetrator during the Oblique Penetration of Monolithic Targets," *Proc. 2nd Charlottesville Conf. on High Density KE Penetrator Materials*, Charlottesville, VA, October 13–17.

Herrmann, W. (1977), "Current Problems in the Finite Difference Solution of Stress Waves," in *Nonlinear Waves in Solids*, T. C. T. Ting, R. J. Clifton, and T. Belytschko (eds.), Proc. Workshop at U. of Illinois at Chicago Circle, March 21–23, Army Research Office.

Johnson, G. R. (1981), "Recent Developments and Analyses Associated with the EPIC-2 and EPIC-3 Codes," in *1981 Advances in Aerospace Structures and Materials,* S. S. Wand and W. J. Renton (eds.), AD-01, New York: American Society of Mechanical Engineers.

Mader, C. L. (1979), *Numerical Modeling of Detonation*, Berkeley, CA: University of California Press.

Mader, C. L. (1987a), "TDL—A Two-Dimensional Reactive Lagrangian Hydrodynamic Code for Personal Computers," Mader Consulting Company, Honolulu, HI

Mader, C. L. (1987b), USERTDL—A Code for Helping the User Develop Input Files for the TDL Code Using Personal Computers," Mader Consulting Company, Honolulu, HI

Maenchen, G., and Sack, S. (1964), "The TENSOR Code," in *Methods in Computational Physics*, Vol. 3, B. Alder, et al. (eds.), New York: Academic Press, pp. 181–210.

Malkus, D. S., and Hughes, T. J. R. (1978), "Mixed Finite Element Methods—Reduced and Selective Integration Techniques: A Unification of Concepts," *Comp. Meth. Appl. Mech. Engng.*, *15*:63–81.

Misey, J. J., Gupta, A. D., and Wortman, J. D. (1980), "Simulation Methods for the Evaluation of Structural Response to High Strain Rates," in *Emerging Technologies in Aerospace Structures, Design, Structural Dynamics and Materials*, J. R. Vinson (ed.), Book H00157, New York: American Society of Mechanical Engineers.

Nimmer, R. P., and Boehman, L. (1981), "Transient Nonlinear Response Analysis of Soft-Bodied Impact on Flat Plates Including Interactive Load Determination," Paper 81-0621-CP, *1981 AIAA / ASME / ASCE / AHS 22nd Structures, Structural Dynamics and Materials Conf.*, Atlanta, April 6–8.

NMAB (1980), *Materials Response to Ultra-High Loading Rates*, National Materials Advisory Board, NMAB-356, Washington, D.C.

Noh, W. F. (1976), Lawrence Livermore Laboratory, Report UCRL-52112.

Schultz, J. C. (1985), "Finite Element Hourglassing Control," *Int. J. Num. Meth. Engng.*, *21*:1039–1048.

von Holle, W. G., and Trimble, J. J. (1976), "Temperature Measurement of Shocked Copper Plates and Shaped Charge Jets by Two-Color IR Radiometry," *J. Appl. Phys.*, *47*:2391–2394.

von Holle, W. G., and Trimble, J. J. (1977), "Temperature Measurements of Copper and Eutectic Metal Shaped-Charge Jets," Ballistic Research Laboratory, BRL-R-2004, August.

Walsh, R. T. (1973), "Finite Difference Methods," in *Dynamic Response of Materials to Intense Impulsive Loading*, P. C. Chou and A. K. Hopkins (eds.), Air Force Materials Laboratory.

Walters, W. P., Jonas, G. H., and Zukas, J. A. (1985), "Explosive Loading of Lead Hemispherical Liners," *Comput. Struct.*, *20*(1–3):615–621.

Weickert, C. A. (1983), "Evaluation of Selected Computer Codes for Impact and Explosive Detonation Calculations," DRES Suffield Memorandum No. 1059, Defence Research Establishment, Suffield, Alberta, Canada.

Weickert, C. S., and Kimsey, K. D. (1983), "Three-Dimensional Computer Simulation of a Linear Self-Forging Fragment Device," *Proc. 7th Intl. Symp. Ballistics,* The Hague, The Netherlands.

Wilkins, M. L. (1980), "Use of Artificial Viscosity in Multidimensional Fluid Dynamic Calculations," *J. Comp. Phys.*, *36*:281–303.

Woodward, R. L. (1987), Course Notes for the Short Course *High Velocity Impact Dynamics*, Computational Mechanics Associates, Baltimore, MD.

Zukas, J. A. (1987), in *High Velocity Impact Dynamics*, course notes, Computational Mechanics Associates, Baltimore, MD.

Zukas, J. A., Nicholas, T., Swift, H. F., Greszczuk, L. B., and Curran, D. R. (1982), *Impact Dynamics*, New York: Wiley-Interscience.

BIBLIOGRAPHY: PRODUCTION COMPUTER CODES

AUTODYN

a. *Manuals*

Demonstration Manual
User Subroutines Manual
Rezoning Tutorial
Jetting Tutorial
Printer and Locator Manual
User Manual
Verification Problems Manual

b. *Computational Results*

Birnbaum, N. K. et al. (1987), "Non-Linear Analysis of Missile Impact with Experimental Verification," *Proc. 9th Intl. Conf. SMIRT.*

Cowler, M. S. et al. (1987), "AUTODYN—An Interactive Non-Linear Analysis Program for Microcomputers Through Supercomputers," *Proc. 9th Intl. Conf. SMIRT.*

Cowler, M. S. et al. (1987), "Numerical Simulation of Impact Phenomena in an Interactive Computing Environment," *Proc. Conf. IMPACT87*, Bremen, W. Germany.

Itoh, M., and Cowler, M. S. (1987), "An Interactive Lagrangian Approach to Two Dimensional Penetration Analysis," *Proc. Conf. IMPACT87*, Bremen, W. Germany.

CSQ

a. *Manuals*

McGlaun, J. M. (1982), "Improvements in CSQII: An Improved Numerical Convection Algorithm," Sandia National Laboratories, SAND82-0051, January.

McGlaun, J. M. (1982), "Improvements in CSQII: A Transmitting Boundary Condition," Sandia National Laboratories, SAND82-1248, June.

Thompson, S. L. (1975), "CSQ—A Two-Dimensional Hydrodynamic Program with Energy Flow and Material Strength," Sandia Laboratories, SAND-74-0122.

Thompson, S. L. (1975), "Input Instructions for CSQII—A Ten Material Version of CSQ," Sandia Laboratories, RS5166/135.

Thompson, S. L. (1977), "CSQII—An Eulerian Finite Difference Program for Two-Dimensional Material Response—Part I. Material Sections," Sandia National Laboratories, SAND77-1339.

Thompson, S. L., and Lauson, H. S. (1972), "Improvements in the CHART D Radiation—Hydrodynamics Code II: A Revised Program," Sandia National Laboratories, SC-RR-71-0173, February.

b. Computational Results

CSQIII is often used in conjunction with the TOODY code. Many of the references cited there contain CSQ results as well.

DEFEL

a. Manuals

A manual describing theoretical development and user's directions is available from the developers.

b. Computational Results

Chou, P. C., and Wu, L. (1986), "A Dynamic Relaxation Finite-Element Method for Metal Forming Processes," *Int. J. Mech. Sci.*, *28*(4):231–250.

Chou, P. C., Ciccarelli, R. D., and Walters, W. P. (1983), "The Formation of Jets from Hemispherical-Liner Warheads," *Proc. 7th Intl. Symp. on Ballistics*, The Hague, Netherlands, April 19–21.

Flis, W. J. (1986), "Advanced Algorithms for Computer Simulation of Hypervelocity Impact," *Proc. 1986 Hypervelocity Impact Symp.*, San Antonio, TX, October 21–24.

DYNA2D

a. Manuals

Hallquist, J. O. (1980), "THOR: A Post-Processor for Two-Dimensional Analysis Codes," Lawrence Livermore National Laboratory, UCRL-52852, April.

Hallquist, J. O. (1981), "MAZE—An Input Generator for DYNA2D and NIKE2D," Lawrence Livermore National Laboratory, UCID-19029, April.

Hallquist, J. O. (1982), "ORION: An Interactive Post-Processor for Analysis Codes NIKE2D, DYNA2D and TACO2D," Lawrence Livermore National Laboratory, UCID-17980, January.

Hallquist, J. O. (1984), "User's Manual for DYNA2D—An Explicit Two-Dimensional Hydrodynamic Finite Element Code with Interactive Rezoning," Lawrence Livermore National Laboratory, UCID-18756, Rev. 2, January.

A very thorough description of sliding interface logic is given in:

Hallquist, J. O. (1976), "A Procedure for the Solution of Finite Deformation Contact-Impact Problems by the Finite Element Method," Lawrence Livermore National Laboratory, UCRL-52066.

Hallquist, J. O. (1978), "A Numerical Treatment of Sliding Interfaces and Impact," in *Computational Techniques for Interface Problems*, K. C. Park and D. K. Gartling (eds.), AMD, Vol 30, New York: ASME.

b. *Computational Results*

Goudreau, G. L., and Hallquist, J. O. (1982), "Recent Developments in Large-Scale Finite Element Lagrangian Hydrocode Technology," *Comp. Methods Appl. Mech. Engr.*, *33*(1–3):725–757.

Murphy, M. J. (1983), "Shaped Charge Penetration in Concrete: A Unified Approach," Lawrence Livermore National Laboratory, UCRL-53393, January.

Murphy, M. J., and Henderson, J. M. (1983), "Computer Simulation of Concrete Penetration by Shaped Charge Jets," *Proc. 7th Intl. Symp. on Ballistics*, The Hague, Netherlands, April.

Tuft, D. B., and Murphy, M. J. (1981), "Computer Design of a High Explosive Velocity Augmented Kinetic Energy Penetrator," *Comput. Struct.*, *13*:303–309.

Werne, R. W. et al. (1980), "An Advanced Analytical and Experimental Investigation of the Hydrodynamic Performance of a Misznay–Shardin Warhead," Lawrence Livermore National Laboratory, UCRL-83406.

DYNA3D

a. *Manuals*

Brown, B. E. (1980), "SPIN: A Program for 3-D Axisymmetric Geometry Generation," Lawrence Livermore National Laboratory, UCID-18799.

Brown, B. E., and Hallquist, J. O. (1982), "TAURUS: An Interactive Post-Processor for the Analysis Codes NIKE3D, DYNA3D, TACO3D and GEMINI," Lawrence Livermore National Laboratory, UCID-19392.

Gerhard, M. A. (1979), "SLIC: An Interactive, Graphic Mesh Generator for Finite-Element and Finite-Difference Application Programs," Lawrence Livermore National Laboratory, UCRL-52823.

Hallquist, J. O. (1981), "MAZE—An Input Generator for DYNA2D and NIKE2D," Lawrence Livermore National Laboratory, UCID-19029, April.

Hallquist, J. O. (1983), "Theoretical Manual for DYNA3D," Lawrence Livermore National Laboratory, UCID-19401, March.

Hallquist, J. O. (1986), "DYNA3D User's Manual (Nonlinear Dynamic Analysis of Solids in Three Dimensions)," Lawrence Livermore National Laboratory, UCID-19592, November 1982; Rev. 1, April 1984; Rev. 2, March.

b. Computational Results

Benson, D. J., and Hallquist, J. O. (1986), "A Simple Rigid Body Algorithm for Structural Dynamics Programs," *Int. J. Num. Meth. Engr.*, *22*:723–749.

Chiesa, M., and Callabresi, M. (1981), "Nonlinear Analysis of a Mitigating Steel Nonsecone," *Comput. Struct.*, *13*:295–301.

Goudreau, G. L., and Hallquist, J. O. (1982), "Recent Development in Large-Scale Finite Element Lagrangian Hydrocode Technology," *J. Comp. Meth. Appl. Mech. Engr.*, *33*:725–757.

Hallquist, J. O., Benson, D. J., and Goudreau, G. L. (1986), "Implementation of a Modified Hughes–Liu Shell into a Fully Vectorized Explicit Finite Element Code," in *Finite Element Methods for Nonlinear Problems*, P. G. Bergan, K.–J. Bathe, and W. Wunderlich (eds.), Heidelberg: Springer-Verlag.

Tuft, D. C., and Godfrey, C. S. (1982), "Computer Analysis of a Three-Dimensional Mass Focus Projectile Device," Lawrence Livermore National Laboratory, UCRL-87678.

DYSMAS

DYSMAS/L

a. Manuals

Internal documentation by G. Bretz, A. Poth, J. Massmann, F. Scharpf, R. Schwarz, J. Sielaff, and W. Jarzab.

b. Computational Results

Bretz, G., Jarzab, W., and Raasch, I. (1986), "Berechnung eines frontalen Crashvorganges bei einer heckangetriebenen Limousine," VDI-Berichte 613, D. Radaj (ed.), pp. 507–525, *Proc. VDI Conf.*, "Berechnung im Automobilbau," Wurzburg, Germany, November, VDI-Verlag, Dusseldorf.

Jarzab, W. (1986), "Mathematical Modeling and Applications in Crash Analysis, in Supercomputer Applications in Automotive Research and Engineering Development," Suppl., C. Marino (ed.), *Proc. Intl. Conf. of Supercomputer Appl. in the Automotive Industry*, Zurich, Switzerland, October, Computational Mechanics Publications, Southhampton.

Jarzab, W. (1987), "Numerical Simulation and Experimental Validation in Crashworthiness Applications," *Proc. COMPAUTO 87*, Geneva, Switzerland, March, Computational Mechanics Publications, Southhampton.

Poth, A. et al. (1981), "Experimental and Numerical Investigation of the Ricocheting of Projectiles from Metallic Surfaces," *Proc. 6th Intl. Symp. on Ballistics*, Orlando, FL.

Poth, A. et al. (1983), "Failure Behavior of an Aluminum Plate under Impact Loading," *Proc. Intl. Conf. on Appl. Of Fract. Mech. to Matls. and Struct.*, Freiburg, W. Germany.

Poth, A. et al. (1985), "Impact Damage Effects and Computational Methods," AGARD, *60th Mtg. of Struct. and Matl. Panel*, April, San Antonio, TX.

Poth, A. et al. (1985), "Structural Response to Weapon Loading—Areas of Application of Eulerian, Lagrangian and Coupled Codes," *2nd Symp. of Interaction of Non-Nuclear Munitions with Struct.*, April, Panama City, FL.

Poth, A. et al. (1985), "Application of Nonliner FE/FD-Methods for Support of Structural Tests," AGARD, *61st Mtg. of Struct. and Matl. Panel*, September, Oberammergau, W. Germany.

Schwarz, R. et al. (1983), "Analysis of Reinforced Concrete Structures Subjected to Aircraft Impact Loading," *Proc. 7th Intl. Conf. on Struct. Mech. in Reactor Technol.*, Chicago.

Schwarz, R. et al. (1985), "Calculation of Impact- and Penetration-Effects on Hardened Reinforced Concrete Structures," *2nd Symp. of Interaction of Non-Nuclear Munitions with Struct.*, April, Panama City, FL.

DYSMAS/E

a. Manuals

Internal documentation by H. J. Diekhoff, B. Fiessler, G. Hausmann, F. Scharpf, and H. J. Schittke.

b. Computational Results

Klaus, M., and Schittke, H. J. (1984), "Anwendung des Hydrodynamik-Codes DYSMAS/E auf Ausbreitung und Wirkung nuklearer Luftstosswellen," IABG-Report B-TF-1633.

Renn, W., Scharpf, F., Schittke, H. J., and Schwarz, R. (1985), "Numerical Simulation of Fuel Spillage Following an Aircraft Impact onto a Nuclear Power Plant," *8th Intl. Conf. on Struct. Mech. in Reactor Tech.*, Brussels, Belgium, August 19–23.

Schittke, H. J., Diekhoff, H. J., and Fiessler, B., "Simulation der Wechselwirkung zwischen Anzundschwaden und einem Inert-Pulverbett," 12. Wehrtechnisches Symposium, "Innenballistik der Rohrwaffen," Mannheim 29.10–31.10.

DYSMAS/ELC

a. Manuals

Internal documentation by B. Fiessler, J. Kinscher, W. Pfrang, A. Poth, F. Scharpf, and H. J. Schittke.

b. Computational Results

Bergerhoff, W., Mohr, W., Pfrang, W., and Scharpf, F. (1985), "The Program DYSMAS/ELC and Its Applications on Underwater Shock Loading of Vessels," in *Maritime Simulation*, M. R. Heller (ed.), Proc. 1st Intercontinental Symp., Munich, June, Berlin: Springer-Verlag.

Fiessler, B. et al. (1983), "Use of DYSMAS/ELC for the 3-D Analysis of PWR Fluid-Structure Interaction Problems," *Proc. 7th Int. Conf. on Struct. Mech. in Reactor Technol.*, Chicago.

Pfrang, W., and Mohr, W. (1985), "Structural Response of a Bucket under Severe Underwater Explosion Loading, Part II: Numerical Investigation," *Vortrag 56th Shock and Vibr. Symp.*, Monterey, CA, October.

Pfrang, W. et al. (1986), "Shock Loading of a Vessel by an Underwater Explosion—A Numerical Simulation Compared with a Full Scale Test," *Vortrag, 57th Shock and Vibr. Symp.*, New Orleans, October.

Pfrang, W. et al. (1987), "Die Numerische Simulation einer verdammten Bodendetonation," *Proc. Intern. Symp. uber Interaktion Konventioneller Munition mit Schutzbauten*, Mannheim, Germany, March.

Scharpf, F. (1985), "Structural Response to Weapon Loadings—Areas of Application of Eulerian, Lagrangian and Coupled Codes," *2nd Symp. on Interaction of Non-Nuclear Munitions with Structures*, University of Florida, Eglin, April.

EPIC-2

a. Manuals

Johnson, G. R. (1978), "EPIC-2, A Computer Program for Elastic-Plastic Impact Computations in Two Dimensions Plus Spin," ARBRL-CR-00373.

Johnson, G. R. (1983), "Development of Strength and Fracture Models for Computations Involving Severe Dynamic Loading. Volume II—Description of Improved EPIC-2 Code," AFATL-TR-83-05.

Johnson, G. R., and Stryk, R. A. (1986), "User Instructions for the EPIC-2 Code," AFATL-TR-86-51.

b. Computational Results

Johnson, G. R. (1976), "Analysis of Elastic-Plastic Impact Involving Severe Distortions," *J. Appl. Mech., Trans. ASME*, *98*(3), September.

Johnson, G. R. (1977), "Liquid-Solid Impact Calculations with Triangular Elements," *J. Fluids Engr., Trans. ASME*, *99*(3), September.

Johnson, G. R. (1979), "Dynamic Response of Axi-Symmetric Solids Subjected to Impact and Spin," *AIAA J.*, September.

Johnson, G. R. (1981), "Dynamic Analysis of a Torsion Test Specimen Including Heat Conduction and Plastic Flow," *J. Engr. Matls. Technol., ASME*, *103*(3), July.

Johnson, G. R. (1981), "Recent Developments and Analyses Associated with the EPIC-2 and EPIC-3 Codes," in *1981 Advances in Aerospace Structures and Materials*, S. S. Wang and W. J. Renton (eds.), AD-01, New York: ASME.

Johnson, G. R. (1982), "Status of EPIC Codes, Material Characterization and New Computing Concepts at Honeywell," in *Proceedings of Computational Aspects of Penetration Mechanics, Lecture Notes in Engineering*, Vol. 3, J. Chandra and J. E. Flaherty (eds.), New York: Springer-Verlag.

Johnson, G. R. (1984), "Computations and Material Characterization for High Velocity Impact and Explosive Detonation," in *Theoretical Foundations for Large-Scale Computations for Nonlinear Material Behavior*, S. Nemat-Nasser, R. J. Asaro, and G. A. Hegemier (eds.), Martinus Nijhoff Publishers, Dordrecht.

Johnson, G. R., Stryk, R. A., and Dodd, J. G. (1986), "Dynamic Lagrangian Computations for Solids, With Variable Nodal Connectivity for Severe Distortions," *Int. J. Num. Meth. Engr.*

Kimsey, K. D. (1980), "Analysis of Hydrodynamic Ram," in *Proc. 1980 Summer Computer Simulation Conf.*, La Jolla, CA: AFIPS Press.

Kimsey, K. D. (1984), "Calculation of Penetration, in *Theoretical Foundations for Large-Scale Computations for Nonlinear Material Behavior*, S. Nemat-Nasser, R. J. Asaro, and G. A. Hegemier (eds.), Martinus Nijhoff Publishers, Dordrecht.

Misey, J. J., Gupta, A. D., and Wortman, J. D. (1980), "Simulation Methods for the Evaluation of Structural Response to High Strain Rates," in *Emerging Technologies in Aerospace Structures, Design, Structural Dynamics and Materials*, J. R. Vinson (ed.), H00157, New York: ASME.

Stecher, F. P., and Johnson, G. R. (1984), "Lagrangian Computations for Projectile Penetration into Thick Plates," *1984 ASME Intl. Computers in Engineering Conf. and Exhibit*, August.

EPIC-3

a. Manuals

Johnson, G. R. (1977), "EPIC-3, A Computer Program For Elastic-Plastic Impact Calculations in 3 Dimensions," BRL CR 343, July.

Johnson, G. R., and Stryk, R. A. (1986), "User Instructions for the EPIC-3 Code," AFATL-TR-86-51.

Johnson, G. R., Colby, D. D., and Vavrick, D. J. (1978) "Further Development of the EPIC-3 Computer Program for Three-Dimensional Analysis of Intense Impulsive Loading," AFATL-TR-78-81, July.

Johnson, G. R., Vavrick, D. J., and Colby, D. D. (1980), "Further Development of EPIC-3 for Anisotropy, Sliding Surfaces, Plotting and Material Models," ARBRL-CR-00429, May.

b. Computational Results

Johnson, G. R. (1977), "Three Dimensional Analysis of Sliding Surfaces During High Velocity Impact," *J. Appl. Mech., Trans. ASME*, *99*(4).

Johnson, G. R. (1981), "Dynamic Analysis of Explosive-Metal Interaction in Three Dimensions," *J. Appl. Mech., Trans. ASME*, *103*(1), March.

Johnson, G. R., Colby, D. D., and Vavrick, D. J. (1979), "Three Dimensional Computer Code for Dynamic Response of Solids to Intense Impulsive Loads," *Int. J. Num. Meth. Engr.*, *14*(12).

Johnson, G. R., and Stryk, R. A. (1986), "Eroding Interface and Improved Tetrahedral Algorithms for High Velocity Impact Calculations in Three Dimensions," *Proc. 1986 Hypervelocity Impact Symp.*, San Antonio, TX.

Kimsey, K. D. et al. (1981), "Computer Simulation of Scaled MK84 Bomb Impact into Concrete," *Proc. Sixth Intl. Symp. on Ballistics*, Oct. 27–29, 1981, Orlando, FL.

Zukas, J. A. (1980), "Impact Dynamics," in *Emerging Technologies in Aerospace Struct., Design, Structural Dynamics and Materials*, J. R. Vinson (ed.), H00157, New York: ASME.

See also references listed in the description of EPIC-2.

HELP

a. Manuals

Hageman, L. J., and Herrmann, R. G. (1977), "Incorporation of the NAG-FRAG Model for Ductile and Brittle Failure into HELP, a 2D MultiMaterial Eulerian Program," Systems, Science and Software, Inc., SSS-R-77-3389, September.

Hageman, L. J., and Sedgwick, R. T. (1972), "Modifications to the HELP Code for Modeling Plugging Failure: User's Manual," USAF Armament Laboratory, AFATL-TR-72-106, June.

Hageman, L. J. et al. (1975), "HELP, A Multi-Material Eulerian Program for Two Compressible Fluid and Elastic-Plastic Flows in Two Space Dimensions and Time," Systems, Science and Software, Inc., SSS-R-75-2654, July.

Walsh, J. M. et al. (1970), "HELP, A Multiple-Material Eulerian Program for Compressible Fluid and Elastic Plastic Flows in Two Space Dimensions and Time," Vols. I & II, Systems, Science and Software, Inc., 3SR-350, June.

b. Computational Results

Arbuckle, A. L., Walters, W. P., and Aseltine, C. L. (1980), "Analysis of Uniform Wall and Tapered Hemispherical Liners With Several Explosive Confinement Geometries," Ballistic Research Laboratory, ARBRL-TR-02222, March.

Chawla, M. S., and Zukas, J. A. (1980), "Numerical Estimation of Stress Intensity Factors by a Finite Difference Eulerian Method (The HELP Code)," Ballistic Research Laboratory, ARBRL-CR-00426, April.

Chou, P. C., Ciccarelli, R. D., Arbuckle, A. L., and Walters, W. P. (1981), "Jet Formation of an Implosively Loaded Hemispherical Liner," Ballistic Research Laboratory, ARBRL-CR-00470, September.

Hageman, J. J., and Walsh, J. M. (1975), "HELP Code Solutions to Two Test Problems in Armor Penetration," Ballistic Research Laboratory, BRL-CR-37.

Kiwan, A. R., and Arbuckle, A. L. (1977), "Study of Liner Collapse, Jet Formation and Characteristics from Implosive Shaped Charge Systems," Ballistic Research Laboratory, BRL-R-2028, November.

Kucher, V., and Harrison, J. (1977), "Shaped Charge Jet Penetration of Discontinuous Media," Ballistic Research Laboratory, BRL-1995.

Misey, J. J., Gupta, A. D., and Wortman, J. D. (1980), "Simulation Methods for the Evaluation of Structural Response to High Strain Rates," in *Emerging Technologies in Aeorspace Structures, Design, Structural Dynamics and Materials*, J. R. Vinson (ed.), New York: ASME.

Schmitt, J. A. (1979), "A New Internal Energy Calculation for the HELP Code and Its Implications to Conical Shaped Charge Simulations," Ballistic Research Laboratory, ARBRL-TR-02168.

Schmitt, J. A. (1980), "Truncation Error Terms in the Kinetic Energy Calculation in the HELP Algorithm and Their Consequences," *J. Comp. Phys.*, *35*(2), April.

Sedgwick, R. T. (1980), "Numerical Techniques for Modeling High Velocity Penetration and Perforation Processes," in *Ballistic Materials and Penetration Mechanics*, R. C. Laible (ed.), Amsterdam: Elsevier. (This reference contains numerous citations to HELP and METRIC code results appearing mainly in government reports.)

Segwick, R. T. et al. (1978), "Numerical Investigations in Penetration Mechanics," *Int. J. Engr. Sci.*, *18*:859–869.

Smith, D. L. (1984) "Speeding Up the HELP Hydrodynamic Code," Materials Research Laboratories, MRL-R-925, May.

Zukas, J. A. et al. (1979), "On the Utility of Plane Strain Approximations for Oblique Impact Calculations," Ballistic Research Laboratory, ARBRL-MR-0269, October.

HEMP

a. Manuals

Giroux, E. D. (1973), "HEMP User's Manual," Lawrence Livermore National Laboratory, UCRL-51079, Rev. 1.

Warren, K. H. (1983), "HEMPDS User's Manual," Lawrence Livermore National Laboratory, UCID-18075, Rev. 1, February.

Wilkins, M. L. (1982), "Calculation of Elastic-Plastic Flow," Lawrence Livermore National Laboratory, UCRL-7322, Rev. 2, February.

b. Computational Results

HEMP has been used extensively since its development in 1964. For representative results, see the following:

Chen, Y. M. (1974), "Numerical Computation of Dynamic Stress Intensity Factors by a Lagrangian Finite-Difference Method (The HEMP Code)," Lawrence Livermore National Laboratory, UCRL-51563, April.

Chen, Y. M., and Wilkins, M. L. (1976), "Stress Analysis of Crack Problems with a Three-Dimensional, Time-Dependent Computer Program," *Int. J. Fracture*, *12*(4): 607–617.

Norris, D. M. et al. (1977), "Mechanics of Long Rod Penetration at High Obliquity," *Proc. High Density Alloys Penetrator Materials Conf.*, Army Materials & Mechanics Research Center, AMMRC-SP-77-3, April.

Norris, D. M. et al. (1978), "A Computer Simulation of the Tension Test," *J. Mech. Phys. Solids*, *26*.

Wilkins, M. L. (1977), "Fracture Studies with Two- and Three-Dimensional Computer Simulation Programs," *Proc. Conf. on Frac. Mech. and Tech.*, Hong Kong, March 21–25, Leyden: Noordhoff.

Wilkins, M. L. (1980), "Computer Simulation of Penetration Phenomena," in *Ballistic Materials and Penetration Mechanics*, R. C. Laible (ed.), North-Holland: Elsevier.

Wilkins, M. L. (1980), "Use of Artificial Viscosity in Multidimensional Fluid Dynamic Calculations," *J. Comp. Phys.*, *36*(3, July).

Wilkins, M. L., and Guinan, M. W. (1973), "Impact of Cylinders on a Rigid Boundary," *J. Appl. Phys.*, *44*(3):1200–1206.

HEMP3D

Wilkins, M. L. et al. (1975), Lawrence Livermore National Laboratory, UCRL-51574, Rev. 1.

HULL

a. Manuals

_______ (1986), "HULL Documentation. Vol. II, HULL User's Guide," Orlando Technology Inc.

_______ (1986), "HULL Documentation. Vol. III, SAIL User's Guide," Orlando Technology Inc.

Durrett, R. E., and Matuska, D. A. (1978), "The HULL Code, Finite Difference Solution to the Equations of Continuum Mechanics," Air Force Armament Laboratory, AFATL-TR-78-125.

Gaby, L. P. (1978), Air Force Weapons Laboratory, C4-C-4041.

Matuska, D. A. (1981), "SAIL User's Guide for Running HULL and EPIC3 Codes," Ballistic Research Laboratory, ARBRL-CR-00466; also AFATL-TR-81-70, September.

Matuska, D. A., and Osborn, J. J. (1986), "HULL Documentation. Vol. I, Technical Discussion," Orlando Technology Inc., Shalimor, FL.

Matuska, D. A., Durrett, R. E., and Osborn, J. J. (1982), "HULL User's Guide for Three-Dimensional Linking with EPIC-3," Ballistic Research Laboratory, ARBRL-CR-00484, July.

Osborn, J. J. (1981), "Improvements in EPIC3—Link to HULL—Improved Equation of State—Improved Fracture Modeling—SAIL Update System—Other Improvements," Air Force Armament Laboratory, AFATL-TR-81-10, June.

Osborn, J. J. (1981), "A Preliminary Model for Loads on a Penetrator Impacting Concrete," Ballistic Research Laboratory, ARBRL-CR-00456; also AFATL-TR-81-53.

Several variants of HULL exist. The code was first written in 1971 as a purely hydrodynamic code and rewritten in 1976 to permit computations involving elastic-plastic flow. In 1979, additional developments were begun to link HULL with the three-dimensional Lagrangian code, EPIC-3. The code was again revised in 1986 and now includes both Eulerian and Lagrangian modules. These can be run separately or linked in a variety of ways.

b. Computational Results

Matuska, D. A., and Osborn, J. J. (1981), "HULL/EPIC3 Linked Eulerian/Lagrangian Calculations in Three Dimensions," Ballistic Research Laboratory, ARBRL-CR-00467; also AFATL-TR-71-81, September.

Nash, M. A., and Cullis, I. G. (1984), "Numerical Modeling of Fracture—A Model for Ductile Fracture in Triaxial States of Stress," in *Proc. 3rd. Conf. on Mechanical Properties at High Rates of Strain*, J. Harding (ed.), Institute of Physics Conference Series 70, Institute of Physics, London.

Osborn, J. J. (1982), "Hydrocode Calculations of High Length-to-Diameter Cylindrical Explosions in Sand," Air Force Armament Laboratory, AFATL-TR-82-10, February.

METRIC

Hageman, L., and Lee, E. P. (1976), "Development of an Ordnance Velocity, Multimaterial, 3D Perforation Code for Finite Plates," Systems, Science and Software, SSS-R-76-2861.

Hageman, L. J., Waddell, J. L., and Herrmann, R. G. (1976), "Application of the Multimaterial, Eulerian, Three-Dimensional METRIC Code to Two Ballistic Impact Situations," Systems, Science & Software, SSS-R-76-2973.

Sedgwick, R. T., Waddell, J. L., and Wilkinson, G. M. (1987), "High Velocity Long Rod Impact: Theory and Experiment," *Proc. 10th Int. Symp. on Ballistics*, San Diego.

PISCES2DELK

a. Manuals

Version 3 manuals

Hancock, S. L. (1976), "Finite Difference Equations for PISCES 2DELK, A Coupled Euler Lagrange Continuum Mechanics Computer Program," Physics International Co., Technical Memorandum TCAM 76-2, April.

Trigg M. et al. (1981), "PISCES 2DELK User's Manual," Physics International Co., April (Version 3).

Version 4 manuals

_______ (1985), "PISCES 2 DELK User's Manual," Version 4, PISCES International, Holland.

Hancock, S. (1985), "PISCES 2DELK Theory Manual," Version 4. Pisces International, Holland.

b. Computational Results

A summary of PISCES code capabilities and extensive computational results are given in two PISCES International brochures:

Buis, J. P. et al. (1984), "The PISCES Software for Nuclear Safety: A Survey of PISCES Code Application to Nuclear Safety Problems," PISCES International B.V., April.

Pohl, W. et al. (1984), "The PISCES Software for Defense: A Survey of PISCES Code Applications for Defense-Oriented Computational Problems," PISCES International B.V., May.

Additional information may be found in:

Bakowsky, T., Coffenberry, J., and Brown, R. E. (1982), "Self-Forging Fragment Design Syntheses," Physics International Co., PIIR-44-82.

Gordon, J. T., and Davison, D. K. (1983), "Calculation of the Shock Wave from a Pentolite Tapered Charge," *The Shock and Vibration Bulletin*, Part 1, Bulletin 52, May.

Hancock, S. L. (1983), "Fluid-Structure Interaction Calculations Using Second Order Upwind Differencing," in *Proc. 7th Intl. Conf. on Struct. Mech. in Reactor Technol.*, Chicago, August.

Hancock, S. L., and Hancock, H. (1977), "A Computatinal Study of Rigid Cones Penetrating Aluminum Targets," Physics International Co., Tech. Memo TCAM 77-4, July.

Hancock, S., Hancock, H., and Behrmann, L. (1982), "Full Lagrange and Lagrange–Euler Shaped Charge Jetting Calculations," Physics International Co., PIIR-3-82.

Kivity, Y., and Hancock, S. L. (1984), "Pebble Impact on Layered targets at High Obliquity," *ASME Intl. Computers in Engr. Conf.*, Las Vegas, Nevada, August.

Kurylo, J., Hancock, S., and Kivity, Y. (1984), "Viscous Flow Calculations of Shock Diffraction and Drag Loads on Arched Structures," *Proc. AIAA 17th Fluid Dynamics, Plasma Dynamics and Lasers Conf.*, June 25–27, Snowmass, CO (AIAA Paper 84-1680).

Schweiger, R., and Pohl, W. (1984), "A Step Towards Computer-Aided Engineering in the Field of Self-Forging Fragment Warhead Design," *Proc. 8th Intl. Ballistic Symp.*, Orlando, FL.

Thomsen, J. M. et al. (1979), "Calculational Investigation of Impact Cratering Dynamics: Early Time Material Motions," in *Proc. Lunar Planet. Sci. Conf. (10th)*, 2741–2756.

PISCES3DELK

a. Manuals

_______ (1981), "PISCES 3DELK User's Manual," PISCES International, Holland.

b. Computational Results

Buis, J. P. et al. (1984), "The PISCES Software for Nuclear Safety: A Survey of PISCES Code Application to Nuclear Safety Problems," PISCES International, B.V., April.

Chu, H. Y., Cowler, M. S., and Hancock, S. L. (1983), "PISCES-3DELK A Coupled Euler-Lagrange Program for Computing Fluid-Structure Interactions in Three Dimensions," in *Proc. 7th Intl. Conf. on Struct. Mech. in Reactor Technol.*, Chicago, August.

Pohl, W. et al. (1984), "The PISCES Software for Defense: A Survey of PISCES Code Applications for Defence-Orientated Computational Problems," PISCES International, B.V., May.

Additional information can be provided upon request for special applications since most of the three-dimensional work done is not published.

SOIL

Contact the code developer regarding the availability of SOIL documentation and examples of computational results.

TOODY

a. Manuals

Swegle, J. W. (1978), "TOODY IV—A Computer Program for Two-Dimensional Wave Propagation," Sandia Laboratories, SAND-78-0552, Sept. 1978 (reprinted April 1984).

Swegle, J. W. (1981), "ARTOO—An Automatically Rezoning Two-Dimensional Lagrangian Finite Difference Wavecode," Sandia Laboratories, SAND81-2235, December.

Swegle, J. W. (1982), "Verification Problems for ARTOO, An Automatically Rezoning Two-Dimensional Finite-Difference Wavecode," SAND81-2236, March.

Swegle, J. W., and Hicks, D. L. (1979), "An Anisotropic Constitutive Equation for Use in Finite Difference Wave Propagation Calculations," Sandia Laboratories, SAND-79-0382, May.

Thorne, B. J., and Holdridge, D. B. (1974), "The TOOREZ Lagrangian Rezoning Code," Sandia Laboratories, SLA-73-1057, April.

b. Computational Results

Numerous results of simulations with TOODY have been published in journal articles and government reports. For a classic application see:

Bertholf, L. D. et al. (1975), "Damage in Steel Plates from Hypervelocity Impact: Part II—Numerical Results and Spall Measurement," *J. Appl. Phys.*, *46*(9):3776–3783.

ZEUS

_______ (1987), "ZEUS Technical Description and User's Manual," Computational Mechanics Consultants, Inc.

CHAPTER 13

SHAPED CHARGE GENERALITIES

In this chapter, the various variables and parameters that govern the formation and performance of lined cavity charges are discussed. Simple analytical models and computer codes used in these studies are presented.

13.1. SHAPED CHARGE VARIABLES

The Liner

Probably, the most important shaped charge design element is the metallic (or nonmetallic) liner. The variables associated with the liner are the liner material and the liner geometry. The liner geometry can consist of a multitude of arcuate devices. The most popular are the cone, hemisphere, tulip, trumpet, the dual-angle cone (also called the biconic liner), Misznay–Schardin liners or ballistic discs or P charge liners (also known as self-forging fragments or explosively formed penetrators), tandem devices, and combinations of all these, such as a cone attached to the open apex of a hemisphere (i.e., a hemi-cone).

Once the geometric configuration is established, a pertinent variable is the liner diameter, where the term *liner diameter* refers to the outer diameter of the liner, in shaped charge notation. In general, the bigger the liner, the longer the jet and the greater the penetration capability, that is, the bigger, the better. (Recall the discussion on scaling.)

In general, liner diameters range from the 1 to 2 in. size used in research devices or bomblets up to 12 in. or so as used in torpedos. However, larger and smaller shaped charges have been employed for special applications. Smaller charges (1–2 in. or less) are difficult to fabricate to the required tolerances.

Large liners are also difficult to fabricate because of their size, and are also difficult to load. Loading is difficult due to the large height and diameter of the explosive fill, which may exceed the capabilities of the explosive pressing or casting facilities. In this case, loading is carried out in stages. In addition, for very large or very small liners, control of the metallurgical and mechanical properties of the liner material is difficult. Usually, army designers and their contractors deal with diameters ranging from about 2.5 in. (light antitank weapons) to 7 in. (heavy antitank weapons). Army rounds sometimes are required to be man portable. This requires the warhead weight (or diameter) to be as small as feasible.

The Liner Wall Thickness

Another critical liner design variable is the wall thickness. Typically, uniform wall thicknesses range from about 1 to 4 % of the charge diameter. However, liner wall thicknesses of up to 8% or so have been used. The charge diameter is the outer diameter of the explosive fill and is, of course, always greater than or equal to the liner diameter. The charge diameter will be discussed later in this chapter. The wall thickness chosen depends on the liner geometry, the liner material, and the required properties of the jet in reference to its intended application. Note that an optimum charge design, fabrication method, or geometry does not exist. The design is governed by the intended application and the imposed constraints. A unique solution or design for any particular problem seldom exists.

In addition, the wall thickness contour need not be uniform but may be tapered. A smooth taper, where the liner is thick at its pole or apex and thin at its equator or base, is simply called a taper. If the smooth taper results in a liner that is thin at its pole or apex and thick at its equator or base, the liner is said to have an inverse taper. The taper, in either direction, does not have to be smooth, but care should be taken to avoid sharp discontinuities or sharp thickness variations in the liner. Otherwise, the liner may particulate early according to the location of these discontinuities resulting in a poorly formed jet. The resulting jet then may not be an effective penetrator. The taper usually occurs on the inside (or air side) of the liner, away from the side of the liner in contact with the explosive, although this is not always the case. Basically, tapering the liner allows the designer to control the jet velocity gradient, jet length, and to an extent, the breakup time. In general, thin walled liners can be accelerated to higher velocities than thick walled liners. As examples, Aseltine et al. (1978) and Arbuckle et al. (1980) present studies of tapered hemispherical liners and Klamer (1964) discusses tapered conical liners.

The Liner Apex Angle

The other pertinent variable necessary to describe the liner is the liner apex angle (in the case of conical-like liners) or the altitude (or depth) for other

geometric shapes. For a cone, the smaller the apex angle, within reason, the faster the jet tip velocity and the lower the jet mass. Liners with a wide apex angle have a slower tip velocity and are more massive. Very wide apex angle cones begin to approximate hemispherical liners or arcuate devices such as explosively formed penetrators. A large depth or altitude of a nonconical liner implies more liner material available and a greater surface area in contact with the high explosive. This should result in a greater length of penetrator and hence a deeper penetration than a device with a shallower depth. Klamer (1964) discusses the effect of liner apex angle.

If one considers the various altitudes, diameters, wall thicknesses, and wall contour tapers that are possible for each of the arcuate geometries mentioned earlier, a multitude of geometric designs are possible. However, the various geometric designs have a different mode of collapse and jet formation, and this can greatly influence the resulting properties of the jet. See, for example, Kolsky et al. (1949), Evans (1950), Evans and Ubbelohde (1950a, 1950b), Kolsky (1949), Kiwan and Arbuckle (1977), and Pugh et al. (1946).

The conical shaped charge liners collapse, form, and breakup in the manner discussed in the earlier chapters. For narrow-angle (low apex angle) cones, the tip velocity and stretch rate are higher than for wide-angle cones. In fact, cylindrical liners, usually tapered to simulate a small apex angle cone, are capable of producing very fast jets. For example, George (1945), Kolsky et al. (1949), Evans (1950), and Evans and Ubbelohde (1950a, 1950b) describe the collapse of various shaped charge liners. Except for cylindrical charges, conical apex angles of 30° to 120°, depending on the liner material, are popular. Variations to the conical liner geometry, other than those already mentioned, include alteration of the conical apex region. The apex may be sharp, rounded, or blunt with a truncated cone. These variations affect the lead particle of the jet, the jet tip velocity, the jet tip mass, and the jet velocity gradient and mass distribution. Carleone et al. (1977) discuss jet formation and the origin of the jet tip for a conical shaped charge.

Nonconical Liners

The tulip and trumpet liners collapse similar to a conical liner, although the tulip liner, or elliptical liner, may behave like a hemispherical liner depending on its overall warhead configuration design. Also, trumpet liners typically have a high tip velocity and do not possess the inverse velocity gradient characteristic of conical liners. The hemispherical liners exhibit an entirely different mode of collapse than conical liners. The hemispherical liner is inverted from the pole or turned inside out. This results in a lower strain rate, less severe deformation process than the violent collision on the axis that conical liners undergo (Aseltine et al. 1978; Arbuckle et al. 1980; Kolsky 1949; Kiwan and Arbuckle 1977; Chou et al. 1981, 1983). Thus, the design of hemispherical and tulip-type liners must take into account the nature of the formation process (Aseltine et al. 1978; Arbuckle et al. 1980; Kolsky 1949; Kiwan and Arbuckle

1977; Chou et al. 1981, 1983, 1985, 1986; Perez et al. 1977). The collapse and formation of the jet from a hemispherical shaped charge liner was studied analytically by Chou et al. (1985). Walters and Golaski (1987) experimentally verified the jet collapse and formation mechanisms depicted by Chou et al. (1985).

For explosively formed penetrators (EFPs), self-forging fragments, P charges, dish-shaped devices, spherical caps, Misznay–Schardin devices, or the like, the collapse and formation depend to a large extent on the explosive geometry, the confinement geometry, and the metallic liner geometry. For example, under the proper conditions, one can form a projectile from a rearward-folding device (pole or apex of the liner emerges first) or a forward-folding device (tail or wings or base of the liner emerge first) or a W-fold device (where the liner forms into a W shape and collapses upon itself). Each of these devices may be generated by various tapers of the liner wall thickness and a confining body. A point focus device employs a uniform wall thickness liner and attempts to focus all liner material into a single point. The W-fold device and the point focus device are used to produce compact spheres or oblate spheroids. Forward- and rearward-folding devices are used to produce continuous rods or projectiles, which hopefully will stretch and elongate, but will not particulate, or if they do break, they will consist of only two or three segments. For the short EFP slugs, the initial stretching rate is much less than for a shaped charge. Thus, the effect of the free ends can propagate through the slug before actual breakup occurs. Therefore, the EFP breakup is more sensitive to small changes in material strength than the breakup of shaped charge jets. In addition to spheres and long rods, other shapes can be formed including hollow caps and rods with a flared, conical base to provide aerodynamic stability.

EFPs typically are low-velocity devices (as compared to shaped charges) and yield a tip velocity of 2–3 km/s. However, they generate large diameter, high mass projectiles and produce large holes in the target material. The penetration does not diminish rapidly over a long standoff (tens of meters) if the projectile is aerodynamically stable. Air drag and tumbling, if the projectile is unstable, are the main causes of degradation of penetration with standoff. At short standoff distances the performance is poor since the penetrator must have time, and hence distance, to form. Optimal penetration (at the appropriate standoff) is usually about one to two charge diameters into steel. Again, confinement effects and explosive geometry also influence the formation and performance. Increasing the L/CD of the EFP warhead increases the jet kinetic energy.

The collapse and formation of a typical EFP configuration is illustrated in the chapter on example applications. Carleone (1987) presents a detailed description of EFP charges.

Combinations of spherical caps or hemispherical liners and conical liners are possible. Such devices are constructed by removing the apex region of a hemispherical liner and covering the opening with a cone or another hemi-

sphere, or using a conical liner with a hemispherical apex region as in Pugh et al. (1946). These devices can be contoured to form continuous jets or to form two distinct jets where one jet leads the other in space and time. Shaped charge devices of this type are useful in producing a "prejet," or precursor jet, to remove elements positioned between the warhead and the target, such as a seeker or guidance package on the missile carrying the shaped charge. (Recall the discussion by Kennedy on the origin of the trumpet liner given in Chapter 3.)

For combinations of charges such as conical–spherical, conical–conical, and so on, the two liners may be blended together to form a smooth transition between them or they may be joined by a sharp geometric discontinuity. If the charges are carefully blended together to form a continuous jet a new geometric configuration may result, for example, the trumpet liner. The old Carnegie group (Pugh et al. 1946) experimented with some of these geometric combinations.

If the apex region of a conical liner is removed and replaced by another conical liner, the resulting liner is called a dual-angle or biconic liner. Note that in the literature, devices of this type are sometimes called tandem liners.

However, in this text, a tandem liner is defined to be two distinct and separate liners that are not in contact. The intent of this device is to provide a one-two punch against the target, that is, one jet followed by another. The tandem liner concept, that is, a series of coaxial shaped charges, was first proposed by Tuck (1943).

Other shaped charge geometries consist of fluted conical liners, as discussed in Chapter 3. A fluted liner contains grooved pleats on the inside (air side) surface of the liner which extend from the apex to the base. The flutes cause the jet to rotate, the idea being to counterbalance the rotation of the warhead in flight. Warheads are often spun in flight to provide aerodynamic stability. If a jet forms while the warhead is spinning, the jet may disperse in a radial direction if the spin rate is high enough. A jet that is spinning as it forms (via flutes, as one example) can be designed to counterbalance the missile spin and avoid radial dispersion of the jet. Such liners are termed spin compensated. Other techniques for spin compensation involve the metallurgical control of the liner material. Thomas (1951) discussed fluted liners and Weickert (1986) used hydrocodes to analyze the effect of the flutes on the liner collapse.

Of course, many other liner shapes and contour variations are possible. Only some of the more popular liner shapes have been described here.

13.2. THE EXPLOSIVE FILL AND INITIATION MODE

The next design variable to be addressed is the explosive fill. Usually, more energetic explosive fills yield faster jets, a greater jet kinetic energy, and deeper penetration. Table 1 summarizes the effects of explosive detonation rate and

TABLE 1. Explosive Properties

	LX-14	PBXW-110	70/30 Octol	Comp B	Pentolite	Amatex 40	TNT
Density (g/cm^3)	1.835	1.75	1.80	1.72	1.67	1.63	1.61
Detonation rate (m/s)	8830	8480	8300	7900	7470	6900	6800
Detonation presure (kbars)	358	315	310	268	233	194	186

From Simon and DiPersio (1971).

detonation pressure. LX-14 is 95% HMX and PBXW-110 is 78% RDX. The Octol is 70/30 (70% HMX, 30% TNT), and Comp B is 60% RDX, 40% TNT. Pentolite is 50% PETN and 50% TNT, and Amatex 40 is 40% RDX, 40% TNT. The densities and detonation velocities are as given earlier in Chapter 4 on Gurney velocity approximations. The detonation pressures are approximated by

$$P \text{ (kbars)} = 0.25\rho \left(\text{g/cm}^3\right) D^2 \text{ (m/s)} \times 10^{-5}.$$

The penetration and lethality effectiveness increase as the detonation rate and/or the detonation pressure increases. From Table 1, LX-14 would be the most effective, and TNT the least effective, explosive for shaped charge studies. The target hole volume increases with specific explosive energy in an approximately linear fashion. The explosives are ranked according to their penetration and lethality effectiveness. Thus, a high detonation velocity and high detonation pressure explosive is desirable although other factors, such as sensitivity, grain size, and homogeneity, must be considered. Additional data are provided by Simon (1983, 1974).

Charge Diameter

The diameter of the explosive charge, referred to as the charge diameter, or CD, not to be confused with the cone diameter as sometimes happens, is an important design variable. The ratio of the liner diameter to the charge diameter is termed the subcalibration ratio. The subcalibration ratio required depends on the liner and confinement geometry as well as the liner and confinement materials and the explosive used. It is generally agreed that explosive near the base of the liner is necessary to enable the wings or base of the liner to adequately collapse and participate in the penetration process. The control of the liner subcalibration ratio is critical in the formation of forward-folding or backward- (rearward-) folding self-forging fragment (SFF) or EFP liners. Additional subcalibration is used to form implosive hemispherical or

near-hemispherical devices [see, e.g., Kiwan and Arbuckle (1977) and Chou et al. (1981)]. The charge diameter (CD), or outer diameter of the explosive fill, is the reference unit for normalizing shaped charge performance. Thus, to allow comparison between rounds one usually plots penetration versus standoff distance both normalized by the CD.

Charge Length

The length of the explosive charge (L) is necessary to provide a sufficient amount of explosive energy for the liner collapse process. The height of explosive between the apex or pole of the liner and the booster is called the head height. The head height must be large enough to allow, as close as possible, a uniform (planar) detonation wave to reach the liner for a point-initiated charge. Too short a head height causes a highly spherical wave to impact the liner and the collapse may be nonuniform. Rarefaction effects are also more likely to be detrimental. Typically, the tip velocity, jet kinetic energy, and penetration of the jet (recall we are only addressing penetration into monolithic targets) increases as the head height increases, up to a point. A head height of about 1.5 CD provides a value beyond which very little improvement in penetration capability is achieved. Usually a 1 CD head height is ample and a head height of $\frac{5}{8}-\frac{3}{4}$ CD results in a very small penalty in penetration power for point-initiated conical or hemispherical lined charges. Klamer (1964) presents data on the effect of charge length and subcalibration. Some investigators use the charge length (the total height of the charge, L) as the pertinent parameter, that is, the charge length is sometimes confused with the head height in the literature. For point-initiated, conventional charges with a subcalibration ratio less than one, adequate L/CD values range from 1.3 to 1.8.

It is usually desirable to keep the head height or charge length to a minimum to reduce the length of the device and to save weight. Several methods are available to accomplish this. This simplest method is to remove unnecessary explosive by tapering the rear of the charge, that is boattailing. A boattailed charge is shown in Figure 1. Care must be exercised in choosing the break point (or point where the geometric discontinuity commences) to avoid the interference of rarefaction waves on the liner collapse. Usually, the break point occurs just aft of the liner apex or pole. The influence of the explosive fill geometry is further discussed by Kolsky et al. (1949), Evans (1950), Evans and Ubbelohde (1950b), Simon and DiPersio (1971), and Simon (1974, 1983). Typically, only about 10–20% of the total explosive chemical energy is translated into penetrator kinetic energy.

Another technique used to shorten the head height is waveshaping. Waveshaping involves inserting a device in the explosive charge, usually near the detonator or near the apex or pole of the liner, to contour, redirect, or shape the detonation wave to the required geometry in a short distance. Waveshapers are also used to alter the collapse of the liner by changing the angle of

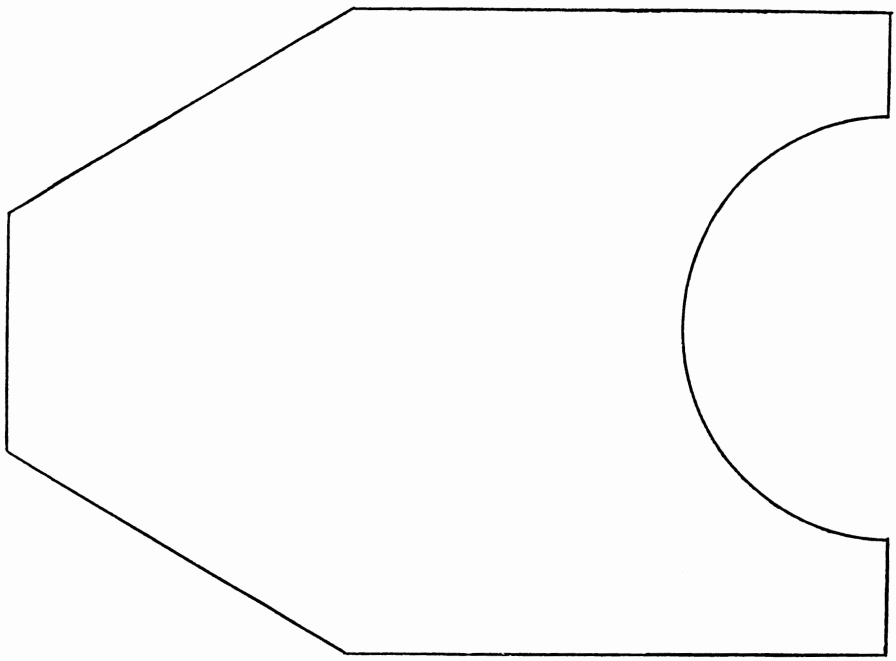

Figure 1. A Boattailed Charge.

incidence of the detonation wave, and thus even enhance performance from a short head height device. Successful waveshapers have been constructed from air, explosives, plastics, ceramics, metals, and even concrete. In addition to the waveshaper material, the other variables involved in waveshaper design are the location of the device in the explosive fill and its geometry and size. Jones (1985) discusses some of the analytical aspects of waveshaping, and Pezzica and Pazienza (1987) and Pezzica et al. (1987) performed computational studies of various waveshaper geometries.

For the explosive fill in general, both cast and pressed explosives are possible, and both are widely used (e.g., Octol and LX-14). In either case, care must be taken to guarantee a uniformity in the density and distribution of the particles (e.g., HMX crystals). Also, it may be necessary to control the grain size of the HMX or RDX particles in the explosive. For example, the median weight average diameter of the HMX grain in 75/25 Octol is about 500 μm and the median weight average diameter of the HMX grain in LX-14 is around 110 μm. A good, tight contact must also be obtained between the explosive and the liner or asymmetries may result.

Also, just as ways of tapering or contouring the metallic liner have been investigated, the explosive can be tapered or contoured, in conjunction with

the confinement body and the liner contour, to control the charge to mass ratio and enhance the collapse of the jet. This is done to optimize the velocity gradient to control jet length, breakup time, and penetration performance.

So far, a point initiation of a shaped charge device has been emphasized. A point initiation consists of a detonator–booster combination attached at a single point, on the centerline of a cylindrical or boattailed explosive charge. Other modes of initation are possible, usually designed to shorten the head height or to enhance the collapse and/or performance of the jet. These alternate methods include peripheral initiation or simultaneous initiation around the circumference of the charge, which is another way to reduce the head height, but can cause detonation wave interactions near the pole or apex of the liner. Peripheral initiation can also be achieved by a single point initiation and a waveshaper.

Various types of lens systems, for example, an air lens (using an air–HE system) or a binary lens (using two different types of HE in contact and of different detonation rates) are also used. These devices reduce the head height, may enhance the performance, and are used in implosion devices, which cause the liner (usually hemispherical) to focus at a given point or region before jetting. See, for example, Kiwan and Arbuckle (1977) and Chou et al. (1981). Also, multipoint initiation devices, which are designed to initiate the secondary explosive at several points simultaneously, and thus form the desired wave contour over a relatively short distance, are sometimes used. Simultaneous initiation over an explosive surface can also be achieved by propagating an explosively generated shock wave through a metal plate. Devices of these types are sometimes termed plane-wave lenses.

In addition, special effects can be achieved by offsetting the detonator–booster combination or by offsetting the liner. Either technique can cause the jet to form at some angle displaced from the centerline of the warhead. Evans and Ubbelohde (1950b) illustrate this case for an offset liner (a spherical cap) where the axis of the jet deviates from the axis of detonation. Other asymmetrical initiation studies were discussed by Trinks (1976), Thomanek (1976), and Walters (1986) for conical liners. Held has also experimented extensively in this field, as reported by Trinks (1976) and Held (1980). Walters (1986) also addressed the asymmetrical initiation of hemispherical shaped charges. Other methods of producing shaped charge jets where the jet particles are intentionally misaligned are discussed by Thomanek (1976), Held (1980), and Segletes (1985). Detonation waves, peripheral initiation, and detonator alignment effects are discussed by Eichelberger and Rostoker (1950). Also, Mayseless et al. (1987) discuss the effects of asymmetries on point initiated and peripherally initiated shaped charges.

The liner and explosive fill combination is also coupled to the confinement or body influence. The confinement, which is a metallic or fiber casing around the explosive charge diameter, is used to assist in loading the charge with a cast explosive; to provide a fragmenting, antipersonnel device based on the

fragmentation of the case; or to keep the detonation pressures high and thus alter or maintain the velocity gradient of the jet. A heavy confinement could allow use of a smaller amount of explosive by preventing the premature release of explosive energy. The outer diameter of the confinement body is called the warhead diameter. It may be thin and of a low-density material such as aluminum (perhaps designed to absorb the launch loads from a gun or missile) or thick and fabricated from a stronger material such as steel. For some applications, such as man-portable rounds, the heavy confinement is usually avoided to save weight. The influence of confinement is discussed, for example, by Klamer (1964), Evans (1950), Chou et al. (1983), and Brown et al. (1987).

The Body Confinement

As coupled with the explosive and liner contour, the material and the geometric shape of the confinement body is critical (e.g., Simon 1983). The body may be tapered to create a localized high-pressure effect, called tamping, or it may be uniform, to uniformly increase the detonation pressure, or tapered to regulate the velocities of the liner and the confinement. The confinement, including its material and geometry is quite influential in determining the method of formation of self-forging-fragments or EFPs, especially forward-folding and rearward-folding devices.

For shaped charge jets the confinement geometry is influential in controlling the jet velocity gradient, and for well-aligned and assembled charges, the performance increases at long standoff distances but is nearly the same as unconfined charges at short and moderate standoff distances. Confinement rings are sometimes required to prevent the detonation products from escaping from the base of the liner. These rings may be as heavy as the confinement thickness. There is an upper limit on the thick confinement of the liner since maintenance of pressure on the liner after collapse is unimportant. Thus, further increase in confinement thickness does not lead to a further increase in jet performance. For steel, a heavy confinement wall thickness of about $\frac{1}{10}$ CD is the maximum reasonable value (Evans 1950). Note that for a fixed warhead (missile) diameter there is a tradeoff between using a light confinement with a larger charge diameter (or liner diameter) and a smaller charge diameter with a heavy confinement. Usually, heavily confined charges are not weight efficient.

Other techniques are available to enhance or inhibit the collapse of shaped charge devices by either varying the explosive–confinement–liner interaction or by introducing additional devices. Localized confinement, that is, a single metallic band around the charge diameter of a warhead can locally enhance the collapse. Extraneous devices such as plastic, or metal, or even liquids positioned inside (on the air side of) the liner can inhibit the collapse process. Other methods of enhancing, disrupting, or inhibiting the collapse to produce specialized jets for specific purposes are possible. See, for example, Kolsky et al. (1949), Kolsky (1949), Merendino et al. (1963), and Held (1980).

13.3. JET CHARACTERISTICS

The liner material, as referred to early in this chapter, is of paramount importance. Favorable jet material properties will be discussed shortly. The material in the liner may even consist of two or more materials. Bimetallic conical and hemispherical liners have been fabricated and successfully tested (Kolsky et al. 1949). Conical liners consisting of a 1 cm LD and 0.37 mm copper and a 0.37 mm steel layer bonded together, with the copper in contact with the HE, were fired into polythene to recover some of the particles. The recovered particles revealed the following: all steel particles (apparently from the inside of the liner and near the tip); particles of steel on the outside and copper on the inside (apparently from midway along the cone slant height); and a slug that was copper on the outside with a steel core. When bimetallic liners of steel outside and copper inside were tested, corresponding results were obtained with the steel and copper roles reversed. See Kolsky et al. (1949) for details. Stratified, that is, layered bimetallic liners were analytically studied by Chou et al. (1985) and experimentally by Walters and Golaski (1987). These latter studies are discussed in the example applications chapter.

The liner material as well as its metallurgy is considered to be important. The characteristics of a good candidate material for a shaped charge liner are listed in Table 2. One requirement is a high melting temperature. Jets from low-boiling-point materials, for example, lead and cadmium, exhibit more marked fluid characteristics than higher-melting-point materials, for example, copper. Von Holle and Trimble (1976, 1977), as discussed earlier, measured the temperature of shaped charge jets. Walsh and Christian (1955) provided a method to determine the shock heating of materials due to explosive loading. Walters et al. (1984a, 1984b) used the EPIC code to calculate the temperature contours of a collapsing lead liner. They concluded that an optimum wall thickness exists for liners of a low melting point. Also, George (1945) performed metallurgical microscopic examinations of recovered slugs from conical liners to deduce the temperatures during deformation or collapse of the liner.

Other desirable characteristics of candidate materials for shaped charge liners include a high density to enhance penetration, a high bulk speed of

TABLE 2. Favorable Characteristics of Shaped Charge Jet Materials

1. High T_M (melt temperature)
2. High ρ (density)
3. High C_B (bulk speed of sound)
4. Fine grain, proper grain orientation, good elongation
5. Availability
6. Cheap
7. Easy to fabricate
8. Nontoxic
9. High dynamic strength

sound to guarantee jet cohesiveness, and a "dynamic" high-strength material. A dynamic high-strength material means a material that exhibits a high degree of strength under severe pressure and high strain rate conditions. Materials of this type do not necessarily correspond to materials of high static strength values. Additional material characteristics are fine-grain materials, with the proper grain orientation, that could result in a high-yield stress material with good elongation characteristics. Note that the yield stress (and strain rate) and material hardness are increased as the grain size decreases according to the Hall–Petch-type response, that is,

$$\sigma = \sigma_0 + KD^{-1/2} \quad \text{or} \quad H = H_0 + K'D^{-1/2},$$

where σ, σ_0 are residual yield stresses, H and H_0 are hardnesses, K, K', σ_0 and H_0 are constants, and D is average grain size or grain diameter. Thus, a fine grain material can produce a high residual stress, or a high hardness, or high strain, or strain rate material according to the Hall–Petch theory (Zerilli and Armstrong 1987).

In addition, the material should be readily available, inexpensive, nontoxic, and easy to fabricate. This requirement precludes elements such as platinum (expensive), osmium (not readily available), and so on.

The characteristics that depict a favorable shaped charge jet are ductility (a smooth, continuous, stretching jet), straightness (not misaligned in reference to the detonation axis), coherency (not overdriven), a favorable velocity gradient, a massive jet (the jet diameter influences the target hole diameter), a fast jet, and a continuous jet or a jet with a long breakup time. Also specialized jets may be required, for example, a spaced jet, or two distinct jets separated in space, a jet with a large tip particle, and so on. Thus, the various design parameters can be used to dramatically alter the properties of the penetrator. For this reason, one liner geometry or warhead configuration is not necessarily superior to any other. The proper design depends on the application and the design constraints.

The factors governing the performance of shaped charges may be summarized as follows: the explosive, the charge length, the charge confinement, the initiation mode, the liner and its shape, the standoff distance (distance between the base of the charge and the target), and any asymmetries present. The effects of air drag were noted earlier; recall DiPersio et al. (1965). The effects of fine grain shaped charge liner material are currently being reported in the open literature (e.g., Dante and Golaski 1985; Zerilli and Armstrong 1987).

Basically, the shaped charge jet performance into RHA targets can be gauged by the jet "factor of merit" (FM) where

$$\text{FM} = \frac{V_j \tau \sqrt{\rho_j}}{\text{CD}}$$

from DiPersio et al. (1967) where V_j is the jet tip velocity, τ is the jet average breakup time, ρ_j is the jet density, and CD is the charge diameter. Thus, for a given charge diameter, penetration is increased by increasing V_j, τ, and ρ_j.

The shaped charge jet parameters that completely describe the jet and hence can be used to model its penetration capability are given in Table 3.

The desired shaped charge jet parameters and the required favorable jet characteristics can be drastically altered by asymmetries. This has been discussed previously in this book; recall Evans (1950), Leidel (1978), Aseltine (1980), and Klamer (1964).

Granted that one is aware of the design variables at his disposal (e.g., liner geometry, explosive fill, etc.) and that one is aware of the jet parameters of importance (e.g., tip velocity, breakup time, jet diameter, etc.), it remains to relate the shaped charge design variables to the jet parameters. Then, the jet parameters can be used as input into one of the penetration models discussed in an earlier chapter to predict the penetration performance of a given shaped charge design. Thus, the problem involves three stages. One first studies the shaped charge liner collapse. Then one uses the results of the liner collapse analysis to study the jet formation. Finally, one uses the free flight or formed jet characteristics to predict penetration, hole growth, and other aspects of terminal ballistics. Hole growth and cratering is a vast field and beyond the basic scope of this book. However, a brief overview of this important area was given in the chapter on penetration.

The jet collapse and jet formation may be estimated by relatively simple analytical models such as those given earlier in the text. These models analyze the jet formation using a PER theory coupled with either a Defourneaux and Taylor angle theory or with a Gurney-type model and a Taylor angle theory.

TABLE 3. Shaped Charge Jet Parameters

1.	V_{j_0}	Velocity gradient	(jet tip velocity)
2.	V_R		(jet tail velocity)
3.	τ or τ distribution (jet breakup time)		
4.	d_j (jet diameter)		
5.	l_j (jet length)		
6.	Lead particle characteristics		
7.	V.O. (for effective S.O., V.O. is virtual origin)		
8.	σ_j and constitutive characterization		
9.	ρ_j and EOS and compressibility effects		
10.	KE_j (jet kinetic energy)		
11.	M_j (jet momentum)		
12.	HE, detonation rate, etc...		
13.	Spin insensitivity		
14.	Penetration—three-dimensional effects Jet drift Sidewall collisions		

(See the chapters on Gurney velocity and jet formation). The analytical codes are used for conical and near conical liner geometries and are not universally valid for highly nonconical liners such as hemispheres. Table 4 lists a few of these codes. Dullum and Haugstad (1986) investigated the liner collapse of five different shaped charges using both simple analytical models and more complex computer codes. Considerable discrepancies were found among the computed results. However, this type of comparison, although interesting, is to be expected since most computer codes or analytical models cannot be applied to problems they were not designed to solve or must be modified or adjusted to accommodate the problem at hand.

Other codes exist and are similar to those given in Table 4. These codes calculate the pertinent jet parameters listed earlier. The code output describes the jet geometry, the jet velocity distribution, and jet mass distribution. The jet formation and development may be described when the jet collapse results are used in conjunction with a jet breakup model such as given by Carleone and Chou, Hirsch, Pfeffer, and so on, as discussed in Chapter 8.

Analyses that address the formation mechanisms of shaped charge jets are given by Chou et al. (1985, 1986) and Perez et al. (1977). Chou et al. (1985, 1986) and Walters and Golaski (1987) also analyze the collapse and formation of hemispherical liners.

More sophisticated studies of the liner collapse, including nonconical liners, may be obtained from the hydrocodes. Eulerian,Lagrangian, and hybrid codes are useful for liner collapse studies. Zukas et al. (1982) discuss the hydrocodes in detail. The codes that are most popular in shaped charge studies include HELP, HULL, HEMP, and EPIC. In addition, a relatively new code called HOIL, which represents a marriage between HOIL (from the OIL family of codes) and HEMP, promises to be a valuable tool for the shaped charge

TABLE 4. Shaped Charge Computer Codes

Code Name	Source	Liner Collapse Model
BASC	Harrison (1981a, 1981b)	Modified Defourneaux, Steady Taylor
DESC-1, DESC-2	Carleone et al. (1975)	Modified Defourneaux, Steady Taylor
DESC-3	Flis (1984)	Gurney–Chanteret, Unsteady Taylor
TB/ISL (version TB/81)	Fauquignon (1981) and Pfeffer (1981)	Defourneaux or Hennequin–Pfeffer–Winawer, Steady Taylor
PISCES 2DELK	Behrmann (1973)	Two-D Eulerian Finite-Difference for Explosive, Mass-Points for Liner and Casing
TEMPS	Dyna East (1978)	Two-D Lagrangian Finite-Difference for Explosive, Mass-Points for Liner and Casing

From Chou and Flis (1986).

designer. HOIL was developed by Harrison of the BRL (1984). An earlier chapter discussed numerical calculations in detail.

Other methods of determining the collapse and formation of a shaped charge liner are experimental in nature. Shaped charge measurement techniques have been adequately covered elsewhere. Basically, the experimental methods consist of flash radiography, which provides an X-ray picture of the jet at predetermined times, and thus can be used to observe jet collapse, growth, and formation; camera coverage using framing cameras or streak cameras; and penetration (penetration–time) measurements, which are useful in themselves and can also be used to "back-calculate" the jet parameters. Held (1981a) gives an excellent overview of shaped charge measurement techniques. Other basic references on the pertinent experimental techniques are given by Zukas et al. (1982), Jamet and Thomer (1976), Johannson and Persson (1970), and Charbonnier (1981). Specific experimental references can be found in the *Flash Radiography Symposia* (e.g., Bryant 1976), the *Detonation Symposia*, and the sixteen volumes of the *Proceedings of the International Congress on High Speed Photography* (1954–1984). Experimental techniques pertinent to hypervelocity jets are given by Kronman and Groff (1973) and the studies by Held and associates (1970, 1976a, 1976b, 1981b, 1983, 1984a, 1984b, 1985a, 1985b, 1986a). The experimental techniques employed by Held and associates are summarized in Held (1986b), and Walters et al. (1987).

General references, useful for shaped charge device design, include Baum et al. (1949), the *Rheinmetall Handbook* (1973), the *Army Materiel Command Pamphlet* (1964) (for introductory material), and the *Manual for Shaped Charge Design* (Brimmer 1950). Carleone et al. (1978) explain a design procedure or synthesis method for the design of a fragmentation charge, an EFP, and a shaped charge. Four types of design tools are discussed, namely, simple design formulas, one-dimensional computer codes, two-dimensional computer codes, and experimentation. A design iteration for an EFP and a shaped charge warhead are illustrated. Held (1980), Leidel (1978), and Cox (1964) describe linear cutting charges.

Also, a multitude of shaped charge test parameters and test results were compiled by Arthur D. Little, Inc. (1959). This comprehensive data base includes a great deal of test results involving shaped charge parametric studies and penetration versus standoff distance studies.

REFERENCES

Arbuckle, A. L., Walters, W. P., and Aseltine, C. L. (1980), "Analysis of Uniform Wall and Tapered Hemispherical Liners with Several Explosive Confinement Geometries," ARBRL-TR-02222, March.

Arthur D. Little, Inc. (1959), "Collection and Arrangement of Shaped Charge Data, Third Interim and Final Report, Volume 1. Parameters, Volume II. Tables of Data, Parts 1, 2 and 3, Volume III. Glossary," Report C-59292, December 31.

Aseltine, C. L. (1980), "Analytical Predictions of the Effect of Warhead Asymmetries on Shaped-Charge Jets," Ballistic Research Laboratory Technical Report ARBRL-TR-02214, February.

Aseltine, C. L., Walters, W. P., Arbuckle, A. L., and Lacetera, J. E. (1978), "Hemispherical Shaped Charges Utilizing Tapered Liners," *Proc. 4th Int. Symp. on Ballistics*, Monterey, CA, October 17–19.

Baum, R. A., Stanykovich, R. P., and Skekter, B. I. (1949), *Physics of an Explosion*, New York: Research Information Service, 546. (AD 400151).

Behrmann, L. (1973), "Calculation of Shaped Charge Jets Using Engineering Approximations and Finite-Difference Computer Codes; Volume I, Generalized Analytical Approach to Shaped-Charge Warhead Design," Air Force Armament Laboratory Report AFATL-TR-73-160, August.

Brimmer, R. A. (1950), "Manual for Shaped-Charge Design," Navord Report 1248, NOTS 311, ADB954297, August.

Brown, J., Cullis, I. G., and Griffiths, N. (1987), "The Effects of Confining Studies on Shaped Charges," *Proc. 10th Int. Symp. on Ballistics*, Vol. 2, San Diego, October.

Bryant, L. E. (ed.) (1976), *Proceedings of the Flash Radiography Symposium*, (LC no. 77-5244, 1977) Houston.

Carleone, J. (1987), Section 3, "Mechanics of Shaped Charges," *Basic Principles of Hypervelocity Impact and Related Topics*, Course Notes, Computational Mechanics Associates, April, Baltimore, MD.

Carleone, J., Jameson, R., and Chou, P. C. (1977), "The Tip Origin of a Shaped Charge Jet," *Propell. Explos.*, *2*:126–130.

Carleone, J., Chou, P. C., and Simpson, R. (1978), "A Synthesis Method for Modern Warhead Design," *Proc. 4th International Symp. on Ballistics*, Monterey, October.

Carleone, J., Chou, P. C., and Tanzio, C. A. (1975), "User's Manual for DESC-2, A One-Dimensional Computer code to Model Shaped Charge Liner Collapse, Jet Formation, and Jet Properties," Dyna East Corporation Technical Report No. DE-TR-75-4, December.

Charbonnier, F. (1981), "Flash Radiography," in *Radiography and Radiation Testing*, Vol. 3, *Nondestructive Testing Handbook*, 2nd ed., L. E. Bryant and P. McIntire (eds.), Columbus, OH; ASNT.

Chou, P. C. and Flis, W. J. (1986), "Recent Developments in Shaped Charge Technology," *Propell., Explos. Pyrotech. 11*:99–114.

Chou, P. C., Ciccarelli, R. D., Arbuckle, A. L., and Walters, W. P. (1981), "Jet Formation of an Implosively Loaded Hemispherical Liner," Contract Report, ARBRL-CR-00470, September.

Chou, P. C., Ciccarelli, R. D., and Walters, W. P. (1983), "The Formation of Jets from Hemispherical Liner Warheads," *Proc. 7th Int. Symp. on Ballistics*, The Hague, Netherlands, April 19–21.

Chou, P. C., Flis, W. J., and Forsyth, C. M. (1986), "A Simplified Model of Jet Formation in Hemispherical Shaped Charges," *Proc. 9th Int. Symp. on Ballistics*, Shrivenham, UK, April–May.

Chou, P. C., Walters, W. P., Ciccarelli, R. D., and Weaver, G. W. (1985), "Jet Formation Mechanics of Hemispherical Warheads," BRL Contractor Report, BRL-CR-545, October.

Cox, C. M. (1964), "Memorandum Report on Linear and Conical Shaped Charge Performances," The Firestone Tire and Rubber Company, Defense Research Division, Report No. DRD-4, May.

Dante, J. G. and Golaski, S. K. (1985), "Micrograin and Amorphous Shaped-Charge Liners," *Proceedings of ADPA Bomb and Warhead Section*, White Oak, MD, May.

DiPersio, R., Jones, W., Merendino, A., and Simon, J. (1967), "Characteristics of Jets from Small Caliber Shaped Charges with Copper and Aluminum Liners," BRL Memorandum Report No. 1866, September.

DiPersio, R., Simon, J., and Merendino, A. (1965), "Penetration of Shaped Charge Jets into Metallic Targets," BRL Report No. 1296, September.

Dullum, O. and Haugstad, B. (1986), "A Comparative Investigation of Various Analytical and Numerical Shaped Charge Liner Collapse Models," *Proc. 9th Int. Symp. on Ballistics*, Shrivenham, UK, April–May.

Dyna East Corporation (1978), "A Two-Dimensional Explosive Mass-Point Computer Code (TEMPS)," Dyna East Corporation Technical Report DE-TR-78-3, June.

Eichelberger, R. J., and Rostoker, N. (1950), "Jet and Target Characteristics," with Introduction by E. M. Pugh, First Bimonthly Report, Fundamentals of Shaped Charges, CIT-ORD-28, August 31 (AD 499747).

Evans, W. M. (1950), "The Hollow Charge Effect," *Bulletin of the Institution of Mining and Metallurgy*, No. 520, March.

Evans, W. M., and Ubbelohde, A. R. (1950a), "Some Kinematic Properties of Munroe Jets," *Res. Supp.*, London, 3-8, May.

Evans, W. M., and Ubbelohde, A. R. (1950b), "Formation of Munroe Jets and Their Action on Massive Targets," *Res. Supp.*, London, 3-7.

Fauquignon, C. (1981), "Modelling Techniques for Shaped-Charges in France and French-German Institute of Saint-Louis," *Proc. 7th Annual Technical Meeting on Physics of Explosives*, Livermore, CA, October 21–23.

Flis, W. J. (1984), "User's Manual for DESC-3, A One-Dimensional Computer Code for Shaped Charge Analysis," Dyna East Report DE-TR-84-01, November.

George, H. P. (1945), "Mechanism of Collapse of Conical Hollow Charge Liners," Frankford Arsenal Report R-667, October.

Harrison, J. T. (1981a), "Improved Analytical Shaped-Charge Code: BASC," Ballistic Research Laboratory Technical Report No. ARBRL-TR-02300, March.

Harrison, J. T. (1981b), "BASC, an Analytical Code for Calculating Shaped Charge Properties," *Proc. 6th Int. Symp. on Ballistics*, Orlando, FL, October 27–29.

Harrison, J. T. (1984), "A Two Stage, Hydrodynamic, Numerical Technique, 'HOIL' and an Analysis of the Results of a Hemispherical, Shaped Charge Liner Collapse," *Proc. of 8th Int. Symp. on Ballistics*, Orlando, FL, October.

Held, M. (1970), "Orthogonal Multistreak Recording Technique," *Ninth Int. Congress on High Speed Photography*, Denver, pp. 126–129.

Held, M. (1976a), "The Performance of the Different Types of Conventional High Explosive Charges," *Second Int. Symposium on Ballistics*, Daytona, FL, March.

Held, M., Ludwig, D., and Nikowitsch, P. (1976b), "SST-Synchro-Streak-Technique," *Twelfth Int. Congress on High Speed Photography*, Toronto, pp. 234–237.

Held, M. (1980), "Cutting Charges," *5th Int. Symp. on Ballistics*, Toulouse, France, April.

Held, M. (1981a), "Shaped Charge Measurement Techniques—Overview," *Proc. 7th Annual Meeting on Physics of Explosives*, Livermore, CA, October.

Held, M. (1981b), "Evaluation of Shaped Charge Penetration Efficiency by Advanced Diagnostic Techniques," *Sixth Int. Sym. on Ballistics*, Orlando, FL, October.

Held, M. (1983), "Characterizing Shaped Charge Performance by Stand-Off Behavior," *Seventh Int. Sym. on Ballistics*, The Hague, 19–21 April.

Held, M. (1984a), "High-Speed Photography in Detonics," *Proc. of the 16th International Congress on High Speed Photography and Photonics*, SPIE, Strasbourg, France.

Held, M. and Nikowitsch, P. (1984b), "Comparative Investigation of Flash X-Ray Pictures and SST-Records for Diagnostic Evaluation of Shaped Charge Jets," *Sixteenth Int. Congress on High Speed Photography and Photonics*, Strasbourg, France, pp. 614–618.

Held, M. (1985a), "Flash X-Radiography in Ballistics," *Mat. Eval.*, *43*:1104–1123.

Held, M. (1985b), "Determination of the Material Quality of Copper Shaped Charge Liners," *Propell., Explos. Pyrotech. 10*:125–128.

Held, M. (1986a), "The Orthogonal Synchro-Streak-Technique as a Diagnostic Tool, Particularly for Shaped Charge Jets," *Propell., Explos., Pyrotech.*, *11*:170–175.

Held, M. (1986b), *Fundamental Aspects of Hypervelocity Impact and Shaped Charge Phenòmena*, Vol. 3, Course Notes, Computational Mechanics Associates, Baltimore, MD, April.

Jamet, F., and Thomer, G. (1976), *Flash Radiography*, New York: Elsevier Scientific.

Johannson, C. H., and Persson, P. A. (1970), *Detonics of High Explosives*, London: Academic.

Jones, D. A. (1985), "Wave Shaping in the MRL 38 mm Shaped Charge," Department of Defense, Materials Research Laboratories, Melbourne, Victoria, Australia, Report MRL-R-980, December.

Kiwan, A. R., and Arbuckle, A. L. (1977), "Study of Liner Collapse, Jet Formation and Characteristics from Implosive Shaped Charge Systems," BRL-R-2028, November.

Klamer, O. A. (1964), "Shaped Charge Scaling," Ammunition Engineering Directorate, Picatinny Arsenal Technical Memorandum 1383, Dover, NJ, March.

Kolsky, H. (1949), "A Study of the Mechanism of Munroe Charges, Part II—Charges with Hemispherical Liners," *Res. Supp.*, London, 2-2:96–98.

Kolsky, H., Snow, C. I., and Shearman, A. C. (1949), "A Study of the Mechanism of Munroe Charges, Part I—Charges with Conical Liners," *Res. Supp.*, London, 2-2:89–95.

Kronman, S., and Groff, R. W. (1973), "A Stereo Segmental Flash Radiographic Technique," BRL-MR-2343, December.

Leidel, D. J. (1978), "A Design Study of An Annular-Jet Charge for Explosive Cutting," Ph.D. Dissertation, Drexel University, Philadelphia, PA, June.

Mayseless, M., Miller, S., Niv, E., and Peretz, D. (1987), "Experimental and Computational Analysis of the Effect of Asymmetries on Peripherally Initiated Shaped Charges," *Proc. 10th Int. Symp. on Ballistics*, Vol. 2, San Diego, October.

Merendino, A., Regan, J. M., and Kronman, S. (1963), "A Method of Obtaining a Massive Hypervelocity Pellet from a Shaped Charge Jet," BRL Memorandum Report No. 1508, August.

Perez, E., Fauquignon, C., and Chanteret, P. (1977), "Fundamental Studies of Shaped Charge Mechanisms," *Proc. 3rd Int. Symp. on Ballistics*, Karlsruhe, Germany, March.

Pezzica, G., and Pazienza, G. (1987), "Calculation of the Wave-Shaper Effects on Detonation Wave in Shaped Charges," *Propell., Explos., Pyrotech.*, *12*:125–129.

Pezzica, G., Pazienza, G., and Vignolo, G. M. (1987), "Numerical Modeling of Shaped Charges With Wave Shapers," *10th Int. Symp. on Ballistics*, San Diego, October.

Pfeffer, M. (1981), "Thompson-Brandt/Institute Saint Louis Computer Code Modelling of Shaped Charge Performance," *Proc. 7th Annual Technical Meeting on Physics of Explosives*, Livermore, CA, October 21–23.

Proceedings of the Int. Symposium on Detonation (*Vols. 1–8*), available from Naval Surface Weapons Center, Silver Spring, MD.

Proceedings of the Int. Congress on High Speed Photography: Vol. 1, Washington, 1952, published HSP, 5, SMPTE, NY, 1954; Vol. 2, Paris, 1954, published Dunod, Paris, 1956; Vol. 3, London, 1956, published Butterworth, London, 1957; Vol. 4, Koln, Germany 1958, published Verlag Helwich, Darmstadt, 1959; Vol. 5, Washington, 1960, published SMPTE, NY, 1962; Vol. 6, The Hague, Netherlands, 1962, published Tjeenk Willink & Zoon, Haarlan, 1963; Vol. 7, Zurich, 1965, published Verlag Helwich, Darmstadt, 1967; Vol. 8, Stockholm, published Almqvist & Wiksell, Stockholm, 1968; Vol. 9, Denver, 1970, published SMPTE, NY, 1971; Vol. 10, Nice, 1972, published ANRT, Paris, 1973; Vol 11, London, 1974, published Chapman & Hall, London, 1975; Vol. 12, Toronto, 1976, published SPIE, Washington, 1977; Vol. 13, Tokyo, 1978, published *J. Soc. Prec. Eng.*, Tokyo, Distribution, SPIE, US, 1979; Vol. 14, Moscow, 1980; Vol. 15, San Diego, 1982, published SPIE, Washington, 1983; Vol. 16, Strasbourg, France, 1984, published SPIE, 1984.

Pugh, E. M. et al. (1946), "Protection Against Shaped Charges," Final Report, Carnegie Institute of Technology, National Defense Research Committee, NRDC Report No. A-384 and Office of Scientific Research and Development, OSRD Report No. 6384, February.

Rheinmetall, (1973), *Rheinmetall Weapons Engineering Handbook*, Dusseldorf, FSTC-HT-23-0500-75.

Segletes, S. B. (1985), "Confinement Fabrication Technique for Asymmetrically Confined Shaped Charge Warheads," United States Patent 4,153,666, April.

Simon, J. (1983), "Shaped Charge Research Circa 1960–1980," presented at MBB, Schrobenhausen, W. Germany, September.

Simon, J. (1974), "The Effect of Explosive Detonation Characteristics on Shaped Charge Performance," *Proceedings of the Army Science Conference*, Vol. 3, pp. 99–112, West Point, NY, June.

Simon, J., and DiPersio, R. (1971), "The Evaluation of the Effect of Explosive Filler on Shaped Charge Performance and Lethality Effectiveness," BRL Report 1552, October.

Thomas, L. H. (1951), "A Zero Order Theory of the Initial Motion of Fluted Hollow Charge Liners," in "Transactions of Symposium on Shaped Charges," held at the Ballistic Research Laboratory, Aberdeen Proving Ground, MD, BRL Report No. 837, November (AD 1531).

Thomanek, F. R. (1976), "Unsymmetrically Affected Rotational Shaped Charges," *Proc. of the 2nd Int. Symp. on Ballistics*, Daytona Beach, FL, March.

Trinks, W. (1976), "Shaped Charges and Armor Protection: Their Alternate, Continuous Development," *Jahrbuch der Wehrtechnik*, 8, (translation FSTC 1375-75, AD B015556), May.

Tuck, J. L. (1943), "Note on the Theory of the Munroe Effect," UK Report, A.C. 3596 (Phys. Ex. 393-WA-638-32), March 27.

U.S. Army Materiel Command (1964), "Engineering Design Handbook, Ammunitions Series, Section 2, Design for Terminal Effects," Pamphlet No. ACMP 706-245, July (AD 389304).

von Holle, W. G., and Trimble, J. J. (1976), "Temperature Measurement of Shocked Copper Plates and Shaped Charge Jets by Two-Color IR Radiometry," *J. Appl. Phys.*, *47*(6).

von Holle, W. G., and Trimble, J. J. (1977), "Temperature Measurements of Copper and Eutectic Metal Shaped Charge Jets," BRL Report R 2004, August.

Walsh, J. M., and Christian, R. H. (1955), "Equation of State of Metals from Shock Wave Measurements," *Phys. Rev.*, *97*(6), March 15.

Walters, W. P. (1986), "Asymmetric Initiation of Shaped-Charges," *SECTAM XIII Proceedings*, *Southeastern Conference on Theoretical and Applied Mechanics*, Columbia, SC, April.

Walters, W. (1987), *Fundamental Aspects of Hypervelocity Impact and Shaped Charge Phenomena*, Course Notes, Computational Mechanics Associates, April, Baltimore, MD.

Walters, W. P., and Golaski, S. K. (1987), "Hemispherical and Conical Shaped Charge Liner Collapse and Jet Formation," BRL Technical Report, BRL-TR-2781, February.

Walters, W. P., Jonas, G. H., and Zukas, J. A. (1984a) "Explosive Loading of Lead," *Proc. of SECTAM XII*, *The Southeastern Conference on Theoretical and Applied Mechanics*, Pine Mountain, GA, May, Auburn, AL: Auburn University Press.

Walters, W. P., Jonas, G. H., and Zukas, J. A. (1984b), "Explosive Loading of Lead Hemispherical Liners," in *Advances and Trends in Structures and Dynamics*, A. K. Noor and R. J. Hayduk (eds.), New York: Pergamon Press.

Weickert, C. A. (1986), "Spinning Self-Forging Fragments and Shaped Charges," Ph.D. Dissertation, Drexel University, Philadelphia, PA, June.

Zerilli, F. J., and Armstrong, R. W. (1987), "Dislocation-Mechanics-Based Constitutive Relations for Material Dynamics Calculations," *J. Appl. Phys.*, *61*(5):1816–1825.

Zukas, J. A., Nicholas, T., Swift, H. F., Greszczuk, L. B., and Curran, D. R. (1982), *Impact Dynamics*, New York: Wiley.

CHAPTER 14

EXAMPLE APPLICATIONS

Shaped charges, as discussed in the earlier chapters, come in all shapes and sizes. That is, a multitude of charges have been designed for various applications over the years. A few of these are depicted in the following figures.

The reader is urged not to draw direct comparison between the flash radiographs of the various jets, except for those intended (and specified as such) for direct comparison. A direct comparison is prohibited by the different magnification factors resulting from diverse experimental setups as well as the various reductions in the photographic/printing process. The flash radiographs contained herein are intended only to illustrate various shaped charge jet characteristics and not detailed measurement of jet properties.

Note also that the reported flash times provide only a relative time measure between the various experiments since the start, or X-ray reference time, may vary from study to study. This time difference is usually of the order of a few microseconds.

The following pages present the "picture book" of shaped charge examples and applications.

14.1. CONICAL SHAPED CHARGE LINERS

Figure 1 depicts the most conventional shaped charge liner geometries, namely, the conical liner, the hemispherical liner, and the trumpet liner. In Figure 1*b* the simulated collapse of the hemispherical liner from the EPIC-2 hydrocode is also shown for times of 46 and 76 μs after detonation.

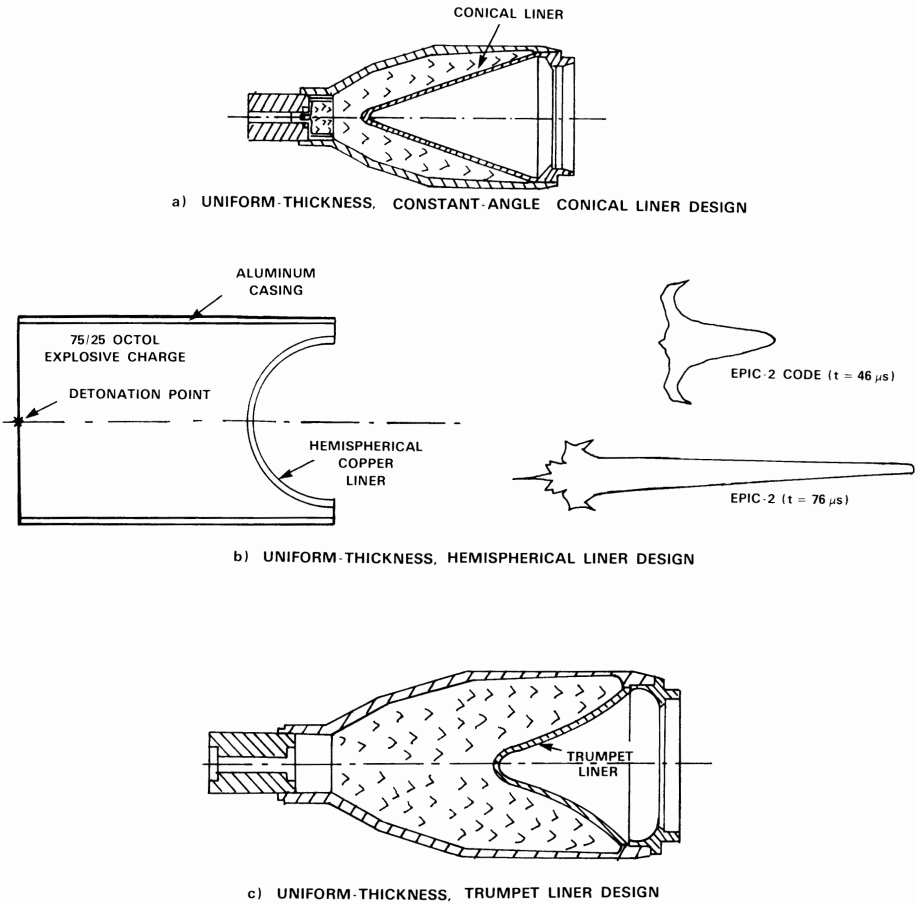

Figure 1. Basic liner designs (a—Arvidsson and Ohlsson 1984, b—Chou et al. 1983, c—Davison and Arvidsson 1985).

Certain specialized liner designs are shown in Figure 2, and the references cited in this figure provide detail regarding the application of these specialized designs. Figure 3 shows another specialized application due to Geiger and Honcia (1977). In this design, the high explosive and liner are both planar symmetric.

Figure 4 illustrates the effect of flutes on a spinning shaped charge liner. A fluted liner spun at optimum frequency gives a jet with characteristics similar to the jet from a smooth (unfluted) liner fired in a static mode (Figure 4*b*). Figure 4*a* shows a distorted jet fired from a smooth liner when the charge was spinning. Fluted liners were discussed earlier, and Weickert (1986) provides additional details.

Figure 5 illustrates the collapse sequence of a conical shaped charge. Figures 6*a* and 6*b* further illustrate the collapse sequence of a conical liner.

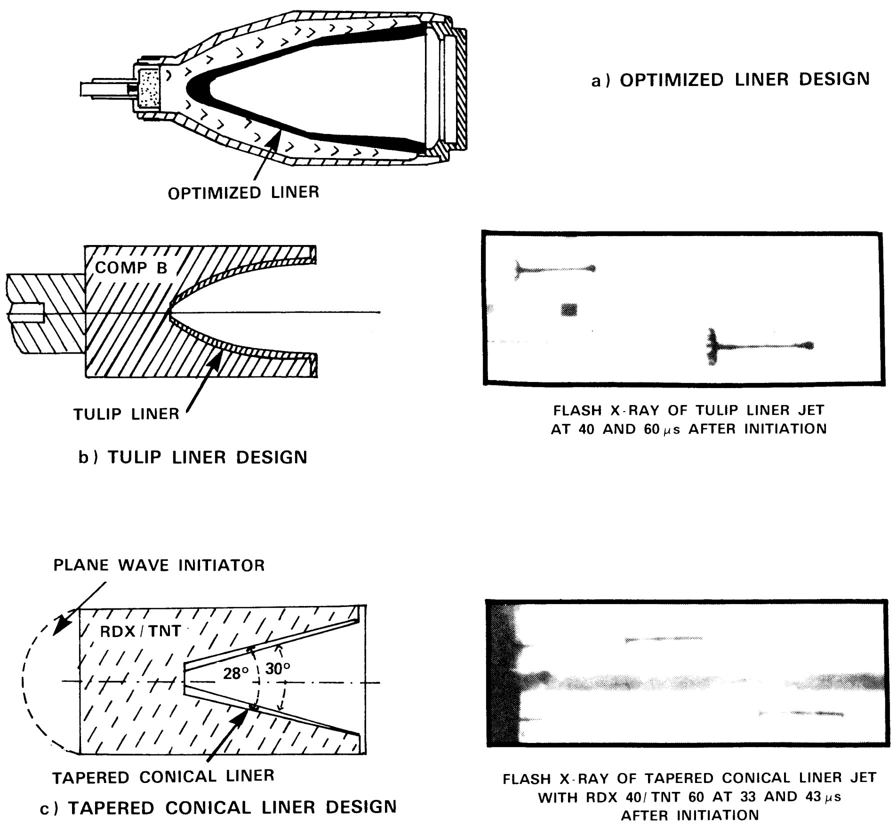

Figure 2. Specialized liner designs (a—Davison and Arvidsson 1985, b and c—Chanteret and Jamet 1984).

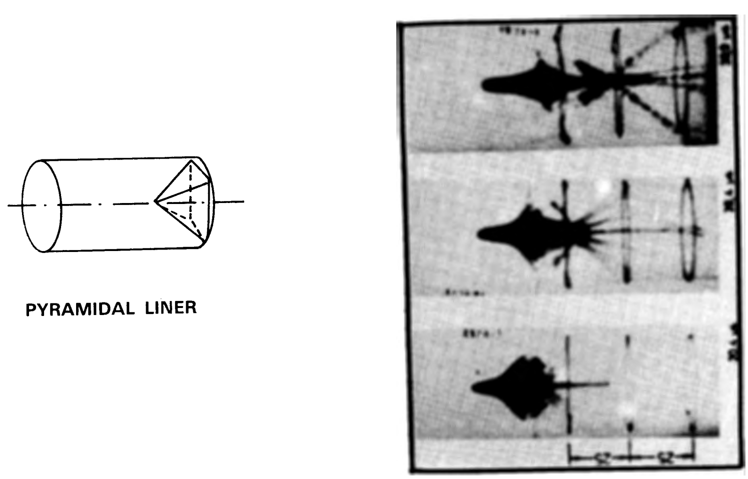

Figure 3. Planar symmetric liner design (Geiger and Honcia 1977).

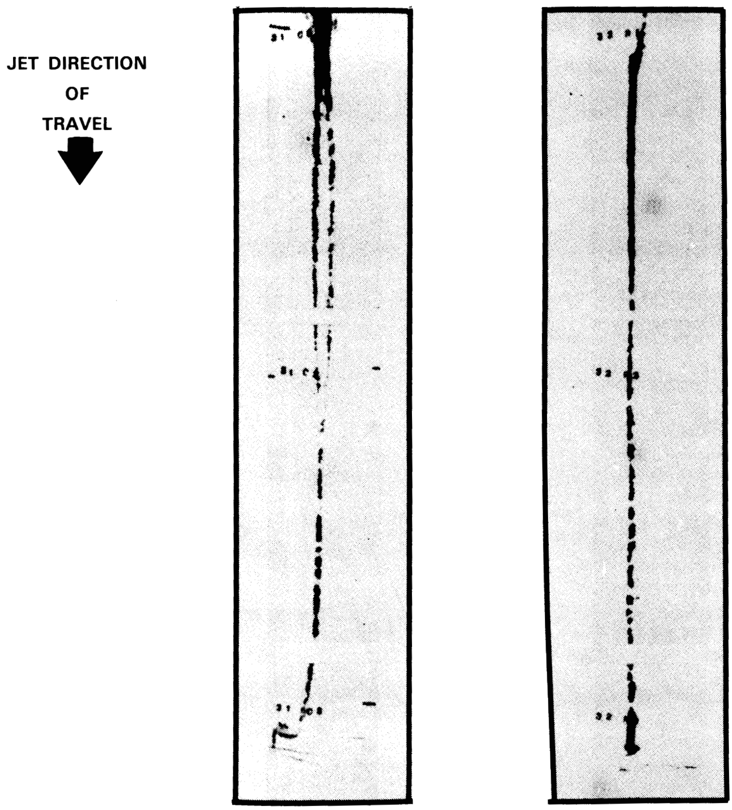

a) SMOOTH LINER b) FLUTED LINER

Figure 4. Jet radiographs showing the effect of flutes (AMCP 1964; Weickert 1986).

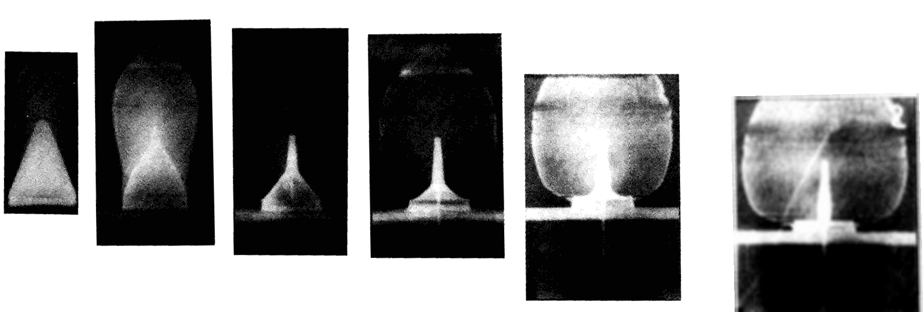

0 25 31 37 43

Delay times are after detonator initiation (microseconds)

Liner-copper, 81 mm, 42°, H.E.-Comp B
Liner–Copper,81mm,42° H.E.–Comp.B

Figure 5. Collapse sequence (from left to right) of a conical shaped charge (courtesy BRL).

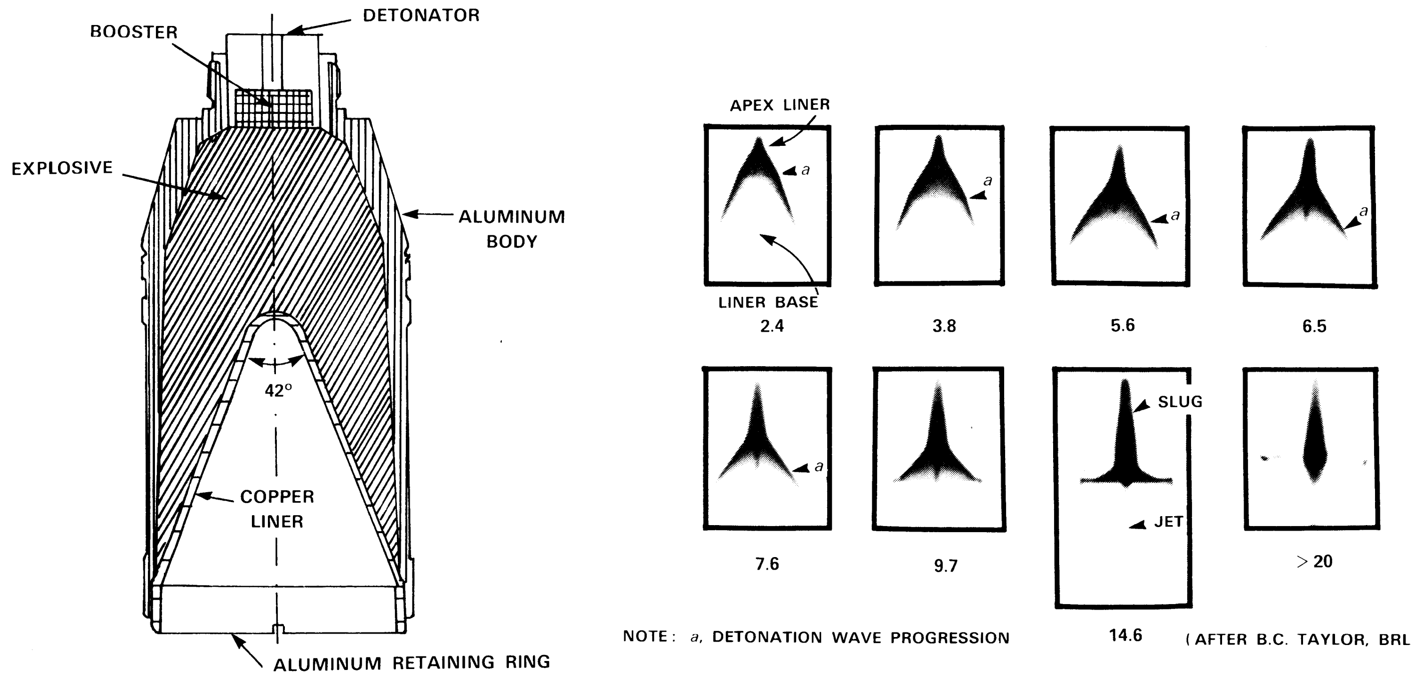

Figure 6. (a) Cross section of a conical shaped charge. **(b)** The sequential copper cone collapse at times indicated in microseconds. Time zero is when detonation wave reaches liner apex (Simon and DiPersio 1972).

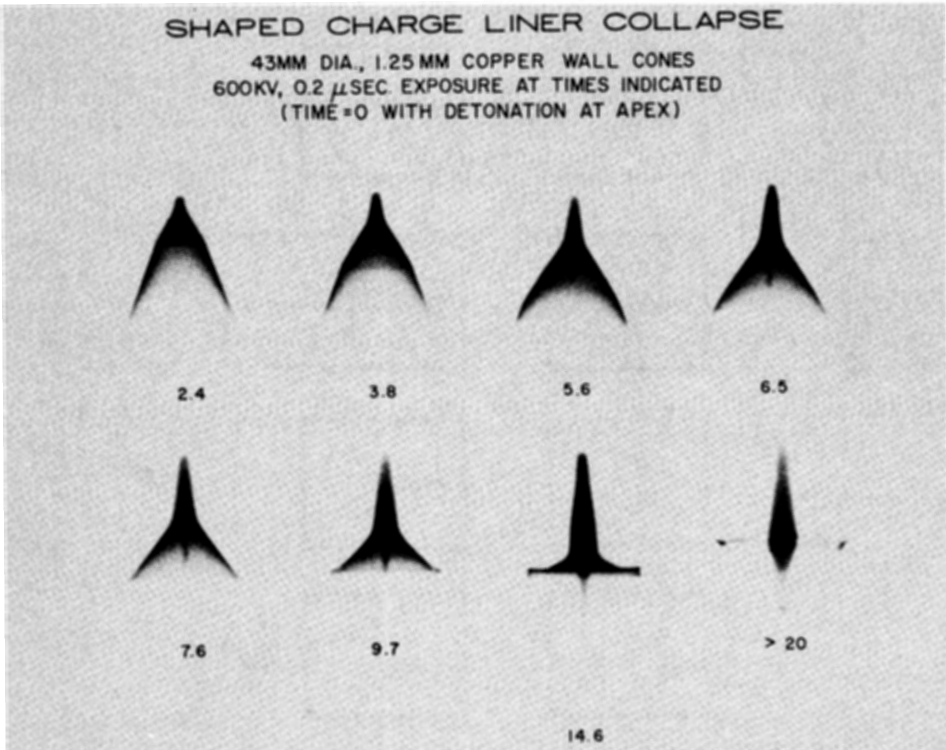

Figure 7. The collapse sequence of a shaped charge with a conical liner (courtesy BRL).

Figure 7 presents a "closeup" of Figure 6*b*. A framing camera sequence of the collapse of a conical liner is shown in Figure 8.

The effect of the conical liner apex angle is illustrated in Figures 9–16. The apex angle study was performed by, and furnished courtesy of, M. Held of Messerschmitt-Bolkow-Blohm Gmbh, (MBB), Schrobenhausen, West Germany.

Figure 9 summarizes the results of the conical apex angle (2α) study for copper liners with a charge and liner diameter of 58 mm and a liner wall thickness of approximately 4 mm. In Figure 9, the X-ray flash time was 35 μs after detonation. The apex angle was varied from 80° to 180°.

Figure 10 presents a detailed view of conical apex angles of 160°, 170°, and 180°. Figure 11 continues the series for apex angles of 130°, 140°, and 150°. Figure 12 completes the series for apex angles of 80°, 90°, 100°, 110°, and 120°. Again, the relevant X-ray flash times were 35 μs after detonation of the charge. Figure 13 highlights selected results from the earlier figures.

Additional conical apex angle studies for a 32 mm liner and charge diameter copper shaped charge with a 1.5 mm liner wall thickness are summarized in Figure 14. The apex angles studied were 30°, 60°, 90°, 120°,

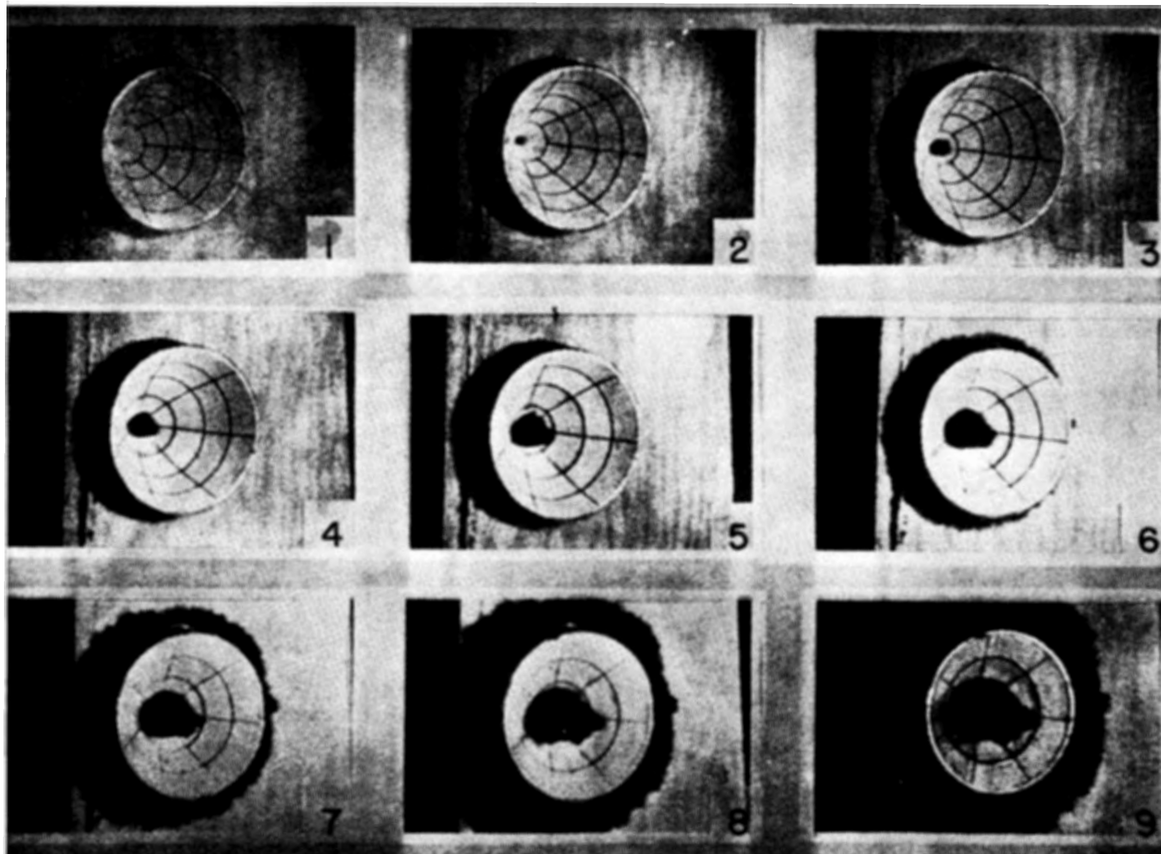

Figure 8. Selected frames of framing camera sequence of cone collapse in 60°, 10 cm aluminum cone (Cook 1958).

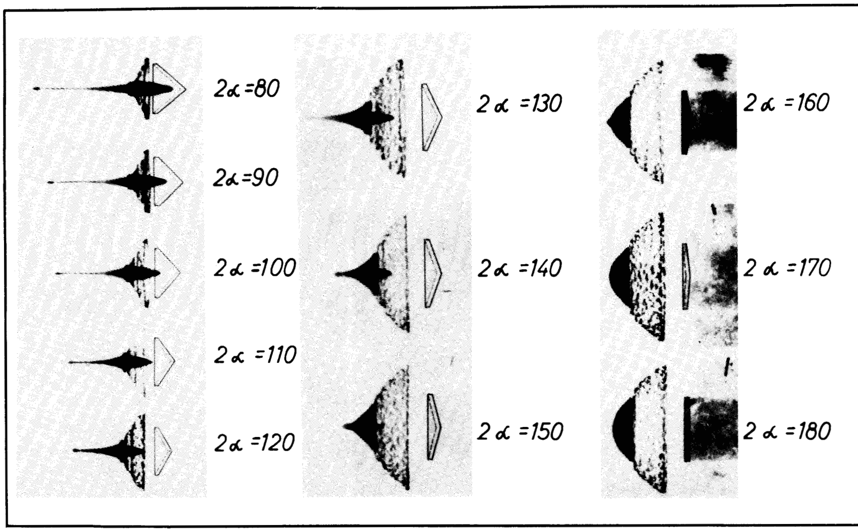

Figure 9. Conical apex angle study 35 μs after detonation (courtesy of M. Held, MBB, Schrobenhausen).

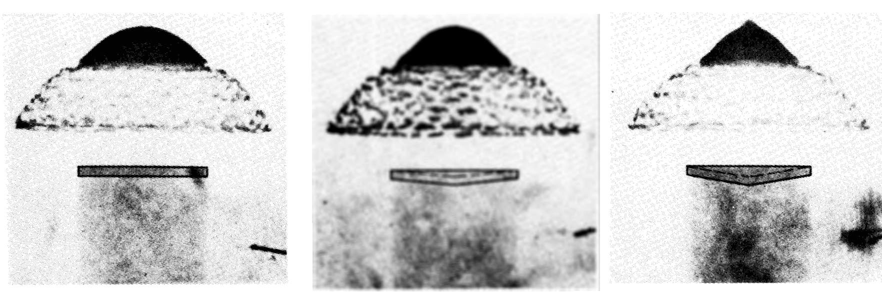

Figure 10. Conical apex angle study for apex angles of 180°, 170°, and 160° (courtesy of M. Held, MBB, Schrobenhausen).

150°, and 180°. The flash times were 15, 30, 45, and 60 μs, as noted in the figure. The jet tip velocity is denoted by V_s.

Figures 15 and 16 illustrate the jet formation of a copper conical lined shaped charge with a 32 mm charge diameter and 1.5 mm wall thickness. The conical apex angle was 60°. The indicated flash times are measured from the arrival of the detonation wave at the tip (apex) of the cone. Note the particulation (breakup) of the jet in Figure 16.

Figure 17 shows the jet from a conical shaped charge just prior to breakup. The necking of the jet is clearly visible.

Figure 18 is a special radiograph designed to show the tip region of the jet from a conical shaped charge. Figure 19 shows the jet formation from a

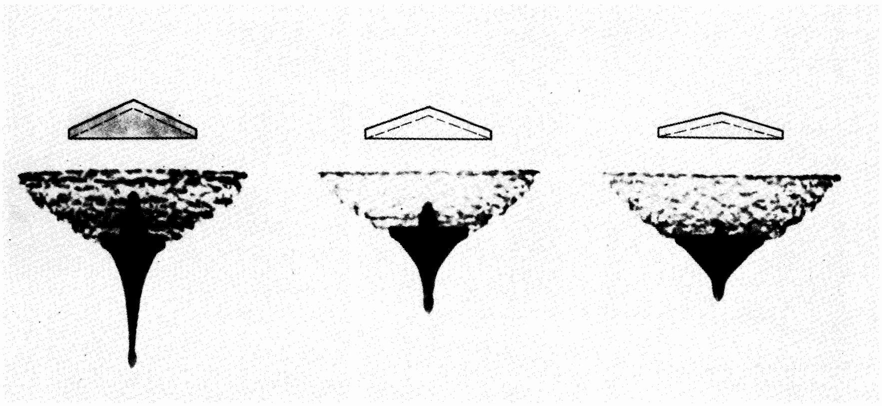

Figure 11. Conical apex angle study for apex angles of 130°, 140°, and 150° (courtesy of M. Held, MBB, Schrobenhausen).

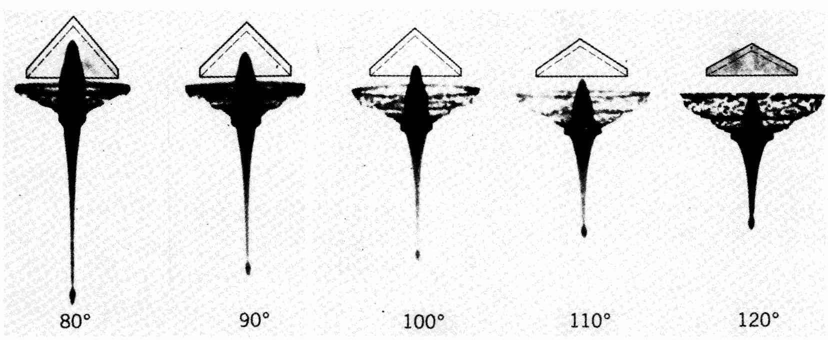

Figure 12. Conical apex angle study for apex angles of 80°, 90°, 100°, 110°, and 120° (courtesy of M. Held, MBB, Schrobenhausen).

heavily confined shaped charge. This radiograph shows the slug or the rear of the jet.

Figure 20 shows a copper jet from a 100 mm diameter shaped charge obtained by the Orthogonal-Synchro-Streak Technique (OSST) (Held 1986). The records on the top of the figure are the direct observations and the lower records were obtained by angle mirrors. The first upper strip shows a dark region in the upper left-hand corner that is artifically introduced by a small electric detonator fired at the edge of the field of view at a predetermined time after the detonation of the shaped charge. This yields an exact correlation between the shaped charge detonation time and the start of the recording. This is one way to allow accurate calculation of the jet tip and jet particle velocities. Held (1986) provides further details.

Note that in these optical records, the tip of the jet is engulfed in a cloud of vapor. This is probably due to ablation of the jet that travels about 9 km/s

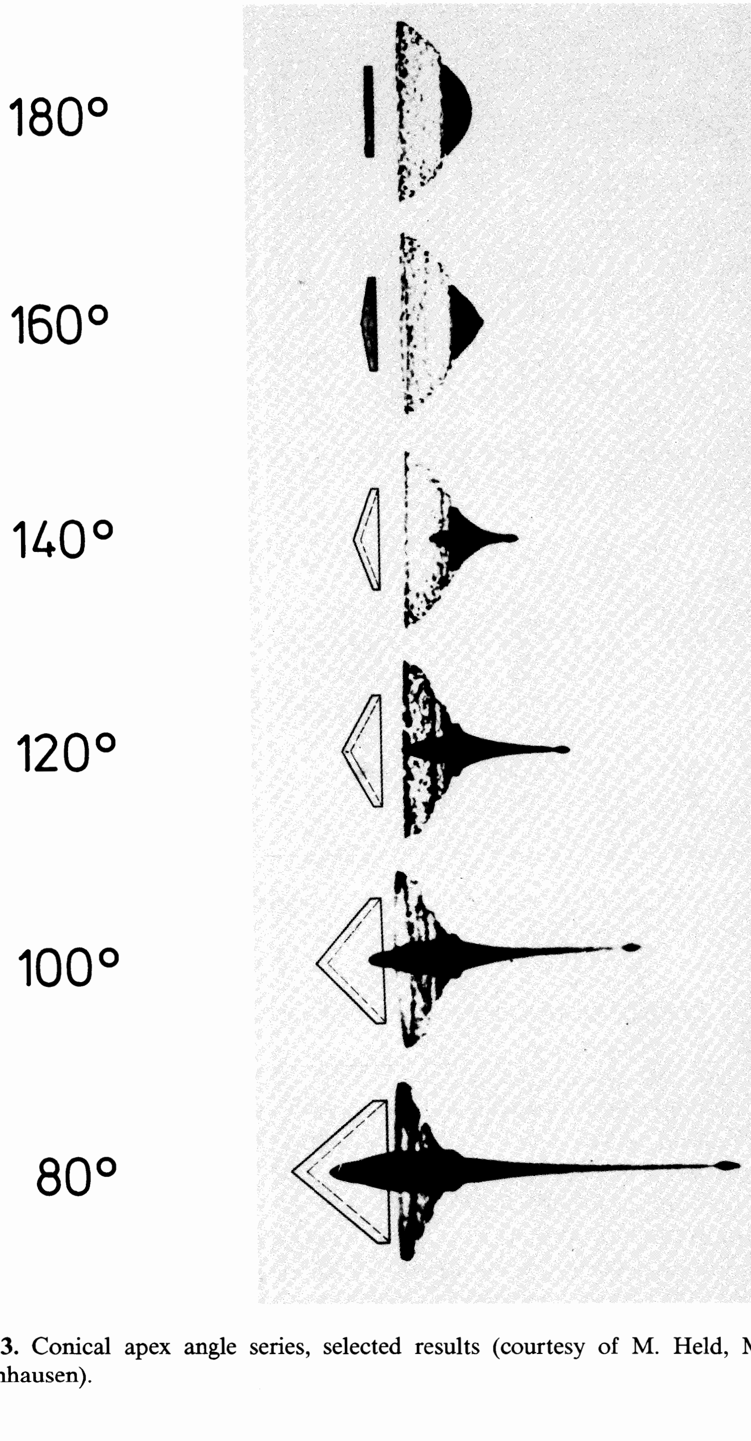

Figure 13. Conical apex angle series, selected results (courtesy of M. Held, MBB, Schrobenhausen).

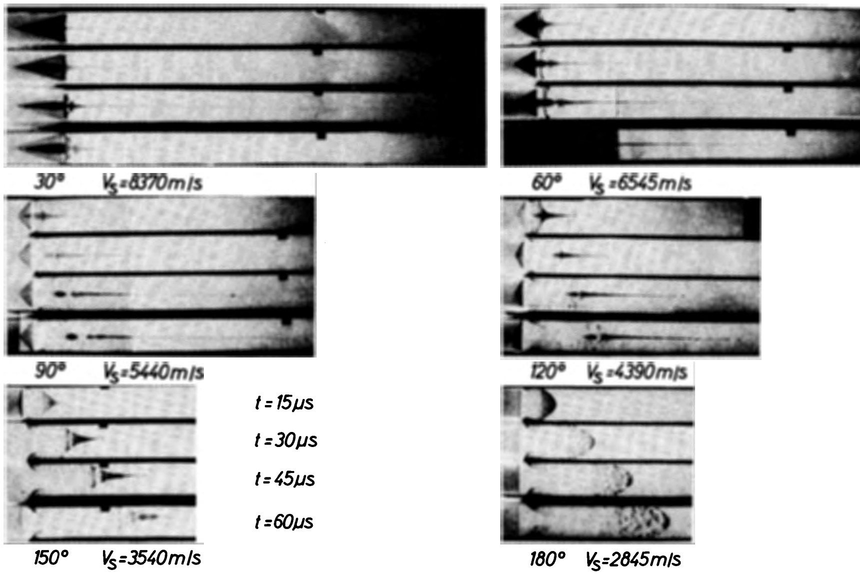

Figure 14. Conical liner apex angle study for apex angles of 30°, 60°, 90°, 120°, 150°, and 180° (courtesy of M. Held, MBB, Schrobenhausen).

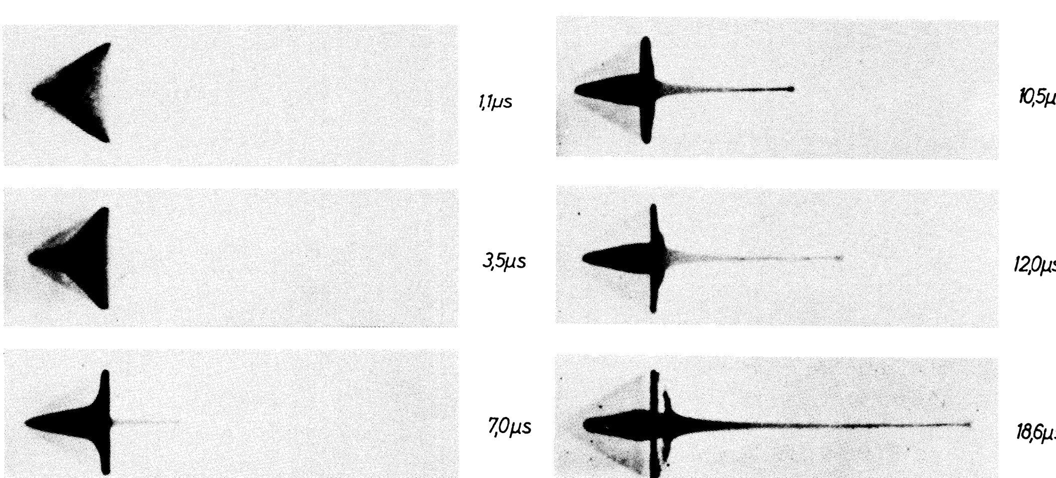

Figure 15. Jet formation of a 60° copper, conical shaped charge (courtesy of M. Held, MBB, Schrobenhausen). The times given are the elapsed time after the detonation wave reached the apex of the liner.

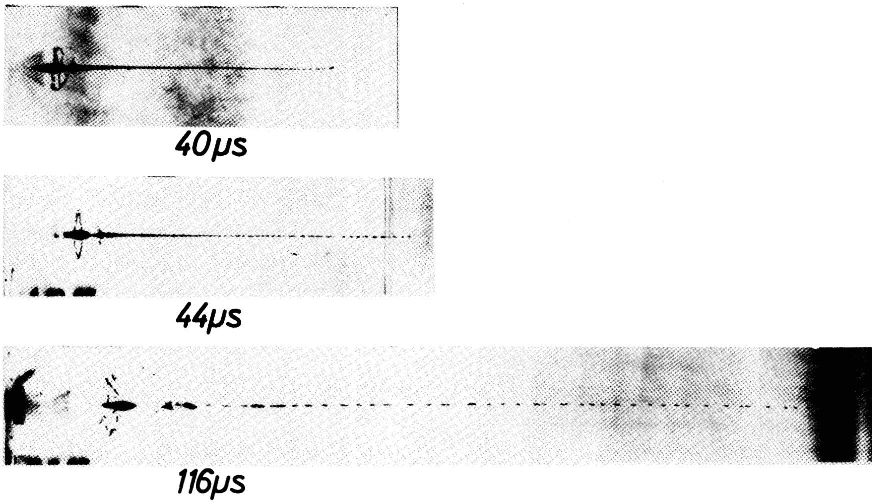

Figure 16. Jet formation and breakup of a 60° copper, conical shaped charge (courtesy of M. Held, MBB, Schrobenhausen). The times given are the elapsed time after the detonation wave reached the apex of the liner.

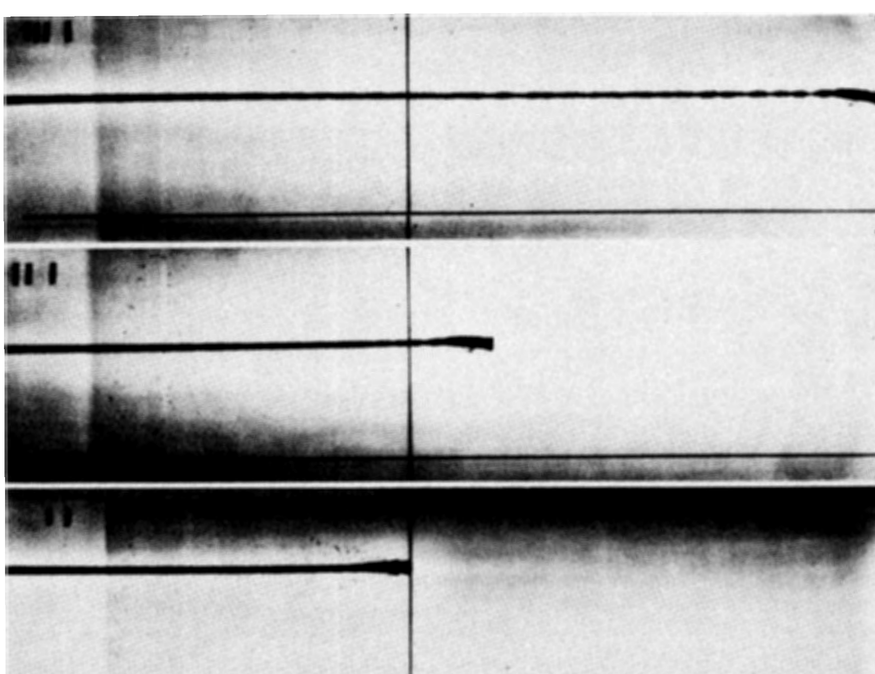

Figure 17. Jet from a conical shaped charge showing early necking just prior to the onset of jet breakup.

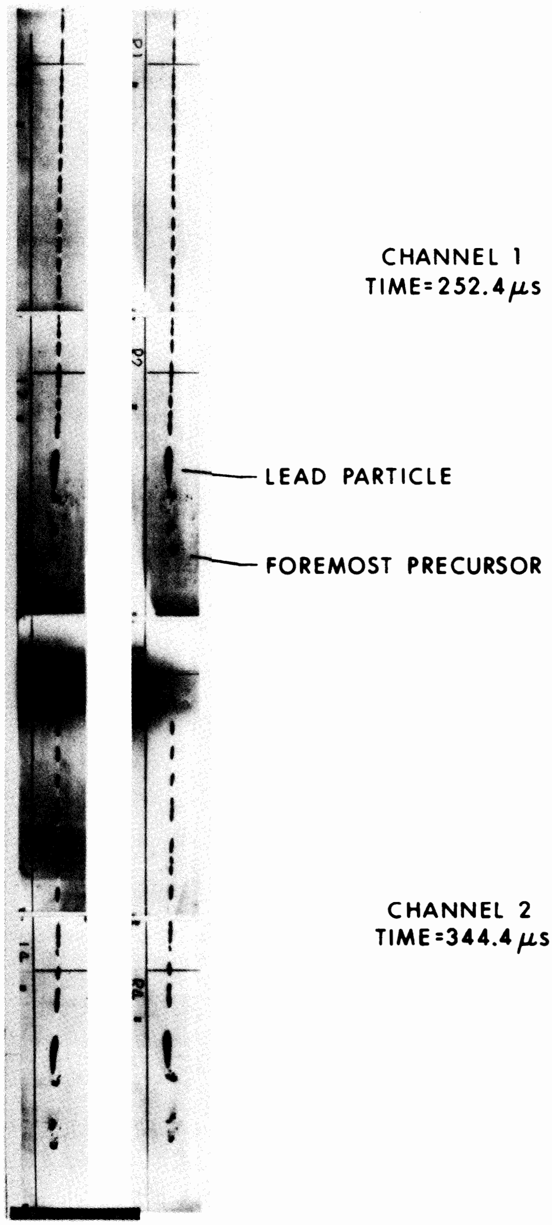

Figure 18. The tip region of a shaped charge jet.

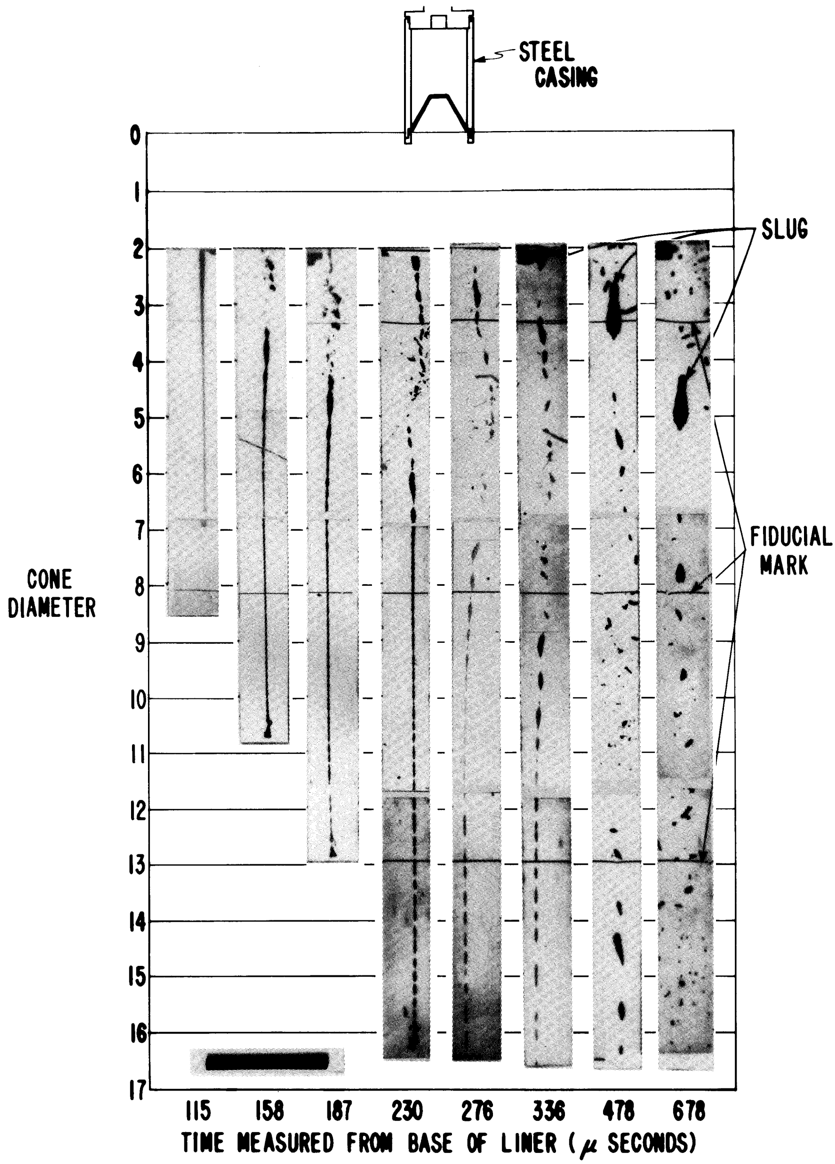

Figure 19. The jet from a heavy confined shaped charge at various distances. Note that the front of the jet was allowed to leave the film in order to radiograph the slug (Simon and DiPersio 1972).

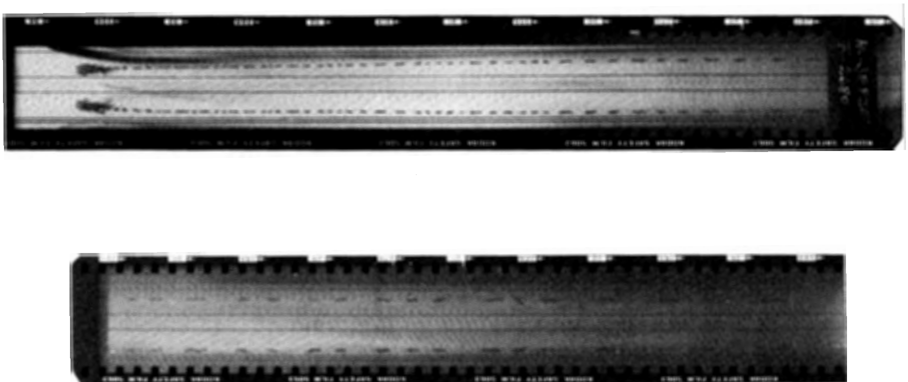

Figure 20. OSST record of a shaped charge jet from a 100 mm diameter, copper shaped charge. The record was taken at 0.5 km/s. The straight horizontal lines are the fiducial lines and are 40 mm apart (1st to 2nd and 3rd to 4th). A continuously writing CORDIN Model 330 camera was used (courtesy M. Held, MBB, Schrobenhausen).

through the air. On an optical record, this ablation phenomenon can be clearly seen. However, due to its low density, this ablation veil is more difficult to see in flash X-ray radiographs.

The tip of the jet is usually surrounded by a multitude of small particles all of which in turn create a trailing ablation veil. Behind the jet tip, the particulated shaped charge jet becomes clearly visible, in general, as can be seen in the lower portion of the record from Figure 20. Again, Held (1986) provides a complete description of the OSST recordings and presents additional examples.

14.2. SHAPED CHARGE LINER COLLAPSE AND JET FORMATION

The following section was extracted from the reports by Chou et al. (1985) and Walters and Golaski (1987). Numerical studies using the HELP and EPIC-2 computer codes (DEFEL is the Dyna East version of EPIC-2) were performed by Chou et al. (1985) that clearly illustrate the shaped charge liner collapse and jet formation for stratified (horizontally layered), bimetallic, copper–nickel shaped charge liners. Both conical and hemispherical liner geometries were considered. Partial experimental verification of the liner collapse and jet formation process was obtained by Walters and Golaski (1987) using a diffusion bonding technique to fabricate the liners and recovering some of the jet particles in water.

Figure 21 shows the stratified, copper–nickel, bimetallic, conical liner. The HELP code numerical simulation, using massless tracer particles to track the flow of the material, is shown in Figure 22. Figure 23 illustrates the cross

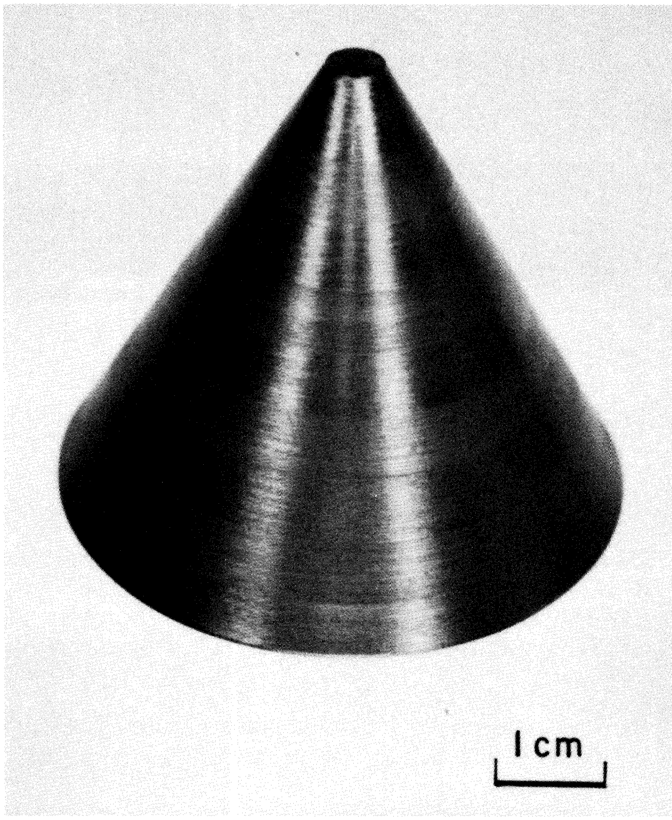

Figure 21. Finish machined, stratified, copper–nickel, conical shaped charge liner (Walters and Golaski 1987).

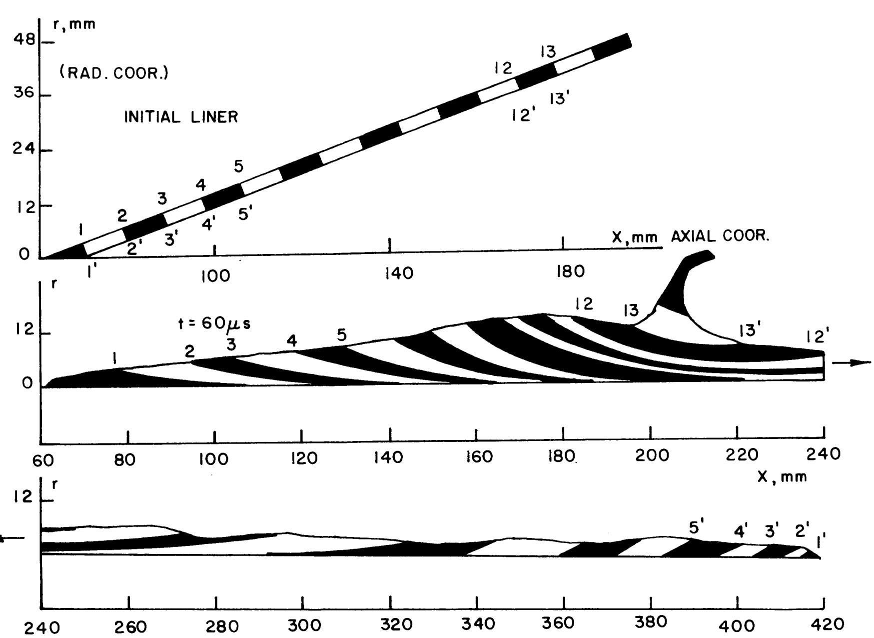

Figure 22. HELP code simulation of a 42° conical liner charge, initial liner geometry (top), jet and slug at 60 μs (center and bottom) (Walters and Golaski 1987).

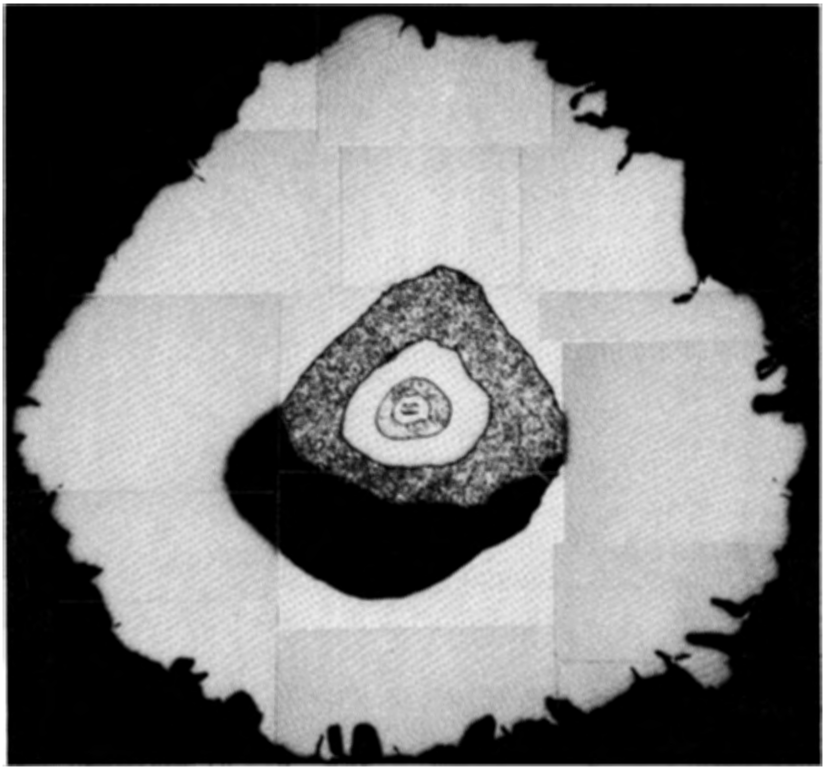

Figure 23. Cross section of jet particle from a stratified copper–nickel conical shaped charge liner (Walters and Golaski 1987).

section of a recovered jet particle revealing the flow of jet material. This particle is probably from the latter half of the jet (since the front-most particles probably eroded during impact with the water). Figure 24 shows a magnified view of the central region of the jet particle in Figure 23. Figure 25 presents a free-flight (in air) flash radiograph from the bimetallic, conical liner. Note that the jet collapses and forms as expected, probably due to the similar behavior of copper and nickel under shock loading conditions as well as the identical densities of copper and nickel. Finally, Figure 26 shows the slug recovered from the stratified, bimetallic liner.

A similar theoretical-experimental study was performed for stratified, bimetallic shape charge liners with the same materials. Figure 27 reveals the unique collapse pattern of point-initiated hemispherical liners, namely, a tubular, layered collapse. Figures 28 and 29 show the agreement between the hydrocodes and show the application of the massless tracer particles to follow the material flow. The late time (76 μs) jet formation is revealed in Figure 30.

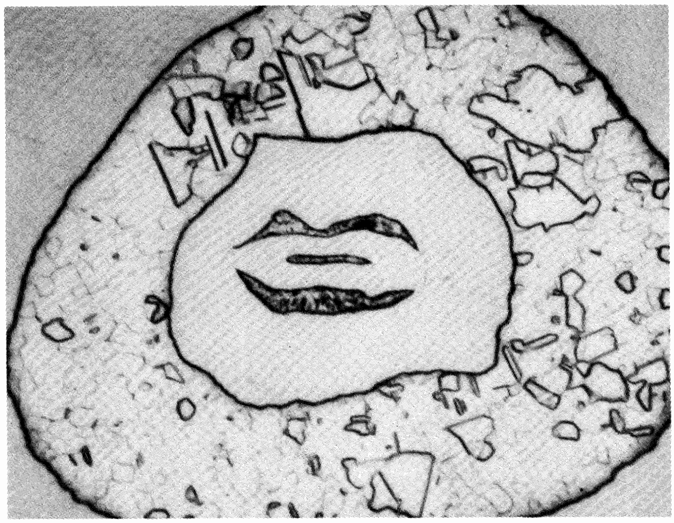

Figure 24. Central region of jet particle from a stratified copper–nickel conical shaped charge liner (Walters and Golaski 1987).

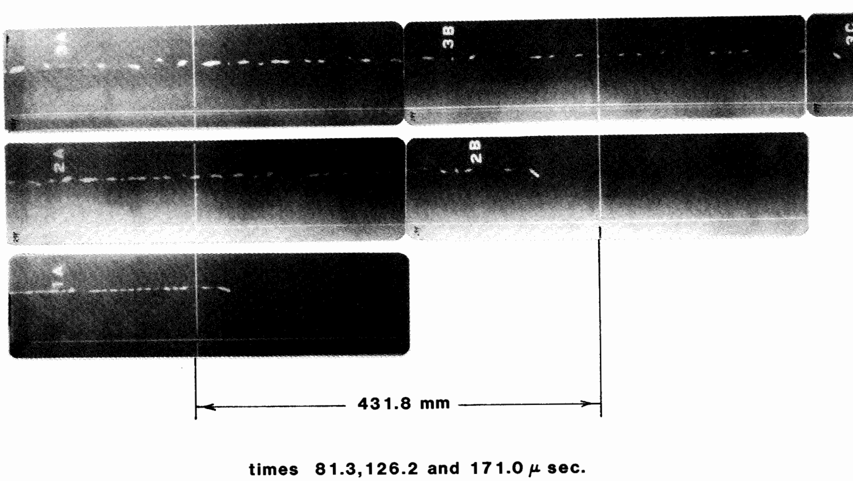

Figure 25. Free-flight flash radiographs of the jet from a stratified copper–nickel conical shaped charge liner (Walters and Golaski 1987).

As illustrated in Figure 31, a surface-initiated charge and a point-initiated charge do not collapse in the same manner.

The stratified, bimetallic, copper–nickel, hemispherical liner is shown in Figure 32. Figure 33 shows the free-flight flash radiograph from the point-ini-

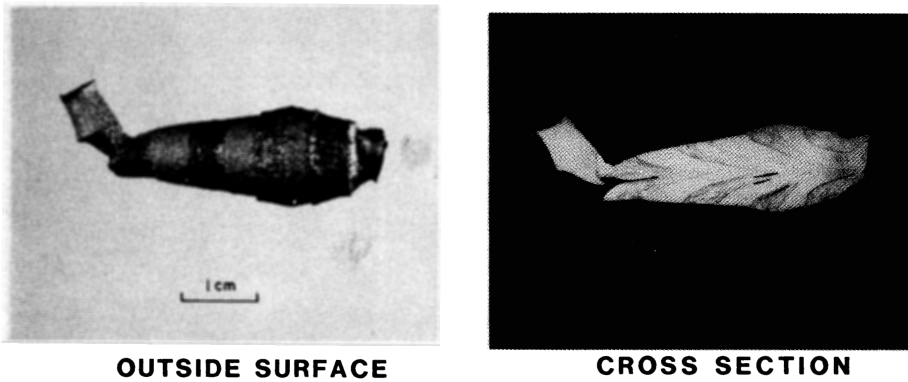

Figure 26. Recovered slug from a stratified copper–nickel conical shaped charge liner (Walters and Golaski 1987).

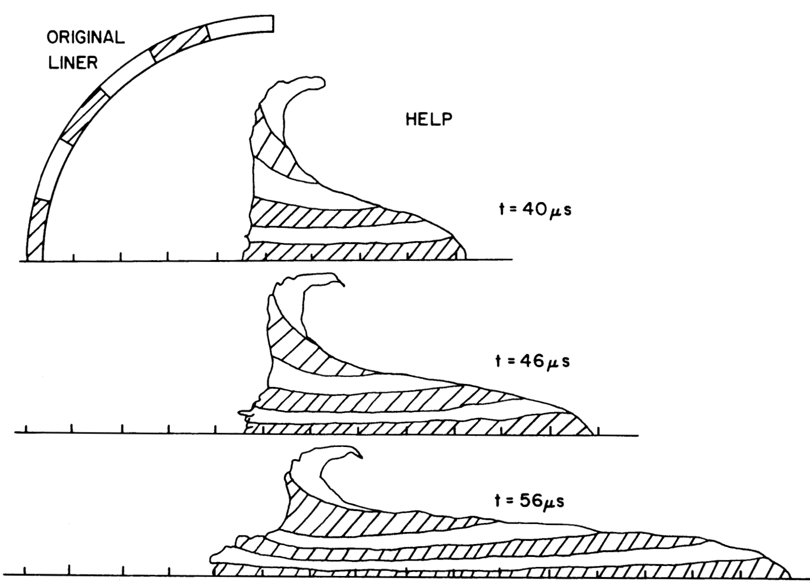

Figure 27. HELP code simulation of jet formation from a hemispherical liner charge for the point-initiated case at three times after detonation (Walters and Golaski 1987).

tiated, hemispherical liner shaped charge. Again, the copper–nickel liner collapses, and the jet forms, as expected.

Figure 34 shows a cross section of a recovered jet particle (again, probably from the latter half of the jet) that reveals the tubular, layered collapse of the point-initiated, hemispherical liner. Figure 35 shows a cross section of one-half of the recovered jet particle that clearly shows the tubular, layered collapse of the liner.

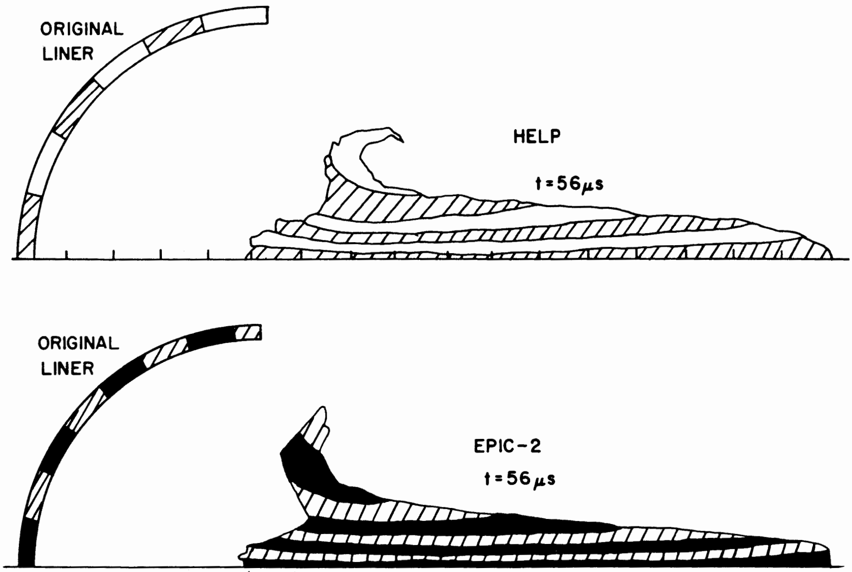

Figure 28. Comparison of HELP and EPIC-2 computer code simulations of jet formation from a hemispherical liner charge for the point-initiated case at $t = 56\ \mu s$ after detonation (Walters and Golaski 1987).

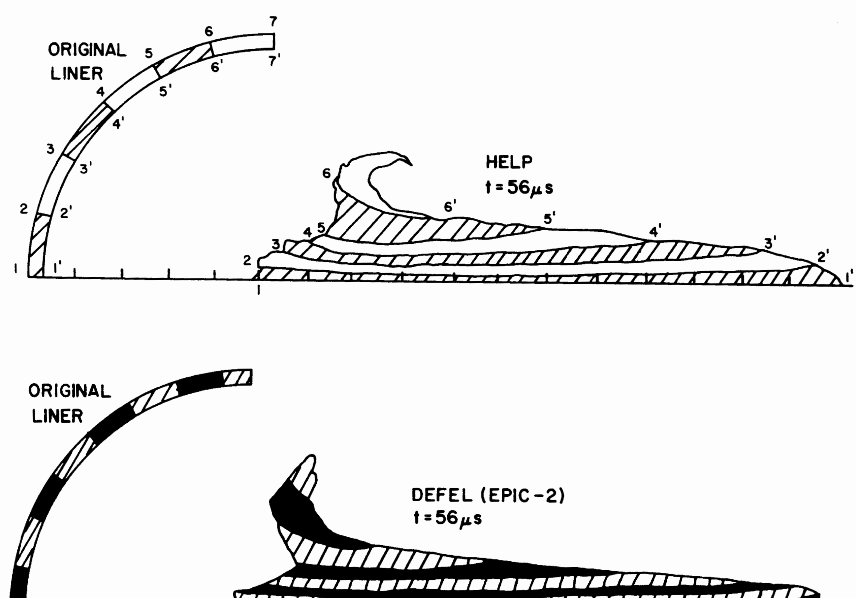

Figure 29. Computer code (HELP and DEFEL) simulation of jet formation of a hemispherical liner charge (Walters and Golaski 1987).

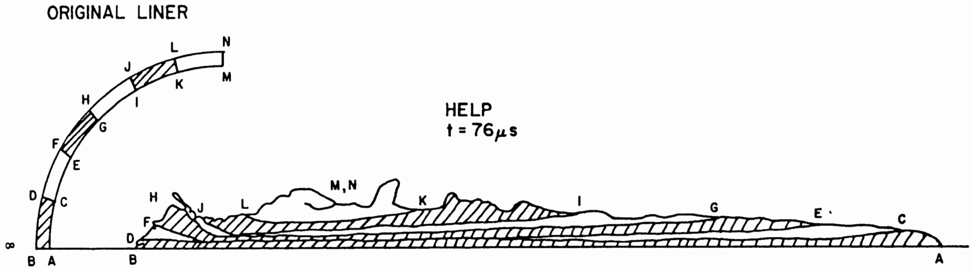

Figure 30. HELP code simulation of jet formation from a hemispherical liner charge for the point-initiated case at $t = 76$ μs after detonation (Walters and Golaski 1987).

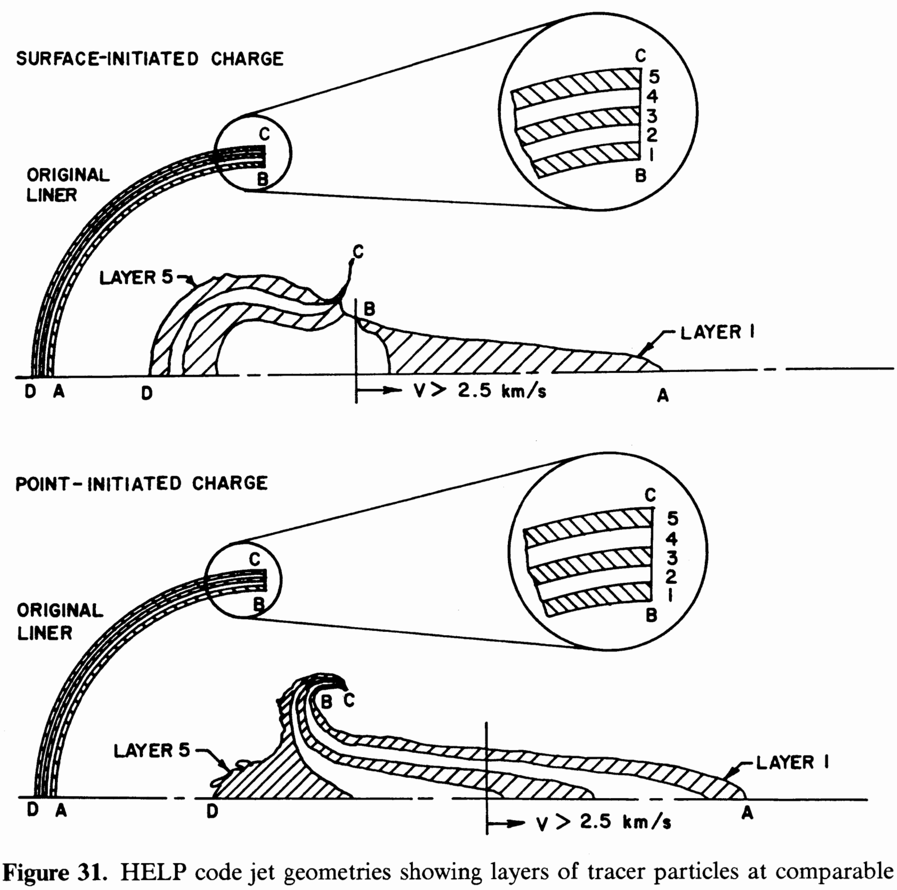

Figure 31. HELP code jet geometries showing layers of tracer particles at comparable times after detonation (Walters and Golaski 1987).

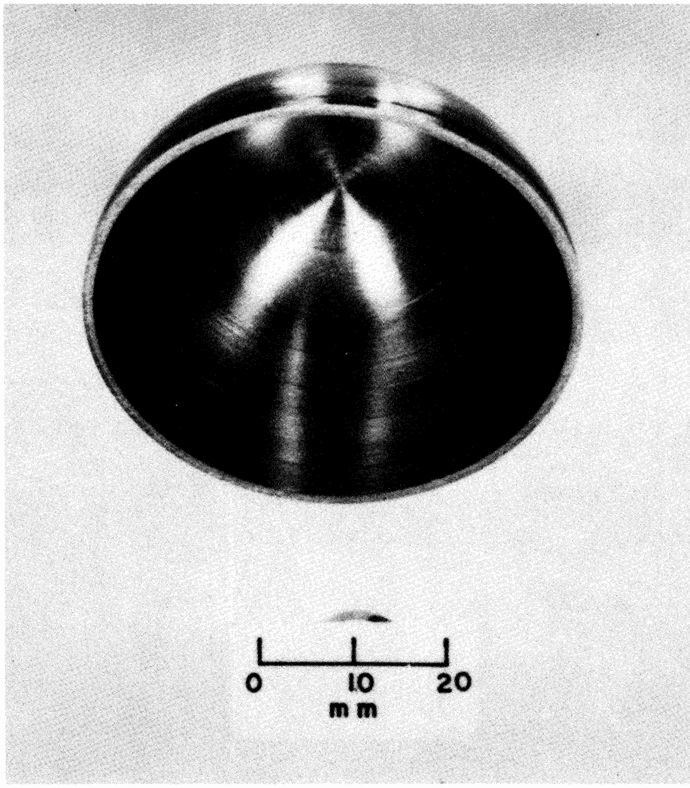

Figure 32. Finish machined, stratified, copper–nickel hemispherical shaped charge liner (Walters and Golaski 1987).

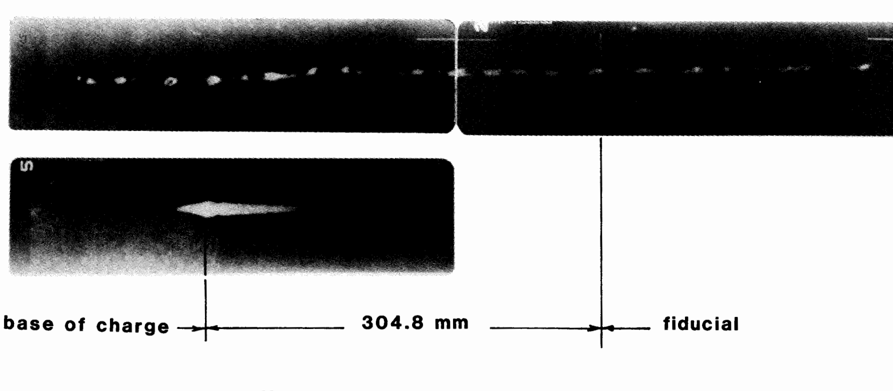

Figure 33. Free-flight flash radiographs of the jet from a stratified copper–nickel hemispherical shaped charge liner (Walters and Golaski 1987).

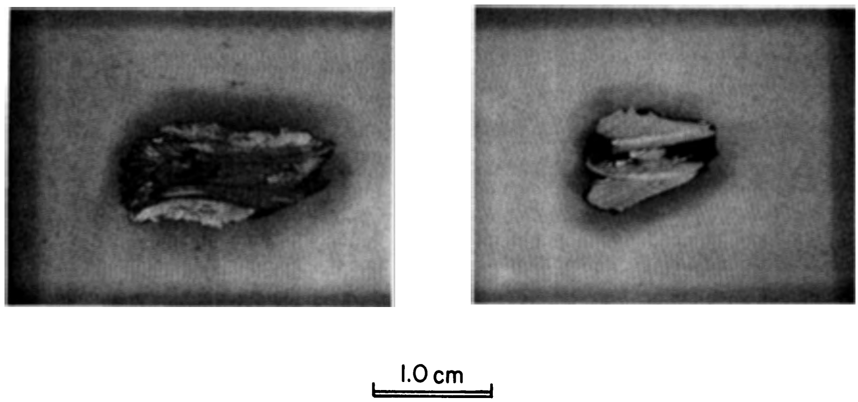

Figure 34. Cross section of recovered jet particles from a stratified copper–nickel hemispherical shaped charge liner (Walters and Golaski 1987).

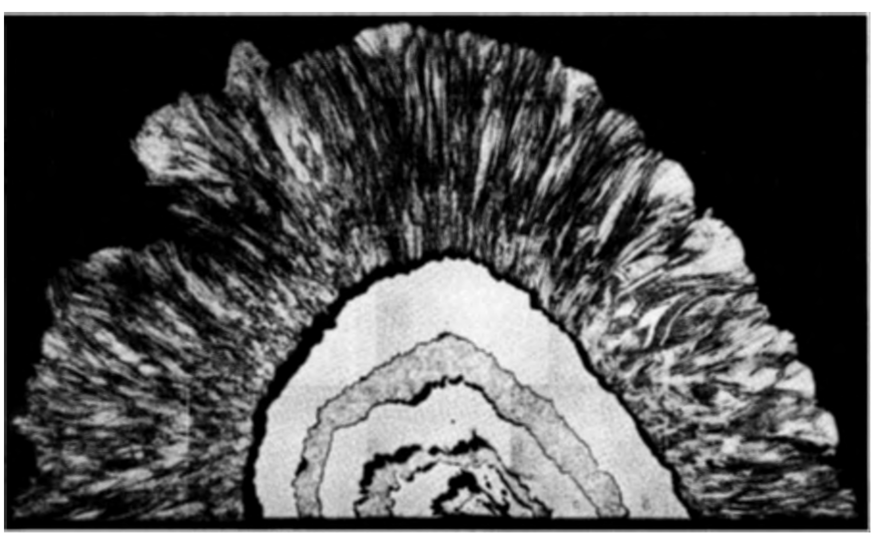

Figure 35. Cross section of one-half of a recovered jet particle from a stratified copper–nickel hemispherical shaped charge liner (Walters and Golaski 1987).

14.3. SHAPED CHARGES WITH HEMISPHERICAL LINERS

The early collapse of a shaped charge with a hemispherical liner is shown in Figure 36. Note that the pole inverts, or the liner turns inside out from the pole. The middle portion of Figure 36 shows the characteristic "Mexican sombrero."

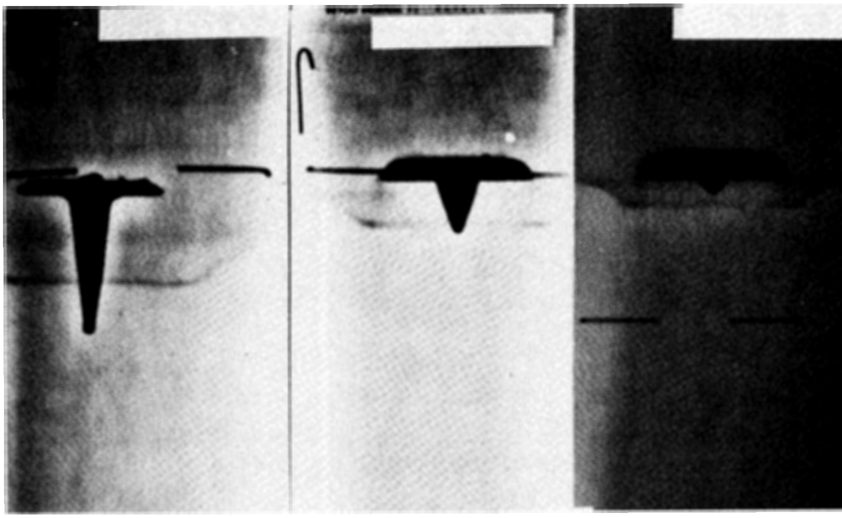

Figure 36. Early collapse of a hemispherical shaped charge liner. Note the inversion of the pole region.

Figures 37 and 38 show the formation and particulation of 127 mm diameter shaped charges with hemispherical liners made from OFHC (oxygen free high conductivity) copper. Figure 37 covers the 300–400 μs time range and Figure 38 covers the 500–600 μs time range. Note the tumbling of the jet particles at the long flash times.

Figures 39 and 40 show the jet from a shaped charge identical to the one shown in Figures 37 and 38, except the liner was fabricated from ETP (electrolytic tough pitch) copper. Note the "jagged" nature of the jet particles, especially at the later times. Comparison of Figures 37–40 reveals that the liner material and metallurgy are important in controlling the shaped charged jet ductility.

Figure 41 shows the jet from a shaped charge with an OFHC copper hemispherical liner, as in Figures 37 and 38, but this liner was simply hydroformed and not finish machined as the others were. Note that the "jagged" particle behavior returns for this nonprecision liner.

Figure 42 shows a framing camera record of the collapse of a hemispherical shaped charge liner. Figures 43*a*–43*d* show a collapse sequence, obtained by a high-speed framing camera, for an ETP copper, hemispherical shaped charge liner. Figure 43*a* shows the initial setup, where a mirror was used to obtain two views of the collapsing jet. The grid and numbers on the liner surface were used to obtain the liner collapse velocities. Note that the pole region forms first. The detonation products were not screened and begin to appear in Figure 43*c*. The jet eventually is obscured by the detonation products and only the

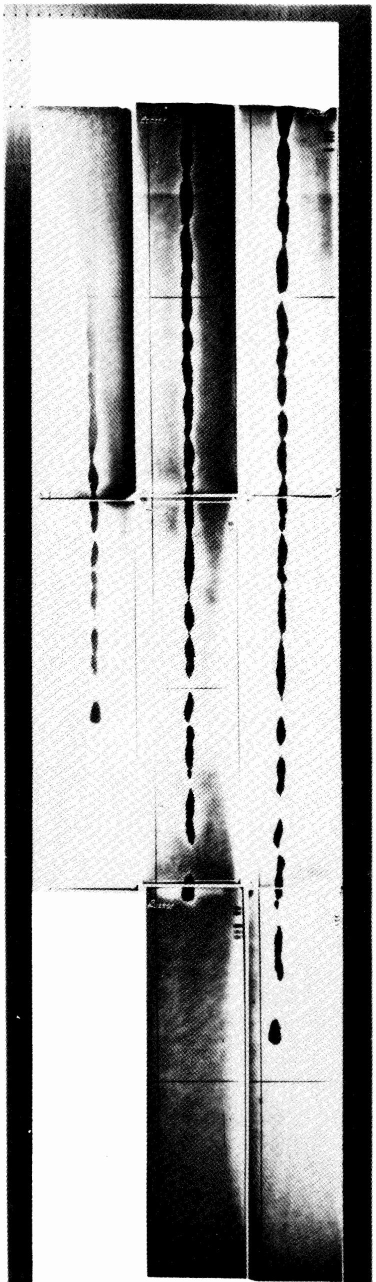

Figure 37. Jet from a shaped charge with an OFHC copper, hemispherical liner. Flash times are 303, 344, and 378 μs.

Figure 38. Jet from a shaped charge with an OFHC copper, hemispherical liner. Flash times are 543, 568, and 593 μs.

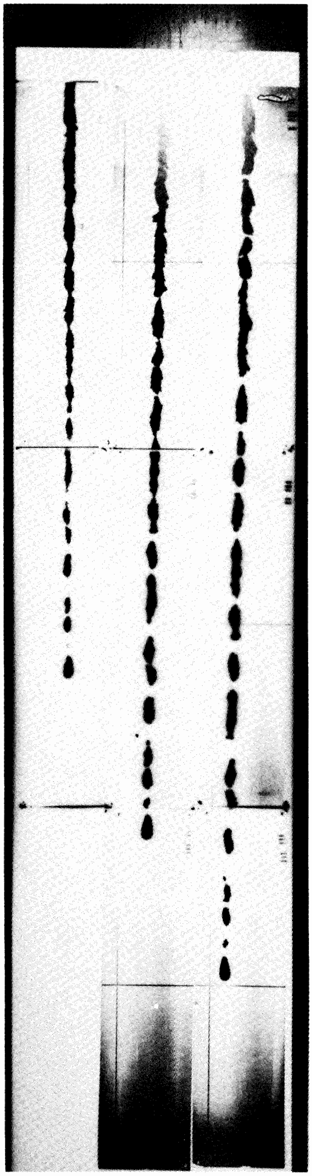

Figure 39. Jet from a shaped charge with an OFHC copper, hemispherical liner. Flash times are 303, 344, and 380 μs.

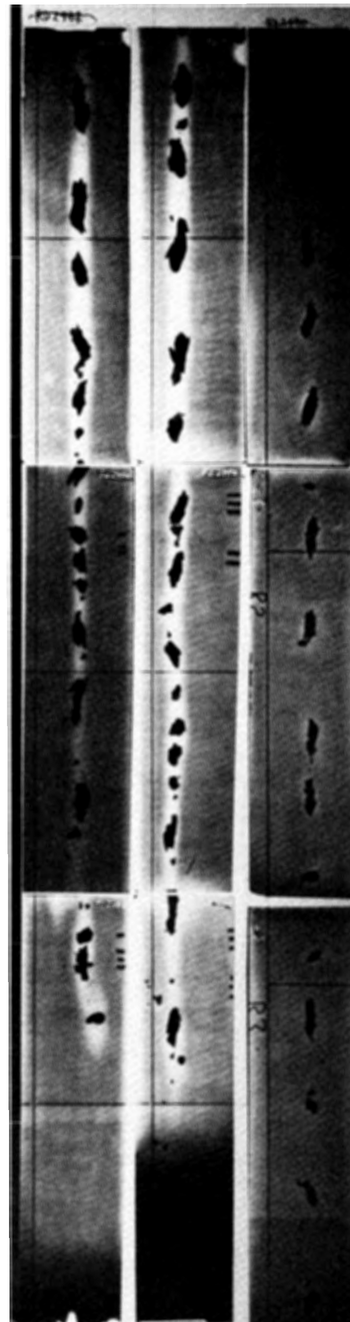

Figure 40. Jet from a shaped charge with an ETP copper, hemispherical liner. Flash times are 450, 476, and 500 μs.

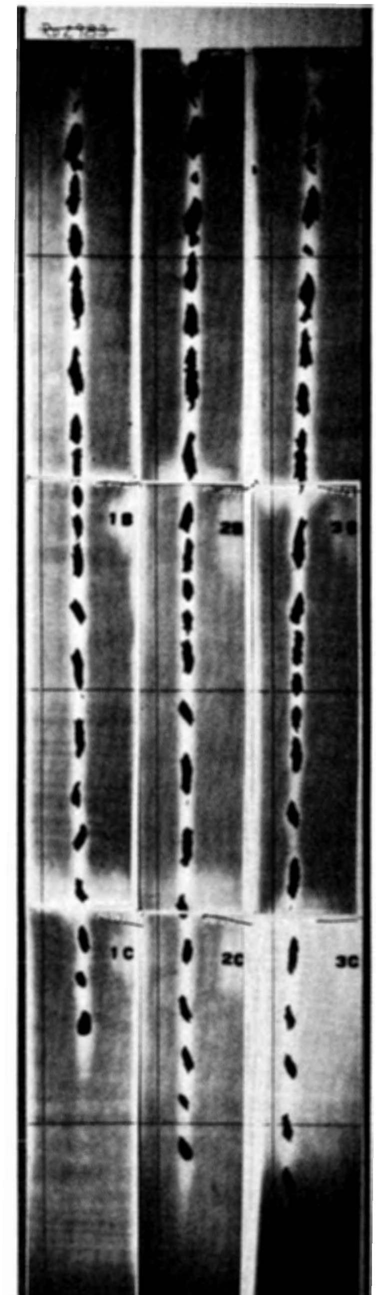

Figure 41. Jet from a shaped charge with an OFHC copper, hemispherical liner. Flash times are 450, 475, and 500 μs. The liner was not finish machined.

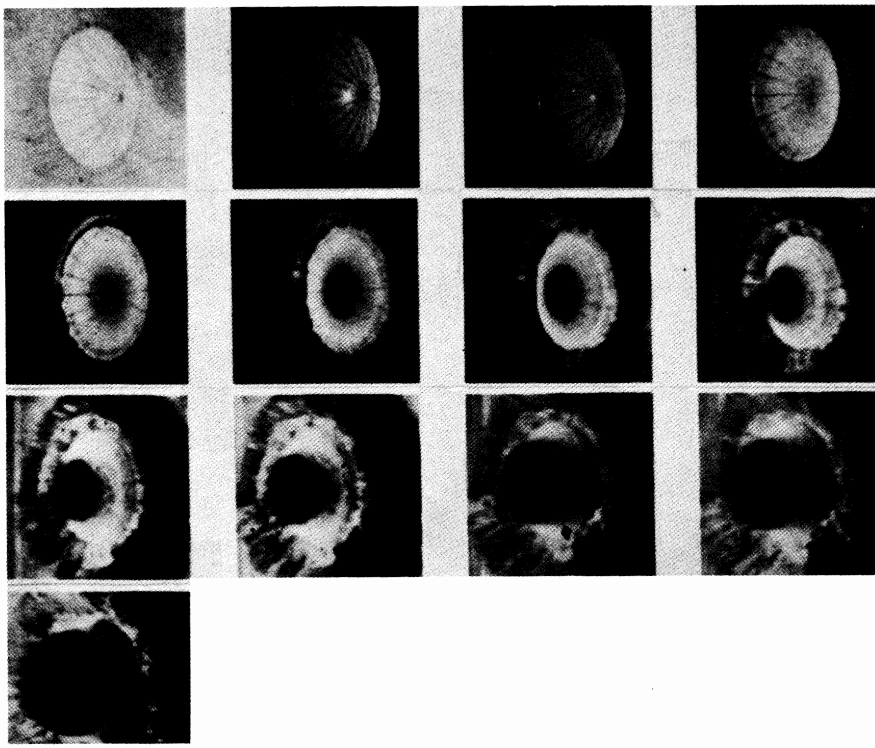

Figure 42. Microsecond, framing camera flash bomb illuminated, sequence of collapse of hemispherical shaped charge liner (Cook 1958).

two views of the jet tip appear. These two views of the tip appear to collide in Figure 43*d* (due to the mirror arrangement). Figure 43*b* represents an elapsed time of about 6.4 μs since Figure 43*a*. Figure 43*c* is about 12.8 μs after the frame shown in Figure 43*a*. Finally, Figure 43*d* occurs at about 32 μs.

Figure 44 depicts a flash radiograph (X-ray) study of the collapse of a shaped charge with a hemispherical liner. Note again the inversion of the pole and the appearance of the "Mexican sombrero" at 15 μs. These flash radiographs were taken by S. Kronman of the BRL several years ago.

14.4. EXPLOSIVELY FORMED PENETRATORS

Numerical simulations of the various self-forging fragments (SFFs) or explosively formed penetrators (EFPs) are shown in this section. Details are given by Weickert (1986).

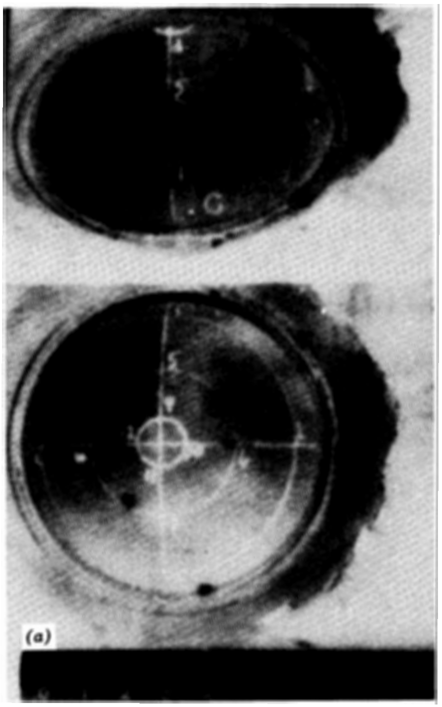

Figure 43a. A framing camera record of the collapse of a shaped charge with a hemispherical liner.

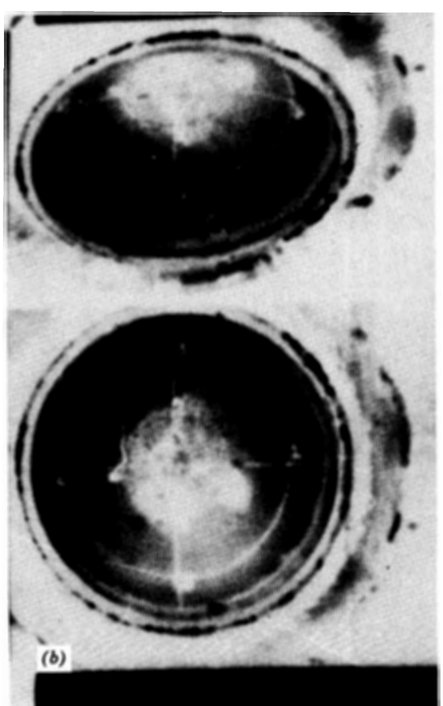

Figure 43b. A framing camera record of the collapse of a shaped charge with a hemispherical liner.

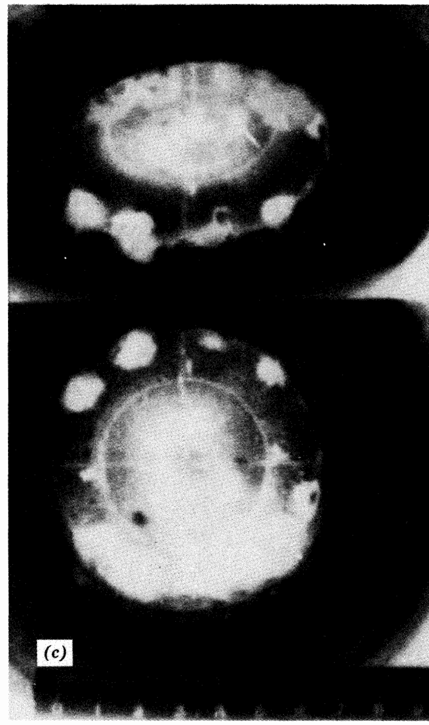

Figure 43c. A framing camera record of the collapse of a shaped charge with a hemispherical liner.

Figure 43d. A framing camera record of the collapse of a shaped charge with a hemispherical liner.

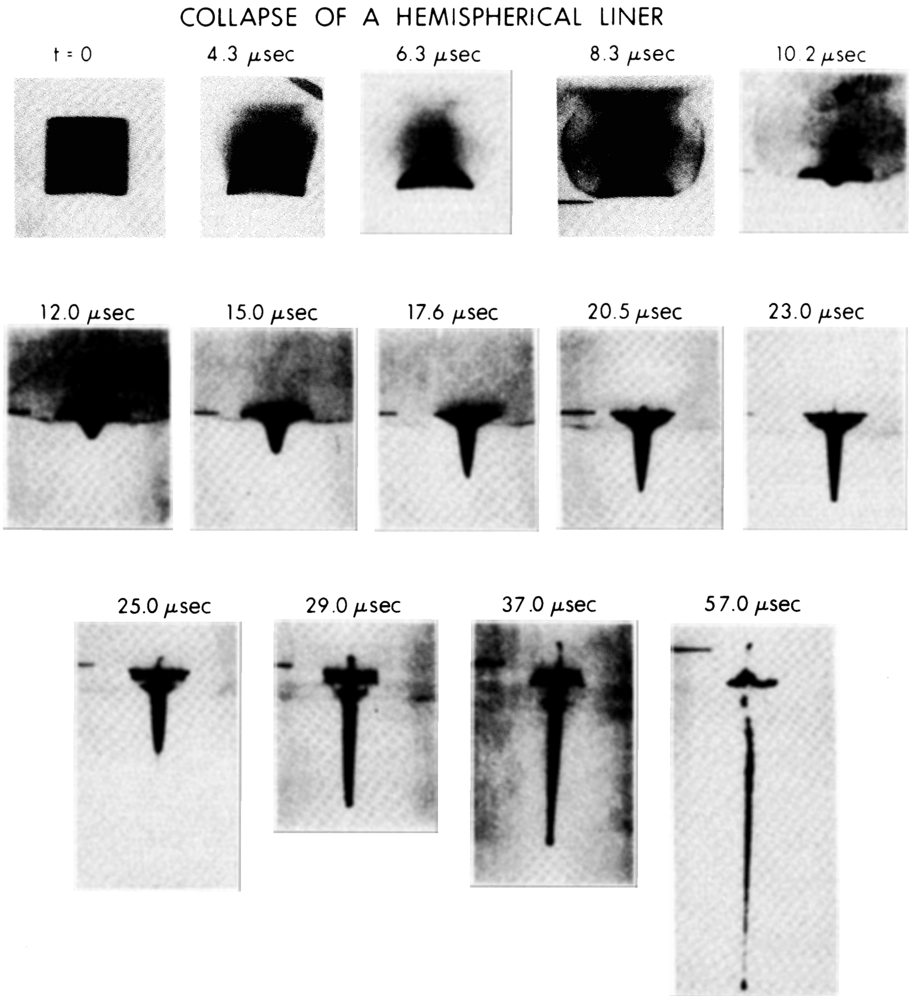

Figure 44. Flash radiograph study of the collapse and formation of a shaped charge with a hemispherical liner (obtained by S. Kronman, BRL).

Figures 45–47 illustrate a forward-folding, a backward-folding, and a W-fold penetrator, respectively.

Figure 48 illustrates various EFP designs, and Figures 49 and 50 show EFPs resulting from confined or cased charges. Figures 51 and 52 further illustrate penetrator shapes resulting from various liner geometries, that is, parabolic and hyperbolic.

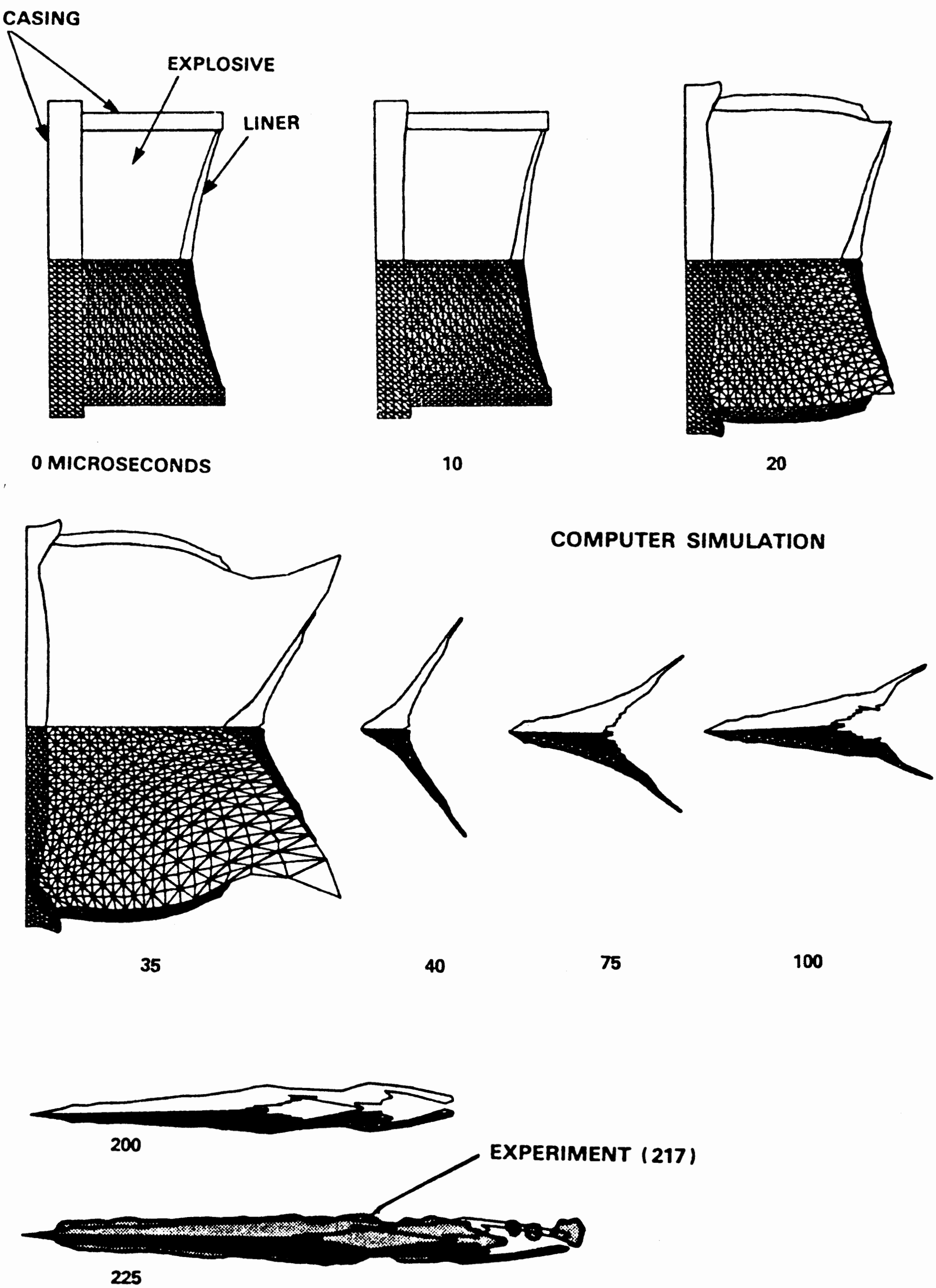

Figure 45. Forward-fold SFF formation (Weickert 1986).

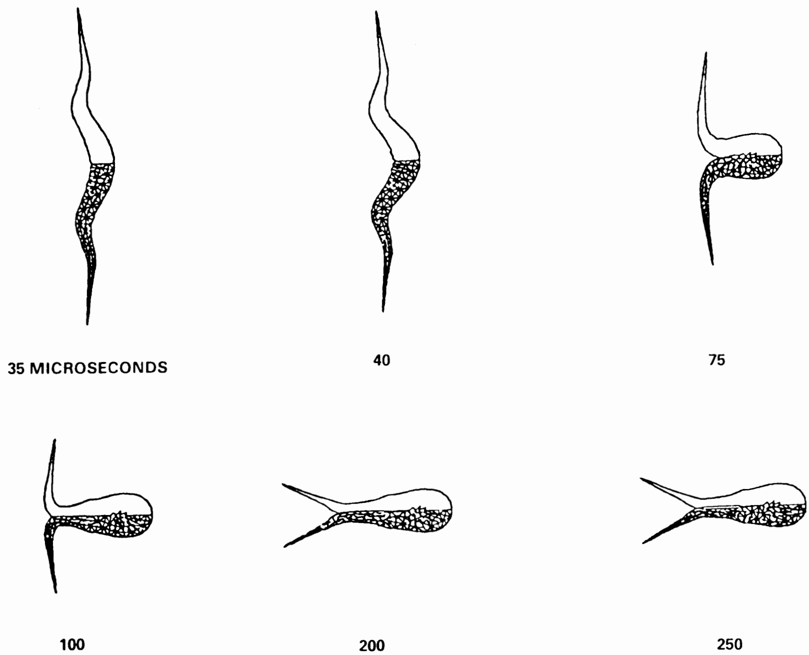

Figure 46. Backward-fold SFF formation (Weickert 1986).

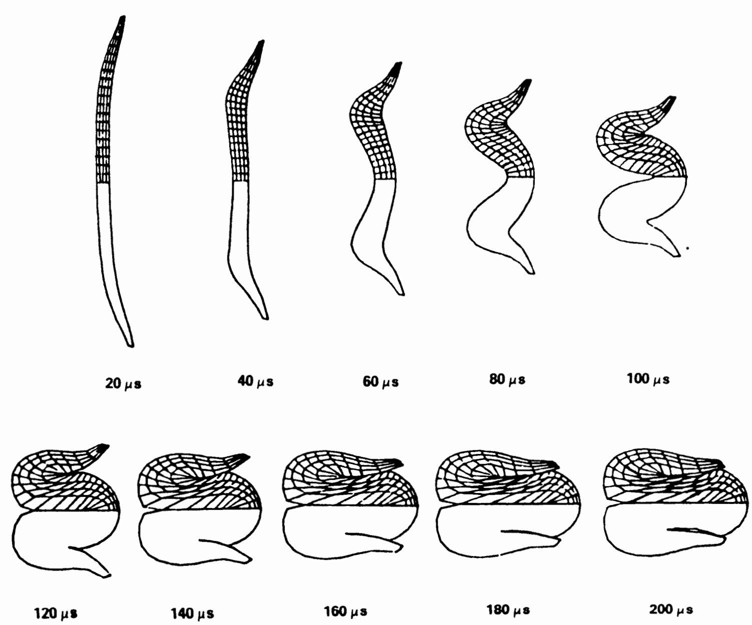

Figure 47. W-fold SFF formation (Hallquist 1980).

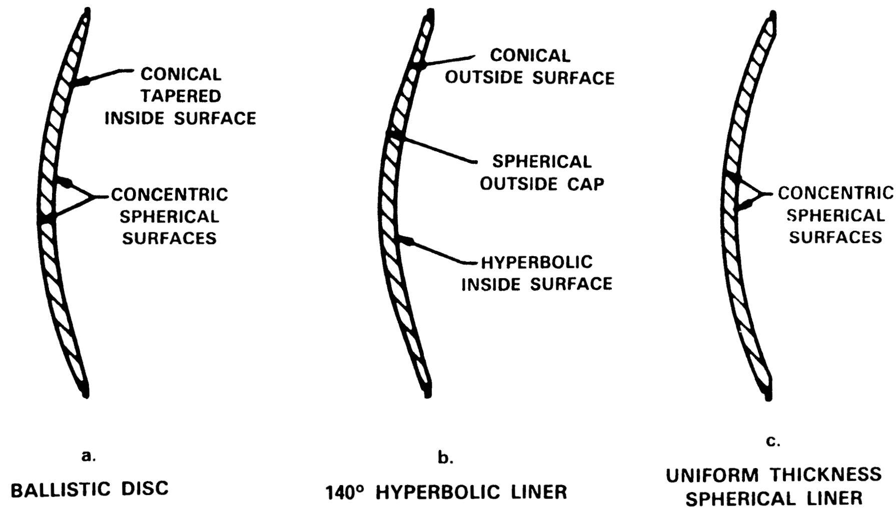

Figure 48. Self-forging fragment liner designs (Hermann et al. 1977).

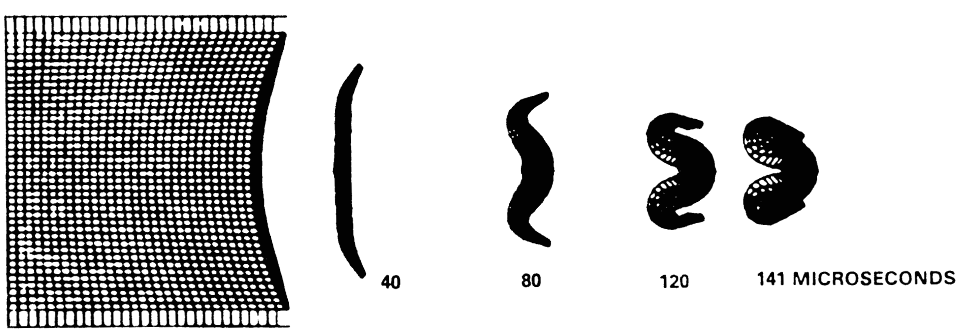

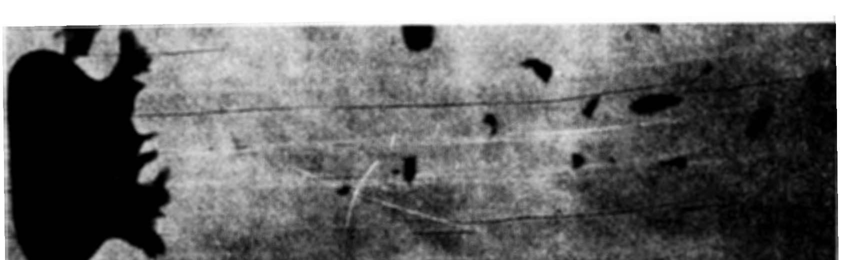

Figure 49. Computer simulation and radiograph of fragment produced from a steel ballistic disk in confined charge (Hermann et al. 1977).

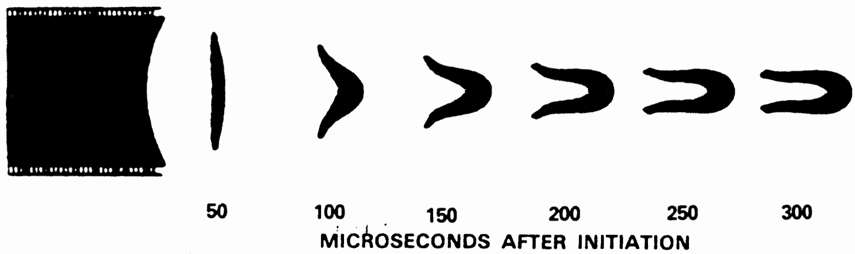

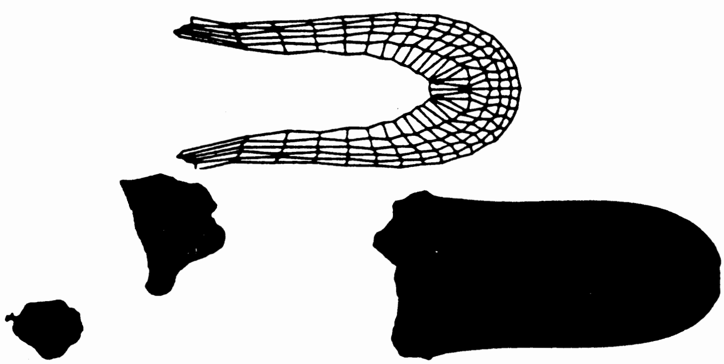

Figure 50. Computer simulation and radiograph of fragment produced from uniform thickness steel liner in confined charge (Hermann et al. 1977).

14.5. BLASTING AND SHAPED CHARGES

The Defense Research Establishment Suffield (DRES) of Canada developed a technique to deploy large craters as obstacles to tanks and vehicles. First, a shaped charge is employed to create a borehole. A typical demolition charge used by the Canadian Armed Forces is shown in Figure 53. Figure 54 shows the demolition charge positioned to create the borehole. The three-prong stand under the shaped charge is designed to provide the appropriate standoff distance.

After the borehole is formed, it is filled with a granular explosive called TRIGAN, developed by the Canadian Defense Research Establishment. Figure 55 shows the granular TRIGAN pellets, which are housed in plastic carrying containers (Figure 56). The TRIGAN is poured into the borehole and primed with C4 to act as a cratering charge. On-site preparation includes adding water to the TRIGAN, which significantly increases its detonation

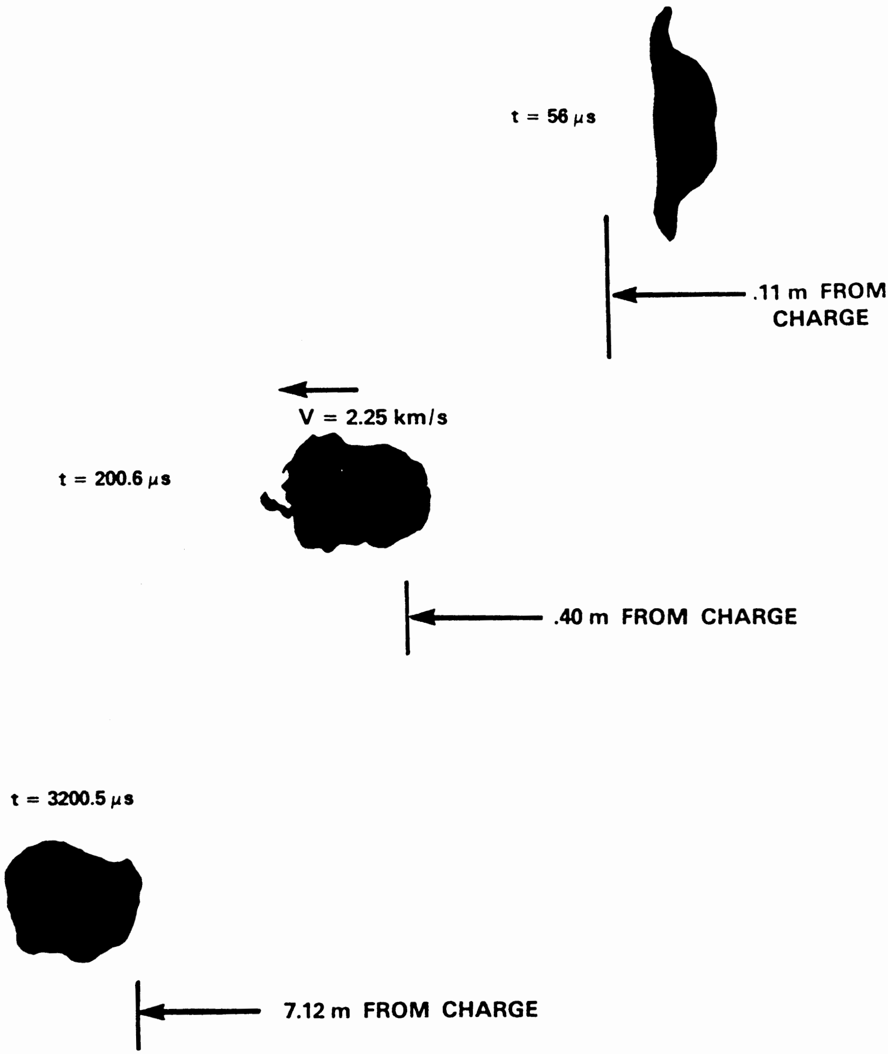

Figure 51. X-radiographic sequences of a parabolic lined SFF charge that generates a ball fragment (PI 1979).

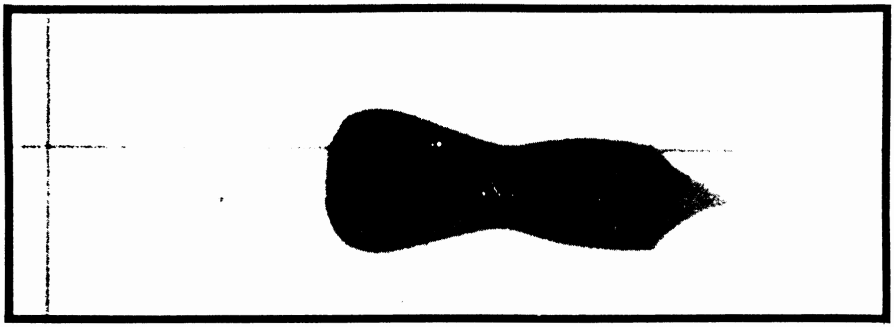

Figure 52. Copper fragment produced by a 140° hyperbolic liner (Weickert 1986).

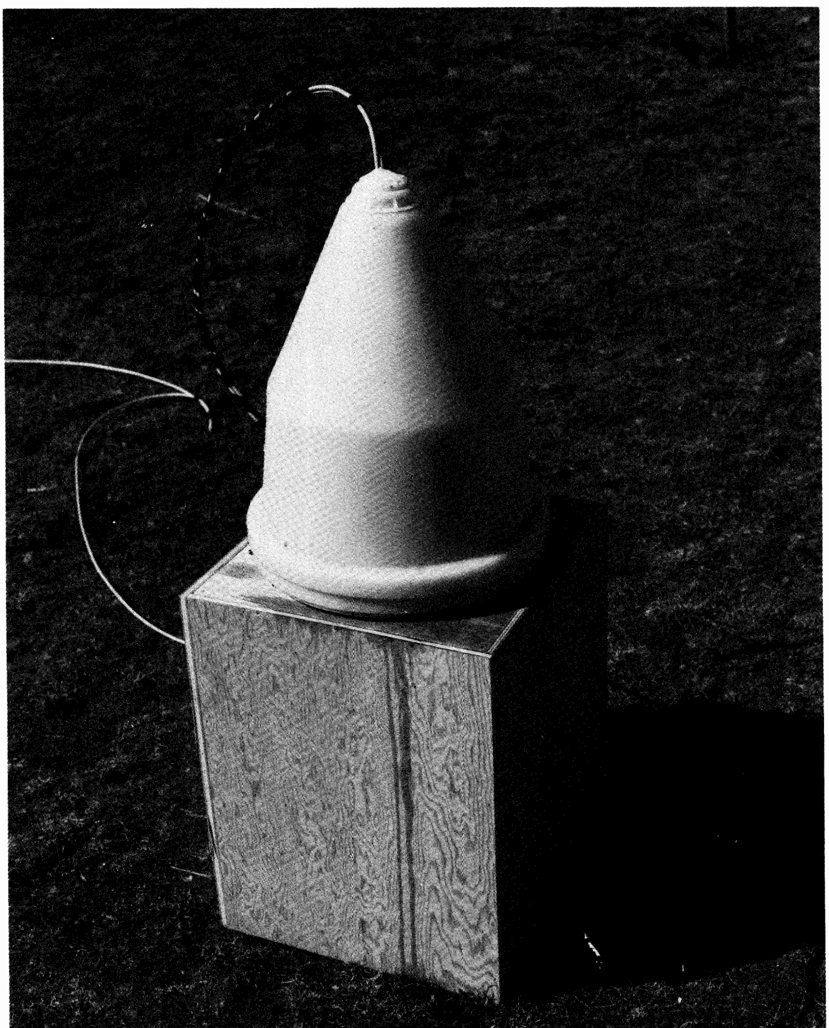

Figure 53. A demolition charge used by the Canadian Armed Forces (courtesy Defense Research Establishment Suffield).

Figure 54. The setup of a shaped charge used for cratering (courtesy Defense Research Establishment Suffield).

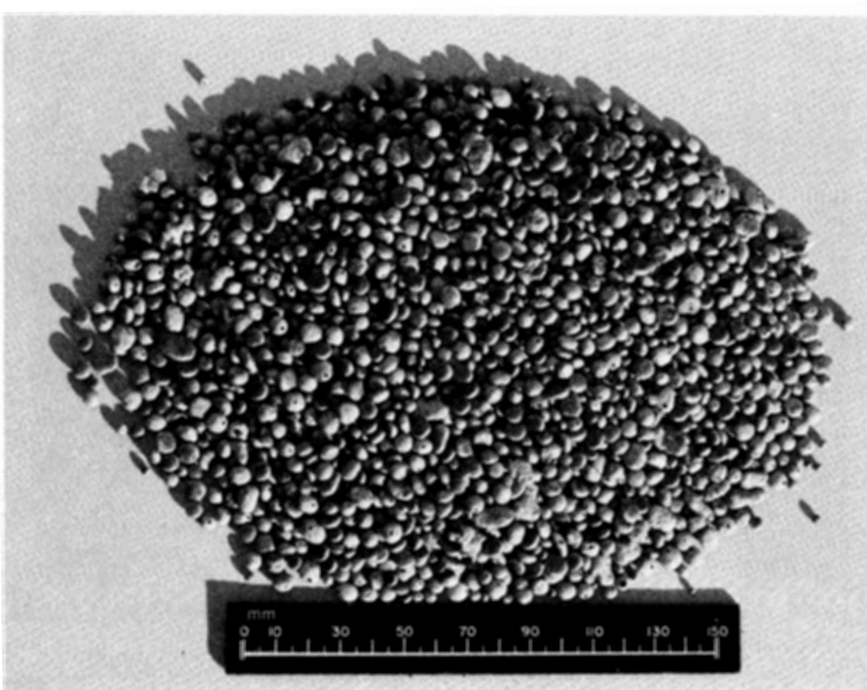

Figure 55. Granular TRIGAN pellets (courtesy Defense Research Establishment Suffield).

Figure 56. TRIGAN is poured from its original plastic containers into a shaped charge borehole (courtesy Defense Research Establishment Suffield)).

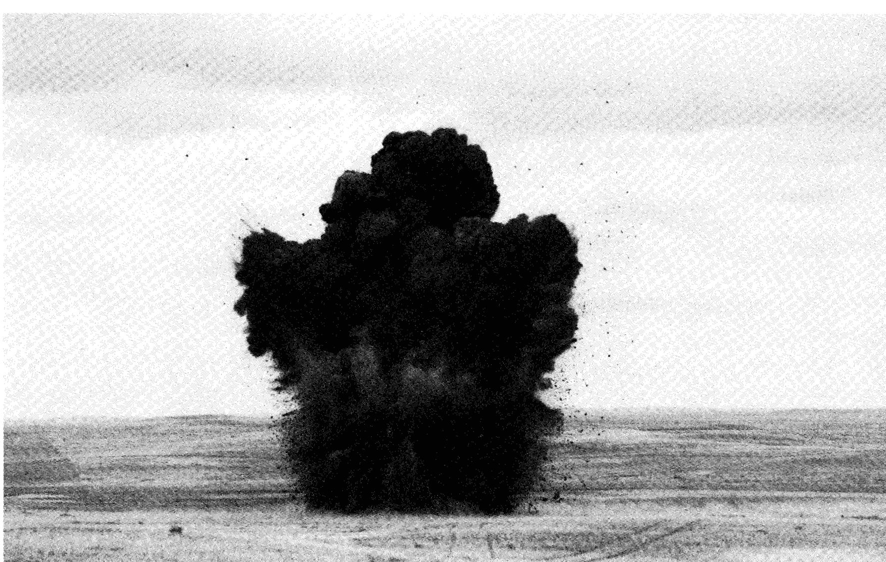

Figure 57. Detonation of TRIGAN cratering charges (courtesy Defense Research Establishment Suffield).

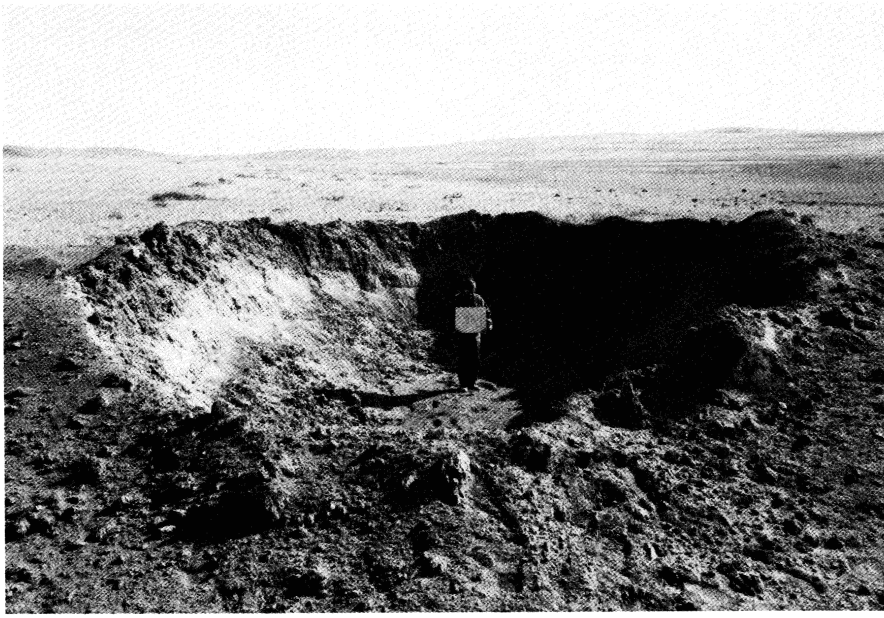

Figure 58. A typical countermobility obstacle produced by the detonation of TRIGAN charges (courtesy Defense Research Establishment Suffield.

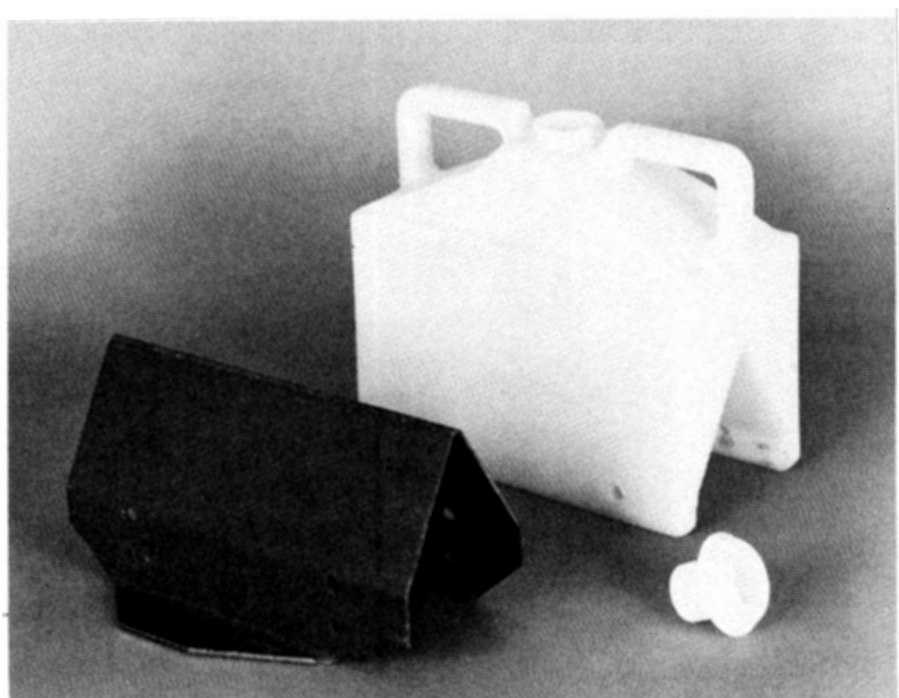

Figure 59. A linear shaped charge container and liner (courtesy Defense Research Establishment Suffield).

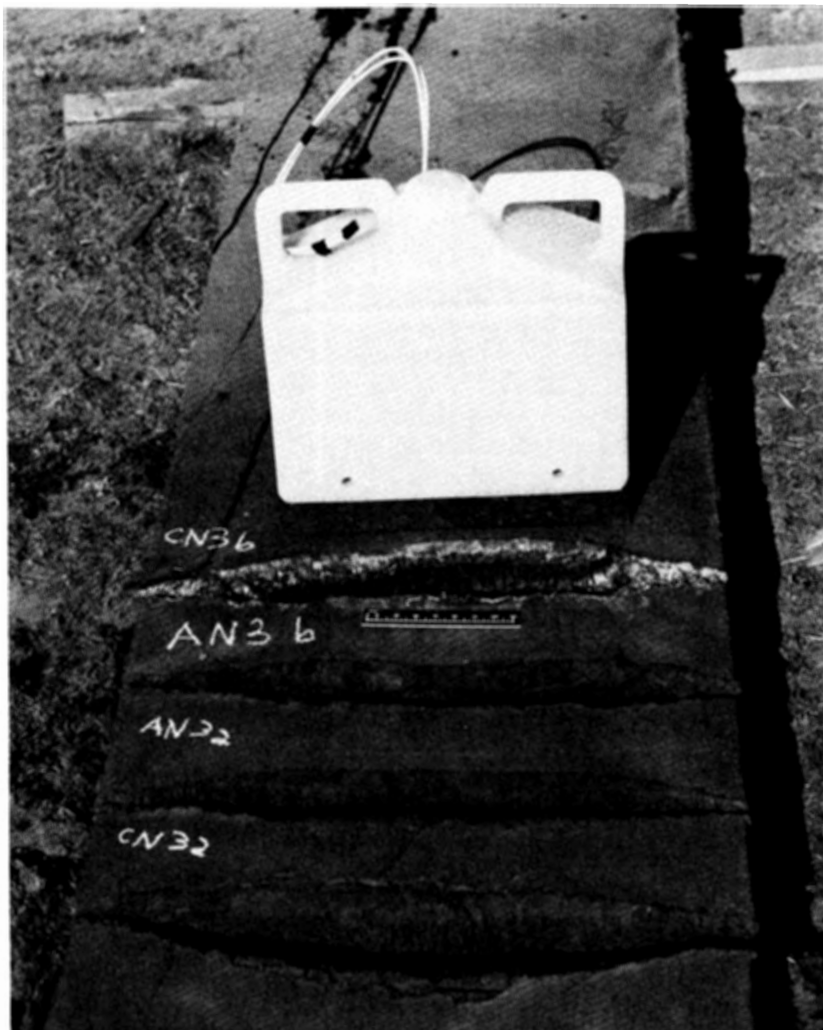

Figure 60. The linear shaped charge mounted on a 20 cm thick steel plate, showing also cuts produced with various thicknesses of the steel liner (courtesy Defense Research Establishment Suffield).

velocity and pressure. Figure 57 shows the resultant blast, and Figure 58 shows the countermobility obstacle (crater) produced.

In addition to the cylindrical shaped charge used for creating boreholes, a linear shape is available for use as a cutting charge. The linear shaped charge can be assembled on site (see Figure 59) and contains 10 kg of TRIGAN and a liner made of mild steel. The liner is also shown in Figure 59. This demolition charge is shown in Figure 60, mounted on a 20 cm thick steel plate and

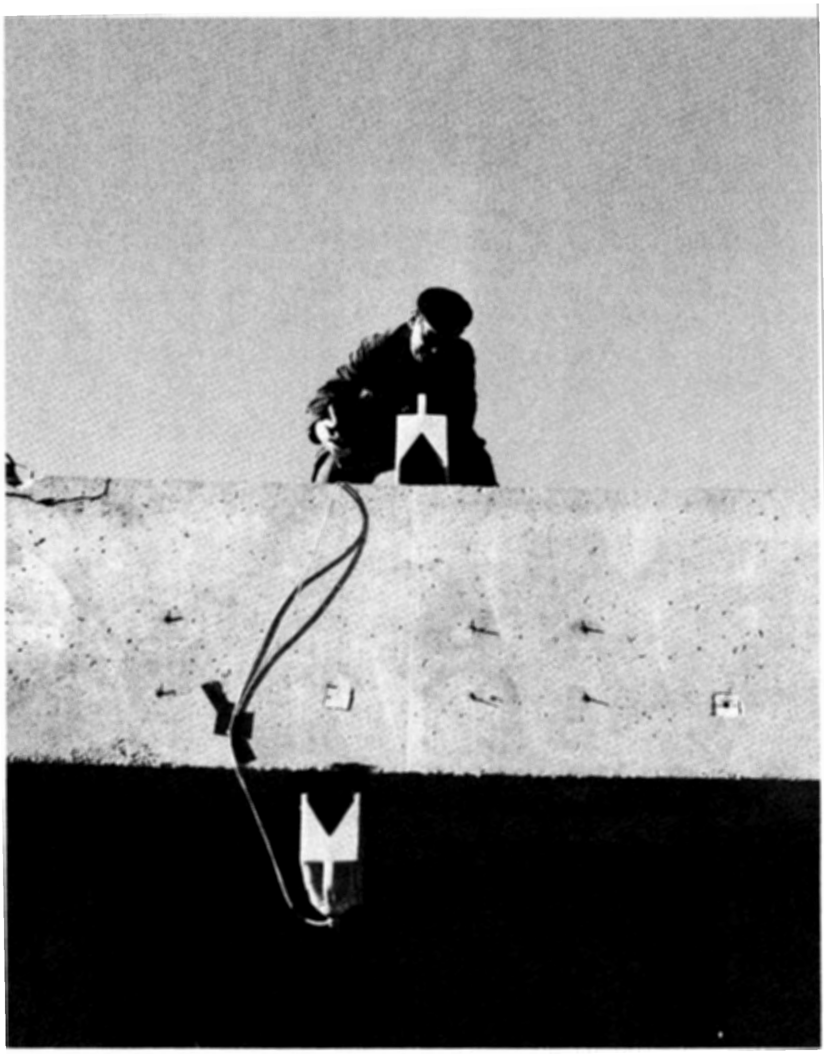

Figure 61. The linear cutting charge attached to a heavily reinforced bridge like structure (courtesy Defense Research Establishment Suffield).

showing cuts in the plate produced by various thicknesses of the mild steel liner.

Figure 61 shows this linear cutting charge used as a demolition charge and attached to a heavily reinforced bridge like structure. Figure 62 shows the structure after demolition. The indentation in the screw cap (Figure 59) is filled with plastic explosive that acts as a primer for the TRIGAN.

The preceding discussion and Figures 53–62 were furnished courtesy of Defense Research Establishment Suffield.

14.6. SPECIAL APPLICATIONS AND EFFECTS

Earlier chapters discussed special applications of shaped charges including linear cutting charges and the like. Figures 63 and 64 illustrate some of these charges. Figure 64 shows typical perforation or cutting performances and representative hole profiles for cutting charges, conventional shaped charges, and self-forging fragment charges.

The effects of charge imperfections on jet formation of conical liners are shown in Figure 65. Charge inhomogeneity (the upper half of the charge loaded with Comp B and the bottom half of the charge loaded with TNT), crossing axes effects (the liner and explosive charge axis of symmetries are not parallel), and offset initiation effects are illustrated.

Figures 66 and 67 illustrate the effect of off-center initiation on a conical liner. The initiation assembly was offset to the maximum possible angle from the charge axis of symmetry, 11.4° in this case. Walters (1986) provides details.

Figures 68–73 present the offset angle study for a shaped charge with a hemispherical liner. Figures 68 and 69 show the reference case, that is, the collapse and formation of the hemispherical shaped charge for a zero offset angle, or the detonator aligned on the charge axis of symmetry. Figures 70 and

Figure 62. The bridge like structure after demolition (courtesy Defense Research Establishment Suffield).

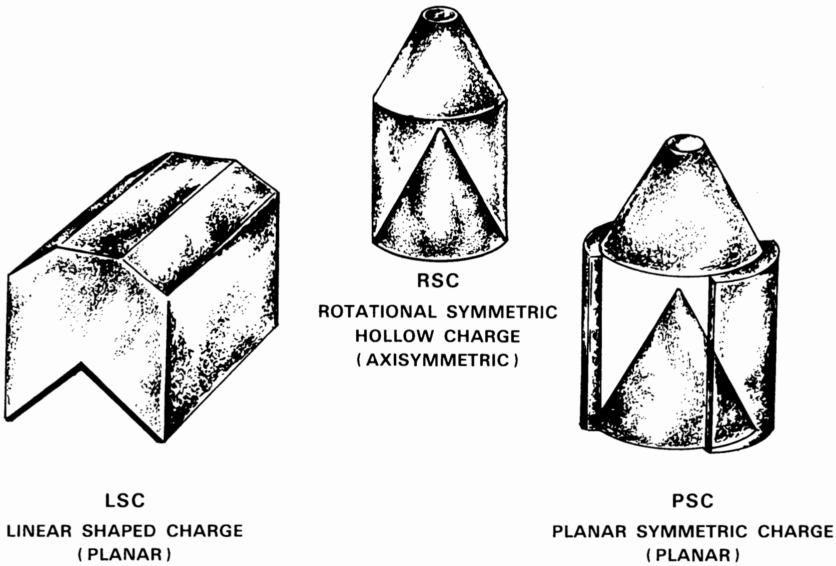

Figure 63. Typical shaped charges for penetration and cutting functions (Held 1980).

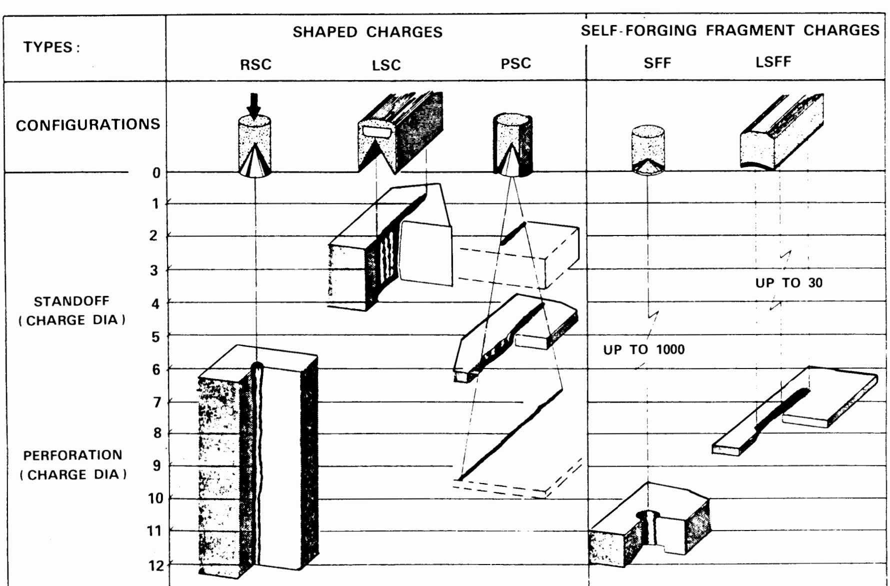

Figure 64. Comparison of the usual standoff and typical perforation or cutting performances and of hole profiles into mild steel for shaped charges and self-forging fragment charges (Held 1980).

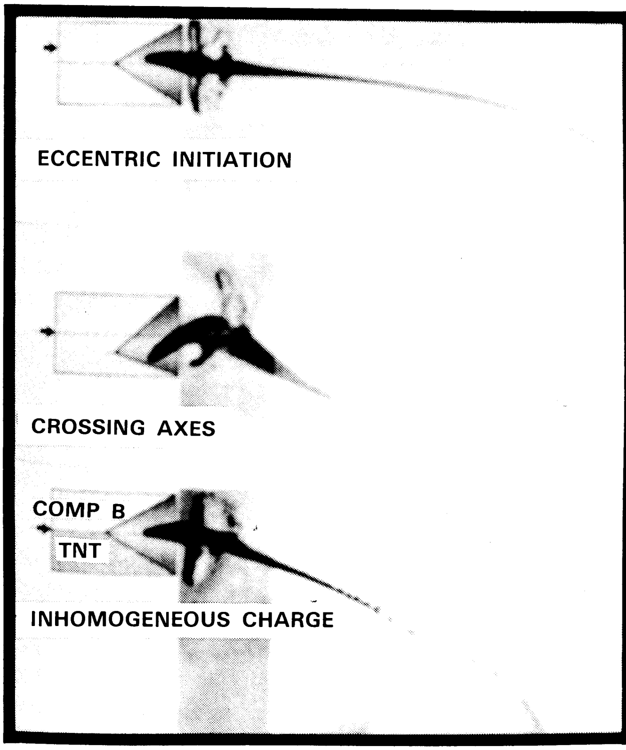

Figure 65. Examples of how charge imperfections, such as eccentric initiation or crossing axes of charge and liner or inhomogeneous high explosive charge effect the jet formation (Held 1983).

71 are for a small offset angle, namely 0.5°. The jet deflects only slightly, and the hemispherical liner is more tolerant of an eccentric initiation than a conical liner.

Figures 72 and 73 show the shaped charge with a hemispherical liner and the maximum possible offset angle, 17.35° in this case. Of course, the jet is severely bowed, as is the jet from a conical liner.

Figures 74 and 75 show the jet from a hemispherical shaped charge liner initiated using a dual-point initiation, that is, two initiation assemblies located at the maximum offset angle and 180° apart. Note how the jet "opens up" as witnessed by the hollow region in Figure 74. At later times (Figure 75) the jet splits and becomes an effective long standoff cutting charge. Again, details are given by Walters (1986).

The quality of the jet obtained from shaped charges with hemispherical, lead liners was studied by Walters et al. (1985). In particular, lead hemispheres of different wall thicknesses were examined under explosive loading conditions. The three wall thicknesses used in the study are given in Table 1,

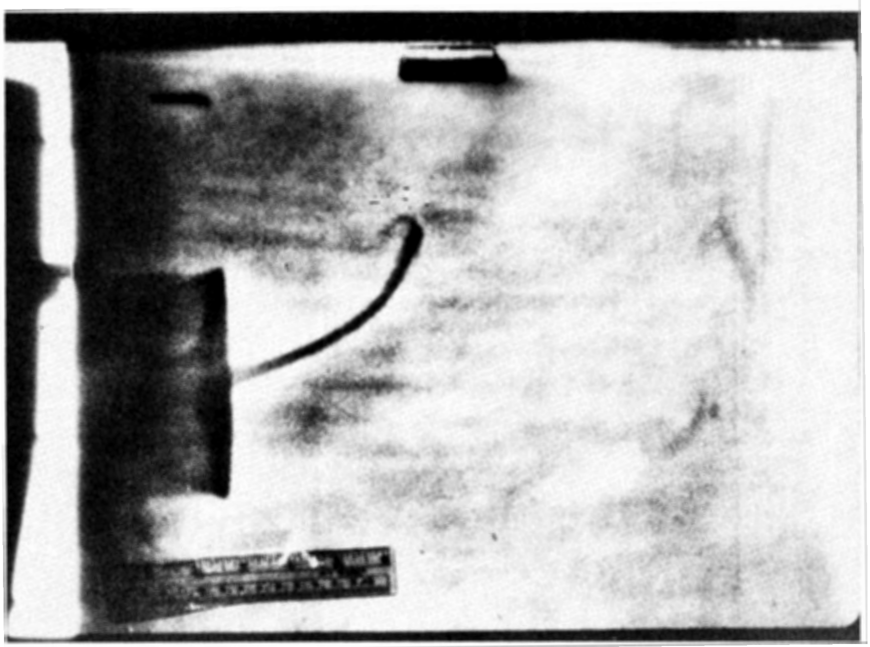

Figure 66. The jet formed from the collapse of a shaped charge with a conical liner. The flash time was 47.0 μs and the offset angle was 11.4° (Walters 1986).

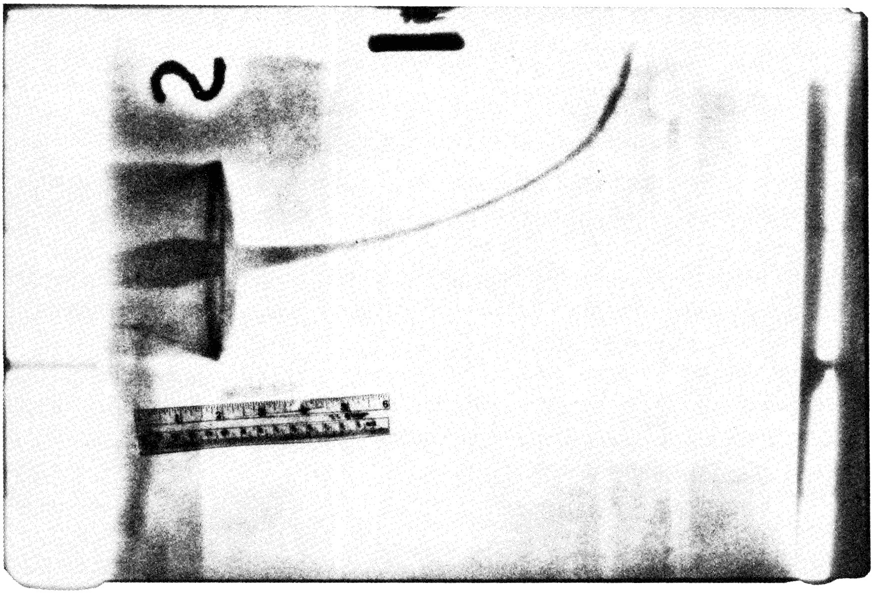

Figure 67. The jet formed from the collapse of a shaped charge with a conical liner. The flash time was 60.3 μs and the offset angle was 11.4° (Walters 1986).

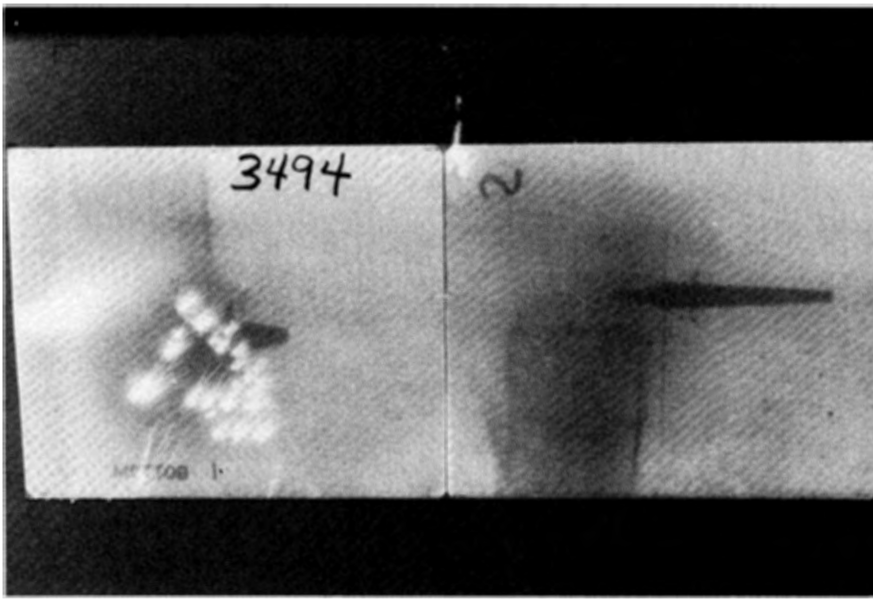

Figure 68. The jet formed from the collapse of a shaped charge with a hemispherical liner, reference case, or 0° offset angle. Flash times were 39.8 and 55.5 μs (Walters 1986).

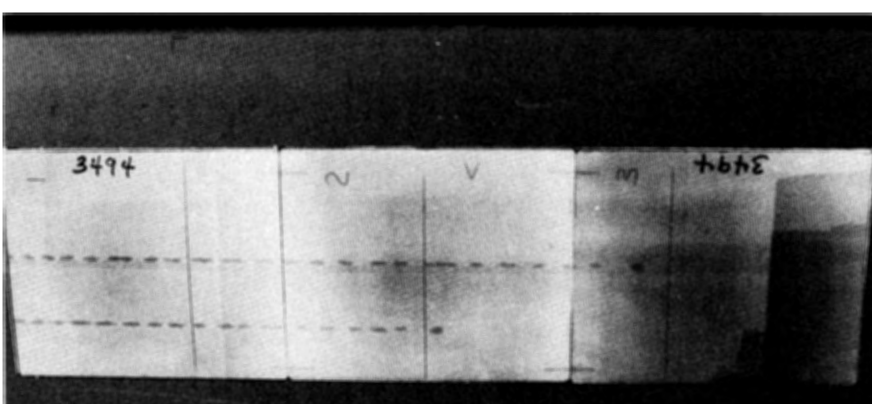

Figure 69. The jet formed from the collapse of a shaped charge with a hemispherical liner, reference case, or 0° offset angle. Flash times were 309.7 and 361.6 μs (Walters 1986).

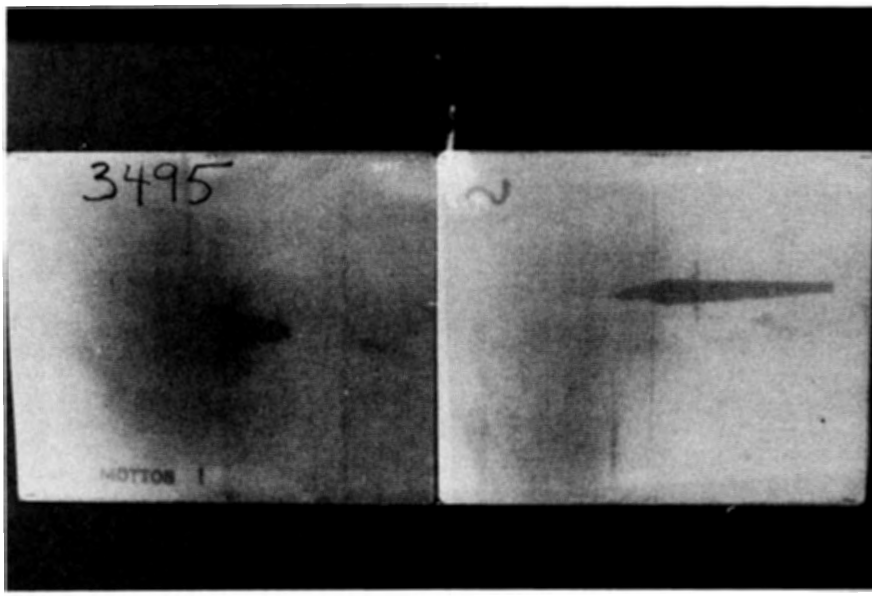

Figure 70. The jet formed from the collapse of a shaped charge with a hemispherical liner. The flash times were 39.9 and 55.5 μs. The offset angle was 0.5° (Walters 1986).

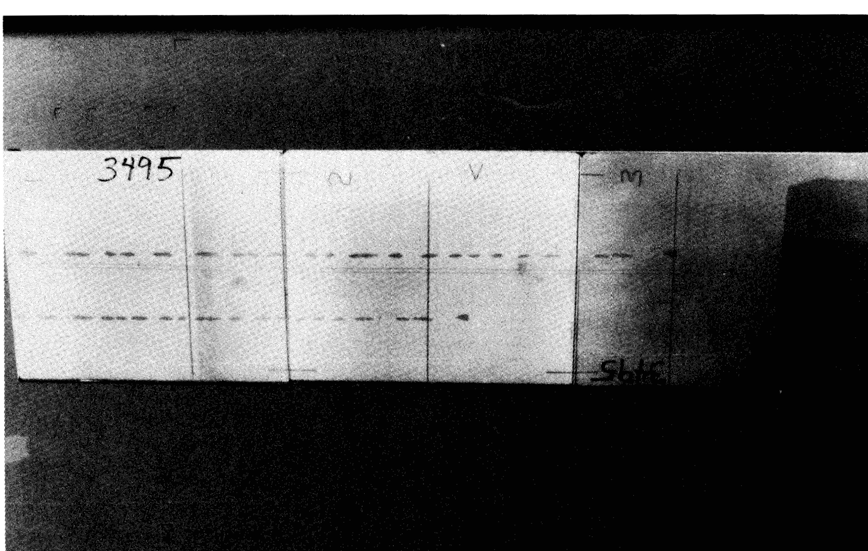

Figure 71. The jet formed from the collapse of a shaped charge with a hemispherical liner. The flash times were 309.3 and 361.6 μs. The offset angle was 0.5° (Walters 1986).

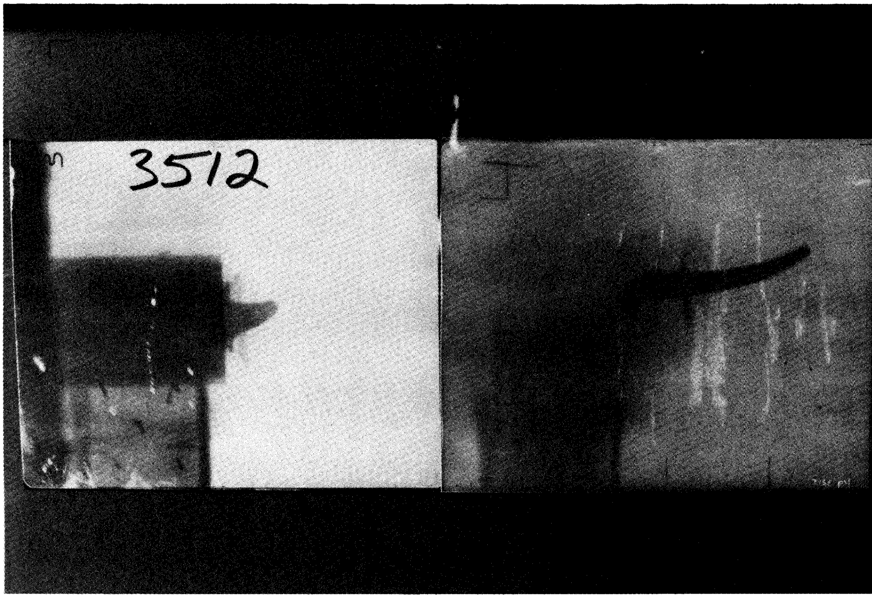

Figure 72. The jet formed from the collapse of a shaped charge with a hemispherical liner. The flash times were 39.4 and 54.4 μs. The offset angle was 17.35° (Walters 1986).

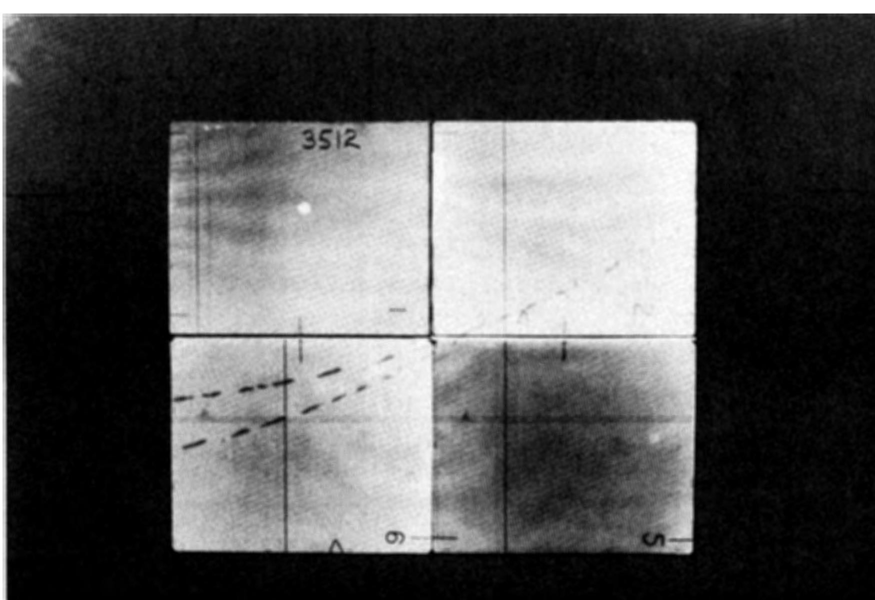

Figure 73. The jet formed from the collapse of a shaped charge with a hemispherical liner. The flash times were 310.1 and 368.1 μs. The offset angle was 17.35° (Walters 1986).

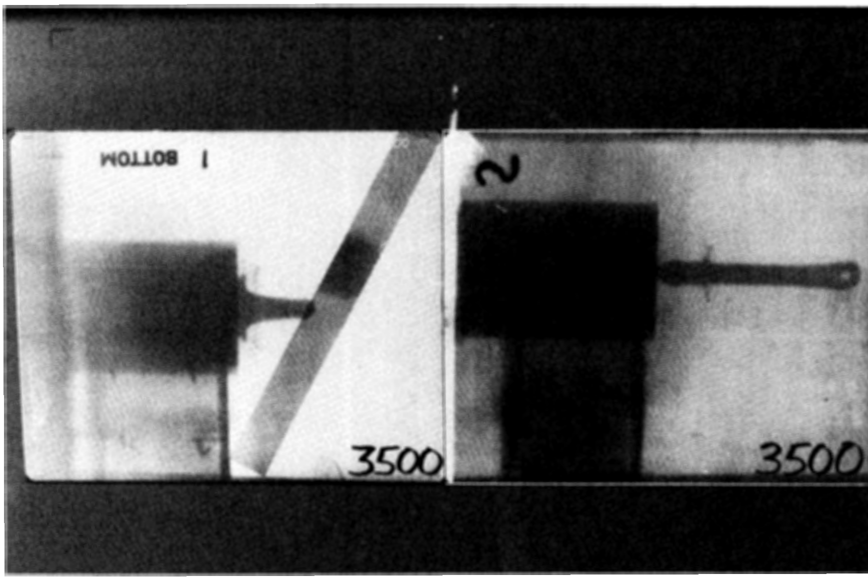

Figure 74. The jet formed from the collapse of a dual-point initiated, maximum offset angle, shaped charge with a hemispherical liner. The flash times were 39.9 and 55.7 μs (Walters 1986).

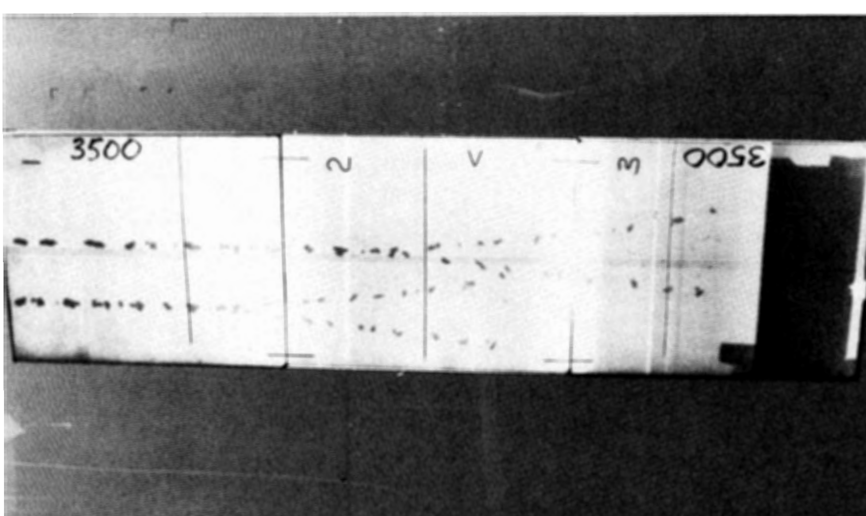

Figure 75. The jet formed from the collapse of a dual-point initiated, maximum offset angle, shaped charge with a hemispherical liner. The flash times were 309.6 and 361.6 μs (Walters 1986).

TABLE 1. Results of the Lead Hemispherical Liner Tests

Round Number	Liner	X-ray Flash Times (s)	Penetration (CD)	Jet Tip Velocity (km/s)
2950	127 mm diameter	408	0.81[a]	4.63
	2.97 mm	433		
	wall thickness	457.9		
	(2.34% wall)			
2951	127 mm diameter	418	3.13[a]	4.57
	3.81 mm wall	443		
	thickness (3% wall)	467.9		
2952	127 mm diameter	418.1	2.03[a]	4.0
	5.08 mm wall	442.9		
	thickness (4% wall)	467.9		
3157	50.8 mm diameter	483.2	0.07[b]	
	1.9 mm wall	505.3		
	thickness (3.75% wall)	524.6		

[a]At a 17.15 CD standoff into 50 mm stacked RHA plates.
[b]At a 31 CD standoff into 50 mm stacked RHA plates.

together with the liner diameter, resulting penetration depths, and the jet tip velocities. Flash radiographs depicting jets from the three configurations are shown in Figures 76 to 78. The associated wall thicknesses and flash times are listed in Table 1. Table 1 also lists the characteristics of a small-diameter lead hemispherical liner as scaled from the 127 mm liner, except that the wall thickness was 1.9 mm. This liner was tested to provide data regarding the rear of the jet. The delay times were altered to allow the tip of the jet to leave the field of view covered by the film in order to provide coverage of the jet tail. Radiographic data for this jet are shown in Figure 79. Details were given in Chapter 12.

Figures 76–78 indicate several interesting features. The same piece of film on the first channel (designated as 1 1, 1 11, and 1 111) was inadvertently used for both rounds 2951 and 2952 (Figures 77 and 78, respectively). Thus, the jets from both these rounds were superimposed on the first channel. Round 2951 has the longest jet, round 2952 the shortest. From the figures, it is evident that jet quality improves as the wall thickness increases (that is, the jet becomes less fluid, more solid in appearance as wall thickness increases). Correspondingly, the jet tip velocity decreases as wall thickness increases (Table 1) since the liner becomes more massive.

Note the obvious transition of the fluid characteristics of the jet as the wall thickness increases. The thin wall liner yields a jet with considerable amounts of vapor present. The vapor content of jets from thicker lines is markedly reduced. Most probably they are in a solid or liquid phase. Information regarding liquefaction of the jet can be obtained by firing the jet into a target

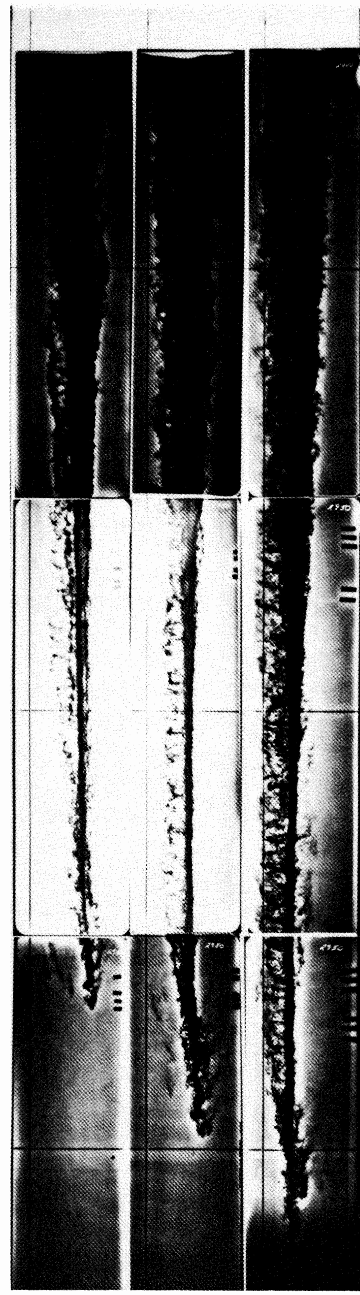

Figure 76. Free-flight flash radiograph of round 2950 of Table 1 (Walters et al. 1985).

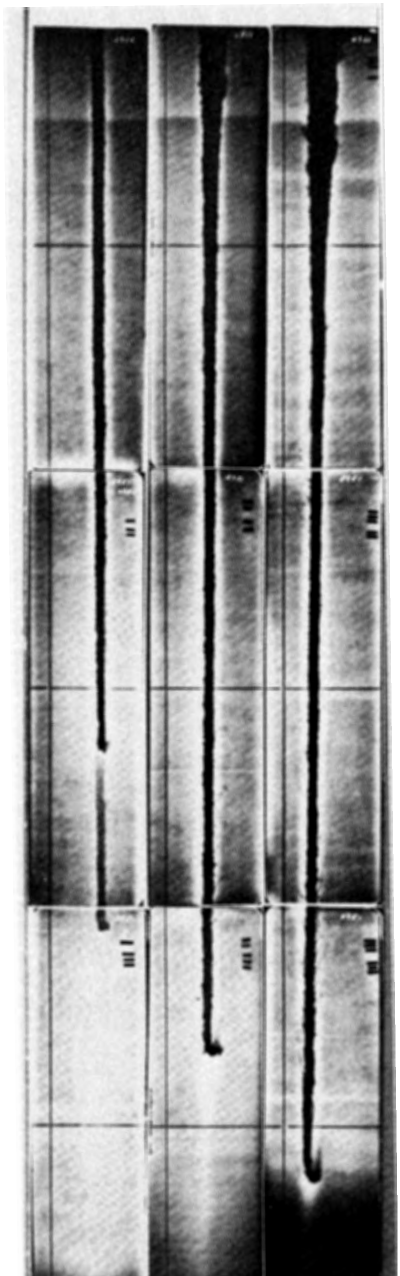

Figure 77. Free-flight flash radiograph of round 2951 of Table 1 (Walters et al. 1985).

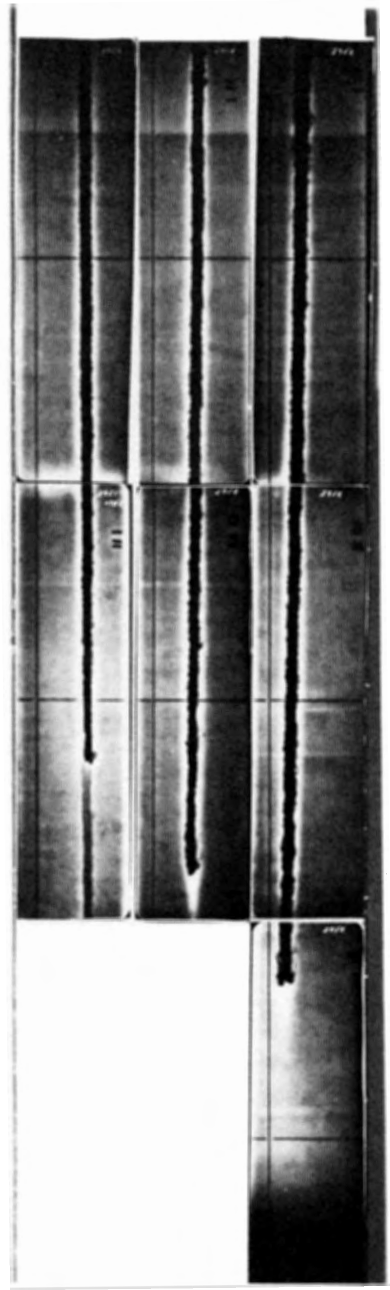

Figure 78. Free-flight flash radiograph of round 2952 of Table 1 (Walters et al. 1985).

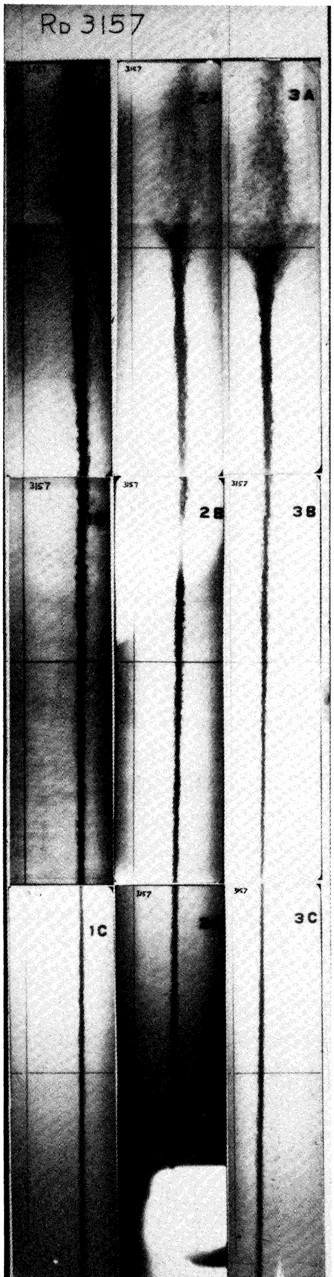

Figure 79. Free-flight flash radiograph of round 3157 of Table 1 (Walters et al. 1985).

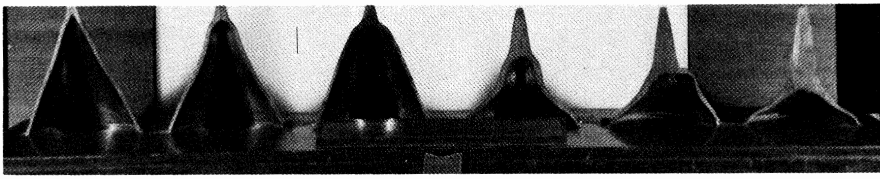

Figure 80. The partial collapse of a conical shaped charge liner, front view (courtesy BRL).

at an oblique angle to the jet axis. A liquid jet would exhibit considerable splatter against an oblique plate, whereas a much cleaner (and deeper) penetration channel would be obtained from a solid jet.

Walters et al. (1985) provide additional detail and present computational results that show the temperature gradients during the collapse and formation of the jets from the lead liners. Note that lead is an ideal material for the study of jet temperatures since the low melting point of lead allows for thermodynamic phase changes. Again, details were given in Chapter 12.

Earlier chapters described methods of inhibiting the collapse of a shaped charge liner in order to study the collapse process. This has been done, using various techniques, as discussed previously. The cross section of a recovered liner, with the collapse arrested at various stages, is shown in Figures 80 and 81. These liners were recovered in an experiment performed by S. Kronman of BRL many years ago. The exact procedure he used to inhibit the collapse is no longer known. However, these experimental results were duplicated by the authors by using a water column (of various heights) to surround the liner in lieu of a high explosive. An explosive pellet was then floated on top of the water column and detonated to propagate a shock wave through the water column. The recovered liners (captured in a bucket of water) were identical to those shown in Figures 80 and 81. Note that the partially collapsed liners agree with the computational pictures of jet formation and early time flash radiographs. Also note that the second liner from the right in Figures 80 and 81 was damaged during the recovery process, which explains its unsymmetric appearance.

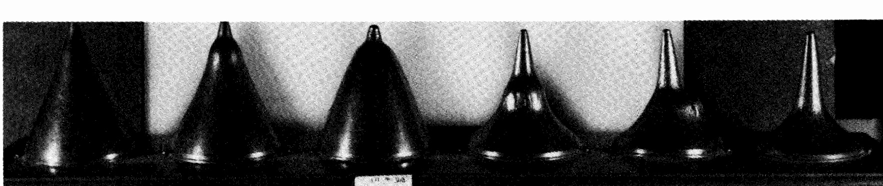

Figure 81. The partial collapse of a conical shaped charge liner, rear view (courtesy BRL).

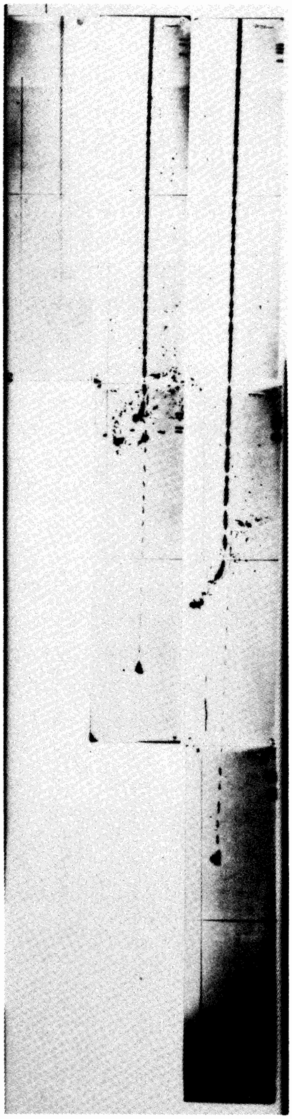

Figure 82. A shaped charge jet overtaking and colliding with another jet.

14.7. SHAPED CHARGE JET COLLISIONS

Figure 82 depicts a shaped charge jet overtaking and colliding with the tail of another shaped charge jet.

Finally, in a classic experiment, Pernick (1965) [also Lukasik and Pernick (1965)] obtained a framing camera record for two shaped charge jets colliding head-on in air. The direction of jet motion was vertical, and a conventional argon bomb was used to provide back lighting for the camera. As shown in Figure 83 the approaching jets first appear from behind the expanding detonation products in the second frame. In Figure 83, the time increases from left to right and top to bottom with 1.4 μs per frame. The jet tips are highly luminous and cometlike in appearance. The highly luminous collision is first observed in the fourteenth frame. The collision region expands in time, and its extreme brightness persists for the duration of the film record. Growing dark areas appear in the last three frames and are probably due to expansion cooling and interaction with the encroaching detonation products (Pernick 1965).

Figure 84 is a streak camera record of a shaped charge jet collision in air. On the left side of the figure is an image of a marker scale located between the two shaped charges. This scale provides a calibration between spatial position at the explosive event and transverse distance on film. The time scale calibration follows from the streak camera rotational speed. The direction of increasing time is from left to right. The camera entrance slit is oriented in the

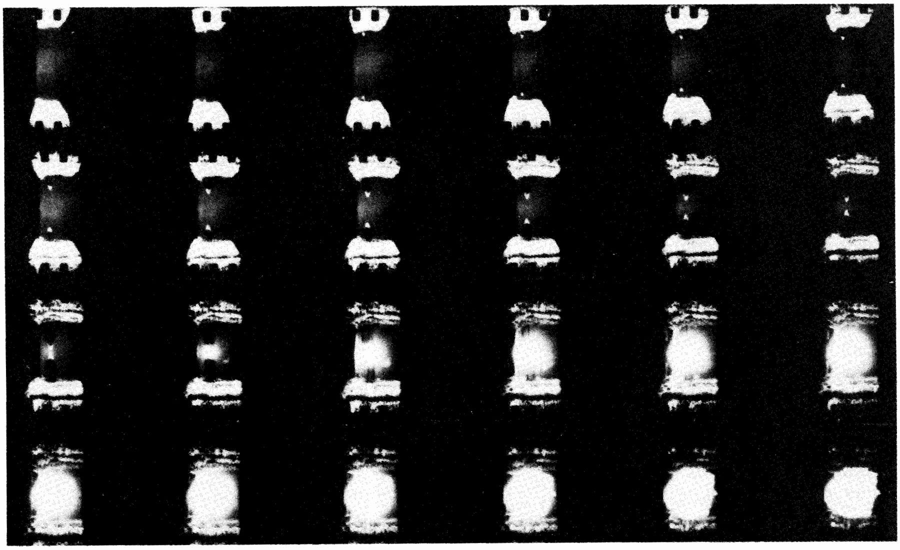

Figure 83. Framing camera record of jet collision in air (courtesy of B. J. Pernick 1965).

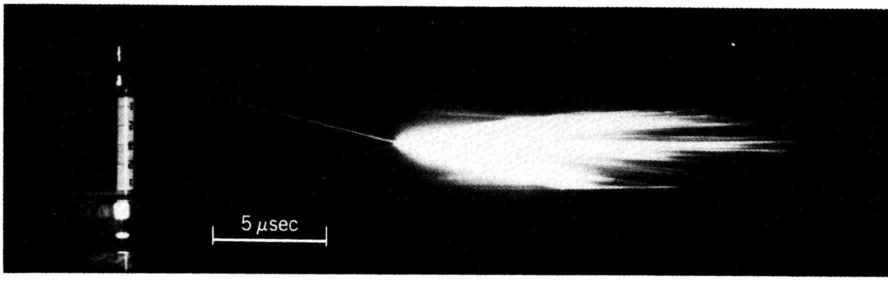

Figure 84. Streak camera record of two copper jets before and after collision in air (courtesy of B. J. Pernick 1965).

direction of jet motion. The two narrow light trails on the left side of the figure represent the approaching jets. The light comes from the luminous jet tips. Jet collision is characterized by the intersection of these trails and subsequent exposure that lasts for about 50 μs. A region of intense luminosity, centered about the impact point, remains roughly localized for the length of the camera record. Aside from the initial jet velocity data contained in a streak record, the extremely high light intensity of the collision products is apparent, even when viewed through a narrow streak camera entrance slit. Pernick (1965) provides additional data on head-on shaped charge jet collisions and the resulting plasma production.

REFERENCES

AMCP (1964), "Ammunition Series Section 2, Design for Terminal Effects," Army Materiel Command Pamphlet, AMCP 706-245, July.

Arvidsson, B., and Ohlsson, H. G. (1984), "Investigation of Liners For Shaped Charges Manufactured from Cu-Powder by X-ray Diffraction and Ultrasonic Techniques," *Proc. 8th Int. Symp. on Ballistics*, Orlando, Florida, 23–25 October.

Chanteret, P. Y., and Jamet, F. (1984), "Quasi Non-Stretching Hypervelocity Jets," *8th Int. Symp. on Ballistics*, Orlando, Florida, 23–25 October.

Chou, P. C., Ciccarelli, R. D., and Walters, W. P. (1983), "The Formation of Jets from Hemispherical-Liner Warheads," *Proc. 7th Int. Symp. on Ballistics*, The Hague, Netherlands, 19–21 April.

Chou, P. C., Walters, W. P., Ciccarelli, R. D., and Weaver, G. W. (1985), "Jet Formation Mechanics of Hemispherical Warheads," Ballistic Research Laboratory Contractor Report, ARBRL-CR-545, October.

Cook, M. A. (1958), *The Science of High Explosives*, New York: Reinhold Publishing.

Davison, D. K., and Arvidsson, B. K. (1985), "Optimization of a 90 mm Shaped Charge Warhead," *2nd Symp. on the Interaction of Non-Nuclear Munitions with Structures*, Panama City Beach, Florida.

Geiger, W., and Honcia, G. (1977), "Shaped Charges with Pyramidal Liners," *3rd Int. Symp. on Ballistics*, Karlsruhe, West Germany, 23–25 March.

Hallquist, J. O. (1980), "User's Manual for DYNA2D—An Explicit Two-Dimensional Hydrodynamic Finite Element Code with Interactive Rezoning," Report UCID-18756, Lawrence Livermore National Laboratory.

Held, M. (1980), "Cutting Charges," *Proc. 5th Int. Symp. on Ballistics*, Toulouse, France, 16–18 April.

Held, M. (1983), "Characterizing Shaped Charge Performance by Stand-Off Behavior," *7th Int. Symp. on Ballistics*, The Hague, Netherlands, 19–21 April.

Held, M. (1986), "The Orthogonal-Synchro-Streak Technique as a Diagnostic Tool, Particularly for Shaped Charge Jets," *Propell. Explos. Pyrotech.*, *11*:170–175.

Hermann, J. W., Jr., Randers-Pehrson, G., and Berus, E. R. (1977), "Experimental and Analytical Investigation of Self-Forging Fragments for the Defeat of Armor at Extremely Long Standoff," *3rd Int. Symp. on Ballistics*, Karlsruhe, West Germany, 23–25 March.

Lukasik, S. J., and Pernick, B. J. (1965), "Plasma Production by Kinetic Impact," Davidson Laboratory Report 850, February.

Pernick, B. J. (1965), "Plasma Production by Kinetic Impact," Ph.D. Dissertation, Stevens Institute of Technology, Hoboken, NJ.

PI (1979), "SFF Design Technology," Physics International, California, January.

Simon, J., and DiPersio, R. (1972), "Jet Formation and Utilization," in *Proc. 12th Annual Symp. on Behavior and Utilization of Explosives in Engineering Design*, L. Davison and J. E. Kennedy (eds.), New Mexico Section of the ASME, March.

Walters, W. P. (1986), "Asymmetric Initiation of Shaped Charges," *Proc. of SECTAM XIII, The Southeastern Conference on Theoretical and Applied Mechanics*, Columbia, South Carolina, April.

Walters, W. P., Jonas, G. H., and Zukas, J. A. (1985), "Explosive Loading of Lead Hemispherical Liners," *Comput. Struct.* *20*(1–3):615–621.

Walters, W. P., and Golaski, S. K. (1987), "Hemispherical and Conical Shaped Charge Liner Collapse and Jet Formation," Ballistic Research Laboratory Technical Report, ARBRL-TR-2781, February.

Weickert, C. A. (1986), "Spinning Self-Forging Fragments and Shaped Charges," Ph.D. Dissertation, Drexel University, Philadelphia, June.

INDEX